Seeking the Lipid Substrate Binding Site: Structural Studies of Eukaryotic Diacylglycerol Kinases

by
Elizabeth Jane Petro

A dissertation submitted to Johns Hopkins University in conformity with the requirements for the degree of Doctor of Philosophy

Baltimore, Maryland
December 2013

Abstract

Very little is known about the structure of the catalytic domain of eukaryotic diacylglycerol kinases (DGKs), a family of interfacial enzymes implicated in a number of physiological roles and human diseases. Constructs of the catalytic domain could be expressed in *Escherichia coli* and extracted, refolded, and purified from inclusion bodies, but when subjected to analytical gel filtration chromatography, these constructs eluted in the void volume in what appeared to be microscopic aggregates unsuitable for x-ray crystallography. Adding glutathione S-transferase, thioredoxin, or maltose binding protein as N-terminal fusion tags did not improve the constructs' solubility. Coexpressing with bacterial chaperones increased the yield in the supernatant after high-speed centrifugation, but the protein still eluted in the void upon analytical gel filtration chromatography. DGK constructs expressed in insect cells were likewise insoluble and unsuitable for x-ray crystallography. Loss of enzymatic activity of purified DGK could be mitigated by including 50% (v/v) glycerol and storing at -80°C, and by including detergent, lipid, and protein activators following thawing. Certain polybasic proteins and substrate analogs increase the *in vitro* enzymatic activity of purified DGK, whereas hirudin decreases its activity under certain conditions. DGK is able to use certain diglyceride analogs as substrates. Bimolecular fluorescence complementation was unable to show whether DGK-theta dimerized or interacted with tau when overexpressed in mammalian cells. Thrombin was able to digest DGK-theta after folding, but none of the washing conditions tested were able to separate the digested fragments, so while digestion with thrombin appeared to activate DGK-theta, whether the activation was due to relief from auto-inhibition or some other effect from the thrombin could not be

resolved. Photoaffinity labels were able to enzymatically inactivate purified DGK-theta in a probe-, ultraviolet-, and time-dependent way, but only when the linker between the substrate analog moiety and the photoactivatable moiety was sufficiently short. Mass spectrometry studies were unable to detect peptides shifted by the predicted molecular weight of the photoaffinity labels or their fragments. This work should guide future studies of the structure of eukaryotic DGKs.

Acknowledgments

Ms. Carol Harker, Mr. Clifton Maddox, Ms. Elizabeth Dixon, and Ms. Sheril Dyer washed glassware, racked and autoclaved pipet tips, and autoclaved medium and water. The Department of Biological Chemistry shared the film developer. The laboratory of Professor Gerald Hart shared their shaking incubator, centrifuges, probe sonicator, spectrophotometer, fluorescent microscope, scintillation counter, plate reader, and tissue culture hood. The laboratory of Professor Jun Liu (Pharmacology and Molecular Sciences) shared their spectrophotometer, microscope, tissue culture hood, cold room, and column parts. The laboratory of Professor Jeffry Corden (Molecular Biology and Genetics) shared their Odyssey® Infrared Imaging System and scintillation counter. The laboratory of Professor Susan Craig shared their multichannel pipettors and tips. I used Microsoft® Excel® and SigmaPlot™ to perform calculations.

Professor L. Mario Amzel (Biophysics and Biophysical Chemistry) pointed out that silver staining unequally stains proteins and thus is not a good way to assess protein purity. Dr. Becky Tu-Sekine suggested the modified silver staining protocol. Dr. Jeremy Rotty of Professor Pierre Coulombe's laboratory taught me how to immunoblot.

Dr. Becky Tu-Sekine taught me how to perform radiometric endpoint DGK assays. Mr. William Petro taught me to "do as you oughter: add acid to water". Professor Daniel M. Raben suggested that salt extraction might be a source of uncertainty in the radiometric endpoint assay.

Dr. Chad Slawson of Professor Gerald Hart's laboratory (Biological Chemistry) suggested using a shaking incubator in the cold room to express bacteria at 16°C, and assisted in setting one up.

Dr. Bryan Geisbrecht, of Professor Daniel Leahy's laboratory (Biophysics and Biophysical Chemistry), provided the pT71myc plasmid. Dr. Rishi Porecha cloned alphacat and epsiloncat into pT71myc. The Synthesis & Sequencing Facility (The Johns Hopkins University School of Medicine) and GENEWIZ® performed DNA sequencing. Dr. Agedi Boto and Professor Sandra Gabelli of Professor L. Mario Amzel's laboratory shared flasks, a shaking incubator, the microfluidizer, and centrifuges, and provided technical assistance with the 4L expression of alphacat in pT71myc. The laboratory of Professor Cynthia Wolberger (Biophysics and Biophysical Chemistry) shared tubes for the microfluidizer. The Department of Cell Biology shared their ultracentrifuge and scintillation counter. Professor Daniel Leahy recommended using analytical gel filtration chromatography as a way to assess the monodispersity of proteins before proceeding to crystallization studies. Professor Albert Mildvan provided the analytical gel filtration resins as well as the columns, caps, and tubing. The laboratory of Professor Fumio Sakane (Chemistry, Chiba University) provided the rabbit anti-DGK-alpha antibody. Professor Daniel M. Raben suggested blocking the analytical gel filtration column with albumin, using a carrier protein to facilitate ethanol precipitation, and concentrating protein samples by dialysis against 15% (w/v) polyethylene glycol (PEG) 17.5k prior to loading onto the analytical gel filtration column. Professor Sandra Gabelli recommended loading at least 1-2 mg per mL protein onto an analytical gel filtration column.

Dr. David Bolduc of Professor Philip Cole's laboratory (Pharmacology and Molecular Sciences) provided the chaperone plasmids. Dr. Becky Tu-Sekine transformed the chaperone plasmids into BL21(DE3). Ms. Hana Goldschmidt performed the protein

electrophoresis shown in Figure 27. Dr. Becky Tu-Sekine performed the protein electrophoresis shown in Figure 30, and retuned the bath sonicator.

Ms. Michele Ostroski cloned alphacat into pGEX-4T2. Ms. Laura Morkowchuk prepared the 5x M9 salts from which I prepared the M9 Minimal Medium. Ms. Ping Hu of Professor Gerald Hart's laboratory provided the anti-GST antibody used in Figure 44, Figure 45, and Figure 203**A**.

Dr. Nadine Samara of Professor Cynthia Wolberger's laboratory provided the pET32a plasmid along with helpful advice for designing primers to use PCR for cloning into the plasmid.

Ms. Tonya Gilbert of Professor Sean Taverna's laboratory (Pharmacology and Molecular Sciences) provided the pET28-HisMBP-FLAGpp plasmid.

Dr. Sabina Muend helped edit the manuscript "Bacterial expression strategies for several *Sus scrofa* diacylglycerol kinase alpha constructs: solubility challenges"[1], and some of those edits are preserved in this dissertation, used under CC BY-NC 2.5.

Ms. Michele Ostroski, with the help of the laboratory of Professor Douglas Robinson (Cell Biology), generated the FLAG-DGKA-overexpressing strain of *D. discoideum*. Dr. Becky Tu-Sekine helped maintain *D. dictyostelium* cells, and provided the activators used in Figure 66.

Dr. Becky Tu-Sekine designed the cloning strategy for generating *R. norvegicus* DGK-alpha in bacmid. Dr. Becky Tu-Sekine generated the pENTR11X plasmid, and performed the EcoRI digestion and subsequent electrophoresis and agarose gel excision. Dr. Becky Tu-Sekine harvested the first round of the initial DGK-alpha baculovirus production and used it to infect more Sf9 cells to produce the second round, which she

also harvested. Saki Phommachanh of Invitrogen™ (now Life Technologies™) provided valuable technical support for Sf9 cell culture.

Dr. Becky Tu-Sekine cloned and produced the DGK-theta baculovirus, performed the immunoblot shown in Figure 75 and prepared the cell pellet showed therein, and prepared the cell pellet shown in Figure 76**A**.

Dr. Becky Tu-Sekine cloned and isolated the plasmid encoding Fc-FLAG-DGK-theta used to transfect 293FT cells. Ms. Hana Goldschmidt transfected the 293T cells with the plasmid encoding myc-tagged DGK-theta, and lysed the cells.

Dr. Becky Tu-Sekine expressed and purified the DGK-theta aliquots assayed in the DGK stability chapter, recommended the 0.4% (v/v) NP-40 preincubation step, and prepared the samples shown in Figure 100. The laboratory of Professor Jun Liu shared the use of their chemical fume hood, water-jacketed quartz cuvette and accompanying stir bar, 360 nm lamp, and steel-probed thermometer. Dr. Wei Shi and Dr. Shridhar Bhat assisted with setting up and using the lamp and cuvette, and Dr. Benjamin Nacev and Ms. Sarah Head shared the use of the lamp. Dr. Becky Tu-Sekine suggested preincubating DGK on ice in the presence of detergent before diluting, suggested testing whether preincubating with histone H1, MgATP, and/or DTT protects purified DGK-theta from inactivation at room temperature, suggested keeping 0.005% (v/v) DDM present at all times, and suggested that DTT breakdown could be the key to DGK inactivation over time. Professor Jed Fisher of Professor Shahriar Mobashery's laboratory (Chemistry & Biochemistry, University of Notre Dame) suggested using a UV LED instead of the 360 nm lamp. Ms. Sarah Head recommended the use of a UV LED flashlight as a circuitry source to power the LED.

Dr. Becky Tu-Sekine purified the tau from BL21 shown in Figure 119.

Dr. Joanna Gajewiak of Professor Glenn Prestwich's laboratory (Medicinal Chemistry, University of Utah) synthesized the JG compounds.

Dr. Becky Tu-Sekine purified the DGK-theta aliquots used in the DGK activation, inhibition, and substrate specificity chapter, with the exception of the protease inhibitor subchapter, in which I purified the DGK-theta. Ms. Courtney Grossman labeled DiC8 vials as DOG vials, allowing the DiC8 substrate tests of alphacat in pT71myc.

Professor Arne Gericke (Department of Chemistry and Biochemistry, Kent State University) presented the conditions for making PIP_2-containing liposomes at the 51st Annual Meeting of the Biophysical Society in Baltimore, MD in March 2007.

Dr. Meng M. Rowland and Mr. Sammy Eni Eni of Professor Michael Best's laboratory (Chemistry, University of Tennessee) provided the photoaffinity labels. Professor Daniel M. Raben suggested charring the TLC plates to visualize the migration patterns of the photoaffinity labels and estimate their concentration. Mr. Morgan B. Stern recommended the use of an acid gas respirator while charring plates. Professor Daniel M. Raben suggested the two-binding site hypothesis for explaining the results shown in Figure 136. Dr. Becky Tu-Sekine provided the isomerized DOG.

The FLAG/YN-Smad3 and FLAG/YC-Smad4 constructs were provided by Professor Suzanne Scarlata (Physiology & Biophysics, Stony Brook University Medical Center), who reportedly[2] obtained them from Professor Thomas Kerppola (Biological Chemistry, University of Michigan). The laboratory of Professor M. Daniel Lane (Biological Chemistry) shared their fluorescent microscope. Dr. Becky Tu-Sekine recommended the use of ApE (A plasmid Editor) software, provided cloning advice for

the DGK-theta BiFC cloning project, and designed and performed the PCR of the first YC constructs using less template, lower annealing temperatures, and longer annealing times. The Zeiss LSM 510 Inverted META was provided by the Johns Hopkins University School of Medicine Institute for Basic Biomedical Sciences Microscope Facility, our laboratory's account for which we shared with the laboratory of Professor Rajini Rao (Physiology).

Dr. Becky Tu-Sekine generated the tau BiFC constructs. The Olympus I fluorescence microscope was provided by the Johns Hopkins University School of Medicine Institute for Basic Biomedical Sciences Microscope Facility, our laboratory's account for which we share with the laboratory of Professor Rajini Rao (Physiology).

Dr. Becky Tu-Sekine expressed and purified the *H. sapiens* DGK-theta shown in Figure 172 - Figure 176 and designed the experiment shown in Figure 173. Professor Daniel M. Raben suggested buying fresh thrombin and using hirudin and PMSF as thrombin inhibitors. Dr. Becky Tu-Sekine recommended reusing primary antibody dilutions for immunoblotting. Professor Daniel M. Raben suggested loading the resin (rather than just comparing the resin + supernatant to the supernatant) in Figure 182**B**.

Dr. Becky Tu-Sekine suggested using sucrose-loaded vesicle (SLV) pulldown as a method to detect covalent crosslinking of photoaffinity labels to DGK, purified the aliquots of DGK-theta used in the Chapter 8: Photoaffinity labeling chapter from HEK293T cells, as described[3], contributed to designing the experiments shown in Figure 188 and Figure 193, suggested focusing on a positive control for SLV pulldown, and recommended the C1b domain of PKCδ specifically as such a positive control. The laboratory of Professor Jun Liu provided the rabbit anti-histidine antibody used in Figure

193**D** and Figure 209. Professor Daniel M. Raben suggested testing DAG-dependent SLV pulldown of eGFP-C1b. Dr. Becky Tu-Sekine suggested that other proteins in HEK293T cytosol might be competing with eGFP-C1b for DAG binding. Dr. Becky Tu-Sekine suggested supplementing PC/PE SLVs to assist in pulling down the experimental SLVs, allowing them to be at a lower concentration. The laboratory of Professor Gerald Hart provided the plate reader used for measuring the fluorescence of SLVs in order to measure lipid recovery. Dr. Becky Tu-Sekine suggested using phorbol 12-myristate 13-acetate (PMA) as a positive control for the positive control.

Professor Natasha Zachara suggested using Triton X-114 (TX-114) partitioning as a method to detect photoaffinity labeling of DGK. Dr. Albert Lee of Professor Natasha Zachara's laboratory provided advice for the TX-114 partitioning experiments. The laboratory of Professor Gerald Hart provided the TX-114.

Dr. Meng M. Rowland recommended shortening the linker between the DAG-like moiety and the benzophenone moiety in the photoaffinity labels. Professor Daniel M. Raben suggested monitoring a delay in the timecourse of photocrosslinking as a way to determine whether DOG was competing for crosslinking, and suggested that changes in humidity could explain the different migration patterns of compound **4** on TLC.

Professor Robert Cole recommended using SDS-PAGE to separate DGK from the other components of the reaction before subjecting the sample to LC/MS/MS. Professor Natasha Zachara recommended the use of a 3-8% tris-acetate gel for measuring a gel shift of crosslinked DGK, and provided the gel and appropriate buffers. Ms. Jennifer Groves of Professor Natasha Zachara's laboratory assisted in performing the electrophoresis. The laboratory of Professor Gerald Hart provided the HPLC-grade methanol for washing

the excised, destained gel pieces prior to LC/MS/MS. Ms. Lauren DeVine of Professor Robert Cole's laboratory performed the protein mass spectrometry experiments, and recommended the use of acetonitrile and water as solvents for mass spectrometry of the lipid probe. The laboratory of Professor Gerald Hart provided the acetonitrile used in the probe solubility test. Professor Veera Venkata Ratnam Bandaru of Professor Norman J. Haughey's laboratory (Neurology) performed the lipid mass spectrometry experiments. The laboratory of Professor Michael Best performed the mass spectrometry shown in Figure 238.

Professor Natasha Zachara recommended using the master document, captions, cross-references, and mirror margins features of Microsoft® Word for writing the dissertation. I used Microsoft® Word, Microsoft® Excel®, Microsoft® PowerPoint®, Adobe® Illustrator®, Adobe® Photoshop®, ChemDoodle®, ImageJ, and SigmaPlot™ to make the figures.

This work was supported by an American Heart Association Predoctoral Fellowship and by Grant GM059251 from the National Institutes of Health.

Abbreviations Used in This Text

A: adenine

A280: absorbance at 280 nm

ADP: adenosine-5'-diphosphate

α: anti

APS: ammonium persulfate

ATP: adenosine-5'-triphosphate

AU: arbitrary units

B: before

BLAST: Basic Local Alignment Search Tool

BME: β-mercaptoethanol

bp: base pairs

BSA: bovine serum albumin

C: cytosine

Cam: chloramphenicol

Carb: carbenicillin

CIP: calf intestinal alkaline phosphatase

CMC: critical micelle concentration

D: detergent phase

DAG: diacylglycerol

DDM: dodecyl-β-D-maltoside

Dicty: *Dictyostelium discoideum*

DGK: diacylglycerol kinase

DiC8: 1,2-dioctanoyl-*sn*-glycerol

DNA: deoxyribonucleic acid

DOC: deoxycholate

DOG: dioleoylglycerol; 1-2-dioleoyl-*sn*-glycerol unless specified otherwise

dpi: dots per inch

dpm: decays per minute

DTT: dithiothreitol

e: eGFP-C1b

F: fresh, or foil

FB: fractionation buffer

FBS: fetal bovine serum

G: guanine

GSH: glutathione

HEK: human embryonic kidney

HEPES: 4-(2-hydroxyethyl)-1-piperazineethanesulfonic acid

His: histidine

HRP: horseradish peroxidase

I: induced, infected, input, or ice

IB: immunoblot

IPTG: isopropyl-β-D-thiogalactopyranoside

Kan: kanamycin

K_i: inhibition constant

$K_{m(surface)}$: surface Michaelis constant

L: lysate

LB: Luria Broth

LC/MS/MS: liquid chromatography followed by tandem mass spectrometry

LDH: lactate dehydrogenase

LED: light-emitting diode

LMW: low molecular-weight

LUV: large unilamellar vesicle

M: mock-transfected

mAb: monoclonal antibody

MBP: maltose binding protein

MOI: multiplicity of infection

MOPS: 3-(*N*-morpholino)propanesulfonic acid

MS: mass spectrometry

MW: molecular weight

MWCO: molecular weight cut-off

NAD^+: oxidized nicotinamide adenine dinucleotide

NADH: reduced nicotinamide adenine dinucleotide

NAG: *N*-acetylglucosamine

$NaPP_i$: sodium pyrophosphate

NBD-PE: 1,2-dioleoyl-*sn*-glycero-3-phosphoethanolamine-*N*-(7-nitro-2-1,3-benzoxadiazol-4-yl)

NCBI: National Center for Biotechnology Information

Ni-NTA: nickel-nitrilotriacetic acid

NMR: nuclear magnetic resonance

NNM: non-nuclear membrane

NP-40: Nonidet P-40

OD: optical density

OG: octyl-β-glucoside

O-GlcNAc: *O*-linked *N*-acetylglucosamine

P: pellet

PA: phosphatidic acid

pAb: polyclonal antibody

PAGE: polyacrylamide gel electrophoresis

PBS: phosphate-buffered saline

PC: phosphatidylcholine

PCR: polymerase chain reaction

PE: phosphatidylethanolamine

PEG: polyethylene glycol

PEI: polyethyleneimine

Pen: penicillin

pfu: plaque-forming unit

PG: phosphatidyl glycerol

pI: isoelectric point

PI: phosphatidylinositol

PIC: protease inhibitor cocktail

PIP_2: phospho-(1'-myo-inositol-4',5'-bisphosphate)

PK: pyruvate kinase

PKC: protein kinase C

PMA: phorbol 12-myristate 13-acetate

PMSF: phenylmethylsulfonyl fluoride

PNS: post-nuclear supernatant

POPA: 1-palmitoyl-2-oleoyl-*sn*-glycero-3-phosphate

POPC: 1-palmitoyl-2-oleoyl-*sn*-glycero-3-phosphocholine

POPE: 1-palmitoyl-2-oleoyl-*sn*-glycero-3-phosphoethanolamine

POPG: 1-palmitoyl-2-oleoyl-*sn*-glycero-3-phospho-(1'-*rac*-glycerol)

POPS: 1-palmitoyl-2-oleoyl-*sn*-glycero-3-phospho-L-serine

PP: PreScission Protease

PS: phosphatidylserine

psi: pounds per square inch

PVDF: polyvinylidene

R: reused, or resuspended

r_{av}: average radius

Rcf: relative centrifugal field

RefSeq: Reference Sequence

R_f: relative front

rpm: rotations per minute

R+S: resin plus supernatant

RT: room temperature

S: supernatant

SD: standard deviation

SDS: sodium dodecyl sulfate

SLV: sucrose-loaded vesicle

stds: standards

Strep: streptomycin

T: thymine

TBS: Tris-buffered saline

TCA: trichloroacetic acid

TEA: triethanolamine

TEMED: *N,N,N',N'*-tetramethylethylenediamine

TES: *N*-tris(hydroxymethyl)methyl-2-aminoethanesulfonic acid

TEV: Tobacco Etch Virus

TF: Trigger Factor

TLC: thin layer chromatography

T_m: phase transition temperature for lipids; melting temperature for DNA

Tris: tris(hydroxymethyl)aminomethane

TRX: thioredoxin

TX-100: Triton X-100

TX-114: Triton X-114

U: uninduced, uninfected, or UV

WR: washed resin

w/v: weight per volume (g per 100 mL)

v/v: volume per volume (mL per 100 mL)

V: vesicles

V_e: elution volume

V_o: void volume

X-Gal: 5-bromo-4-chloro-3-indolyl β-D-galactopyranoside

Chapter 1: Introduction

DGKs are a family of enzymes in eukaryotes that catalyze the transfer of the γ-phosphoryl from ATP onto the hydroxyl of DAG to produce ADP and PA. Most mammalian DGKs are interfacial enzymes, catalyzing reactions at the two-dimensional interface between the membrane and the aqueous phase.

Eukaryotic DGKs have been implicated in a number of physiological roles and human diseases[4,5]. Understanding the structure of these enzymes would bring insight into their activity, open doors to DGK modulator production and impact not only lipid signaling research but also medicine. Furthermore, little is known about the function of lipid kinases. Unlike their relatives with soluble substrates, the interfacial properties of these kinases greatly increase the technical difficulty for research. Lessons learned from DGKs might be applied to other lipid kinases, or indeed other interfacial enzymes. Most research to date revolves around protein-protein interactions, whereas much less concentrates on activity between lipids and proteins. Purification techniques and structural studies between DGKs interactions with DAG may be applied to other proteins that interact with lipids. Applications for this research are endless: not only could *de novo* protein lipid interactions be developed, but also improvements to drug delivery systems would further advance medicine into a new era.

Most work on eukaryotic DGKs has been conducted on those isolated from endogenous sources. Eukaryotic DGKs have been partially purified from rat liver[6], rat brain[7–9], bovine brain[10], bovine thymus[11], human platelets[12], porcine brain[8], porcine testis[13,14], porcine submaxillary glands[15,16], baboon brain[17], 3T3 mouse fibroblast

cells[8,15,16,18–21], *Drosophila* heads[22], and *Caltharanthus roseus* suspension-cultured cells[23], and they have been purified to apparent homogeneity from porcine brain[24–26], porcine thymus[15,16,19,27–29], bovine brain[30], bovine testis[15,16,18,19], rat brain[31–33], human platelets[12], human white blood cells[34], and *Microsporum gypseum* suspension-cultured cells[35]. While purified DGKs from endogenous sources have been invaluable for studying their enzymology, these sources are not amenable to producing enough protein for pursuing structural studies.

Recombinant forms of eukaryotic DGKs have been expressed in *E. coli*[36,37], in COS-7[36,38,39] and COS-1 *Chlorocebus aethiops* kidney cells[15,16], in Jurkat human T cells[38,40], in HEK293 human embryonic kidney cells[38,41], and in Sf21 *Spodoptera frugiperda* cells[42,43], and have been partially purified from HEK293 cells[44], COS-7 cells[45], *Dictyostelium discoideum*[46,47], *E. coli*[44,48–52], and Sf21 cells[53]. In only two cases to our knowledge has a eukaryotic DGK been purified to apparent homogeneity from a recombinant source: porcine DGK alpha was purified to apparent homogeneity after being expressed in the *Saccharomyces cerevisiae* strain WY294[15], and human DGK-theta was purified to apparent homogeneity after being expressed in HEK293 cells[3]. Truncations of the accessory (not catalytic) domains of eukaryotic DGKs have been expressed recombinantly with more success[16,39,54].

As such, little is known about the structure of DGKs, particularly of the catalytic domain. The catalytic domain is so-called because it is a region of primary sequence homology that makes up the gene family. Furthermore, this domain from *S. scrofa* DGK-alpha, when expressed in COS-7 cells, was reported to be catalytically competent[45], possessing similar enzymatic properties to the full-length enzyme, demonstrating that all

of the determinants for the catalytic reaction, including binding sites for the two substrates, are located in this region of the protein. But whereas a nuclear magnetic resonance (NMR) structure of the N-terminus of *Homo sapiens* DGK-alpha has been reported[62], as have an NMR structure of the second C1 domain[56] and an x-ray crystal structure of the SAM domain from *H. sapiens* DGK-delta[57], no structures of any part of the catalytic domain from any eukaryotic DGK have yet been published.

I therefore set out to recombinantly express and purify various eukaryotic DGK constructs in bacteria, *Dictyostelium discoideum*, insect cells, and mammalian cells. In order to use enzymatic activity to study DGK structure and enzymology, I developed methods to preserve DGK activity during storage and experimental manipulation. In order to gain insight into structural requirements for DGK's enzymology, as well as to optimize methods for experimental manipulation, I studied the effects of activators and inhibitors as well as substrate specificity. In order to probe intermolecular structural interactions of eukaryotic DGKs, I used bimolecular fluorescence complementation (BiFC). In addition to studying genetic truncations of eukaryotic DGKs, I also used proteolysis to generate such truncations, in case the entire protein sequence was required for proper folding. I also used a photoaffinity labeling approach in order to map the diacylglycerol binding site on the surface of eukaryotic DGKs. This work should guide future studies not only of the structure of eukaryotic DGKs, but also of other interfacial enzymes, and other protein-lipid interactions.

Chapter 2: General Methods

Introduction

The methods described in this chapter are general methods used throughout the different projects described in each of the dissertation chapters. Methods specific to each chapter will be described in that chapter.

Measuring Protein Concentration

I measured protein concentration using the Bio-Rad Protein Assay (Bio-Rad 500-0006), which works by the principle that the absorbance of Coomassie® Brilliant Blue G-250 dye in an acidic solution at 595 nm (A595) increases upon binding protein[58], and the protein concentration in a sample can thus be measured colorimetrically. I blanked with buffer, and used known concentrations of bovine serum albumin (BSA) as a standard to calibrate the A595 reading as a function of protein concentration. For the protein sample whose concentration I was measuring, I diluted it if necessary to interpolate into a good linear fit of the BSA, including zero.

Sodium Dodecyl Sulfate Polyacrylamide Gel Electrophoresis (SDS-PAGE)

SDS-PAGE is a method to separate macromolecules, such as proteins, by their size. Because SDS, an anionic detergent, coats most proteins in a constant ratio of 1.4 g SDS per g protein[59], the relative migration in SDS-PAGE is a linear function of the logarithm of molecular weight for most proteins[60], so the relative migration compared to molecular weight standards can be used to measure the molecular weights of proteins in a sample. After electrophoresis, the migration pattern of the proteins can be detected either

by nonspecific staining, such as by Coomassie dyes[61] or silver staining[62], or immunoblotting can be used to detect the migration pattern of specific proteins.

In general, I first prepared a protein sample by diluting it into SDS-gel loading buffer (for a final concentration of 28.125 mM tris(hydroxymethyl)aminomethane (Tris), pH 6.8, 11.25% (v/v) glycerol (for helping the sample sink to the bottom of the well, by increasing its density), 0.9% (w/v) SDS, 0.01125% (w/v) bromophenol blue (for visually tracking the sample as it is loaded and electrophoreses), 2.5% (v/v) β-mercaptoethanol (BME)), adapted from Bio-Rad's "A Guide to Polyacrylamide Gel Electrophoresis and Detection") and heating at ~95°C for several minutes to ensure that the proteins were fully denatured and coated with SDS. When loading an equivalent volume (to compare, for example, the amount of protein in a lysate to the amount of protein in a subsequent preparation, which may have been resuspended in a different volume), I calculated the equivalent volume according to Equation 1.

$$L_b = L_a * \left(\frac{R_b}{R_a}\right)$$

Equation 1. I calculated the equivalent volume (L_b) of sample **b** to load based on the volume loaded of sample **a** (L_a), the volume in which sample **a** was originally resuspended (R_a), and the volume in which sample **b** was resuspended (R_b). For example, if the cell pellet were resuspended in 1 mL lysis buffer to produce 1 mL of lysate, and if after removing the supernatant I extracted the pellet with 0.2 mL of extraction buffer to produce 0.2 mL of extracted protein, and if I loaded 1 µL of lysate, the equivalent volumes of supernatant and extracted protein would be 1 µL and 0.2 µL, respectively.

I then loaded the samples into PAGs I had cast myself. For the separating phase of the gel, which resolves the samples by molecular weight, the percentage of acrylamide varied, and the rest of the gel was made of 375 mM Tris, pH 8.8, 0.1% (w/v) SDS, 0.1% (w/v) ammonium persulfate (APS), and 0.04% (v/v) *N,N,N',N'*-tetramethylethylenediamine (TEMED) (except for 8% acrylamide gels, in which case TEMED was increased to 0.06%, and 6% acrylamide gels, in which case TEMED was

increased to .08%). The stacking phase of the gel, which sweeps the proteins from the well into a tight band due to the differential mobility of anions at the lower pH[63], was made of 250 mM Tris, pH 6.8, 0.1% (w/v) SDS, 0.1% (w/v) APS, and 0.01% (v/v) TEMED. I used the gels within one week so that the buffers between the stacking and separating phases had not mixed by diffusion[64]. I electrophoresed in electrophoresis buffer (30.3 g per L Tris base, 144.0 g glycine, and 10.0 g SDS) (also from Bio-Rad's "A Guide to Polyacrylamide Gel Electrophoresis and Detection") in a Mini-PROTEAN® apparatus (Bio-Rad) between 30 and 200 V until the dye front left the gel.

Coomassie is an anionic dye that, as SDS does, binds nonspecifically to proteins, and as such has the advantage that the intensity of Coomassie staining can be used to estimate protein abundance. Coomassie staining is thus a useful tool for assessing the purity of a protein sample, if the protein is sufficiently abundant, as in bacterial overexpression of recombinant protein. If a gel's destiny was Coomassie staining, after electrophoresis I destained the gel in ultrapure (Type I) water for several minutes, gently shaking at room temperature, in order to remove the SDS, which can interfere with the protein-Coomassie interaction. Then I incubated the gel overnight, gently shaking at room temperature, in either ProtoBlue Safe (National Diagnostics EC-722) (combined in a 9:1::ProtoBlue Safe:ethanol ratio, as recommended by the manufacturer) (which, in my experience, was a more sensitive dye) or Bio-Safe Coomassie Stain (Bio-Rad 161-0786) (which, in my experience, was a less sensitive dye). In order to reduce background staining, I destained the gel by gently shaking in ultrapure water for several hours, with a wadded up Kimwipe™ (Kimberly-Clark® TW31KWPCS) in the corner, and usually changed Kimwipes™ once or twice over the course of the destaining. I sandwiched the

destained gel between two clear plastic sheet protectors (Office Depot® #498811) and scanned an image of it at 300 dots per inch (dpi).

Silver staining is another method to visualize proteins following SDS-PAGE. It can be treacherous for estimating protein concentration, not only because the degree of staining depends not only on the chemical composition of the protein[65] but also because the degree of staining depends nonlinearly on the concentration of protein present. Silver ions complexed to protein is less reactive than free ions, which is why the silver needs to be washed briefly from the gel in order to get positive and not negative staining of protein bands, which means not only that the degree of staining is very sensitive to the degree of washing after staining, but also that more concentrated protein can stain less intensely than less concentrated protein[66]. On the other hand, silver staining can be up to thirty times more sensitive than Coomassie staining, so it can be a useful technique for observing the electrophoretic migration of protein purified from a mammalian expression system, where the protein's concentration is below the threshold of detection of Coomassie staining. Because of the high sensitivity of silver staining, I was careful to use clean containers and ultrapure water, to keep keratins (from human skin, and thus dust) or other abundant proteins from the environment from contaminating the gel. I stained gels using the SilverQuest™ Silver Staining Kit (Life Technologies™ LC6070) following the manufacturer's protocol with the following modifications: I reduced the sensitizing step from ten minutes to seven minutes, and I added a brief wash with ultrapure water between the post-sensitization 30% ethanol ten-minute wash step and the ten-minute ultrapure water wash step. I also made sure during these water wash steps to vigorously shake the dish, if necessary, so that by the end of the ten-minute water wash

the solvent had sufficiently exchanged in the gel such that the gel was submerged and no longer floated on top of the water. After staining, as above, I sandwiched the destained gel between two clear plastic sheet protectors and scanned at 300 dpi.

A technique that can be even more sensitive than silver staining is immunoblotting, which, unlike Coomassie or silver staining, detects specific epitopes (particular surfaces of a particular protein). Immunoblotting thus can be useful for detecting the migration patterns of proteins of very low concentration, such as protein purified from a mammalian expression system. It can also be very useful to detect whether a specific protein is present in a complex mixture, even at low relative concentrations compared to the other proteins, and even when other proteins of similar size are present, such as detecting whether a recombinant protein is successfully expressing in a lysate. I transferred protein from the gel to a nitrocellulose membrane that had been presoaked in transfer buffer (30.3 g per L Tris base, 14.4 g per L glycine, 10% (v/v) methanol, pH 8.3), or else a polyvinylidene (PVDF) membrane, which I first briefly soaked in methanol before soaking in transfer buffer, in a GENIE® Electrophoretic Transfer apparatus (Idea Scientific 4017) at 12 V for ninety minutes or so.

I used two general methods for detecting the proteins on the membrane. One method was chemiluminescent. For these membranes, if I wanted to visualize all the protein nonspecifically (to, for example, estimate how much of the total protein my protein of interest is, or check whether a bubble obstructed the transfer), I rinsed the membrane with ultrapure water, briefly stained with the dye Ponceau S (which binds proteins reversibly, and does not seem to be deleterious to later immunoblotting), then

briefly washed the membrane with water. In order to reduce nonspecific interaction of the primary antibody with the membrane and other proteins on the membrane, I first blocked the membrane with 3% (w/v) BSA in TBS/T (8 g per L NaCl, 0.2 g per L KCl, 3 g per L Tris base, 0.1% (v/v) Tween-20, adapted from Sambrook, Fritsch, and Maniatis's *Molecular Cloning: A Laboratory Manual*[67]), gently shaking either at room temperature for an hour, or as long as overnight (or longer) at 4°C. After blocking, I incubated the membrane in either blocking buffer or TBS/T along with a primary antibody raised against the epitope of interest, gently shaking for four hours, or as long as overnight (or longer) at 4°C. The primary antibody dilution also included sodium azide as a preservative: I eventually learned that I produced the best results, however, when I always used a fresh primary antibody dilution, so the preservative was unnecessary. After incubation with the primary antibody, I rinsed the membrane by vigorously shaking in TBS/T, then incubated in the appropriate secondary antibody, raised against the species of the primary antibody, which was also conjugated to horseradish peroxidase (HRP). After incubation with the primary antibody, I rinsed the membrane by vigorously shaking in TBS/T, and then incubated briefly in a chemiluminescent substrate for the HRP (either SuperSignal West Pico Chemiluminescent Substrate (Thermo Scientific), or else Immobilon Western Chemiluminescent HRP Substrate (EMD Millipore)). The HRP used the chemiluminescent substrate to produce photons emanating from the region of the gel to which the secondary antibody had bound (which, in turn, indicated where the primary antibody bound, which, in turn, indicated where the epitope of interest had migrated), so I therefore sandwiched the membrane between plastic binder sheets and exposed it to film. For each membrane, I tried multiple exposure times to optimize

visualization of the immunoblot signal. If I was going to perform densitometry on a film, I chose exposures faint enough that I could read text through the bands of interest. Most films I scanned at 300 dpi, but films selected for densitometry I scanned as 1200 dpi .tiff files. I measured the densitometry of these scans with ImageJ[68] (v1.46r) without calibration, three times from the same film. The relative densitometry of each lane was normalized to the total densitometry of all the lanes on that replicate.

Alternatively, I used the Odyssey® Infrared Imaging System (LI-COR®) to detect the proteins on immunoblots. Those membranes I did not Ponceau S stain, because the dye gives high background in the infrared. I was careful to keep these membranes in containers that were never used for Coomassie staining, because Coomassie likewise gives high background in the infrared. I blocked these membranes with Odyssey Blocking Buffer (LI-COR®) and washed the membranes with phosphate-buffered saline (PBS) (Cellgro® 21-040-CV). I used secondary antibodies conjugated to infrared fluorophores (such as IRDye® 680LT goat anti-mouse IgG (LI-COR® 926-68020) or IRDye® 800CW goat anti-rabbit IgG (LI-COR® 926-32211)) in Odyssey Blocking Buffer with 0.2% (v/v) Tween-20 and 0.01% (w/v) SDS. I scanned the membranes using the Odyssey® Infrared Imaging System running Odyssey® v3.0 (LI-COR®), with a resolution of 169 μm, quality of medium, offset of 0.0, and intensity of 5.

Sometimes it was necessary to strip primary antibodies off the blot and reprobe with another primary antibody or a fresher aliquot of the same antibody. For PVDF membranes, I incubated the membrane in 5 mL of fivefold diluted NewBlot™ PVDF Stripping Buffer (LI-COR® 928-40032) for twenty minutes, shaking at ~80 rotations per minute (rpm) at room temperature. For nitrocellulose membranes, I used NewBlot™

Nitro Stripping Buffer (LI-COR® 928-40030). I generally redeveloped stripped membranes (and, when I remembered, reprobed with secondary antibody) to ensure the stripping worked, and, if necessary, stripped again and reassessed again until most of signal was gone.

Protein Precipitation

Because SDS precipitates with guanidine and with potassium, I removed any guanidine and/or potassium from guanidine or potassium-containing samples by ethanol-precipitation. I added 225 µL cold ethanol to 25 µL of protein sample, vortexed to mix, and stored at -20°C for ten minutes to keep cold. If I were precipitating a protein in order to increase its concentration, I increased the volumes for this initial step proportionately. For very dilute samples, I sometimes added a carrier protein such as BSA to nucleate precipitation. To pellet the precipitated proteins, I microfuged at maximum speed at 4°C for five minutes. I then washed the pellet by resuspending in 250 µL cold 90% (v/v) ethanol, vortexing to mix, and microfuging at maximum speed at 4°C for five minutes. I then resuspended the pellet in 25 µL SDS gel-loading-buffer, vortexed to mix, and heated to 95°C to fully solubilize the pellet.

Alternatively, I used trichloroacetic acid (TCA) to precipitate protein. I prepared the TCA by dissolving 5 g in 2.5 mL of ultrapure water. I added 100 µL TCA solution to 400 µL protein sample, and incubated at 4°C for five minutes. I microfuged at maximum speed for five minutes to pellet the protein, and discarded the supernatant. I washed the pellet twice by resuspending it in 200 µL acetone, once again pelleting the protein by microfuging at maximum speed for five minutes and discarding the supernatant. I

evaporated any remaining acetone by placing the tube on a 95°C heating block, and resuspended the pelleted protein in 1 mL Bio-Rad Protein Assay buffer.

Diacylglycerol Kinase (DGK) Activity Assays

Radiometric Endpoint DGK Assay

I used a radiometric endpoint assay for determining the specific activity of DGK. The general principle was to incubate DGK in the presence of [γ-^{32}P]-adenosine-5'-triphosphate (ATP), then isolate the lipids and measure the [γ-^{32}P]-phosphatidic acid (PA) produced.

I incorporated the lipid substrate into either detergent micelles[69] or liposomes (lipid bilayer spheroids 100 nm in diameter, also called large unilamellar vesicles (LUVs)). I measured out the lipid required into a borosilicate glass tube using a steel-and-glass syringe, dried the lipid into a film under nitrogen gas, and stored the lipid film under vacuum for at least one hour prior to hydration. For micelles, I used either octyl-β-glucoside (OG) or else Triton X-100 (TX-100). In order to calculate the amount of detergent to add, I added enough such that the mol% plus all the lipids would be 100%, plus the critical micelle concentration (CMC), which is the concentration of monomer that must be in solution before the detergent will aggregate into micelles. I added the appropriate volume of buffer and detergent, and alternately bath-sonicated and vigorously vortexed the solution until the micelles were completely clear. Aqueous dilutions of dithiothreitol (DTT), a reducing agent with limited stability in solution, were stored in small aliquots at -20°C, and thawed aliquots were discarded and not refrozen.

In order to prepare liposomes, I hydrated the lipid film in the appropriate buffer at a temperature higher than the highest phase transition temperature (T_m) of the included lipids for at least thirty minutes, bath-sonicating for thirty seconds every ten minutes, and vortexing if necessary, until the lipids appeared uniformly resuspended. For all buffers, I generally adjusted the pH at the same temperature at which I planned to later use them. I then extruded the lipids at least nine times (but always an odd number of times, so that the final liposomes ended up on the opposite site from where they started) through a polycarbonate membrane with a pore size of 100 nm (Avanti® Polar Lipids, Inc. 610005) using a Mini-Extruder set (Avanti® Polar Lipids, Inc. 610023) on a heating block at a temperature likewise higher than the highest T_m, until the resuspended lipids appeared translucent. I always checked the membrane after extruding to make sure that it had not ruptured or slipped during extrusion or assembly of the Mini-Extruder.

When making liposomes, I experienced a perhaps one in four or five chance that the liposomes would be inexplicably bad (either they were exceedingly difficult to extrude, or looked terrible, or the assayed DGK activity would be extremely low, and when I went back to look at the liposomes I had made, the lipids had fallen out of solution and sunk to the bottom of the tube, even though they had looked fine when I had made them). Sometimes I would be able to attribute a cause to the bad liposomes (one vial of dioleoylglycerol (DOG) produced bad liposomes, for example, or a miscalculation of lipid would lead to a lipid composition not amenable to extrusion), but most often, the bad liposomes still occasionally occurred despite my best efforts to prevent them (treating the tubes with Sigmacote® (Sigma-Aldrich® SL2), visually comparing different sets of liposomes after extrusion to make sure they appeared the same (if they were supposed to

be the same concentration), being patient and not using too much force to extrude, buying a new Mini-Extruder and cleaning it only with water and dilute detergent and no organic solvents, etc.). To this day I am unsure of all of the variables that contribute to good extrusion, and as such, any single assay must be regarded cautiously, especially when comparing different sets of liposomes.

After incubating in various reaction conditions, temperatures and times (noted in each figure legend), I quenched the reaction by adding to the 50-100 μL reaction volume in a 13x100 mm borosilicate glass test tube 1 mL of 1 M NaCl (aqueous), 2 mL of methanol, and 1 mL of chloroform, and gently vortexing to mix. I took care to set the vortexer to the on position, and not the touch position, to ensure that the vortexer was on a low enough setting to not spatter radioactive fluid. In this proportion the solvents formed a single phase.

I then extracted the lipids by adding another 1 mL each of chloroform and 1 M NaCl, and vortexing again to mix. In this proportion, the solvents formed two distinct phases. To improve phase separation, I briefly centrifuged the samples at room temperature before removing the aqueous (top) phase by aspiration. I washed the lipids by adding 2 more mL 1 M NaCl and vortexing, and separated the phases by centrifuging again. I removed the lipids to a clean tube using a 9" borosilicate glass Pasteur pipet, and evaporated the solvent by placing the tube under a stream of nitrogen gas on a heating block, leaving a film of lipid, and some salt, on the bottom of the tube.

I could not merely count the radioactivity at this point, because although most of the unreacted [γ-^{32}P]-ATP should have been removed by the aqueous washes, not necessarily all of it had. I therefore separated the lipids from the other chemical

components of the film by resuspending the film in 30 μL 95:5::chloroform:methanol and spotting onto either aluminum (EMD Millipore 5582-7) or glass (Analtech 31911) thin layer chromatography (TLC) plates. TLC works by the principle that different solvents have different affinities for the matrix on the plate: as the solvent rises up the plate by capillary action, the solvents will separate based on their relative affinity. Likewise, any molecules dissolved in the solvent (such as lipids spotted onto the plate) have different affinities for the different solvents and for the matrix on the plate, and will therefore migrate at different rates, thus separating the chemicals. Even when scoring a 2 mm buffer region between each lane on the aluminum plates, I always achieved better resolution between lanes using glass plates with channels between the lanes than I did with aluminum plates, so I later learned to use only glass plates. Initially I would spot in the presence of hot air from a hair dryer, but this included the risk of the radioactive lipid spattering into another lane or even off the plate altogether. In later experiments, I therefore streaked the lipid in a region between 0.2 mm below the top of the preadsorbent zone and 0.5 mm above the bottom of the plate: this was a large enough area that the 30 μL easily evaporated in the time it took to streak it and did not leak outside this region. To separate PA from the other lipids (including other radiolabeled lipids, as might be observed when assaying a sample that might contain other lipid kinase activities, such as a whole lysate), I developed the TLC plate in a solvent system consisting of 50:20:15:10:5::chloroform:acetone:methanol:acetic acid:water, no more than two weeks old. When making the TLC solvent, I was careful to add the acetic acid after adding the water. Aluminum plates I ran about ninety minutes, and glass plates I ran about sixty minutes, or until the solvent front was within a few centimeters of the top of the plate.

I used autoradiography in order to visualize the location of the radioactive spots on the plate. After allowing the plate to dry briefly (at least ten minutes, but sometimes as long as overnight) I would expose the plate to film. ^{32}P decays to ^{32}S via β decay: the emitted electron interacts with the film so that when the film is developed the region adjacent to the radioactive material appears as a dark spot. I found that if I did not let the plate dry too long, some of the silica would come off on the film, which could be helpful for aligning the film to the plate later. I wrapped the plate and film together either in aluminum foil or else in a black plastic bag to protect the film from light, then stored overnight or longer at -20°C. After developing the film, I aligned the film and the plate, annotated the film to record how the spots aligned to the plate, and marked on the plate the region corresponding to the radioactive spots. In this solvent system, PA usually migrates at a relative front (R_f) of ~0.85. For aluminum plates, I cut the region of the plate with the radioactive spot and placed that region of the lane in a scintillation vial with 4 mL scintillation fluid, taking care to capture as much of the silica as possible in the vial. For glass plates, I scraped the silica from the region of interest onto a piece of clean aluminum foil, and then transferred the radioactive silica from the aluminum foil to a scintillation vial with 4 mL scintillation fluid, likewise taking care to capture as much of the silica as possible in the vial. When there were enough lanes on the plate, I would include empty lanes as blanks; otherwise, I used scintillation fluid as blanks. While cutting and scraping plates, I wore a surgical mask (Secure-Gard AT7509) to reduce the amount of radioactive dust I inhaled. In later experiments, I also measured out [γ-^{32}P]-ATP directly into scintillation fluid to calibrate the scintillation counter.

I measured the decays per minute (dpm) using a liquid scintillation counter (Wallac 1410). I subtracted the average of the blank vials' counts from each of the samples' counts. Initially, I counted on the swipes setting and summed the ^{32}P and ^{35}S channels and used that number as the counts. In later experiments, I counted on the ^{32}P setting, but also counted a known volume of [γ-^{32}P]-ATP. I measured the ratio of the counted activity of the [γ-^{32}P]-ATP sample to its predicted activity assuming 2.2×10^9 dpm per mCi, and divided the counts of the experimental samples by that ratio in order to calibrate the scintillation counter. In this case, I propagated the uncertainty from the scintillation counter calibration into the final measurement of DGK activity. Assuming a 1:1 ratio of ATP to PA in the reaction, using the counts, the total concentration of ATP, and the specific activity of the [γ-^{32}P]-ATP in the reaction, I could calculate the nmol PA produced. From the amount of DGK used and the time of the reaction, assuming that the reaction was linear with time, I could calculate the specific activity of DGK in nmol PA per minute per μg DGK.

For all experiments using radioactivity, I performed the experiment in a region of the laboratory approved for radioactivity, wore a laboratory coat, gloves, and radiation badge, and, when possible, worked behind a shield. When working with liquid radioactivity, I wore a second pair of gloves (one size larger) over the first pair. Before leaving the radioactivity room, I checked my person, including the soles of my shoes, for radioactivity by Geiger counter. I removed any detectable radioactive contamination by washing with Radiacwash™ and water. I disposed solid radioactive waste (double-bagged in especially thick plastic bags to prevent puncture by broken glass) in the short

half-life drum down the hall, liquid radioactive waste by calling Radiation Safety for pickup, and scintillation vials in the scintillation vial drum down the hall.

1,2-Diacylglycerol (DAG) Isomerization to 1,3-DAG

1,2-DAG, the lipid substrate of DGK, will spontaneously isomerize to 1,3-DAG, so in general I would try to proceed quickly after liposome extrusion to the rest of the assay, and always used DAG-containing liposomes on the same day I made them. When I measured a timecourse of DAG isomerization under the conditions they face as liposomes, I did observe a time-dependent increase in the signal of 1,3-DAG as a proportion of 1,2-DAG (Figure 1), although this observation was largely a result of a decrease in the 1,2-DAG signal rather than an increase of the 1,3-DAG signal. A decrease in signal might be a result of oxidation of the unsaturated bonds in the fatty acid moieties, and thus decreased affinity for the iodine vapor used to visualize the spots[70]. Even after 48 hours, only about a quarter of the 1,2-DAG had isomerized to 1,3-DAG, and at the timescales relevant to the DGK assay, less than a fifth had.

A

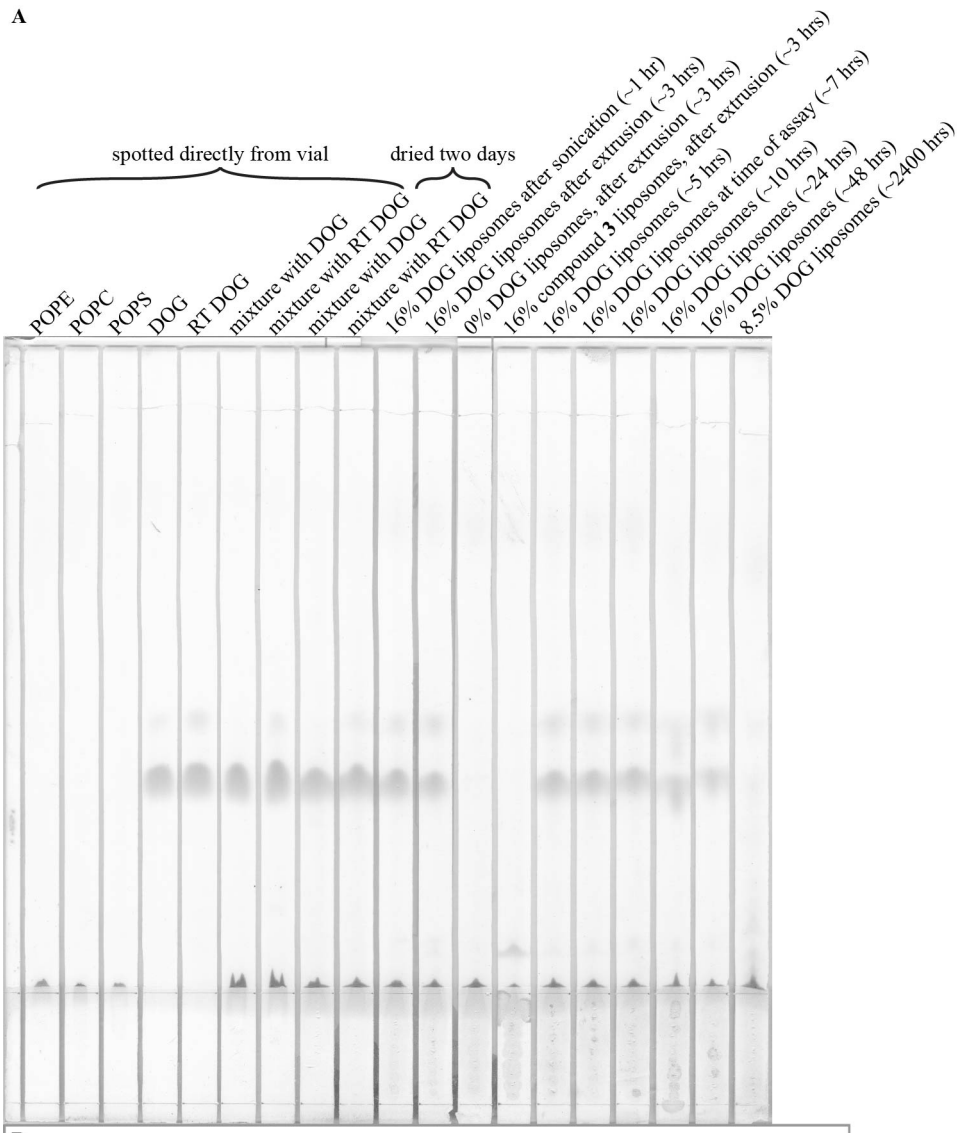
spotted directly from vial
dried two days
POPE
POPC
POPS
DOG
RT DOG
mixture with DOG
mixture with RT DOG
mixture with DOG
mixture with RT DOG
16% DOG liposomes after sonication (~1 hr)
16% DOG liposomes after extrusion (~3 hrs)
0% DOG liposomes, after extrusion (~3 hrs)
16% compound 3 liposomes, after extrusion (~3 hrs)
16% DOG liposomes (~5 hrs)
16% DOG liposomes at time of assay (~7 hrs)
16% DOG liposomes (~10 hrs)
16% DOG liposomes (~24 hrs)
16% DOG liposomes (~48 hrs)
8.5% DOG liposomes (~2400 hrs)

B

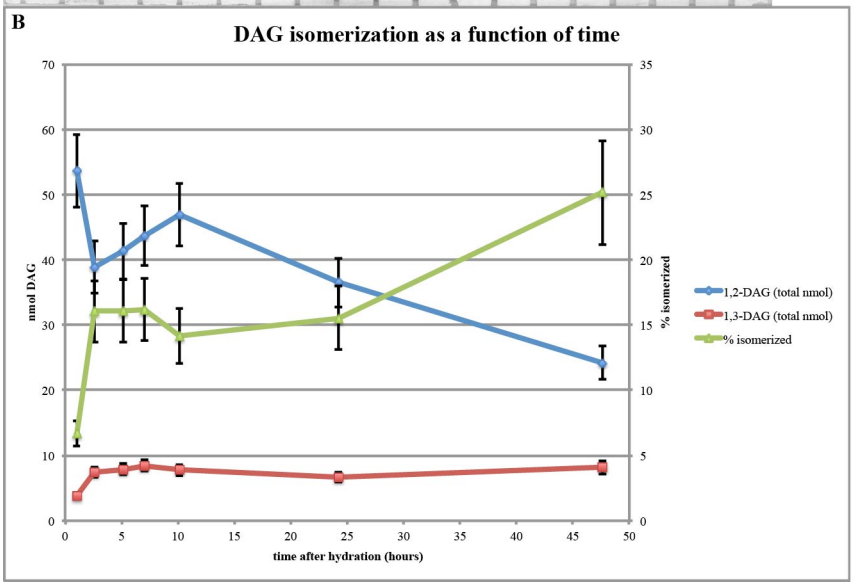
DAG isomerization as a function of time
nmol DAG
% isomerized
time after hydration (hours)
1,2-DAG (total nmol)
1,3-DAG (total nmol)
% isomerized

Figure 1. Timecourse of DAG isomerization. I made 15.1 mM liposomes (42.7:21.3:20:16::1-palmitoyl-2-oleoyl-sn-glycero-3-phosphoethanolamine(POPE):1-palmitoyl-2-oleoyl-sn-glycero-3-phosphocholine(POPC):1-palmitoyl-2-oleoyl-sn-glycero-3-phospho-L-serine(POPS):1-2-dioleoyl-sn-glycerol(DOG)). I took aliquots over time, extracted the lipids, and stored the dried lipids as a film until all had been collected. **(A)** TLC plate of spotted lipids. I resuspended the lipid films and spotted a volume of liposomes such that 64 nmol DOG would be spotted. I also spotted standards of an equivalent amount directly from the lipid standard vials, either separately or together ("mixture"), either directly from the vial onto the plate, or else dried as a film for two days. "RT DOG" signifies a vial of DOG (in chloroform) stored at room temperature rather than at -20°C. The 8.5% DOG liposomes had been made previously, and the 0% DOG and 16% compound 3 liposomes were liposomes extruded at the same time, to compare recovery. I ran the plates in fresh 85:15:5::toluene:chloroform:methanol, a solvent system predicted to separate 1,2- from 1,3-diacylglycerol[71]. After briefly allowing to dry, I visualized the spots on the plate by incubating in a tank with iodine crystals, which produce iodine vapor, which stains isolated double bonds[70], such as in the oleoyl fatty acid chains. The predominant spot corresponds to 1,2-diacylglycerol; the fainter, upper spot corresponds to 1,3-diacylglycerol. I sandwiched the plate between two clear plastic sheets and scanned as a 600 dpi greyscale .tiff file. **(B)** Quantification of the signal from (A). I performed densitometry on the spots using ImageJ, as described in the **"Sodium Dodecyl Sulfate Polyacrylamide Gel Electrophoresis (SDS-PAGE)"** subchapter of the "General Methods" subchapter. In triplicate, mean ± standard deviation (SD).

Extracting Lipids with 1 M NaCl vs. 1% $HClO_4$

Published protocols for DGK assays commonly extract the lipids after quenching the reaction by washing with acid[72,29,73], whereas our laboratory washes with 1 M NaCl. I therefore tested whether this salt wash was contributing to uncertainty in my assay results by quenching and extracting either with 1 M NaCl, as usual, or else with 1% $HClO_4$. The method of extraction did not appear to affect the total recovered activity, in either micelles or liposomes and, if anything, quenching and extracting with 1% $HClO_4$ produced more uncertainty than 1 M NaCl, not less (Figure 2). I therefore concluded that the 1 M NaCl extraction step was fine in the radiometric endpoint DGK assay, and continued to use 1 M NaCl.

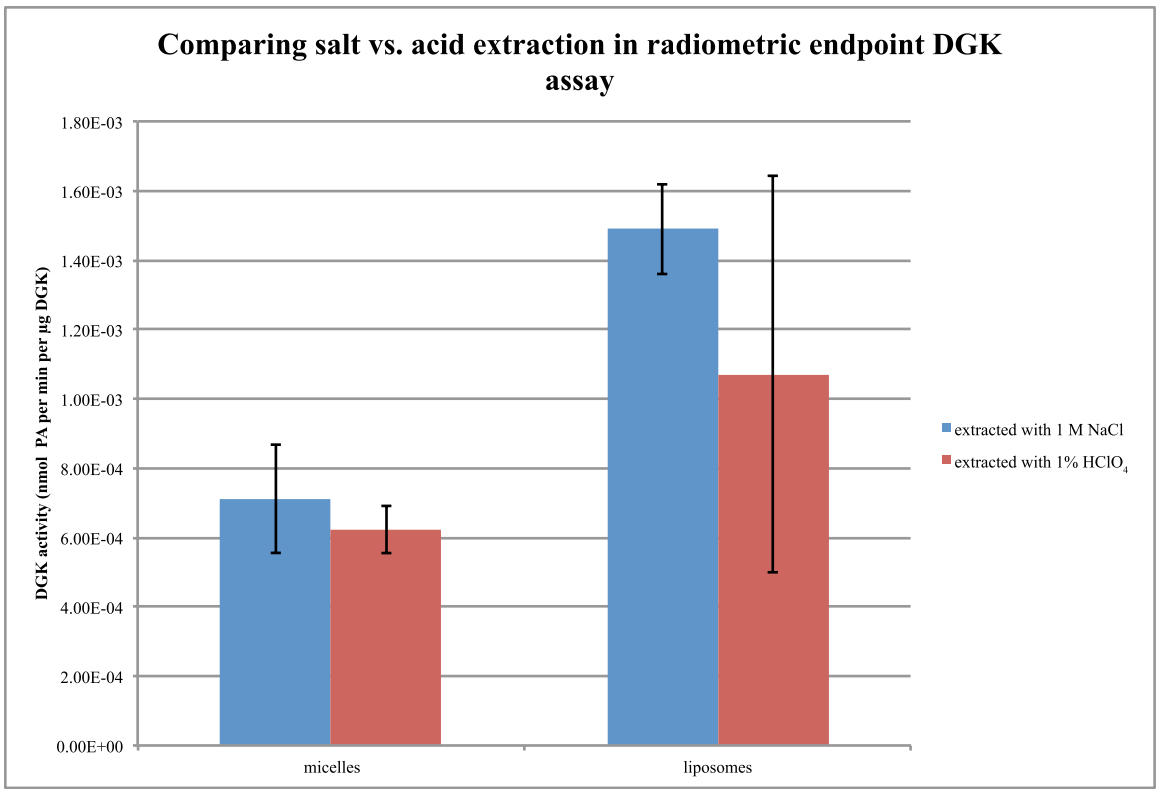

Figure 2. Comparing salt vs. acid extraction in the radiometric endpoint DGK assay. DGK activity assay. The sample assayed was the non-nuclear membrane (NNM) fraction from 293FT human embryonic kidney (HEK) cells that had been transiently transfected with Fc-FLAG-DGK-theta (shown in **Figure 84C** and **D**) at a concentration of 15.4 ng per µL. Micelles: 4.8 mM Triton X-100 (TX-100) micelles (9.4 mol% POPS, 6.3 mol% DOG). Liposomes: 7.5 mM (53:22:17:8::POPE:POPC:POPS:DOG). The assay included 49 mM 4-(2-hydroxyethyl)-1-piperazineethanesulfonic acid (HEPES), pH 7.0, 134 mM NaCl, 4.4 mM $MgCl_2$, 1 mM DTT, 1 mM ATP, 119 Ci per mmol [γ-^{32}P]-ATP, and, from the diluted NNM, 25 ng per µL total protein (as measured by the Bio-Rad Protein Assay), 1.5 mM N-acetylglucosamine (NAG) (to inhibit O-linked N-acetylglucosamine (O-GlcNAc) transferase during lysis), 154 µM NaF (to inhibit serine and threonine phosphatases), 44 µM $NaVO_4$ (to inhibit tyrosine phosphatases), 62 ng/mL quinacrine (to inhibit phospholipase), 0.02x protease inhibitor cocktail (PIC) (Roche 11873580001), 0.004% Nonidet P-40 (NP-40) (a detergent to help lyse the cell membrane), and 0.8% glycerol (to help stabilize the enzyme while frozen). The reaction proceeded for 15 minutes at 37°C. In triplicate, mean ± SD.

Developing Continuous DGK Assays

The radiometric assay has the advantage of being relatively sensitive, independent of pH or cation concentration, and specific for DGK activity. It has the disadvantage of using ^{32}P, including the associated risks in health and environmental contamination, and associated expense, but also of being an endpoint assay, and taking at least one and a half days (for the smallest assays) and as long as three days (for the larger assays). A

continuous assay could have the advantage of being able to monitor the reaction in real time, could be much faster, and could use other substrates besides DOG without having to first optimize TLC conditions. One common approach to designing a continuous assay is to couple the reaction of interest (in our case, the transfer of the γ-phosphoryl from ATP onto DAG to produce adenosine-5'-diphosphate (ADP) and PA) to another reaction that can be followed with a spectrophotometer. Therefore, one possible future direction for our laboratory would be the development of a continuous assay, to complement our radiometric endpoint assay, for the analysis of DGK activity.

One such coupled assay is the ADP Quest™ assay (DiscoveRx), which couples ADP production to a pyruvate kinase (PK) reaction, which uses ADP to produce pyruvate, which is then coupled to a pyruvate oxidase reaction, which uses the produced pyruvate to produce hydrogen peroxide, which is then coupled to a peroxidase reaction, which uses the produced hydrogen peroxide to produce resorufin, whose accumulation can be measured at 590 nm[74]. I therefore performed a preliminary investigation toward adapting the ADP Quest™ HS kit (DiscoveRx 90-0087S) as a DGK assay. I found that while the signal at 590 nm depended linearly with good fit on the concentration of ADP in the buffer provided by the ADP Quest™ HS kit, the fit was much worse in our assay buffer (Figure 3**A**). The signal at 590 nm in our buffer also drifted considerably over time, and while the linear fit of this drift had a high correlation coefficient (Figure 3**B**), the residuals to the fit over time were clearly nonuniformly distributed (Figure 3**C**), showing that the drift was not, in fact, linear. Taken together, these results show that our assay buffer is not amenable to quantitatively measuring ADP production, and thereby DGK activity, using the ADP Quest™ HS kit, even without sulfonic acid-containing

buffers such as HEPES, reducing agents such as DTT, or ADP contamination from ATP. I contacted DiscoveRx, and they could not identify any of our buffer components as problematic for their kit. Future directions for adapting ADP Quest™ as a DGK assay would require testing the individual components of our assay buffer to see which one(s) interfere with the proprietary reagents, finding alternatives for those components, and then confirming with the radiometric endpoint assay that those components do not interfere with DGK activity.

A

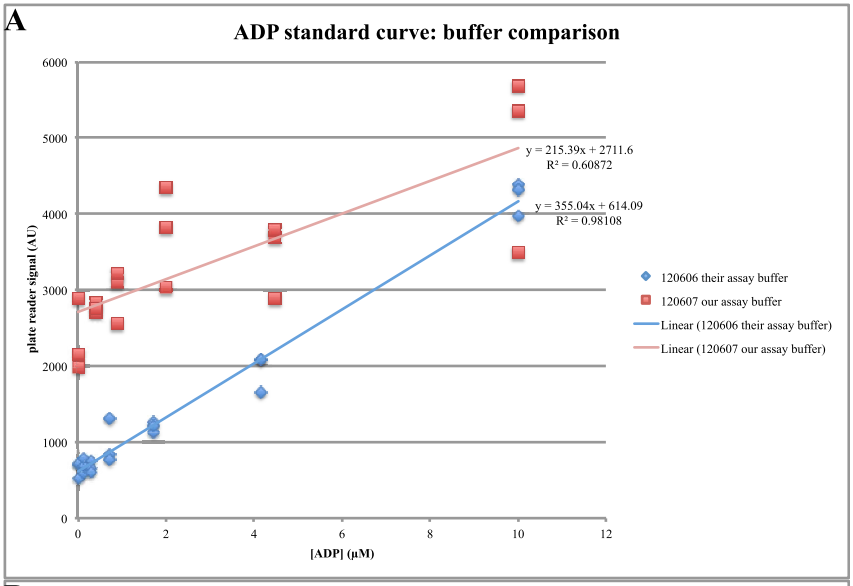
ADP standard curve: buffer comparison
plate reader signal (AU)
[ADP] (µM)
y = 215.39x + 2711.6
R² = 0.60872
y = 355.04x + 614.09
R² = 0.98108
120606 their assay buffer
120607 our assay buffer
Linear (120606 their assay buffer)
Linear (120607 our assay buffer)

B

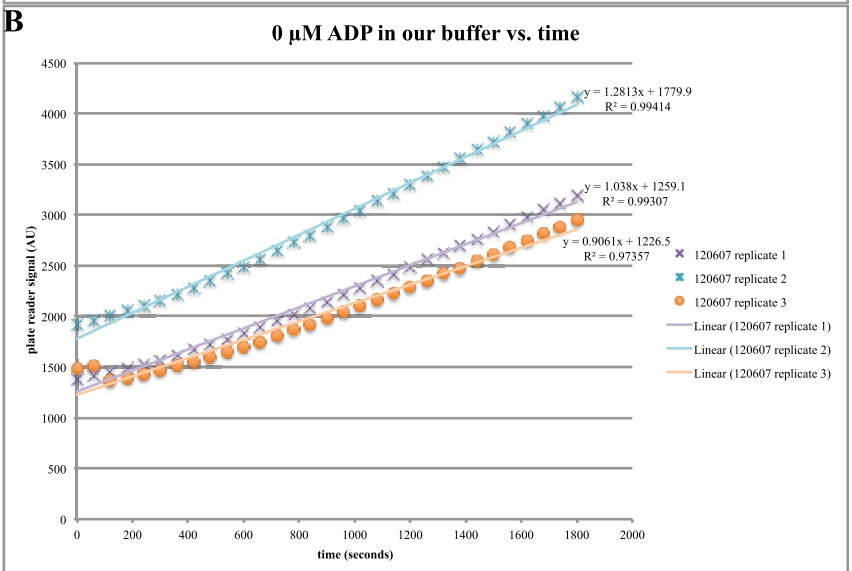
0 µM ADP in our buffer vs. time
plate reader signal (AU)
time (seconds)
y = 1.2813x + 1779.9
R² = 0.99414
y = 1.038x + 1259.1
R² = 0.99307
y = 0.9061x + 1226.5
R² = 0.97357
120607 replicate 1
120607 replicate 2
120607 replicate 3
Linear (120607 replicate 1)
Linear (120607 replicate 2)
Linear (120607 replicate 3)

C

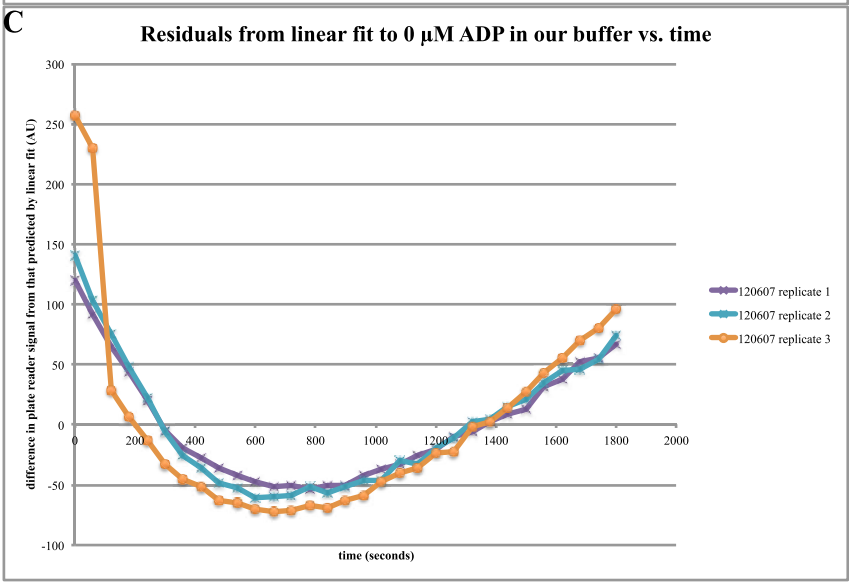
Residuals from linear fit to 0 µM ADP in our buffer vs. time
difference in plate reader signal from that predicted by linear fit (AU)
time (seconds)
120607 replicate 1
120607 replicate 2
120607 replicate 3

Figure 3. The ADP Quest™ HS kit is not compatible with our assay buffer. I combined 15 µL of either their assay buffer (the assay buffer included with the kit) or our assay buffer (final concentration of 50 mM triethanolamine (TEA), pH 7.5, 100 mM NaCl, 1 mM liposomes (48:24:20:8::POPE:POPC:POPS:DOG), 0.6% (v/v) glycerol, 0.1 mg per mL ovalbumin, 0.005% (v/v) NP-40) with 5 µL of different ADP standards in a black 384-well plate (freshly cleaned with ultrapure water, methanol, and compressed air), then added 10 µL Reagent A and 20 µL Reagent B. I read on the plate reader at 37°C with preheating, with an excitation filter at 530 nm and an emission filter at 590 nm, reading every sixty seconds for thirty minutes, scaled to an empty well for auto sensitivity, reading from the top of the plate, for a plate type of Nunc 384 flat bottom size 16x24, with a top probe vertical offset of 1 mm, and shaking one second before each reading. I performed the experiments with their buffer on one day (120606), but there was a problem with the samples using our buffer on that day, so I repeated the experiment with our buffer the next day (120607): because of limited reagents, I was unable to repeat the experiment with their buffer that day. **(A)** The signal at 590 nm as a function of ADP concentration, 15 minutes into the experiment. I used Microsoft® Excel® to calculate the linear regression. AU, arbitrary units. **(B)** The signal at 590 nm as a function of time, of the three replicates of our buffer, with 0 µM ADP. **(C)** The residuals from the previous figure (I subtracted the measured signal from that predicted by the linear fit) as a function of time.

Kinase reactions are commonly coupled to PK, which uses the produced ADP to produce pyruvate, and then coupled to lactate dehydrogenase (LDH), which uses the produced pyruvate to oxidize nicotinamide adenine dinucleotide (NADH) to NAD^+, which can be monitored spectrophotometrically[75]. In preliminary investigations to determine whether such a LK/PDH coupled assay could be adapted for assaying DGK activity, I measured the sensitivity of our spectrophotometer using a clear plastic (but not advertised as optically clear) 384-well plate measuring the absorbance at 340 nm of various concentrations of NADH. The absorbance at 340 nm depended linearly on the concentration of NADH with an excellent fit under the conditions tested, and from the sensitivity measured, I calculated that in order to observe a change in 0.01 absorbance units over thirty minutes, 1 ng of DGK in the assay would need a specific activity of at least 6.9 nmol per minute per µg DGK (Figure 4). This assay would therefore not be nearly as sensitive as the radiometric assay but its greater speed and safety and consequent lower expense could make it useful for concentrated samples of high activity. The next step to adapting the PK/LDH assay as a DGK assay would be, as above with the ADP Quest™ assay, to determine whether NADH can be quantitatively measured in the

context of the DGK assay buffer, and if not, to then determine which component(s) interfere with the assay, find alternatives for those components, and confirm that the alternatives do not interfere with DGK activity as measured by the radiometric endpoint assay.

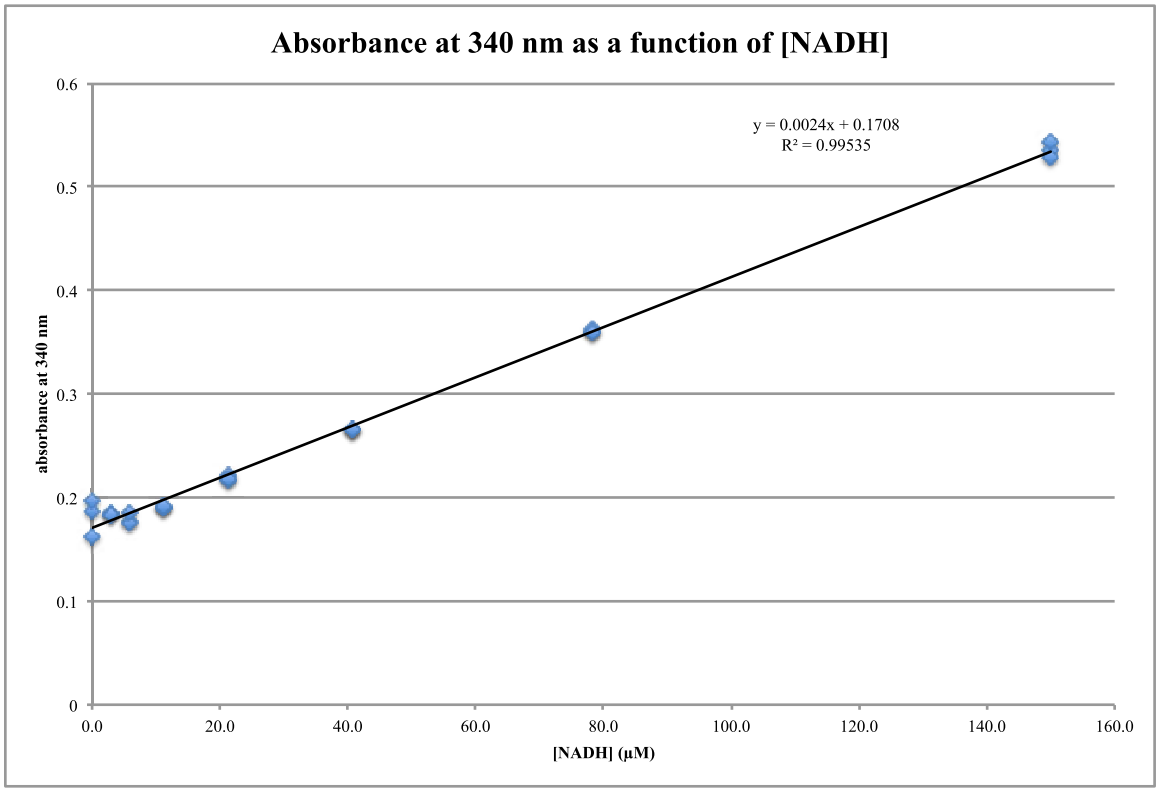

Figure 4. Absorbance at 340 nm of varying concentrations of NADH (Sigma-Aldrich® N8129-50MG) in 50 mM HEPES, pH 7.5 in a volume of 100 µL in a 384-well clear plastic plate. I used Microsoft® Excel® to calculate the linear regression.

Although coupled continuous assays could have considerable advantages over the radiometric assay, they are also limited to reaction conditions such that the activities of the downstream enzymes are not rate-limiting. As such, the pH or cationic dependence of DGK could not be measured with a coupled assay. Still, for high-activity, high-purity samples, such continuous assays could be useful enough, due to their reduced expense and increased speed and safety, to be worth developing for DGK.

Calculating Relative Centrifugal Fields (Rcfs)

Centrifugation is a commonly used method to separate materials in a mixture based on their density. In order to calculate the relative centrifugal field (Rcf) reported in a figure legend in this dissertation, I used the table found in the manual for the rotor in question to convert the rotor speed (in rpm) to the Rcf at the average radius (r_{av}). When using a rotor speed not explicitly tabulated, I used Equation 2 to interpolate between the tabulated Rcfs.

$$Rcf = \left(\frac{\left(\frac{Rcf_1}{{v_1}^2}\right) + \left(\frac{Rcf_2}{{v_2}^2}\right)}{2} \right) * v^2$$

Equation 2. I calculated the *Rcf* for a given rotor speed *v* as a function of the *Rcf*s corresponding to the rotor speeds in the table above and below v. For example, to calculate the *Rcf* for 31,000 rpm, I looked up the *Rcf*s for 30,000 rpm and 35,000 rpm, and interpolated according to **Equation 2**.

Charring TLC Plates

In order to visualize spots on TLC plates, I used two methods. As previously mentioned, iodine crystals produce iodine vapor, which stains isolated double bonds[70]. In order to visualize other molecules that may not have such isolated double bonds, I sprayed the plate with 40% (v/v) sulfuric acid in water using a TLC sprayer kit (Analtech 40-01), then incubated the plate in a 120°C oven until the lipids appeared as brown spots. Once charred, I allowed the plate to cool in a fume hood before placing into plastic binder sheets and scanning at 300 dpi. While charring plates, I wore personal protective equipment including a laboratory coat, gloves, safety goggles, and a half facepiece drop down respirator (3M 6000DD) with organic vapor / acid gas cartridge P100 filters (3M 60923).

DNA Electrophoresis

To separate DNA by size, I used agarose gel electrophoresis. I generally used 1%-1.5% (w/v) agarose in TAE buffer. I microwaved to melt the agarose, and when the agarose was uniformly melted, I added ethidium bromide, a fluorescent molecule that stains DNA by intercalating between base pairs, to 7 μg per 100 mL. Because ethidium bromide intercalates into DNA, it is also a potent mutagen, and must be handled carefully. While the gel was still liquid, I poured the gel into a cast and let the gel cool at room temperature to solidify. If I did not plan to use the gel right away, I stored the gel wrapped in cellophane and moistened with TAE buffer at 4°C.

I generally electrophoresed DNA gels in TAE buffer at 100 V until the dye front had run one-third to halfway down the gel. Sometimes it was necessary to run the gel at a lower voltage (if I couldn't supervise the gel because I was at a seminar, for example), or for longer times (if I needed to resolved a difference in size between two similarly-sized molecules, for example). I visualized the location of DNA in the gel by setting the gel on a UV box, and photographed the gel using an AlphaImager® HP System (proteinsimple)™.

Chapter 3: Expressing and Purifying DGKs

Introduction

In order to begin structural studies of eukaryotic DGKs, I needed to produce some DGK to study. In order to be confident that the phenomena I observed were due to DGK and not other components of the cells, I needed to purify the DGK from the other cellular components. X-ray crystallography, a common method for studying protein structure, in particular requires highly concentrated and purified protein. I therefore set out to recombinantly express and purify various eukaryotic DGK constructs in bacteria, *Dictyostelium discoideum*, insect cells, and mammalian cells.

Expression and Purification Methods

Bacterial Expression Methods

To produce and maintain deoxyribonucleic acid (DNA), I transformed expression plasmids into One Shot® TOP10 Chemically Competent *Escherichia coli* (Life Technologies™), a strain especially engineered for high-efficiency plasmid propagation, including features such as the *endA1* mutation, which inactivates periplasmic DNA-specific endonuclease, which reduces nonspecific digestion and therefore enhances DNA stability during transformation[76], and the *recA1* mutation in the master regulator of recombination[77], which inhibits the homologous recombination system and therefore reduces nonspecific recombination in cloned DNA. I transformed the bacteria by incubating 2 μL of purified DNA with 20 μL just-thawed bacteria on ice in a BD Falcon™ round-bottom culture tube for thirty minutes before heat-shocking by incubating the tube in a 42°C water bath for 45 seconds and then plunging back into ice.

The incubation on ice allows time for the plasmid to interact with the outside of the cell membrane, and the heat shock causes a rapid change in the fluidity of the membrane, which allows the plasmid to cross the membrane at zones of adhesion (sites where the inner and outer membrane have fused through the cell wall layer)[78]. I then added 200 μL of S.O.C. medium (2% tryptone, 0.5% yeast extract, 10 mM NaCl, 2.5 mM KCl, 10 mM $MgCl_2$, 10 mM $MgSO_4$, 20 mM glucose) to the tube and shook at 225 rpm for one hour at 37°C to allow the antibiotic resistance gene to express the gene product, so that when I plated the reaction on Bacto™ agar (BD 214010) (1.5% (w/v)) with the appropriate antibiotic, the bacteria with the transformed plasmid were able to survive. The antibiotics I used included kanamycin (Kan) (30 μg/mL) for pT71myc and pET28-HisMBP-FLAGpp, chloramphenicol (Cam) (35 μg/mL) for the chaperones, and carbenicillin (Carb) (100 μg/mL) for pGEX-4T2 and pET32a. Carb selects against the ampicillin resistance gene, but is less labile to β-lactamase than ampicillin[79]. I incubated these plates overnight at 37°C until distinct colonies formed: if necessary, I restreaked the plates until the colonies were well-isolated.

For long-term storage of bacterial strains, I made glycerol stocks from these plates. I picked an individual colony and grew overnight in 4 mL Luria Broth (LB) with the appropriate antibiotic, shaking at 225 rpm overnight at 37°C. The following morning, I combined 700 μL of the fresh culture with 300 μL autoclaved (and therefore sterile) 50% glycerol in a sterile cryogenic vial. I stored the cells at cold temperatures so that the metabolism and structure of the cells would change little, if at all, over the course of years. Freezing damages cells both by dehydration and the consequent increase of concentration of certain electrolytes, because ice crystals outside cells exert osmotic

pressure on the water inside cells, as well as by physical disruption from ice crystals[80]. Glycerol acts as a cryoprotectant by acting as a solute during dehydration and thus preventing the increase in electrolyte concentration and has the added benefits of not being toxic to the cells even at high concentrations, having high solubility in water over a variety of temperatures, and being able to permeate the cells[81]. I flash-froze the glycerol stock by incubating the cryogenic tube in a methanol / dry ice (solid CO_2) bath. Rapid freezing can prevent the formation of ice crystals, which also damage cells: instead the water forms a glassy solid. I took care that the tubes were labeled with alcohol-resistant ink, such that the labels remained legible. I then stored the frozen tubes at -80°C. When starting colonies from the glycerol stock, I did not allow the stock to thaw, but rather scraped at the frozen culture with a freshly flamed (and therefore sterile) steel loop and either streaked onto a plate to produce well-isolated colonies, or else directly inoculated an LB (plus antibiotic) liquid culture.

To express protein, instead of the TOP10 strain of *E. coli*, I used the BL21(DE3) or Rosetta™(DE3) (Novagen®) strains of *E. coli*. BL21(DE3) is deficient in the *lon* and *ompT* proteases[82] and is therefore especially well-suited for recombinant protein expression. Rosetta™(DE3) also includes a chloramphenicol-resistant plasmid that encodes the transfer ribonucleic acids (tRNAs) for the AGG, AGA, AUA, CUA, CCC, and GGA codons, which are commonly used in eukaryotes but rarely used in bacteria[83]. In order to transform plasmids into BL21(DE3), I first made the cells competent for transformation by pelleting the cells from a 4 mL overnight culture, then resuspending in 25 mL cold, 0.22 μM filtered 100 mM $CaCl_2$, and incubating on ice for two hours. I harvested the cells by pelleting and resuspended again in 5 mL cold, 0.22 μM filtered 100

mM $CaCl_2$. I made glycerol stocks from these competent cells and then transformed in the same way as I did with the One Shot® TOP10 cells.

To express protein, I generally inoculated LB medium (along with the appropriate antibiotic) either from a single colony from a freshly grown plate, or else from a glycerol stock, and then shook the culture at 225 rpm overnight at 37°C. The following morning, I inoculated a larger culture with the starter culture, and shook it at 37°C until the absorbance (optical density) at 600 nm (OD600) reached 0.3-1, at which point I added isopropyl-β-D-thiogalactopyranoside (IPTG) to 0.1-1 mM to induce expression of the plasmid. IPTG is a non-hydrolyzable analog of lactose, and, like lactose, binds to the lac repressor and allosterically releases it from the lac operator[84]. By relieving inhibition, IPTG induces expression of genes regulated by the lac operon, such as in some recombinant plasmids. I periodically measured the OD600 of samples of the culture, and used Equation 3 to predict when the OD600 would reach the desired value. I did not include IPTG for uninduced controls. I then shook the cultures either at 37°C for three hours, or at 16°C overnight (12-22 hours).

$$A_t = A_0(2^{kt})$$

Equation 3. A_t is the absorbance at 600 nm at time t; A_0 is the absorbance at time zero; and k is the growth rate. By measuring the absorbance at multiple timepoints, I could estimate k and predict approximately when the absorbance would reach a given value.

To harvest the expressed protein, the following morning I pelleted the cells by centrifugation (15 minutes at ~300-20,000 x *g* at 4°C). I resuspended the cell pellets in lysis buffer, generally 4 mL per gram cell pellet. When time allowed, I froze the resuspended cell pellet at -80°C, and then rethawed to ensure complete lysis. I added egg white lysozyme to 1 mg per mL. Lysozyme catalyzes the hydrolysis of 1,4-β-linkages in

peptidoglycan, a key component of the bacterial cell wall, and thereby damages the cell wall, and this effect at least partially contributes to cell wall lysis (although its muramidase activity is actually not required to kill bacteria[85], so lysozyme may also have additional, as of yet undescribed mechanisms for cell killing, possibly including activation of the CpxA-CpxR two-component system, which then leads to membrane depolarization and oxidative stress[86]). I incubated the resuspended cell pellet on ice for thirty minutes, vortexing occasionally to mix. I then lysed the resuspended cell pellet by probe sonication in at least ten ten-second bursts, resting on ice between each burst, until no longer viscous. I removed the insoluble fraction by centrifuging at 40,000-120,000 x *g* for 65-90 minutes at 4°C.

Dictyostelium Discoideum *Expression Methods*

FLAG-DGKA-overexpressing *Dictyostelium discoideum* cells were stored either at -80°C. I maintained *D. discoideum* cells as adherent cultures on tissue culture plates at room temperature in a plastic, Tupperware®-style container covered with aluminum foil. Any time I lifted the lid of the plate (to thaw down, feed, or split the cells), I did so in a tissue culture hood. I grew the cells in enriched Dicty medium (43 mL FM Defined Minimal Media (Formedium™ FMM0101), 500 mL 1.5x HL5 with Glucose (MP Biomedicals, LLC #3090-322), 15 µg per mL G418 (a drug to select for FLAG-DGKA-expressing cells), 20 U per mL penicillin (Pen) (an antibiotic, to prevent the growth of bacteria), 20 µg per mL streptomycin (Strep) (another antibiotic, to likewise prevent the growth of bacteria)). When the cells grew overconfluent, I split them to a new plate by using a pipet to use a stream of medium to displace the cells from the plate, and then re-

seeded the new plate a lower density, usually as a function of the density of the previous plate (e.g., 1:10).

Insect Cell Expression Methods

I maintained Sf9 *Spodoptera frugiperda* cells as adherent cultures on tissue culture plates in a 27°C incubator in Sf9 medium (500 mL Grace's 1x Supplemented Insect Medium (Gibco® (Life Technologies™) 11605), 50 mL Premium fetal bovine serum (FBS) (Atlanta Biologicals S11150), 5.6 mL 10,000 U/mL Penicillin-Streptomycin (Pen-Strep) (Gibco® 15140)). I used 10 mL medium per 10 cm plate. If the cells had not been split for three days but were not yet confluent, I replaced the medium on the plate with fresh medium.

In order to split Sf9 cells, I followed a method recommended by Saki Phommachanh of Invitrogen™. I first removed the medium by aspiration (using a sterile pipet in a tissue culture hood), then gently washed 5 mL of insect cell medium over the cells. I removed the medium (including released cells) to a 50 mL conical tube, then repeated with another 5 mL of insect medium, and continued repeating until all of the cells had appeared to have let go of the plate. I then pelleted the collected cells by centrifuging at minimum speed at room temperature for five minutes. I removed all but 5 mL of the resulting supernatant by aspiration, then gently tapped the tube to resuspend the cells. I removed the resuspended cells to a clean plate at the desired density, then supplemented medium as necessary. For example, for maintaining the cell lines, I generally used a 1:5 split, which means that I would take 1 mL (of the 5 resuspended mL) and add that to a new 10 cm dish already containing 9 mL of medium.

While splitting Sf9 cells, I generally monitored cell viability using a dye exclusion method. I added trypan blue to 1x to 20 μL of resuspended cells, and gently pipetted the mixture into the notch on a hemocytometer, such that the resuspended cells filled the chamber by capillary action. I counted the number of cells in the large square and multiplied by 10,000 to estimate the number of cells per mL. Living cells are able to exclude trypan blue; therefore only dead cells appeared blue. I calculated the viability by dividing the number of blue cells by the number of total cells.

I measured the concentration of baculovirus using a plaque-forming assay. I added 2 mL of resuspended 4.4 x 10^5 Sf9 cells per mL to each well of a six-well plate. I allowed to adhere for one hour, then replaced the medium on the wells with 1 mL of virus-containing media, in 10x serial dilutions, and allowed to infect for one hour. I then replaced the medium with 2 mL per well of warm plaquing medium (22.5 mL Grace's 2x supplemented, 1.5 mL FBS, 12.5 mL sterile ultrapure water, 12.5 mL 4% (w/v) agarose), and allowed to solidify for twenty minutes at room temperature. I then incubated the cells at room temperature in a humidified chamber (a plastic Tupperware®-style container with a wet Kimwipe™ in the corner, rehydrating the Kimwipe™ as necessary). After one week, I visualized the plaques by staining with 0.5 mL per well 0.1% (w/v) neutral red for two hours at room temperature.

I maintained High Five™ *Trichoplusia ni* ovary cells as adherent cultures on tissue culture plates in a 27°C incubator in High Five™ medium (500 mL Grace's 1x Supplemented Insect Medium, 50 mL FBS, 5.5 mL Pen-Strep). I used 10 mL medium per 10 cm plate. If the cells had not been split for three days but were not yet confluent, I replaced the medium on the plate with fresh medium.

I split High Five™ cells using a sloughing method: in a tissue culture hood, I used a sterile pipet to gently flow the medium of the plate over the cells until all the cells had released and were resuspended in the medium. I removed the resuspended cells to a clean plate at the desired density, with supplemented medium as necessary. I generally used a 1:15 split to maintain the High Five™ cells.

Mammalian Cell Expression Methods

I maintained 293FT human embryonic kidney cells, which are a fast-growing variant of 293T cells, which include SV40 large T antigen, which allows very high levels of protein to be expressed from vectors containing the SV40 origin, as adherent cultures on tissue culture plates in a 37°C incubator. I used 10 mL medium per 10 cm plate. I first grew the cells in either 293FT growth medium 1 (0.88x DMEM, high glucose (Gibco® (Life Technologies™) 11965), 25 mL FBS). However, without antibiotics, the cells were prone to bacterial infection. I therefore switched to 293FT growth medium 2 (500 mL DMEM, high glucose (Gibco® (Life Technologies™) 11965), 10% (v/v) FBS, 100 U or μg per mL Pen-Strep, 1 mM sodium pyruvate (Gibco® (Life Technologies™) 11360), 1x non-essential amino acids (Gibco® (Life Technologies™) 11140), 2 mM L-glutamine (Gibco® (Life Technologies™) 25030), 500 μg per mL G418). I maintained 293T and COS-7 *Chlorocebus aethiops* kidney cells in 293T growth medium (0.89x DMEM, high glucose, 10% (v/v) FBS, 100 U or μg per mL Pen-Strep).

If the cells had not been split for three days but were not yet confluent, I replaced the medium on the plate with fresh medium. To split the cells, I prewarmed the bottles of medium, PBS, and aliquots of 0.05% Trypsin-EDTA (Gibco® (Life Technologies™) 25300) (trypsin, a protease, disrupts cell-cell interactions and the extracellular matrix, and

EDTA chelates divalent cations, which promote cell-cell interactions: together, they help loosen the cells of the plate) in a 37°C water bath. I used a sterile pipet to remove the medium by aspiration from the plate of cells. I very gently washed the cells with PBS (being sure to pipet the PBS onto the wall of the dish, and not directly onto the cells), and removed the PBS by aspiration. I then trypsinized the cells by adding 1 mL per 10 cm plate trypsin-EDTA, gently swishing the plate such that all the cells contacted the trypsin-EDTA, then immediately removing excess trypsin-EDTA by aspiration. I incubated the (dry) plate at 37°C for ~2-3 minutes (in practice, the time it took to label the plates for the split cells and aliquot medium into them), then resuspended the cells in the desired volume of medium, and added to the appropriate density to medium already aliquoted into plates.

To express protein recombinantly in mammalian cells, I performed a transient transfection. For each 15 cm plate to transfect, I combined 20 μg of purified DNA with Opti-MEM® I Reduced Serum Medium (Gibco® (Life Technologies™) 31985) and 40 μg of polyethyleneimine (PEI) with Opti-MEM®, then added the PEI solution to the DNA solution, and incubated at room temperature for 15 minutes. I then added the mixture directly to a 15 cm plate of 293FT cells (in growth medium). I incubated the plate for four hours at 37°C, then replaced the medium with growth medium.

Alternatively, I transfected with HiFect® Reagent (Lonza VBA-1001). I preheated the HiFect® to 55°C prior to use. For each well of a 6-well plate to transfect, I combined 2 μg of purified DNA with Opti-MEM® and 3 μL HiFect® with Opti-MEM®, then added the HiFect® to the DNA solution, vortexing to mix, and incubated at room temperature for 15 minutes. I replaced the medium on the cells with prewarmed Opti-

MEM®, and added the HiFect®/DNA solution, rocking the plate gently to thoroughly mix. After several hours, I replaced the medium with growth medium.

Protein Purification: Batch Affinity Chromatography

In general, I purified proteins by using affinity chromatography. The principle of affinity chromatography is that the resin includes a component (such as nickel-nitrilotriacetic acid (Ni-NTA)) that has high affinity to part of the target protein, or to an epitope tag engineered into the protein for just such a purpose (such as a hexahistidine (His_6) tag). Incubating the protein sample with the resin and then washing the resin would thus be predicted to enrich for the target protein, as the other proteins in the sample with lower affinity for the resin would wash off. The purified protein can be removed by washing the resin with an elution buffer, which contains a component (such as imidazole) that competes with the protein for binding to the resin and therefore displaces the protein.

Because of the small scale of most of my experiments, and because I was generally the only person in the laboratory using these methods for purifying protein, I generally found it more convenient to use batch chromatography rather than pouring columns. In general, I would add the affinity resin to the sample to be purified, mix and incubate, then collect the resin by centrifugation. The supernatant from this centrifugation I designated as the "flowthrough", and it would include proteins with low affinity to the resin, as well as extra affinity-tagged protein if the binding sites on the resin had been saturated. I would then wash the resin by resuspending it with various wash buffers, mixing, and incubating, and then collect the resin by centrifugation. The supernatant from these steps I designated as "washes", and it would include proteins with

weak affinity to the resin. To remove the purified protein from the resin, I would resuspend the resin in elution buffer, and once again mix, incubate, and collect the resin by centrifugation. The supernatant from this step I designated the "eluate", and while it would be enriched for the target protein with the affinity tag, it could also include other proteins with relatively high affinity for the resin. To determine how much protein had remained bound to the resin (or, because these are batch methods, precipitated and come down in the pellet with the resin), I resuspended the remaining resin with elution buffer and also included that as a sample in the SDS-PAG or activity assay.

Because the MagneGST™ glutathione particles (Promega V8611) are magnetic, instead of centrifuging the resin as I did with Ni-NTA agarose, I rather used a MagneSphere® Technology Magnetic Separation Stand (Promega Z5343) to collect the resin.

I generally stored purified samples for DGK activity assays in small aliquots in 50% glycerol at -80°C, and other samples at -20°C, although sometimes I briefly stored samples at 4°C.

Analytical Gel Filtration

Gel filtration (also known as size exclusion) is a method used to separate molecules by their size and shape. The gel filtration particles include an interior space, accessible by pores. Molecules that are too large to fit through the pores will be excluded from the interior space, and elute in the void volume of the resin[87]. Blue dextran is a large molecule with a molecular weight of 2000 kD, and is thus commonly used to mark the void volume of a resin, especially since its elution is easily measured at 620 nm, and its progression can be easily seen by eye to make sure that molecules are moving through

the column in a uniform manner. If a molecule is small enough to fit inside the pore to access the interior space, it will interact with the particles, and it will elute more slowly from the column, in a larger elution volume. The ratio of the elution volume of a protein on a particular column to the void volume of the column depends roughly linearly on the logarithm of the molecular weight of the protein[88]. By comparing to the elution profile of molecular weight standards, therefore, the molecular weight of a protein eluting from the column can be estimated using its elution volume, and a protein of a known molecular weight can be predicted to elute at a particular volume. The elution volume of a protein will also depend on its shape and on its interaction with other molecules present in the sample (for example, a dimer of proteins would be predicted to elute at a volume corresponding to a molecular weight approximately twice that of the monomer).

I used gel filtration column to determine whether the protein I had enriched was monodisperse, i.e., whether it was eluting as a single population, at a size consistent with either its molecular weight or at the molecular weight corresponding to that of an oligomer. Large aggregations of protein would be predicted to elute at the void volume. Because I was not using the protein in any downstream applications, the column I used was small, and the technique was thus analytical gel filtration, as opposed to preparative.

Because the order of elution is key to interpreting the results of gel filtration chromatography, I could not, as I did with the affinity chromatography, use batch methods, but rather needed to find a column. Because resolution is best when the sample volume is smaller than 1% of the total volume of the column, but there is no additional benefit to sample sizes smaller than 1% of the total volume[89], and because I expected to elute in volumes of ~250 uL, I chose a 20 mL column. I first hydrated the resin in gel

filtration buffer, then poured the resin into the column, then settled the resin by connecting the column via a tube to a beaker of buffer on a platform above the column, and draining the bottom of the column into another beaker, so that the buffer flowed into the column by gravity. I made sure that I was able to see the top of the resin at the top of the column, that the surface of the resin was smooth and flat, and that there were no bubbles in the resin.

I loaded a sample by first draining the buffer to the surface of the resin. I generally removed all but the last few milliliters of buffer from the headspace with a pipet, taking great care not to disturb the surface of the resin. If I did disturb the surface, I uniformly resuspended the entire top of the resin (as much as I could conveniently reach with a pipet), and then allow it to settle before proceeding. I allowed the last few milliliters of buffer to drain by gravity. When the last of the buffer was absorbed, but before the resin started to dry and crack, I loaded the sample in a volume no more than 200 μL (1% of the volume of the column). I then immediately started the fraction collector (LKB Bromma 2212 Helirac). Once the sample had been absorbed by the resin, but before the resin started to dry and crack, I loaded another ~200 μL of buffer, which would dilute any remaining sample that had not yet been absorbed. After this buffer absorbed, I gently filled the headspace with buffer using a pipet, taking great care not to disturb the surface of the resin, and then attached the headspace via a tube to a beaker of buffer on a platform above the column, and the column eluted by gravity. In this way I minimized any spreading of the signal caused by dilution of any unabsorbed sample into the buffer later loaded onto the column.

To measure void volumes, I used a fraction collector. In order to make sure that the column was eluting into the proper fraction, I attached a tube to the bottom of the column. The volume of the tube was ~0.5 mL, which probably led to some longitudinal mixing, but the length of the tube was required by the geometry of the setup. I programmed the fraction collector to change collection tubes as a function of time. However, the fraction collector did not always shift the full distance between two tubes, and sometimes shifted before the appointed time, so I had to closely supervise the machine at all times during the elution to make sure that the eluting drops were being collected into tubes and not pouring onto the floor. To measure elution volumes, I measured the volume of each fraction using a pipettor, and transferred the fraction to an Eppendorf for later analysis. The elution volume of a fraction is thus the sum of the volumes of all the preceding fractions on that run.

I determined the elution profile for a molecule by measuring the absorbance at 620 nm or visually (for blue dextran), at 280 nm (for proteins, especially the molecular weight standards, which were at a relatively high concentration), by SDS-PAGE followed by Coomassie staining, silver staining, or immunoblotting, or by measuring the protein concentration using the Bio-Rad Protein Assay.

In order to predict in what volume a protein of a particular size would elute (for, for example, selecting which fractions to load on a gel), or in order to estimate the molecular weight corresponding to an observed peak, I first ran molecular weight standards on the column, including blue dextran (Sigma-Aldrich® D4772), whose elution volume is the void volume. Other molecular weight markers included sweet potato β-amylase (200 kD) (Sigma-Aldrich® A8781), yeast alcohol dehydrogenase (150 kD)

(Sigma-Aldrich® A8656), bovine serum albumin (66 kD) (Sigma-Aldrich® A8531), bovine erythrocyte carbonic anhydrase (29 kD) (Sigma-Aldrich® C7025), and horse heart cytochrome c (12.4 kD) (Sigma-Aldrich® C7150). I then plotted those elution volumes, represented as a ratio to the void volume of the column, as a function of the logarithm of each protein standard's molecular weight. I used Microsoft® Excel® to calculate a linear fit for this plot, according to Equation 4. I then used this linear fit to predict the elution volume of a particular molecular weight, or to predict the molecular weight of a particular elution volume.

$$\frac{V_e}{V_o} = (k * \log_{10} MW) + b$$

Equation 4. The elution volume of a protein depends linearly on the logarithm of its molecular weight. V_e is the elution volume of a protein, V_o is the void volume (the elution volume of blue dextran), k is the slope of the linear fit, MW is the molecular weight of the protein, and b is the y-intercept of the linear fit.

I later added a blocking step between calibration and loading experimental samples, in which I loaded 200 µL (~1% of the column volume) of 10 mg per mL albumin or another molecular weight standard, and then washed the column with at least as much gel filtration buffer as that standard's elution volume. This step appeared to improve detection of the target protein in the analytical gel filtration fractions shown in Figure 12 and Figure 13.

Expressing and Purifying DGK Constructs from *E. coli*

Bacterial Expression Introduction

As mentioned in the Introduction, I set out to express the catalytic domain of a eukaryotic DGK. My approach was to express either full-length or just the catalytic domain of *S. scrofa* DGK-alpha (the first to be discovered and therefore best-studied of

the eukaryotic DGKs) in *E. coli* with the purpose of producing large amounts of soluble protein for structural studies.

Expressing and Purifying Alphacat in pT71myc

Introduction

The alphacat construct consists of residues 333-733 of *Sus scrofa* DGK alpha (accession number NP_999197.1), and is so named because it includes the catalytic domain, which is annotated on the Conserved Domain Database[90] as LCB5. The missing N-terminal residues include the EF-hand motifs and C1 domains; alphacat also lacks the C-terminal cysteine (Figure 5).

Results

Alphacat was cloned into pT71myc, which adds to the N-terminus of the protein a fusion tag consisting of hexahistidine, a thrombin proteolytic site, a myc tag, and a Tobacco Etch Virus (TEV) protease site. The total mass of this protein construct (including the fusion tag) is predicted to be 49.8 kD, and the isoelectric point (pI) is 6.99.

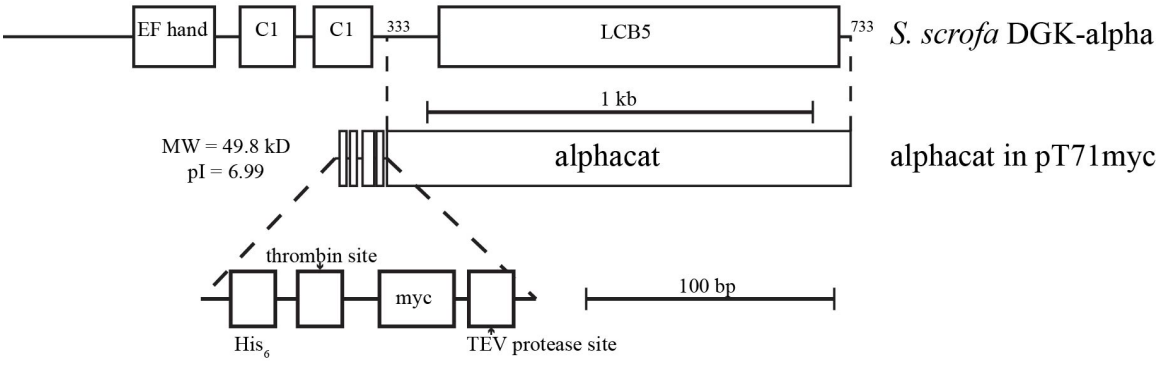

Figure 5. Schematic of alphacat in pT71myc construct. Top, a schematic of *S. scrofa* DGK-alpha. Middle, a schematic of "alphacat", which consists of residues 333-733 of DGK-alpha, including the LCB5 domain, but missing the C-terminal cysteine. Bottom, a magnification of the epitope tag region of alphacat in pT71myc. pT71myc adds to the N-terminus of the protein a fusion tag consisting of a hexahistidine, a thrombin proteolytic site, a myc tag, and a TEV protease site. The total mass of this protein construct

(including the fusion tag) and pI are predicted to be 49.8 kD and 6.99, respectively. This figure has been modified from Petro and Raben[1] and is used under CC BY-NC 2.5.

I induced the expression of alphacat in the Rosetta™(DE3) (Novagen®) strain of *E. coli* by adding IPTG. When compared to uninduced control, the induced lysate expressed an additional band, easily detectable by Coomassie staining, that migrated between the 40 kD and 50 kD molecular weight standards during SDS-PAGE, consistent with the predicted size of the fusion protein of 49.8 kD (Figure 6). This band was also recognized by an anti(α)-histidine antibody on immunoblots (Figure 6), consistent with its expressing the epitope tag. I therefore concluded that alphacat in pT71myc was expressing.

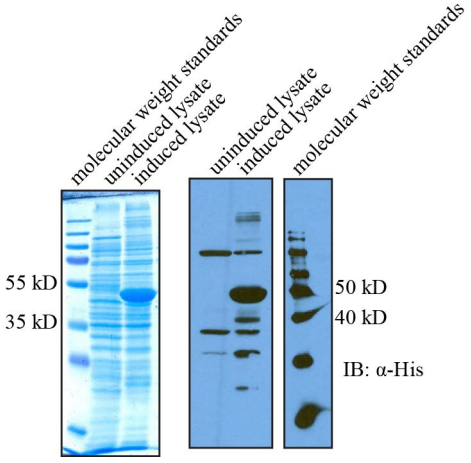

Figure 6. Alphacat in pT71myc expresses when induced by IPTG, is of the appropriate size, and is recognized by an anti-histidine antibody. SDS-PAGE of 12% acrylamide gels followed by: left, Coomassie staining; right, immunoblot against histidine (mouse α-His_6 (abcam® ab6196 (1:2500 (v/v)))). IB, immunoblot. I inoculated 25 mL cultures of LB Kan with overnight cultures of alphacat in pT71myc in Rosetta™(DE3). When the OD600 was predicted to reach 1.0, I added IPTG to 0.5 mM and shook the cultures overnight at 16°C, then pelleted the cells and resuspended in lysis buffer (50 mM Tris, pH 8.0, 300 mM NaCl, 10 mM imidazole, 1 mM $CaCl_2$, 0.5% (v/v) NP-40, 1x PIC, 25 U per µL lysozyme, 0.1% B-PER Bacterial Protein Extraction Reagent (Thermo Scientific 78243)). I loaded 24 µL per lane onto the Coomassie, and 5 µL onto the immunoblot. This figure has been modified from Petro and Raben[1] and is used under CC BY-NC 2.5.

When I assayed the DGK activity, Rosetta™(DE3) lysates that had been transformed with alphacat in pT71myc and induced with IPTG showed greater enzymatic activity than either untransformed BL21(DE3) lysates or lysates that had not been

induced with IPTG (Figure 7), suggesting not only that the construct was successfully expressing, but also that at least some of the expressed protein was catalytically competent, consistent with previous reports that expressed the catalytic domain in COS-7 cells[45].

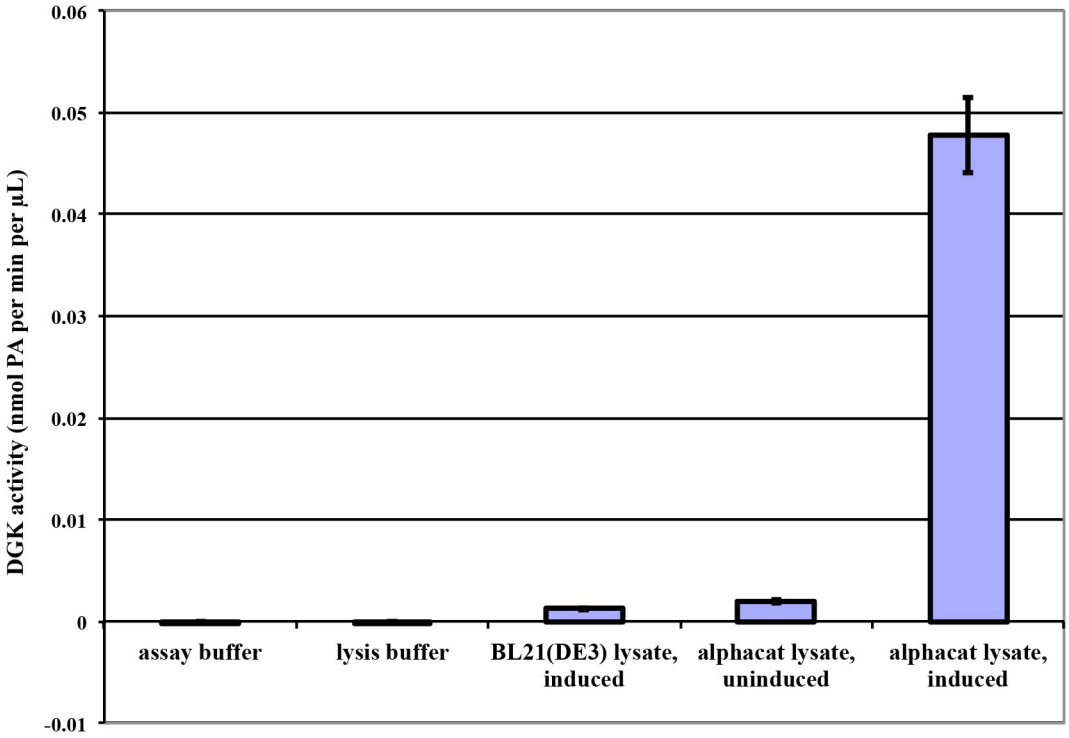

Figure 7. Lysates of Rosetta™(DE3) transformed with alphacat in pT71myc have DGK activity. I inoculated 25 mL LB Kan cultures with overnight cultures of either alphacat in pT71myc in Rosetta™(DE3) or else untransformed BL21(DE3). When the OD600 was predicted to reach 1.0, I added IPTG to 0.5 mM and shook the cultures overnight (~21 hours) at 16°C, then pelleted the cells by centrifugation and resuspended in lysis buffer (50 mM Tris, pH 8.0, 300 mM NaCl, 10 mM imidazole, 1 mM $CaCl_2$, 0.5% NP-40, 1x PIC, 1 mM DTT, 1 mg per mL lysozyme) and incubated on ice for thirty minutes. I lysed the cells by probe-sonicating six times on ice for ten seconds each, resting on ice for ten seconds between each burst. DGK activity assay, in 7.5 mM liposomes (53:22:17:8::PE:PC:PS:DOG), 48.4 mM HEPES, 4.84 mM $MgCl_2$, 0.968 mM $CaCl_2$, 2 mM DTT, 1 mM ATP, 60.5 mCi/mmol [γ-^{32}P]-ATP; 15 minutes at 30°C. I used 1 µL of lysate (or buffer) in each 50 µL reaction.

In order to determine whether alphacat was soluble, I first needed to make sure the cells actually lysed. Bath sonication for five minutes in the presence of 0.5% NP-40 was insufficient to completely lyse the cells, as evidenced by the fact that most of the

cellular proteins visible in the lysate by Coomassie were not visible in the supernatant (Figure 8**A**). Probe sonicating for six fifteen-second bursts, followed by a thirty-minute incubation at 4°C with an old aliquot of lysozyme, is likewise insufficient to lyse the cells (Figure 8**B**).

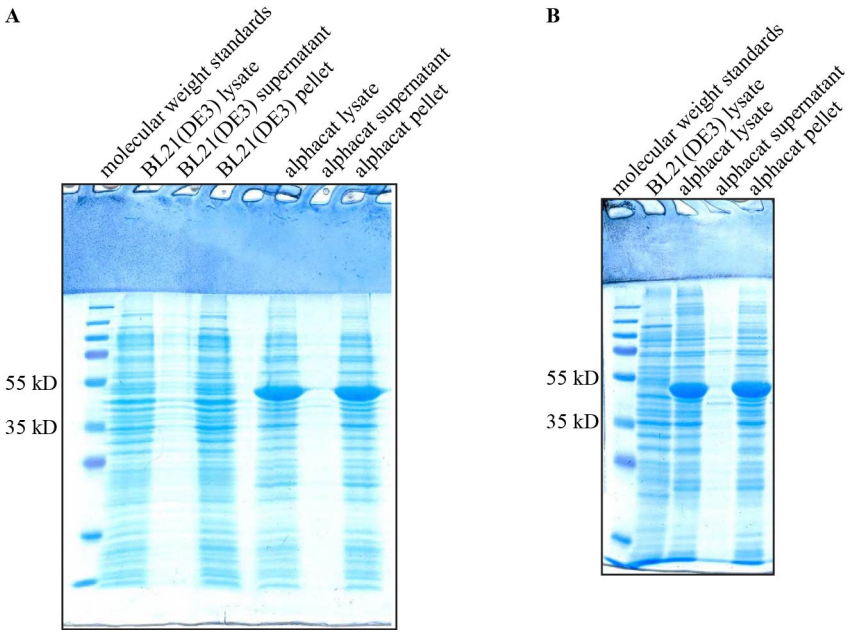

Figure 8. Bath sonication, or probe-sonication with an old aliquot of lysozyme, is inadequate to lyse BL21(DE3) cells. SDS-PAGE of 15% acrylamide gels followed by Coomassie staining. **(A)** I inoculated a 4 mL culture of LB Kan with overnight cultures of alphacat in pT71myc in Rosetta™(DE3), or a 4 mL culture of LB with overnight cultures of BL21(DE3). When the OD600 was predicted to reach 1.0, I added IPTG to 0.5 mM and shook the cultures overnight at 16°C, then pelleted the cells and resuspended in lysis buffer (55 mM Tris, pH 8.0, 5.5 mM $MgCl_2$, 1 mM $CaCl_2$, 0.5% (v/v) NP-40, 1x PIC). I bath-sonicated for five minutes, adding ice to the water to keep it cool, and separated the supernatant from the pellet by microfuging at maximum speed for ten minutes at 4°C. I loaded 10 µL per lane. **(B)** The same samples as shown in **Figure 6**. I lysed by probe-sonicating (on setting 2.5) six times for fifteen seconds each, resting on ice for fifteen seconds between each burst, and inverting to mix. I then added (old) lysozyme to 25 U per mL, and rotated for thirty minutes at 4°C. I loaded 4 µL per lane.

When I replaced the old lysozyme with fresh egg white lysozyme, six ten-second bursts from the probe sonicator were sufficient to lyse the cells (Figure 9). After lysis, however, although almost all of the Coomassie-staining cellular proteins were in the supernatant after centrifugation, the band corresponding to alphacat remained in the pellet, suggesting that it was insoluble. When washed with 2 M urea and 2% (v/v) Triton

X-100, the vast majority of alphacat remained in the pellet rather than the supernatant (Figure 9**A**), leading me to conclude that the expressed protein went into inclusion bodies[91]. Washing the pellet of insoluble protein with 4 M urea (instead of 2 M) and 2% (v/v) Triton X-100 solubilized some, but not all, of the alphacat (Figure 9**B**).

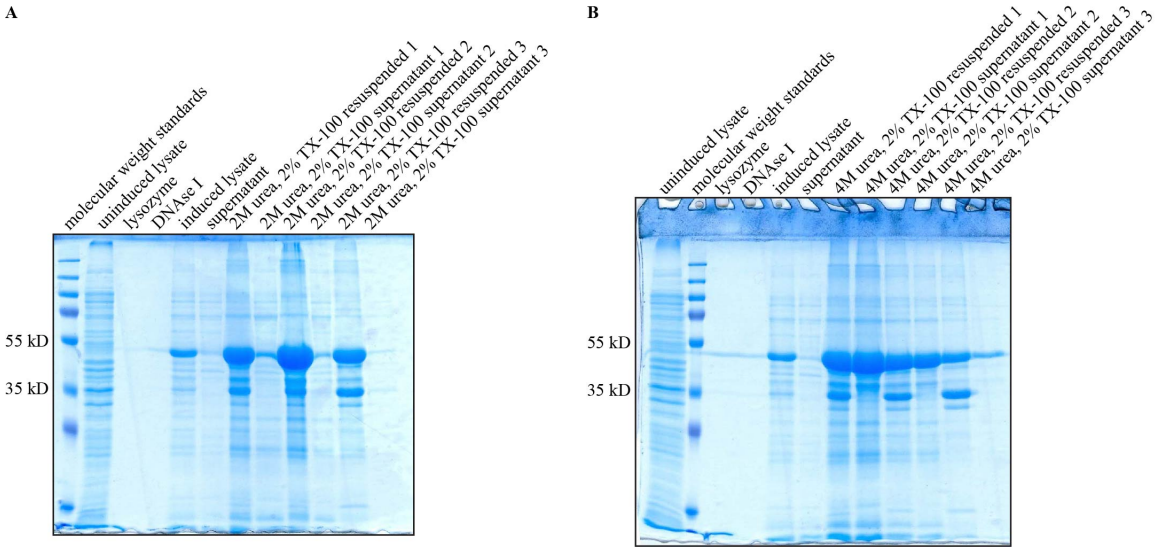

Figure 9. Alphacat in pT71myc goes into inclusion bodies. SDS-PAGE of 12% acrylamide gels followed by Coomassie staining. I inoculated 25 mL cultures of LB Kan with overnight cultures of alphacat in pT71myc in Rosetta™(DE3). When the OD600 was predicted to reach 1.0, I added IPTG to 0.5 mM and shook the cultures overnight (~21.5 hours) at 16-20°C, then pelleted the cells and resuspended in 4 mL per gram wet cell pellet lysis buffer (50 mM Tris, pH 8.0, 300 mM NaCl, 10 mM imidazole, 5 mM $MgCl_2$, 1 mM $CaCl_2$, 0.5% (v/v) NP-40, 1x PIC, 1 mM DTT, 1 mg per mL egg white lysozyme, 10 U per mL DNAse I). I incubated on ice for thirty minutes, then probe-sonicated with six ten-second bursts, resting on ice for ten seconds between each burst. I separated the supernatant from the pellet by centrifuging at 14,500 x *g* for one hour at 4°C. I washed the pellet three times either in **(A)** 2M urea wash buffer (50 mM Tris, 300 mM NaCl, 10 mM imidazole, 1 mM $CaCl_2$, 1 mM DTT, 2 M urea, 2% (v/v) Triton X-100), or **(B)** 4 M urea wash buffer (the same as 2 M urea wash buffer, but urea increased to 4 M). I loaded 0.5 µL per lane. This figure has been modified from Petro and Raben[1] and is used under CC BY-NC 2.5.

I could solubilize some, but not all, of the alphacat from inclusion bodies using guanidine hydrochloride, a chaotropic agent that unfolds proteins (Figure 10). After diluting into buffer (which, by reducing the guanidine concentration, is predicted to cause the protein to refold), I could enrich alphacat by nickel-nitrilotriacetic acid (Ni-NTA) chromatography. NTA is a tridendate molecule that, when attached to agarose beads,

chelates Ni. The His_6 tag on alphacat is also predicted to chelate Ni, and thus Ni-NTA chromatography is predicted to be able to enrich alphacat. After enrichment, some of the alphacat remained in the pellet with the resin, which could be because the alphacat-Ni-NTA interaction was too strong to be eluted with 250 mM imidazole, but was more likely because the alphacat was precipitating and coming down in the pellet as insoluble protein.

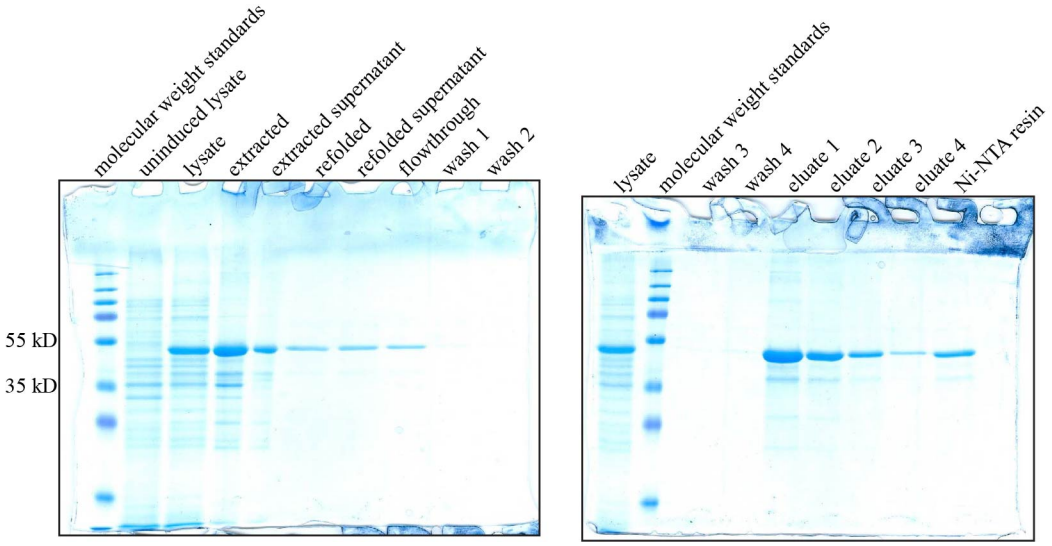

Figure 10. Alphacat can be partially solubilized from inclusion bodies, and enriched on Ni-NTA. SDS-PAGE of 12% acrylamide gels followed by Coomassie staining. These are the same samples that are shown in **Figure 9A**. I resuspended the washed pellets (that had been previously washed with 2 M urea) in extraction buffer (50 mM Tris, pH 8.0, 300 mM NaCl, 10 mM imidazole, 1 mM $CaCl_2$, 1 mM DTT, 6.7 M guanidine chloride) and sonicated until the pellet vanished and the solution appeared clear. I removed the insoluble fraction by centrifuging at 110,000 x *g* for one hour at 4°C. I then refolded the extracted supernatant by diluting 63.5-fold into loading buffer (50 mM Tris, pH 8.0, 300 mM NaCl, 10 mM imidazole, 1 mM $CaCl_2$, 1 mM DTT), and once again removed the insoluble fraction by centrifuging at 110,000 x *g* for one hour at 4°C. I added Ni-NTA agarose (QIAGEN 30210) 1:200 (v/v) and incubated for one hour, rocking at 4°C. I washed the resin with wash buffer (same as loading buffer, but DTT reduced to 0.5 mM) and eluted with elution buffer (same as loading buffer, but imidazole increased to 250 mM). I loaded 0.5 µL of the lysates and extracted samples, and 22.5 µL of the other samples.

Because monodispersity is considered a valuable quality of proteins expressed for structural studies, I subjected the affinity-purified fraction (Figure 11) to analytical gel filtration. If a protein is monodisperse, it is predicted elute as a single peak at the appropriate molecular weight: for alphacat in pT71myc, this would be at 49.8 kD

(between the 29 kD carbonic anhydrase and the 66 kD albumin molecular weight standards) if it is a monomer, at 99.6 kD (between albumin and the 150 kD alcohol dehydrogenase) if it is a dimer, etc. After analytical gel filtration on Sephadex® G-100 resin (Sigma-Aldrich®), any alphacat that eluted from the resin was undetectable by Coomassie staining (Figure 12**A**). I tried to transfer the proteins from the Coomassie-stained gel to nitrocellulose for immunoblotting, to see whether I could detect the analytical gel filtration fractions by the more sensitive method, but even though the alphacat lysate was easily detectable by Coomassie staining, apparently Coomassie-stained proteins either do not transfer well or are not detected by immunoblot, because I was unable to detect even the alphacat lysate on the immunoblot (Figure 12**B**). When I ran the gel filtration fractions on a new, fresh immunoblot, the alphacat that had eluted from the Ni-NTA resin was clearly detectable by an anti-DGK-alpha antibody (Figure 12**C**) but not an anti-His antibody (Figure 12**D**) (note that this is a different anti-His antibody than the one that detected alphacat in pT71myc lysate in Figure 6). In either blot, none of the gel filtration fractions were detectable, nor were they detectable by silver staining (Figure 12**E**). (The band that migrates between the 60 kD and 70 kD molecular weight markers is probably albumin (66 kD) that had not been completely washed off the column following calibration. Alphacat is the predominant band in the fraction that eluted from the Ni-NTA resin, which migrated between 50 and 60 kD on this gel.) I concentrated the gel filtration fractions by ethanol-precipitating the protein, and still could not detect any alphacat eluting from the column by silver stain (Figure 12**F**).

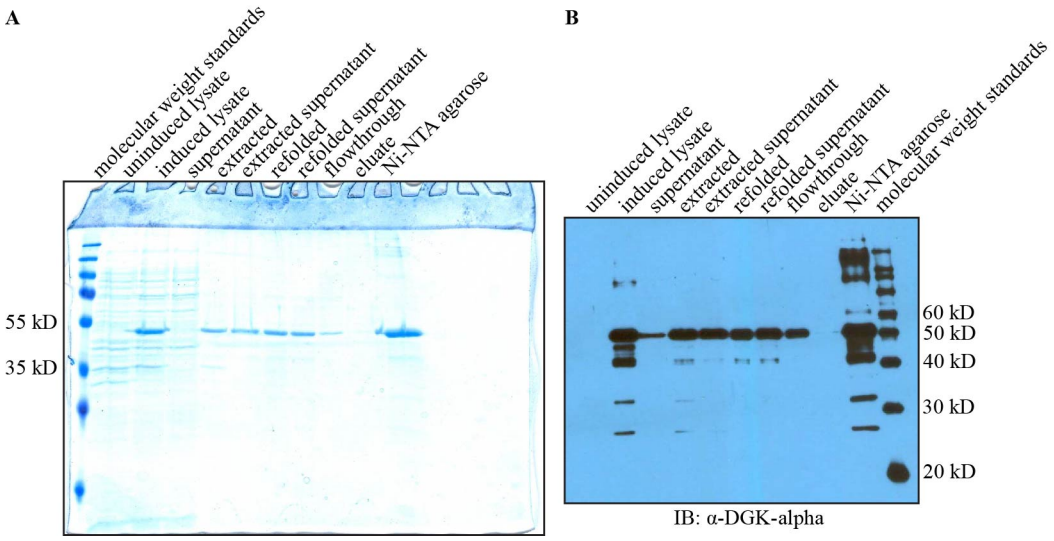

Figure 11. Expression of alphacat in pT71myc, extraction from the pellet, and purification on Ni-NTA. I inoculated 25 mL cultures of LB Kan with overnight cultures of alphacat in pT71myc in Rosetta™(DE3). When the OD600 was predicted to reach 1.0, I added IPTG to 0.5 mM and shook the cultures overnight 16°C, then pelleted the cells and resuspended in 4 mL per gram wet cell pellet lysis buffer (50 mM Tris, pH 8.0, 300 mM NaCl, 10 mM imidazole, 5 mM $MgCl_2$, 1 mM $CaCl_2$, 0.5% (v/v) NP-40, 1x PIC, 1 mM DTT, 1 mg per mL egg white lysozyme, 20 U per mL DNAse I). I incubated on ice for five hours. I separated the supernatant from the pellet by centrifuging at 22,000 x *g* for one hour at 4°C. I extracted the pellets with extraction buffer (50 mM Tris, pH 8.0, 300 mM NaCl, 10 mM imidazole, 1 mM $CaCl_2$, 0.5 mM DTT, 6.7 M guanidine chloride) and vortexed and pipetted until the pellet had mostly vanished. I removed the insoluble fraction by centrifuging at 22,000 x *g* for one hour at 4°C. I then refolded the extracted supernatant by diluting 56.6-fold into loading buffer (50 mM Tris, pH 8.0, 300 mM NaCl, 10 mM imidazole, 1 mM $CaCl_2$, 0.5 mM DTT), and removed the insoluble fraction by centrifuging at 110,000 x *g* for one hour at 4°C. I added Ni-NTA agarose 1:200 (v/v) and incubated for two hours, rocking at 4°C. I washed the resin with wash buffer (same as loading buffer, but imidazole increased to 20 mM) and eluted with elution buffer (same as loading buffer, but imidazole increased to 250 mM). **(A)** SDS-PAGE of a 12% acrylamide gel followed by Coomassie staining. I loaded 0.5 µg of each lysate and equivalent volumes (see **Equation 1**) of the other samples. **(B)** SDS-PAGE of a 12% acrylamide gel followed by immunoblotting against DGK-alpha (rabbit antibody from the Sakane lab (1:5000 (v/v))).

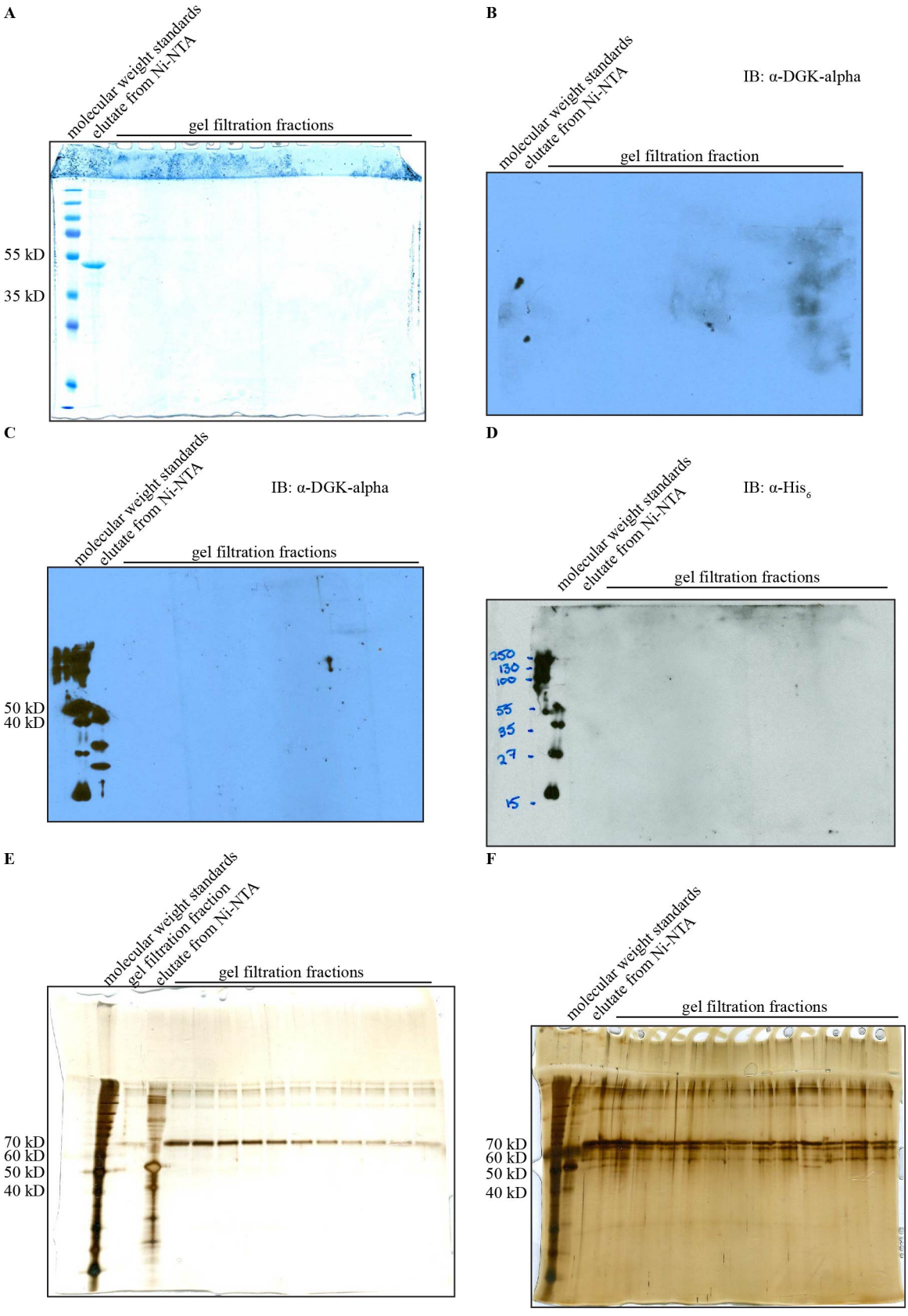
A
molecular weight standards
elutate from Ni-NTA
gel filtration fractions
55 kD
35 kD
B
molecular weight standards
elutate from Ni-NTA
IB: α-DGK-alpha
gel filtration fraction
C
molecular weight standards
elutate from Ni-NTA
IB: α-DGK-alpha
gel filtration fractions
50 kD
40 kD
D
molecular weight standards
elutate from Ni-NTA
IB: α-His6
gel filtration fractions
250
130
100
55
35
27
15
E
molecular weight standards
gel filtration fraction
elutate from Ni-NTA
gel filtration fractions
70 kD
60 kD
50 kD
40 kD
F
molecular weight standards
elutate from Ni-NTA
gel filtration fractions
70 kD
60 kD
50 kD
40 kD

Figure 12. Analytical gel filtration chromatography without first blocking the column results in undetectable gel filtration fractions. I loaded 130 μL of the elution shown in **Figure 11** onto a Sephadex® G-100 column that I had previously calibrated with blue dextran, alcohol dehydrogenase, carbonic anhydrase, and albumin, eluting by gravity in gel filtration buffer (55 mM HEPES, 55 mM $MgCl_2$, 1.1 mM $CaCl_2$, pH 8.0) and collected fractions every five minutes. **(A)** SDS-PAGE of a 12% acrylamide gel followed by Coomassie staining. I loaded 4 μL of eluate and 18 μL per lane of fractions 14-26 (corresponding to predicted molecular weights of 206 kD to 16.5 kD). **(B)** The same gel shown in (A) transferred to nitrocellulose and immunoblotted against DGK-alpha (rabbit antibody from the Sakane lab (1:5000 (v/v))). **(C)** SDS-PAGE of a 12% acrylamide gel followed by immunoblotting against DGK-alpha (rabbit antibody from the Sakane lab (1:5000 (v/v))). I tore the gel while assembling the transfer apparatus, causing the lanes to shift partway down the membrane. The labeling of the lanes coincides with bottom region of the membrane, where alphacat is predicted to migrate. **(D)** The same membrane shown in (C), immunoblotted against His_6 (Clontech Laboratories, Inc. 631212 (1:2500 (v/v))). **(E)** SDS-PAGE of a 12% acrylamide gel followed by silver staining. **(F)** SDS-PAGE of a 12% acrylamide gel followed by silver staining. I ethanol-precipitated 180 μL of each gel filtration fraction and loaded 83%, and I loaded 1 μL of eluate.

One potential reason for why I could not detect alphacat eluting from the Sephadex® G-100 column could have been that the alphacat had adsorbed to the resin and never eluted off. I therefore blocked the analytical gel filtration column with albumin and washed extensively (more than ten column volumes) with buffer. I also ultracentrifuged the alphacat eluted from Ni-NTA (from the same preparation shown in Figure 12) to remove any insoluble material immediately before loading onto the analytical gel filtration column. This time, I could clearly detect alphacat by immunoblotting in gel filtration fractions corresponding to the void volume of the column (Figure 13). In fact, the alphacat eluted a little earlier than the blue dextran: this result could be explained by compression of the Sephadex® G-100 resin in the thirty-one days that elapsed between when I ran the blue dextran and when I ran the alphacat. The calibration of the Sephadex® G-100 column gave a good linear fit (Figure 13**C**), suggesting that the analytical gel filtration column was working properly. I therefore concluded that the alphacat was aggregating, which would explain why it eluted in the void volume.

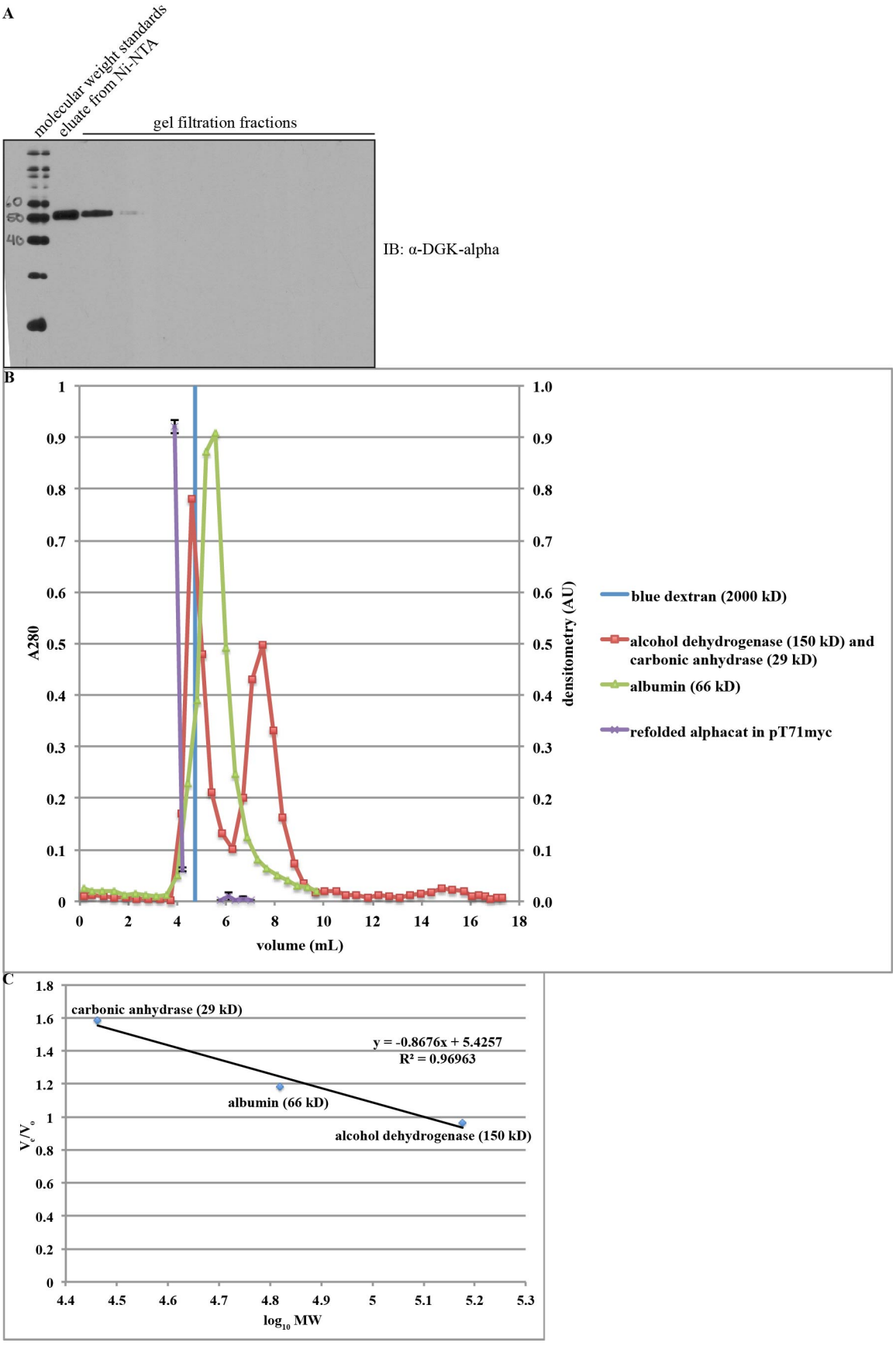
A
molecular weight standards
eluate from Ni-NTA
gel filtration fractions
IB: α-DGK-alpha
B
A280
densitometry (AU)
volume (mL)
blue dextran (2000 kD)
alcohol dehydrogenase (150 kD) and carbonic anhydrase (29 kD)
albumin (66 kD)
refolded alphacat in pT71myc
C
carbonic anhydrase (29 kD)
y = -0.8676x + 5.4257
R² = 0.96963
albumin (66 kD)
alcohol dehydrogenase (150 kD)
Ve/Vo
log10 MW

Figure 13. Previously blocking the column improves detection of alphacat eluting from a Sephadex® G-100 analytical gel filtration column, from which it elutes in the void volume. I loaded 200 μL of the same elution that I used in **Figure 12**, except that I had added glycerol to 50% and stored it for seventeen days at -80°C, onto the same Sephadex® G-100 column shown in **Figure 12**, eluting by gravity in gel filtration buffer (55 mM HEPES, 5.5 mM $MgCl_2$, 1.1 mM $CaCl_2$, pH 7.0), and collected fractions every five minutes. **(A)** SDS-PAGE of a 12% acrylamide gel followed by immunoblotting against DGK-alpha (rabbit antibody from the Sakane lab (1:5000 (v/v))). **(B)** The elution of molecular weight markers as a function of elution volume. I detected the elution of the proteins standards by measuring the absorbance at 280 nm (A280) of the gel filtration fractions. I detected the elution of the blue dextran visually: the vertical line marks the volume of the fraction that appeared the bluest. To measure the elution volume of alphacat, I performed densitometry three times on the film shown in (A). Mean ± SD. **(C)** Calibration of the Sephadex® G-100 column: elution volume (presented as a ratio of the void volume) of the molecular weight standards as a function of logarithm molecular weight. I calculated the linear regression using Microsoft® Excel®.

In case the reason that alphacat was eluting in the void was because the fraction that had eluted from Ni-NTA had been frozen and thawed before I had loaded it onto the analytical gel filtration column, and the freeze-thaw cycles were causing the protein to aggregate, I repeated the Sephadex® G-100 analytical gel filtration chromatography with alphacat I had freshly expressed and purified. This time, I could easily detect alphacat in the gel filtration fractions, but it once again eluted in the void volume (Figure 14).

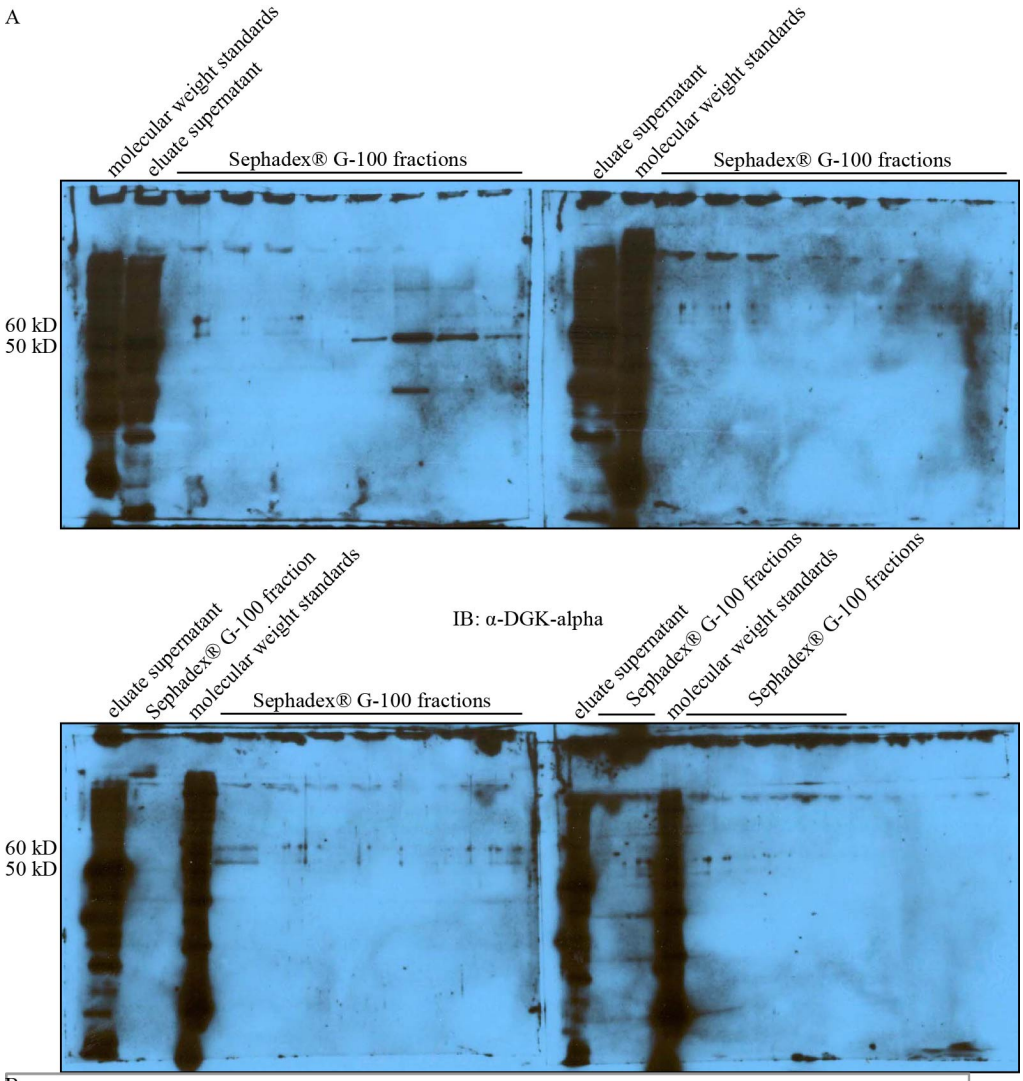
A
molecular weight standards
eluate supernatant
Sephadex® G-100 fractions
eluate supernatant
molecular weight standards
Sephadex® G-100 fractions
60 kD
50 kD
IB: α-DGK-alpha
eluate supernatant
Sephadex® G-100 fraction
molecular weight standards
Sephadex® G-100 fractions
eluate supernatant
Sephadex® G-100 fractions
molecular weight standards
Sephadex® G-100 fractions
60 kD
50 kD

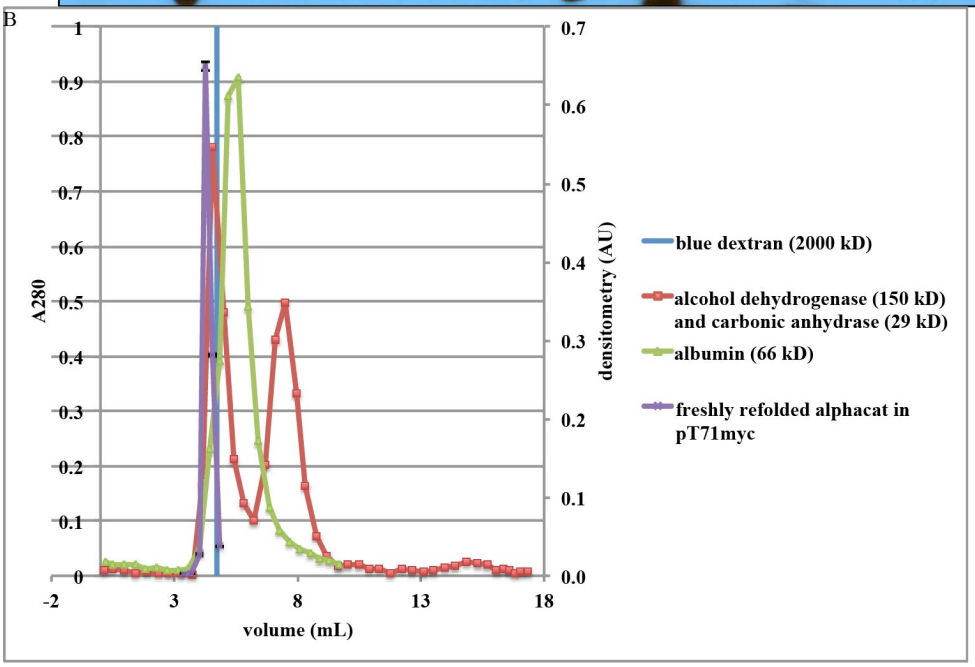
B
A280
densitometry (AU)
volume (mL)
blue dextran (2000 kD)
alcohol dehydrogenase (150 kD) and carbonic anhydrase (29 kD)
albumin (66 kD)
freshly refolded alphacat in pT71myc

Figure 14. Freshly expressed and purified alphacat in pT71myc elutes from Sephadex® G-100 in the void volume. I inoculated a 50 mL culture of LB Kan with an overnight culture of alphacat in pT71myc in Rosetta™(DE3). When the OD600 was predicted to reach 1.0, I added IPTG to 0.5 mM and shook the cultures for 21 hours at 15°C, then pelleted the cells and resuspended in 4 mL per gram wet cell pellet lysis buffer (50 mM Tris, pH 8.0, 300 mM NaCl, 10 mM imidazole, 5 mM $MgCl_2$, 1 mM $CaCl_2$, 0.5% (v/v) NP-40, 1x PIC, 1 mM DTT, 1 mg per mL egg white lysozyme). I incubated on ice for two hours. I separated the supernatant from the pellet by centrifuging at 43,000 x *g* for ninety minutes at 4°C. I extracted the pellets with extraction buffer (50 mM Tris, pH 8.0, 300 mM NaCl, 10 mM imidazole, 1 mM $CaCl_2$, 0.5 mM DTT, 6.7 M guanidine chloride) and probe-sonicated until the pellet had vanished and the solution was clear. I removed the insoluble fraction by centrifuging at 17,900 x *g* for two hours at 4°C. I then refolded the extracted supernatant by diluting fifty-fold into loading buffer (50 mM HEPES, pH 7.0, 300 mM NaCl, 10 mM imidazole, 1 mM $CaCl_2$, 0.5 mM DTT), and removed the insoluble fraction by centrifuging at 30,000 x *g* for ninety minutes at 4°C. I added Ni-NTA agarose 1:240 (v/v) and incubated for one hour, rocking at 4°C. I washed the resin with wash buffer (same as loading buffer, but imidazole increased to 20 mM) and eluted with elution buffer (same as loading buffer, but imidazole increased to 250 mM). I removed the insoluble fraction by centrifuging at 43,000 x *g* for ninety minutes at 4°C, and loaded 200 µL of the eluate's supernatant onto the same Sephadex® G-100 column shown in **Figure 12** and **Figure 13**, and collected fractions every five minutes, eluting by gravity in gel filtration buffer (50 mM HEPES, 5 mM $MgCl_2$, 1 mM $CaCl_2$, pH 7.0). **(A)** SDS-PAGE of 12% acrylamide gels followed by immunoblotting against DGK-alpha (rabbit antibody from the Sakane lab (1:5000 (v/v))). I loaded 24 µL per lane of the gel filtration fractions of elution volumes corresponding to molecular weights of 270 to 2.4 kD. **(B)** To quantify the alphacat in the gel filtration fractions, I performed densitometry, using a shorter exposure of the first membrane shown in (A), three times on the same film. Mean ± SD.

Even though the vast majority of alphacat was in the pellet after cell lysis, I also recovered a small amount in the supernatant. I wondered whether this small amount of soluble protein could be sufficiently enriched to detect its elution from an analytical gel filtration column, and whether that soluble protein would be monodisperse. I therefore purified the supernatant from alphacat-expressing Rosetta™(DE3) on Ni-NTA and found that, indeed, alphacat could be enriched from the supernatant (Figure 15**A** and **B**). When I loaded this enriched fraction onto the Sephadex® G-100 analytical gel filtration column, however, alphacat continued to elute in the void volume (Figure 15**B** and **C**).

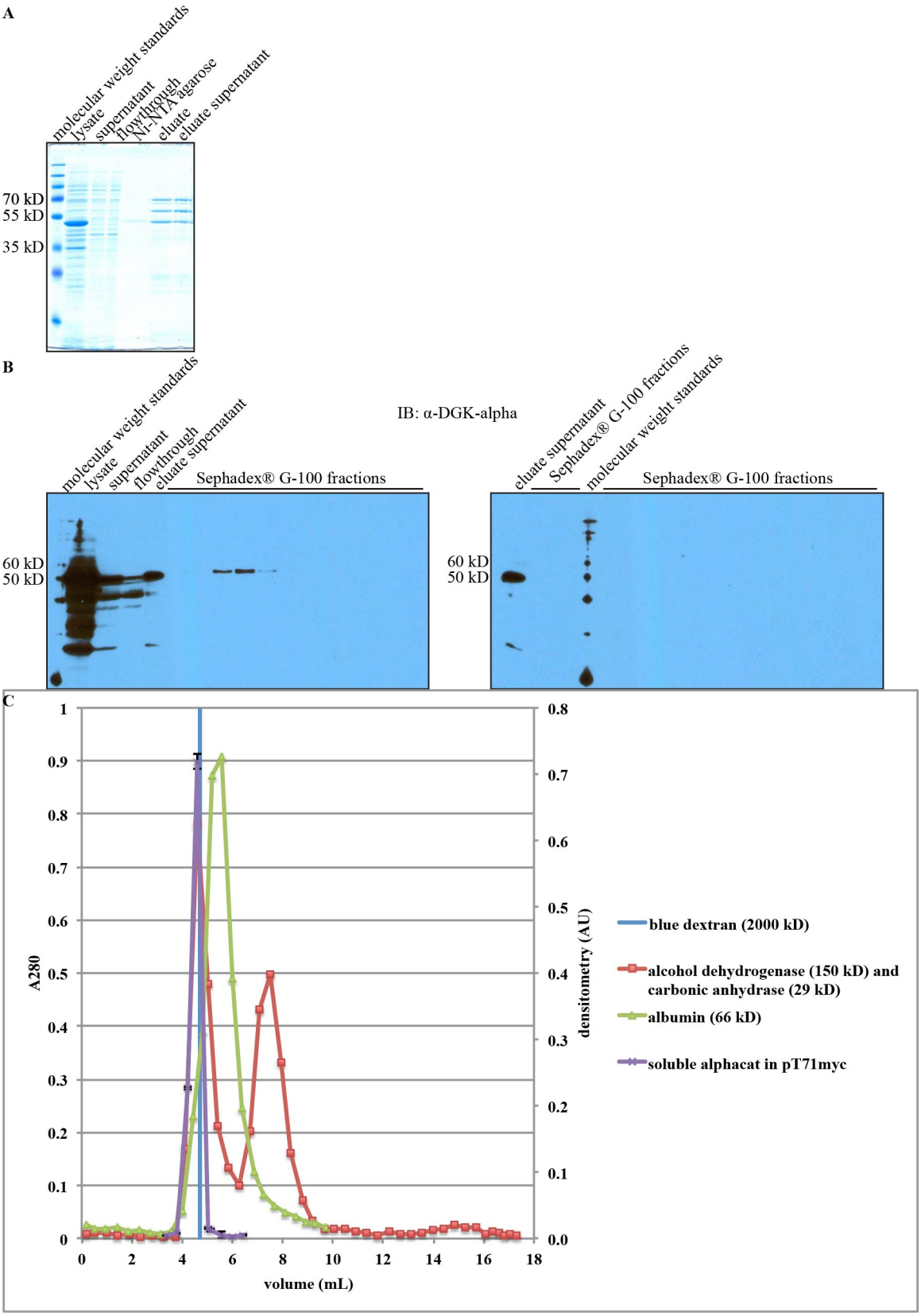
A
molecular weight standards
lysate
supernatant
flowthrough
Ni-NTA agarose
eluate
eluate supernatant
70 kD
55 kD
35 kD
B
IB: α-DGK-alpha
molecular weight standards
lysate
supernatant
flowthrough
eluate supernatant
Sephadex® G-100 fractions
60 kD
50 kD
eluate supernatant
Sephadex® G-100 fractions
molecular weight standards
Sephadex® G-100 fractions
60 kD
50 kD
C
A280
densitometry (AU)
volume (mL)
blue dextran (2000 kD)
alcohol dehydrogenase (150 kD) and carbonic anhydrase (29 kD)
albumin (66 kD)
soluble alphacat in pT71myc

Figure 15. Soluble alphacat in pT1myc can be enriched by Ni-NTA chromatography, but it elutes from Sephadex® G-100 in the void volume. I inoculated a 50 mL culture of LB Kan with an overnight culture of alphacat in pT71myc in Rosetta™(DE3). When the OD600 was predicted to reach 1.0, I added IPTG to 0.5 mM and shook the cultures for 21 hours at 15°C, then pelleted the cells and resuspended in 4 mL per gram wet cell pellet lysis buffer (50 mM Tris, pH 8.0, 300 mM NaCl, 10 mM imidazole, 5 mM $MgCl_2$, 1 mM $CaCl_2$, 0.5% (v/v) NP-40, 1x PIC, 0.5 mM DTT, 1 mg per mL egg white lysozyme, 20 U per mL DNAse I). I incubated on ice for one hour. I removed the insoluble fraction by centrifuging at 43,000 x *g* for ninety minutes at 4°C. I added Ni-NTA agarose 1:12 (v/v) and incubated for 135 minutes, rocking at 4°C. I washed the resin with wash buffer 1 (50 mM Tris, pH 8.0, 300 mM NaCl, 10 mM imidazole, 1 mM $CaCl_2$, 0.5 mM DTT) followed by wash buffer 2 (same as wash buffer 1, but imidazole increased to 20 mM), and eluted with elution buffer (same as the wash buffers, but imidazole increased to 250 mM). I removed the insoluble fraction by centrifuging at 43,000 x *g* for ninety minutes at 4°C, and loaded 200 µL of the eluate's supernatant onto the same Sephadex® G-100 column shown in **Figure 12** - **Figure 14**, and collected fractions every seven minutes, eluting by gravity in gel filtration buffer (55 mM HEPES, 5.5 mM $MgCl_2$, 1.1 mM $CaCl_2$, pH 8.0). **(A)** SDS-PAGE of a 12% acrylamide gel followed by Coomassie staining. **(B)** SDS-PAGE of 12% acrylamide gels followed by immunoblotting against DGK-alpha (rabbit antibody from the Sakane lab (1:5000 (v/v))). I loaded 24 µL per lane of the gel filtration fractions of elution volumes corresponding to molecular weights of 274 to 38 kD. **(C)** To quantify the alphacat in the gel filtration fractions, I performed densitometry, using a shorter exposure of the first membrane shown in (B), three times on the same film. Mean ± SD.

Oligomerization of LCB5 family proteins is not unprecedented: purified *Salmonella typhimurium* YegS recombinantly expressed in *E. coli* elutes as a dimer from a Superdex G200 resin[92], *E. coli* YegS[93] and *Staphylococcus aureus* DgkB[94] recombinantly expressed in *E. coli* each crystallize as dimers, and *H. sapiens* DGK-epsilon recombinantly expressed in COS-7 cells has been reported to dimerize based on its migration in perfluorooctanoic acid (PFO)-PAGE[43]. (PFO is weaker detergent than SDS, and hence some protein-protein interactions are maintained during electrophoresis with PFO[95]: however, because this result was observed with DGK-epsilon-overexpressing COS-7 lysates[43] and not purified protein, the possibility cannot be ruled out that DGK-epsilon was not dimerizing but rather interacting with another cellular protein of approximately the same size as itself.) If alphacat dimerized, however, the predicted size of the dimer would be 99.6 kD, which could be difficult to distinguish from the void volume on a Sephadex® G-100 resin. I therefore tested where refolded alphacat in pT71myc eluted from Sephadex® G-150 resin, a resin with a larger exclusion

volume and hence able to resolve differences in molecular weight among larger macromolecules. When I loaded refolded alphacat in pT71myc onto a Sephadex® G-150 column, however, alphacat continued to elute in the void volume (Figure 16).

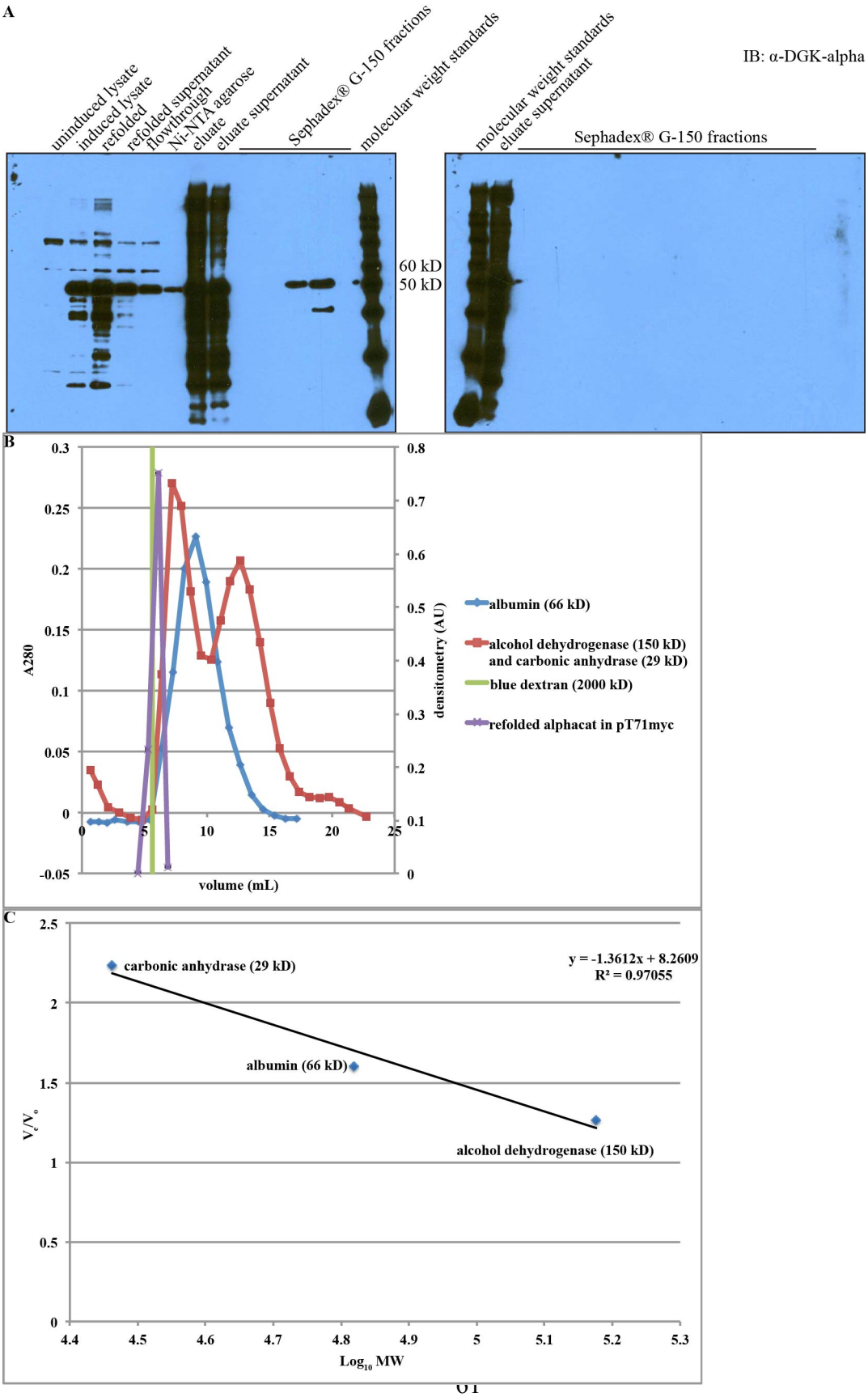
A
uninduced lysate
induced lysate
refolded
refolded supernatant
flowthrough
Ni-NTA agarose
eluate
eluate supernatant
Sephadex® G-150 fractions
molecular weight standards
IB: α-DGK-alpha
60 kD
50 kD
molecular weight standards
eluate supernatant
Sephadex® G-150 fractions
B
A280
densitometry (AU)
volume (mL)
albumin (66 kD)
alcohol dehydrogenase (150 kD) and carbonic anhydrase (29 kD)
blue dextran (2000 kD)
refolded alphacat in pT71myc
C
carbonic anhydrase (29 kD)
albumin (66 kD)
alcohol dehydrogenase (150 kD)
y = -1.3612x + 8.2609
R² = 0.97055
Ve/Vo
Log10 MW

Figure 16. Refolded alphacat elutes from Sephadex® G-150 in the void volume. I inoculated a 72.5 mL culture of LB Kan with an overnight culture of alphacat in pT71myc in Rosetta™(DE3). When the OD600 was predicted to reach 1.0, I added IPTG to 0.5 mM and shook the cultures for 21 hours at 14°C, then pelleted the cells and resuspended in 4 mL per gram wet cell pellet lysis buffer (50 mM Tris, pH 8.0, 300 mM NaCl, 10 mM imidazole, 1 mM $CaCl_2$, 0.5% (v/v) NP-40, 1x PIC, 0.5 mM DTT, 1 mg per mL egg white lysozyme, 20 U per mL DNAse I). I incubated on ice for one hour, then added DNAseI to 27 U per mL, then incubated on ice for another thirty minutes, then added $MgCl_2$ to 5 mM, then incubated on ice for another thirty minutes, then drew through a 22-gauge needle five times. I separated the supernatant from the pellet by centrifuging at 43,000 x *g* for twenty minutes at 4°C. I extracted the pellets with 2.5 mL per gram original cell pellet extraction buffer (50 mM Tris, pH 8.0, 300 mM NaCl, 10 mM imidazole, 1 mM $CaCl_2$, 0.5 mM DTT, 6.7 M guanidinium chloride) and probe-sonicated until completely clear. I removed the insoluble fraction by centrifuging at 19,700 x *g* for thirty minutes at 4°C. I then refolded the extracted supernatant by diluting fifty-fold into loading buffer (50 mM Tris, pH 8.0, 300 mM NaCl, 10 mM imidazole, 1 mM $CaCl_2$, 0.5 mM DTT), and removed the insoluble fraction by centrifuging at 18,000 x *g* for thirty minutes at 4°C. I added Ni-NTA agarose 1:600 (v/v) and incubated for two hours, rocking at 4°C. I washed the resin with loading buffer, followed by wash buffer (same as loading buffer, but imidazole increased to 20 mM), and eluted with elution buffer (same as wash buffer, but imidazole increased to 250 mM). I removed the insoluble fraction by centrifuging at 43,000 x *g* for ninety minutes at 4°C, and loaded 200 µL of the eluate's supernatant onto a Sephadex® G-150 column that had been previously calibrated with blue dextran, alcohol dehydrogenase, carbonic anhydrase, and albumin, and collected fractions every 3.5 minutes, eluting by gravity in gel filtration buffer (55 mM HEPES, 5.5 mM $MgCl_2$, 1.1 mM $CaCl_2$, pH 8.0). **(A)** SDS-PAGE of 12% acrylamide gels followed by immunoblotting against DGK-alpha (rabbit antibody from the Sakane lab (1:5000 (v/v))). I loaded 24 µL per lane of the gel filtration fractions of elution volumes corresponding to molecular weights of 305 to 8.6 kD. **(B)** To quantify the alphacat in the gel filtration fractions, I performed densitometry, using a shorter exposure of the first membrane shown in (A), three times on the same film. Mean ± SD. **(C)** Calibration of the Sephadex® G-150 column: elution volume (presented as a ratio of the void volume) of the molecular weight standards as a function of logarithm molecular weight. I calculated the linear regression using Microsoft® Excel®.

Chelating agents such as imidazole have been reported to reverse the aggregation of histidine-tagged proteins[96]. However, when I included 250 mM imidazole in the gel filtration buffer, refolded alphacat in pT71myc continued to elute in the void volume (Figure 17).

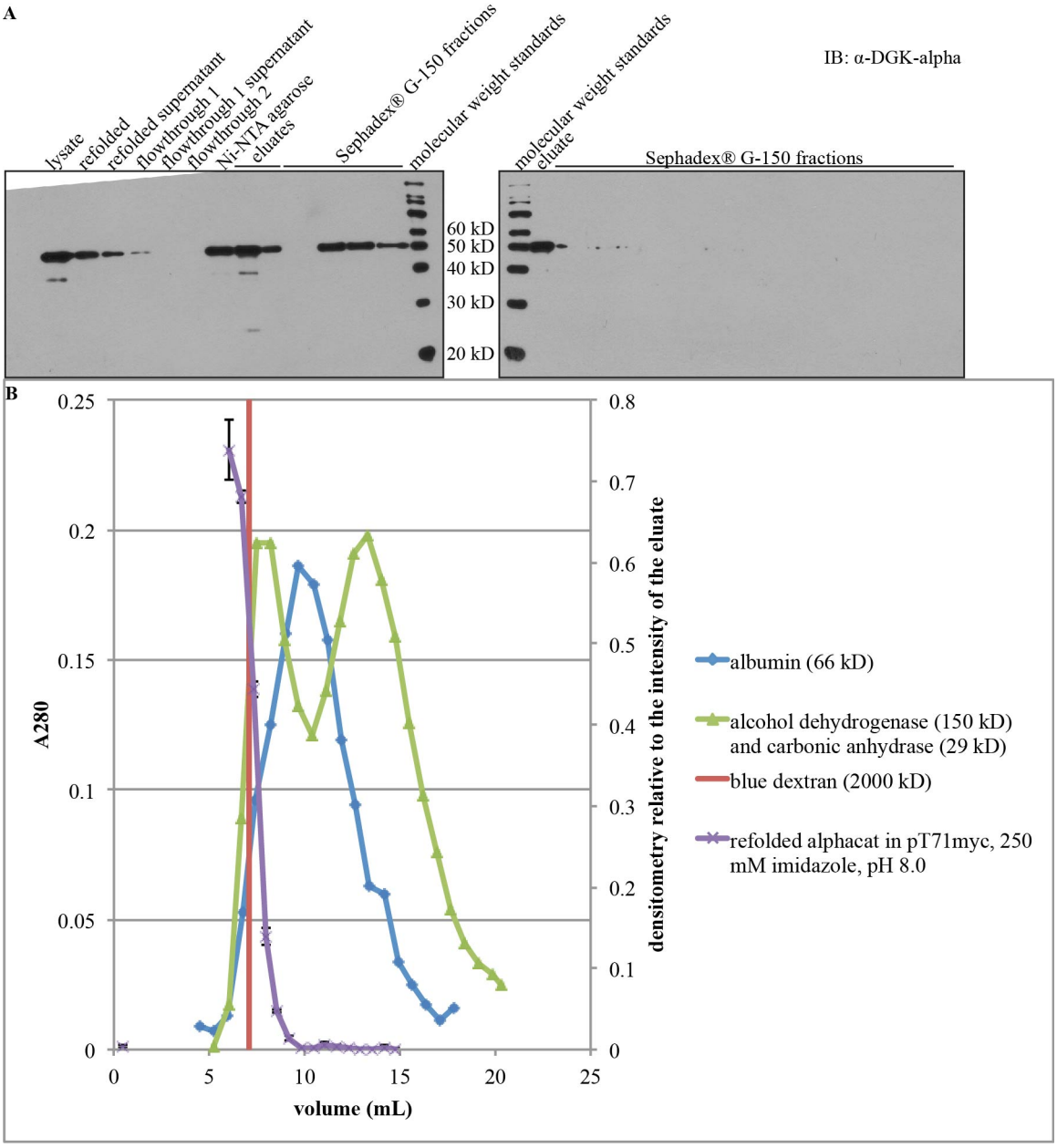

Figure 17. In the presence of 250 mM imidazole, refolded alphacat in pT71myc continues to elute in the void volume from a Sephadex® G-150 analytical gel filtration column. I inoculated a 62.5 mL culture of LB Kan with an overnight culture of alphacat in pT71myc in Rosetta™(DE3). When the OD600 was predicted to reach 1.0, I added IPTG to 0.5 mM and shook the cultures for 21 hours at 15°C, then pelleted the cells and froze the pellets at -80°C for a bit over seven months. I thawed the cell pellets by gently shaking the tube in room-temperature until just thawed, and resuspended in 4 mL per gram wet cell pellet lysis buffer (50 mM Tris, pH 8.0, 300 mM NaCl, 10 mM imidazole, 5 mM $MgCl_2$, 1 mM $CaCl_2$, 0.5% (v/v) NP-40, 1x PIC, 1 mg per mL egg white lysozyme, 20 U per mL DNAse I). I incubated on ice for thirty minutes, then separated the supernatant from the pellet by centrifuging at 43,000 x *g* for ninety minutes at 4°C. I extracted the pellets with 2 mL per gram original cell pellet extraction buffer (50 mM Tris, pH 8.0, 300 mM NaCl, 10 mM imidazole, 1 mM $CaCl_2$, 0.5 mM DTT, 6.7 M guanidine chloride) and probe-sonicated until completely clear. I then refolded the extracted alphacat by diluting fifty-fold into loading buffer (50 mM Tris, pH 8.0, 300 mM NaCl, 10 mM imidazole, 1 mM $CaCl_2$, 0.5 mM DTT), and

removed the insoluble fraction by centrifuging at 110,000 x *g* for one hour at 4°C. I added Ni-NTA agarose 1:500 (v/v) and incubated for one hour, rocking at 4°C. I stored the flowthrough (flowthrough 1) at -80°C for one week, then thawed by gently shaking the tube in room-temperature until just thawed, and removed the insoluble fraction by centrifuging at 110,000 x *g* for one hour at 4°C. I repurified the flowthrough by adding Ni-NTA agarose 1:500 (v/v) and incubating overnight, rocking at 4°C. I washed the resin with loading buffer, followed by wash buffer (same as loading buffer, but imidazole increased to 20 mM), and eluted with elution buffer (same as wash buffer, but imidazole increased to 250 mM). I removed the insoluble fraction by microfuging, and loaded 200 µL of the eluate's supernatant onto a Sephadex® G-150 column that had been previously calibrated with blue dextran, albumin, alcohol dehydrogenase, carbonic anhydrase, and blocked with albumin, and I collected fractions every two minutes, eluting by gravity in gel filtration buffer (55 mM HEPES, 5.5 mM $MgCl_2$, 1.1 mM $CaCl_2$, 250 mM imidazole, pH 8.0). **(A)** SDS-PAGE of 12% acrylamide gels followed by immunoblotting against DGK-alpha (rabbit antibody from the Sakane lab (1:5000 (v/v))). I loaded 24 µL per lane of the gel filtration fractions of elution volumes corresponding to molecular weights of 231 to 17 kD. **(B)** Elution profile of molecular weight standards and alphacat. I measured the A280 of the protein molecular weight standards. I observed blue dextran elution visually: the elution volume of the bluest fraction is represented by a vertical line. In order to quantify the alphacat in the gel filtration fractions, I performed densitometry on the films shown in (A), three times on the same film. In order to compare the two immunoblots, I calculated the signal as a proportion of the signal from the eluate on the same blot. Mean ± SD.

Proteins have been reported to aggregate at pHs around their pI[97]. After sequencing the DNA of the alphacat in pT71myc construct I later learned that the pI of this construct is 6.99, but at the time of these experiments I was under the mistaken impression that the pI of the construct was 8.4. (Not realizing that the fusion tag added by pT71myc included more than just the histidine tag, I had calculated the pI from the sequence of alphacat, plus six histidines. I later sequenced the alphacat in pT71myc construct using the T7 primer: it is on this sequence that the schematic in Figure 5 is based.) I had conducted the previous purifications and analytical gel filtration chromatography at pH 8.0. Concerned that being too close to the pI was contributing to alphacat's aggregation (at pH 8.0, approximately 40% of a protein whose pI is 8.4 would be uncharged), I dropped the pH of lysis, purification, and analytical gel filtration to 6.4 (so that only 1% of a protein whose pI is 8.4 would be uncharged), in the hopes that doing so would increase the proportion of alphacat that eluted from the analytical gel filtration column in a volume corresponding to that predicted for a dimer. (However, I was still using Tris to buffer the pH, even though 6.4 is well outside the buffering range

of Tris[98], so the actual pH is uncertain.) Under these conditions for analytical gel filtration, although some of the alphacat continued to elute in the void volume, some also eluted at a volume corresponding to about 79 kD, somewhat later than the predicted elution volume of a dimer (predicted size 99.6 kD) (Figure 18). Any quantitative comparison of the immunoblot signal of two peaks would require that the two populations have equal affinity for the antibody, which I have no reason to believe.

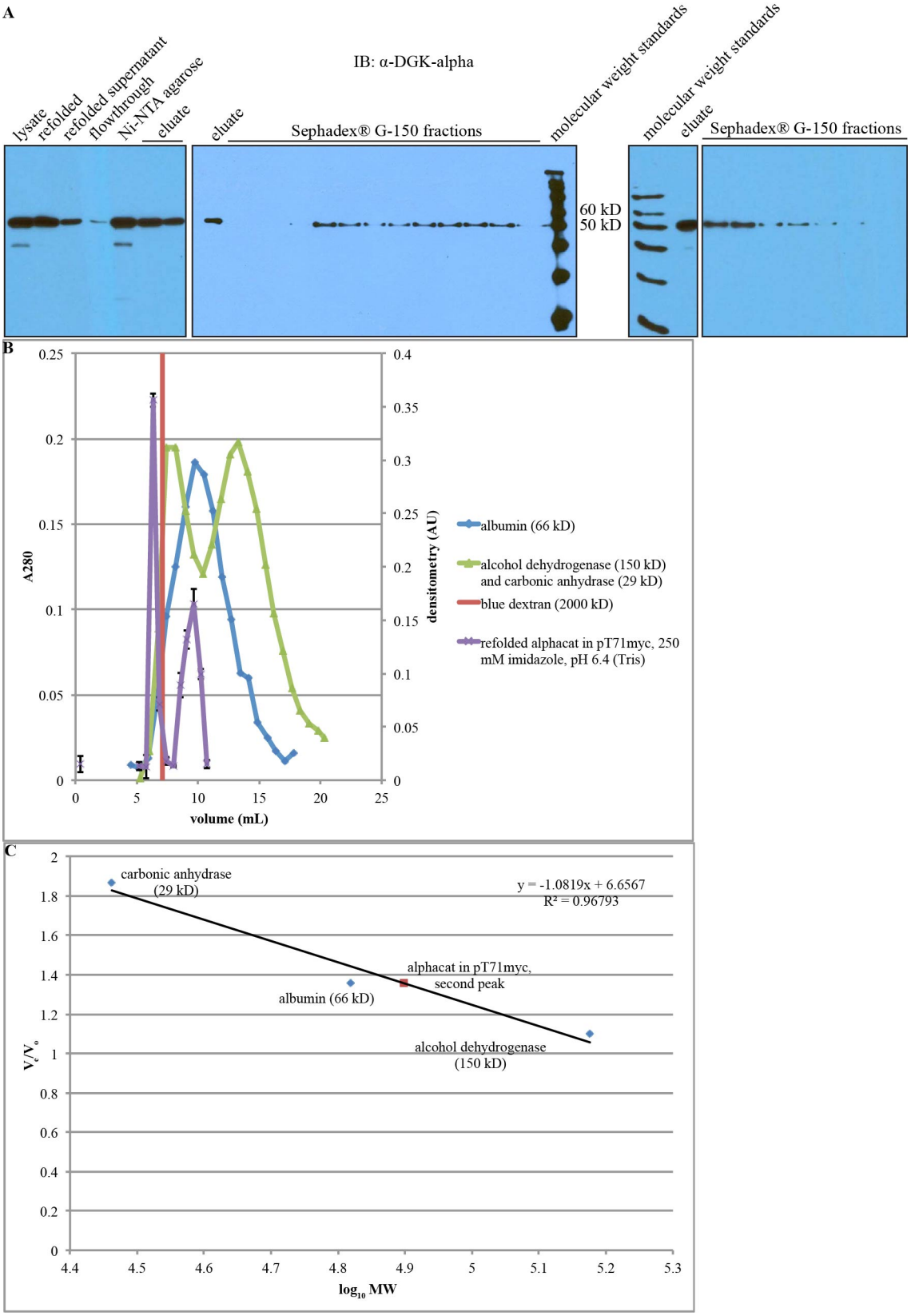
A
IB: α-DGK-alpha
lysate
refolded
refolded supernatant
flowthrough
Ni-NTA agarose
eluate
eluate
Sephadex® G-150 fractions
molecular weight standards
60 kD
50 kD
molecular weight standards
eluate
Sephadex® G-150 fractions
B
A280
densitometry (AU)
volume (mL)
albumin (66 kD)
alcohol dehydrogenase (150 kD) and carbonic anhydrase (29 kD)
blue dextran (2000 kD)
refolded alphacat in pT71myc, 250 mM imidazole, pH 6.4 (Tris)
C
carbonic anhydrase (29 kD)
y = -1.0819x + 6.6567
R² = 0.96793
alphacat in pT71myc, second peak
albumin (66 kD)
alcohol dehydrogenase (150 kD)
Ve/Vo
log10 MW

Figure 18. In the presence of 250 mM imidazole at pH 6.4, refolded alphacat in pT71myc elutes from a Sephadex® G-150 analytical gel filtration column in two peaks. The protein used in this experiment was purified from the same cell pellets used in **Figure 17**. I thawed the cell pellets by gently shaking the tube in room-temperature until just thawed, and resuspended in 4 mL per gram wet cell pellet lysis buffer (50 mM Tris, pH 6.4, 300 mM NaCl, 10 mM imidazole, 5 mM $MgCl_2$, 1 mM $CaCl_2$, 0.5% (v/v) NP-40, 1x PIC, 0.5 mM DTT, 1 mg per mL egg white lysozyme, 20 U per mL DNAse I). I incubated on ice for one hour, vortexing halfway through, then separated the supernatant from the pellet by centrifuging at 43,000 x *g* for ninety minutes at 4°C. I extracted the pellets with 2 mL per gram original cell pellet extraction buffer (50 mM Tris, pH 6.4, 300 mM NaCl, 10 mM imidazole, 1 mM $CaCl_2$, 0.5 mM DTT, 6.7 M guanidine chloride) and probe-sonicated until completely clear. I then refolded the extracted alphacat by diluting fifty-fold into loading buffer (50 mM Tris, pH 6.4, 300 mM NaCl, 10 mM imidazole, 1 mM $CaCl_2$, 0.5 mM DTT), and removed the insoluble fraction by centrifuging at 110,000 x *g* for one hour at 4°C. I added Ni-NTA agarose 1:500 (v/v) and incubated overnight, rocking at 4°C. I washed the resin with loading buffer, followed by wash buffer (same as loading buffer, but imidazole increased to 20 mM), and eluted with elution buffer (same as wash buffer, but imidazole increased to 250 mM). I removed the insoluble fraction by microfuging, and loaded 200 µL of the eluate's supernatant onto the same Sephadex® G-150 column shown in **Figure 17**, freshly reblocked with albumin, and I collected fractions every two minutes, eluting by gravity in gel filtration buffer (55 mM HEPES, 5.5 mM $MgCl_2$, 1.1 mM $CaCl_2$, 250 mM imidazole, pH 6.4). **(A)** SDS-PAGE of 12% acrylamide gels followed by immunoblotting against DGK-alpha (rabbit antibody from the Sakane lab (1:5000 (v/v))). I loaded 24 µL per lane of the gel filtration fractions of elution volumes corresponding to molecular weights of 301 to 18 kD. **(B)** The elution of molecular weight markers as a function of elution volume. I detected the elution of the proteins standards by measuring the absorbance at 280 nm (A280) of the gel filtration fractions. I detected the elution of the blue dextran visually: the vertical line marks the volume of the fraction that appeared the bluest. To quantify the alphacat in the gel filtration fractions, I performed densitometry, using a shorter exposure of the middle membrane shown in (A), three times on the same film. Mean ± SD. **(C)** Calibration of the Sephadex® G-150 column: elution volume (presented as a ratio of the void volume) of the molecular weight standards as a function of logarithm molecular weight. I calculated the linear regression using Microsoft® Excel®. The elution volume of the second peak of alphacat (as measured by densitometry from the blot shown in (A)), plotted onto the linear fit of the protein molecular weight standards, gives a predicted molecular weight of 79 kD.

In order to make sure these results were reproducible, I repeated with a fresh and larger-scale expression of alphacat in pT71myc. Once again, when lysed and purified at pH 6.4 (Figure 19**A**), and when loaded onto the analytical gel filtration column in 250 mM imidazole, alphacat eluted in two distinct peaks, one corresponding to the void volume, and one eluting somewhat later (Figure 19**B-C**). This time the predicted molecular weight of the second peak is 127 kD: one possible explanation for the change in predicted molecular weight could be that the gel filtration resin compressed in volume during the nearly six weeks that elapsed between calibration and the chromatography shown in Figure 19. However, when I replotted alphacat's elution onto a fresh calibration of the same column, the predicted molecular weight of the second peak was

nearly the same, at 128 kD (Figure 20). The discrepancy in the elution volumes in the experiments shown in Figure 18 and Figure 19 is therefore unlikely to be a result of compression of the Sephadex® G-150 resin. Another possible explanation for the difference in elution volumes could be that in the later experiment, alphacat was purified in the presence of 5 mM $MgCl_2$. Other LCB5 family proteins have Mg^{2+} binding sites[92,94], so it is possible that the presence of Mg^{2+} affects alphacat's conformation, which could influence its elution profile from an analytical gel filtration column. Yet another possible explanation is that alphacat's conformation is pH-dependent, and the pH varied between these experiments because of Tris's poor buffering capacity at 6.4. 127 kD is considerably larger than the predicted mass of a dimer (99.6 kD), but also smaller than the predicted mass of a trimer (149.4 kD).

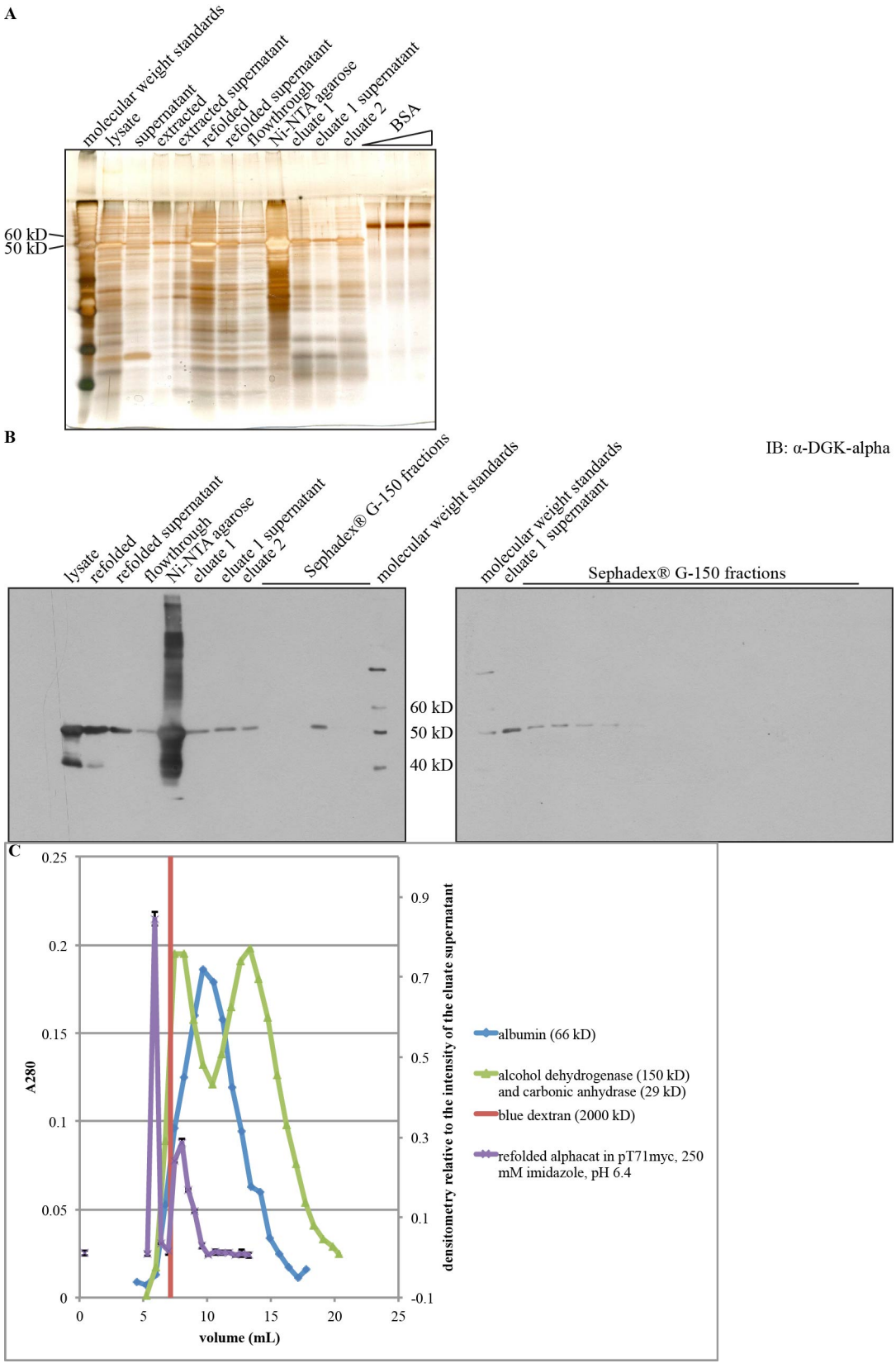
A
molecular weight standards
lysate
supernatant
extracted
extracted supernatant
refolded
refolded supernatant
flowthrough
Ni-NTA agarose
eluate 1
eluate 1 supernatant
eluate 2
BSA
60 kD
50 kD
B
IB: α-DGK-alpha
lysate
refolded
refolded supernatant
flowthrough
Ni-NTA agarose
eluate 1
eluate 1 supernatant
eluate 2
Sephadex® G-150 fractions
molecular weight standards
molecular weight standards
eluate 1 supernatant
Sephadex® G-150 fractions
60 kD
50 kD
40 kD
C
A280
densitometry relative to the intensity of the eluate supernatant
volume (mL)
albumin (66 kD)
alcohol dehydrogenase (150 kD) and carbonic anhydrase (29 kD)
blue dextran (2000 kD)
refolded alphacat in pT71myc, 250 mM imidazole, pH 6.4

Figure 19. In the presence of 250 mM imidazole at pH 6.4, refolded alphacat in pT71myc reproducibly elutes from a Sephadex® G-150 analytical gel filtration column in two peaks. I inoculated three 62.5 mL cultures of LB Kan with an overnight culture of alphacat in pT71myc in Rosetta™(DE3). When the OD600 was predicted to reach 1.0, I added IPTG to 0.5 mM and shook the cultures for 20.5 hours at 22°C, then pelleted the cells and resuspended in 4 mL per gram wet cell pellet lysis buffer (50 mM Tris, pH 6.4, 300 mM NaCl, 10 mM imidazole, 5 mM $MgCl_2$, 1 mM $CaCl_2$, 0.5% (v/v) NP-40, 0.5 mM DTT, 1x PIC, 1 mg per mL egg white lysozyme, 20 U per mL DNAse I). I incubated on ice for thirty minutes, vortexing occasionally to mix, then separated the supernatant from the pellet by centrifuging at 43,000 x *g* for ninety minutes at 4°C. I extracted the pellets with extraction buffer (50 mM Tris, pH 6.4, 300 mM NaCl, 10 mM imidazole, 5 mM $MgCl_2$, 1 mM $CaCl_2$, 0.5 mM DTT, 6.7 M guanidine chloride) and probe-sonicated until completely clear. I removed the insoluble fraction by centrifuging at 43,000 x *g* for ninety minutes at 4°C. I then refolded the extracted alphacat by diluting fifty-fold into loading buffer (50 mM Tris, pH 6.4, 300 mM NaCl, 10 mM imidazole, 5 mM $MgCl_2$, 1 mM $CaCl_2$, 0.5 mM DTT), and removed the insoluble fraction by centrifuging at 110,000 x *g* for one hour at 4°C. I added Ni-NTA agarose 1:500 (v/v) and incubated overnight, rocking at 4°C. I washed the resin with loading buffer, followed by wash buffer (same as loading buffer, but imidazole increased to 20 mM), and eluted with elution buffer (same as wash buffer, but imidazole increased to 250 mM). I removed the insoluble fraction by centrifuging at 43,000 x *g* for ninety minutes at 4°C, and loaded 200 µL of the eluate's supernatant onto the same Sephadex® G-150 column shown in **Figure 17** and **Figure 18**, freshly reblocked with albumin, and I collected fractions every two minutes, eluting by gravity in gel filtration buffer (55 mM HEPES, 5.5 mM $MgCl_2$, 1.1 mM $CaCl_2$, 250 mM imidazole, pH 6.4). **(A)** SDS-PAGE of a 12% acrylamide gel followed by silver staining. **(B)** SDS-PAGE of 12% acrylamide gels followed by immunoblotting against DGK-alpha (rabbit antibody from the Sakane lab (1:5000 (v/v))). I loaded 24 µL per lane of the gel filtration fractions of elution volumes corresponding to molecular weights of 287 to 27 kD. **(C)** Elution profile of molecular weight standards and alphacat. In order to quantify the alphacat in the gel filtration fractions, I performed densitometry on the films shown in (B), three times on the same film. In order to compare the two immunoblots, I calculated the signal as a proportion of the signal from the eluate supernatant on the same blot. Mean ± SD.

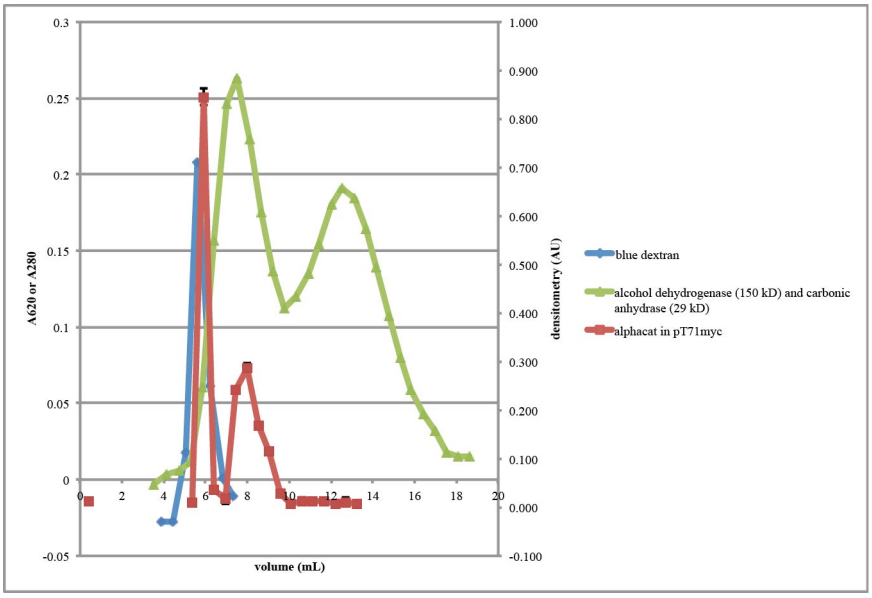

Figure 20. The second peak of refolded alphacat in pT71myc in 250 mM imidazole, pH 6.4 (Tris) elutes from a freshly recalibrated Sephadex® G-150 analytical gel filtration column at a volume consistent with a molecular weight of 128 kD. The same column shown in **Figure 17 - Figure 19**, but

recalibrated. Elution profile of molecular weight standards and alphacat. I measured the A280 of the protein molecular weight standards, and A620 of the blue dextran fractions. The alphacat data is the same shown in **Figure 19**C, but replotted onto the fresh calibration.

When I scaled the expression up to 4 L of culture, alphacat remained insoluble, but I was once again able to extract some alphacat from protein pellets using guanidine chloride, and could purify the refolded protein on Ni-NTA resin (Figure 21**A**). Most of the purified protein either remained bound to the Ni-NTA resin or else precipitated and thus pelleted with the Ni-NTA resin. The yield of eluted protein was very low, even after eluting overnight (eluate 3 E), suggesting that the low yield was not a result of the elutions' being too short. When I loaded the purified protein onto the Sephadex® G-150 analytical gel filtration column, alphacat once again eluted in two distinct peaks (Figure 21**B-C**). The predicted molecular weight of the second peak, based on the calibration, was 122 kD, once again considerably larger than the predicted mass of a dimer (99.6 kD), but also smaller than the predicted mass of a trimer (149.4 kD), and consistent with the previously observed elution volumes consistent with molecular weights of 127-128 kD (Figure 19 and Figure 20).

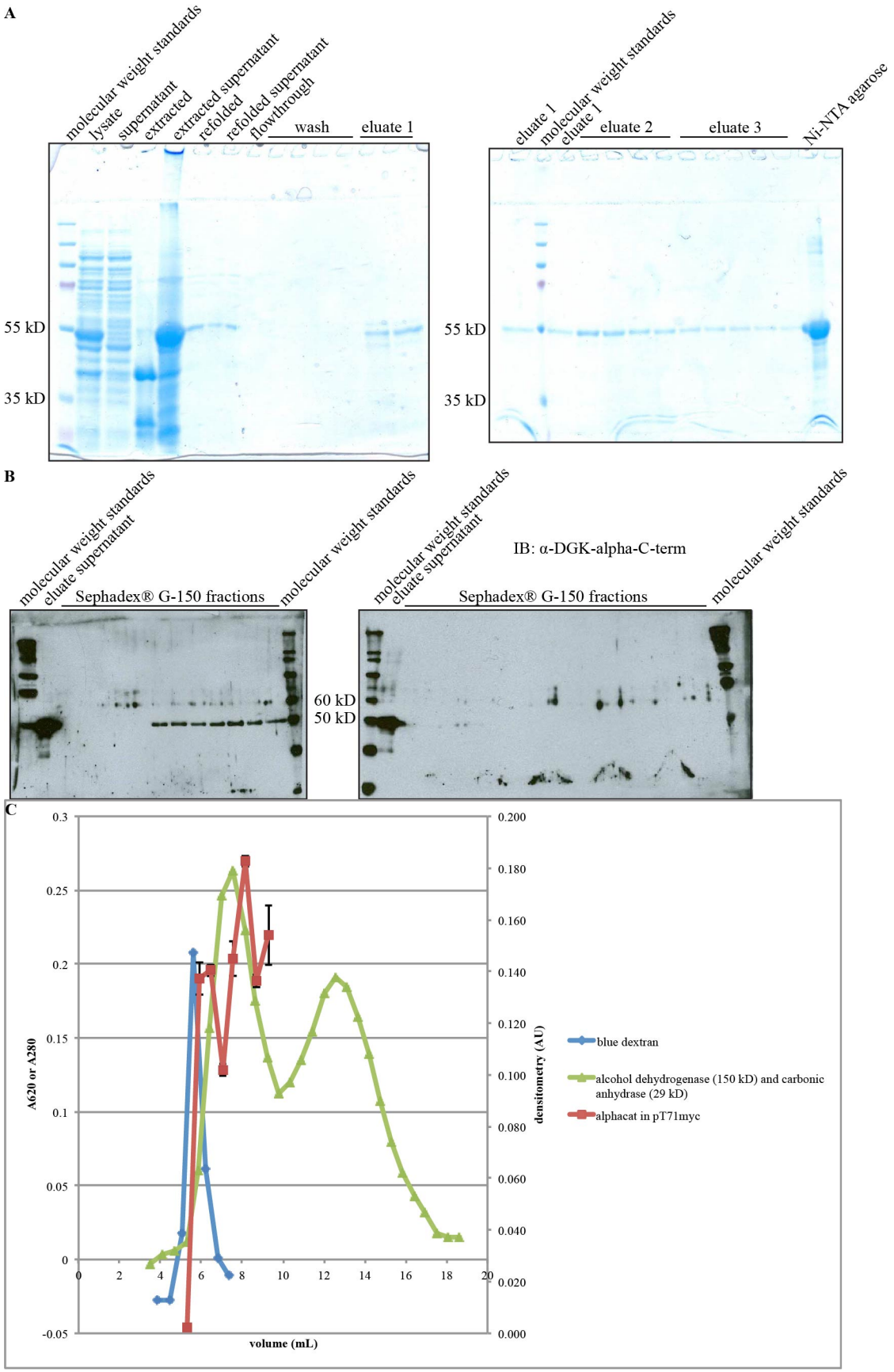
A
molecular weight standards
lysate
supernatant
extracted
extracted supernatant
refolded
refolded supernatant
flowthrough
wash
eluate 1
55 kD
35 kD
eluate 1
molecular weight standards
eluate 1
eluate 2
eluate 3
Ni-NTA agarose
55 kD
35 kD
B
molecular weight standards
eluate supernatant
Sephadex® G-150 fractions
molecular weight standards
IB: α-DGK-alpha-C-term
60 kD
50 kD
molecular weight standards
eluate supernatant
Sephadex® G-150 fractions
molecular weight standards
C
A620 or A280
densitometry (AU)
volume (mL)
blue dextran
alcohol dehydrogenase (150 kD) and carbonic anhydrase (29 kD)
alphacat in pT71myc

Figure 21. The second peak of refolded alphacat in pT71myc in 250 mM imidazole, pH 6.4 (Tris) from a scaled-up expression elutes from a Sephadex® G-150 analytical gel filtration column at a volume consistent with a molecular weight of 122 kD. I inoculated four 1 L cultures of LB Kan with an overnight culture of alphacat in pT71myc in Rosetta™(DE3). When the OD600 was predicted to reach 1.0, I added IPTG to 0.38 mM and shook the cultures overnight at 16°C, then pelleted the cells and resuspended in 0.8 mL per gram wet cell pellet lysis buffer (50 mM HEPES, pH 6.0, 300 mM NaCl, 10 mM imidazole, 5 mM $MgCl_2$, 1 mM $CaCl_2$, 0.5 mM DTT), and stored overnight at -80°C. I thawed the frozen lysates by shaking the tubes gently in room-temperature water. I added lysis buffer to 10 mL per gram wet cell pellet. I lysed the cells by microfluidizing them twice at > 10,000 pounds per square inch (psi). The supernatant was separated from the pellet by centrifuging at 23,500 x *g* for thirty minutes. I extracted the pellets with 2 mL per gram original cell pellet extraction buffer (50 mM HEPES, pH 6.4, 300 mM NaCl, 10 mM imidazole, 5 mM $MgCl_2$, 1 mM $CaCl_2$, 0.5 mM DTT, 6.7 M guanidine chloride) and probe-sonicated and vortexed until the pellet mostly went into solution. I removed the insoluble fraction by centrifuging at 110,000 x *g* for one hour at 4°C. I then refolded the extracted alphacat by diluting twenty-fold into loading buffer (50 mM HEPES, pH 6.4, 300 mM NaCl, 10 mM imidazole, 5 mM $MgCl_2$, 1 mM $CaCl_2$), and removed the insoluble fraction by centrifuging at 23,500 x *g* for thirty minutes. I added Ni-NTA agarose 1:3040 (v/v) and incubated overnight, rocking at 4°C. I washed the resin with loading buffer, followed by wash buffer (same as loading buffer, but imidazole increased to 20 mM). I eluted in three steps, with elution buffer 1 (same as wash buffer, but imidazole increased to 100 mM), elution buffer 2 (200 mM imidazole), and elution buffer 3 (250 mM imidazole). Because the second elution appeared the most pure, I selected that fraction for analytical gel filtration chromatography. I removed the insoluble fraction by centrifuging at 43,000 x *g* for ninety minutes at 4°C, and loaded 200 µL of the eluate's supernatant onto the same Sephadex® G-150 column shown in **Figure 20**, freshly blocked with 670 µL of 10 mg per mL cytochrome c, and I collected fractions every 2.5 minutes, eluting by gravity in gel filtration buffer (55 mM HEPES, 5.5 mM $MgCl_2$, 1.1 mM $CaCl_2$, 250 mM imidazole, pH 6.4). **(A)** SDS-PAGE of 12% acrylamide gels followed by Coomassie staining. **(B)** SDS-PAGE of 12% acrylamide gels followed by immunoblotting against DGK-alpha-C-term (Abgent AP8128b (1:300 (v/v))). **(C)** Elution profile of molecular weight standards and alphacat from the same column shown in **Figure 20**. In order to quantify the alphacat in the gel filtration fractions, I performed densitometry three times on the film shown in (B). Mean ± SD.

In an effort to get more concentrated alphacat so that I could measure its concentration with confidence in order to measure its specific activity with confidence, I repurified the flowthrough shown in Figure 21, this time eluting with each elution buffer until the Bio-Rad Protein Assay reading at 595 nm dropped below 0.010 (Figure 23**A**). Two factors seemed to contribute to the concentration of alphacat in pT71myc eluted from Ni-NTA. The first is that alphacat in pT71myc appeared to be more concentrated after longer elution times, as expected, although this effect appeared to be more dramatic in elution buffer containing 250 mM imidazole than in 70 mM imidazole (Figure 23**B**). The second factor is that of buffer composition: freshly made elution buffer dramatically increased the concentration of alphacat eluted from the resin, in some cases. Although

the reducing agent I used, tris(chloroethyl)phosphate (TCEP), has been reported to remain more than 80% reduced after three weeks at room temperature in a variety of buffers[99], I took the precaution of adding fresh TCEP to elutions following elution 4 Z, in case that was the key buffer component. Another issue could be the pH: 6.4 is outside the range of HEPES's buffering capacity as well, so a freshly made buffer might have a different pH than the previous buffer.

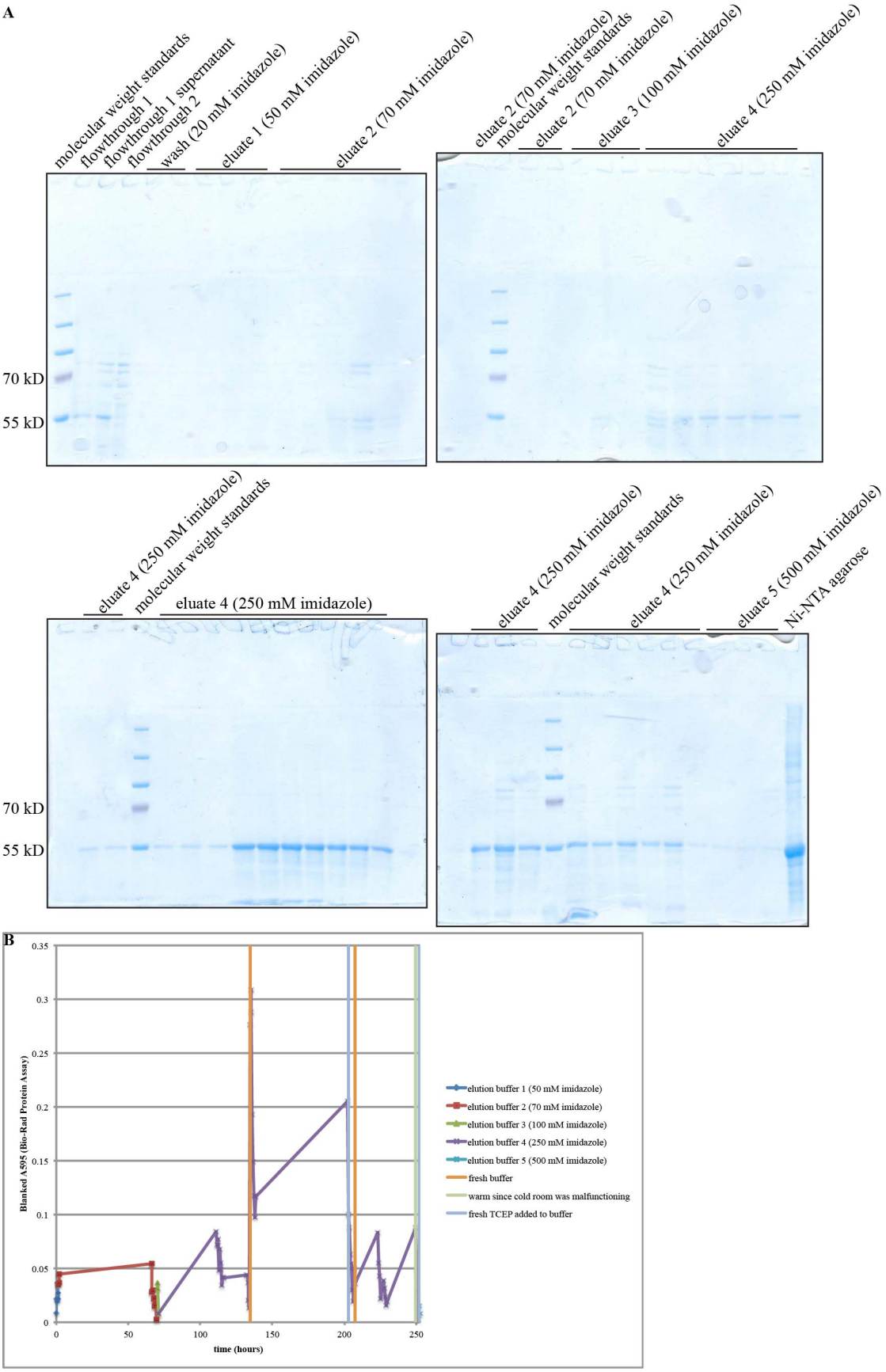
A
molecular weight standards
flowthrough 1
flowthrough 1 supernatant
flowthrough 2
wash (20 mM imidazole)
eluate 1 (50 mM imidazole)
eluate 2 (70 mM imidazole)
70 kD
55 kD
eluate 2 (70 mM imidazole)
molecular weight standards
eluate 2 (70 mM imidazole)
eluate 3 (100 mM imidazole)
eluate 4 (250 mM imidazole)
eluate 4 (250 mM imidazole)
molecular weight standards
eluate 4 (250 mM imidazole)
70 kD
55 kD
eluate 4 (250 mM imidazole)
molecular weight standards
eluate 4 (250 mM imidazole)
eluate 5 (500 mM imidazole)
Ni-NTA agarose
B
Blanked A595 (Bio-Rad Protein Assay)
time (hours)
elution buffer 1 (50 mM imidazole)
elution buffer 2 (70 mM imidazole)
elution buffer 3 (100 mM imidazole)
elution buffer 4 (250 mM imidazole)
elution buffer 5 (500 mM imidazole)
fresh buffer
warm since cold room was malfunctioning
fresh TCEP added to buffer

Figure 22. Alphacat in pT71myc's elution from Ni-NTA agarose depends on the time of the elution and on the batch of elution buffer. I removed the insoluble fraction from the flowthrough shown in **Figure 21**, which had been stored for thirteen days at 4°C, by centrifuging at 21,000 x *g* for thirty minutes at 4°C. I added Ni-NTA agarose 1:2700 and rocked for ~36 hours at 4°C. I washed with wash buffer (50 mM HEPES, pH 6.4, 20 mM imidazole, 300 mM NaCl, 1 mM $CaCl_2$, 5 mM $MgCl_2$, 0.1 mM TCEP), and eluted with elution buffer 1 (same as wash buffer, but with imidazole increased to 50 mM), elution buffer 2 (70 mM imidazole), elution buffer 3 (100 mM imidazole), elution buffer 4 (250 mM imidazole), and elution buffer 5 (500 mM imidazole), continuing to elute until the A595 as measured by the Bio-Rad Protein Assay was less than 0.010. Starting with elution 4 Z, I also added TCEP fresh to the previously made buffers. **(A)** SDS-PAGE of 12% acrylamide gels followed by Coomassie staining. I ethanol-precipitated the flowthrough 1, flowthrough 1 supernatant, and flowthrough 2 to remove the guanidine prior to loading onto the gel. I loaded 25 µL into each lane. **(B)** Blanked A595 of the Bio-Rad Protein Assay of eluates, plotted as a function of time and color-coded by elution buffer. Vertical lines mark those eluate fractions that coincided with a change in buffer or temperature.

I loaded the thus purified alphacat onto the Sephadex® G-150 analytical gel filtration column, but even after concentrating the gel filtration fractions by TCA precipitation, the protein concentration remained undetectable by the Bio-Rad Protein Assay, a method that, unlike immunoblotting, should be able to quantitatively compare the concentration of different populations of alphacat. An alternative method for concentrating protein is to dialyze against a buffer with a high concentration of a solute that is too large to pass through the pores: by osmosis, water will leave the dialysis tubing, which concentrates the protein inside the dialysis tubing. I therefore concentrated the purified alphacat by dialyzing against 15% polyethylene glycol (PEG) 17.5kD in the hopes that would improve the detection of the subsequent analytical gel filtration chromatography fractions, but dropped the tubing and thereby contaminated the purified protein with PEG. PEG-SDS interactions have been reported[100], and I confirmed that PEG disrupts the electrophoresis of alphacat (Figure 23). I was therefore unable to interpret the Coomassie staining or immunoblots of analytical gel filtration fractions from the contaminated protein.

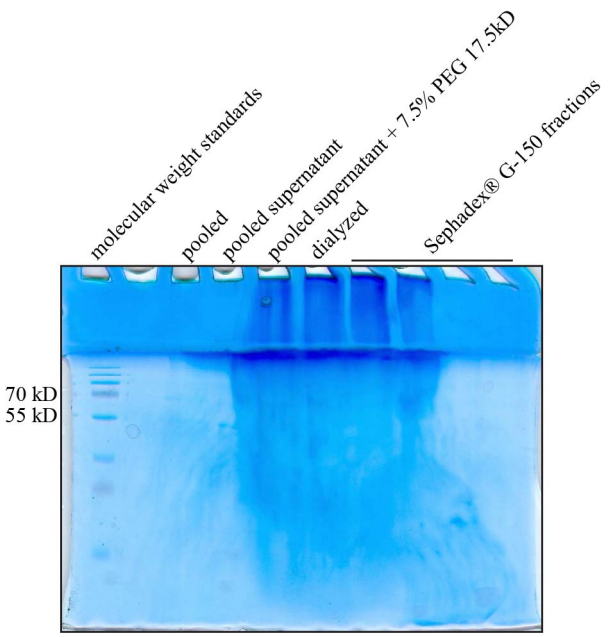

Figure 23. PEG contamination disrupts the electrophoresis of alphacat. I pooled the fourth elution (250 mM imidazole) from **Figure 22** ("pooled"), which had been stored at 4°C for two weeks, and removed the insoluble fraction by centrifuging at 118,000 x *g* for one hour at 4°C. I dialyzed the supernatant ("pooled supernatant") against dialysis buffer (55 mM HEPES, 5 mM $MgCl_2$, 1 mM $CaCl_2$, 250 mM imidazole, 15% (w/v) 17.5kD PEG) using 3500 molecular weight cut-off (MWCO) dialysis tubing (Thermo Scientific 68035) at 4°C for ten total hours. While I was putting the protein sample into the dialysis tubing, I dropped the tubing and thereby contaminated the protein with PEG. I removed the insoluble fraction from the dialyzed sample by centrifuging at 54,900 x *g* for ninety minutes at 4°C. I loaded 200 µL of the supernatant onto a Sephadex® G-150 column, freshly blocked with 1.19 mL of 10 mg per mL BSA, and I collected fractions every 2.5 minutes, eluting by gravity in gel filtration buffer (55 mM HEPES, 5.5 mM $MgCl_2$, 1.1 mM $CaCl_2$, 250 mM imidazole, pH 6.4). I loaded 48 µL of each gel filtration fraction, and tested whether PEG disrupts PAGE by adding PEG to 7.5% to the pooled supernatant sample. SDS-PAGE of a 12% acrylamide SDS-PAG followed by Coomassie staining. The sample with the added PEG shows distinctly more streaking in the stacking region of the gel than the sample without, showing that PEG is disrupting electrophoresis and staining.

I went back and purified leftover cell pellets from the expression shown in Figure 19, with the hopes of purifying enough alphacat to be able to concentrate with PEG before loading onto the column (this time without contaminating it), but the yield (as measured by the Bio-Rad Protein Assay) was only 0.177 mg, which was not enough for 200 µL of a 1-2 mg per mL solution, which would be necessary to be able to reliably detect the eluting protein.

With a fresh, one-liter expression, I once again extracted alphacat from protein pellets in buffer adjusted to pH 6.4 using HEPES as a buffer (the pH was later measured to be 6.0, consistent with being outside HEPES's buffering range), and purified on Ni-NTA (Figure 24). By re-extracting the insoluble pellets and purifying those as well, and combining the washes and the eluates, and by dialyzing against 15% PEG 17.5kD, I was eventually able to concentrate alphacat to a concentration of 1.2 mg per mL in a volume of 40 uL. After removing the insoluble, I loaded it onto a Sephadex® G-200 analytical gel filtration column (in the hopes of being able to distinguish a 199.2 kD dimer from the void volume), but alphacat eluted in the void volume (Figure 25). I therefore concluded that the His-tagged alphacat was forming aggregates unsuitable for pursuit for structural studies.

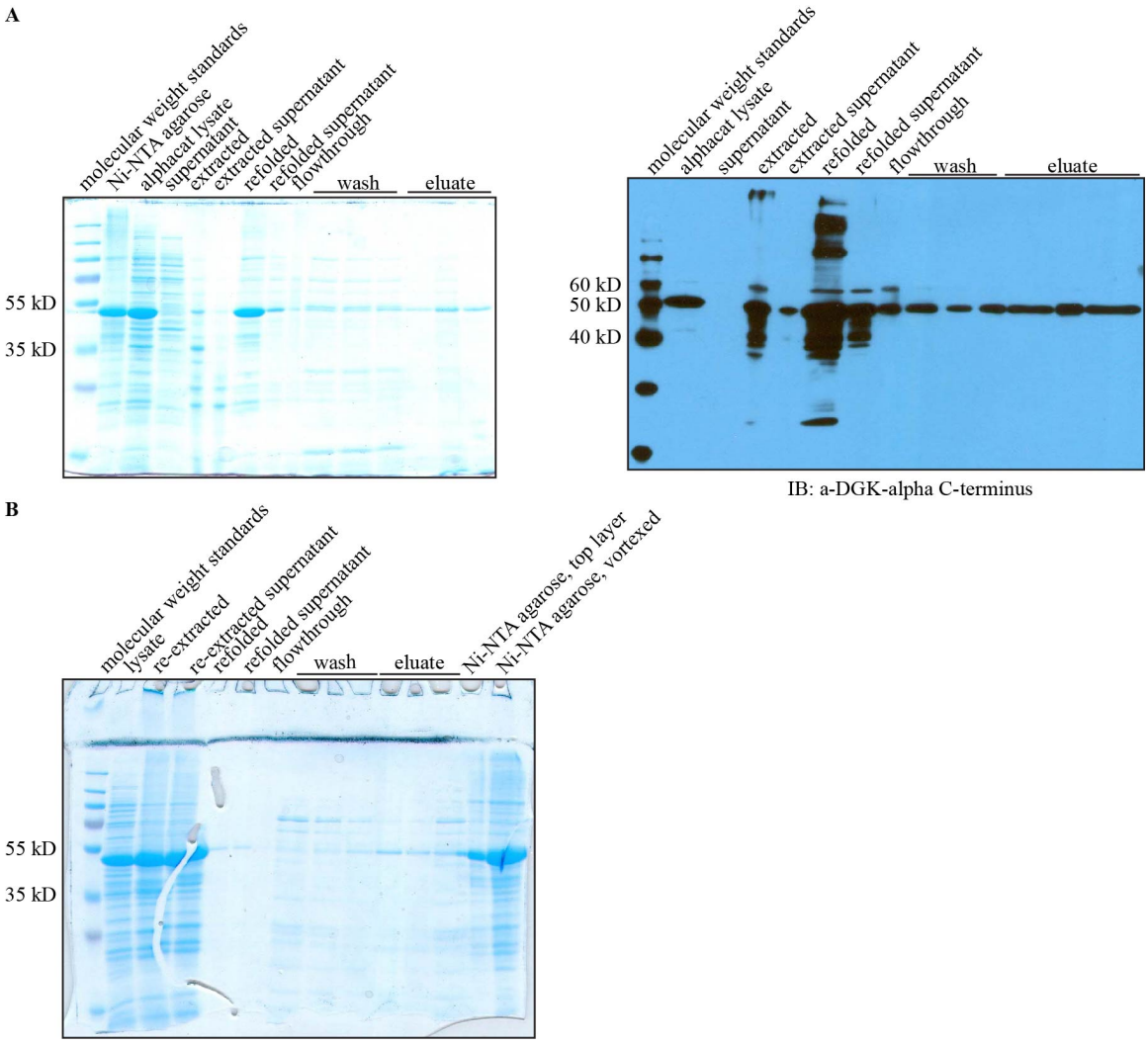

Figure 24. Alphacat in pT71myc, expressed in a one-liter culture of Rosetta™(DE3), extracted from the pellet, and purified on Ni-NTA. I inoculated two 500 mL cultures of LB Kan with an overnight culture of alphacat in pT71myc in Rosetta™(DE3). When the OD600 was predicted to reach 1.0, I added IPTG to 0.5 mM and shook the cultures for 17 hours at 16°C, then pelleted the cells and resuspended in 4 mL per gram wet cell pellet lysis buffer (50 mM HEPES, pH 6.4, 300 mM NaCl, 10 mM imidazole, 5 mM $MgCl_2$, 1 mM $CaCl_2$, 0.5% (v/v) NP-40, 0.5 mM DTT, 1x PIC), and froze at -80°C. I thawed the resuspended cells, shaking gently in room-temperature water, and added egg white lysozyme to 1 mg per mL. I incubated on ice for thirty minutes, then probe-sonicated eleven times for ten seconds each, resting on ice between each pulse. I separated the supernatant from the pellet by centrifuging at 118,000 x *g* for 65 minutes at 4°C. I extracted the pellets with extraction buffer (50 mM HEPES, pH 6.4, 300 mM NaCl, 10 mM imidazole, 5 mM $MgCl_2$, 1 mM $CaCl_2$, 6.8 M guanidine chloride) and probe-sonicated until mostly clear. I removed the insoluble fraction by centrifuging at 118,000 x *g* for 65 minutes at 4°C. I then refolded the extracted alphacat by diluting fifty-fold into loading buffer (50 mM HEPES, pH 6.4, 300 mM NaCl, 10 mM imidazole, 5 mM $MgCl_2$, 1 mM $CaCl_2$, 0.5 mM DTT), and removed the insoluble fraction by centrifuging at 20,000 x *g* for thirty minutes at 4°C. I added Ni-NTA agarose 1:4000 (v/v) and incubated for three days, rocking at 4°C. I washed the resin with wash buffer (50 mM HEPES, pH 6.4, 300 mM NaCl, 70 mM imidazole, 5 mM $MgCl_2$, 1 mM $CaCl_2$, 0.1 mM TCEP), and eluted with elution buffer (same as wash buffer, but imidazole increased to 250 mM). The yield was low, so I re-extracted the same pellets, which had been stored for nine days at -80°C, with extraction buffer, pipetting until all of the pellets had

been resuspended, and probe-sonicating eleven times for 15 seconds each, resting on ice between each pulse. I refolded the extracted alphacat by diluting fifty-fold into loading buffer, and removed the insoluble fraction by centrifuging at 20,000 x *g* for thirty minutes at 4°C. I added Ni-NTA agarose 1:4000 (v/v) and incubated for four days, rocking at 4°C. I washed the resin with wash buffer, and eluted with elution buffer. **(A)** SDS-PAGE of 12% acrylamide gels followed by: left, Coomassie staining; right, immunoblotting against DGK alpha C-terminus (Abgent AP8128b (1:300 (v/v))). **(B)** SDS-PAGE of a 12% acrylamide gel followed by Coomassie staining. After centrifuging the Ni-NTA agarose following purification, I removed the top layer (predicting that it would contain more Ni-NTA agarose and less precipitated protein), and then vortexed it to mix. This figure has been modified from Petro and Raben[1] and is used under CC BY-NC 2.5.

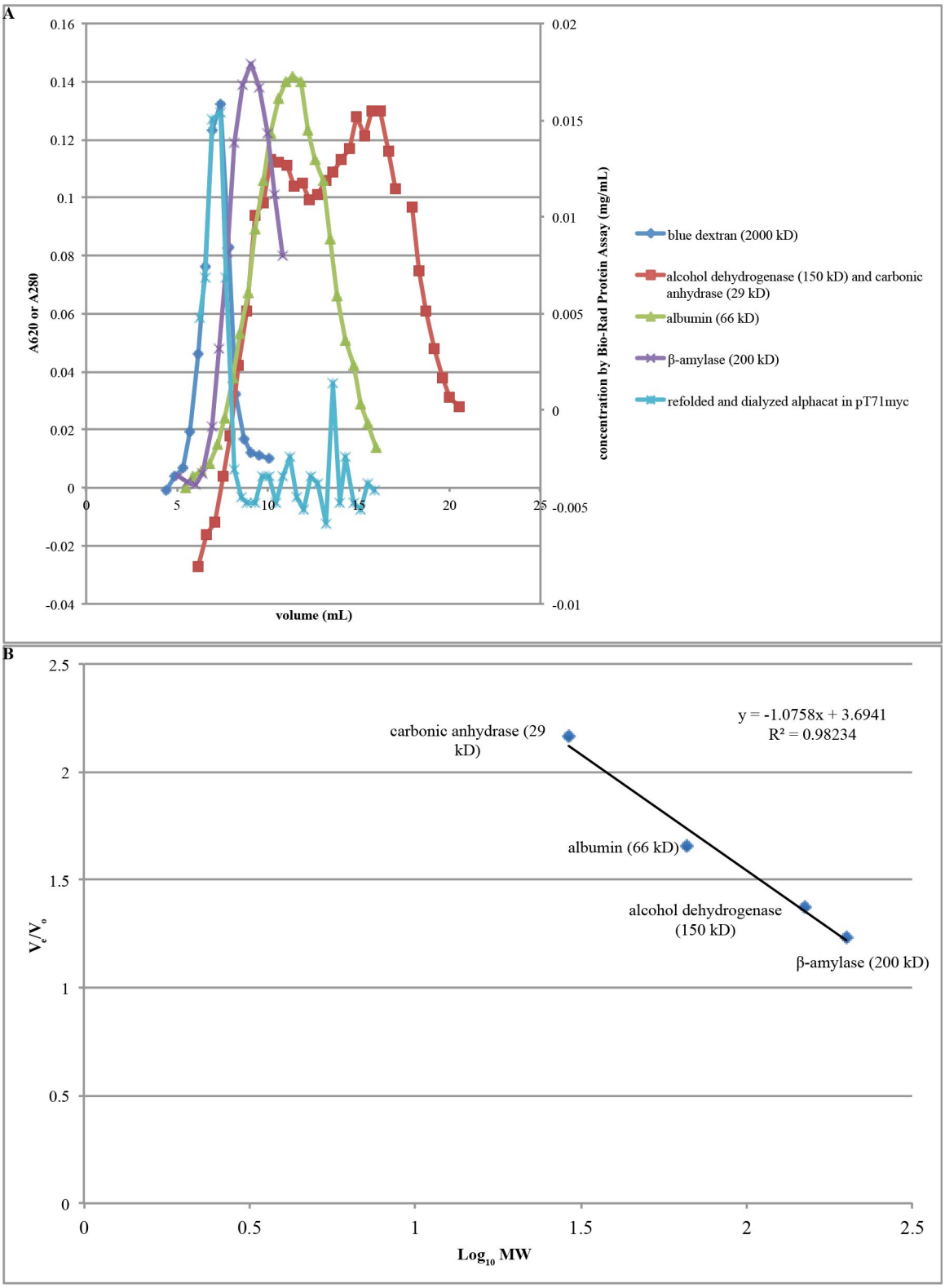

Figure 25. Purified alphacat in pT71myc elutes from a Sephadex® G-200 column in the void volume. I pooled all the eluates from both extractions shown in **Figure 24**, and removed the insoluble fraction by centrifuging at 29,400 x *g* for 2.5 hours at 4°C. The yield was still lower than I would have liked to load

onto the gel filtration column, so I also added all of the washes, and removed the insoluble fraction by centrifuging at 54,900 x *g* for ninety minutes at 4°C. I dialyzed the supernatant against dialysis buffer (55 mM HEPES, 5 mM $MgCl_2$, 1 mM $CaCl_2$, 250 mM imidazole, 15% (w/v) 17.5kD PEG, pH 6.4) using 3500 MWCO dialysis tubing at 4°C for ~twenty total hours, followed by using a 10,000 MWCO dialysis cassette (Thermo Scientific 66383) at 4°C for ~eight hours, until the protein concentration was ~1.2 mg/mL. I removed the insoluble fraction by centrifuging at 43,000 x *g* for ninety minutes at 4°C, and loaded 200 µL of the supernatant onto a Sephadex® G-200 column that had been freshly blocked with 0.9 mL of 10 mg/mL albumin, and had been previously calibrated with blue dextran, alcohol dehydrogenase, carbonic anhydrase, β-amylase, and albumin, and I collected fractions every 110 seconds, eluting by gravity in gel filtration buffer (55 mM HEPES, 5.5 mM $MgCl_2$, 1.1 mM $CaCl_2$, 250 mM imidazole, pH 6.4). **(A)** Elution volumes of molecular weight standards and of purified alphacat from a Sephadex® G-200 column. Left vertical axis, A280 of the protein molecular weight standards, and A620 of the blue dextran fractions. Right vertical axis, protein concentration of eluted alphacat, as measured by the Bio-Rad Protein Assay. **(B)** Calibration of the Sephadex® G-200 column: elution volume (presented as a ratio of the void volume) of the molecular weight standards as a function of logarithm molecular weight. I calculated the linear regression using Microsoft® Excel®. This figure has been modified from Petro and Raben[1] and is used under CC BY-NC 2.5.

Discussion

An alternative explanation is that the alphacat oligomerizes into a complex large enough to elute in the void volume of the Sephadex® G-200 resin. As previously mentioned, other LCB5 proteins have been shown to oligomerize. The smallest of the constructs studied in this report is alphacat in pT71myc, with a molecular weight of 49.8 kD. In order for oligomerized alphacat in pT71myc to be larger than β-amylase (200 kD), in front of which we observe it to elute from the Sephadex® G-200 resin, its oligomerization state would have to be at least that of a pentamer (249 kD). Because the most plausible oligomerization states of alphacat would be either a dimer or else a dimer of dimers, I find the microscopic aggregate hypothesis more convincing.

It was not entirely clear which conditions led to the appearance of a second peak in the analytical gel filtration fractions detectable by immunoblot. 6.4 is below the buffering range of both Tris and HEPES, so it could very well be a pH reproducibility issue. Alternatively, the second peak could have a much higher affinity for the antibody than the peak eluting in the void volume: if the population in the second peak were much smaller than that in the void volume peak, then that would explain why a second peak

would be detectable by immunoblot (Figure 18 - Figure 21), but not by the Bio-Rad Protein Assay (Figure 25).

Conclusions

In conclusion, I was able to express alphacat in pT71myc, but it was mostly insoluble. I was able to extract it from the pellet and purify it by Ni-NTA chromatography, or purify the small amount that was soluble, but in either case it eluted in the void volume on an analytical gel filtration column. Adding imidazole to 250 mM and dropping the pH to 6.4 led to the appearance of a second peak that eluted from the analytical gel filtration column at an elution volume consistent with a molecular weight of ~120-130 kD, which is between the size predicted for a dimer and a trimer. This second peak, while detectable by immunoblotting, was undetectable by the Bio-Rad Protein Assay, suggesting that this population was small compared to that eluting in the void volume. I therefore concluded that the vast majority of the expressed alphacat in pT71myc was forming large aggregates unsuitable for pursuit for x-ray crystallography. Furthermore, the yield of soluble alphacat extracted from inclusion bodies even to load onto the analytical gel filtration column was very low, even though alphacat was expressed in large amounts. I therefore considered strategies to improve the solubility of alphacat.

Cloning, Expression, Purification, and Analytical Gel Filtration of Alphacat in pT71myc Coexpressed with Bacterial Chaperones

Introduction

Coexpression with bacterial chaperones is a commonly used strategy to improve the yield and solubility of recombinantly expressed proteins in *E. coli*[101–103]. In an attempt to improve the solubility of alphacat, I therefore coexpressed it with each of five sets of bacterial chaperones: GroEL/ES, Trigger Factor (TF), GroEL/ES/TF, DnaK/DnaJ/GrpE, and DnaK/DnaJ/GrpE/ClpB.

Results

The chaperone-containing plasmids were provided by Professor Philip Cole's laboratory (Pharmacology and Molecular Sciences, The Johns Hopkins University School of Medicine). In order to verify the identity, insertion of the chaperones into the provided plasmids, and sequence of the shorter chaperones (GroES and GrpE), I designed DNA sequencing primers. The plasmids were unknown, so I designed sequencing primers from within the purported genes. I looked up the genes in *E. coli* on the National Center for Biotechnology Information (NCBI)'s web site[104], went to "Genomic regions, transcripts, and products", and looked up the sequence (in FASTA format) of the Reference Sequence (RefSeq). I then designed sequencing primers with an appropriate length, guanine-cytosine (GC) content, melting temperature (T_m), low predicted tendency to hairpin or self-dimerize, and good site-specificity with the sequence of that chaperone and the other chaperone genes in the same plasmid. For GroEL, the sequencing primers were CCAACGAGGACCAGAACCA and GACTTCCTTGACCATCTGCG; for GroES,

they were GCCGCTGGATGTGAAAGT and CGATGGCTACGGTGTGAAA; for TF, they were TTATCCGCACCAACGAGC and TGCTGCTGGGCGAAGTTA; for DnaJ, they were AGGGTGATTTGCTGTGCC and ATGCCACCTTGCTCAAACG; for DnaK, they were AAGAAGCAGGCGACAAACT and TTTGCGGGTTCGTCACTG; for ClpB, they were TGAACAGCACATTGCCTCG and AATAAAGGACTAACCGAACCCC; and for GrpE, they were CGATGCTGGATGTTGTGCG and TTCACGGGTCTGGGCTTCA. Of these sequencing primers, all except the GroEL forward primer successfully sequenced their chaperone gene targets.

From the generated sequences, I performed a protein-protein Basic Local Alignment Search Tool (BLAST) search[105] to identify GroEL to be from either *Plesiomonas shigelloides* (GenBank: BAE95977.1) or *E. coli* (NCBI Reference Sequence: YP_006093740.1) with at least two nonsynonymous point mutations. (This turned out to be a different GroEL sequence from the one that I had used to design the sequencing primers, which may explain why the forward primer did not successfully sequence.) I likewise identified GroES, TF, DnaK, GrpE, and ClpB to be from *E. coli* (NCBI Reference Sequences NP_290775.1, NP_286178.1, NP_285706.1, NP_417104.1, and NP_289147.1, respectively), and DnaJ to be from either *E. coli* (NCBI Reference Sequence: NP_414556.1) or from *Shigella flexneri* (NCBI Reference Sequence: NP_835756.1). TF had an extra codon in the GroEL/ES plasmid. The molecular weights of the bacterial chaperones are as follows: GroEL = 57.4 kD; GroES, = 10.4 kD; TF = 48.1 kD (or 48.3 kD when in the GroEL/ES plasmid); DnaK = 69.1 kD; DnaJ = 41.1 kD; GrpE = 21.8 kD; ClpB = 95.9 kD. Each chaperone plasmid included a chloramphenicol resistance gene, a T7 promoter, and the *lac* operator (LacO). In a single set, all the

chaperones are encoded in the plasmid in series (but each with their own stop codon) behind a single promoter, with the exception of GroEL/ES/TF, in which case TF follows a second copy of T7/LacO.

The Rosetta™(DE3) strain of *E. coli*, which had been used to express the alphacat in pT71myc above, contains pRARE, a plasmid encoding the tRNAs for codons that are commonly used by eukaryotes but rarely used by *E. coli*. pRARE, however, contains the same antibiotic resistance gene as the plasmid encoding the chaperones; therefore, to be able to select for expression of the chaperones, I switched to the BL21(DE3) strain of *E. coli*. I transformed the alphacat in pT71myc plasmid into BL21(DE3) cells that had been previously transformed with each of the sets of chaperones. Alphacat coexpressed with GroEL, GroES, TF, and DnaK robustly expressed when induced with IPTG, as detected by Coomassie staining after SDS-PAGE (Figure 26). DnaJ, GrpE, and ClpB expression were not detectable by Coomassie staining. To identify which chaperone constructs enhanced solubility of alphacat, they were coexpressed either at 37°C for three hours, or at 16°C overnight. Coexpression of either GroEL/ES or GroEL/ES/TF at 16°C overnight, and to a lesser extent, coexpression of GroEL/ES/TF at 37°C for three hours, resulted in an increase in alphacat detected in the supernatant following centrifugation of the lysate (Figure 26).

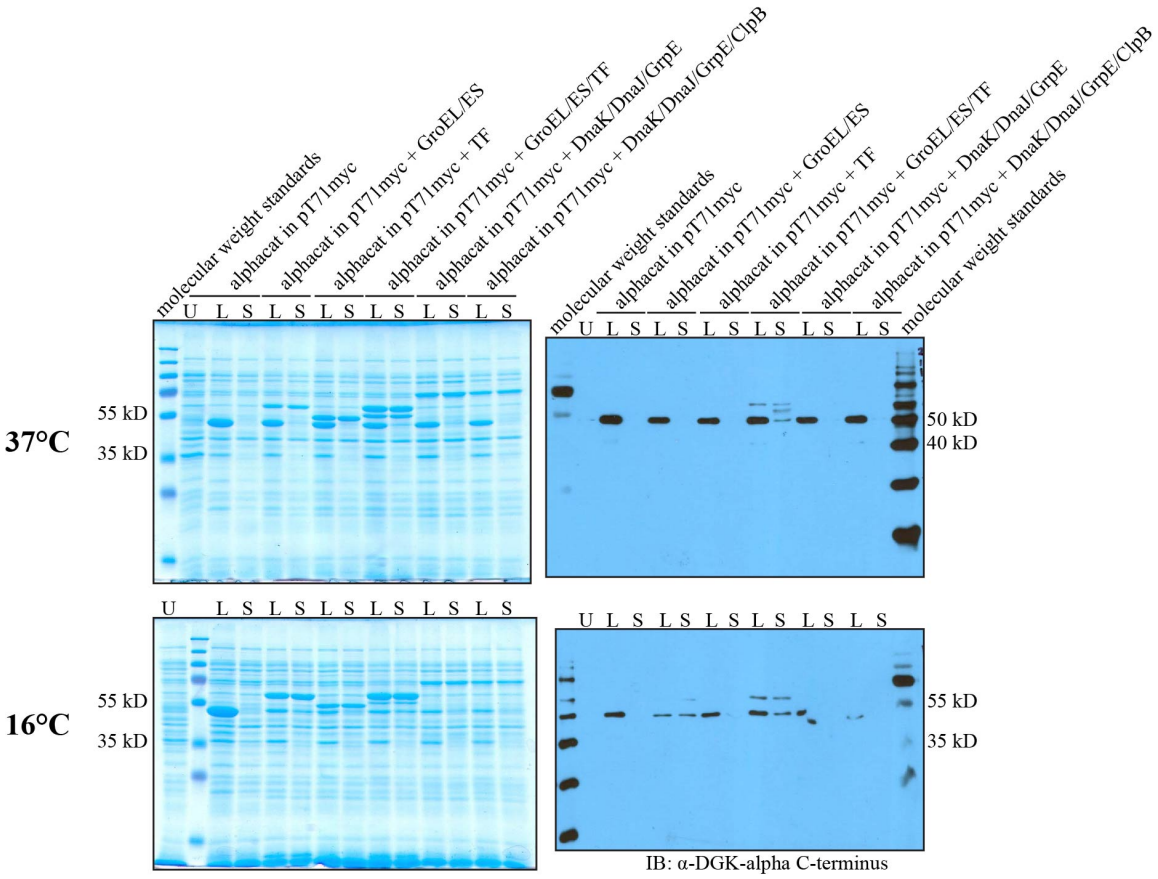

Figure 26. Apparent solubility of alphacat in pT71myc increases when coexpressed with bacterial chaperones. I inoculated 4 mL LB Kan cultures with overnight cultures of alphacat in pT71myc in Rosetta™(DE3), and 4 mL LB Kan Cam cultures with overnight cultures of alphacat in pT71myc cotransformed with each of the sets of chaperones in BL21(DE3). When the OD600 was predicted to reach 0.3, I added IPTG to 0.1 mM and shook the cultures for either three hours at 37°C (top) or 21 hours at 16°C (bottom), then pelleted the cells and resuspended in either 42.7 (for 37°C expression) or 32.3 (for 16°C expression) mL per gram wet cell pellet lysis buffer (50 mM Tris, pH 8.0, 300 mM NaCl, 10 mM imidazole, 1 mM $CaCl_2$, 0.25% (v/v) TX-100, 0.5 mM DTT, 1x PIC), and froze at -80°C. I thawed the cells by gently shaking the tube in room temperature water, added egg white lysozyme to 1 mg per mL, and incubated on ice for thirty minutes. I lysed the cells by probe-sonicating ten times for ten seconds each, resting on ice for fifteen seconds between each pulse. I removed the insoluble fraction by centrifuging at 45,900 x *g* for ninety minutes at 4°C. SDS-PAGE of 12% acrylamide gels followed by: left, Coomassie staining; right, immunoblot against DGK alpha C-terminus; top, induced at 37°C for three hours; bottom, induced at 16°C overnight. U, uninduced; L, lysate; S, supernatant (after removing insoluble from lysate). I loaded 5 µg total protein per lane in the Coomassie-stained gels, and 0.2 µg per lane in the immunoblots. The molecular weights of the bacterial chaperones are as follows: GroEL = 57.4 kD; GroES, = 10.4 kD; TF = 48.1 kD (or 48.3 kD when in the GroEL/ES plasmid); DnaK = 69.1 kD; DnaJ = 41.1 kD; GrpE = 21.8 kD; ClpB = 95.9 kD. This figure has been modified from Petro and Raben[1] and is used under CC BY-NC 2.5.

As can be seen in Figure 26, in addition to the alphacat band, the anti-DGK-alpha antibody recognizes higher-molecular weight bands in the GroEL-containing lanes of the

immunoblots. Because the anti-DGK-alpha antibody recognizes GroEL (Figure 27), I concluded that the 60 kD bands in the immunoblot in Figure 26 are GroEL.

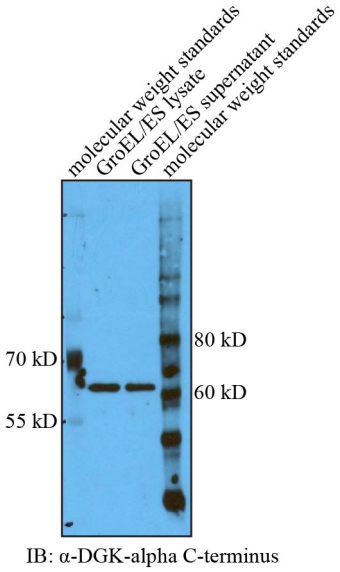

Figure 27. The anti-DGK-alpha C-terminus antibody also recognizes GroEL. SDS-PAGE of an 8% acrylamide gel followed by immunoblotting against DGK alpha C-terminus (Abgent AP8128b (1:300 (v/v))). I loaded 0.2 µg of the lysate, and an equivalent volume of the supernatant. This figure has been modified from Petro and Raben[1] and is used under CC BY-NC 2.5.

I partially purified alphacat coexpressed with GroEL/ES at 16°C overnight by Ni-NTA chromatography. As above, I purified it at pH 6.4, but this time I used sodium citrate to buffer; 6.4 is well within sodium citrate's buffering range, so the pH of these experiments was actually 6.4. GroEL (the upper band) coeluted with alphacat (the lower band) from the Ni-NTA resin (Figure 28). As above, the ~60 kD band is GroEL, and the ~50 kD band is alphacat.

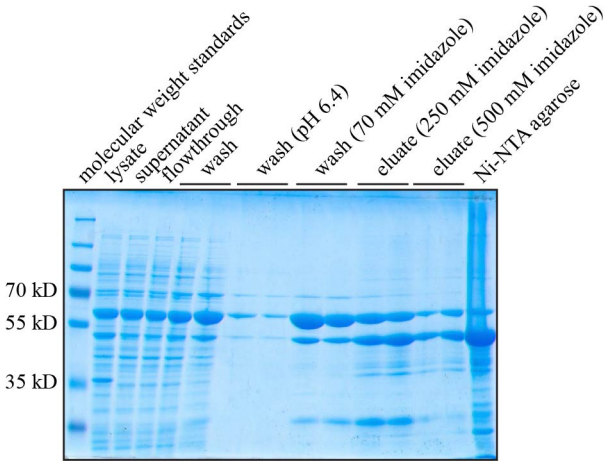

Figure 28. GroEL copurifies with alphacat in pT71myc on Ni-NTA. I inoculated two 500 mL LB Kan Cam cultures with a freshly growing culture of alphacat in pT71myc + GroEL/ES in BL21(DE3). When the OD600 was predicted to reach 0.3, I added IPTG to 0.1 mM and shook the cultures for 14.5 hours at 16°C, then pelleted the cells and resuspended in 4 mL per gram wet cell pellet lysis buffer (50 mM Tris, pH 8.0, 300 mM NaCl, 10 mM imidazole, 1 mM $CaCl_2$, 0.25% (v/v) TX-100, 0.5 mM DTT, 1x PIC), and froze at -80°C. I thawed the cells by gently shaking the tube in room temperature water, added egg white lysozyme to 1 mg per mL, and incubated on ice for thirty minutes, vortexing occasionally to mix. I lysed the cells by probe-sonicating in ten second bursts until no longer viscous. I removed the insoluble fraction by centrifuging at 118,000 x *g* for 65 minutes at 4°C. I added Ni-NTA agarose 1:170 (v/v) to the supernatant and incubated for two hours, rotating at 4°C. I washed the resin with wash buffer 1 (50 mM Tris, pH 8.0, 300 mM NaCl, 10 mM imidazole, 1 mM $CaCl_2$, 0.5 mM DTT), wash buffer 2 (same as wash buffer 1, but replacing the Tris with 55 mM sodium citrate and buffered to pH 6.4), and wash buffer 3 (same as wash buffer 2, but imidazole increased to 70 mM), and eluted with elution buffer 1 (250 mM imidazole) and elution buffer 2 (500 mM imidazole). SDS-PAGE of a 10% acrylamide gel followed by Coomassie staining. I loaded 5 µg of the lysate, equivalent volumes of the supernatant and flowthrough, 5 µg of wash 1 (pH 8.0) and the first wash 3 (70 mM imidazole), and 24 µL of the other washes and eluates. This figure has been modified from Petro and Raben[1] and is used under CC BY-NC 2.5.

When I subjected the Ni-NTA eluate to Sephadex® G-200 size-exclusion chromatography, also buffered to pH 6.4 with sodium citrate, and in the presence of 250 mM imidazole, alphacat and GroEL coeluted in the void volume (Figure 29). Once again, the ~60 kD band is GroEL, and the ~50 kD band is alphacat.

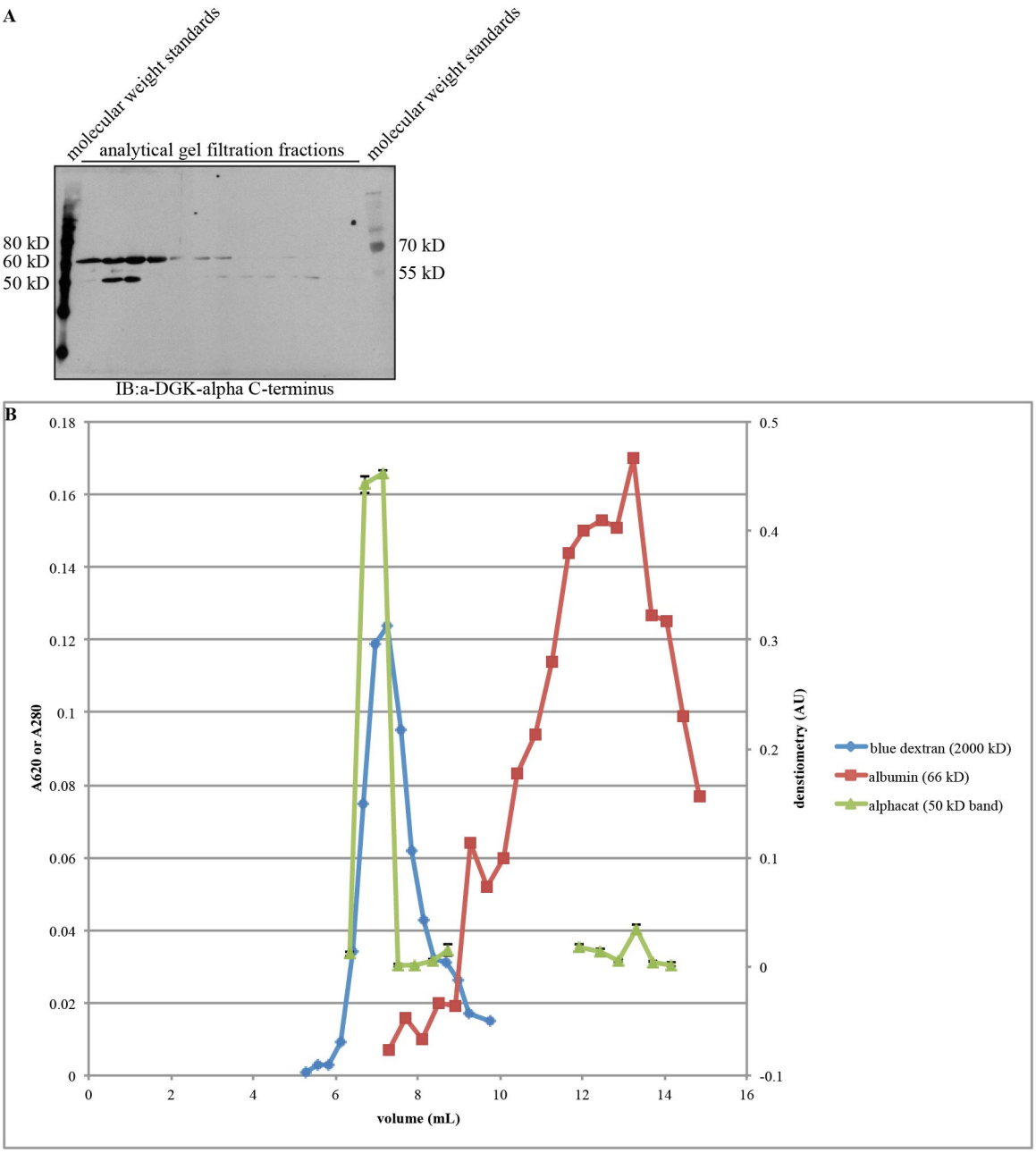

Figure 29. Purified alphacat in pT71myc coexpressed with GroEL/ES elutes from an analytical gel filtration column in the void volume. I pooled the 250 mM imidazole eluates shown in **Figure 28** and removed the insoluble fraction by centrifuging at 43,000 x *g* for ninety minutes at 4°C. I loaded 200 µL of the resulting supernatant onto a Sephadex® G-200 column that had been freshly blocked with 1.07 mL of 10 mg/mL fresh albumin, and had been previously calibrated with blue dextran and albumin, and I collected fractions every 158 seconds, eluting by gravity in gel filtration buffer (55 mM sodium citrate, 5 mM $MgCl_2$, 1 mM $CaCl_2$, 250 mM imidazole, pH 6.4). **(A)** SDS-PAGE of a 10% acrylamide gel followed by immunoblotting against DGK alpha C-terminus (Abgent AP8128b (1:300 (v/v))). I loaded 24 µL per lane of the analytical gel filtration fractions. **(B)** Elution volumes of molecular weight standards and of purified alphacat from a Sephadex® G-200 column. Left vertical axis, A620 of blue dextran elution and A280 of protein standard elutions. Right vertical axis, quantification of the immunoblot signal from the blot shown in (A), mean ± SD. Densitometry of the ~50 kD band was measured three times from the same

film using ImageJ. This figure has been modified from Petro and Raben[1] and is used under CC BY-NC 2.5.

When the partially purified alphacat was subjected to native PAGE as an alternate method to measure monodispersity, it presented a smear (Figure 30), possibly suggesting a population of heterogeneous aggregates, even when coexpressed with chaperones. Adding different detergents to the partially purified protein did not cause it to migrate as a single well-resolved band, but did appear to improve recognition by the antibody. Seeing as the anti-DGK alpha antibody recognizes both alphacat and GroEL, it is unclear of which protein the detergent improved antibody recognition.

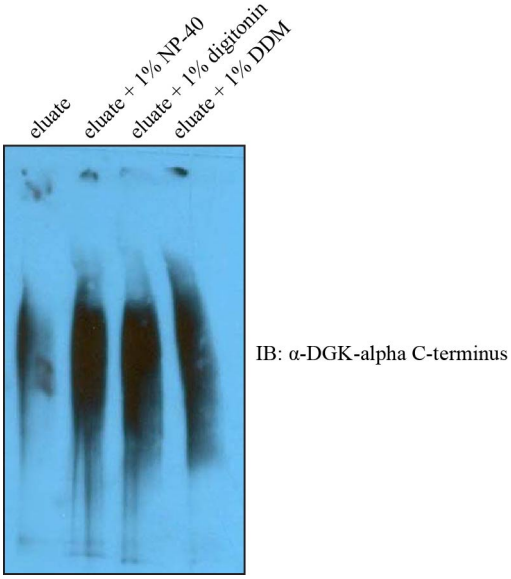

Figure 30. Partially purified alphacat coexpressed with GroEL/ES migrates on native PAGE as a heterogeneous population. I pooled the 250 mM imidazole eluates shown in **Figure 28**, which had been stored for 79 days at 4°C. Native PAGE of a 3-12% acrylamide gradient native gel (Invitrogen™) at 4°C followed by immunoblotting against DGK-alpha (Abgent AP8128b (1:300 (v/v))). DDM: dodecyl-β-D-maltoside.

If the GroEL/ES complex had never released alphacat, it would be predicted to form a complex made of fourteen GroEL monomers and seven GroES monomers, plus the alphacat. This complex would be at least 920 kD in size, which is indeed larger than the ~200-kD void volume of the Sephadex® G-200 resin. 1 mM ATP has been reported

to be sufficient to cause GroEL to release its substrates[106]. To test whether 1 mM ATP would cause GroEL to release alphacat, I lysed and purified alphacat from the co-expressing lysates in the presence of 1 mM ATP. 1 mM ATP has no effect on the Ni-NTA purification of alphacat and GroEL/ES, and GroEL continued to coelute with alphacat from the Ni-NTA resin (Figure 31).

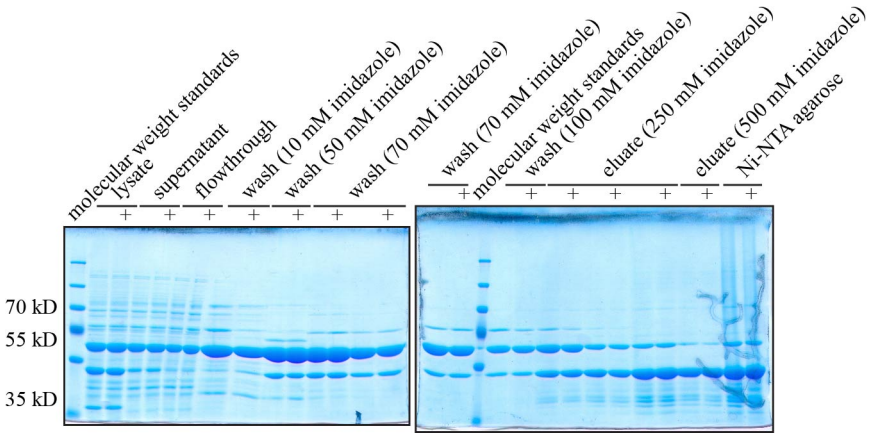

Figure 31. 1 mM ATP has no effect on the purification of alphacat in pT71myc coexpressed with GroEL/ES. I inoculated a 500 mL LB Kan Cam culture with a freshly growing culture of alphacat in pT71myc + GroEL/ES in BL21(DE3). When the OD600 was predicted to reach 0.3, I added IPTG to 0.3 mM and shook the cultures for 17 hours at 16°C, then pelleted the cells and resuspended in 4 mL per gram wet cell pellet lysis buffer (50 mM Tris, pH 8.0, 300 mM NaCl, 10 mM imidazole, 1 mM $CaCl_2$, 0.25% (v/v) TX-100, 0.5 mM DTT, 1x PIC, with or without 1 mM ATP), and froze at -80°C for 19 days. I thawed the cells by gently shaking the tube in room temperature water, added egg white lysozyme to 1 mg per mL, and incubated on ice for thirty minutes, vortexing occasionally to mix. I lysed the cells by probe-sonicating ten times for ten seconds each, resting on ice for fifteen seconds between each pulse. I removed the insoluble fraction by centrifuging at 118,000 x *g* for 65 minutes at 4°C. I added Ni-NTA agarose 1:13 (v/v) to the supernatant without ATP and 1:15 to the supernatant with ATP, and incubated for two hours, rotating at 4°C. I washed the resin with wash buffer 1 (50 mM sodium citrate, pH 6.4, 300 mM NaCl, 10 mM imidazole, 5 mM $MgCl_2$, 1 mM $CaCl_2$, 0.5 mM DTT, with or without 1 mM DTT), wash buffer 2 (same as wash buffer 1, but imidazole increased to 50 mM), wash buffer 3 (70 mM imidazole), and wash buffer 4 (100 mM imidazole), and eluted with elution buffer 1 (250 mM imidazole) and elution buffer 2 (500 mM imidazole). SDS-PAGE of a 10% acrylamide gel followed by Coomassie staining. The lanes marked "+" were purified in the presence of 1 mM ATP. This figure has been modified from Petro and Raben[1] and is used under CC BY-NC 2.5.

I loaded partially purified alphacat onto the Sephadex® G-200 analytical gel filtration column, but when I immunoblotted the analytical gel filtration fractions to determine the elution volume of alphacat, the anti-histidine antibody recognized a ~50 immunoreactive band in the GroEL/ES lysate in addition to the alphacat and analytical

gel filtration columns (Figure 32), suggesting that while casting the gel, the interface between the stacking and separating phases and dried out and the wells' contents had leaked into adjacent wells. As such, the immunoblot is inconclusive (because what may appear to be a preponderance of alphacat in the void volume may just be contamination from the eluate's supernatant lane).

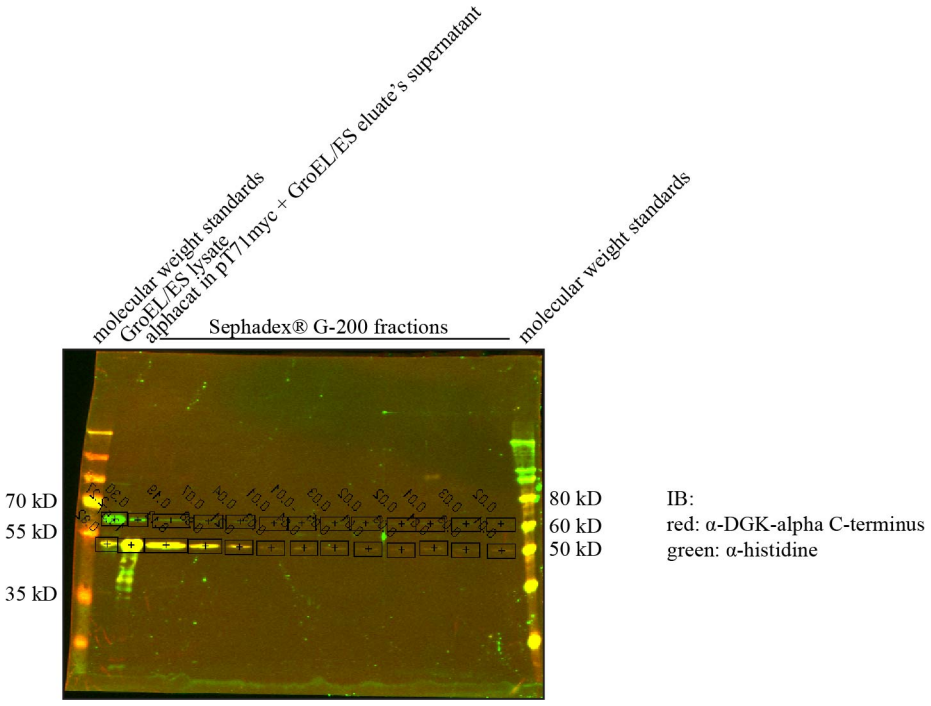

Figure 32. The presence of the 50 kD immunoreactive band in the GroEL/ES lane suggests interwell contamination of the immunoblot of Sephadex® G-200 analytical gel filtration chromatography of partially purified alphacat in pT71myc + GroEL/ES in the presence of 1 mM ATP. I pooled the 250 mM imidazole eluate in the presence of 1 mM ATP, shown in **Figure 31**, and removed the insoluble fraction by centrifuging at 61,400 x *g* for one hour at 4°C. I loaded 200 µL of the resulting supernatant onto a Sephadex® G-200 column that had been freshly blocked with 0.91 mL of 10 mg/mL fresh albumin, and had been previously calibrated with blue dextran, albumin, and β-amylase, and I collected fractions every 260 seconds, eluting by gravity in gel filtration buffer (50 mM Tris, 300 mM NaCl, 5 mM $MgCl_2$, 1 mM $CaCl_2$, 250 mM imidazole, pH 8.0). SDS-PAGE of a 10% acrylamide gel, followed by immunoblotting against DGK-alpha (Abgent AP8128b (1:300 (v/v))) (red) and histidine (BD Biosciences 631212 (1:5000 (v/v))) (green). Yellow indicates red/green overlay. The ~60 kD band is GroEL; the ~50 kD band is alphacat. The boxes and numbers were produced by the Odyssey® v3.0 software.

Discussion and Conclusions

To summarize, coexpressing alphacat in pT71myc with bacterial chaperones increased its yield in the soluble fraction (Figure 26), which is promising for large-scale

expressions for crystallography. Unfortunately, alphacat in this soluble fraction still eluted in the void volume during analytical gel filtration chromatography (Figure 29). One reason that alphacat coexpressed with GroEL/ES eluted in the void volume could be explained by its being complexed to the GroEL, based on our evidence that the two proteins copurify on Ni-NTA (Figure 28 and Figure 31), and they coelute from the analytical gel filtration column (Figure 29). If the alphacat is in fact complexed with GroEL/ES, the predicted molecular weight of the complex would be greater than 900 kD, and thus would indeed be predicted to elute in the void on the Sephadex® G-200 column. Lysis and purification in the presence of 1 mM ATP was apparently insufficient to cause the GroEL to release alphacat (Figure 31). Another possibility is that while coexpressing alphacat with bacterial chaperones was sufficient to increase its yield in the supernatant, alphacat still remained in microscopic aggregates. As such, I decided to pursue other constructs for expressing soluble alphacat for the purpose of x-ray crystallography.

Cloning and Expression of Full-Length DGK-Alpha in pT71myc

Introduction

In order to know whether bacterially expressed alphacat was properly folded, I needed to demonstrate that it had calcium-independent enzymatic activity[49]. As a positive control, I needed a source of full-length DGK-alpha that demonstrated calcium-dependent enzymatic activity. I therefore set out to express full-length DGK-alpha. Because the pT71myc construct robustly expressed alphacat, I tested whether I could use the pT71myc plasmid to express full-length *S. scrofa* DGK-alpha in *E. coli*.

Results

In order to clone full-length *S. scrofa* DGK-alpha into pT71myc, I designed primers to add restriction digest sites, via the polymerase chain reaction (PCR), on either side of DGK-alpha. PCR is a method used to amplify a short section of DNA[107]: by adding desired features via the primers, the amplified DNA will include those features. I designed the forward primer, GTAAGTCGACATCCAAGGAGAGGGGG, to add a SalI restriction site just N-terminal to DGK-alpha. SalI is an enzyme from *Streptomyces albus* that cuts DNA at a particular sequence (GTCGAC)[108]: if that site has been added, the enzyme will cut the DNA at that sequence on both strands (because the site is palindromic), leaving a sticky end, which can be ligated to another sticky end left at another digested SalI site. By digesting and ligating, therefore, pieces of DNA can be cut and pasted together at particular places. Following the SalI site, the primer included a single nucleotide to make sure that DGK-alpha would be in the appropriate reading frame in pT71myc. I included a four-nucleotide overhang in front of the restriction site to improve the efficiency of the digestion of the PCR product[109], and I chose the nucleotide content of the overhang both to provide a GC anchor to the end of the PCR product, as well as to keep the overall GC content of the primer below 60%. I designed the reverse primer, GCAGCGGCCGCTCAGCACAAGAAGCCAAAGAAATTG, to add a NotI (a restriction enzyme from *Nocardia otitidis-caviarum*[110]) site immediately C-terminal to DGK-alpha's stop codon, along with a three-nucleotide overhang including a GC anchor. The PCR product from using these primers, however, produced only a short insert, not the entire *S. scrofa* DGK-alpha gene.

To improve PCR product quality, I therefore designed a new forward primer, GTAAGTCGACATCCAAGGAGAGGGGGCTGATAAG, which increased the length of the homologous region of the primer from fifteen to twenty-three nucleotides, increased the predicted melting temperature (T_m) of the primer from 61.9°C to 64.3°C (so that it was now within 5°C of the T_m of the reverse primer, 68.9°C), and decreased the GC content from 57.7% to 52.9%. This primer, in conjunction with the same reverse primer, successfully generated the proper PCR product, and incorporation of the DGK-alpha insert in the PCR product was confirmed by DNA sequencing.

The pT71myc vector added the same N-terminal fusion tag to DGK-alpha as described above for the alphacat construct, consisting of a hexahistidine, a thrombin proteolytic site, a myc tag, and a TEV protease site (Figure 33). The total mass of this protein construct (including the fusion tag) and the pI are predicted to be 87.5 kD and 6.10 respectively.

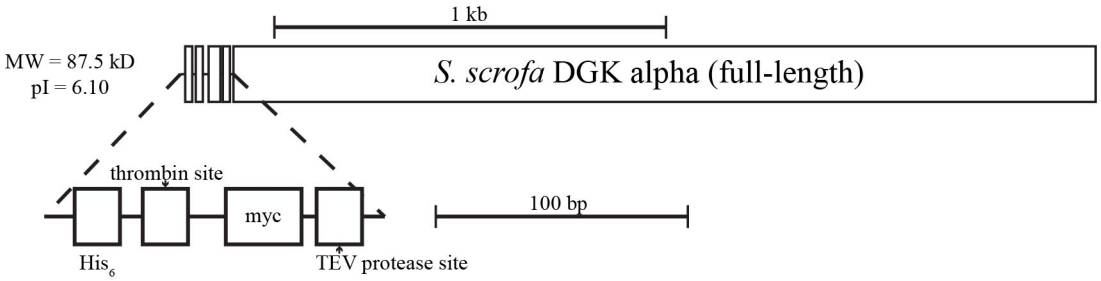

Figure 33. Schematic of the full-length DGK-alpha in pT71myc construct. Top, schematic of full-length *S. scrofa* DGK alpha in pT71myc. Bottom, a magnification of the epitope tag region of alpha in pT71myc. pT71myc adds to the N-terminus of the protein a fusion tag consisting of a hexahistidine, a thrombin proteolytic site, a myc tag, and a TEV protease site. The total mass of this protein construct (including the fusion tag) and pI are predicted to be 87.5 kD and 6.10, respectively. The epitope-tagged region of the construct is magnified for clarity. This figure has been modified from Petro and Raben[1] and is used under CC BY-NC 2.5.

When I transformed full-length DGK alpha in pT71myc into the BL21(DE3) strain of *E. coli*, it expressed readily following induction with IPTG, producing a band,

easily detectable by Coomassie staining following SDS-PAGE, that migrated between the 70 kD and 100 kD molecular weight markers, consistent with the predicted size of 87.5 kD, and was recognized by an anti-histidine antibody on immunoblots (Figure 34), consistent with its expressing the epitope tag, as expected. This construct, however, as alphacat in pT71myc did, also produced insoluble protein: when the bacterial lysate was centrifuged, the protein remained in the pellet.

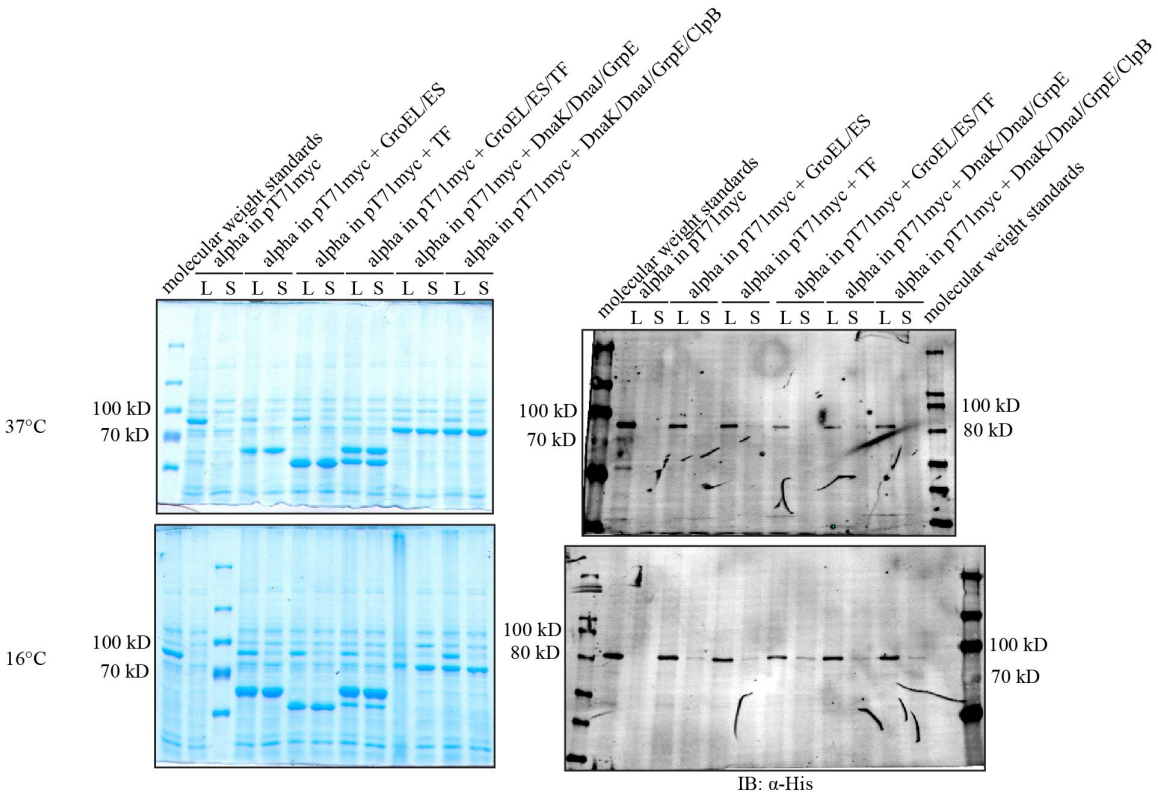

Figure 34. Full-length DGK alpha in pT71myc expressed a band of the correct size that was recognized by the anti-histidine antibody, and its apparent solubility increases when coexpressed with bacterial chaperones. I inoculated two 4 mL LB Kan cultures with a freshly growing culture of full-length DGK-alpha in pT71myc in BL21(DE3), and two 4 mL LB Kan Cam cultures each with freshly growing culture of full-length DGK-alpha in pT71myc transformed into BL21(DE3) previously transformed with each of the sets of chaperones. When the OD600 was predicted to reach 0.4, I added IPTG to 0.5 mM and shook the cultures either for three hours at 37°C or 15.5 hours at 16°C, then pelleted the cells and stored at -80°C overnight. I resuspended each cell pellet in 1 mL lysis buffer (50 mM Tris, pH 8.0, 300 mM NaCl, 10 mM imidazole, 5 mM $MgCl_2$, 1 mM $CaCl_2$, 0.25% (v/v) TX-100, 0.5 mM DTT, 1x PIC), and added egg white lysozyme to 1 mg per mL, and incubated on ice for thirty minutes, vortexing occasionally to mix. I lysed the cells by probe-sonicating ten times for ten seconds each, resting on ice for fifteen seconds between each pulse. I removed the insoluble fraction by centrifuging at 54,900 x *g* for 65 minutes at 4°C. SDS-PAGE of 8% acrylamide gels followed by: left, Coomassie staining; right,

immunoblotting against hexahistidine (BD Biosciences 631212 (1:5000 (v/v))); top, induced at 37°C for three hours; bottom, induced at 16°C overnight. L, lysate; S, supernatant (following removal of the insoluble fraction from the lysate). This figure has been modified from Petro and Raben[1] and is used under CC BY-NC 2.5.

In order to determine whether any of the sets of chaperones could improve this construct's solubility, I coexpressed DGK-alpha in pT71myc and each of the sets of chaperones either at 37°C for three hours or at 16°C overnight. At 16°C, coexpression of each of the sets of plasmids increased the amount DGK-alpha detected in the supernatant following centrifugation (Figure 34). The set that increased the amount to the greatest extent was GroEL/ES/TF, but even in this case, most of the protein remained in the pellet (Figure 34).

In order to determine the best induction conditions for full-length DGK-alpha coexpressed with GroEL/ES/TF, and in order to produce fresh enzyme with which to test its enzymatic activity, I grew a single culture of DGK-alpha in pT71myc coexpressed with GroEL/ES/TF, and removed aliquots at different OD600s and added IPTG to different concentrations, and induced at 16°C overnight. The induction conditions that produced the most soluble DGK-alpha appeared to be inducing at OD600 of 0.5 and an IPTG concentration of 0.5 mM (Figure 35).

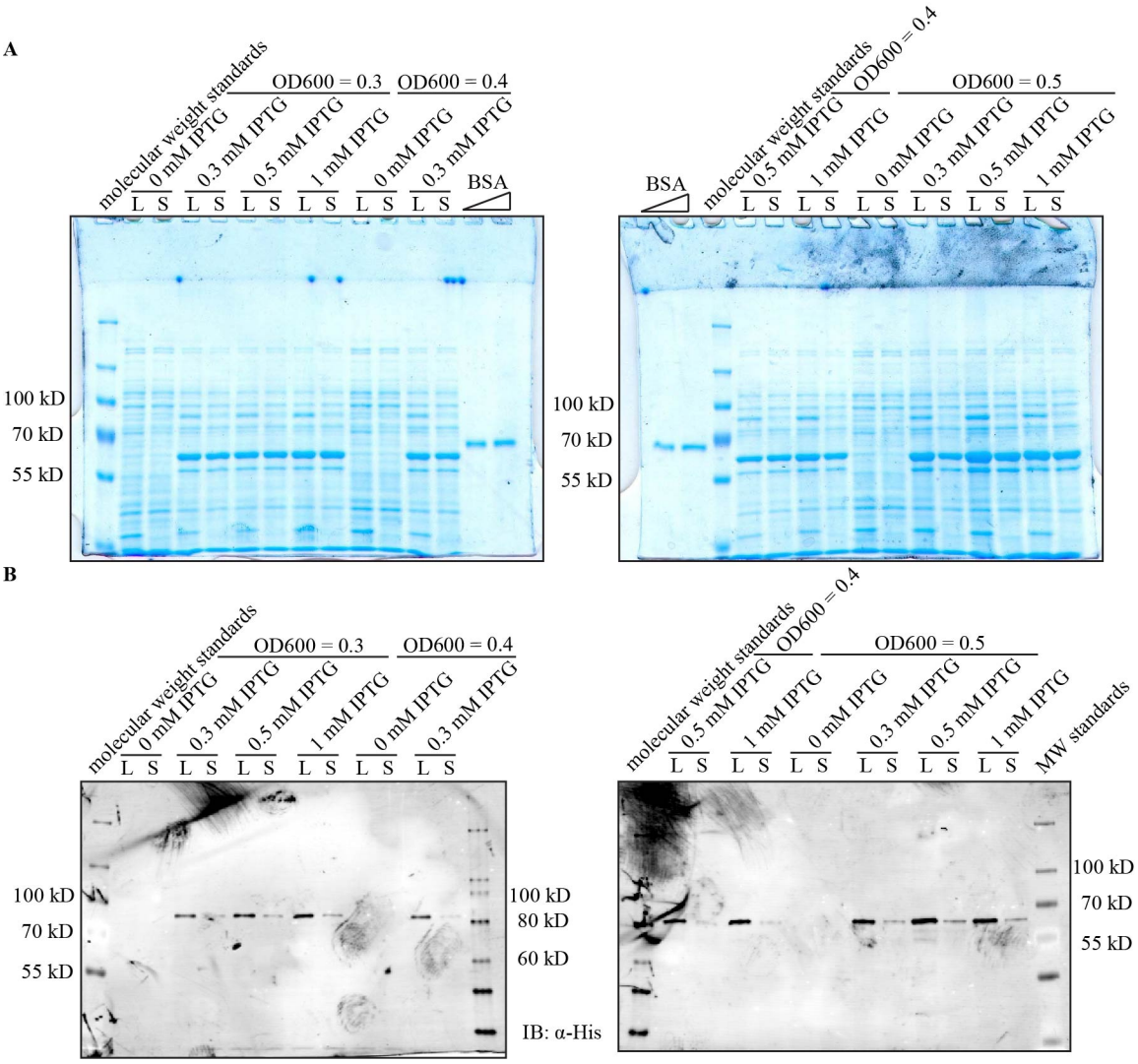

Figure 35. Induction test of full-length DGK-alpha in pT71myc coexpressed with GroEL/ES/TF. I inoculated a 78.5 mL LB Kan Cam cultures each with freshly growing culture of full-length DGK-alpha in pT71myc plus GroEL/ES/TF in BL21(DE3). When the OD600 was predicted to reach the indicated values, I removed 4 mL aliquots, added IPTG to the indicated concentration, and shook the cultures overnight at 16°C, then pelleted the cells and froze at -80°C. I resuspended each cell pellet in 666 µL lysis buffer (50 mM Tris, pH 8.0, 300 mM NaCl, 10 mM imidazole, 5 mM $MgCl_2$, 1 mM $CaCl_2$, 0.25% (v/v) TX-100, 0.5 mM DTT, 1x PIC), and added egg white lysozyme to 1 mg per mL, and incubated on ice for thirty minutes, vortexing occasionally to mix. I lysed the cells by probe-sonicating ten times for ten seconds each, resting on ice for fifteen seconds between each pulse. I removed the insoluble fraction by centrifuging at 71,700 x *g* for 90 minutes at 4°C. SDS-PAGE followed by **(A)** Coomassie staining and **(B)** immunoblotting against histidine (BD Biosciences 631212 (1:5000 (v/v))). The membranes had been previously probed with an older aliquot of primary antibody, then stripped using NewBlot™ PVDF Stripping Buffer. I redeveloped the membranes to check that the signal from the primary decreased, then reblocked and proceeded with a fresh aliquot of primary antibody.

When I tried to assay the activity of these lysates, however, the liposomes I produced for the assay were bad, for reasons that I never clearly identified. By the time

the liposome situation had resolved itself (possibly in part due to a retuned bath sonicator), I had used up the aliquots of DGK-alpha in pT71myc coexpressed with GroEL/ES/TF induced at OD600 of 0.5 and an IPTG concentration of 0.5 mM (the conditions that appeared to produce the most soluble DGK-alpha (Figure 35)) that had been stored in 50% glycerol at -80°C. When I assayed the supernatant that had been induced at OD600 of 0.5 and an IPTG concentration of 1 mM, although the sample did show greater DGK activity than the uninduced supernatant, and although this activity was EGTA-dependent (as would be predicted for full-length DGK-alpha), the additional measured DGK activity was very low.

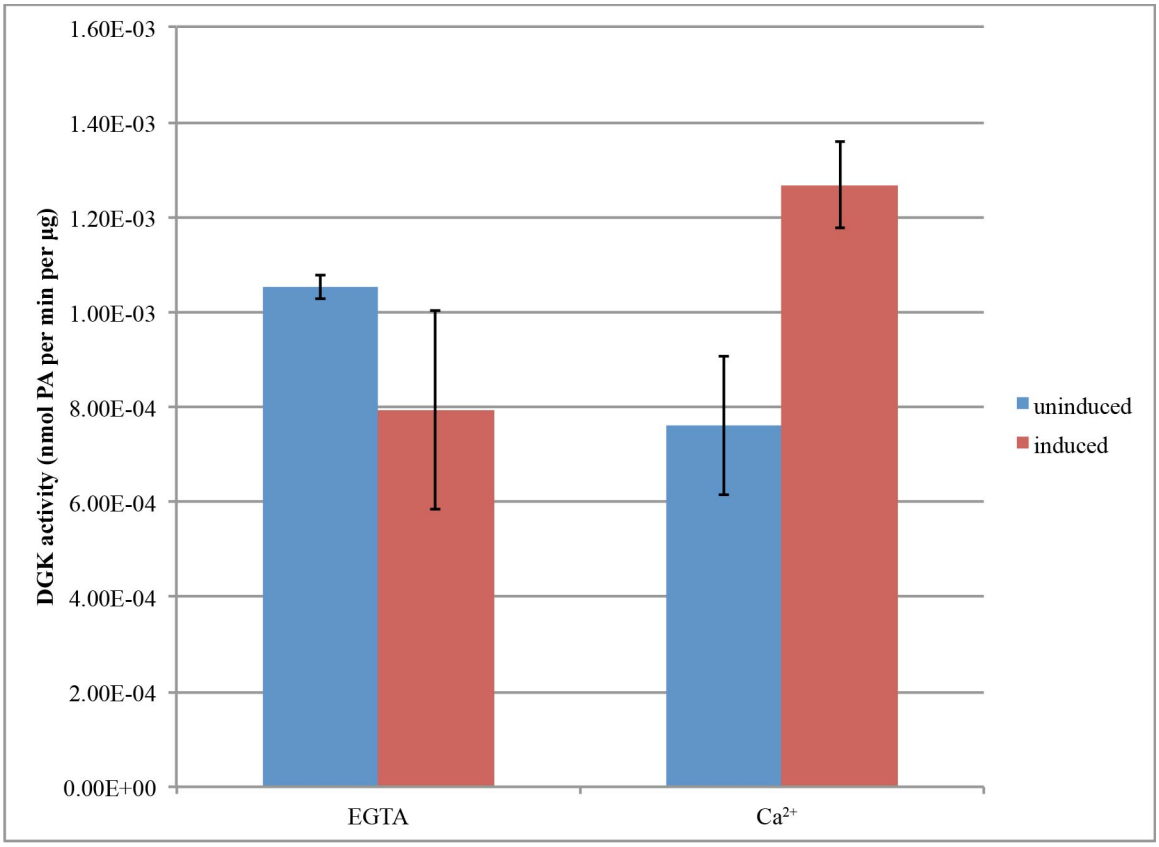

Figure 36. Full-length DGK-alpha in pT71myc has low but measurable and Ca^{2+}-dependent DGK activity. DGK activity assay of the supernatant of full-length DGK-alpha coexpressed with GroEL/ES/TF, induced at an OD600 of 0.5 with 1 mM IPTG, shown in **Figure 35**. The uninduced sample was aliquoted and moved to the 16°C shaker at an OD600 of 0.4 (because I had used up the aliquots of the uninduced at an OD600 of 0.5 while troubleshooting the liposomes). I stored the samples in 50% glycerol (v/v) at -80°C

for twenty days prior to assaying. The reaction included 40 ng per μL protein (as measured by the Bio-Rad Protein Assay), 5 mM liposomes (53:22:17:8::POPE:POPC:POPS:DOG), 2.5 mM Tris, 102.5 mM NaCl, 0.5 mM imidazole, 2.35 mM $MgCl_2$, 0.225 mM $CaCl_2$, 0.0125% (v/v) Triton X-100, 0.05x PIC, 1 mM DTT, 5% (v/v) glycerol, 43.75 mM 3-(N-morpholino)propanesulfonic acid (MOPS), pH 7.1, 1 mM ATP, and 52.3 Ci per mmol [γ-^{32}P]-ATP. The sample marked "EGTA" also included 0.875 mM EGTA, and $MgCl_2$ increased to 2.46, for a predicted concentration of 0.9 mM MgATP and 0.2 μM free Ca^{2+}[111]. The reaction proceeded for 15 minutes at 30°C. In triplicate, mean ± SD.

Discussion and Conclusions

At this point, my strategy was to compare the properties of alphacat and full-length DGK-alpha, which meant that I needed "good" full-length DGK-alpha. My criterion for determining whether DGK-alpha was "good" was whether it showed Ca^{2+}-dependent activation[36]. Because the enzymatic activity of full-length DGK-alpha in pT71myc was so low, I decided to pursue other constructs that might improve the expression of soluble full-length DGK-alpha.

Expressing and Purifying Epsiloncat in pT71myc

Introduction

I thought perhaps the catalytic domain of another eukaryotic DGK might express more solubly than alphacat, and therefore decided to try to express the catalytic domain of *H. sapiens* DGK-epsilon in pT71myc, the same plasmid that had robustly expressed alphacat.

Results

The epsiloncat construct consists of residues 201-567 of *H. sapiens* DGK-epsilon. This construct was cloned into the plasmid pT71myc, which adds to the N-terminus of the protein a fusion tag consisting of hexahistidine, a thrombin proteolytic site, a myc tag, and a TEV protease site. The total mass of this protein construct (including the fusion tag) and pI are predicted to be 45.2 kD and 5.97, respectively. I could induce the

expression of epsiloncat in Rosetta™(DE3) by adding IPTG to the growth medium. When compared to uninduced control, the induced lysate expressed an additional band, easily detectable by Coomassie staining, that migrated between the 35 kD and 55 kD molecular weight standards during SDS-PAGE, consistent with the predicted size of the fusion protein of 45.2 kD (Figure 37**A**). This band was also recognized by an anti-histidine antibody (Figure 37**B**), an anti-DGK-epsilon antibody (Figure 37**C**), and an anti-myc antibody (Figure 37**D**) on immunoblots, consistent with its expressing in frame and with the proper epitope tags. In fact, the anti-DGK-epsilon antibody and the anti-myc antibody recognized multiple bands in the induced, but not the uninduced lysate. These multiple bands might be a result of ribosome pausing, frameshifts, deletions, mistranslations, or aborted translation products. Rosetta™(DE3) contains the pRARE plasmid, but it may not have been maintained during this expression, because the bacteria were cultured in the absence of Cam. The cDNA of epsiloncat does in fact include a number of rare codons: three AGG, three AGA, seven CTA, five ATA, five CGA, three CCC, and seventeen GGA.

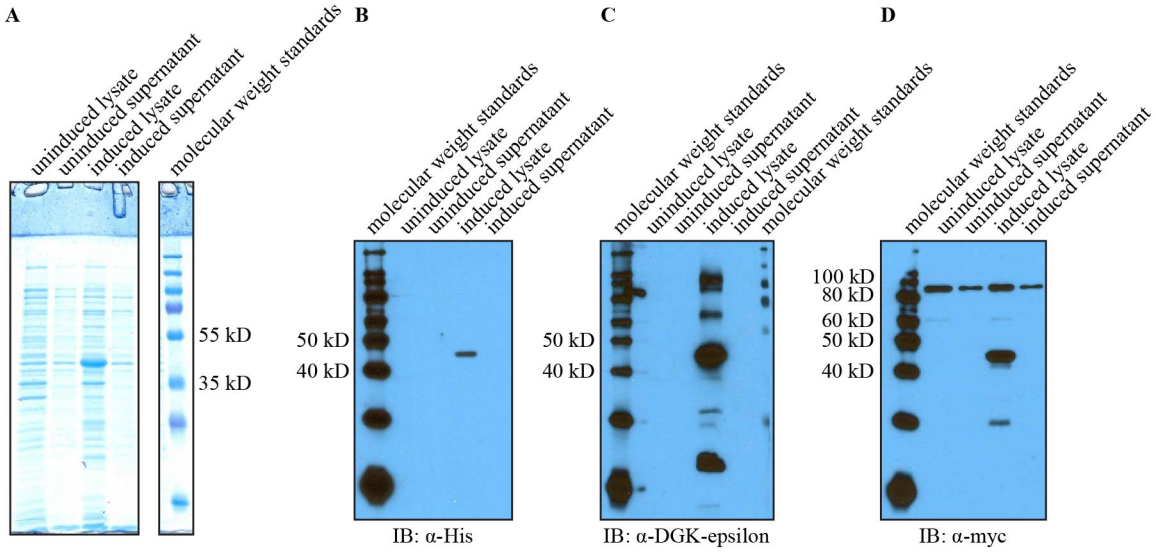

Figure 37. Epsiloncat in pT71myc expresses when induced by IPTG, is of the appropriate size, and is recognized by anti-histidine, DGK-epsilon, and myc antibodies. I inoculated two 50 mL LB Kan cultures each with an overnight culture of epsiloncat in pT71myc in Rosetta™(DE3). When the OD600 was predicted to reach 1.0, I added IPTG to 0.5 mM, and shook the cultures for 21 hours at 15°C, then pelleted the cells. I resuspended each cell pellet in 4 mL per gram wet cell pellet lysis buffer (50 mM Tris, pH 8.0, 300 mM NaCl, 10 mM imidazole, 5 mM $MgCl_2$, 1 mM $CaCl_2$, 0. 5% (v/v) NP-40, 0.5 mM DTT, 1x PIC, 10 U per mL DNAse I, and 1 mg per mL egg white lysozyme), and incubated on ice for thirty minutes. I lysed the cells by probe-sonicating three times for ten seconds each, resting on ice for ten seconds between each pulse. I removed the insoluble fraction by centrifuging at 115,000 x *g* for 90 minutes at 4°C. SDS-PAGE of 12% acrylamide gels followed by **(A)** Coomassie staining, **(B)** immunoblotting against His_6 (abcam® ab6196 (1:2500 (v/v))), **(C)** immunoblotting against DGK-epsilon (1:2000 (v/v)), and **(D)** immunoblotting against myc (abcam® ab9106 (1:250 (v/v))).

Because the bacteria had appeared to not entirely lyse, I re-lysed the pellets and purified the supernatant on Ni-NTA (Figure 38). Even when the cells are entirely lysed, most of the epsiloncat remains in the pellet. However, the small amount of epsiloncat that partitions into the supernatant can be enriched on Ni-NTA.

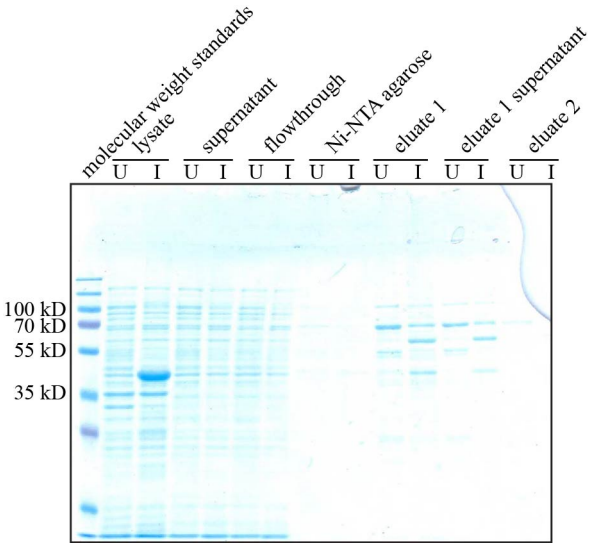

Figure 38. Epsiloncat in pT71myc is mostly insoluble, but the small portion that is soluble can be enriched on Ni-NTA. I re-lysed the pellets shown in **Figure 37**, which had been stored at -80°C for eleven days, by adding another 4 mL per gram original cell pellet lysis buffer, incubating on ice for thirty minutes, and probe-sonicating in ten-second bursts, resting on ice for ten seconds between each burst, until no longer viscous. I removed the insoluble fraction by centrifuging at 43,000 x *g* for ninety minutes at 4°C. I added Ni-NTA agarose 1:4 (v/v) to the supernatant and incubated overnight, rotating at 4°C. I washed the resin with wash buffer 1 (50 mM Tris, pH 8.0, 300 mM NaCl, 10 mM imidazole, 1 mM $CaCl_2$, 0.5 mM DTT) and wash buffer 2 (same as wash buffer 1, but imidazole increased to 20 mM), and eluted with elution buffer (250 mM imidazole). SDS-PAGE followed by Coomassie staining. I tore the gel following electrophoresis such that most of the rightmost lane (induced eluate 2) was missing. U, uninduced; I, induced.

Although the epsiloncat was soluble after purification on Ni-NTA in that it remained in the supernatant after ultracentrifugation, it eluted in the void volume when loaded onto a Sephadex® G-150 column (Figure 39). (I am uncertain why the uninduced eluate 1 supernatant shows immunoreactivity to the anti-DGK-epsilon antibody in this immunoblot while the uninduced lysate shows no immunoreactivity in Figure 37. This immunoblot used a dilution of the same antibody aliquot (which means the antibody was older), and a shorter incubation time for the secondary antibody, which should produce less, not more, sensitivity. If the interface between the stacking and separating phases dried out and caused interwell contamination from the induced eluate 1 supernatant lane, I would expect immunoreactivity in the lane to the right as well, when there is none. One

possibility is that the immunoreactive band is a background band from *E. coli* that also migrates between the 40 and 50 kD molecular weight standards that was enriched by Ni-NTA and therefore not seen in the lysate, in which case the protein that elutes in the void volume could be this background band and not epsiloncat after all. However, because a band of the right size was seen differentially in the induced vs. uninduced samples in Figure 38 (suggesting that epsiloncat is indeed present and enriching in Ni-NTA), and because the induced lysate was recognized by the antibody differentially in Figure 37 (suggesting that the anti-DGK-epsilon antibody recognizes epsiloncat), the appearance of a background band of the correct size dominating antibody recognition seems unlikely. The most likely explanation is that some of the induced eluate 1 supernatant overflowed from the well into the well to the left (and not to the right) while I loaded the gel. If that is the case, that should not impact the interpretation that the enriched epsiloncat eluted from the analytical gel filtration column in the void volume.) I therefore deemed epsiloncat in pT71myc unsuitable for pursuit for x-ray crystallography.

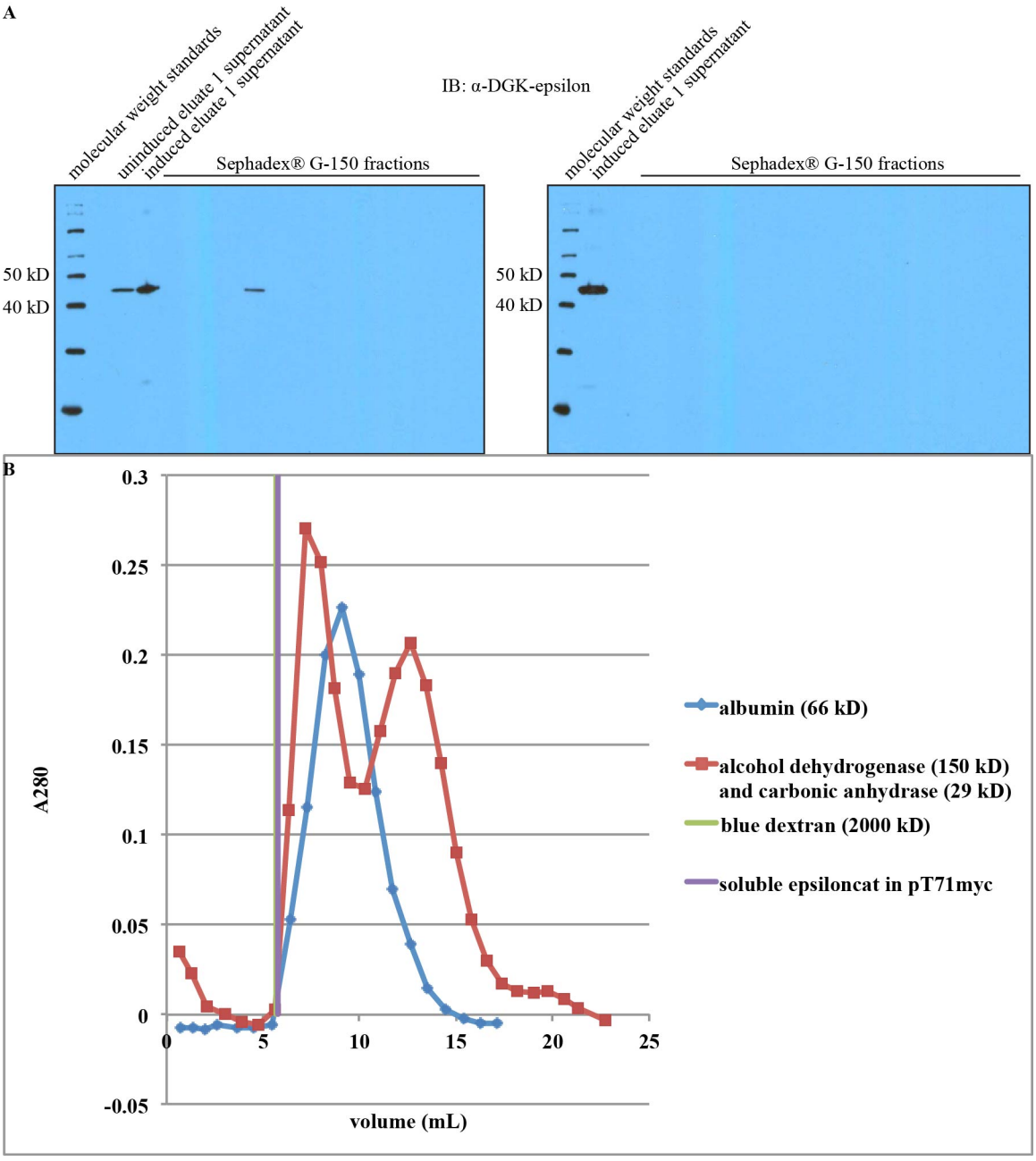

Figure 39. Soluble epsiloncat elutes from Sephadex® G-150 in the void volume. I loaded 200 µL of eluate 1's supernatant (shown in **Figure 38**) onto the same Sephadex® G-150 column shown in **Figure 16**, and collected fractions every 260 seconds, eluting by gravity in gel filtration buffer (55 mM HEPES, 5.5 mM $MgCl_2$, 1.1 mM $CaCl_2$, pH 8.0). **(A)** SDS-PAGE followed by immunoblotting against DGK-epsilon (1:4000 (v/v)). I loaded the gel filtration fractions of elution volumes corresponding to molecular weights of 336 to 3.9 kD. **(B)** The elution of molecular weight markers as a function of elution volume. I detected the elution of the proteins standards by measuring the A280 of the gel filtration fractions. A vertical line marks the volume of the fraction that appeared bluest during blue dextran elution: this is the void volume. A vertical line also marks the volume of the fraction with the greatest anti-DGK-epsilon detection from the immunoblot shown in (A).

Conclusions

Because the enriched epsiloncat in pT71myc eluted from the Sephadex® G-150 column in the void volume, I concluded that epsiloncat in pT71myc was unsuitable for pursuit for x-ray crystallography.

Cloning, Expression, Purification, and Analytical Gel Filtration of Alphacat in pGEX-4T2 Coexpressed with Bacterial Chaperones

Introduction

Translational folding partners have been reported to improve the solubility of proteins expressed in *E. coli*[112–115]. In addition to being a useful epitope tag for affinity purification[116], the protein glutathione-S-transferase (GST) is one such fusion tag that has been reported to improve the solubility of target proteins to which it has been fused[117]. In fact, GST fusion tags have been successfully used to express the EF-hands of DGK-alpha and gamma (although not beta) in *E. coli*[54]. In an attempt to improve the solubility of recombinantly expressed alphacat, alphacat was therefore cloned into a GST-containing plasmid.

Results

The pGEX-4T2 vector (Figure 40) introduces GST from *Schistosoma japonicum*, followed by a thrombin proteolytic site, at the N-terminus of the protein. The total mass of this protein construct (including the fusion tag) and pI are predicted to be 71.6 kD and 6.97, respectively.

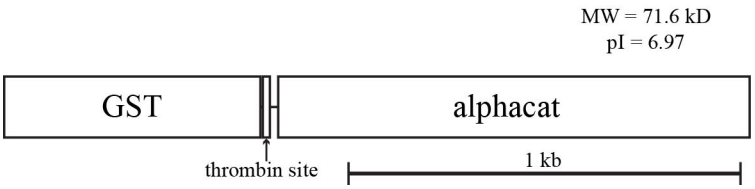

Figure 40. Schematic of alphacat in pGEX-4T2 construct. "Alphacat" consists of residues 333-733 of *S. scrofa* DGK alpha. pGEX-4T2 adds to the N-terminus of the protein a fusion tag consisting of *S. japonicum* GST followed by a thrombin proteolytic site. The total mass of this protein construct (including the fusion tag) and pI are predicted to be 71.6 kD and 6.97, respectively. This figure has been modified from Petro and Raben[1] and is used under CC BY-NC 2.5.

I transformed alphacat in pGEX-4T2 into BL21(DE3) strain of *E. coli*, as well as into BL21(DE3) competent cells that had already been transformed with each of the sets of bacterial chaperones. I tested the expression in LB and in Minimal Media. The cultures in Minimal Media started to grow until they reached an OD600 of ~0.02, at which point they stopped growing. As can be seen in Figure 41, alphacat in pGEX-4T2 expressed readily after induction with IPTG, producing a band, easily detectable by Coomassie staining following SDS-PAGE, that ran between the 60 kD and 70 kD molecular weight markers, slightly faster than its predicted size of 71.6 kD, and was recognized by an α-DGK-alpha antibody, but not an anti-histidine antibody, by immunoblot. As I observed with alphacat in pT71myc, the alphacat in pGEX-4T2 construct produced insoluble protein, as measured by detection in the supernatant either by Coomassie staining or immunoblot following SDS-PAGE following centrifugation of the bacterial lysate. As I also observed with alphacat in pT71myc, coexpressing GroEL/ES increased the amount of GST-tagged alphacat detected (either by Coomassie or immunoblot) in the supernatant following centrifugation. As above, GroEL is recognized by the α-DGK-alpha antibody; in this case, GroEL is the lower band, and alphacat is the upper band.

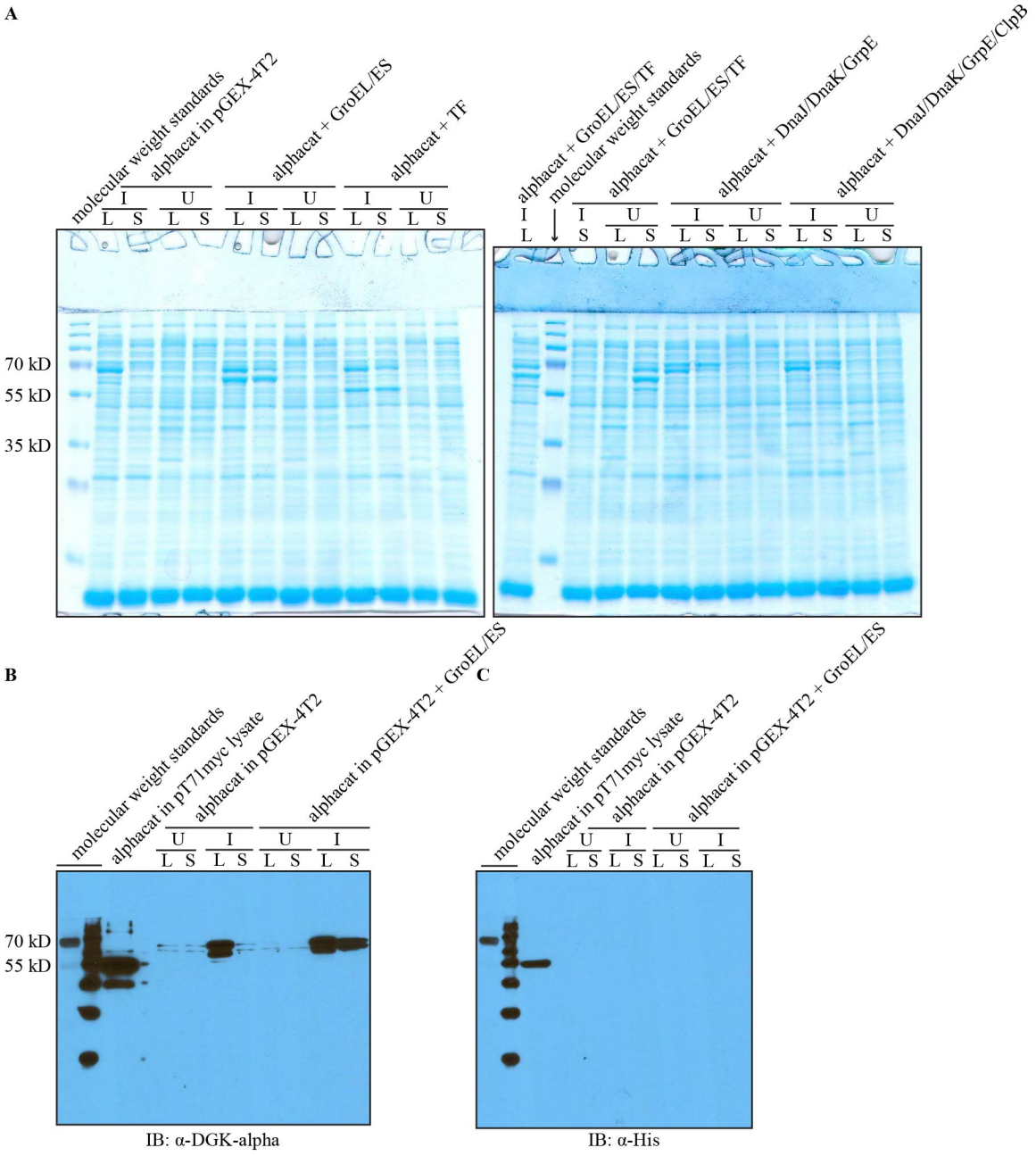

Figure 41. Alphacat in pGEX-4T2 expresses that runs slightly faster than predicted that is recognized by the anti-DGK-alpha antibody, and its apparent solubility increases when coexpressed with GroEL/ES. I inoculated two 4 mL LB Carb cultures and two 4 mL M9 Minimal Media (12.8 g per L $Na_2HPO_4 \bullet 7H_2O$, 3 g per L KH_2PO_4, 0.5 g per L NaCl, 1 g per L NH_4Cl, 0.4% (w/v) glucose) Carb cultures each with an overnight culture of alphacat in pGEX-4T2 in BL21(DE3), and two LB Carb Cam cultures and two M9 Minimal Media Carb Cam cultures each with overnight cultures of alphacat in pGEX-4T2 coexpressing with each of the sets of chaperones in BL21(DE3). When the OD600 of the LB cultures was predicted to reach 0.3, I added IPTG to 0.1 mM, and shook the cultures for 21 hours at 16°C. I pelleted the cells and froze at -80°C overnight. I resuspended each cell pellet in 40 mL per gram wet cell pellet lysis buffer (50 mM HEPES, pH 6.4, 300 mM NaCl, 10 mM imidazole, 5 mM $MgCl_2$, 1 mM $CaCl_2$, 0.5% (v/v) NP-40, 0.5 mM DTT, 1x PIC), and added egg white lysozyme to 1 mg per mL and DNAse I to 20 U per

mL, and incubated on ice for thirty minutes. I lysed the cells by probe-sonicating three times for ten seconds each, resting on ice for fifteen seconds between each pulse. I removed the insoluble fraction by centrifuging at 54,900 x *g* for 20 minutes at 4°C. SDS-PAGE of 12% acrylamide gels followed by: **(A)** Coomassie staining, **(B)** immunoblotting against DGK-alpha C-terminus (Abgent AP8128b (1:300 (v/v))), or **(C)** immunoblotting against His_6 (abcam® ab6196 (1:2500 (v/v))). I, induced; U, uninduced; L, lysate; S, supernatant (after removing insoluble from lysate). This figure has been modified from Petro and Raben[1] and is used under CC BY-NC 2.5.

Because coexpressing with GroEL/ES/TF appeared to increase the solubility of alphacat in pGEX-4T2, I expressed it fresh in order to assay its enzymatic activity (Figure 42**A**). Activity in micelles was noisy (Figure 42**B**); the detergent may have solubilized endogenous *E. coli* DGKA, which is an integral membrane protein, allowing it to access the DOG in the micelles and contribute to the observed enzymatic activity. As such, I also assayed the DGK activity using liposomes as a substrate (Figure 42**C**). I was able to detect greater activity in the lysate and especially in the supernatant of the alphacat in pGEX-4T2 coexpressed with GroEL/ES/TF, suggesting that the bacterial chaperones allowed more of the alphacat in a catalytically competent way, but the magnitude of the increase was small, especially when considering the large amount of alphacat expressed detected by Coomassie.

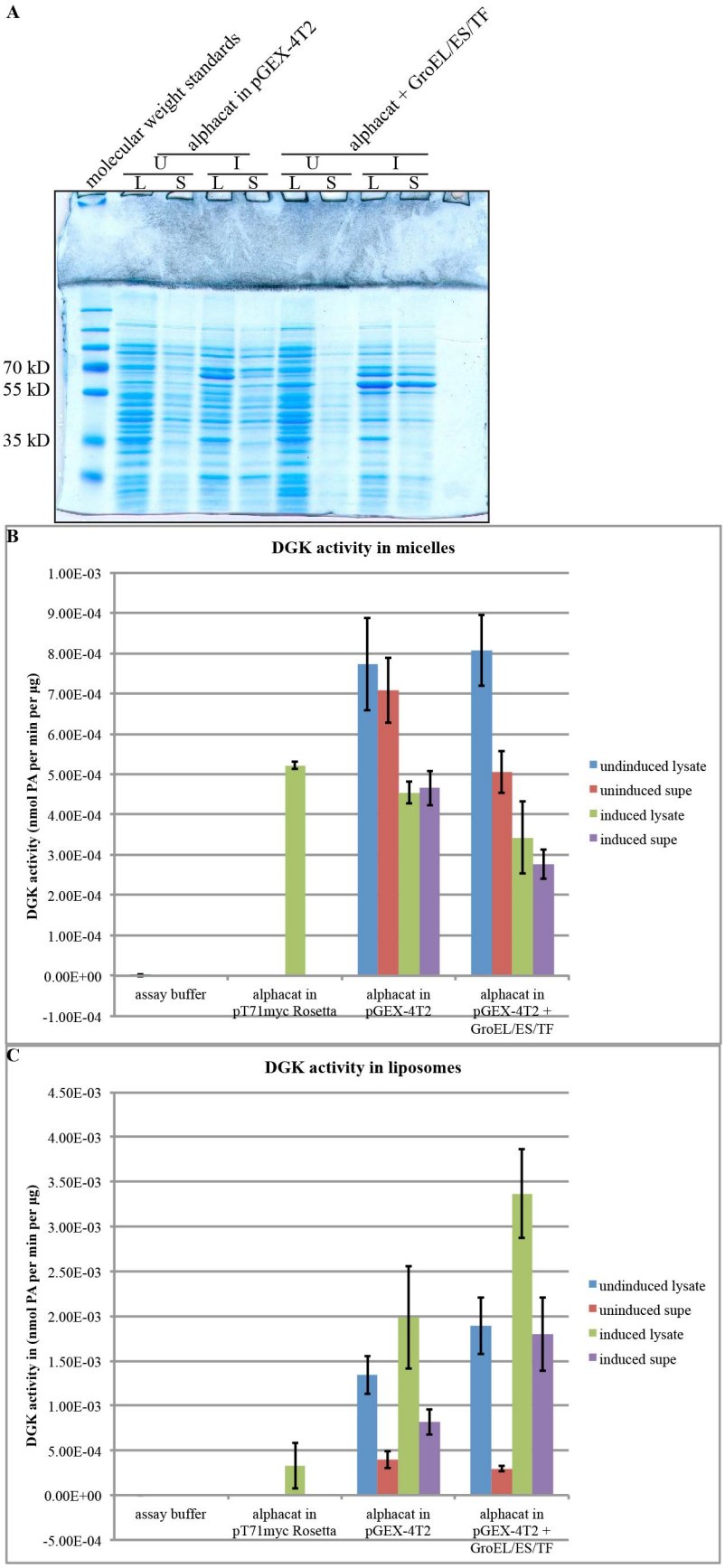
A
molecular weight standards
alphacat in pGEX-4T2
alphacat + GroEL/ES/TF
U
I
U
I
L
S
L
S
L
S
L
S
70 kD
55 kD
35 kD
B
DGK activity in micelles
DGK activity (nmol PA per min per µg)
1.00E-03
9.00E-04
8.00E-04
7.00E-04
6.00E-04
5.00E-04
4.00E-04
3.00E-04
2.00E-04
1.00E-04
0.00E+00
-1.00E-04
assay buffer
alphacat in pT71myc Rosetta
alphacat in pGEX-4T2
alphacat in pGEX-4T2 + GroEL/ES/TF
undinduced lysate
uninduced supe
induced lysate
induced supe
C
DGK activity in liposomes
DGK activity in (nmol PA per min per µg)
4.50E-03
4.00E-03
3.50E-03
3.00E-03
2.50E-03
2.00E-03
1.50E-03
1.00E-03
5.00E-04
0.00E+00
-5.00E-04
assay buffer
alphacat in pT71myc Rosetta
alphacat in pGEX-4T2
alphacat in pGEX-4T2 + GroEL/ES/TF
undinduced lysate
uninduced supe
induced lysate
induced supe

Figure 42. Coexpression with GroEL/ES/TF increases the DGK activity of alphacat in pGEX-4T2 in BL21(DE3) lysates. I inoculated two 125 mL LB Carb cultures with an overnight culture of alphacat in pGEX-4T2 in BL21(DE3), and two 125 mL LB Carb Cam cultures with an overnight culture of alphacat in pGEX-4T2 + GroEL/ES/TF in BL21(DE3). When the OD600 reached 0.5, I added IPTG to 0.1 mM (or not) and shook the cultures for 21 hours at 16°C, then pelleted the cells. I resuspended each cell pellet in 1 mL lysis buffer (50 mM HEPES, pH 6.4, 300 mM NaCl, 10 mM imidazole, 5 mM $MgCl_2$, 1 mM $CaCl_2$, 0.5% (v/v) NP-40, 0.5 mM DTT, 1x PIC), and added DNAse I to 20 U per mL and egg white lysozyme to 1 mg per mL, and incubated on ice for thirty minutes. I lysed the cells by probe-sonicating three times for ten seconds each, resting on ice for fifteen seconds between each pulse. I removed the insoluble fraction by centrifuging at 54,900 x *g* for 65 minutes at 4°C. **(A)** SDS-PAGE followed by Coomassie staining. I loaded 2 µg per well, as measured by the Bio-Rad Protein Assay. **(B)** DGK activity assay in Triton X-100 detergent micelles. I stored the samples in 50% glycerol (v/v) at -80°C overnight prior to assaying. The reaction included 40 ng per µL protein (as measured by the Bio-Rad Protein Assay), 7.3 mM Triton X-100 micelles (6.3 mol% DOG, 18.8% mol% POPS), 5 mM HEPES, 110 mM NaCl, 1 mM imidazole, 8.5 mM $MgCl_2$, 0.26 mM $CaCl_2$, 0.05% (v/v) NP-40, 0.1x PIC, 1.3 mM DTT, 5% (v/v) glycerol, 40 mM MOPS, pH 7.4, 1 mM ATP, and 119 Ci per mmol [γ-^{32}P]-ATP. The reaction proceeded for 15 minutes at 30°C. In triplicate, mean ± SD. **(C)** DGK activity assay in liposomes. I stored the samples in 50% glycerol (v/v) at -80°C for seven days prior to assaying. The reaction included 40 ng per µL protein (as measured by the Bio-Rad Protein Assay), 7.5 mM liposomes (53:22:17:8::POPE:POPC:POPS:DOG), 5 mM HEPES, 110 mM NaCl, 1 mM imidazole, 8.5 mM $MgCl_2$, 0.26 mM $CaCl_2$, 0.05% (v/v) NP-40, 0.1x PIC, 1 mM DTT, 5% (v/v) glycerol, 40 mM MOPS, pH 7.4, 1 mM ATP, and 41.7 Ci per mmol [γ-^{32}P]-ATP. The reaction proceeded for 15 minutes at 30°C. In triplicate, mean ± SD.

In order to optimize expression before purification, I tested the effects of temperature and pH on the expression of alphacat in pGEX-4T2, coexpressed with GroEL/ES. Because the pI is predicted to be 6.97, I tested the solubility of lysis at either pH 5 (buffered with sodium succinate) or pH 9 (buffered with glycine), in order to be at least two pH units away from the pI (so that only 1% of the protein would be uncharged). I also tested the effect of the temperature of induction: I tested expression at 37°C, and meant to test the expression at 16°C, but the shaking incubator had been moved to a new cold room, and the temperature setting that had been 16°C in the previous cold room was now only 6°C. Once again, alphacat is the upper band, and GroEL is the lower band. More alphacat was expressed, and, as a result, more alphacat remained in the soluble fraction, in the 6°C expression than in the 37°C expression (Figure 43). Under the conditions tested, alphacat remained mostly insoluble: the yield of alphacat is less than the supernatant than in the lysate as detected by Coomassie staining (Figure 43**A**), and is

not even detectable by immunoblotting, even though the alphacat in the lysate is easily detectable (Figure 43**B**).

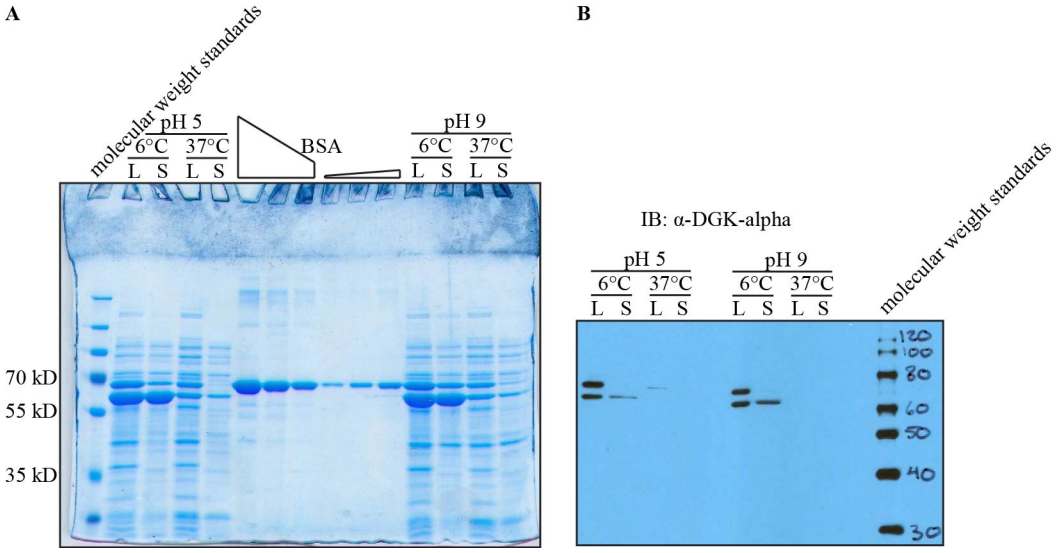

Figure 43. Testing the effect of pH and induction temperature on the expression of alphacat in pGEX-4T2 coexpressed with GroEL/ES. I inoculated two 12.5 mL LB Carb Cam cultures with an overnight culture of alphacat in pGEX-4T2 + GroEL/ES in BL21(DE3). When the OD600 was predicted to reach 0.3, I added IPTG to 0.1 mM (or not) and shook the cultures either for three hours at 37°C or else for 21.5 hours at 6°C, then pelleted the cells. I resuspended each cell pellet in either 17.4 mL per gram wet cell pellet (for 37°C expression) or else 450 µL (for 16°C expression) pH 5 lysis buffer (50 mM sodium succinate, pH 5.0, 100 mM NaCl, 20 mM NaF, 10 mM $MgCl_2$, 0.2 mM $CaCl_2$, 0.5% (v/v) NP-40, 1 mM DTT, 1x PIC) or pH 9 lysis buffer (same as pH 5 lysis buffer, except buffered with 50 mM glycine, instead of sodium succinate, to pH 9.0), and added egg white lysozyme to 1 mg per mL, and incubated on ice for thirty minutes, vortexing occasionally to mix. I lysed the cells by probe-sonicating ten times for ten seconds each, resting on ice for fifteen seconds between each pulse. I removed the insoluble fraction by centrifuging at 40,300 x *g* for ninety minutes at 4°C. SDS-PAGE of 10% acrylamide gels followed by **(A)** Coomassie staining, or **(B)** immunoblotting against DGK-alpha C-terminus (Abgent AP8128b (1:300 (v/v))). L, lysate; S, supernatant.

In an effort to determine as soon as possible whether the alphacat in pGEX-4T2 coexpressed with GroEL/ES was a promising construct to pursue for x-ray crystallography studies, I loaded the soluble fraction of a fresh expression directly onto a freshly blocked Sephadex® G-200 analytical gel filtration column, with no additional prior purification steps. However, I was unable to detect alphacat in any of the gel filtration fractions, by Coomassie staining (Figure 44**A**) or by immunoblotting against

either DGK-alpha (Figure 44**B**) or GST (Figure 44**C**). Clearly I needed to enrich alphacat in pGEX-4T2 before loading it onto the analytical gel filtration column.

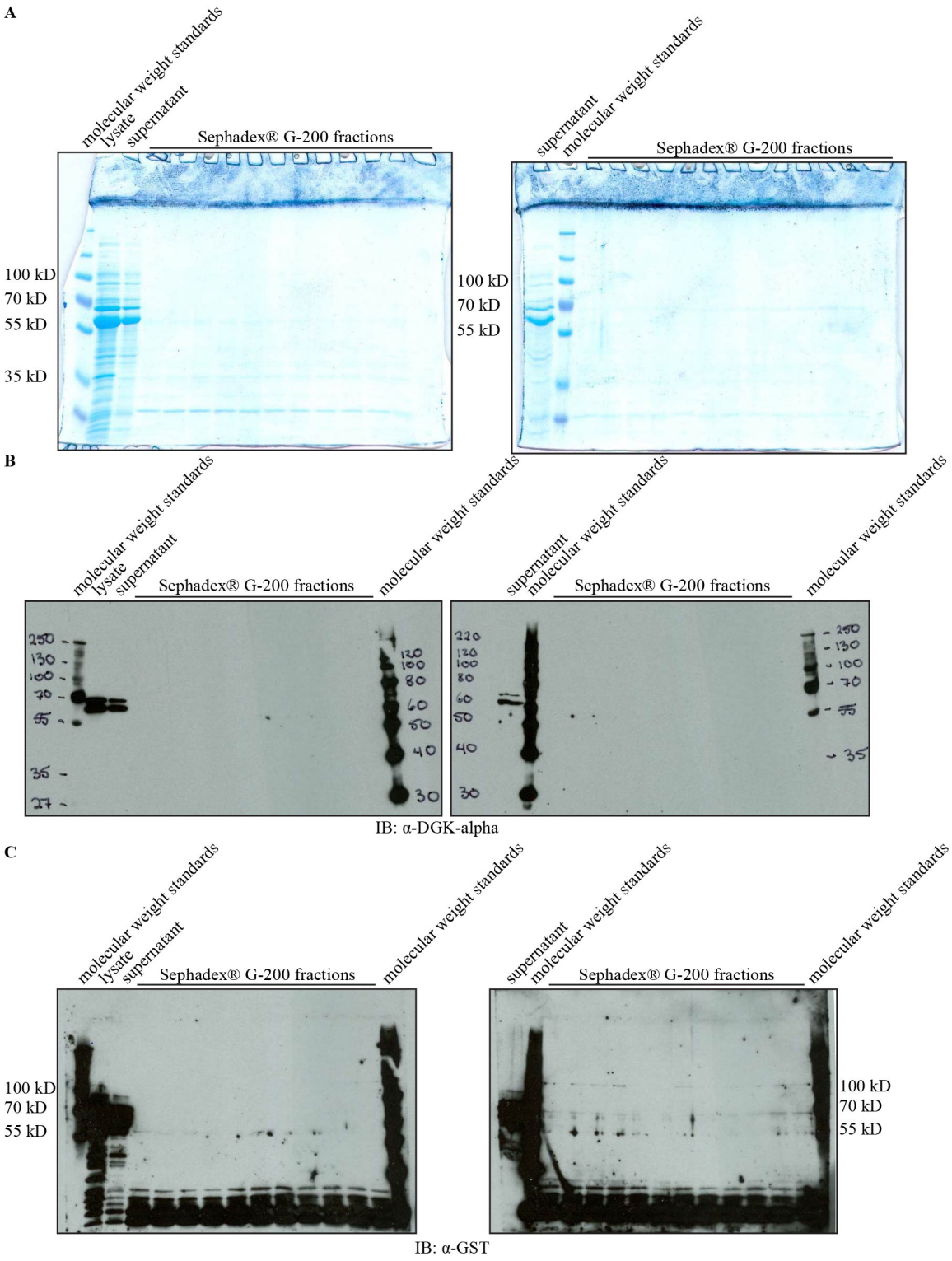

Figure 44. When the supernatant of alphacat in pGEX-4T2 coexpressed with GroEL/ES in BL21(DE3) is loaded directly onto a Sephadex® G-200 analytical gel filtration column, alphacat is undetectable in the eluate. I inoculated a 100 mL LB Carb Cam culture with an overnight culture of alphacat in pGEX-4T2 + GroEL/ES in BL21(DE3). When the OD600 was predicted to reach 0.3, I added

IPTG to 0.1 mM and shook the cultures for 22 hours at 16°C, then pelleted the cells. I resuspended the cell pellet in 4 mL lysis buffer (50 mM glycine, pH 9.0, 100 mM NaCl, 20 mM NaF, 10 mM $MgCl_2$, 0.2 mM $CaCl_2$, 0.5% (v/v) NP-40, 1 mM DTT, 1x PIC) and added egg white lysozyme to 1 mg per mL, and incubated on ice for 45 minutes. I lysed the cells by probe-sonicating ten times for ten seconds each, resting on ice for fifteen seconds between each pulse. I removed the insoluble fraction by centrifuging at 40,300 x *g* for ninety minutes at 4°C. I loaded 200 µL of the resulting supernatant onto a Sephadex® G-200 column that had been freshly blocked with 240 µL of 10 mg/mL fresh albumin, and I collected fractions every three minutes, eluting by gravity in gel filtration buffer (50 mM glycine, 100 mM NaCl, 20 mM NaF, 10 mM $MgCl_2$, 0.2 mM $CaCl_2$, pH 9.0). SDS-PAGE of 10% acrylamide gels followed by **(A)** Coomassie staining (I loaded 5 µg of the lysate, an equivalent volume of the supernatant, and 24 µL of each of gel filtration fraction), **(B)** immunoblotting against DGK-alpha C-terminus (Abgent AP8128b (1:300 (v/v))), and **(C)** immunoblotting (using the same membranes shown in (B)) against GST (1:50,000(v/v)).

I chose to use MagneGST™ glutathione particles (Promega V8611) to affinity purify alphacat via its N-terminal GST tag. Although I had tested the solubility of alphacat in pGEX-4T2 coexpressed with GroEL/ES at pH 5 and at pH 9, the manufacturer's guide warned that buffers with pHs above 8.0 may inhibit binding of the GST epitope tag to the MagneGST™ glutathione particles. Furthermore, alphacat coexpressed with GroEL/ES appeared more soluble at pH the solubility looks better at pH 6.4 (Figure 41 (although, to be fair, that lysis buffer was buffered with HEPES, whose buffering capacity does not extend to 6.4, so I am uncertain what the actual pH was)) than at pH 9.0 (Figure 43). I therefore lysed a fresh expression of alphacat in pGEX-4T2 plus GroEL/ES at pH 8.0, and tested its solubility under different expression conditions. More alphacat appeared to be in the supernatant following centrifugation when induced at 16°C overnight than when induced at 37°C for three hours (Figure 45).

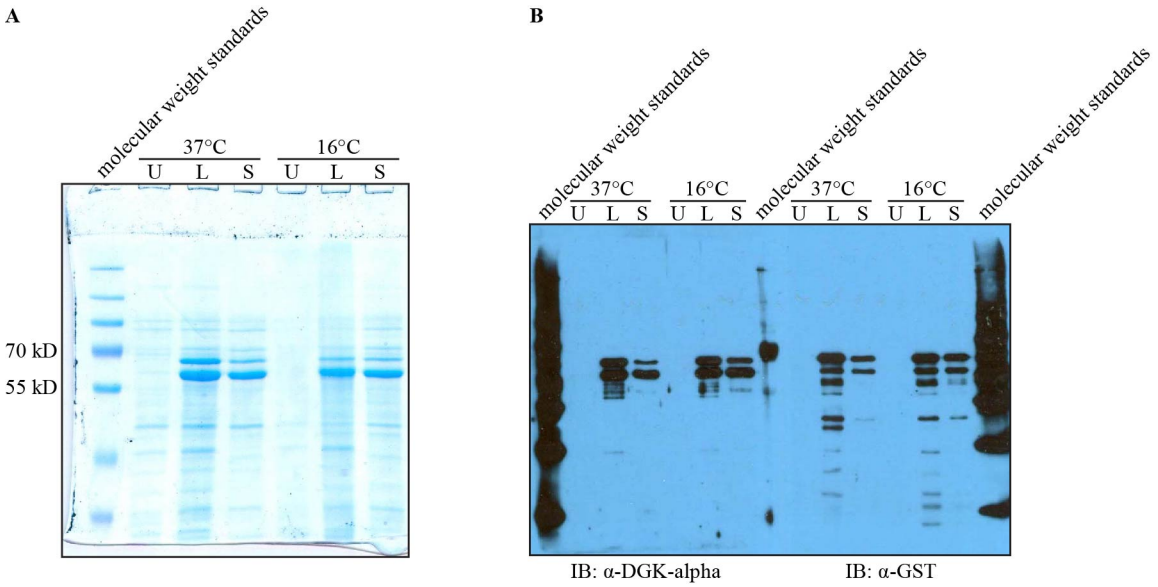

Figure 45. When lysed at pH 8, more alphacat coexpressed with GroEL/ES is soluble when induced at 16°C overnight than at 37°C for three hours. I inoculated two 100 mL LB Carb Cam cultures with an overnight culture of alphacat in pGEX-4T2 + GroEL/ES in BL21(DE3). When the OD600 was predicted to reach 0.3, I removed an aliquot as uninduced, and added IPTG to 0.1 mM to the remaining culture and shook either at 37°C for three hours or else at 16°C overnight, then pelleted the cells. I resuspended the cell pellet in 4 mL per gram wet cell pellet lysis buffer (50 mM Tris, pH 8.0, 1 mM $CaCl_2$, 0.25% (v/v) TX-100, 5 mM DTT, 1x PIC), froze at -80°C for three hours, then thawed by shaking the tube in water gently. I added egg white lysozyme to 1 mg per mL, and incubated on ice for thirty minutes, vortexing occasionally to mix. I lysed the cells by probe-sonicating ten times for ten seconds each, resting on ice between each pulse. I removed the insoluble fraction by centrifuging at 110,000 x *g* for one hour at 4°C. SDS-PAGE of 10% acrylamide SDS-PAGs followed by **(A)** Coomassie staining (I loaded 5 µg in each lane) and **(B)** immunoblotting against DGK-alpha C-terminus (Abgent AP8128b (1:300 (v/v))) (left) or GST (1:50,000(v/v)) (right). I loaded 0.2 µg in each lane of the immunoblots. U, uninduced; L, induced lysate; S, induced supernatant.

I purified the supernatant of alphacat in pGEX-4T2 coexpressed with GroEL/ES using MagneGST™ glutathione particles according to the manufacturer's instructions. Most of the protein flowed through, never adhering to the MagneGST™ glutathione particles in the first place, and the rest eluted off at very low concentrations glutathione (Figure 46), suggesting that alphacat in pGEX-4T2 had a lower than predicted affinity for the glutathione particles.

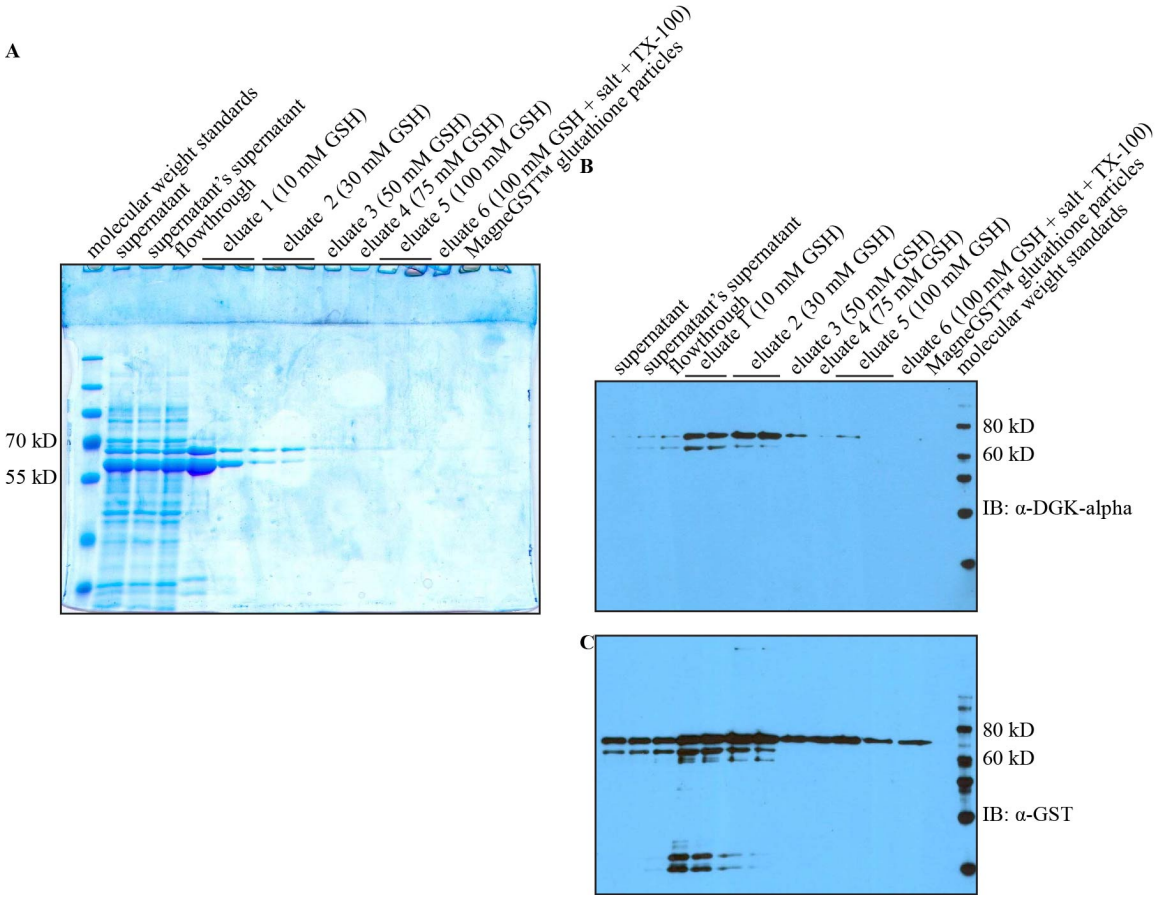

Figure 46. Alphacat in pGEX-4T2 coexpressed with GroEL/ES has lower than expected affinity for MagneGST™ glutathione particles. I thawed the 16°C supernatant (shown in **Figure 45**), which had been stored at -80°C in 20% glycerol for six days, by gently shaking the tube in water. I removed the insoluble fraction by centrifuging at 110,000 x *g* for 65 minutes at 4°C. I added MagneGST™ glutathione particles 1:24 (v/v) and rotated at 4°C for thirty minutes. I washed the particles with wash buffer (50 mM Tris, pH 8.0, 140 mM NaCl, 10 mM KCl, 1 mM $CaCl_2$, 0.1% (v/v) TX-100, 5 mM DTT), and eluted with elution buffer 1 (same as wash buffer, but with glutathione added to 10 mM), elution buffer 2 (30 mM glutathione), elution buffer 3 (50 mM glutathione), elution buffer 4 (75 mM glutathione), elution buffer 5 (100 mM glutathione), and elution buffer 6 (same as elution buffer 5, but NaCl increased to 490 mM and TX-100 increased to 1%). SDS-PAGE of 10% acrylamide gels followed by **(A)** Coomassie staining, **(B)** immunoblotting against DGK-alpha C-terminus (Abgent AP8128b (1:300 (v/v))), and **(C)** immunoblotting against GST (1:50,000(v/v)) (same membrane as shown in (B)). GSH, glutathione.

In an effort to enrich enough alphacat to be able to detect its elution from an analytical gel filtration column, I therefore repurified the flowthrough on MagneGST™ glutathione particles, eluting with lower concentrations of glutathione. Because I was unsure whether MagneGST™ glutathione particles could be reused, I repurified on both the previously used particles as well as fresh particles, at two different concentrations, to

compare (Figure 47**A**). Perhaps slightly more alphacat flowed through the previously used resin, and perhaps slightly more adhered to and then eluted from the fresh resin, but overall Figure 47A shows that MagneGST™ glutathione particles can be reused to purify alphacat. As observed previously with alphacat in pT71myc purification on Ni-NTA, longer elution times produced more concentrated eluted protein (E4 eluted over the weekend, whereas the other elution steps were fifteen minutes) (Figure 47). As in Figure 46, most of the alphacat eluted at the lowest concentration of glutathione.

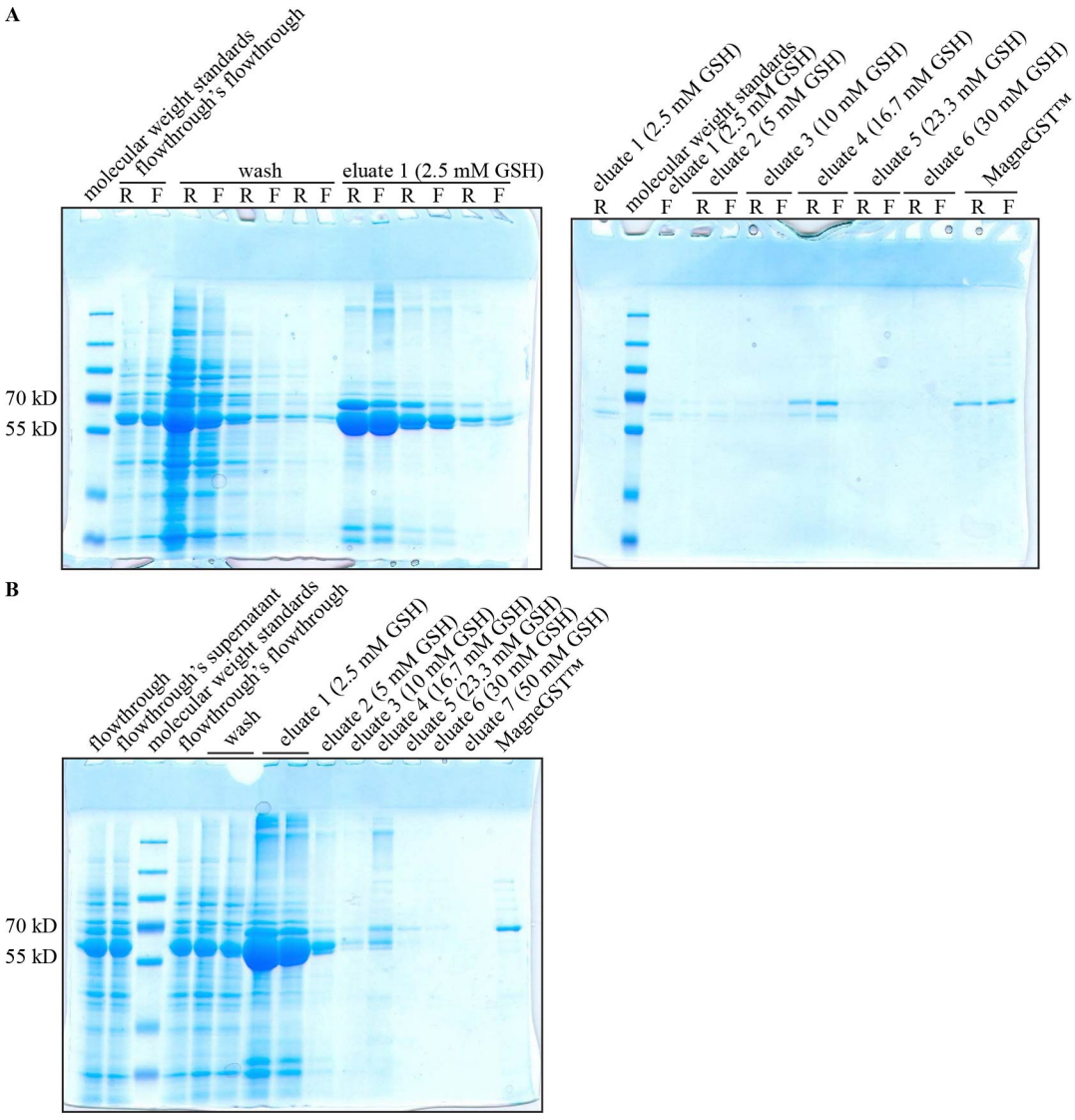

Figure 47. MagneGST™ glutathione particles can be reused to purify alphacat in pGEX-4T2 coexpressed with GroEL/ES. I had stored the flowthrough from **Figure 46** frozen for nine days, and thawed it by shaking the tube in water gently. I removed the insoluble fraction by centrifuging at 110,000 x *g* for 65 minutes at 4°C. I then divided the resulting supernatant into fifths. To one-fifth, I added the previously used MagneGST™ glutathione particles (**Figure 46**) 1:6 (v/v). To another fifth, I added fresh MagneGST™ glutathione particles 1:6 (v/v), in order to determine whether the particles could be reused. To the remaining three-fifths, I added fresh MagneGST™ glutathione particles 1:3 (v/v). I rotated the samples at 4°C for one hour, washed the particles with wash buffer (50 mM Tris, pH 8.0, 140 mM NaCl, 10 mM KCl, 1 mM $CaCl_2$, 0.1% (v/v) TX-100, 5 mM DTT), and eluted with elution buffer 1 (same as wash buffer, but with glutathione added to 2.5 mM), elution buffer 2 (5 mM glutathione), elution buffer 3 (10 mM glutathione), elution buffer 4 (16.7 mM glutathione), elution buffer 5 (23.3 mM glutathione), elution buffer 6 (30 mM glutathione), and elution buffer 7 (75 mM glutathione). SDS PAGE of 10% acrylamide gels followed by Coomassie staining. **(A)** Comparison of 1:6 (v/v) reused vs. fresh MagneGST™ glutathione particles. R, reused; F, fresh. **(B)** 1:3 (v/v) fresh glutathione particles.

Elution E1A from the elution on fresh MagneGST™ glutathione particles using the higher ratio of protein to particles (Figure 47**B**) was sufficiently concentrated (1 mg per mL by the Bio-Rad Protein Assay) to load directly onto the Sephadex® G-200 analytical gel filtration column. In order to match the MagneGST™ elution buffer, prior to loading the partially purified alphacat, I first washed the column with a new gel filtration buffer (50 mM Tris, 140 mM NaCl, 10 mM KCl, 1 mM $CaCl_2$, 0.1% Triton X-100, 5 mM DTT, pH 8.0), then blocked the column with cytochrome c. Instead of a small pink band traveling down the white column, which was what I expected to observe, the entire column turned pink. When the top of the column turned white again, I loaded the partially purified alphacat. I was unable to detect alphacat in any of the eluting gel filtration fractions by immunoblotting against DGK-alpha C-terminus (Figure 48).

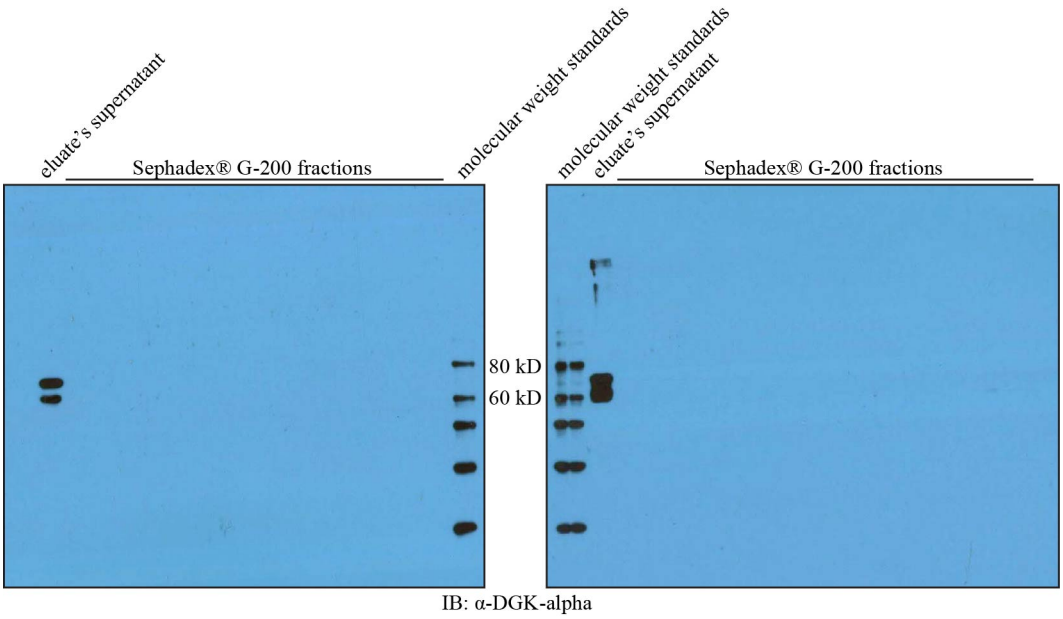

Figure 48. When partially purified alphacat in pGEX-4T2 coexpressed with GroEL/ES in BL21(DE3) is loaded onto a Sephadex® G-200 analytical gel filtration column using a gel filtration buffer that includes 0.1% TX-100, alphacat is undetectable in the eluate. Eluate 1A from the purification using 1:3 (v/v) fresh glutathione particles (**Figure 47**B) was stored at 4°C for four days before I removed the insoluble fraction by centrifuging at 54,900 x *g* for ninety minutes at 4°C. I loaded 200 µL of the resulting supernatant onto a Sephadex® G-200 column that had been freshly blocked with 220 µL of 10 mg/mL cytochrome c, and I collected fractions every 5.5 minutes, eluting by gravity in gel filtration buffer

(50 mM Tris, 140 mM NaCl, 10 mM KCl, 1 mM CaCl2, 0.1% Triton X-100, 5 mM DTT, pH 8.0). SDS-PAGE followed by immunoblotting against DGK-alpha C-terminus (Abgent AP8128b (1:300 (v/v))).

After running the partially purified alphacat on the column, I set out to calibrate the column in the new gel filtration buffer. Unlike previous calibrations, loading blue dextran on the column did not produce any visibly blue fractions. I poured a fresh Sephadex® G-200 column, but once again the blue dextran diffused into the column during calibration rather than producing a discrete blue band. Dropping the Triton X-100 concentration in the gel filtration buffer from 0.1% to 0.01% produced a wide blue peak for blue dextran, and removing Triton X-100 altogether from the gel filtration buffer returned the blue dextran peak to its normal narrow size (Figure 49). I therefore concluded that the Sephadex® G-200 resin was incompatible with Triton X-100 concentrations as low as 0.01%, and that it was the Triton X-100 in the sample that prevented detection of alphacat in pGEX-4T2 in the immunoblots in Figure 48.

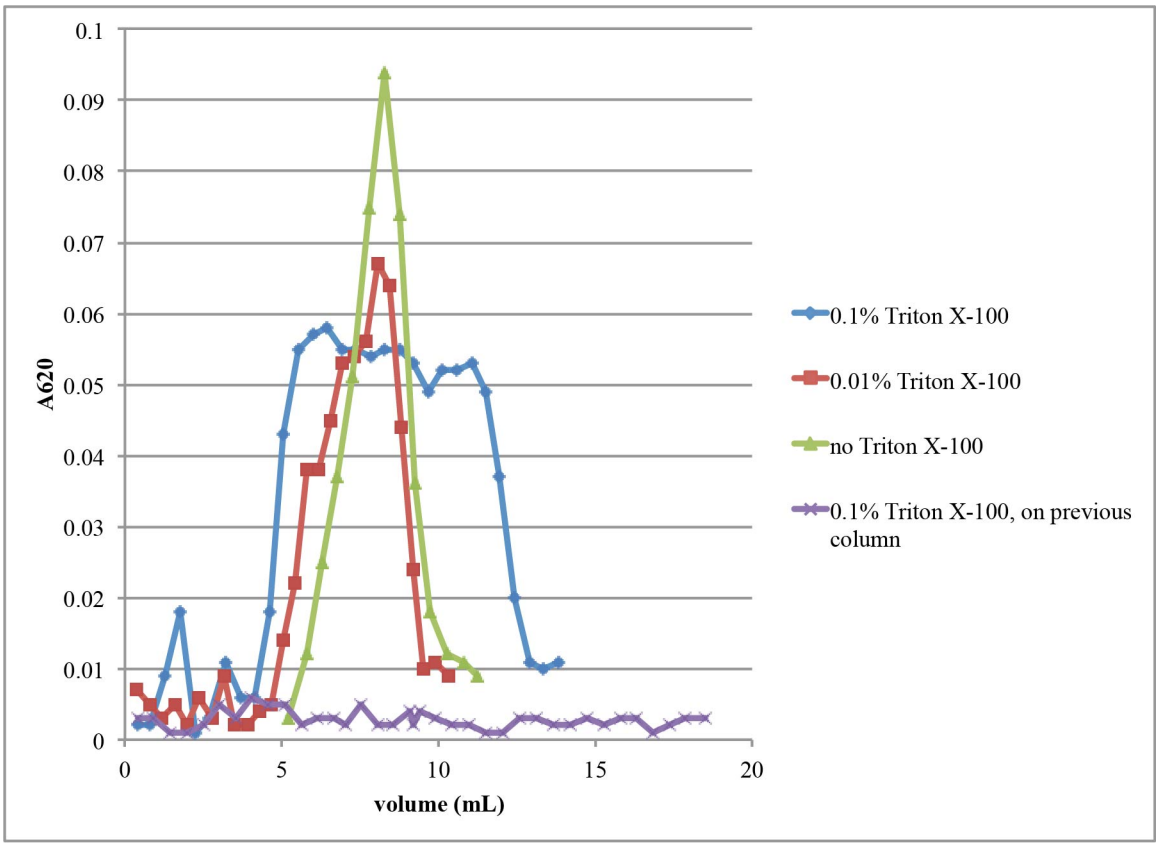

Figure 49. Sephadex® G-200 resin was incompatible with TX-100 concentrations as low as 0.01%. The elution of blue dextran (as monitored by A620) from a Sephadex® G-200 column in gel filtration buffer with differing concentrations of TX-100.

I therefore expressed more alphacat in pGEX-4T2 plus GroEL/ES, and this time purified on MagneGST™ without Triton X-100, seeing as the detergent appeared to be incompatible with the analytical gel filtration resin that I was eventually going to use to determine whether alphacat in pGEX-4T2 was monodisperse. I also eluted in even lower concentrations of glutathione, seeing as most of the alphacat eluted from the glutathione particles at the lowest concentration of glutathione in the previous purification (Figure 47). Although I was able to enrich alphacat using the MagneGST™, once again much of the alphacat flowed through the particles, and the rest eluted at the lowest concentration of glutathione (Figure 50**A**). The partially purified alphacat was not sufficiently

concentrated to load onto the analytical gel filtration column, so I repurified the flowthrough on MagneGST™, and eluted in even lower concentrations of glutathione (Figure 50**B**). I could enrich for alphacat, but, once again, as with alphacat in pT71myc, GroEL coeluted with alphacat from the glutathione particles.

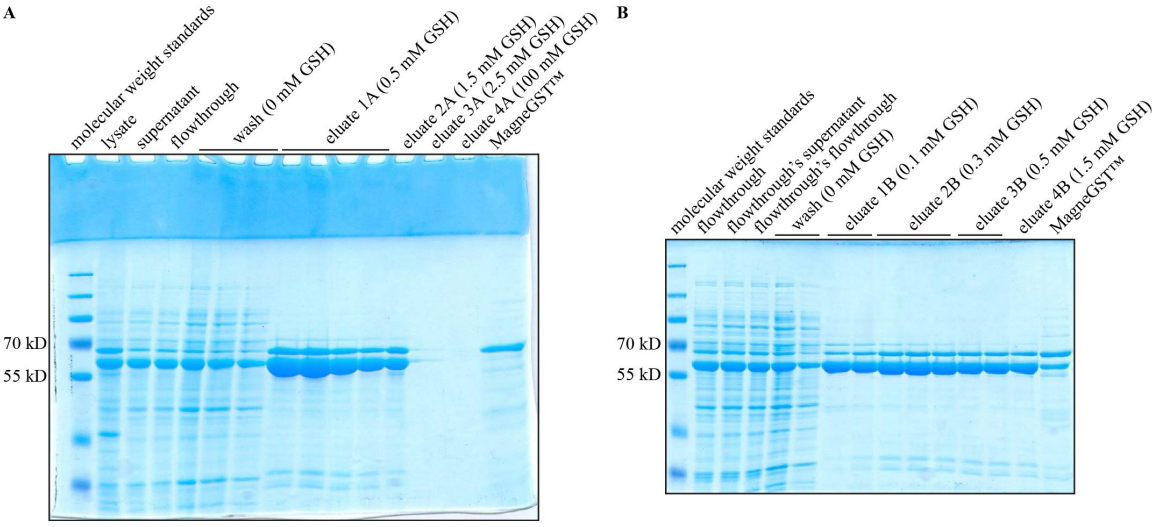

Figure 50. Alphacat in pGEX-4T2 coexpressed with GroEL/ES can be enriched on MagneGST™. I inoculated two 500 mL LB Carb Cam cultures with a freshly growing culture of alphacat in pGEX-4T2 + GroEL/ES in BL21(DE3). When the OD600 reached 0.4, I added IPTG to 0.1 mM and shook at 16°C for fourteen hours, then pelleted the cells. I resuspended the cell pellet in 4 mL per gram wet cell pellet lysis buffer (50 mM Tris, pH 8.0, 1 mM $CaCl_2$, 0.25% (v/v) TX-100, 5 mM DTT, 1x PIC), froze at -80°C overnight, then thawed by shaking the tube in water gently. I added egg white lysozyme to 1 mg per mL, and incubated on ice for thirty minutes, vortexing occasionally to mix. I lysed the cells by probe-sonicating in ten-second bursts until no longer viscous. I removed the insoluble fraction by centrifuging at 110,000 x *g* for 65 minutes at 4°C. I added the previously used MagneGST™ glutathione particles (**Figure 47**) 1:92 (v/v), and rotated at 4°C for 110 minutes. I washed the particles with wash buffer (50 mM Tris, pH 8.0, 140 mM NaCl, 10 mM KCl, 1 mM $CaCl_2$, 5 mM DTT), and eluted with elution buffer 1A (same as wash buffer, but with glutathione added to 0.5 mM), elution buffer 2A (1.5 mM glutathione), elution buffer 3A (2.5 mM glutathione), and elution buffer 4A (100 mM glutathione). I forgot to pH the 200 mM glutathione stock that I used to make the elution buffers, so the pH of elution buffer 4 was probably considerably less than 8.0, especially considering that the gel-loading buffer turned yellow for the eluate 4 samples. I stored the flowthrough at -80°C in 20% glycerol for two days, then thawed in water shaking in order to repurify. I added back the previously used MagneGST™ glutathione particles, and rotated at 4°C for 75 minutes. I washed the particles with wash buffer and eluted with elution buffer 1B (same as wash buffer, but with glutathione added to 0.1 mM), elution buffer 2B (0.3 mM glutathione), elution buffer 3B (0.5 mM glutathione), elution buffer 4B (1.5 mM glutathione), and elution buffer 5B (100 mM glutathione, this time using a 200 mM glutathione stock whose pH had been adjusted to 8.0 using NaOH). SDS-PAGE of 10% acrylamide gels. **(A)** First purification. I added NaOH to the eluate 4 and MagneGST™ samples prior to loading into the SDS-PAGs. **(B)** Repurification of the flowthrough shown in (A). This figure has been modified from Petro and Raben[1] and is used under CC BY-NC 2.5.

I pooled the eluates of both purifications and concentrated alphacat by dialyzing against 15% PEG 17.5 kD. I also took that opportunity to change the buffer from elution buffer to the gel filtration buffer recommended by the manufacturer of the molecular weight standards, plus calcium in case it was required for the proper conformation of alphacat (50 mM Tris, 100 mM KCl, 1 mM $CaCl_2$, pH 8.0). When I loaded the concentrated partially purified alphacat onto the Sephadex® G-200 analytical gel filtration column, alphacat and GroEL coeluted in the void volume (Figure 51). I therefore concluded that the GST-tagged alphacat also formed aggregates unsuitable for pursuit for structural studies.

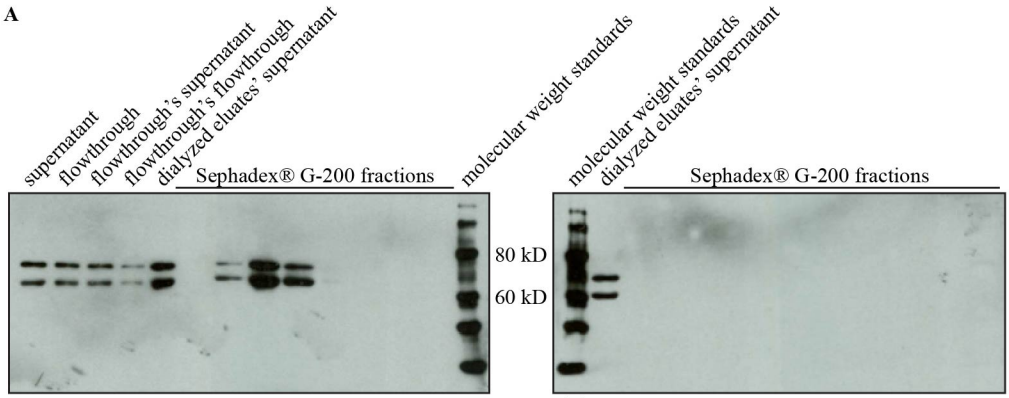
A
supernatant
flowthrough
flowthrough's supernatant
flowthrough's flowthrough
dialyzed eluates' supernatant
Sephadex® G-200 fractions
molecular weight standards
molecular weight standards
dialyzed eluates' supernatant
Sephadex® G-200 fractions
80 kD
60 kD
IB: α-DGK-alpha

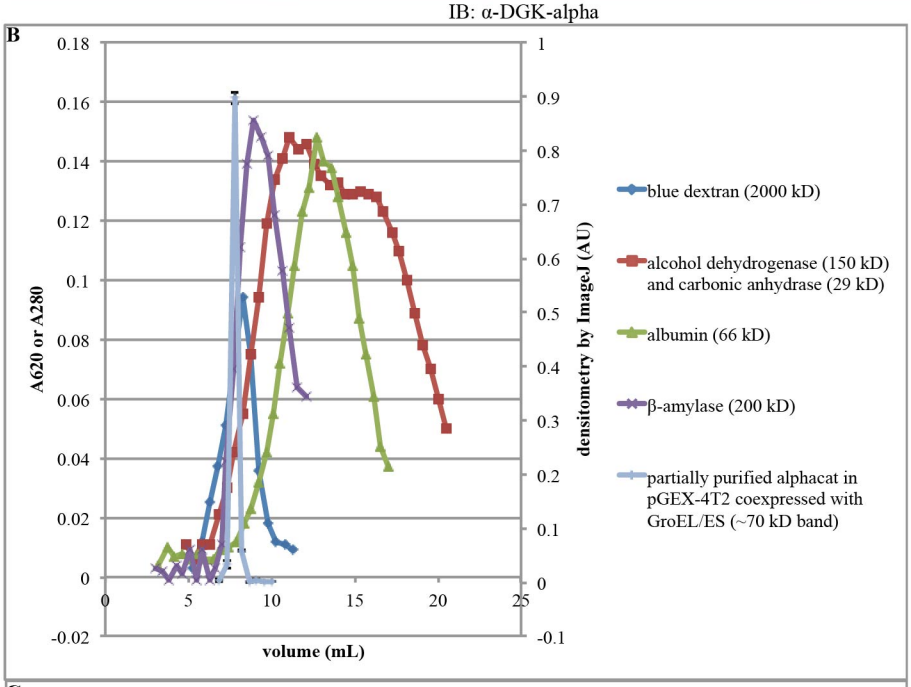
B
A620 or A280
densitometry by ImageJ (AU)
volume (mL)
blue dextran (2000 kD)
alcohol dehydrogenase (150 kD) and carbonic anhydrase (29 kD)
albumin (66 kD)
β-amylase (200 kD)
partially purified alphacat in pGEX-4T2 coexpressed with GroEL/ES (~70 kD band)

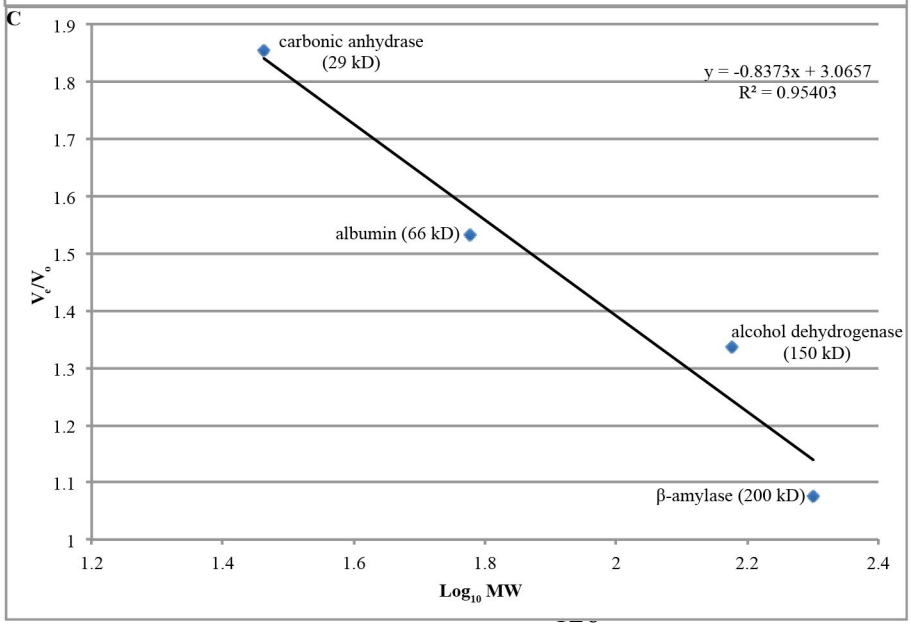
C
carbonic anhydrase (29 kD)
y = -0.8373x + 3.0657
R² = 0.95403
albumin (66 kD)
alcohol dehydrogenase (150 kD)
β-amylase (200 kD)
Ve/Vo
Log10 MW

Figure 51. Partially purified alphacat in pGEX-4T2 coexpressed with GroEL/ES elutes from a Sephadex® G-200 analytical gel filtration column in the void volume. I pooled all the eluates of the repurification (**Figure 50**B) and eluates 1 and 2 of the original purification (**Figure 50**A) and removed the insoluble fraction by centrifuging at 43,000 x *g* for ninety minutes at 4°C. I dialyzed the resulting supernatant against dialysis buffer (50 mM Tris, 100 mM KCl, 1 mM CaCl2, pH 8.0, 15% (w/v) PEG-17.5kD) using 3.5 kD MWCO dialysis tubing at 4°C to concentrate the protein. I removed the insoluble fraction by centrifuging at 43,000 x *g* for ninety minutes at 4°C, and loaded 200 µL of the resulting supernatant onto a Sephadex® G-200 column that had been freshly blocked with 610 µL of 10 mg/mL albumin and previously calibrated with alcohol dehydrogenase, carbonic anhydrase, albumin, and β-amylase. I collected fractions every 124 seconds, eluting by gravity in gel filtration buffer (50 mM Tris, 100 mM KCl, pH 8.0). **(A)** SDS-PAGE of an 8% acrylamide gel followed by immunoblotting against DGK-alpha C-terminus (Abgent AP8128b (1:300 (v/v))). Because the gel filtration buffer included potassium, and because potassium precipitates SDS, I ethanol-precipitated 32 µL of each of the gel filtration fractions of elution volumes corresponding to molecular weights of 441 kD to 28.8 kD, and resuspended in gel-loading buffer before loading onto the gel. **(B)** Elution volumes of molecular weight standards and of purified alphacat from a Sephadex® G-200 column. Left vertical axis, A280 of the protein molecular weight standards, and A620 of the blue dextran fractions. Right vertical axis, densitometry of the ~70 kD band using a shorter exposure of the membrane shown in (A). **(C)** Calibration of the Sephadex® G-200 column: elution volume (presented as a ratio of the void volume) of the molecular weight standards as a function of logarithm molecular weight. I calculated the linear regression using Microsoft® Excel®. A good linear fit suggests a good calibration. This figure has been modified from Petro and Raben[1] and is used under CC BY-NC 2.5.

Because alphacat in pGEX-4T2 migrated faster on SDS-PAGE than would be predicted by its supposed molecular weight (Figure 40-Figure 47 and Figure 50), and because alphacat in pGEX-4T2 exhibited a lower than predicted affinity for glutathione particles (Figure 46, Figure 47, and Figure 50), I wondered whether the entire GST epitope tag was actually present in the clone. When I sent the construct to have its DNA sequenced, however, the proper leader sequence, including the entire GST gene and the thrombin proteolytic site, was clearly present, and alphacat was inserted in the proper location. The protein sequence of alphacat in pGEX-4T2 contains several methionines: perhaps translation starts at a later methionine, thus expressing only part of the GST tag, which would explain the aberrant size and reduced affinity.

Conclusions

Because the concentrated partially purified alphacat in pGEX-4T2 eluted from the Sephadex® G-200 analytical gel filtration column in the void volume (Figure 51), I

concluded that the GST-tagged alphacat also formed aggregates unsuitable for pursuit for structural studies.

Cloning, Expression, and Purification of Alphacat and Full-Length DGK-Alpha in pET32a Coexpressed with Bacterial Chaperones

Introduction

In another attempt to improve the solubility of alphacat and full-length DGK alpha, I decided to clone each of these proteins into a plasmid that would add a fusion tag consisting of *E. coli* thioredoxin (TRX), which has been reported to improve the solubility of target proteins[112,118].

Results

The pET32a plasmid adds to the N-terminus of the protein not only TRX, but also hexahistidine, which can be used to facilitate affinity purification by Ni-NTA chromatography (Figure 52).

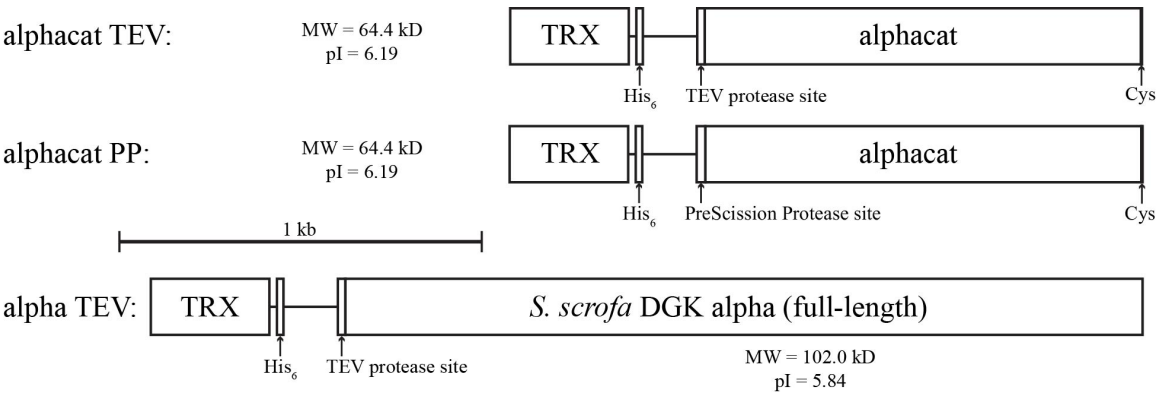

Figure 52. Schematic of alphacat and full-length alpha in pET32a constructs. Top: schematic of alphacat TEV in pET32a construct. "Alphacat" consists of residues 333-733 of *S. scrofa* DGK alpha; for this construct, the 734th residue of *S. scrofa* DGK alpha, cysteine, was added back. pET32a adds to the N-terminus of the protein a fusion tag consisting of *E. coli* TRX followed by a hexahistidine tag. For alphacat TEV, I added a TEV protease site between the fusion tag and alphacat. The total mass of this protein construct (including the fusion tag) and pI are predicted to be 64.4 kD and 6.19, respectively. Middle: schematic of alphacat PP in pET32a construct. Instead of a TEV protease site, I added a PreScission

Protease site between the fusion tag and alphacat. The total mass of this protein construct (including the fusion tag) and pI are predicted to be 64.4 kD and 6.19, respectively. Bottom: schematic of full-length *S. scrofa* DGK alpha TEV in pET32a construct. I added a TEV protease site between the fusion tag and DGK alpha, and I removed the initial methionine from DGK alpha. The total mass of this protein construct (including the fusion tag) and pI are predicted to be 102.0 kD and 5.84, respectively. This figure has been modified from Petro and Raben[1] and is used under CC BY-NC 2.5.

In order to clone alphacat into pET32a, I designed the forward PCR primers GCAAGTCGACAAGAAAACCTGTATTTTCAGGGAATCTATCCCAGTGTCCTGG and GCAAGTCGACAACTGGAAGTTCTGTTCCAGGGGCCCATCTATCCCAGTGTCCTGG. Both begin with a GC anchor, to promote efficient priming during the PCR reaction. The GC anchor is followed by a two-nucleotide spacer: that, plus the GC anchor, provides a four nucleotide overhang adjacent to the restriction site to promote efficient digestion. I chose the two-nucleotide spacer to be AA in order to keep the total GC content of the primer low. The restriction site is followed by another two-nucleotide spacer in order to ensure that the protease consensus sequence as well as the alphacat are in the same reading frame as the start codon encoded in the plasmid. The second two-nucleotide spacer is followed by either a TEV protease site or a PreScission Protease (PP) site, which is immediately followed by the first nineteen nucleotides of alphacat, ending in a GG anchor to promote efficient priming.

In order to clone full-length DGK-alpha into pET32a, I designed the forward PCR primers GCAAGTCGACAAGAAAACCTGTATTTTCAGGGATCCAAGGAGAGGGGG and GCAAGTCGACAACTGGAAGTTCTGTTCCAGGGGCCCTCCAAGGAGAGGGGG. They are identical to the alphacat primers with the exception of instead of ending with the

first nineteen nucleotides of alphacat, they encode the beginning of DGK-alpha, except for the initial methionine (in order to remove competing start sites for translation).

For the reverse primer, I used GCAGCGGCCGCTCAGCACAAGAAGCCAAAGAAATTG, the same reverse primer I used to add a NotI site downstream of full-length DGK-alpha for cloning into pT71myc. This primer adds a NotI site immediately downstream of DGK-alpha or alphacat. As such, it also restores to alphacat the terminal cysteine.

The total mass of the alphacat construct (including the fusion tag, and with either protease site) is predicted to be 64.4 kD, and the pI is predicted to be 6.19. The total mass and pI of the full-length DGK alpha construct are predicted to be 102.0 kD and 5.84, respectively. While the cloning strategy worked for both alphacat constructs and for the alpha TEV construct, I was unable to produce the alpha PP construct. Before working on optimizing PCR conditions to produce the alpha PP construct, I checked the pET32a constructs I did have to see whether the TRX-tagged DGK was any more soluble than the other constructs.

When I transformed these pET32a constructs into the BL21(DE3) strain of *E. coli*, they each expressed readily after induction with IPTG and were easily detectable by Coomassie staining following SDS-PAGE (Figure 53). For each of the alphacat constructs, the predominant band migrated between the 55 and 70 kD molecular weight markers, consistent with its predicted molecular weight of 64.4 kD. For the alpha TEV construct, the predominant band migrated evenly with the 100 kD molecular weight marker, consistent with its predicted molecular weight of 102.0 kD. The full-length alpha band was less robust than the alphacat constructs, but was still easily detectable.

Although all of these constructs robustly expressed in the lysates, following centrifugation, the constructs were undetectable in the supernatant by Coomassie staining. The cells appeared to lyse well, because all of the cellular proteins except the recombinant constructs appear in the supernatant at approximately the same intensity at which they appear in the lysate, so I concluded that these constructs were insoluble, not merely left behind in unlysed cells, and that the TRX fusion tag did not improve the solubility of these DGK alpha constructs.

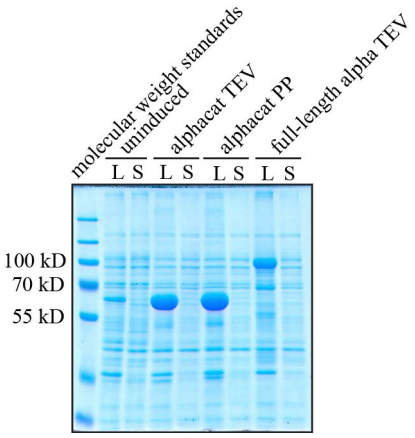

Figure 53. Alphacat and full-length alpha each robustly express a band of the correct size in the pET32a construct, but this band remains insoluble after centrifugation. I inoculated 4 mL LB Carb cultures with overnight cultures of the constructs shown, which I had previously transformed into BL21(DE3). When the OD600 reached 0.3, I added IPTG to 0.1 mM (or not) and shook at 16°C for 22.5 hours, then pelleted the cells. I resuspended the cell pellet in 40 mL per gram wet cell pellet lysis buffer (50 mM Tris, pH 8.0, 300 mM NaCl, 10 mM imidazole, 5 mM $MgCl_2$, 1 mM $CaCl_2$, 0.25% (v/v) TX-100, 0.5 mM DTT, 1x PIC), added egg white lysozyme to 1 mg per mL, and incubated on ice for thirty minutes, vortexing occasionally to mix. I lysed the cells by probe-sonicating ten times for ten seconds each, resting on ice for fifteen seconds between each burst. I removed the insoluble fraction by centrifuging at 43,000 x *g* for ninety minutes at 4°C. SDS-PAGE of a 10% acrylamide gel followed by Coomassie staining. L, lysate; S, supernatant (after removing insoluble from lysate). Uninduced: alphacat TEV. This figure has been modified from Petro and Raben[1] and is used under CC BY-NC 2.5.

Because GroEL/ES appeared to be the most promising bacterial chaperone for improving the solubility of alphacat in pT71myc and alphacat in pGEX-4T2, I likewise tested whether coexpression with GroEL/ES improved the solubility of each of the pET32a constructs. Alpha TEV in pET32a remained undetectable in the supernatant by

Coomassie (Figure 54). A small amount of either alphacat construct was visible in the supernatant by Coomassie (Figure 54), suggesting that coexpression with GroEL did improve their solubility, seeing as none was detectable when expressed without also overexpressing GroEL/ES (Figure 53), but the vast majority of the alphacat expressed remained in the pellet.

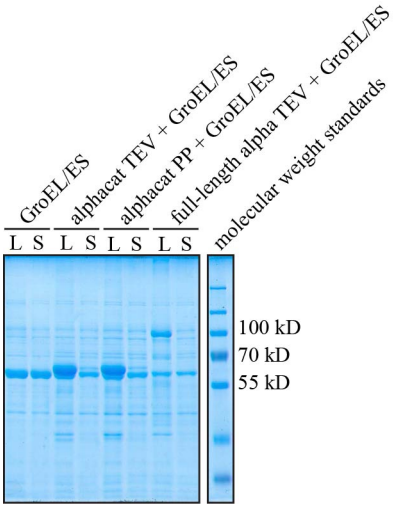

Figure 54. Coexpression with GroEL/ES does not greatly improve the solubility of DGK constructs in pET32a. I inoculated 4 mL LB Carb cultures with overnight cultures of the constructs shown, which I had previously transformed into BL21(DE3). When the OD600 was predicted to reach 0.3, I added IPTG to 1 mM and shook at 16°C overnight, then pelleted the cells. I resuspended the cell pellet in 40 mL per gram wet cell pellet lysis buffer (50 mM Tris, pH 8.0, 300 mM NaCl, 10 mM imidazole, 5 mM $MgCl_2$, 1 mM $CaCl_2$, 0.25% (v/v) TX-100, 0.5 mM DTT, 1x PIC), added egg white lysozyme to 1 mg per mL, and incubated on ice for thirty minutes. I lysed the cells by probe-sonicating ten times for ten seconds each, resting on ice for fifteen seconds between each burst. I removed the insoluble fraction by centrifuging at 43,000 x *g* for ninety minutes at 4°C. SDS-PAGE of a 10% acrylamide gel followed by Coomassie staining. L, lysate; S, supernatant (after removing insoluble from lysate). This figure has been modified from Petro and Raben[1] and is used under CC BY-NC 2.5.

Because alphacat expressed to a greater degree than full-length alpha, I decided to pursue alphacat for trying to maximize the production of soluble protein. I tested the coexpression of each of the sets of chaperones with alphacat TEV to see whether any of the other chaperones besides GroEL/ES improved its solubility. Coexpression with GroEL/ES and, to a lesser extent, TF increased by a small amount the quantity of alphacat TEV visible in the supernatant by Coomassie (Figure 55**A**), but alphacat TEV in

the supernatant remained undetectable by immunoblot (Figure 55**B**). Once again, GroEL was recognized by the α-DGK-alpha antibody; in this case, GroEL is the lower band, and alphacat is the upper band. GroEL is soluble after centrifugation, whereas alphacat TEV in pET32a is not. I concluded that coexpression with bacterial chaperones improved the solubility of TRX-tagged DGK constructs less than it did of alphacat in pT71myc or pGEX-4T2.

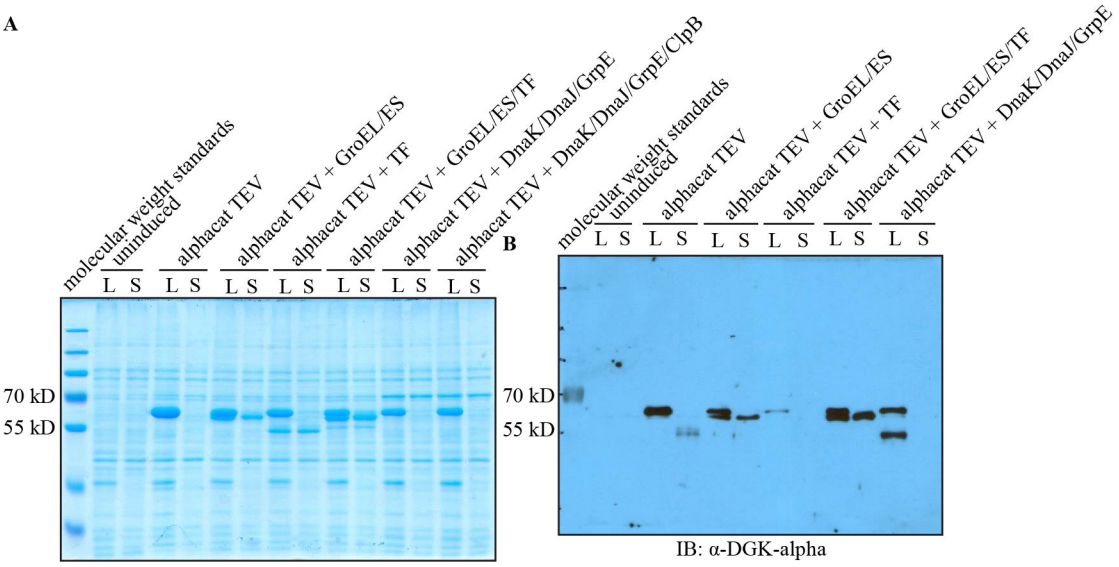

Figure 55. Coexpression with bacterial chaperones does not greatly improve the solubility of alphacat TEV in pET32a. I inoculated one 4 mL LB Carb culture with alphacat TEV in pET32a, and 4 mL LB Carb Cam cultures with overnight cultures of the constructs shown, all in BL21(DE3). When the OD600 was predicted to reach 0.3, I added IPTG to 0.1 mM and shook at 16°C for seventeen hours, then pelleted the cells. I resuspended the cell pellet in 40 mL per gram wet cell pellet lysis buffer (50 mM Tris, pH 8.0, 300 mM NaCl, 10 mM imidazole, 5 mM $MgCl_2$, 1 mM $CaCl_2$, 0.25% (v/v) TX-100, 0.5 mM DTT, 1x PIC), added egg white lysozyme to 1 mg per mL, and incubated on ice for 2.5 hours. I lysed the cells by probe-sonicating ten times for ten seconds each, resting on ice for fifteen seconds between each burst. I removed the insoluble fraction by centrifuging at 43,000 x *g* for ninety minutes at 4°C. SDS-PAGE of 10% acrylamide gels followed by **(A)** Coomassie staining and **(B)** immunoblotting against DGK alpha C-terminus (Abgent AP8128b (1:300 (v/v))). L, lysate; S, supernatant (after removing insoluble from lysate). Uninduced: alphacat TEV in pET32a + GroEL/ES. This figure has been modified from Petro and Raben[1] and is used under CC BY-NC 2.5.

I had previously observed that alphacat in pT71myc could be enriched from the supernatant by Ni-NTA even though the vast majority of alphacat in pT71myc is in the pellet, not the supernatant (Figure 15). I therefore wondered whether the DGK constructs

in pET32a could likewise be enriched from the supernatant, even though the vast majority of the protein was insoluble. I thus purified each of alphacat TEV and full-length DGK-alpha TEV in pET32a on Ni-NTA agarose. Alphacat TEV could clearly be enriched on Ni-NTA agarose (Figure 56). During the course of enrichment, a second, lower band, migrating between the alphacat band and the 60 kD molecular weight standard, appeared, which was also immunoreactive to the anti-DGK-alpha antibody (Figure 56**B**). This band could be a proteolytic fragment of alphacat, but is also the correct size to be endogenous GroEL, which also recognizes the DGK-alpha antibody (Figure 27), and could be associating to the overexpressed and possibly misfolded alphacat. Although I was able to enrich alphacat, the enriched alphacat was insufficiently concentrated to load onto the analytical gel filtration column. Full-length DGK-alpha TEV, as before (Figure 53), did not express as robustly as alphacat, and could not even be detected in the lysate by immunoblot (Figure 56**D**). Although it appeared slightly enriched by Coomassie (Figure 56**C**), full-length alpha TEV remained undetectable by immunoblot even following enrichment (Figure 56**D**).

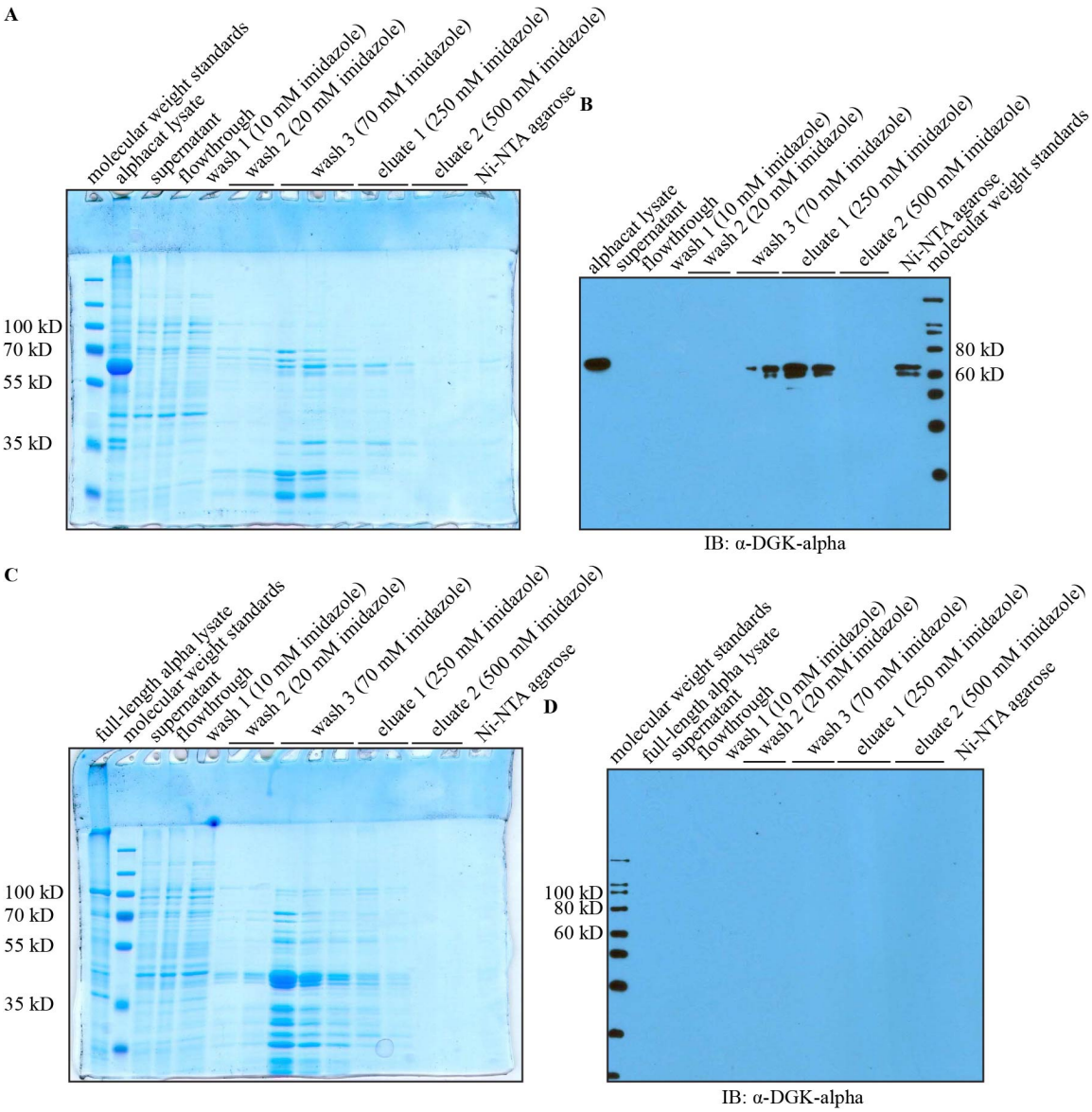

Figure 56. Alphacat TEV, but not full-length DGK-alpha TEV, in pET32a can be enriched on Ni-NTA, but the yield is low. I inoculated one 500 mL LB Carb culture with a freshly growing culture of either alphacat TEV or else full-length DGK-alpha TEV in pET32a in BL21(DE3). When the OD600 was predicted to reach 0.4, I added IPTG to 0.3 mM and shook at 16°C for 18 hours, then pelleted the cells. I resuspended the cell pellet in 24 mL lysis buffer (50 mM Tris, pH 8.0, 300 mM NaCl, 10 mM imidazole, 5 mM $MgCl_2$, 1 mM $CaCl_2$, 0.25% (v/v) TX-100, 0.5 mM DTT, 1x PIC), divided into three tubes, and froze at -80°C. I thawed one tube of each by shaking the tube gently in water. I added egg white lysozyme to 1 mg per mL, and incubated on ice for thirty minutes, vortexing occasionally to mix. I lysed the cells by probe-sonicating ten times for ten seconds each, resting on ice for fifteen seconds between each burst. I removed the insoluble fraction by centrifuging at 110,000 x *g* for 65 minutes at 4°C. I added Ni-NTA agarose 1:15 (v/v) and incubated for two hours, rotating at 4°C. I washed the resin with wash buffer 1 (50 mM Tris, pH 8.0, 300 mM NaCl, 10 mM imidazole, 5 mM $MgCl_2$, 1 mM $CaCl_2$, 0.5 mM DTT), wash buffer 2 (same as wash buffer 1, but imidazole increased to 20 mM), and wash buffer 3 (70 mM imidazole), and eluted with elution buffer 1 (250 mM imidazole), and elution buffer 2 (500 mM imidazole). **(A)**, **(B)**: enrichment of alphacat TEV. **(C)**, **(D)**: enrichment of full-length DGK-alpha TEV. SDS-PAGE of 10%

acrylamide gels followed by **(A)**, **(C)**: Coomassie staining; **(B)**, **(D)**: immunoblotting against DGK-alpha C-terminus (Abgent AP8128b (1:300 (v/v))).

Conclusions

I concluded that the TRX tag did not improve the solubility of our DGK constructs as we had hoped, and decided to pursue another solubility tag.

Cloning, Expression, Purification, and Analytical Gel Filtration of Alphacat and Full-Length DGK-Alpha in pET28-HisMBP-FLAGpp

Introduction

Maltose binding protein (MBP) has been reported to improve the solubility of target proteins to which it has been fused[113,119,120]. I therefore cloned both alphacat and full-length DGK-alpha into an MBP-containing plasmid.

Results

The pET28-HisMBP-FLAGpp plasmid adds to the N-terminus of the protein a fusion tag that includes hexahistidine, *Pyrococcus furiosus* MBP, a FLAG tag, and a PreScission Protease site (Figure 57). In order to clone alphacat and full-length DGK-alpha into pET28-HisMBP-FLAGpp, I designed the forward PCR primer GCAAGTCGACAAATCTATCCCAGTGTCCTGG for alphacat and GCAAGTCGACAATCCAAGGAGAGGGGG for full-length DGK-alpha. Both these primers begin with a GC anchor to promote more efficient priming during the PCR reaction. The GC anchor is followed by two spacer nucleotides: the four nucleotides in total provide an overhang to promote more efficient digestion by the restriction enzyme SalI. I chose these two spacer nucleotides to be AA in order to keep the GC content of the primer low. Following the spacer is a SalI restriction site: following digestion with

SalI, the digested PCR product could then be ligated into the SalI site of the pET28-HisMBP-FLAGpp plasmid that had been likewise digested. Following the SalI site is another two-nucleotide spacer, to ensure that the DGK insert is translated in the same reading frame as the start codon encoded in the pET28-HisMBP-FLAGpp plasmid. Once again, I chose these two spacer nucleotides to be AA in order to keep the GC content of the primer low. For full-length DGK-alpha, this forward primer removes the initial methionine, to prevent the production of untagged DGK-alpha at the second start site. For the reverse primer, I used GCAGCGGCCGCTCAGCACAAGAAGCCAAAGAAATTG, the same reverse primer I used to add a NotI site downstream of full-length DGK-alpha for cloning into pT71myc, and of both full-length DGK-alpha and alphacat for cloning into pET32a. As in the pET32a cloning, this reverse primer restores the terminal cysteine to alphacat.

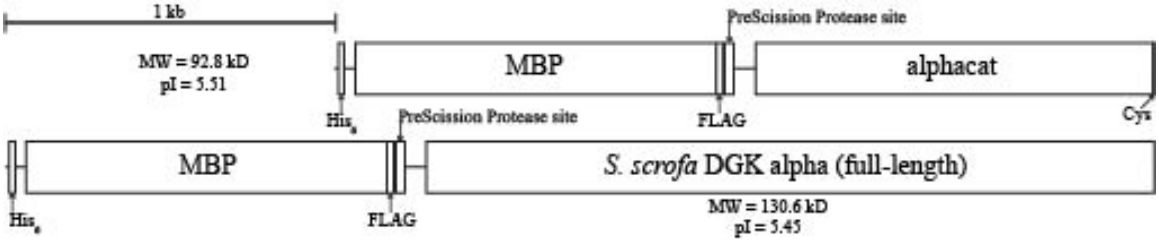

Figure 57. Schematic of alphacat and full-length DGK alpha in pET28-HisMBP-FLAGpp construct. Top, schematic of alphacat in HisMBP-FLAGpp construct. "Alphacat" consists of residues 333-733 of *S. scrofa* DGK alpha; for this construct, the 734th residue of *S. scrofa* DGK alpha, cysteine, was added back. pET28-HisMBP-FLAGpp adds to the N-terminus of the protein a fusion tag consisting of a hexahistidine tag, followed by *P. furiosus* maltose-binding protein (MBP) fusion tag, followed by a FLAG tag, followed by a PreScission Protease site. The total mass of the protein construct (including the fusion tag) and pI are predicted to be 92.8 kD and 5.51, respectively. Bottom, schematic of full-length *S. scrofa* DGK alpha construct. The total mass of the protein construct (including the fusion tag) and pI are predicted to be 130.6 kD and 5.45, respectively. This figure has been modified from Petro and Raben[1] and is used under CC BY-NC 2.5.

When I transformed MBP-tagged alphacat or full-length DGK alpha into the BL21(DE3) strain of *E. coli*, they each expressed readily after induction with IPTG, producing a band, easily detectable by Coomassie staining following SDS-PAGE, that

was recognized by the anti-DGK-alpha antibody (Figure 58). For alphacat, the predominant band migrated between the 80 and 100 kD molecular weight markers, consistent with its predicted molecular weight of 92.8 kD. For full-length DGK-alpha, the predominant band migrated between the 120 and 130 kD molecular weight markers, slightly faster than its predicted molecular weight of 130.6 kD. Both constructs also produced lower-molecular weight bands not seen in the uninduced cells, some of which were also immunoreactive to the anti-DGK-alpha antibody. The MBP tag did not appear to improve DGK-alpha's solubility: the fusion-tagged protein, either alphacat or full-length DGK-alpha, while easily detectable in the lysate, remained undetectable by immunoblotting the supernatant following centrifugation (Figure 58**C**).

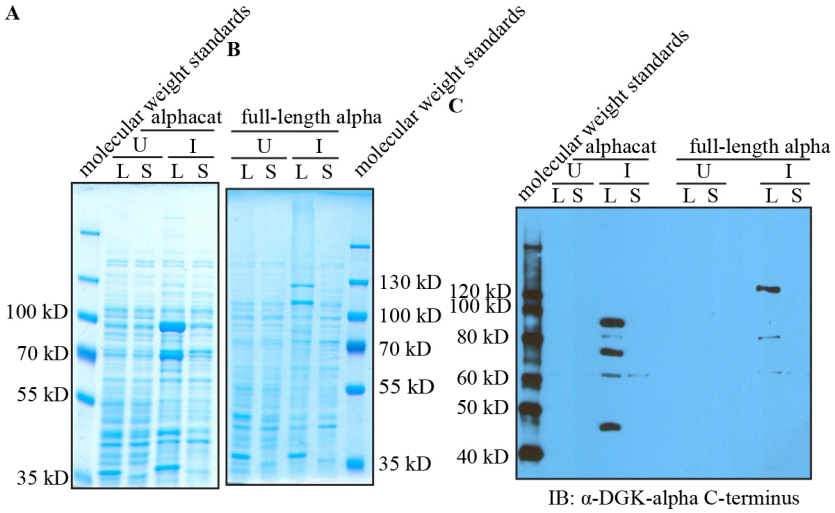

Figure 58. Both alphacat and full-length alpha in pET28-HisMBP-FLAGpp express a band of the correct size that is recognized by the DGK-alpha antibody, but both protein constructs remain in the pellet after centrifugation. I inoculated two 25 mL LB Kan cultures with overnight cultures of alphacat in pET28-HisMBP-FLAGpp in Bl21(DE3), and two 50 mL LB Kan cultures with overnight cultures of full-length DGK-alpha in pET28-HisMBP-FLAGpp in BL21(DE3). When the OD600 was predicted to reach 0.3, I added IPTG to 0.1 mM (or not) and shook overnight (18 hours for alphacat, and 19 hours for full-length DGK-alpha) at 16°C, then pelleted the cells. I resuspended the cell pellet in 4 mL per gram wet cell pellet lysis buffer (50 mM Tris, pH 8.0, 300 mM NaCl, 10 mM imidazole, 1 mM $CaCl_2$, 0.25% (v/v) TX-100, 0.5 mM DTT, 1x PIC), added egg white lysozyme to 1 mg per mL, and incubated on ice for thirty minutes, vortexing occasionally to mix. I lysed the cells by probe-sonicating ten times for ten seconds each, resting on ice for fifteen seconds between each burst. I removed the insoluble fraction by centrifuging at 43,000 x *g* for ninety minutes at 4°C. SDS-PAGE of 8% acrylamide gels followed by: **(A)** and **(B)** Coomassie staining; **(C)** immunoblotting against DGK-alpha C-terminus (Abgent AP8128b (1:300

(v/v))). U, uninduced; I, induced; L, lysate; S, supernatant (after removing insoluble from lysate). This figure has been modified from Petro and Raben[1] and is used under CC BY-NC 2.5.

I had been under the impression that MBP fusion tags targeted the attached protein to the periplasmic space, and that the subsequent isolation from making inappropriate contacts from other cellular proteins was part of the mechanism by which MBP's solubilization worked. It turns out that the targeting to the periplasmic space came from a signal peptide contained in another MBP-containing plasmid I had previously worked with, and MBP itself has no such properties, but at the time I tested whether the MBP-tagged constructs went to the periplasmic space. Following New England BioLabs® Inc.'s Protein Expression & Analysis instruction manual "pMAL™ Protein Fusion & Purification System" (New England BioLabs® Inc. #E8200S), I extracted the periplasmic space from fresh expressions of alphacat and of full-length DGK-alpha in pET28-HisMBP-FLAGpp. Horizontal streaking in the Coomassie-stained gels suggests that the interface between the stacking and separating phases dried out during casting, and caused the wells to leak during electrophoresis (Figure 59**A**). For each construct, a predominant, lower-molecular weight immunoreactive band is seen in the first resuspension (R1) but not the second (R2) (a more precise estimate of the molecular weight of these bands is complicated by the fact that the two sets of molecular weight standards migrate differently on the immunoblot): the fate of these proteins is unclear. Because the periplasmic extraction did not include protease inhibitors, one possibility is that these bands were proteolytically digested during the periplasmic extraction, although this interpretation seems unlikely, seeing as the samples were stored at 4C overnight prior to electrophoresis (and hence, any proteases present in R2 during the periplasmic extraction were also present in the R1 samples waiting for

electrophoresis: one possible explanation could be that endogenous protease inhibitors were removed in the supernatant (S1)). The immunoreactive bands are clearly in the resuspended periplasm but not the supernatant (Figure 59**B**), showing that the MBP-tagged DGK-alpha constructs did not travel to the periplasmic space.

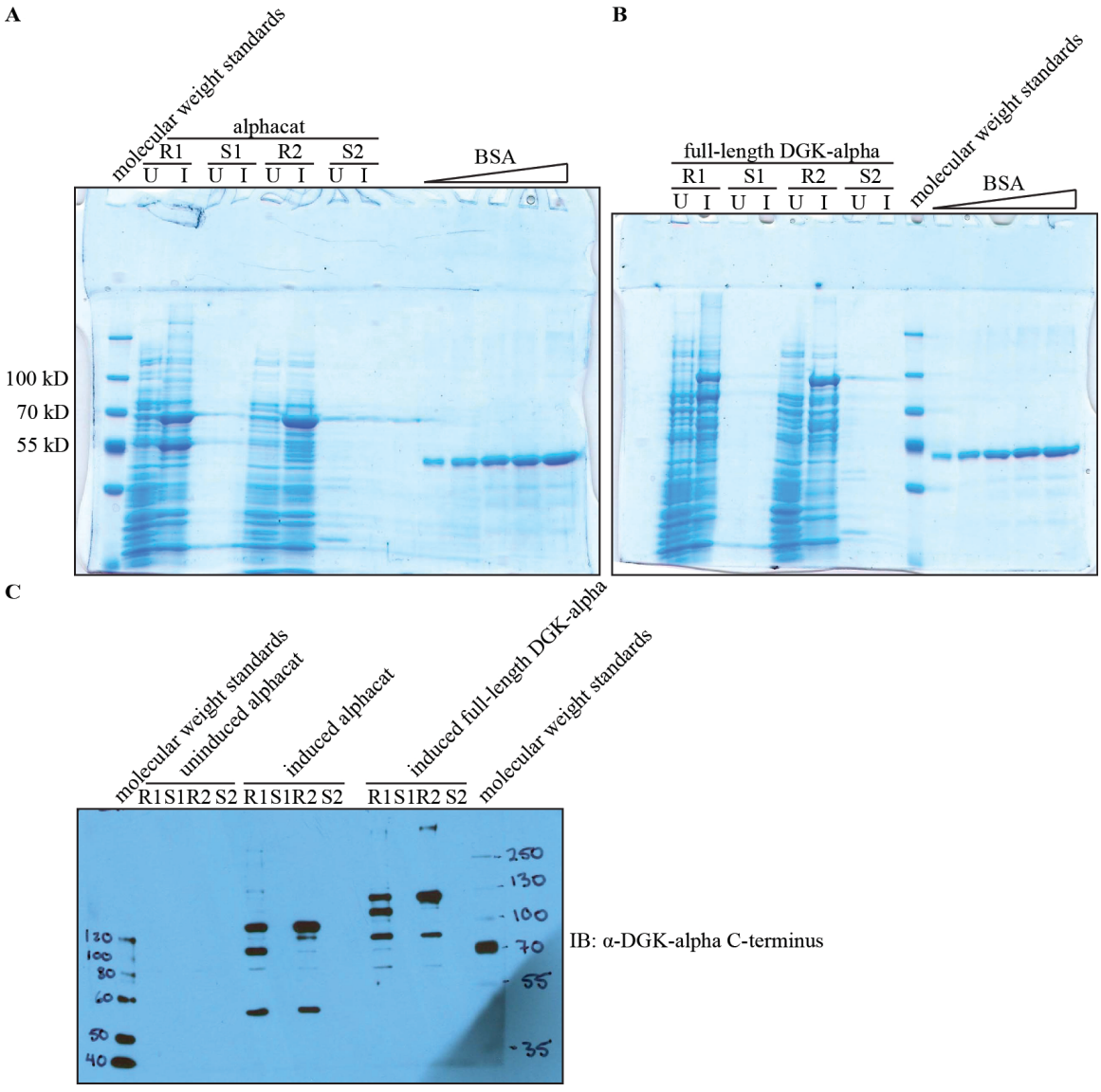

Figure 59. Alphacat and full-length DGK-alpha in pET28-HisMBP-FLAGpp in Bl21(DE3) are not in the periplasmic space. I inoculated two 50 mL LB Kan cultures each with overnight cultures of alphacat in pET28-HisMBP-FLAGpp or full-length DGK-alpha in pET28-HisMBP-FLAGpp in BL21(DE3). When the OD600 was predicted to reach 0.5, I added IPTG to 0.3 mM (or not) and shook for seventeen hours at 16°C, then pelleted the cells. To extract the periplasmic space, I resuspended the cell pellet in 80 mL per gram wet cell pellet resuspension buffer 1 (30 mM Tris, 20% sucrose (w/v), pH 8.0), and removed an aliquot as resuspended 1 (R1). I then added EDTA to 1 mM, and shook at room temperature for five

minutes. I removed the insoluble fraction by centrifuging at 8,000 x *g* for twenty minutes at 4°C, and removed an aliquot of the resulting supernatant as supernatant 1 (S1). I resuspended the pellet in 80 mL per gram ice cold 5 mM $MgSO_4$, and removed an aliquot as resuspended 2 (R2). I shook in an ice bath for five minutes, then removed the insoluble fraction by centrifuging at 8,000 x *g* for twenty minutes at 4°C, and removed an aliquot of the resulting supernatant as supernatant 2 (S2), the osmotic shock fluid. SDS-PAGE of 8% acrylamide gels followed by **(A)** Coomassie staining, and **(B)** immunoblotting against DGK-alpha C-terminus (Abgent AP8128b (1:300 (v/v))). The reason for the discrepancy in the migration patterns between the two sets of molecular weight standards in the immunoblot is unclear.

I had previously observed that alphacat in pT71myc could be enriched from the supernatant by Ni-NTA even though the vast majority of alphacat in pT71myc was in the pellet, not the supernatant (Figure 15). I therefore wondered whether the DGK constructs in pET28-HisMBP-FLAGpp could likewise be enriched from the supernatant, even though the vast majority of the protein was insoluble, as I had done with the pET32a constructs. I thus purified the supernatants of both alphacat in pET28-HisMBP-FLAGpp expressions (both the expression test shown in Figure 58 and the periplasmic expression test shown in Figure 59) on Ni-NTA agarose. Even though alphacat was undetectable in the supernatant in Figure 58, I could indeed enrich alphacat in pET28-HisMBP-FLAGpp on Ni-NTA agarose (Figure 60**A** and **B**). The concentration in alphacat in the supernatant from the periplasmic extraction, however, was so low that even after Ni-NTA agarose enrichment, it was undetectable by immunoblotting (Figure 60C and D).

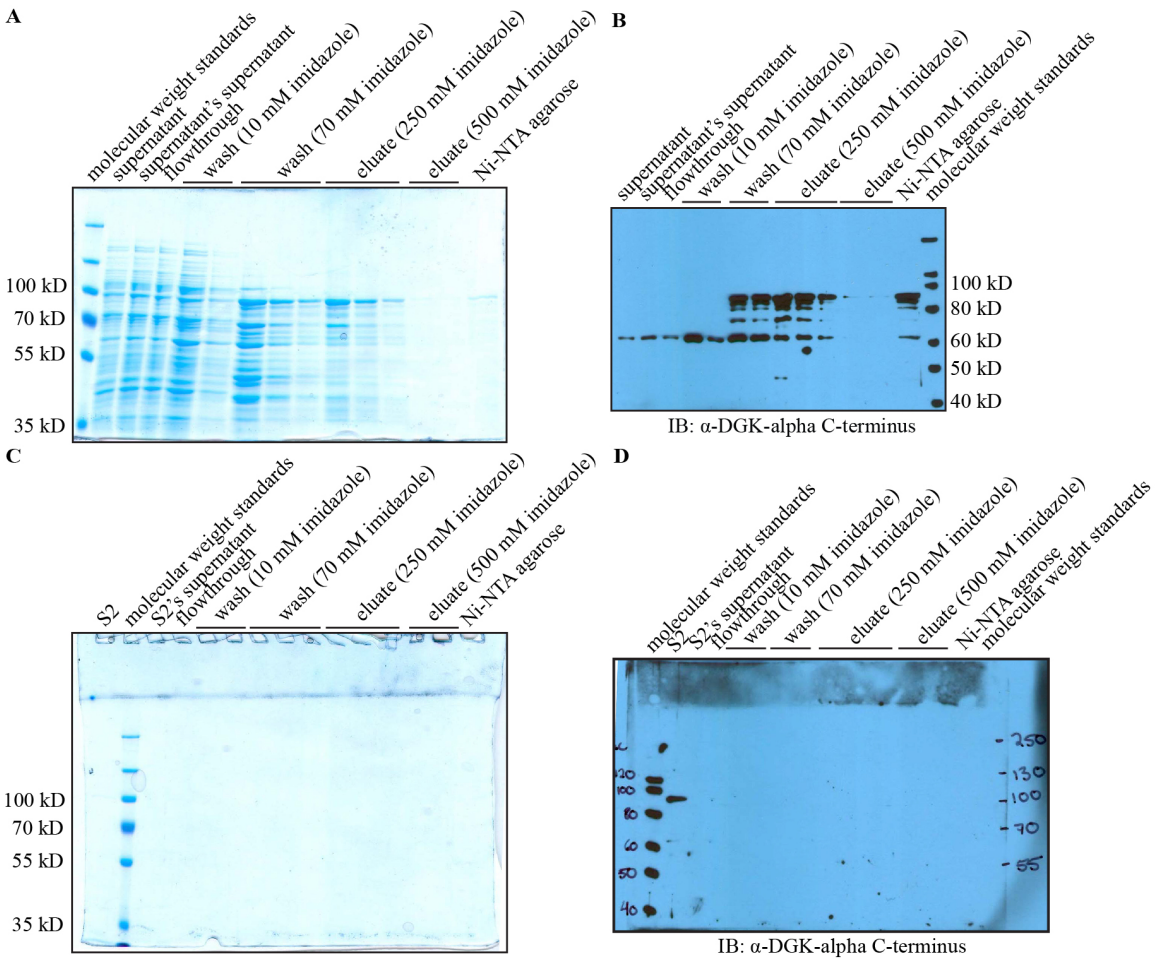

Figure 60. Alphacat in pET28-HisMBP-FLAGpp can be enriched from BL21(DE3) supernatant, but not osmotic shock fluid, by Ni-NTA chromatography. I stored the supernatant from **Figure 58** for two weeks and the osmotic shock fluid (S2) from **Figure 59** for eleven days at -80°C (in 20% glycerol, plus 1.6 mL per gram 1 M Tris, pH 8.0), then thawed by gently shaking the tubes in water. I removed the insoluble fraction by centrifuging at 110,000 x *g* for one hour at 4°C. I added Ni-NTA agarose 1:14 (v/v) to the supernatant (from **Figure 58**) and 1:408 (v/v) to the osmotic shock fluid (from **Figure 59**) and incubated for 4.5 hours, rotating or rocking at 4°C. I washed the resin with wash buffer 1 (50 mM Tris, pH 8.0, 300 mM NaCl, 10 mM imidazole, 5 mM $MgCl_2$, 1 mM $CaCl_2$, 0.5 mM DTT) and wash buffer 2 (same as wash buffer 1, but imidazole increased to 70 mM), and eluted with elution buffer 1 (250 mM imidazole) and elution buffer 2 (500 mM imidazole). SDS-PAGE followed by: **(A)**, **(C)**, Coomassie staining; **(B)**, **(D)**, immunoblotting against DGK-alpha C-terminus (Abgent AP8128b (1:300 (v/v))). **(A)** and **(B)** show the purification from the supernatant shown in **Figure 58**. **(C)** and **(D)** show the purification from the osmotic shock fluid (S2) shown in **Figure 59**. I loaded a larger volume of S2 into the immunoblot shown in (D) than I did into the immunoblot shown in **Figure 59**, which may explain why the antibody was able to detect it in this blot but not in the previous one. This figure has been modified from Petro and Raben[1] and is used under CC BY-NC 2.5.

Although the enriched alphacat was clearly not purified to homogeneity (Figure 60), the yield was sufficient that I could load it onto the Sephadex® G-200 analytical gel

filtration column, after first concentrating it by dialyzing against 15% PEG 17.5k. The eluting MBP-tagged alphacat was clearly detectable by immunoblotting, along with several other immunoreactive bands (consistent with the presence of other immunoreactive bands in the partially purified fraction (Figure 60)) (Figure 61). The predominant immunoreactive band migrates between 60 and 70 kD, so could very well be endogenous GroEL (which also recognizes the anti-DGK-alpha antibody (Figure 27)) associating with the overexpressed and possibly recombinant protein, similarly to what I observed with partially purified alphacat in pET32a (Figure 56**B**). Alphacat in pET28-HisMBP-FLAGpp's predicted molecular weight is consistent with the top, ~90 kD band, and it is on this band that I performed densitometry. Alphacat was not monodisperse, but rather eluted in two populations, one in the void volume, and one at an elution volume corresponding to a molecular weight of 124 kD (Figure 61), between the predicted molecular weights of a monomer and of a dimer. Because alphacat in pET28-HisMBP-FLAGpp was not monodisperse, I therefore concluded that the MBP-tagged alphacat also formed aggregates unsuitable for pursuit for structural studies.

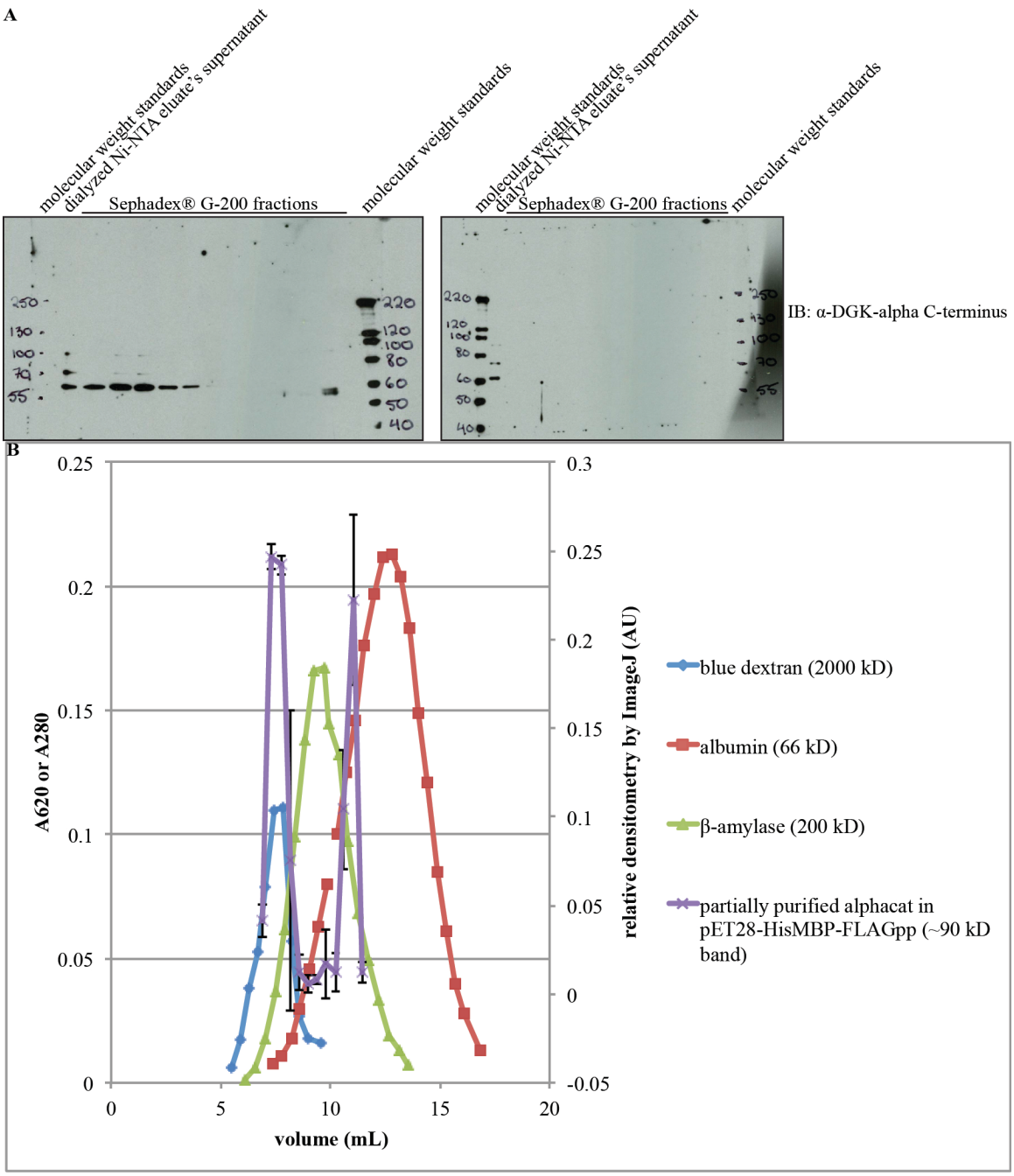

Figure 61. Partially purified alphacat in pET28-HisMBP-FLAGpp is not monodisperse a Sephadex® G-200 analytical gel filtration column. The second wash (70 mM) of the supernatant (shown in **Figure 60**A and B appeared to have the highest yield of alphacat, so, after storing for two days at 4°C, I removed the insoluble fraction by centrifuging at 43,000 x *g* for ninety minutes at 4°C, and then dialyzed the resulting supernatant against dialysis buffer (50 mM tris, 100 mM KCl, 1 mM $CaCl_2$, pH 8.0, 15% (w/v) PEG 17.5 kD) for two hours at 4°C using a 10,000 MWCO cassette to concentrate it. I stored the sample overnight at 4°C, then removed the insoluble fraction by centrifuging at 43,000 x *g* for ninety minutes at 4°C. I loaded 200 µL of the resulting supernatant onto a Sephadex® G-200 column that had been freshly blocked with 930 µL of 10 mg/mL albumin and previously calibrated with albumin and β-amylase. I collected fractions every four minutes, eluting by gravity in gel filtration buffer (50 mM Tris, 300 mM

NaCl, 5 mM $MgCl_2$, 1 mM $CaCl_2$, 250 mM imidazole, pH 8.0). **(A)** SDS-PAGE followed by immunoblotting against DGK-alpha C-terminus (Abgent AP8128b (1:300 (v/v))) of gel filtration fractions of elution volumes corresponding to molecular weights of 549 to 19.2 kD. **(B)** Elution volumes of molecular weight standards and of purified alphacat from a Sephadex® G-200 column. Left vertical axis, A280 of the protein molecular weight standards, and A620 of the blue dextran fractions. Right vertical axis, densitometry performed three times on the ~90 kD band using the film shown in (A), mean ± SD. This figure has been modified from Petro and Raben[1] and is used under CC BY-NC 2.5.

In another attempt to improve the protein constructs' solubility, after inducing expression in *E. coli* with IPTG I added chloramphenicol to arrest translation, which has been reported in to improve the solubility of other proteins prone to aggregation[121]. Treating the cells with chloramphenicol did not appear to improve the recovery of MBP-tagged alphacat or full-length DGK alpha in the supernatant following centrifugation, as measured by either Coomassie staining or immunoblotting following SDS-PAGE (Figure 6e).

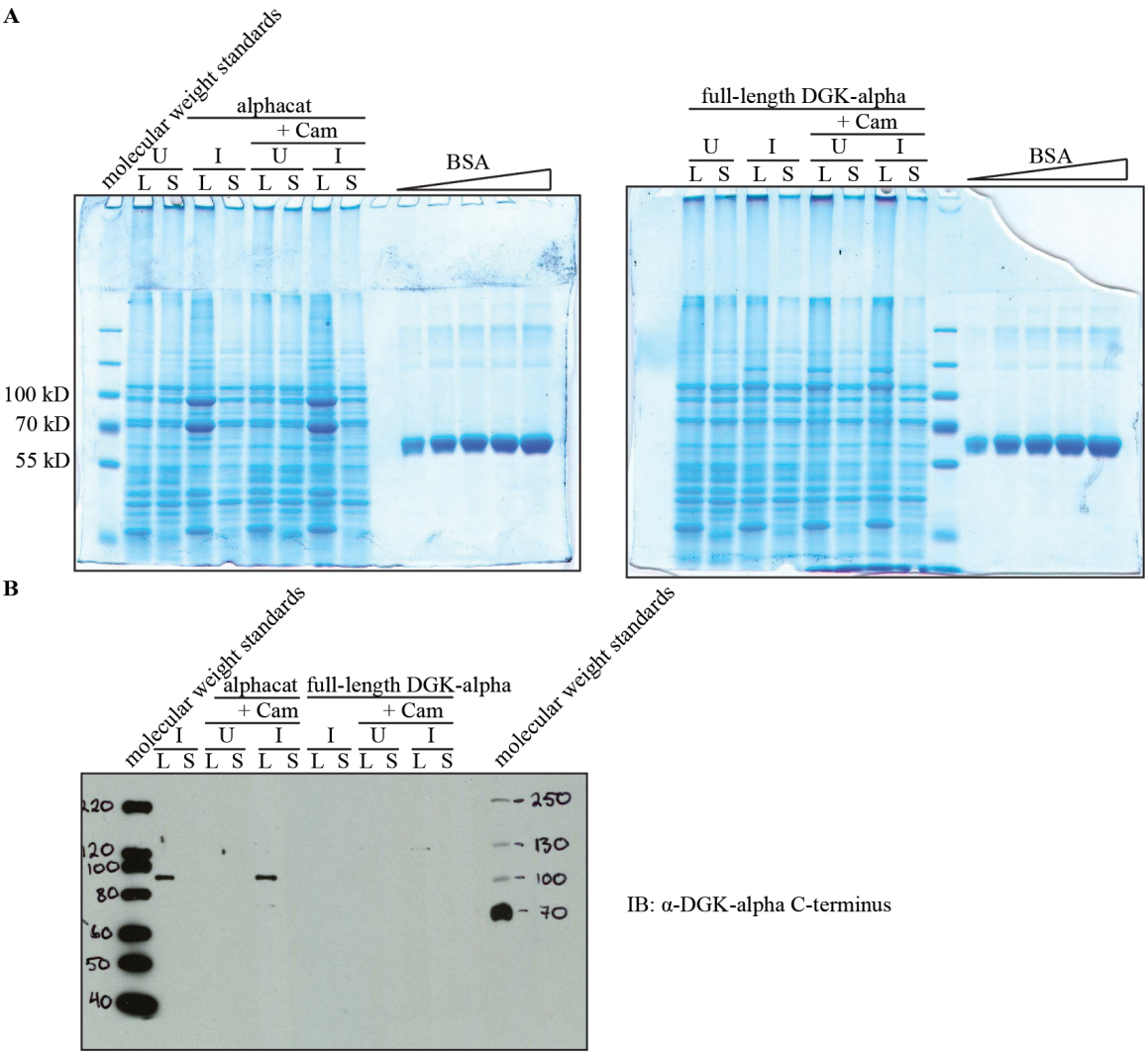

Figure 62. Arresting protein translation with chloramphenicol during expression does not improve the solubility following centrifugation of either alphacat or full-length DGK-alpha in pET28-HisMBP-FLAGpp. I inoculated four 4 mL LB Kan cultures with an overnight culture of either alphacat or else full-length DGK-alpha in pET28-HisMBP-FLAGpp. When the OD600 was predicted to reach 0.8, I added IPTG to 0.1 mM (or not), and shook for fifteen hours at 20°C, then pelleted the cells. I resuspended the uninduced cell pellets in the same volume as original cell culture in either LB Kan Cam (to control for the effects of translation arrest in BL21(DE3) not overexpressing a recombinant protein) or LB Kan plus ethanol (to control for the addition of ethanol, since that is the solvent in which our concentrated chloramphenicol stocks are stored), and I resuspended the induced cell pellets in either LB Kan Cam (to test whether translation arrest improved the solubility of the recombinant proteins) or else LB Kan plus ethanol plus 0.1 mM IPTG. I returned the resuspended cells to culture tubes and continued to shake at 20°C for two more hours, then pelleted the cells and froze at -80°C for two hours. I thawed the cells by gently shaking the tubes in water, then resuspended the cells in 20 mL per gram wet cell pellet lysis buffer (50 mM Tris, pH 8.0, 300 mM NaCl, 10 mM imidazole, 1 mM $CaCl_2$, 0.25% (v/v) TX-100, 0.5 mM DTT, 1x PIC), added egg white lysozyme to 1 mg per mL, and incubated on ice for thirty minutes, vortexing occasionally to mix. I lysed the cells by probe-sonicating ten times for ten seconds each, resting on ice for between each burst. I removed the insoluble fraction by centrifuging at 43,000 x *g* for ninety minutes at 4°C. SDS-PAGE of 8% acrylamide gels followed by: (A), Coomassie staining; (B), immunoblotting

against DGK-alpha C-terminus (Abgent AP8128b (1:300 (v/v))). U, uninduced; I, induced; L, lysate; S, supernatant (after removing insoluble from lysate). Cam, chloramphenicol.

Conclusions

I concluded that the MBP tag did not improve the solubility of the DGK constructs as I had hoped.

Bacterial Expression Discussion and Conclusions

Solubility challenges with expressing eukaryotic DGKs recombinantly in *E. coli* have been previously reported. In one case *S. scrofa* DGK alpha purified from inclusion bodies had no detectable DGK activity[49] (even though *E. coli* lysate overexpressing the same protein does have DGK activity[36]); in another, AtDGK2 from the plant *Arabidopsis thaliana* required a NusA tag in order to express in *E. coli*[51]. Takahashi *et al.* report that they were unable to express the C-terminal domain of *S. scrofa* DGK alpha in *E. coli* because the cysteine-rich C1 domain rendered it insoluble[39]. Recombinantly expressing LCB5 family proteins in *E. coli* has generally been more successful when those family members are prokaryotic[92–94].

One possible explanation for why recombinant expression of prokaryotic LCB5 family proteins has been more successful than eukaryotic is that prokaryotes have different codon abundances than eukaryotes. Insufficient availability of the appropriate tRNA can lead to ribosome pausing, frameshifts, deletions, mistranslations, aborted translation products, and decreased expression of the target protein, even in response to only a single rare codon[122,123]. The cDNA of alphacat does in fact have a number of rare codons: two AGG, five AGA, eight CTA, one ATA, four CGA, twelve CCC, eight GGA, and three CGG. Alphacat TEV in pET32a, when coexpressed with the

DnaK/DnaJ/GrpE/ClpB set of chaperones, produces, in addition to the predominant band of the predicted size, an additional, lower band that is recognized by the anti-DGK-alpha-C-terminus antibody (Figure 55**B**); alphacat in pET28-HisMBP-FLAGpp (Figure 58**C**, Figure 59**B**, and Figure 60**B**) and alphacat in pT71myc (Figure 6**B** and Figure 16**A**) likewise produce several recognized bands. These additional bands could indeed be truncations produced by aborted translation or by frameshifting during translation.

Size may be another factor limiting the success of recombinantly expressing eukaryotic DGKs in prokaryotic systems. *S. typhimurium* YegS and *S. aureus* DgkB are 32 and 35 kD, respectively, smaller than any of the eukaryotic DGKs. Although no absolute upper limit has been reported for the size of proteins that can be recombinantly expressed in *E. coli*, in general, larger proteins express less well. My own observations are consistent with this rule of thumb: the smallest construct tested, alphacat in pT71myc, expresses the most robustly, and the alphacat constructs always express at higher levels than their full-length DGK alpha counterparts.

Translational folding partners are frequently used to improve the solubility of proteins expressed in *E. coli*[112–115]. However, my work has demonstrated that adding GST, TRX, or MBP as a fusion tag did not improve the solubility of either full-length DGK-alpha or alphacat. All of the constructs in the bacterial expression studies are tagged on the N-terminus. The position of a fusion tag can greatly affect a protein's expression and function[124,125]; perhaps exposure of the N-terminus of full-length DGK alpha is required for stability, and a C-terminally tagged construct would express better or be more stable. Alternatively, as discussed above, even the smallest constructs used in this study is large by prokaryotic standards, and perhaps any additional solubility

conferred by the fusion tag was counteracted by the fact that the tagged protein was larger in size.

Progress is being made in the ability to predict the ideal fusion tag to solubilize target proteins; however, much work remains to be done. Protein solubility prediction servers[126,127] are invaluable tools, but they sometimes disagree in their predictions. For example, PROSO[127] predicts our full-length DGK alpha in pT71myc construct to be soluble with a probability of 0.520, whereas SOLpro[126] predicts it to be insoluble with a probability of 0.550540. Their predictions may not be always accurate, either: SOLpro[126], for example, predicts the alphacat in pET28-HisMBP-FLAGpp construct to be soluble with a probability of 0.771506, which is contrary to the data shown in Figure 58. Given the difficulty in predicting which solubility tags will work, it is entirely possible that alternative solubility tags could help increase the soluble yield of mammalian DGKs, and perhaps even cause them to elute as a monodisperse population from an analytical gel filtration column. As mentioned above, the NusA tag proved helpful for expressing *A. thaliana* AtDGK2 in *E. coli*[51]; however, this report does not mention whether the purified AtDGK2 was monodisperse. Solubility predictions by SOLpro[126] for NusA-tagged alphacat and full-length DGK alpha are very optimistic, predicting them to be soluble with probabilities of 0.922228 and 0.870324, respectively, whereas predictions by PROSO[127] are more measured: 0.561 and 0.532, respectively, possibly owing to the large size of these constructs (110 and 148 kD, respectively). Tags specifically engineered to improve the solubility of target proteins have been successfully developed in some systems[115], and could be useful for DGK studies; however, at this

juncture, improving the solubility of eukaryotic DGKs remains a process of trial-and-error.

Coexpressing alphacat with bacterial chaperones, especially GroEL/ES, increases the yield of some, but not all, of the tested constructs in the soluble fraction, which is promising for large-scale expressions for crystallography. Unfortunately, alphacat in this soluble fraction still elutes in the void volume during analytical gel filtration chromatography. One reason that alphacat coexpressed with GroEL/ES elutes in the void volume could be explained by its being complexed to the GroEL, based on the evidence that the two proteins copurify on Ni-NTA (Figure 28, Figure 31, Figure 46, Figure 47, and Figure 50), and they coelute from the analytical gel filtration column (Figure 29 and Figure 51). If the alphacat is in fact complexed with GroEL/ES, the predicted molecular weight of the complex would be greater than 900 kD, and thus would indeed be predicted to elute in the void on the Sephadex® G-200 column. Another possibility is that while coexpressing alphacat with bacterial chaperones is sufficient to increase its yield in the supernatant, it still remains in microscopic aggregates.

The maximum size of a protein to fit in the *cis*-cavity of GroEL has been reported to be 57 kD[128]; on the other hand, GroEL has also been reported to help fold substrates as large as 150 kD[129]. Therefore, it is not entirely surprising that the GroEL/ES sets of chaperones did not improve the solubility of any of the full-length DGK alpha constructs, or of the alphacat in pET32a constructs, although coexpression with GroEL/ES clearly improved the yield of alphacat in pGEX-4T2 in the supernatant after centrifugation, even though the size of the GST-tagged alphacat construct is 71.6 kD.

Analysis of the chaperone data is further complicated by the fact that GroEL is recognized by the α-DGK-alpha antibody (Figure 27). Endogenous GroEL could thus be the identity of the predominant 60 kD immunoreactive band seen in the partially purified alphacat in pET32a (Figure 56) and in the partially purified alphacat in pET28-HisMBP-FLAGpp (Figure 60 and Figure 61), in which case, GroEL's failing to release alphacat could once again explain why alphacat in pET28-HisMBP-FLAGpp elutes in the void volume from the analytical gel filtration column (Figure 61), even though GroEL was not overexpressed in this preparation.

It is not surprising that the DnaK/DnaJ/GrpE and DnaK/DnaJ/GrpE/ClpB sets of chaperones did not improve the solubility of either alphacat or full-length DGK alpha in any of the constructs tested, seeing as only DnaK appeared to overexpress (Figure 26**A**, Figure 34, Figure 41, and Figure 55), and its cochaperones DnaJ (which stimulates DnaK's ATPase activity[130]) and GrpE (which acts as a nucleotide exchange factor for DnaK[130]) are not expressed proportionately. DnaK has also been reported to induce proteolysis in response to overproduction of a recombinant protein[131], which may be the reason we observe new, smaller, immunoreactive bands in alphacat TEV in pET32a lysates when coexpressed with the DnaK set of chaperones (Figure 55).

It is entirely possible that coexpression with alternative sets of chaperones could also enhance the solubility of these proteins, but the process of choosing a set of chaperones to coexpress with a given protein remains largely empirical. Other proteins reported to have chaperone activity, and thus potential candidates for coexpression to improve the solubility of eukaryotic DGKs, include Hsp90[132], α-crystallins[133], and dehydrins[134]. DnaK itself indeed would also be a candidate for consideration, as long as

its cochaperones DnaJ and GrpE are also appropriately expressed, and could even be coexpressed with GroEL/ES, given that these chaperones can work in parallel[135], thereby delivering the driving force needed to solubilize DGK-alpha.

Detergents have often been reported to improve the solubility of recalcitrant proteins[136–138]. Our method for determining monodispersity, analytical gel filtration using a Sephadex® G-200 resin, however, is incompatible with Triton X-100 concentrations as low as 0.01% (v/v) because the detergent causes an unacceptable loss of resolution in the molecular weight standards (Figure 49). Future studies wishing to monitor the monodispersity of eukaryotic DGKs may wish to consider alternative resin/detergent combinations.

Given the challenges of expressing DGKs in prokaryotic hosts, I also tried to express and purify DGKs from eukaryotic expression systems.

Expressing and Purifying *Dictyostelium discoideum* FLAG-DGKA from *D. discoideum*

Introduction

A partially finished collaboration started previously in the laboratory sought to answer the question of whether four synthetic diglyceride analogs produced by the laboratory of Professor Glenn Prestwich (Department of Medicinal Chemistry, University of Utah), whose structures are shown in Figure 120, activated, inhibited, or could serve as substrates for eukaryotic DGKs. This work was begun by Ms. Michele Ostroski using FLAG-DGKA expressed and purified from *D. discoideum* as the eukaryotic DGK. In

order to continue the project, I therefore also needed to express and purify FLAG-DGKA from *Dictyostelium discoideum*.

Results

When I followed Ostroski et al.[47]'s methods for purifying FLAG-DGKA from the eukaryote and slime mold *D. discoideum*, the recombinant protein was enriched on the anti-FLAG agarose, but did not elute from the resin (Figure 63). One important difference between my approach and that of Ostroski et al.[47] was that while they grew their D. discoideum cultures in suspension in liter quantities, I maintained the D. discoideum as an adherent culture on tissue culture plates and therefore expressed much smaller quantities of protein. I was unable to maintain *D. discoideum* as a suspension culture.

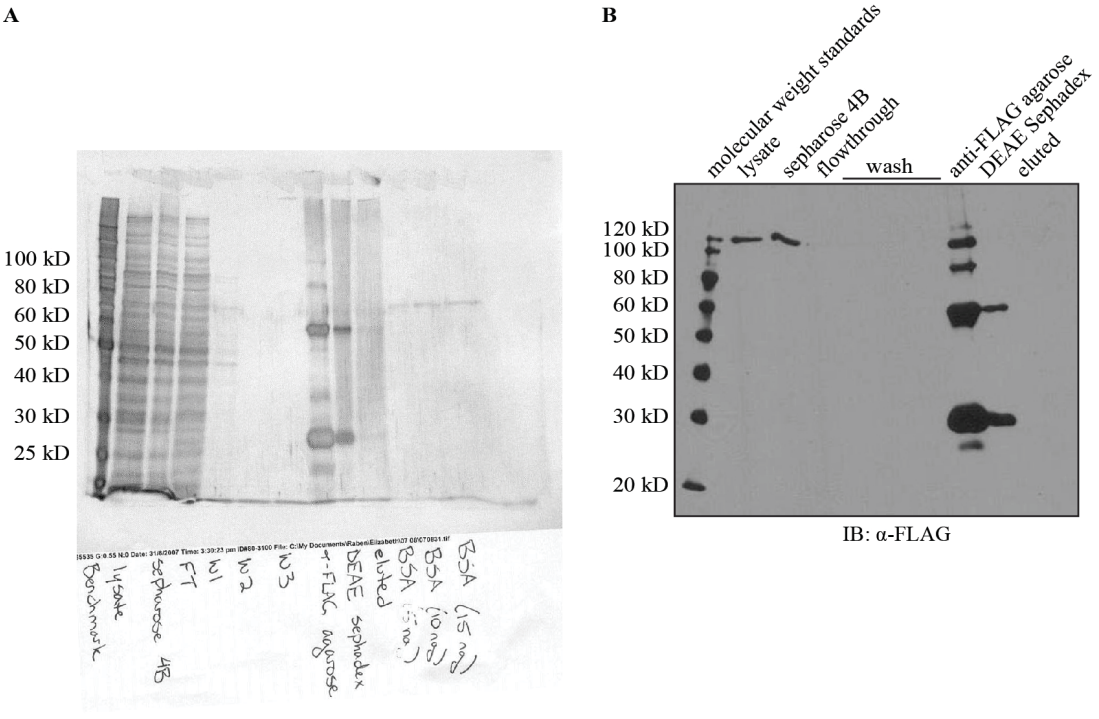

Figure 63. Following protocol Ostroski *et al*[47] to purify FLAG-DGKA from *D. discoideum* gives low yield. I resuspended FLAG-DGKA-expressing *D. discoideum* cells in their own medium. I pelleted the cells and washed with cell wash buffer (50 mM *N*-tris(hydroxymethyl)methyl-2-aminoethanesulfonic

acid (TES), 3x PIC, pH 7.3), then resuspended the cells in lysis buffer (50 mM TES, 200 mM NaCl, 10 mM EDTA, 1 mM DTT, 3x PIC, pH 7.3), and filtered the cells through a 5 μm membrane. I removed the insoluble fraction by centrifuging at 115,000 x *g* for one hour at 4°C. I precleared the resulting supernatant with packed 1:20 (v/v) sepharose 4B and rotated at 4°C for 45 minutes. I then added anti-FLAG agarose (which I had previously washed with anti-FLAG agarose wash buffer (50 mM TES, 400 mM NaCl, 1 mM EDTA, 1 mM DTT, 3x PIC, pH 7.0) 1:45 (v/v) and rotated at 4°C for two hours. I washed the resin with wash buffer and eluted with 200 μg per mL FLAG peptide, and postcleared the eluate with 1:45 (v/v) DEAE Sephadex. SDS PAGE of 8% acrylamide gels, followed by **(A)** silver staining, and **(B)** immunoblotting against FLAG (1:500 (v/v)).

Following the manufacturer's protocol was more productive for using anti-FLAG agarose to purify FLAG-DGKA from adherent cultures. After initial success from a single 15-cm plate expression (Figure 64), I scaled up the expression to five 15-cm plates and removed the insoluble fraction before purifying on anti-FLAG agarose (Figure 65). Recognition by the anti-FLAG antibody in the immunoblot (Figure 64**B** and Figure 65**B**) was consistent with the major band detected in the silver stain's being, in fact, FLAG-DGKA. I could readily detect DGK enzymatic activity of purified FLAG-DGKA (Figure 66), both in micelles and in liposomes, but only in the presence of activators, as has been previously shown for its mammalian homolog DGK-theta[3].

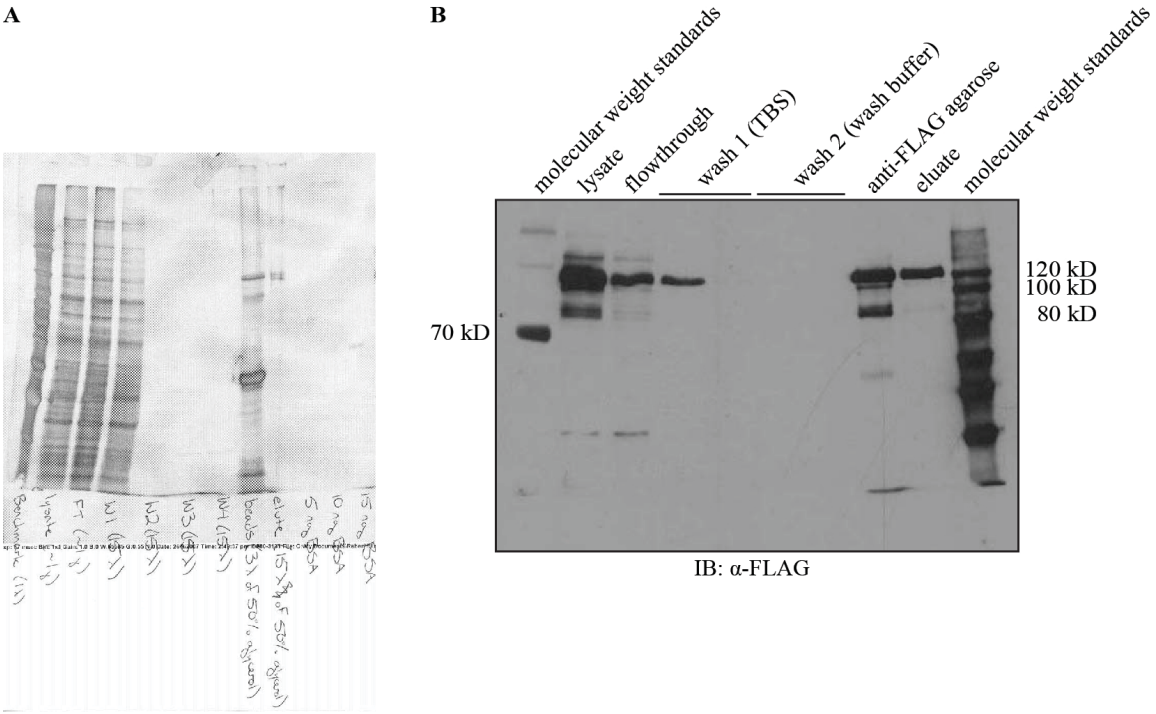

Figure 64. FLAG-DGKA can be purified from *D. discoideum* following the FLAG-agarose manufacturer's protocol. I rinsed one 15 cm plate of FLAG-DGKA-expressing *D. discoideum* cells with PBS, added lysis buffer (50 mM Tris, 150 mM NaCl, 1 mM EDTA, 1% TX-100, 5x PIC, pH 7.4), and rocked at room temperature for 15 minutes. I resuspended the cells in the lysis buffer, then removed the insoluble fraction by centrifuging at 115,000 x *g* for one hour at 4°C. I added anti-FLAG agarose (which I had previously washed with agarose wash buffer (Tris-buffered saline (TBS) (50 mM Tris, 150 mM NaCl, pH 7.4), 5x PIC)) 1:25 (v/v) and rotated at 4°C for two hours. I washed the resin with TBS and with wash buffer 2 (50 mM TES, 5x PIC, pH 7.3), and eluted with elution buffer (50 mM TES, pH 7.3, 200 µg per mL FLAG peptide). SDS-PAGE of 8% acrylamide gels, followed by (A) silver staining, and (B) immunoblotting against FLAG (1:500 (v/v)).

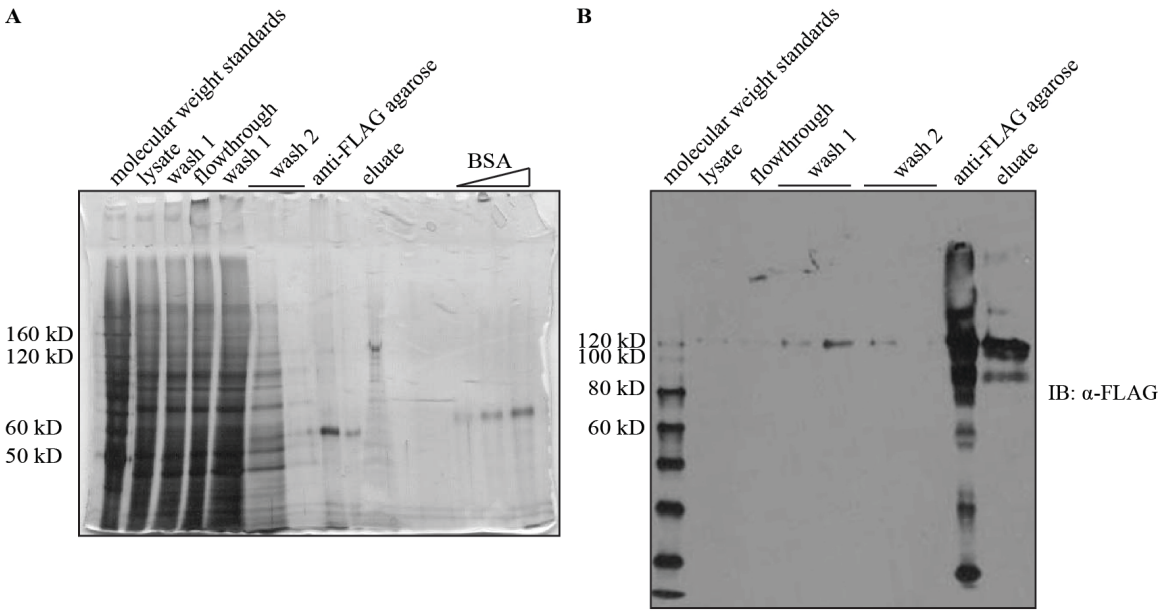

Figure 65. Scaled-up purification of FLAG-DGKA from *D. discoideum*. I rinsed five 15 cm plate of FLAG-DGKA-expressing *D. discoideum* cells with PBS, added lysis buffer (50 mM Tris, 150 mM NaCl, 1 mM EDTA, 1% TX-100, 5x PIC, pH 7.4), and rocked at room temperature for 15 minutes. I resuspended the cells in the lysis buffer, then removed the insoluble fraction by centrifuging at 115,000 x *g* for one hour at 4°C. I froze the resulting supernatant overnight at -80°C. I added anti-FLAG agarose (which I had previously washed with wash buffer 1 (TBS, 5x PIC)) 1:25 (v/v) and rotated at 4°C for two hours. I washed the resin with wash buffer 1 and with wash buffer 2 (50 mM TES, 5x PIC, pH 7.3), and eluted with elution buffer (50 mM TES, pH 7.4, 200 µg per mL FLAG peptide, 5x PIC). SDS-PAGE of 8% acrylamide gels followed by **(A)** silver staining, and **(B)** immunoblotting against FLAG (1:500 (v/v)).

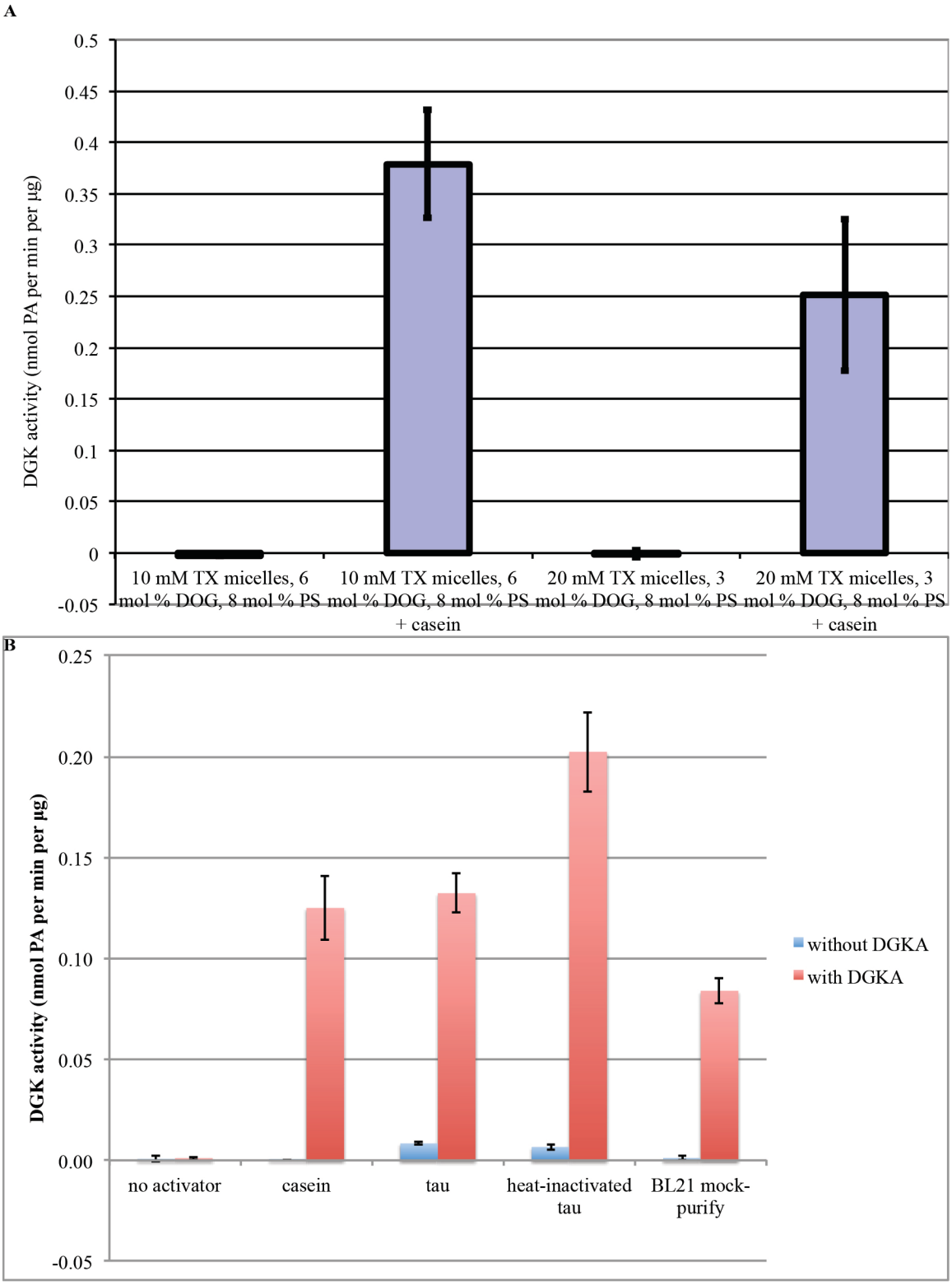

Figure 66. Purified FLAG-DGKA's enzymatic activity depends on the presence of an activator. (A) DGK activity in Triton-X micelles. The reaction included micelles of the composition shown, 47 mM Tris, pH 7.4, 4.7 mM $MgCl_2$, 0.7 ng per µL purified DGKA (as estimated from the silver stain in **Figure 65**A), 2

mM TES, 0.2x PIC, 8 μg per μL FLAG peptide, 2% (v/v) glycerol, 1 mM ATP, and 114 Ci per mmol [γ-^{32}P]-ATP, and proceeded for 7.5 minutes at 37°C. Where indicated, 3 μL of concentrated casein stock solution was included per 50 μL reaction. In duplicate: mean ± SD. The DGKA had been stored at -80°C in 50% glycerol for six weeks prior to assaying. **(B)** DGK activity in liposomes. The reaction included 2 mM liposomes (40:40:12:8::POPE:POPS:PI:DOG), 42 mM Tris, pH 7.0, 8.4 mM $MgCl_2$, 8.4 mM NaF, 0.7 ng per μL purified DGKA (as estimated from the silver stain in **Figure 65**A), 2 mM TES, 0.2x PIC, 8 μg per μL FLAG peptide, 2% (v/v) glycerol, 1 mM ATP, and 114 Ci per mmol [γ-^{32}P]-ATP, and proceeded for 7.5 minutes at 37°C. 1 μL of concentrated stock solutions of the indicated activators was included per 50 μL reaction, where indicated. In triplicate: mean ± SD. The DGKA had been stored at -80°C in 50% glycerol for six weeks prior to assaying.

Discussion and Conclusions

By following the manufacturer's protocol, I was able to express and purify FLAG-DGKA. This purified fraction was recognized by an anti-FLAG antibody, and gave detectable enzymatic activity, but only in the presence of an activator. The antibody recognition and the detectable DGK activity not only support the interpretation that the major band was, in fact, FLAG-DGKA, but also suggests that the recombinant enzyme was properly folded and had experienced any post-translational processing necessary for activity.

Expressing and Purifying DGK Constructs from Insect Cells

Insect Cell Expression Introduction

While prokaryotic expression systems can produce recombinant protein abundantly, which can be useful for producing the highly concentrated protein required for x-ray crystallography, eukaryotic expression systems have a number of advantages over prokaryotic expression systems for expressing eukaryotic proteins, including the proper codon preference, the proper machinery for expressing large proteins, and the proper post-translational modifications, which might be important for solubility. Eukaryotic expression systems generally produce less protein than prokaryotic expression systems, but insect cell lines have nonetheless been successfully used to express proteins

for x-ray crystallography. I therefore set out to express and purify eukaryotic DGK constructs in two different insect cell lines in an effort to produce enough protein for structural studies.

Cloning, Expressing, and Purifying Rattus norvegicus *DGK-Alpha from Sf9 Cells*

Cloning *R. norvegicus* DGK-Alpha into the Bacmid

The pENTR™11X vector was made by removing a SalI site from the pENTR™11 vector (Invitrogen™), in order to produce the proper reading frame for a previous cloning project. *R. norvegicus* DGK-alpha in GFPC2 and pENTR™11X were previously digested with the restriction endonuclease EcoRI, electrophoresed, and excised from the agarose gel. After extracting the DNA from the agarose, I treated the digested pENTR™11X vector with calf intestinal alkaline phosphatase (CIP) to remove the 5' phosphoryl termini to prevent self-ligation[139], electrophoresed, excised from the agarose gel, and extracted the DNA from the gel. I then estimated the concentration of the DNA by comparing to molecular weight standards in agarose gel electrophoresis, ligated the DGK-alpha insert into the pENTR™11X plasmid, transformed the construct into the TOP10 strain of *E. coli*, and selected for kanamycin resistance (conferred by the pENTR™11X plasmid). I extracted the DNA from successful transformants and confirmed successful insertion of DGK-alpha into pENTR™11X by diagnostic digest with EcoRI and SalI, and with EcoRV and HindIII.

I used LR Clonase™ II to recombine DGK-alpha from pENTR™11X via its *att*L1 and *att*L2 sites into pDEST™10 (Invitrogen™) via its *att*R1 and *att*R2 sites. After terminating the reaction with Proteinase K, I transformed the construct into the TOP10

strain of *E. coli*, and selected for carbenicillin resistance (conferred by the ampicillin resistance gene in pDEST™10). I extracted the DNA from successful transformants and confirmed successful insertion of DGK-alpha into pDEST™10 by diagnostic digest with EcoRI.

I then transformed the construct (*R. norvegicus* DGK-alpha in pDEST™10) into the DH10Bac™ strain of *E. coli* (Invitrogen), and selected for the parent bacmid bMON14272 with kanamycin, for the helper plasmid pMON7124 with tetracycline, and for pDEST™10 with gentamycin. I selected recombinant bacmids as white colonies (not blue) in the presence of IPTG (to induce expression of β-galactosidase) and 5-bromo-4-chloro-3-indolyl β-D-galactopyranoside (X-Gal) (a chromogenic substrate of β-galactosidase), because successful insertion of DGK-alpha into pDEST™10 was predicted to disrupt the β-galactosidase gene. I extracted the (large) bacmid DNA, and confirmed successful insertion of DGK-alpha by diagnostic PCR using the M13 universal primer to complement the bacmid and another primer to complement the insert.

Expressing and Purifying *R. norvegicus* DGK-Alpha from Sf9 Cells

With the help of Dr. Becky Tu-Sekine, I first cloned *R. norvegicus* DGK-alpha from the GFPC2 plasmid into pENTR™11X, a variant of the pENTR™11 vector, to provide donor recombination sites in the proper frame around DGK-alpha. I then recombined DGK-alpha from pENTR™11X into the pDEST10™ baculoviral vector, which produces a protein with an N-terminal hexahistidine fusion tag followed by a TEV protease site, and confirmed successful incorporation of the insert by diagnostic PCR. I transfected the baculoviral vector into Sf9 *Spodoptera frugiperda* cells, which then produced baculovirus from the baculoviral vector.

After infecting Sf9 cells with baculovirus encoding DGK-alpha in pDEST10™, the infected Sf9 cell lysates expressed a band easily detectable by silver staining that migrated between 80 and 90 kD, consistent with the predicted molecular weight of the fusion protein of 88.8 kD, and whose intensity increased with increasing multiplicity of infection (MOI) and increasing time of infection (Figure 67**A**). A band migrating between 80 and 100 kD in the infected lysate but not the uninfected lysate was recognized by antibodies against DGK-alpha (Figure 67**B**) and DGK-alpha C-terminus (Figure 69), but not by antibodies against DGK-alpha N-terminus or histidine (Figure 67**B**). By DGK enzymatic activity assay, I measured greater DGK activity in Sf9 lysates that had been infected with the baculovirus than uninfected lysates, with greater activity in detergent micelles than in liposomes (Figure 68), consistent with the expressed bands' identity being that of DGK-alpha.

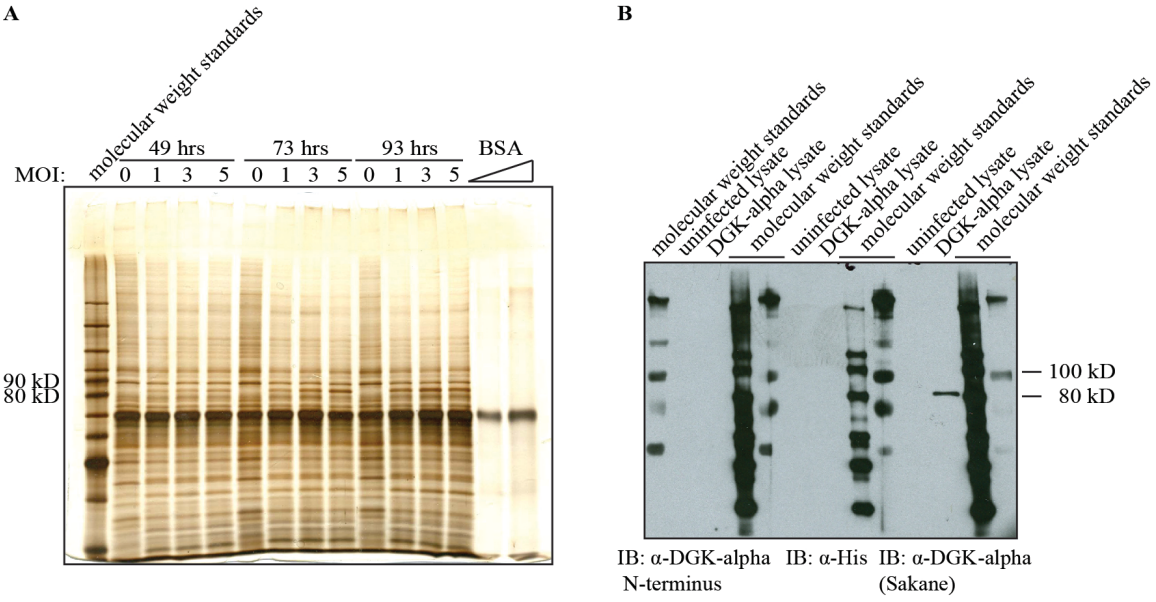

Figure 67. Sf9 cells infected with DGK-alpha in pDEST10™ express a band whose migration pattern consistent with the predicted molecular weight and whose intensity increases with increasing MOI and increasing time of infection, and which is recognized by antibodies against DGK-alpha, but not by antibodies against DGK-alpha N-terminus or histidine. (A) I infected a freshly fed 12-well plate of Sf9 cells with DGK-alpha in pDEST10™ at the indicated MOIs. At the indicated timepoints, I removed

the medium by aspiration, resuspended the cells in lysis buffer (50 mM Tris, pH 8.0, 300 mM NaCl, 10 mM imidazole, 1 mM $CaCl_2$, 0.5% NP-40, 1x PIC, 0.5 mM DTT), and stored at -20°C. SDS-PAGE of an 8% acrylamide gel followed by silver staining. **(B)** I infected a 15 cm plate of Sf9 cells with 10^5 plaque-forming units (pfu) per mL DGK-alpha in pDEST10™ for two days, then removed the medium by aspiration. I added cold lysis buffer to the cells and allowed them to sit on ice for a few minutes before scraping and homogenizing twenty times with a glass cell homogenizer. SDS-PAGE followed by immunoblotting against DGK-alpha N-terminus (Abgent AP8128a (1:200 (v/v)) (left), against His_6 (abcam® ab6196 (1:2500 (v/v)) (middle), and against DGK-alpha (Sakane (1:5000 (v/v)) (right). I loaded 0.5 µg protein (as measured by the Bio-Rad Protein Assay) per well.

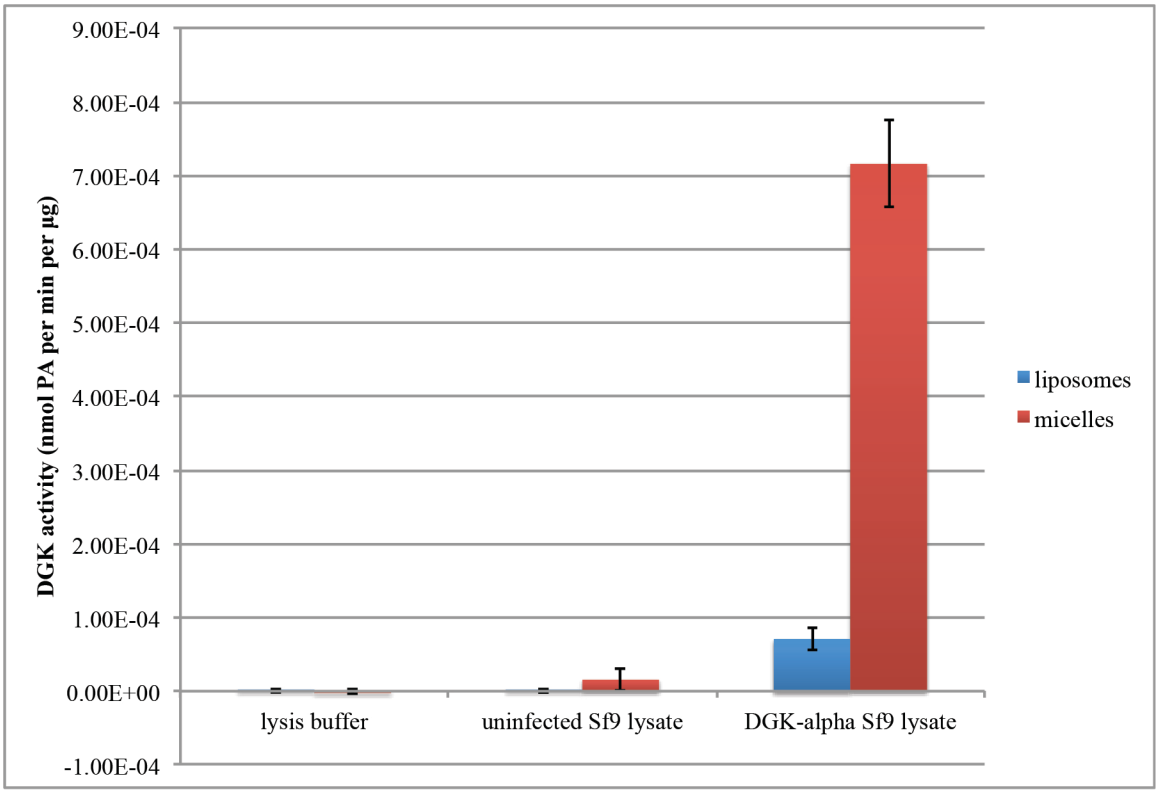

Figure 68. The lysates of Sf9 cells infected with DGK-alpha in pDEST10™ have greater DGK activity than uninfected lysates. The sample used is that shown in **Figure 67**, and had been stored overnight in 50% glycerol at -80°C prior to assaying. Detergent micelles were 5 mM Triton X-100 micelles with 6 mol% DOG and 9 mol% PS. Liposomes were 7.5 mM, 53:22:17:8::PE:PC:PS:DOG. The reaction included 47 mM HEPES, pH 8.0, 4.7 mM $MgCl_2$, 1 mM $CaCl_2$, 1 mM ATP, 2 mM Tris, 12 mM NaCl, 0.4 mM imidazole, 0.02% NP-40, 0.2x PIC, 40 ng per µL total protein (as measured by the Bio-Rad Protein Assay), and 29.3 Ci per mmol [γ-^{32}P]-ATP, and proceeded for 15 minutes at 30°C. In duplicate: mean ± SD.

I estimated my maximum yield of fusion protein to be 5 ng DGK-alpha per 0.5 µg total protein (Figure 67**A**), or 1% by weight, or approximately 0.46 µg per square centimeter of adherent Sf9 culture. However, while total fusion protein yield increased

as a function of time after expression (Figure 67), fusion protein solubility decreased (Figure 69), so the maximum yield of soluble fusion protein would be quite a bit less.

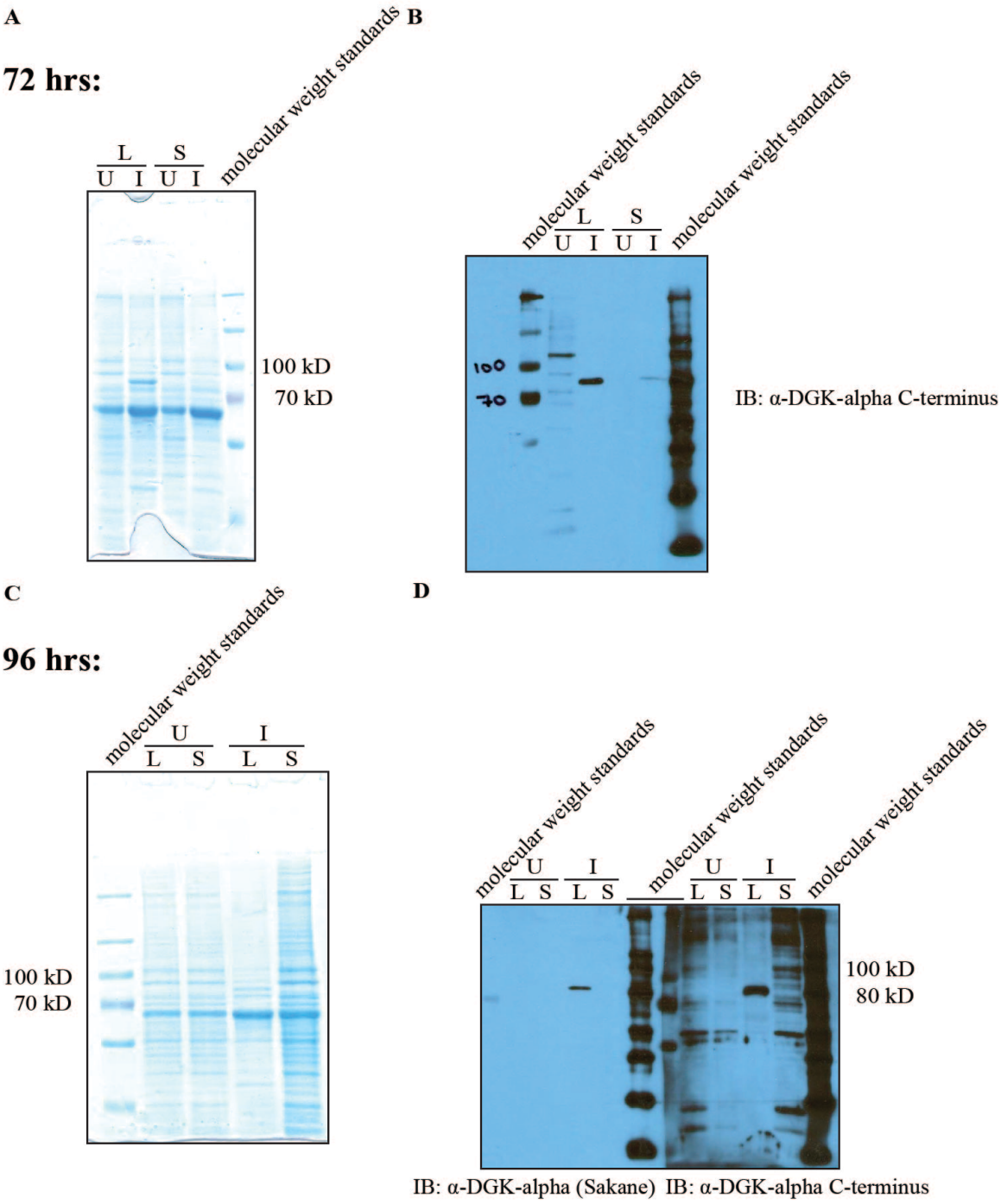

Figure 69. The solubility of DGK-alpha in pDEST10™ decreases with decreasing time of infection. I infected one ten cm plate of Sf9 cells with DGK-alpha in pDEST10™ at a MOI of ~5. At the indicated timepoints, I removed the medium by aspiration, added cold lysis buffer (50 mM Tris, pH 8.0,

300 mM NaCl, 10 mM imidazole, 1 mM $CaCl_2$, 0.5% NP-40, 1x PIC) to the cells, and allowed them to sit on ice for a few minutes before scraping and homogenizing twenty times with a glass cell homogenizer. For the 96-hour infection, the lysis buffer also included 0.5 mM DTT. I removed the insoluble fraction by centrifuging at maximum speed in a tabletop centrifuge for 15 minutes. SDS-PAGE of 8% acrylamide gels followed by **(A)** Coomassie staining (of the 72-hour infection), **(B)** immunoblotting against DGK-alpha C-terminus (Abgent AP8128b (1:300 (v/v))) (of the 72-hour infection), **(C)** Coomassie (of the 96-hour infection), and **(D)** immunoblotting against DGK-alpha (left: Sakane (1:5000 (v/v)); right: DGK-alpha C-terminus Abgent AP8128b (1:200 (v/v)). L, lysate; S, supernatant; U, uninfected; I, infected with DGK-alpha in pDEST10™.

After ultracentrifugation for one hour at 115,000 x *g*, some of the DGK-alpha fusion protein remained in the soluble fraction (Figure 70). When I tried to enrich the DGK-alpha in that soluble fraction on Ni-NTA agarose, however, the protein flowed through the resin. One possible explanation for why the DGK-alpha had no apparent affinity for the Ni-NTA resin could be that DGK-alpha might require calcium to fold in such a way that the hexahistidine tag is exposed and competent for binding to Ni-NTA. Another possible explanation is that the histidine tag might be occluded or indeed not even present in the protein, which would also explain why the anti-histidine antibody did not recognize the fusion protein (Figure 67). The incorporation of the fusion protein into the plasmid was confirmed by diagnostic PCR, but not by sequencing: it is entirely possible that the hexahistidine tag was truncated or missing altogether because of a deletion or frameshift. Any such genetic modification, however, would have to be small in magnitude, because the expressed protein was still between 80 and 90 kD in size, was recognized by the anti-DGK-alpha antibody, and showed detectable DGK enzymatic activity (Figure 67 - Figure 70).

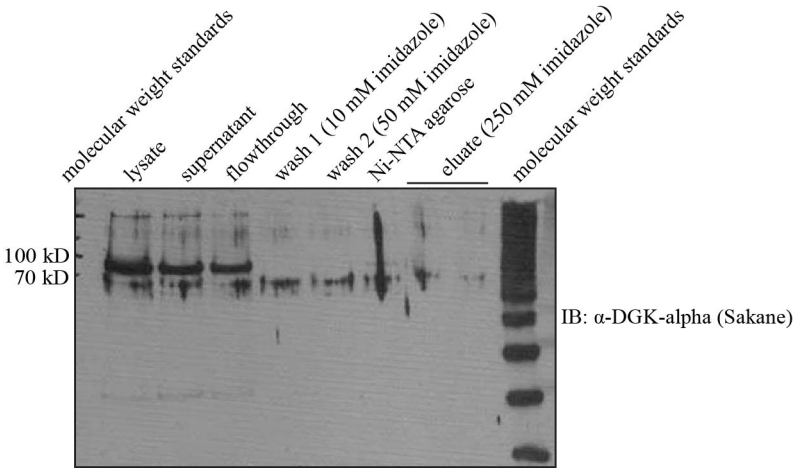

Figure 70. DGK-alpha in pDEST10™ expressed in Sf9 cells has very low affinity for Ni-NTA agarose. I infected one ten cm plate of Sf9 cells with DGK-alpha in pDEST10™ 1:10 (v/v). After 48 hours, I removed the medium by aspiration, gently washed the cells with PBS, resuspended in lysis buffer (50 mM Tris, pH 8.0, 300 mM NaCl, 10 mM imidazole, 0.1% TX-100, 1x PIC), and homogenized ten times with a glass cell homogenizer. I froze the lysates at -80°C for four days, then thawed and removed the insoluble fraction by centrifuging 115,000 x *g* for one hour. I added Ni-NTA agarose 1:10 (v/v) to the resulting supernatant, and rotated for two hours at 4°C. I washed the resin with loading buffer (50 mM Tris, 300 mM NaCl, 10 mM imidazole, 1x PIC, 1 mM DTT) and wash buffer (same as loading buffer, but imidazole increased to 50 mM imidazole), and eluted in elution buffer (250 mM imidazole). SDS-PAGE of an 8% acrylamide gel followed by immunoblotting against DGK-alpha (Sakane (1:5000 (v/v))).

Discussion and Conclusions

I was able to express in Sf9 cells a band that was between 80 and 90 kD in size, was recognized by the anti-DGK-alpha antibody, and showed detectable DGK enzymatic activity (Figure 67 - Figure 70). This protein, however, did not recognize an anti-histidine antibody (Figure 67) and had no apparent affinity for a Ni-NTA resin (Figure 70), suggesting that while at least most of the DGK was present, the histidine tag may have been improperly folded, occluded, or not even present. Because I was unable to purify this protein, and because its solubility was poor to begin with, I therefore decided to pursue another construct for expression in insect cells for structural studies.

Expressing and Purifying **Homo sapiens** *DGK-Theta from High Five™ Cells*

Introduction

H. sapiens DGK-theta is currently the best-studied DGK in our laboratory[3,140,141]. Although *H. sapiens* DGK-theta can be expressed and purified from mammalian cells, insect cells have the potential to produce larger amounts of protein, which would be amenable for structural studies requiring large amounts of protein. We were interested in learning more about the structure of DGK-theta, and therefore set out to express *H. sapiens* DGK-theta in insect cells.

Results

After I infected High Five™ *Trichoplusia ni* ovary cells with baculovirus encoding *H. sapiens* DGK-theta in pDEST10™, infected lysates expressed a band easily detectable by Coomassie staining, not seen in the uninfected cell lysate, that migrated between the 130 and 160 kD molecular weight markers, a bit higher than its predicted molecular weight of 110.0 kD (Figure 71). Less prominent new bands, one between 35 and 55 kD in size, and one between 55 and 70 kD in size, also appeared. I was also able to detect much greater DGK enzymatic activity in the infected lysates than in the uninfected lysates, using either detergent micelles or liposomes as a substrate (Figure 72). I therefore concluded that the infected lysates were successfully expressing DGK-theta.

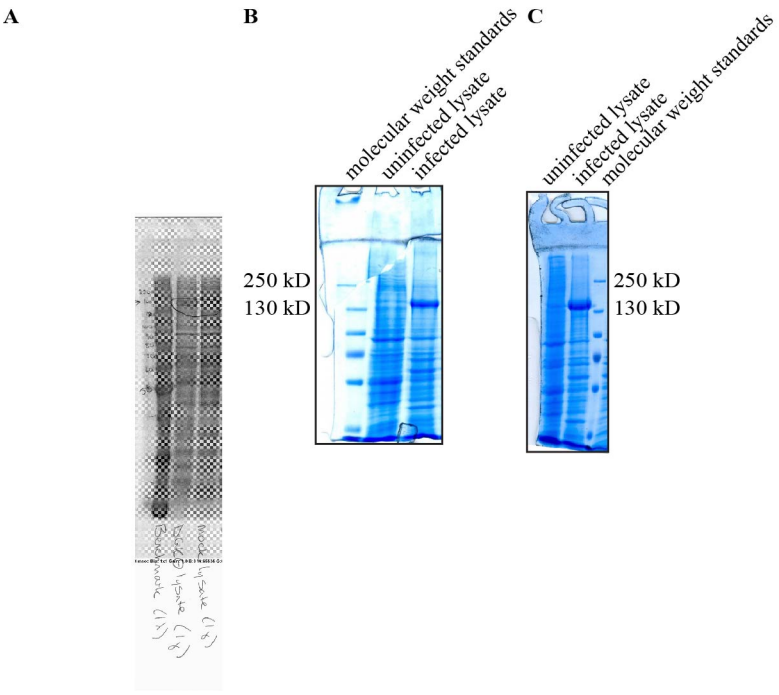

Figure 71. High Five™ cells infected with DGK-theta in pDEST10™ express a band whose migration pattern is slightly slower than that of the predicted molecular weight: three representative expressions. **(A)** I infected one of two fifteen cm plates of High Five™ cells with DGK-theta in pDEST10™ 1:100 (v/v). After 23 hours, I replaced the medium on the cells. The next day, I removed the medium by aspiration, washed the cells with PBS, resuspended the cells in cold lysis buffer (100 mM NaH_2PO_4, pH 8.0, 10 mM Tris, 0.5% NP-40, 1 mM DTT, 1x PIC), and homogenized ten times with a glass cell homogenizer. SDS-PAGE of an 8% acrylamide gel followed by silver staining. **(B)** I infected one of two fifteen cm plates of High Five™ cells with 300 µL DGK-theta in pDEST10™. After two days, I removed the medium by aspiration, washed the cells with cold fractionation buffer (FB) (10 mM HEPES, pH 7.4, 1 mM EDTA, 0.5 mM EGTA), added cold lysis buffer (FB, 100 mM NaCl, 1x PIC, 30 mM NAG, 1 mM $NaVO_4$, 0.5% NP-40) to the cells, and allowed them to sit on ice for ~20 minutes before scraping and homogenizing twenty times with a glass cell homogenizer. SDS-PAGE of an 8% acrylamide gel followed by Coomassie staining. **(C)** I infected one of two fifteen cm plates of High Five™ cells with 300 µL DGK-theta in pDEST10™. After two days, I washed the cells with cold FB, added cold lysis buffer, and allowed them to sit on ice for ten minutes before scraping and homogenizing twenty times with a glass cell homogenizer. SDS-PAGE of an 8% acrylamide gel followed by Coomassie staining.

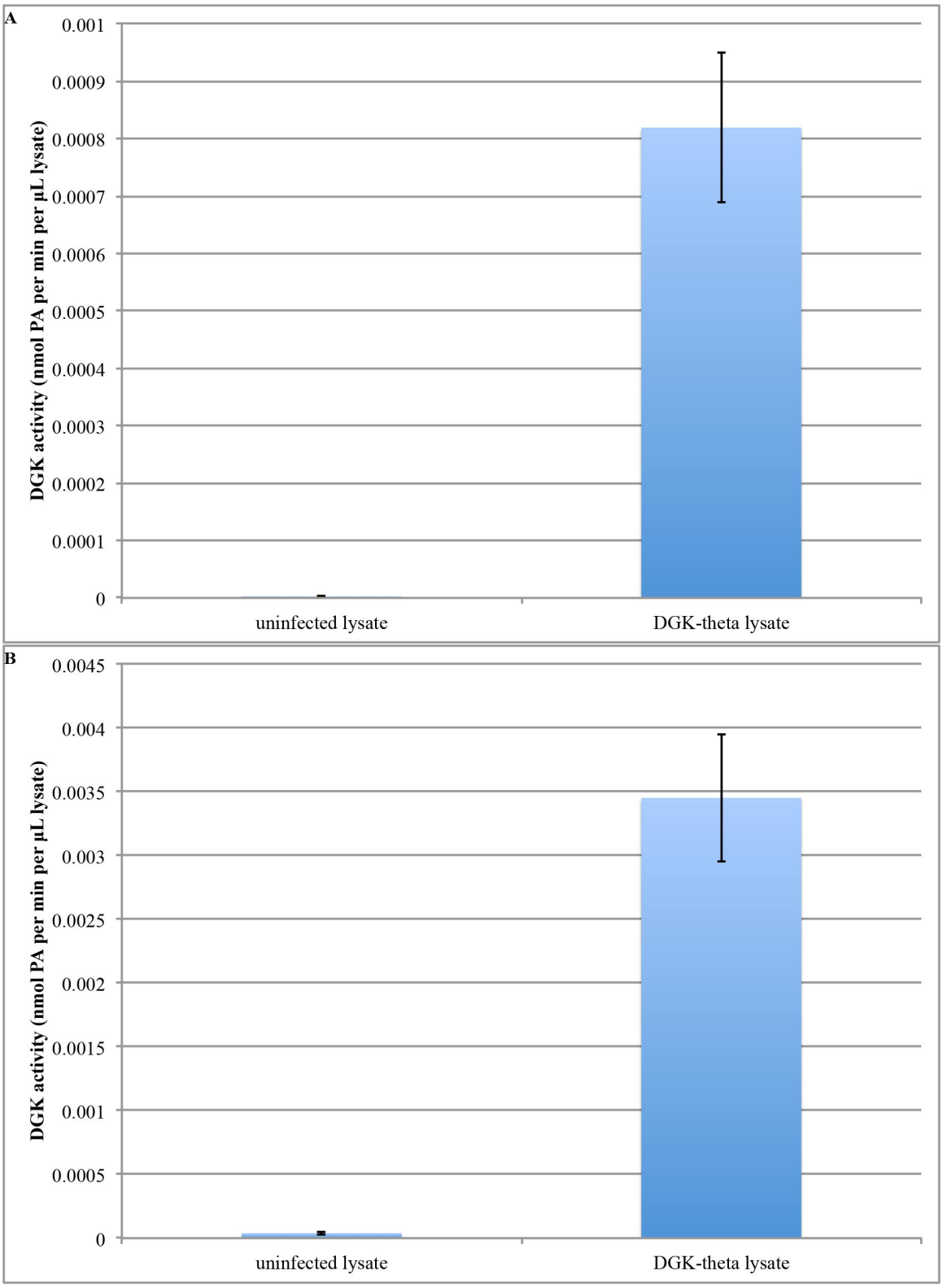

Figure 72. High Five™ cells infected with DGK-theta in pDEST10™ have higher DGK activity than uninfected lysates. DGK activity assays. **(A)** In detergent micelles. I stored the lysates shown in **Figure**

71B in 50% glycerol at -80°C for eleven days prior to assaying. The reaction included 7 mM TX-100 micelles (9 mol% POPS, 6 mol% DOG), 44 mM Tris, pH 7.4, 4.4 mM $MgCl_2$, 1 mM ATP, 0.5 mM HEPES, 47 μM EDTA, 23 μM EGTA, 5 mM NaCl, 1.5 mM NAG, 50 μM $NaVO_4$, 0.025% (v/v) NP-40, 0.05x PIC, 2.5% (v/v) glycerol, 2.5 μL original lysate (prior to adding glycerol per 50 μL reaction, and 43.1 Ci per mmol [γ-^{32}P]-ATP, and proceeded for 15 minutes at 37°C. In duplicate: mean ± SD. **(B)** In liposomes. I stored the lysates shown in **Figure 71**C in 50% glycerol at -80°C for two days prior to assaying. The reaction included 5.25 mM liposomes (53:22:17:8::POPE:POPC:POPS:DOG), 44 mM HEPES, pH 7.5, 4.4 mM $MgCl_2$, 1 mM ATP, 0.5 mM HEPES, 47 μM EDTA, 23 μM EGTA, 85 mM NaCl, 1.5 mM NAG, 50 μM $NaVO_4$, 0.025% (v/v) NP-40, 0.05x PIC, 2.5% (v/v) glycerol, 2.5 μL original lysate (prior to adding glycerol) per 50 μL reaction, and 66.7 Ci per mmol [γ-^{32}P]-ATP, and proceeded for 15 minutes at 37°C. In duplicate: mean ± SD.

An antibody against DGK-theta was able to recognize bands in the infected lysate not detected in the uninfected lysate immunoblotting, consistent with the infected lysate's successfully expressing DGK-theta. However, frequently the antibody detected many bands of different sizes, or else bands that ran much higher than the predicted molecular weight (Figure 73). The cells from which the lysate with the high-running bands was derived were infected were lysed in a different buffer and more lysate was loaded onto the gel: it is not entirely clear which of these differences is responsible for the difference in antibody detection. More puzzlingly, these high-running bands were detected in the very same samples in which the predominant band by silver staining ran at a lower molecular weight (Figure 71**A**): perhaps the antibody-recognizing bands were resistant to silver staining, or perhaps the silver-staining bands were resistant to recognition by the antibody. Following sonication, an antibody-recognizing band of the appropriate size appeared (Figure 73**B**). Denaturation by urea greatly enhanced antibody recognition (less protein was loaded into the urea pellet lane than in the lysate or supernatant lane, yet far more protein was recognized by the antibody), and also increased the number of recognized bands. Following gradual renaturation by serially dialyzing into buffers with lower urea concentrations, the band of the correct size was enriched relative to the higher-running band, but the higher-running band never completely disappeared.

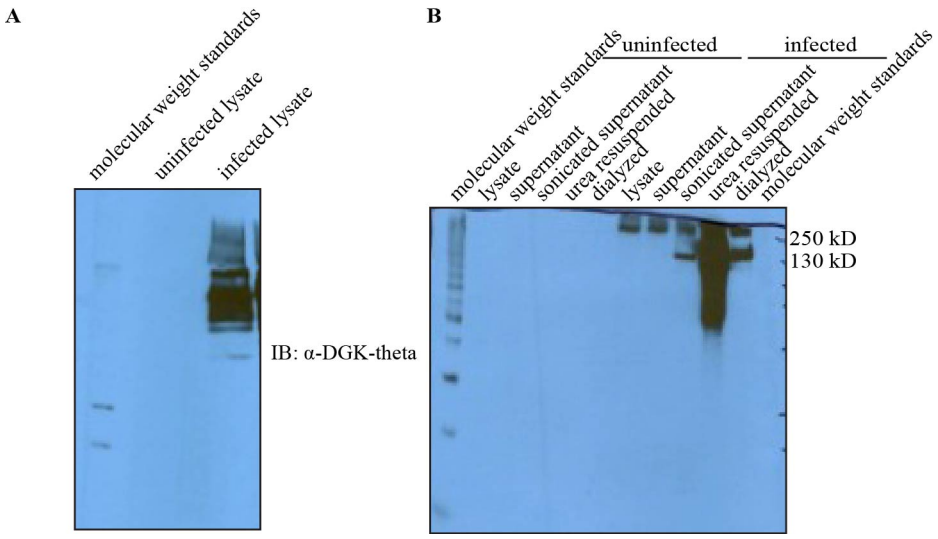

Figure 73. An anti-DGK-theta antibody recognizes bands in lysates infected with DGK-theta that are not present in uninfected lysates, but migration in SDS-PAGE varies among expressions. (A) I infected one of two 15 cm plates of High Five™ cells with 464 µL DGK-theta in pDEST10™. The following day, I replaced the medium on the cells. The day after that, I removed the medium by aspiration, washed the cells with PBS, resuspended the cells in cold lysis buffer (FB, 1x PIC), and homogenized ten times with a glass cell homogenizer. SDS-PAGE of an 8% acrylamide gel followed by immunoblotting against DGK-theta (1:350 (v/v)). **(B)** I collected the aggregates from the lysates shown in **Figure 71A** by centrifugation, resuspended them in lysis buffer (100 mM NaH_2PO_4, pH 8.0, 10 mM Tris, 0.5% NP-40, 1 mM DTT, 1x PIC), and probe-sonicated eight times for fifteen seconds each, resting on ice for fifteen seconds between each burst. I microfuged to collect the pellet, and resuspended the pellet in Buffer B (8 M urea, 100 mM NaH_2PO_4, 10 mM Tris, pH 8.0, 1x PIC, 1 mM DTT). I added Ni-NTA agarose 1:5 (v/v) to the resuspended pellet, then washed the resin with wash buffer (same as Buffer B, but pH reduced to 6.3) and eluted with elution buffer (pH 4.5). I dialyzed the eluate overnight against dialysis buffer 1 (4 M urea, 100 mM NaH_2PO_4, 10 mM Tris, pH 7.4) at 4°C using 3500 MWCO dialysis tubing. The next day, I gradually dripped in dialysis buffer 2 (10% (w/v) sucrose, 100 mM NaH_2PO_4, 10 mM Tris, pH 7.4), such that the final buffer composition was 5% sucrose and 2 M urea. Two days later, I removed half the dialysis buffer, and dripped in more dialysis buffer 2, such that the final buffer composition was 7.5% sucrose and 1 M urea. The next day, I transferred the dialysis tubing to dialysis buffer 3 (same as dialysis buffer 2, but urea increased to 500 mM). After four hours, I transferred the dialysis tubing to dialysis buffer 2. The next day, I transferred the dialysis tubing to dialysis buffer 4 (same as dialysis buffer 2, but with 50 µM $ZnCl_2$). SDS-PAGE of an 8% acrylamide gel followed by immunoblotting against DGK-theta (1:350 (v/v)).

The fraction of DGK-theta expressed in High Five™ cells that remained in the pellet after low-speed centrifugation gave a much higher immunoblot signal than that in the supernatant (Figure 74). Any quantitative comparison by immunoblot requires assuming that the antibody has equal affinity for the soluble and insoluble populations of DGK-theta, but given that it seems unlikely the antibody would have considerably higher affinity for the insoluble population than for the soluble population, it seems reasonable

to conclude that DGK-theta expressed in High Five™ cells is mostly insoluble. I could solubilize some DGK-theta from these pellets by washing with salt (Figure 75). $MgCl_2$ was more effective than NaCl for salting in DGK-theta, but not because of its higher ionic strength. When I removed the salt from these samples by dialysis and assayed their DGK activity in micelles, however, their activity was so low that the radiolabeled lipids extracted from the assay did not even produce spots when exposed to film.

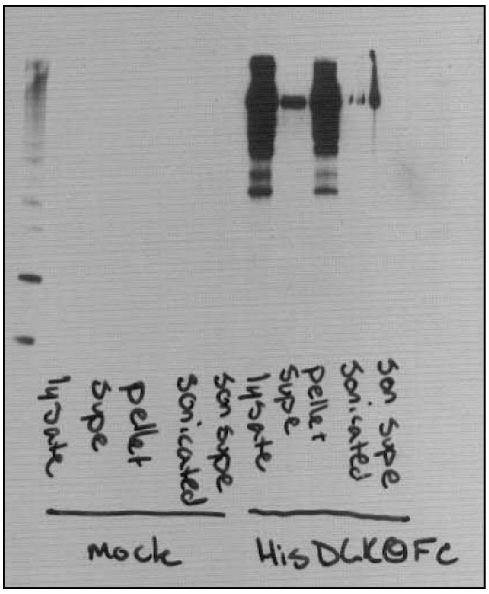

IB: α-DGK-theta

Figure 74. DGK-theta expressed in High Five™ cells is mostly insoluble. I stored the lysates shown in **Figure 73**A at -80°C overnight, the thawed and collected the aggregates by centrifugation, resuspended in lysis buffer (FB, 10 mM DTT, 1x PIC), and probe-sonicated eight times for fifteen seconds each, resting on ice for thirty seconds between each burst. I added NaCl to 1 M and deoxycholate (DOC) to 2% (w/v), rotated at 4°C for thirty minutes, and microfuged to remove the insoluble fraction. SDS-PAGE of an 8% acrylamide gel followed by immunoblotting against DGK-theta (1:350 (v/v)).

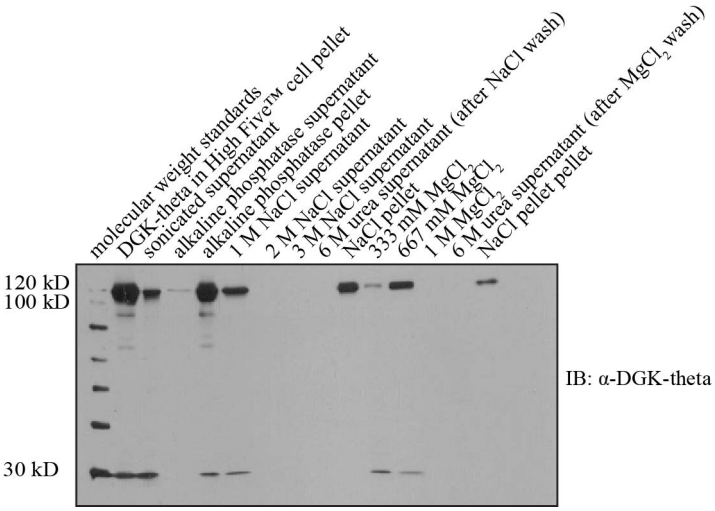

Figure 75. DGK-theta expressed in High Five™ cells can be partially solubilized by salting in. I resuspended the pellets from High Five™ cells infected with DGK-theta in pDEST10™ in DNAseI buffer, then probe-sonicated five times for five seconds each, resting on ice for fifteen seconds between each burst. I collected the pellet by centrifugation, then resuspended in DNAse I buffer. I added DNAse I to 0.1 U per μL and incubated at 37°C for fifteen minutes. I divided into three equal portions, then collected the pellet by centrifugation. The first pellet I resuspended in alkaline phosphatase buffer, added alkaline phosphatase to 0.5 U per μL, and incubated at 37°C for fifteen minutes. The second pellet I washed with 1 M NaCl (in DNAse I buffer), then 2 M NaCl, then 3 M NaCl, then 6 M urea in FP buffer. The third pellet I resuspended in 333 mM $MgCl_2$ (in DNAse I buffer), then 667 M $MgCl_2$, then 1 M $MgCl_2$, then 6 M urea in FP buffer. SDS-PAGE of an 8% acrylamide gel followed by immunoblotting against DGK-theta (1:350 (v/v)).

I could also solubilize DGK-theta from pellets using urea. After slowly removing the urea by dialysis, however, the protein precipitated when transferred to dialysis buffer that contained 50 μM $ZnCl_2$ at pH 7.2. Adding EDTA to 1.5 mM in the dialysis buffer was insufficient to resolubilize the protein, but I could resolubilize the protein by dialyzing against buffer that included 4 M urea at pH 9.5. The protein remained soluble as the urea was dialyzed out, and as $ZnCl_2$ was dialyzed in to 50 μM at pH 9.5. Despite reports that insoluble pellets from DGK-theta-overexpressing High Five™ cells were so enriched for DGK-theta that additional purification steps were unnecessary, the final dialyzed DGK-theta contained, in addition to the predominant band between 100 and 120 kD, many other bands detectable by silver staining (Figure 76**A**). In another expression, washing the pelleted protein with 1 M NaCl and 2% deoxycholate (DOC) before

solubilizing it into a buffer containing 8 M urea, pH 12.5 was insufficient to produce purified dialyzed DGK-theta after the urea was removed (Figure 76**B**). In fact, adding DOC caused protein to crash out of solution and thereby increased, not decreased, the contents of the pellet. In order to produce purified protein, then, I needed additional enrichment steps.

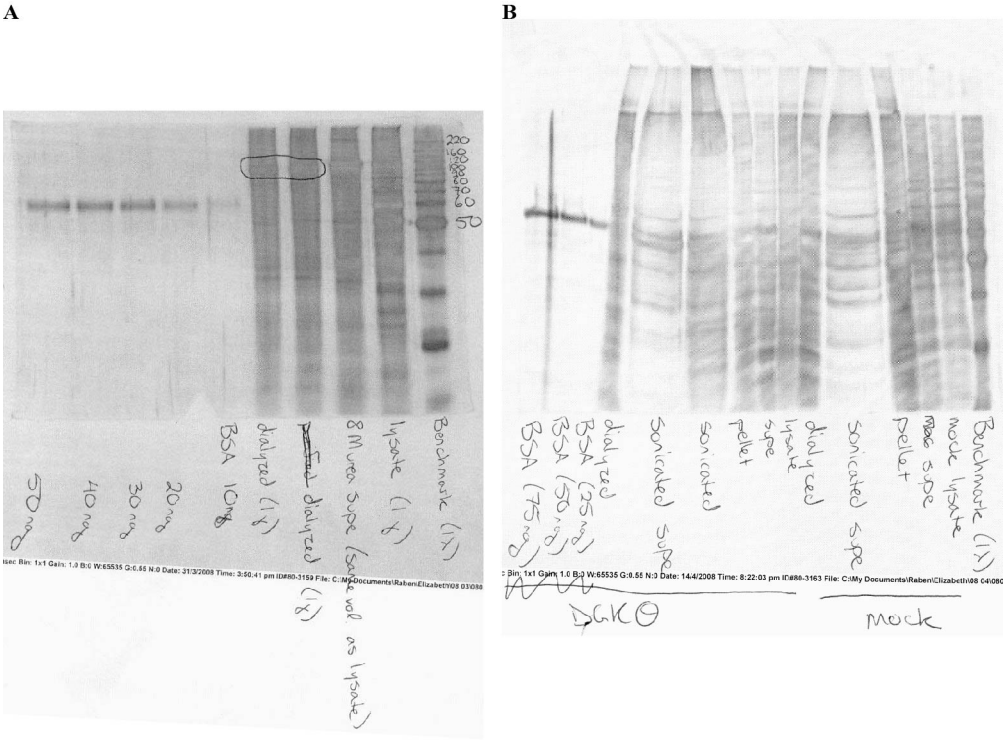

Figure 76. Insoluble pellets from two different expressions of DGK-theta-overexpressing High Five™ cells require additional enrichment steps in order to produce purified DGK-theta. (A) I resuspended the pellets from High Five™ cells infected with DGK-theta in pDEST10™ in extraction buffer (9.89 M urea, 1.1 mM TCEP, 1.24 mM EDTA, pH 12.2), then removed the insoluble fraction by microfuging at maximum speed for ten minutes at room temperature. I dialyzed overnight into dialysis buffer 1 (3 M urea, 1 mM TCEP, 50 mM Tris, 10% sucrose, pH 9.5) at 4°C using 3500 MWCO dialysis tubing. The next day, I poured out about a third of the dialysis buffer, then gradually dripped in dialysis buffer 2 (same as dialysis buffer 1, but urea reduced to 2 M). The next day, I poured out about a third of the dialysis buffer, then gradually dripped in dialysis buffer 3 (1 M urea). At the end of the day, I poured out about two-thirds of the dialysis buffer, then gradually dripped in dialysis buffer 4 (500 mM urea). The next day, I gradually dripped in dialysis buffer 5 (0 mM urea, plus 50 μM $ZnCl_2$). The next day, I transferred the dialysis tubing to dialysis buffer 5, adjusted the pH to 7.2, and, after 3.5 hours, the protein precipitated. I added EDTA to the dialysis buffer to 1.5 mM, but after an hour the protein still had not gone into solution. I transferred the dialysis tubing to dialysis buffer 6 (same as dialysis buffer 1, but urea increased to 4 M), which did cause the protein go back into solution. I gradually dripped in dialysis buffer 7 (0 mM urea), such that the final concentration of urea was 2 M. The next day, I removed half the dialysis buffer, and gradually dripped in dialysis buffer 7, such that the final concentration of urea was 1 M. The

next day, I removed half the dialysis buffer, and gradually dripped in dialysis buffer 7, such that the final concentration of urea was 500 mM. The next day, I removed half the dialysis buffer, and gradually dripped in dialysis buffer 7, such that the final concentration of urea was 250 mM. The next day, I transferred the dialysis tubing to dialysis buffer 8 (100 mM urea), and after three hours, I transferred the dialysis tubing to dialysis buffer 7. I gradually dripped in buffer 5, such that the final concentration of $ZnCl_2$ was 25 μM. SDS-PAGE followed by silver staining. **(B)** SDS-PAGE of the same samples shown in **Figure 74** on an 8% acrylamide gel, followed by silver staining.

I was able to enrich DGK-theta overexpressed in High Five™ cells by non-native affinity chromatography against the hexahistidine epitope tag conferred by the pDEST10™ expression vector using Ni-NTA affinity chromatography (Figure 77). Although DGK-theta was clearly enriched, although the purified DGK-theta was recognized by the anti-DGK-theta antibody (Figure 73B), and although the overexpressing lysates had much greater DGK enzymatic activity than the uninfected lysates, by the time the DGK-theta was purified, it was no longer any more active than protein that had been similarly isolated from uninfected cells (Figure 78). Adding tau to the reaction, which has been shown to activate DGK-theta purified from mammalian cells[3], did not increase the activity of purified DGK-theta. This loss of activity over the course of purification was not simply due to the time it had spent at 4°C, because lysate stored at 4°C lost only a fraction of its activity as compared to lysate stored at -80°C in 50% glycerol. Although by immunoblot more DGK-theta appeared to be in the pellet than in the supernatant (Figure 74 and Figure 77), most of the activity was retained in the supernatant (Figure 78), suggesting that the DGK-theta in the insoluble fraction is not very active to begin with, which might explain why enriching that insoluble protein does not give a very active fraction.

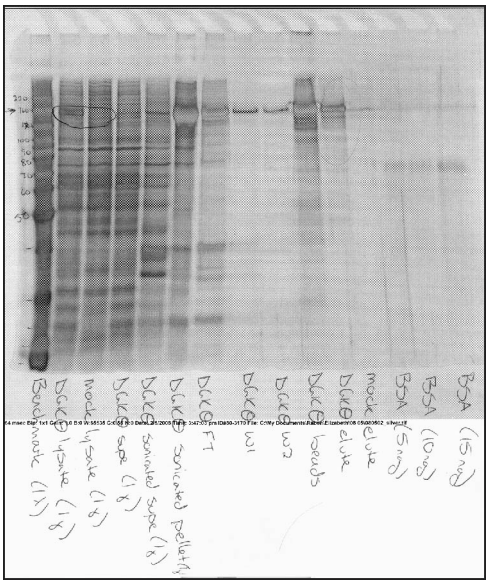

Figure 77. DGK-theta in pDEST10™ can be enriched from High Five™ cells by Ni-NTA affinity chromatography. Purification of DGK-theta from High Five™ cells on Ni-NTA. The band presumed to be DGK-theta, because it is clearly detectable in infected but not uninfected lysates, has been circled. The accompanying immunoblot for this purification may be seen in **Figure 73**B.

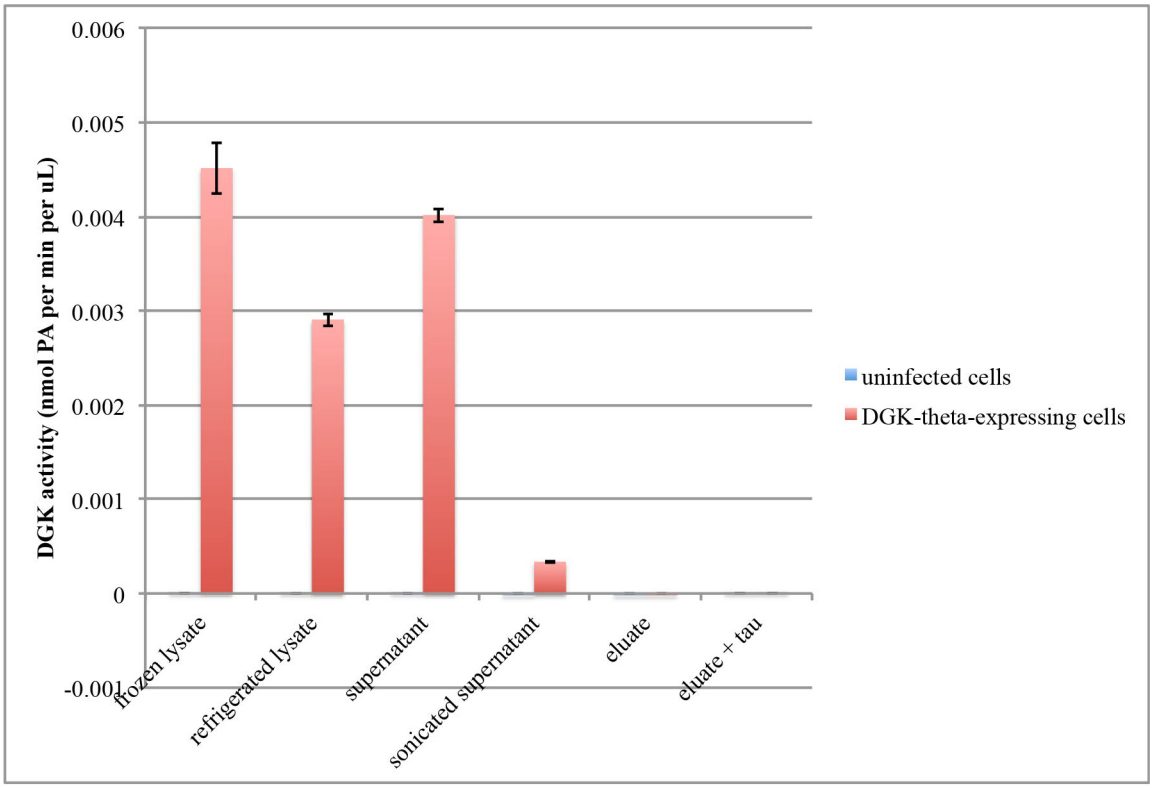

Figure 78. DGK-theta purified from High Five™ cells has no more DGK activity than uninfected High Five™ cells that had been mock-purified. I stored the samples shown in **Figure 77** in 50% glycerol at -80°C for five days prior to assaying. The reaction included 5 mM liposomes

(53:22:17:8::POPE:POPC:POPS:DOG), 44 mM Tris, pH 7.4, 4.4 mM $MgCl_2$, 8 mM NaF, 1 mM ATP, 4 mM NaH_2PO_4, 1 mM DTT, 2 μM $ZnCl_2$, 2% (v/v) glycerol, 2 μL original lysate (prior to adding glycerol) per 50 μL reaction, and 125 Ci per mmol [γ-^{32}P]-ATP, and proceeded for 15 minutes at 37°C. In duplicate: mean ± SD.

I attempted, multiple times, to reproduce efforts in the lab reported to solubilize enzymatically active DGK-theta from the insoluble fraction from High Five™ cells. One representative attempt is shown in Figure 79. After washing the pellet with B-PER, I could solubilize the pellet in 25 mM glycine, 10 mM BME, 1 mM OG, pH 13.7. Because DGK-theta was reported to be in an "SDS-resistant network of enzyme" at this stage (as in Figure 73**B**), I then denatured the protein by adding urea to 8 M, after first dropping the pH to 9.0, which had been reported to cause DGK to migrate appropriately on SDS-PAGE. After dropping the pH to 9.0, some, but not all, of the DGK had been solubilized (Figure 79**A**). After slowly dialyzing out the urea, however, no DGK activity remained (Figure 79**B**). In fact, the activity had been lost even before denaturation by urea (Figure 79**C**). As before, adding activators such as β-casein, protamine, or histone H1 were unable to increase the activity of purified DGK-theta to detectable levels.

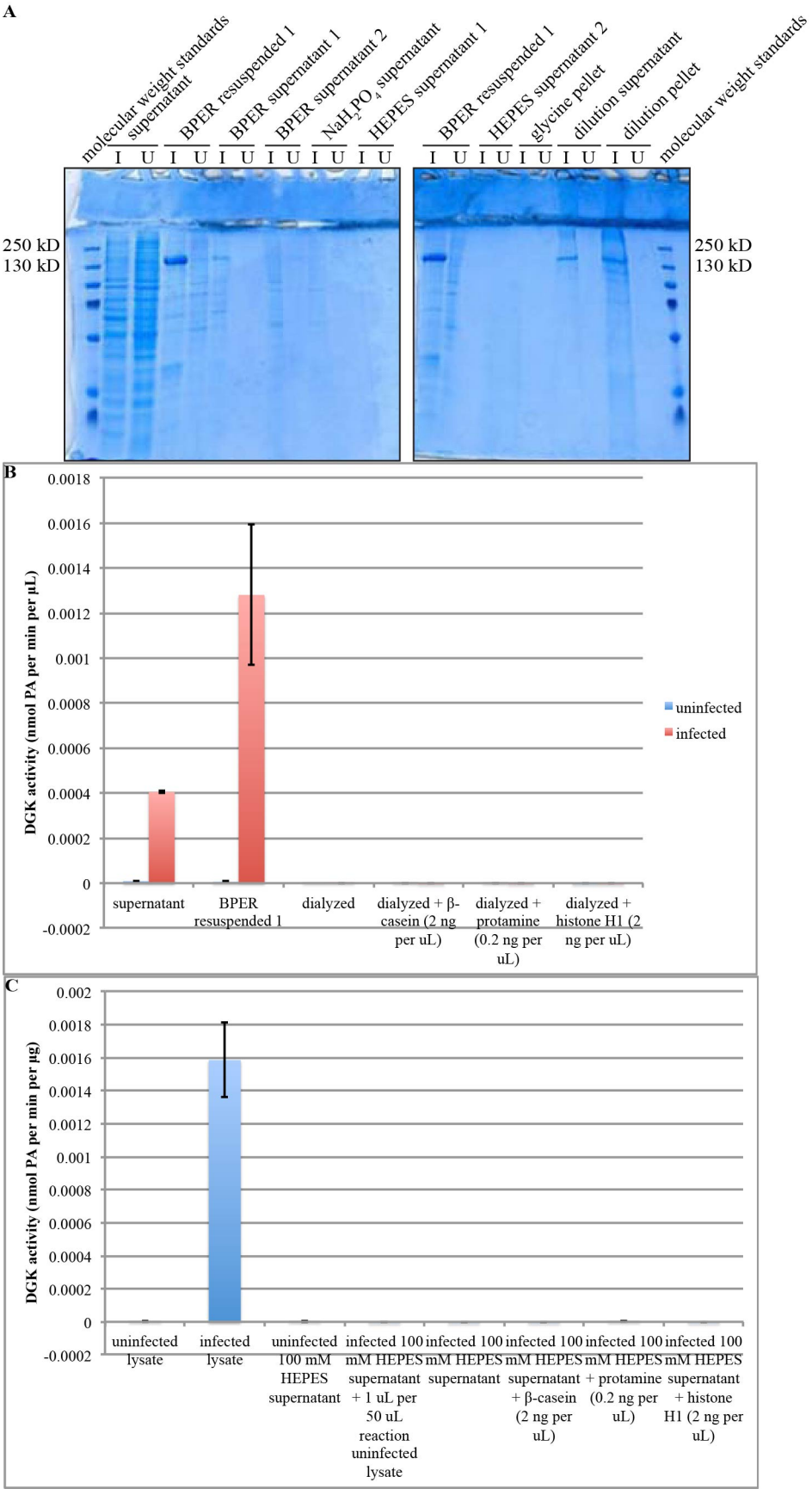
A
molecular weight standards
supernatant
BPER resuspended 1
BPER supernatant 1
BPER supernatant 2
NaH_2PO_4 supernatant
HEPES supernatant 1
BPER resuspended 1
HEPES supernatant 2
glycine pellet
dilution supernatant
dilution pellet
molecular weight standards
I U I U I U I U I U I U I U I U I U I U I U
250 kD
130 kD
250 kD
130 kD
B
DGK activity (nmol PA per min per µL)
0.0018
0.0016
0.0014
0.0012
0.001
0.0008
0.0006
0.0004
0.0002
0
-0.0002
uninfected
infected
supernatant
BPER resuspended 1
dialyzed
dialyzed + β-casein (2 ng per uL)
dialyzed + protamine (0.2 ng per uL)
dialyzed + histone H1 (2 ng per uL)
C
DGK activity (nmol PA per min per µg)
0.002
0.0018
0.0016
0.0014
0.0012
0.001
0.0008
0.0006
0.0004
0.0002
0
-0.0002
uninfected lysate
infected lysate
uninfected 100 mM HEPES supernatant
infected 100 mM HEPES supernatant + 1 uL per 50 uL reaction uninfected lysate
infected 100 mM HEPES supernatant
infected 100 mM HEPES supernatant + β-casein (2 ng per uL)
infected 100 mM HEPES supernatant + protamine (0.2 ng per uL)
infected 100 mM HEPES supernatant + histone H1 (2 ng per uL)

Figure 79. Some of the DGK-theta from the insoluble fraction of infected High Five™ cells can be solubilized, but this solubilized protein has no more DGK activity than protein similarly isolated from uninfected cells. I infected one of two 15 cm plates of High Five™ cells with 300 µL DGK-theta in pDEST10™. After two days, I washed the cells with cold FB, added cold lysis buffer (FB, 100 mM NaCl, 1x PIC, 1 mM $NaVO_4$, 0.5% NP-40) to the cells, and allowed them to sit on ice for ~30 minutes before scraping and homogenizing ten times with a glass cell homogenizer. I stored the lysates at -80°C for six days, then thawed by shaking the tubes gently in water. I collected the aggregates by centrifugation and washed with B-PER (Thermo Scientific), wash buffer 1 (10 mM NaH_2PO_4, pH 8.0), and wash buffer 2 (10 mM HEPES, pH 8.0). I solubilized the pellet by incubating with extraction buffer (25 mM glycine, 10 mM BME, 1 mM OG, pH 13.7) for ten minutes at 37°C, and removed the insoluble fraction by microfuging at maximum speed for five minutes at room temperature. I diluted the resulting supernatant fivefold into dilution buffer 1 (100 mM HEPES, pH 9.0), then removed the insoluble fraction by centrifuging at 46,000 x *g* for one hour at 25°C. I diluted the resulting supernatant into dilution buffer 2 (8 M urea, 25 mM glycine, 1 mM EDTA, 10 mM BME, pH 9.0), then dialyzed overnight into dialysis buffer 1 (same as dilution buffer 2, but without EDTA). I gradually dripped in dialysis buffer 2 (3 M urea, 10% sucrose, 25 mM HEPES, 10 mM BME, pH 9.0), such that the final concentration of urea was 3.6 M, and then I gradually dripped in dialysis buffer 3 (same as dialysis buffer 2, except that the urea was reduced to 2 M), such that the final concentration of urea was 2.9 M. The next day, I poured out most of the buffer and gradually dripped in dialysis buffer 4 (1 M urea), such that the final concentration of urea was 1.9 M, and then I gradually dripped in dialysis buffer 5 (500 mM urea), such that the final concentration of urea was 1.3 M. The next day, I poured out most of the buffer and gradually dripped in dialysis buffer 6 (0 M urea), such that the final concentration of urea was 330 mM. The next day, I poured out about half of the buffer and gradually dripped in dialysis buffer 7 (same as dialysis buffer 6, plus 50 µM $ZnCl_2$), such that the final concentration was 170 mM urea and 25 µM $ZnCl_2$. The next day, I transferred the dialysis tubing to dialysis buffer 8 (25 µM $ZnCl_2$), and dialyzed all day. **(A)** SDS-PAGE of 8% acrylamide gels followed by Coomassie staining. I, infected; U, uninfected. **(B)** DGK activity assay, in detergent micelles. The reaction included 5 mM TX-100 micelles (9 mol% POPS, 6 mol% DOG), 44 mM Tris, pH 7.4, 4.4 mM $MgCl_2$, 8 mM NaF, 1 mM ATP, 0.8% (w/v) sucrose, 2 mM HEPES, 0.8 mM BME, 2 µM $ZnCl_2$, 4 µL dialyzed sample per 50 µL reaction, and 66.7 Ci per mmol [γ-^{32}P]-ATP, and proceeded for 15 minutes at 37°C. In duplicate: mean ± SD. One of the two replicates of the uninfected dialyzed sample appeared to have been contaminated by the sample in the adjacent lane (this was before I included the 0.2 mm buffer zone between lanes on aluminum plates), so that replicate has been omitted and, as such, no SD is shown. **(C)** DGK activity assay, in liposomes. The samples were stored at 4°C for five days prior to assaying. The reaction included 5 mM liposomes (53:22:17:8::POPE:POPC:POPS:DOG), 44 mM Tris, pH 7.4, 4.4 mM $MgCl_2$, 8 mM NaF, 1 mM ATP, 0.4 mM glycine, 0.4 mM BME, 6 mM HEPES, 20 µM OG, 0.8 mM BME, 4 µL dialyzed sample per 50 µL reaction, and 47.5 Ci per mmol [γ-^{32}P]-ATP, and proceeded for 15 minutes at 37°C. In duplicate: mean ± SD.

In an effort to pinpoint precisely when the activity was lost, I tried again with a fresh expression of DGK-theta, with only small changes in the solubilization protocol (the lysis buffer included NAG; the cell pellet was not frozen before lysis; the cells were homogenized twenty times instead of ten; the protein pellets were washed in a larger volume; after the B-PER wash the pellets were washed with a HEPES buffer instead of a phosphate buffer; and I incubated the pellet for a longer time in the high-pH, OG-containing buffer to solubilize it), but this time collected aliquots at each step of the

process, and stored them at -80°C in 50% glycerol in order to later assay the enzymatic activity. Although the vast majority of the DGK-theta was in the pellet, not the supernatant (Figure 80**A** and Figure 81**B**), only about half of the DGK activity was recovered in the supernatant (Figure 80**B**). As the protein pellet was washed, it quickly lost all of its DGK activity (consistent with some small amount of soluble, active DGK having been trapped within the protein pellet, and then removed upon washing, even though the vast majority of the DGK remained in the insoluble pellet), leaving no detectable activity even before the solubilization at pH 13.7. I could detect no activity in the DGK that had been solubilized at pH 13.7, in either micelles (Figure 80**B**) or liposomes (Figure 81**B**), even in the presence of activators such as casein (Figure 80**B**), protamine, or the lysates of uninfected High Five™ cells (Figure 81**B**) in multiple attempts with multiple expressions, in contrast to what had previously been reported.

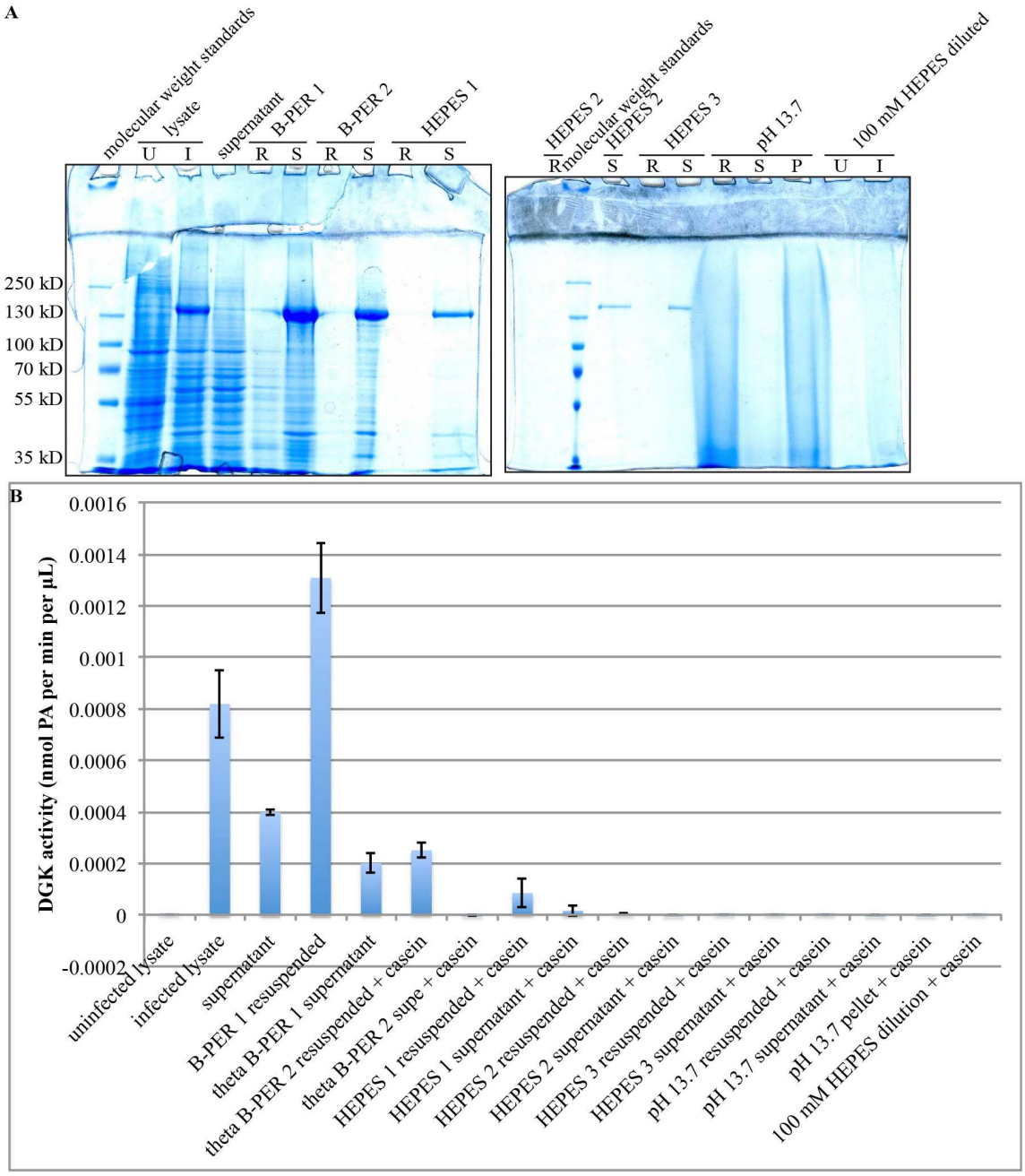

Figure 80. DGK-theta solubilized from High Five™ cells has no detectable DGK activity in detergent micelles. The same expression as shown in **Figure 71**B. I collected the aggregates by centrifugation, and washed with B-PER and wash buffer (10 mM HEPES, pH 8.0), vortexing for one minute for each wash. I solubilized the aggregates by resuspending them in solubilization buffer (25 mM glycine, 1 mM OG, pH 13.7), removed the insoluble fraction by microfuging at maximum speed for five minutes at room temperature, and diluted the resulting supernatant 1:4.2 in resuspension buffer (100 mM HEPES, pH 9.0). **(A)** SDS-PAGE of an 8% acrylamide gel followed by Coomassie staining. U, uninfected; I, infected; R, resuspended; S, supernatant; P, pellet. **(B)** I stored the lysates shown in **Figure 71**B in 50% glycerol at -80°C for eleven days prior to assaying. The reaction included 7 mM TX-100 micelles (9 mol% POPS, 6 mol% DOG), 44 mM Tris, pH 7.4, 4.4 mM $MgCl_2$, 1 mM ATP, 2.5% (v/v) glycerol, 2.5 µL protein sample

(prior to adding glycerol) per 50 µL reaction, and 43.1 Ci per mmol [γ-^{32}P]-ATP, and proceeded for 15 minutes at 37°C. In duplicate: mean ± SD.

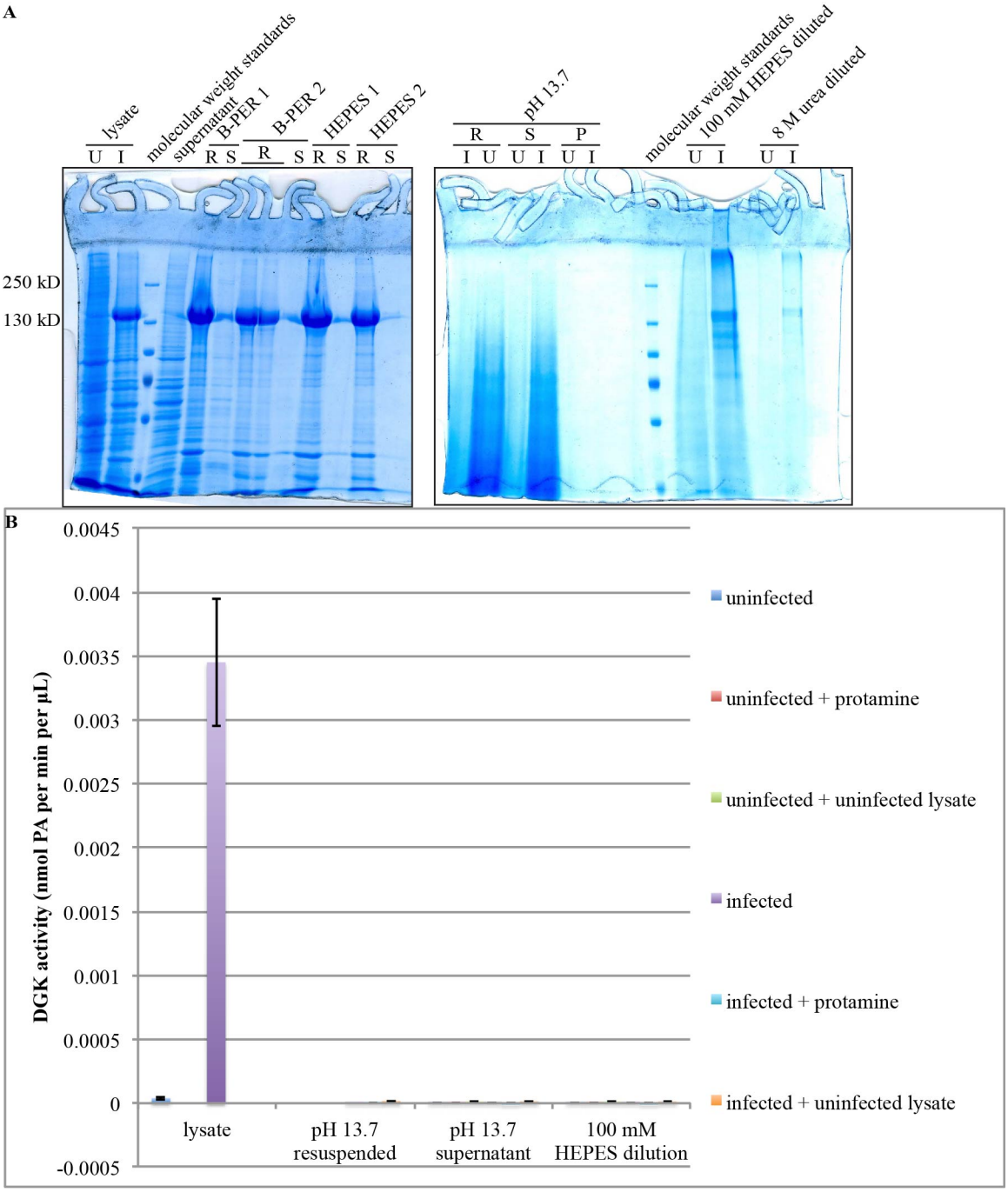

Figure 81. DGK-theta solubilized from High Five™ cells has no detectable DGK activity in liposomes. The same expression as shown in **Figure 71C**. I collected the aggregates by centrifugation, and washed with B-PER and wash buffer (10 mM HEPES, pH 8.0), vortexing for one minute for each wash. I solubilized the aggregates by resuspending them in solubilization buffer (25 mM glycine, pH 13.7), removed the insoluble fraction by microfuging at maximum speed for five minutes at room temperature, and diluted the resulting supernatant 1:5 in resuspension buffer (100 mM HEPES, pH 9.0),

then diluted that 1:6.25 into 8 M urea. **(A)** SDS-PAGE of 8% acrylamide gels followed by Coomassie staining. **(B)** DGK activity assay. I stored the samples in 50% glycerol at -80°C overnight prior to assaying. The reaction included 7 mM liposomes (53:22:17:8::POPE:POPC:POPS:DOG), 44 mM Tris, pH 7.5, 4.4 mM $MgCl_2$, 1 mM ATP, 2.5% (v/v) glycerol, 2.5 μL protein sample (prior to adding glycerol) per 50 μL reaction, and 66.7 Ci per mmol [γ-^{32}P]-ATP, and proceeded for 15 minutes at 37°C. In duplicate: mean ± SD.

I lowered the temperature of expression from 27°C to room temperature (approximately 24°C) to see whether a lower temperature would improve protein quality and hence enzymatic activity of solubilized protein. The vast majority to DGK-theta remained insoluble (Figure 82). I could, as with the higher-temperature expressions, solubilize DGK-theta from this insoluble fraction, but, also as before, the solubilized DGK-theta had no detectable DGK activity.

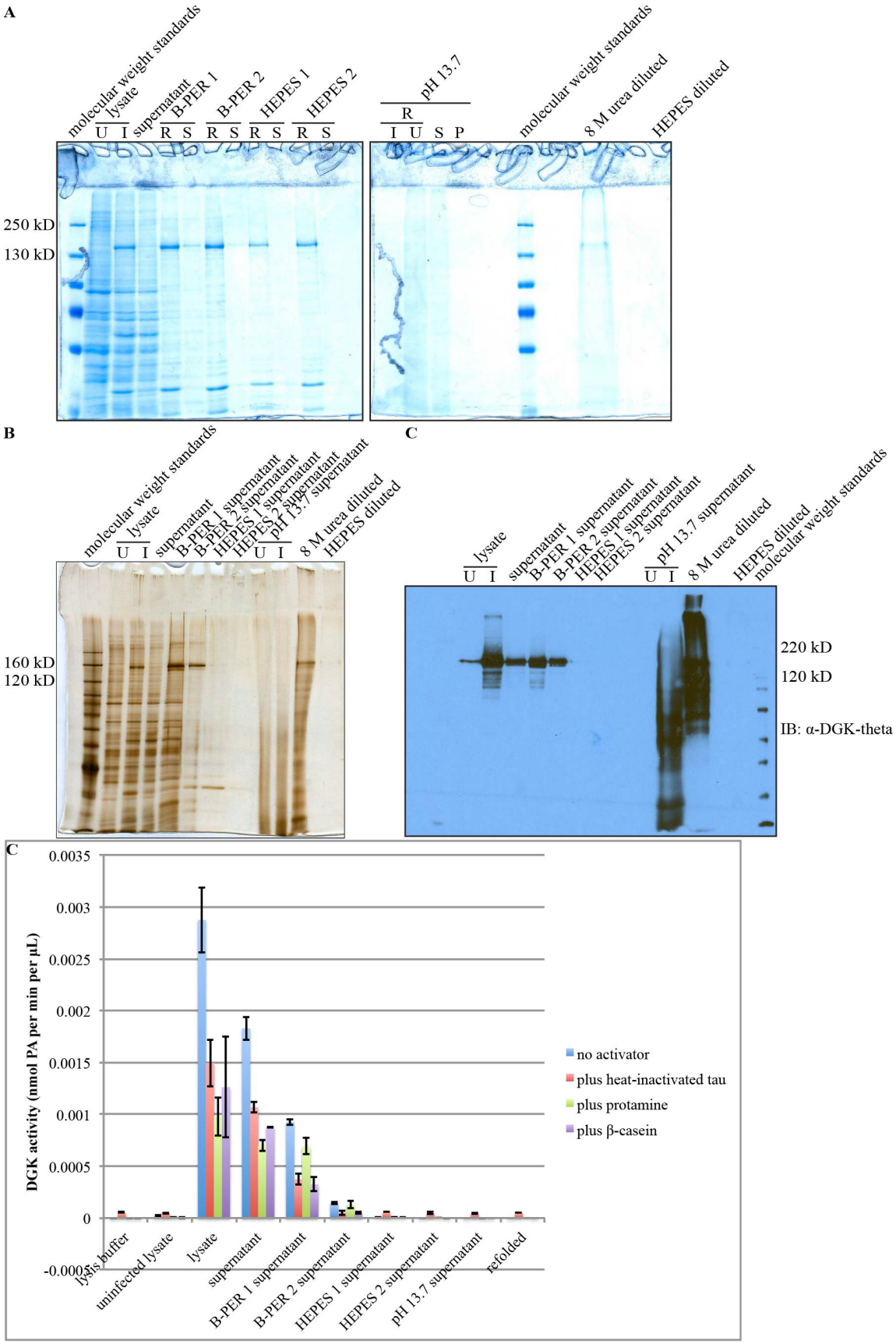
A
molecular weight standards
lysate
U I
supernatant
B-PER 1
R S
B-PER 2
R S
HEPES 1
R S
HEPES 2
R S
pH 13.7
R
I U S P
molecular weight standards
8 M urea diluted
HEPES diluted
250 kD
130 kD
B
molecular weight standards
lysate
U I
supernatant
B-PER 1 supernatant
B-PER 2 supernatant
HEPES 1 supernatant
HEPES 2 supernatant
pH 13.7 supernatant
U I
8 M urea diluted
HEPES diluted
160 kD
120 kD
C
lysate
U I
supernatant
B-PER 1 supernatant
B-PER 2 supernatant
HEPES 1 supernatant
HEPES 2 supernatant
pH 13.7 supernatant
U I
8 M urea diluted
HEPES diluted
molecular weight standards
220 kD
120 kD
IB: α-DGK-theta
C
DGK activity (nmol PA per min per µL)
0.0035
0.003
0.0025
0.002
0.0015
0.001
0.0005
0
-0.0005
lysis buffer
uninfected lysate
lysate
supernatant
B-PER 1 supernatant
B-PER 2 supernatant
HEPES 1 supernatant
HEPES 2 supernatant
pH 13.7 supernatant
refolded
no activator
plus heat-inactivated tau
plus protamine
plus β-casein

Figure 82. DGK-theta solubilized from High Five™ cells grown at a lower temperature has no detectable DGK activity in liposomes. I infected one of two 15 cm plates of High Five™ cells with 300 μL DGK-theta in pDEST10™. Two days later, I washed the cells with FB, added lysis buffer (FB, 1x PIC, 30 mM NAG, 1 mM $NaVO_4$, 0.5% NP-40), and incubated on ice for fifteen minutes before scraping and homogenizing ten times with a glass cell homogenizer. I collected the aggregates by centrifugation, and washed them with B-PER and with wash buffer (10 mM HEPES, pH 8.0). I solubilized the aggregates by resuspending in solubilization buffer (25 mM glycine, 10 mM fresh BME, 1 mM OG, pH 13.7). I removed the insoluble fraction by microfuging at maximum speed for five minutes at room temperature, diluted the resulting supernatant 1:5 into 8 M urea. I then refolded the protein by diluting an additional 1:40 into wash buffer, such that the final concentration was 4 mM urea. SDS-PAGE of 8% acrylamide gels followed by **(A)** Coomassie staining, **(B)** silver staining, and **(C)** immunoblotting against DGK-theta (1:350 (v/v)). U, uninfected; I, infected; R, resuspended; S, supernatant; P, pellet. **(D)** DGK activity assay. I stored the samples in 50% glycerol at -80°C for 18 days prior to assaying. The reaction included 7.5 mM liposomes (53:22:17:8::POPE:POPC:POPS:DOG), 44 mM Tris, pH 7.5, 4.4 mM $MgCl_2$, 80 mM NaCl, 1 mM ATP, 2% (v/v) glycerol, 2.5 μL protein sample (prior to adding glycerol) per 50 μL reaction, and 125 Ci per mmol [γ-^{32}P]-ATP, and proceeded for 15 minutes at 37°C. In duplicate: mean ± SD.

Conclusions

Because the DGK-theta expressed in High Five™ cells was inactive, it was deemed unsuitable for structural studies (since it would be unclear whether any structural information derived from inactive enzyme would be relevant to the turnover-competent molecule).

Insect Cell Expression Conclusions

Although eukaryotic expression systems are predicted to have several advantages over prokaryotic expression systems, the eukaryotic DGK constructs tested expressed in insect cells with poor quality. *R. norvegicus* DGK-alpha in pDEST10™ in Sf9 cells did not properly express the histidine tag and therefore could not be enriched by Ni-NTA chromatography, and *H. sapiens* DGK-theta in pDEST10™ in High Five™ cells was enzymatically inactive. Insect cell expression therefore proved no more useful than bacterial expression did.

Expressing and Purifying *Homo sapiens* DGK-Theta from 293FT Human Embryonic Kidney Cells

Introduction

Although mammalian cell lines produce less protein than other expression systems, they also include all of the proper machinery for expressing mammalian proteins such as mammalian DGKs. The very fact that less protein is produced may also contribute to higher protein quality: it is possible that eukaryotic DGKs have exposed hydrophobic patches to help facilitate lipid binding, and while at endogenous levels of protein the exposed hydrophobic patches might not impair DGK function, when too much DGK is produced in too small a space the exposed hydrophobic patches at a high density might promote aggregation. Although the lower levels of protein produced make mammalian cells an unlikely source for producing protein for x-ray crystallography, the higher quality of produced protein make them an ideal candidate for expressing protein for enzymological studies. For the enzymological studies to answer questions about eukaryotic DGK chemistry, therefore, I set out to express and purify DGKs from mammalian cells.

Results

The Fc-FLAG-DGK-theta in pCDNA3.1 (+) construct begins with an N-terminal fusion tag of *H. sapiens* Ig heavy chain (Fc), followed by a TEV protease site, followed by a FLAG tag (Figure 83). The MW and pI of this construct are predicted to be 129.5 kD and 7.22, respectively.

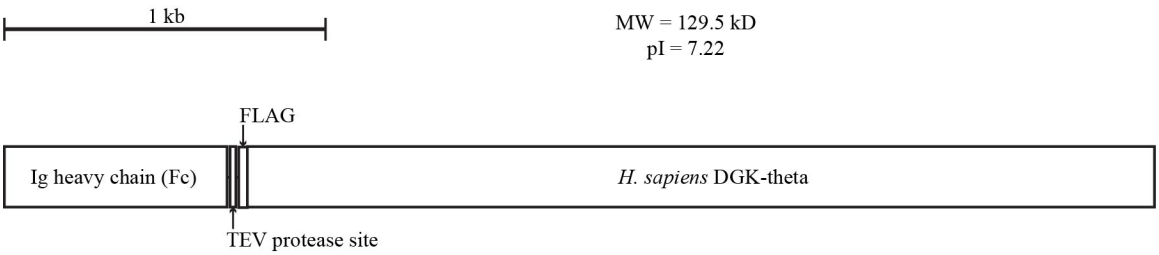

Figure 83. Schematic of Fc-FLAG-DGK-theta in pCDNA 3.1 (+) construct.

I was able to express Fc-FLAG-DGK-theta in 293FT human embryonic kidney (HEK) cells via transient transfection. After fractionating the cells, I was able to use the Fc tag to batch-purify DGK-theta from either cytosol or non-nuclear membranes by affinity chromatography using sepharose conjugated to Protein A, a bacterial protein with high affinity for immunoglobulins. After batch purification, I was able to enrich a band that migrated between the 120 and 160 kD molecular weight markers, consistent with the predicted molecular weight of Fc-FLAG-DGK-theta, that recognized the anti-DGK-theta antibody (Figure 84): I concluded that this band was Fc-FLAG-DGK-theta. While Protein A sepharose could enrich Fc-FLAG-DGK-theta, it was not purified to homogeneity. Small changes in the purification protocol did not greatly affect purity or yield (Figure 84). Fc-FLAG-DGK-theta enriched on protein A sepharose beads had detectable DGK enzymatic activity using either micelles or liposomes as a substrate and could be activated by low molecular-weight (LMW) polylysine (Figure 85).

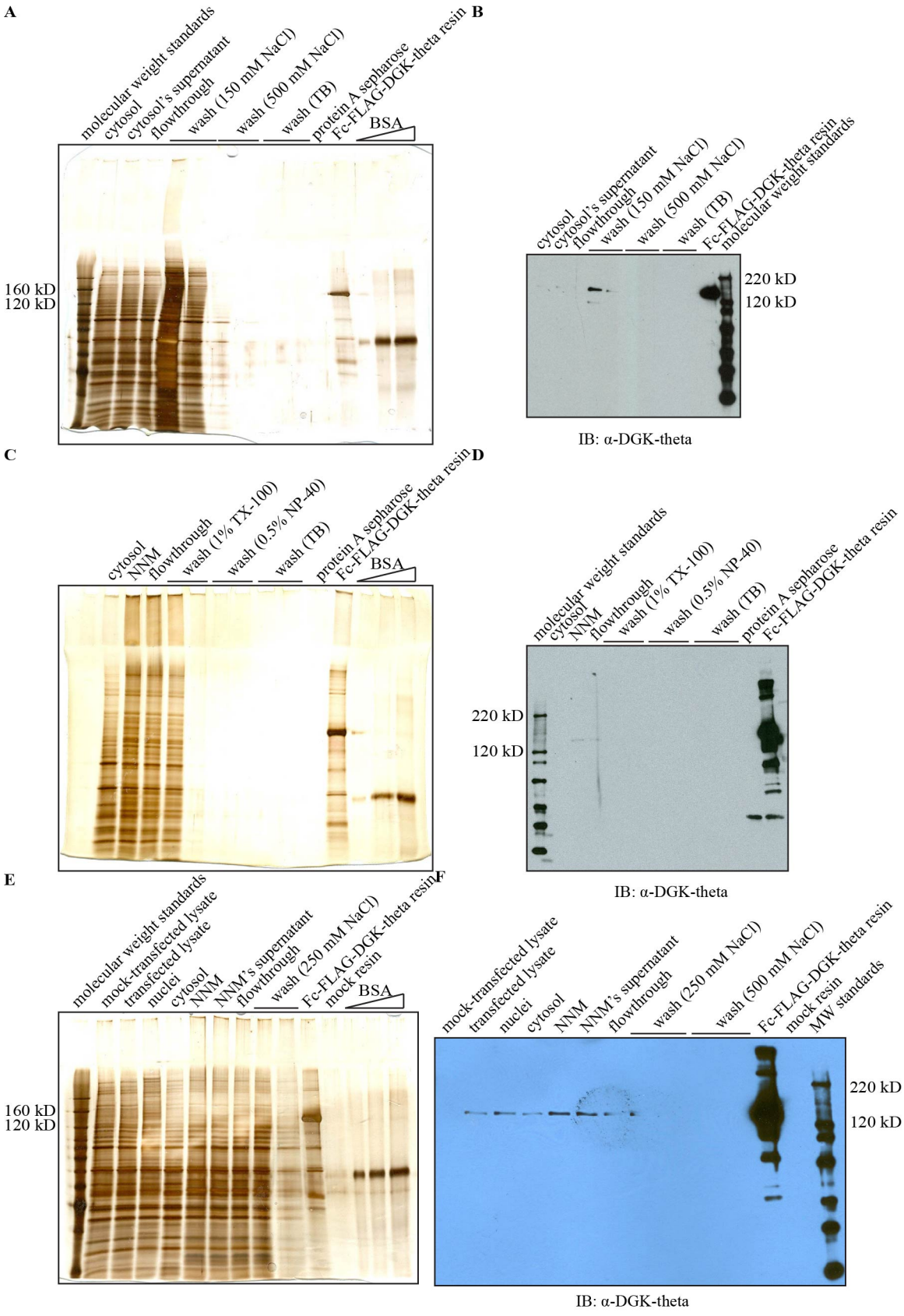
A
molecular weight standards
cytosol
cytosol's supernatant
flowthrough
wash (150 mM NaCl)
wash (500 mM NaCl)
wash (TB)
protein A sepharose
Fc-FLAG-DGK-theta resin
BSA
160 kD
120 kD
B
cytosol
cytosol's supernatant
flowthrough
wash (150 mM NaCl)
wash (500 mM NaCl)
wash (TB)
Fc-FLAG-DGK-theta resin
molecular weight standards
220 kD
120 kD
IB: α-DGK-theta
C
cytosol
NNM
flowthrough
wash (1% TX-100)
wash (0.5% NP-40)
wash (TB)
protein A sepharose
Fc-FLAG-DGK-theta resin
BSA
D
molecular weight standards
cytosol
NNM
flowthrough
wash (1% TX-100)
wash (0.5% NP-40)
wash (TB)
protein A sepharose
Fc-FLAG-DGK-theta resin
220 kD
120 kD
IB: α-DGK-theta
E
molecular weight standards
mock-transfected lysate
transfected lysate
nuclei
cytosol
NNM
NNM's supernatant
flowthrough
wash (250 mM NaCl)
Fc-FLAG-DGK-theta resin
mock resin
BSA
160 kD
120 kD
F
mock-transfected lysate
transfected lysate
nuclei
cytosol
NNM
NNM's supernatant
flowthrough
wash (250 mM NaCl)
wash (500 mM NaCl)
Fc-FLAG-DGK-theta resin
mock resin
MW standards
220 kD
120 kD
IB: α-DGK-theta

Figure 84. Fc-FLAG-DGK-theta in pCDNA3.1 (+) can be enriched from HEK293FT via protein A sepharose affinity chromatography. I transfected five 15 cm 293FT flasks, which had been grown in 293FT growth medium 1, with Fc-FLAG-DGK-theta in pCDNA3.1 (+) for four hours. Three days later, I washed the cells with FB. I added cold lysis buffer (18 mM HEPES, pH 7.4, 92 mM NaCl, 0.5 mM EGTA, 0.9 mM EDTA, 4 μg per mL quinacrine, 1x PIC, 100 mM NAG, 5 mM $NaVO_4$, 10 mM NaF, 5 mM DTT, 0.25% (v/v) NP-40), scraped the plates, and allowed to sit on ice for seven minutes before homogenizing seven times with a glass cell homogenizer. I removed the insoluble fraction by centrifugation. I fractionated the resulting supernatant by centrifuging at 115,000 x *g* for 65 minutes: the resulting supernatant was the cytosol, and the resulting pellet was the non-nuclear membranes (NNM). I stored the cytosol in 20% glycerol at -80°C for two weeks, then thawed by shaking the tube gently in water. I removed the insoluble fraction by centrifugation, then added protein A sepharose 1:125 (v/v) and rotated at 4°C for two hours. I washed the resin with wash buffer 1 (20 mM HEPES, pH 7.4, 150 mM NaCl, 0.5% NP-40), wash buffer 2 (same as wash buffer 1, but NaCl increased to 500 mM), and TB (20 mM HEPES, pH 8.4, 1 mM DTT). SDS-PAGE followed by **(A)** silver staining, and **(B)** immunoblotting against DGK-theta (1:350 (v/v)). From the same expression shown in (A) and (B), I resuspended the NNM in lysis buffer and probe-sonicated three times for tens seconds each, and stored in 20% glycerol at -80°C overnight. I thawed by shaking the tube gently in water, removed the insoluble fraction by centrifugation, then added protein A sepharose 1:50 (v/v) and rotated at 4°C for three hours. I washed the resin with wash buffer 3 (20 mM HEPES, pH 7.4, 5 mM DTT, 250 mM NaCl, 1% (v/v) TX-100), wash buffer 4 (same as wash buffer 3, but TX-100 replaced with 0.5% (v/v) NP-40), and TB. SDS-PAGE followed by **(C)** silver staining, and **(D)** immunoblotting against DGK-theta (1:350 (v/v)). I transfected five 15 cm 293FT plates, which had been grown in 293FT growth medium 2, with Fc-FLAG-DGK-theta in pCDNA3.1 (+). Two days later, I replaced the medium, and the next day, washed the cells with FB. I added cold lysis buffer, scraped the plates, and homogenized twelve times with a glass cell homogenizer. I removed the insoluble fraction by centrifugation, and fractionated the resulting supernatant into cytosol and NNM by centrifuging at 115,000 x *g* for 65 minutes. I resuspended the NNM in lysis buffer and probe-sonicated five times for tens seconds each, and stored in 20% glycerol at -80°C for one month. I thawed by shaking the tube gently in water, removed the insoluble fraction by centrifugation, then added protein A sepharose 1:50 (v/v) and rotated at 4°C for three hours. I washed the resin with wash buffer 5 (same as wash buffer 3, but NP-40 increased to 1% (v/v)), wash buffer 6 (same as wash buffer 5, but NaCl increased to 250 mM), and thrombin buffer (10 mM HEPES, pH 7.5, 10 mM Tris, 100 mM NaCl, 0.1% (w/v) PEG-8000). SDS-PAGE of 8% acrylamide gels followed by **(E)** silver staining, and **(F)** immunoblotting against DGK-theta (1:350 (v/v)).

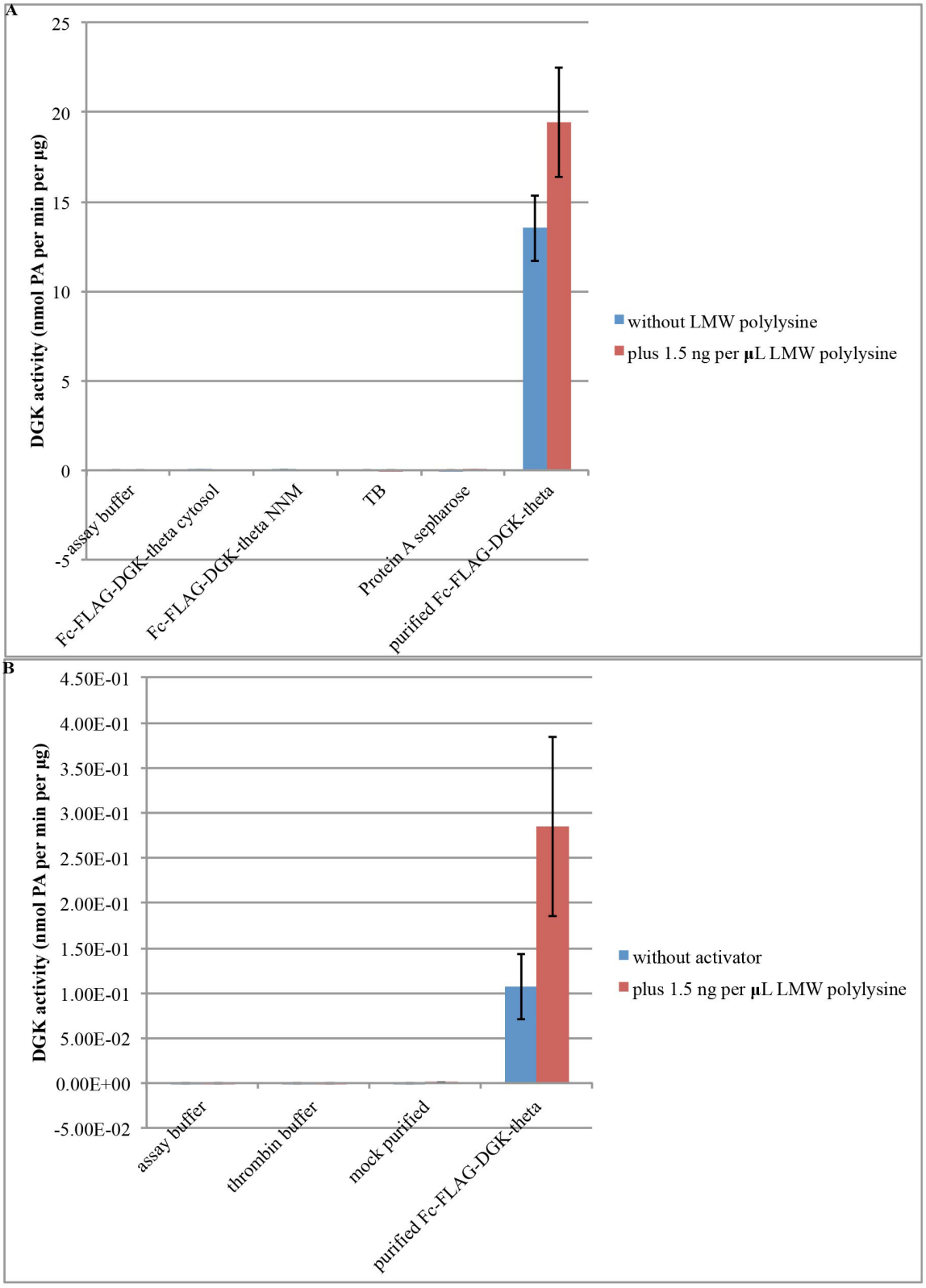
A
25
20
15
10
5
0
-5
DGK activity (nmol PA per min per µg)
assay buffer
Fc-FLAG-DGK-theta cytosol
Fc-FLAG-DGK-theta NNM
TB
Protein A sepharose
purified Fc-FLAG-DGK-theta
without LMW polylysine
plus 1.5 ng per µL LMW polylysine
B
4.50E-01
4.00E-01
3.50E-01
3.00E-01
2.50E-01
2.00E-01
1.50E-01
1.00E-01
5.00E-02
0.00E+00
-5.00E-02
DGK activity (nmol PA per min per µg)
assay buffer
thrombin buffer
mock purified
purified Fc-FLAG-DGK-theta
without activator
plus 1.5 ng per µL LMW polylysine

Figure 85. Fc-FLAG-DGK-theta enriched from 293FT non-nuclear membranes has detectable DGK activity. (A) The samples shown in **Figure 84**(**C**-**D**) were stored in 50% glycerol at -80°C for six weeks prior to assaying. The reaction included 5 mM TX-100 micelles (9 mol% POPS, 6 mol% DOG), 49 mM HEPES, pH 7.0, 4.8 mM $MgCl_2$, 132 mM NaCl, 1 mM ATP, 0.5% (v/v) glycerol, 23 pg protein sample per 50 μL reaction, and 98.3 Ci per mmol [γ-^{32}P]-ATP, and proceeded for 15 minutes at 37°C. In duplicate: mean ± SD. **(B)** The samples shown in **Figure 84**(**E**-**F**) were stored in 50% glycerol at -80°C for three weeks prior to assaying. The reaction included 7.5 mM liposomes (53:22:17:8::POPE:POPC:POPS:DOG), 44 mM HEPES, pH 7.0, 4.4 mM $MgCl_2$, 123 mM NaCl, 1 mM ATP, 0.25 mM Tris, 1% (v/v) glycerol, 1 ng per μL protein sample per 50 μL reaction, and 66.7 Ci per mmol [γ-^{32}P]-ATP, and proceeded for 15 minutes at 37°C. In duplicate: mean ± SD.

We were also interested in learning whether DGK expressed in a mammalian system, presumably with its appropriate post-translational processing, was monodisperse, or whether it would elute in the void volume from a Sephadex G200 analytical gel filtration resin. When I loaded supernatant from 293T cells overexpressing myc-tagged DGK-theta onto the resin, DGK eluted slightly before the void volume, as detected by Western blotting against either the myc tag or DGK-theta (Figure 86). We concluded that, under these particular conditions, DGK expressed in a mammalian system is also not monodisperse.

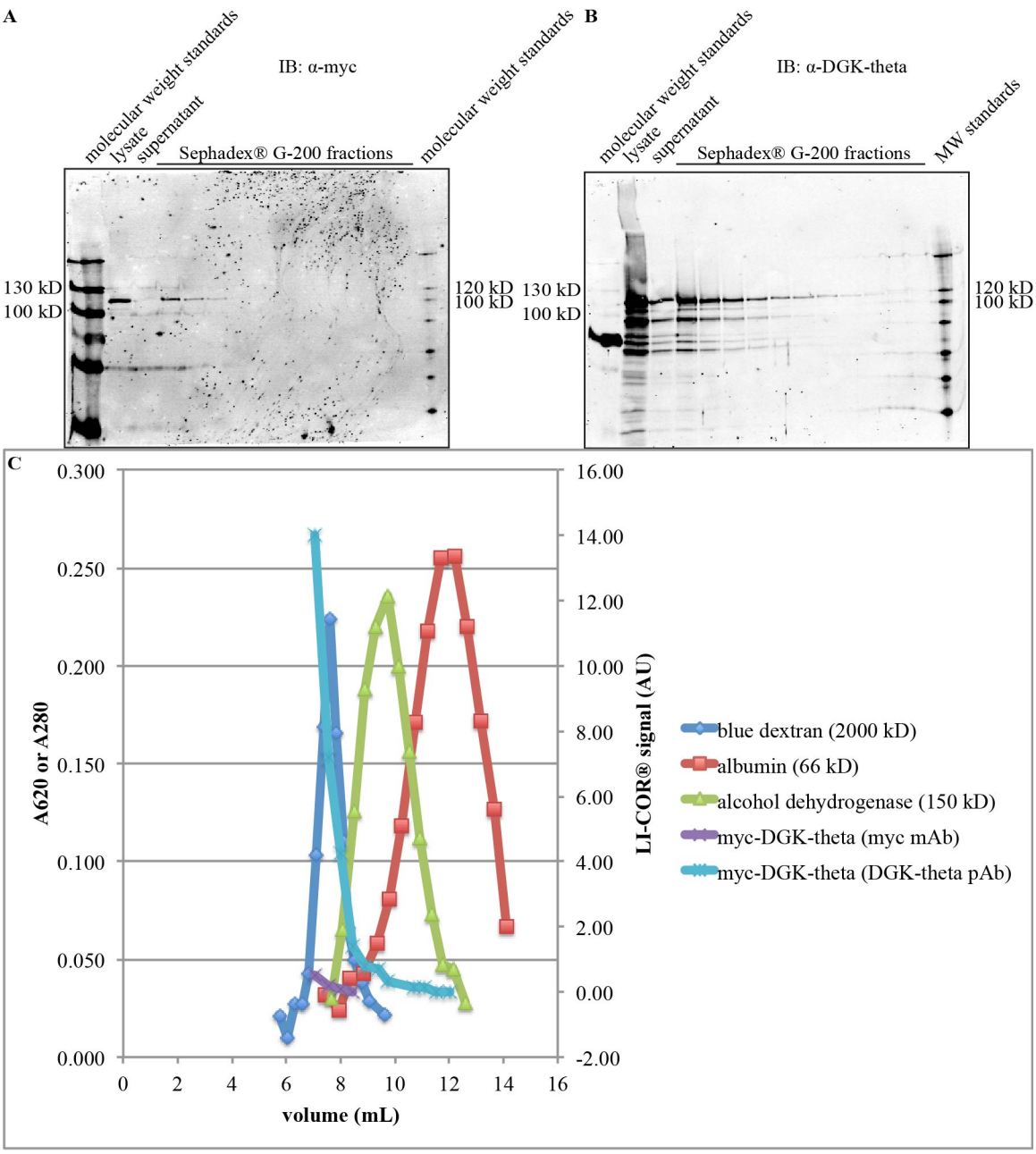

Figure 86. DGK expressed in a mammalian system elutes in the void volume from a Sephadex® G-200 column under the conditions tested. Two 10 cm plates of 293T cells were washed with PBS, then resuspended in lysis buffer (4 mM HEPES, 130 mM sucrose, pH 7.4), scraped, and homogenized 18 times with a glass cell homogenizer. I removed the insoluble fraction by centrifuging at 16,000 x *g* for ten minutes at 4°C, and loaded 200 µL of the resulting supernatant onto a Sephadex® G-200 column that had been previously calibrated with blue dextran, albumin, and alcohol dehydrogenase, and I collected fractions every 7.5 minutes, eluting by gravity in lysis buffer. SDS-PAGE of an 8% acrylamide gel followed by immunoblotting against **(A)** myc (mouse 1:1000 (v/v)), and **(B)** DGK-theta (rabbit 1:200 (v/v)). I loaded 15 µL per well of gel filtration fractions of elution volumes corresponding to molecular weights of 364 to 70 kD. The same membrane was incubated in both antibodies simultaneously, since their signals could be distinguished on the LI-COR® detection system. **(C)** Elution of molecular weight standards (left vertical

axis, A620 for blue dextran and A280 for protein standards) and myc-DGK-theta (immunoblot signal from (A) and (B), quantified by LI-COR®).

Mammalian Cell Expression Conclusions

I was able to express and enrich Fc-FLAG-DGK-theta in 293FT HEK cells. Although this protein eluted in the void volume from an analytical gel filtration column and thus was not promising for x-ray crystallography studies, the limited amount of protein produced by mammalian cells would have been a challenge for such studies anyway. The enriched protein was enzymatically active, and was therefore suitable for enzymological studies.

Expressing and Purifying DGKs Discussion and Conclusions

Recombinantly expressed eukaryotic DGKs face major solubility challenges, not only in bacteria but also in insect cells, a eukaryotic expression system. The protein quality of the DGKs expressed in insect cells is so poor that insect cell expression appears to be a no more promising approach than bacterial expression, despite its purported advantages. Mammalian cells, possibly because of the lower abundance of proteins overexpressed therein, are able to produce enzymatically active DGK, but even DGK recombinantly expressed in mammalian cells elutes from an analytical gel filtration column in the void volume under the conditions tested, suggesting that DGK expressed in mammalian cells likewise faces solubility challenges. Perhaps this tendency toward aggregation is telling us something about how these enzymes work: they are, after all, lipid-handling enzymes, so it is possible that they are exposing hydrophobic patches that, when the concentration of DGK rises too high in a cell, such as when recombinantly expressed, the density of these hydrophobic patches promotes aggregation. Future

studies wishing to produce large amounts of eukaryotic DGKs will face these challenges. It is my hope that this work will help guide future research into more productive directions, so that anyone wishing to express these proteins know which strategies have already been tried. It is also my hope that this work will help inform future efforts to predict which expression strategies will be amenable for which proteins, so that not every method will have to be empirically tested for every protein to be expressed, but rather the proper method can be recommended based on the primary sequence of a protein alone.

Chapter 4: DGK stability

DGK Storage Conditions

Introduction

Purifying and expressing DGKs takes time, and it is impractical to do all experiments on DGK immediately after expressing and purifying it. Therefore, in order to study the activity of DGK, it became plainly apparent that it was imperative to find conditions under which DGK could be stored between expression and experiment that mitigated the loss of DGK activity.

Results

I compared how alphacat in pT71myc from freshly lysed Rosetta™(DE3) cells vs. a lysate that had been stored at -80°C in 20% glycerol for thirteen days fractionated upon washing with 2 M or 4 M urea. When monitored by SDS-PAGE followed by Coomassie staining, how the alphacat fractionated did not appear to depend on whether the lysate was fresh or had been previously frozen (Figure 87**A-D**). When monitored by SDS-PAGE followed by immunoblotting against histidine, the lysates and supernatants did not appear different fresh vs. frozen; however, more alphacat appeared to wash off in the first 2 M urea wash in the freshly expressed sample, and more alphacat appeared to wash off in the first 4 M urea wash in the sample that had been frozen (Figure 87**E**), suggesting that freezing may transfer some of the alphacat to a population that is insoluble at 2 M urea but soluble at 4 M urea. I also immunoblotted against DGK-alpha (Figure 87**F**), but the interpretation of this immunoblot is limited by the fact that the immunoreactive band of the appropriate size to be alphacat was also faintly detected in the uninduced lysate,

suggesting that the interface between the stacking and separating phases of the gel may have dried out during casting, causing the wells' contents to leak and contaminate other lanes. I also assayed the DGK activity of these fractionations, but interpretation of this activity assay is severely limited by two factors. Firstly, the vial of lipid that had been labeled as "DOG" and used as substrate was not, in fact, dioleoylglycerol, but rather dioctanoylglycerol (DiC8), as evidenced by the fact that instead of the single spot usually produced at a relative front (R_f) of 0.85, this substrate produced two spots: a stronger one with an average R_f of 0.54, and a weaker one with an average R_f of 0.75 (Figure 88**A**). Secondly, the lysate that had been left on ice for the duration of the assay showed nearly as high DGK activity as the lysate that had been incubated at 30°C for 15 minutes (Figure 88**B**). Considerable activity on ice makes the results of the assay difficult to interpret because, due to the logistics of large assays, some of the samples spend more time than others in the presence of [γ-^{32}P]-ATP on ice. A higher readout of the DGK assay may, in this case, say more about the amount of time the sample spent on ice with the assay components before being moved into the water bath than it does about the specific activity of the sample.

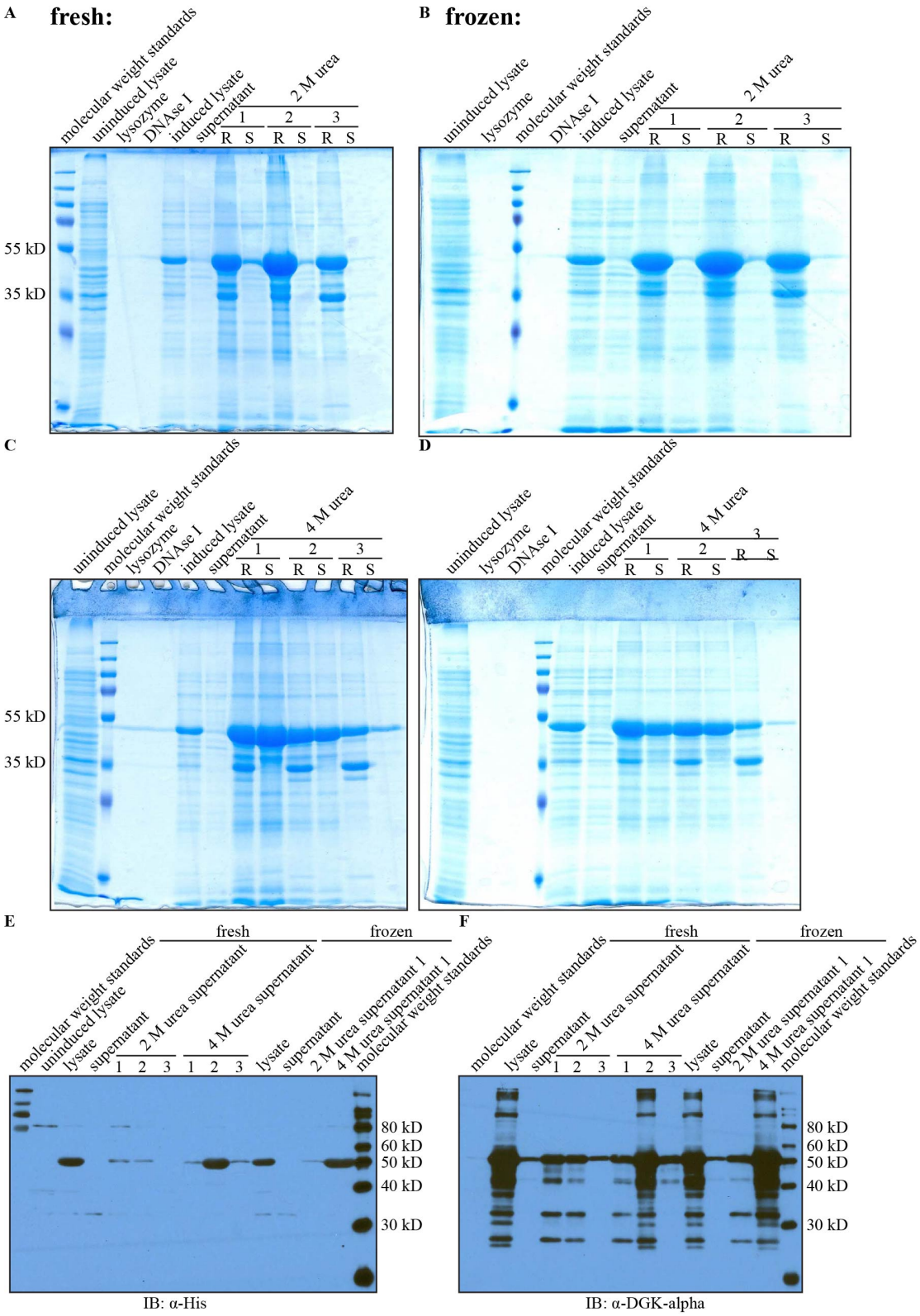
A
fresh:
molecular weight standards
uninduced lysate
lysozyme
DNAse I
induced lysate
supernatant
2 M urea
1
2
3
R S R S R S
55 kD
35 kD
B
frozen:
uninduced lysate
lysozyme
molecular weight standards
DNAse I
induced lysate
supernatant
2 M urea
1
2
3
R S R S R S
C
uninduced lysate
molecular weight standards
lysozyme
DNAse I
induced lysate
supernatant
4 M urea
1
2
3
R S R S R S
55 kD
35 kD
D
uninduced lysate
lysozyme
DNAse I
molecular weight standards
induced lysate
supernatant
4 M urea
1
2
3
R S R S R S
E
fresh
frozen
molecular weight standards
uninduced lysate
lysate
supernatant
2 M urea supernatant
4 M urea supernatant
lysate
supernatant
2 M urea supernatant 1
4 M urea supernatant 1
molecular weight standards
1 2 3 1 2 3
80 kD
60 kD
50 kD
40 kD
30 kD
IB: α-His
F
fresh
frozen
molecular weight standards
lysate
supernatant
2 M urea supernatant
4 M urea supernatant
lysate
supernatant
2 M urea supernatant 1
4 M urea supernatant 1
molecular weight standards
1 2 3 1 2 3
80 kD
60 kD
50 kD
40 kD
30 kD
IB: α-DGK-alpha

Figure 87. Storing at -80°C in 20% glycerol for thirteen days may transfer some of the alphacat in pT71myc in Rosetta™(DE3) to a population that is insoluble at 2 M urea but soluble at 4 M urea, as compared to a fresh lysate. The fresh expression is the same as shown in **Figure 9**. The frozen expression is the same as shown in **Figure 7**. I stored the lysates in 20% glycerol for thirteen days at -80C before fractionating as described in the figure legend to **Figure 9**. SDS-PAGE followed by **(A)-(D)** Coomassie staining, **(E)** immunoblotting against His_6 (abcam® ab6196 (1:2500 (v/v))), and **(F)** immunoblotting against DGK-alpha (Sakane (1:5000 (v/v))). **(A)** and **(C)** show the fractionation of the fresh lysate; **(B)** and **(D)** show the fractionation of the frozen lysate.

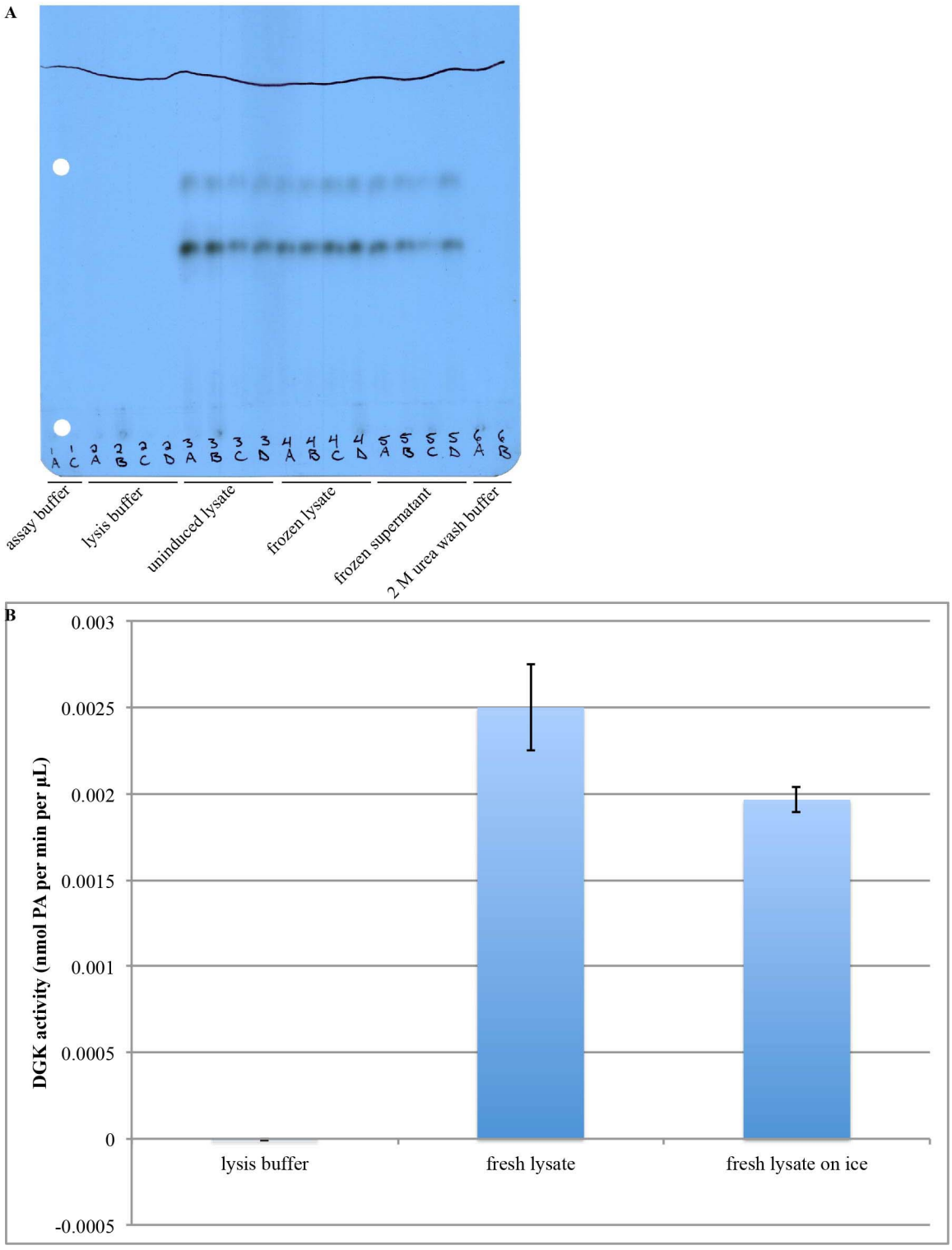

Figure 88. Rosetta™(DE3) lysate overexpressing alphacat in pT71myc shows considerable DGK activity on ice using DiC8 as a substrate. The samples (**Figure 87**) had been stored in 50% glycerol at -80°C for three weeks prior to assaying their DGK activity. The reaction included 7.5 mM liposomes (53:22:17:8::POPE:POPC:POPS:"DOG"), 49 mM HEPES, pH 8.0, 4.9 mM $MgCl_2$, 1 mM $CaCl_2$, 1 mM ATP, 0.25 mM Tris, 1.5 mM NaCl, 50 µM imidazole, 0.0025% (v/v) NP-40, 0.005x PIC, 0.25% (v/v)

glycerol, 0.5 μL protein sample per 50 μL reaction, and 37.3 Ci per mmol [γ-^{32}P]-ATP, and proceeded for 15 minutes at 30°C. Forty minutes elapsed between combining the reaction mix for "fresh lysate on ice" and placing the "fresh lysate" tube in the 30°C water bath. **(A)** Autoradiograph. The marked line indicates the solvent front. A,B: no activator. C,D: plus heat-inactivated tau. **(B)** DGK activity assay. In duplicate: mean ± SD.

Because of the DOG/DiC8 mix-up, I thought that the alphacat in pT71myc lysates were losing activity when stored at -80°C, and thus became concerned about storage conditions, and therefore set out to test those expressly. In these same experiments, I also tested a range of protein concentrations to determine the linear range of the assay. I was unable to test the lysate fresh because the PE vial had been mislabeled as 25 mg/mL when it was in fact 10 mg/mL, meaning that the lipids dried for liposomes had too high a PC:PE ratio to be able to successfully extrude. I dried down fresh lipids of the correct composition for liposomes, but as such I had to store the lysate overnight at 4°C before I was able to assay it. These liposomes also included DiC8 instead of DOG (because of the mislabeled vial of lipid mentioned previously). After one night at 4°C, the bacterial lysate overexpressing alphacat in pT71myc demonstrated more DGK activity toward DiC8 than the uninduced lysate, and this activity depended linearly on the concentration of the enzyme at least up through 60 ng per μL of total protein (Figure 89).

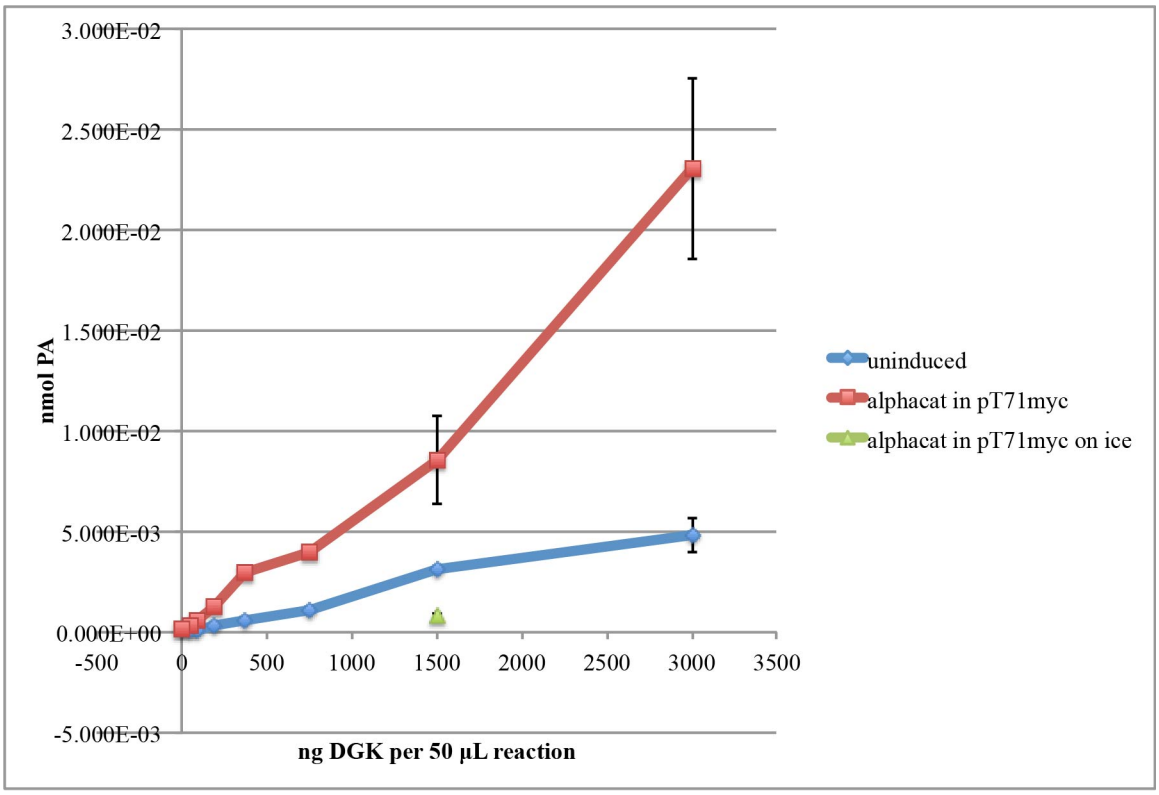

Figure 89. Rosetta™(DE3) lysate overexpressing alphacat in pT71myc shows greater DGK activity toward DiC8 than uninduced lysate, and this activity depends linearly on the concentration of the enzyme at least up through 60 ng per µL of total protein. I inoculated two 25 mL LB Kan cultures with an overnight culture of alphacat in pT71myc in Rosetta™(DE3). When the OD600 was predicted to reach 1.0, I added IPTG to 0.5 mM (or not) and shook the cultures for 21.5 hours at ~18°C, then pelleted the cells by centrifugation and resuspended in 6 mL each cold lysis buffer (50 mM Tris, pH 8.0, 300 mM NaCl, 10 mM imidazole, 1 mM $CaCl_2$, 0.5% NP-40, 1x PIC, 1 mM DTT, 1 mg per mL lysozyme) and incubated on ice for thirty minutes. I lysed the cells by probe-sonicating six times on ice for ten seconds each, resting on ice for ten seconds between each burst. I stored the lysates overnight at 4°C prior to assaying their DGK activity. The reaction included 7.5 mM liposomes (53:22:17:8::POPE:POPC:POPS:"DOG"), 49 mM HEPES, pH 8.0, 4.9 mM $MgCl_2$, 1 mM $CaCl_2$, 1 mM ATP, 98.3 Ci per mmol [γ-^{32}P]-ATP, and, from the lysates, up to 0.9 mM Tris, 5.4 mM NaCl, 180 µM imidazole, 0.009% (v/v) NP-40, and 0.018x PIC, and proceeded for 16 minutes at 30°C. 23 minutes elapsed between combining the reaction mix for "alphacat in pT71myc on ice" and placing the other tubes in the 30°C water bath. I calculated the nmol PA as the total of the two radiolabeled spots produced from DiC8. In duplicate: mean ± SD.

After the initial storage at 4°C overnight, I stored aliquots of the lysates either at 4°C, at -80°C in 20% (v/v) glycerol, and at -80°C in 50% glycerol. After one week, I assayed the activity again in liposomes: this time DOG was used as a substrate, although the R_f remained lower than expected (~0.7). Because the substrate was different, the specific activity cannot be compared quantitatively to the activity one week previously,

so I cannot conclude whether or not the alphacat lost activity during the course of the week, or by how much. I can, however, conclude that for all three storage methods, the activity of alphacat-overexpressing lysates remained higher than that of uninduced lysates (Figure 90). The activity was the highest for alphacat that had been stored at -80°C in 50% glycerol; the activity of lysates stored at 4°C or at -80°C in 20% glycerol were comparable to one another. The activity on DiC8 after one night at 4°C for the induced lysate was more than four times the activity of the uninduced lysate (Figure 89), but the activity on DOG after one week of any of the tested storage conditions was less than four times that of the uninduced lysate (Figure 90); however, as mentioned, any interpretation of these results is limited by the fact that the activity was measured on different substrates.

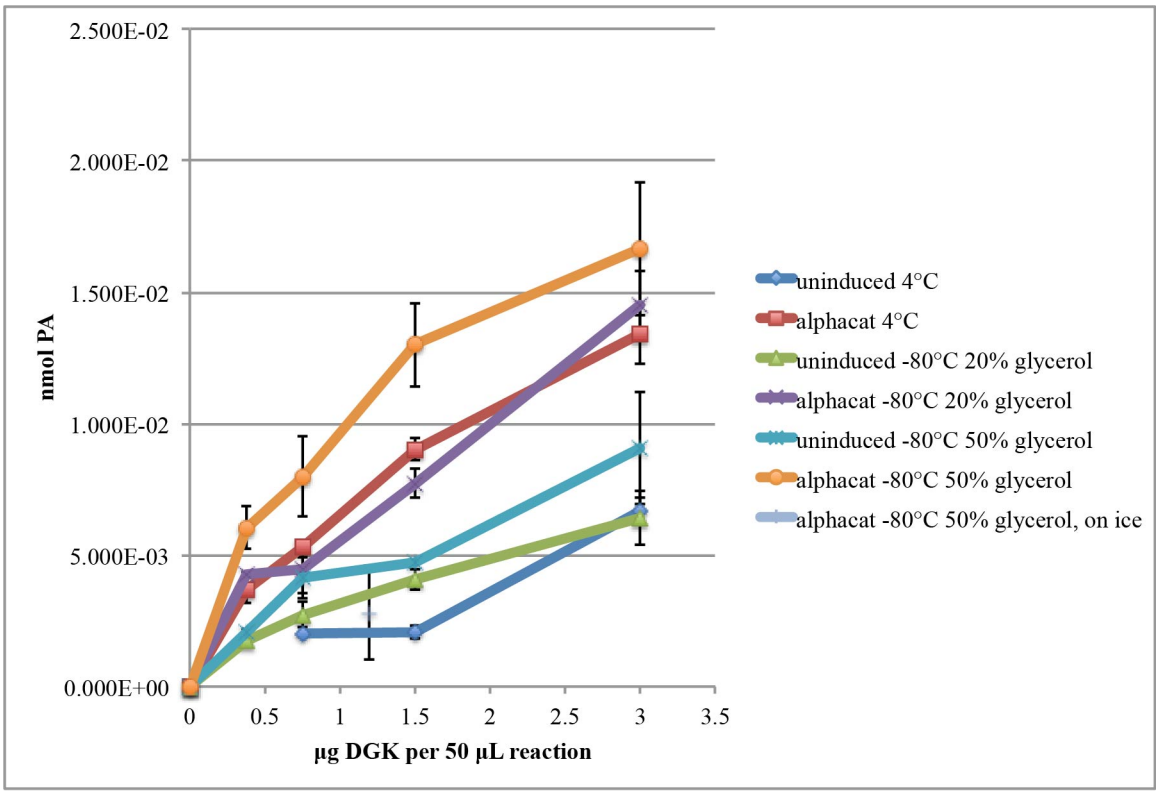

Figure 90. For all three storage methods tested, the activity of alphacat-overexpressing Rosetta™(DE3) lysates remained higher than that of uninduced lysates. DGK activity assay. The samples used were the same as shown in **Figure 89**, stored for one week under the conditions shown. The reaction included 7.5 mM liposomes (53:22:17:8::POPE:POPC:POPS:DOG), 49 mM HEPES, pH 8.0, 4.9 mM $MgCl_2$, 1 mM $CaCl_2$, 1 mM ATP, 76.2 Ci per mmol [γ-^{32}P]-ATP, and, from the lysates, up to 0.9 mM Tris, 5.4 mM NaCl, 180 µM imidazole, 0.009% (v/v) NP-40, 0.018x PIC, and 0.9% (v/v) glycerol, and proceeded for 15 minutes at 30°C. Twenty minutes elapsed between combining the reaction mix for "alphacat -80°C 50% glycerol on ice" and placing the other tubes in the 30°C water bath. In duplicate: mean ± SD.

After two weeks' storage, the activity of all the samples had fallen as compared to their activity after one week's storage (Figure 91) (although caution must be urged in any quantitative comparison between two different assays). Once again, the induced lysates show higher DGK activity than their uninduced counterparts. As opposed to storage after one week (Figure 90), after two weeks' storage, the highest activity is shown by the alphacat that had been stored at 4°C, and the lowest is shown by that stored at -80°C in 50% glycerol (Figure 91). Once again, however, the interpretation of these data is limited by the fact that, even though this assay was relatively fast, the lysate stored on ice

for the time of the assay, plus twenty minutes, showed considerable activity, and the 4°C lysate's high activity may merely reflect the fact that ^{32}P-γ-ATP had been added to those samples first, and they spent longer sitting on ice before being moved to the 30°C water bath.

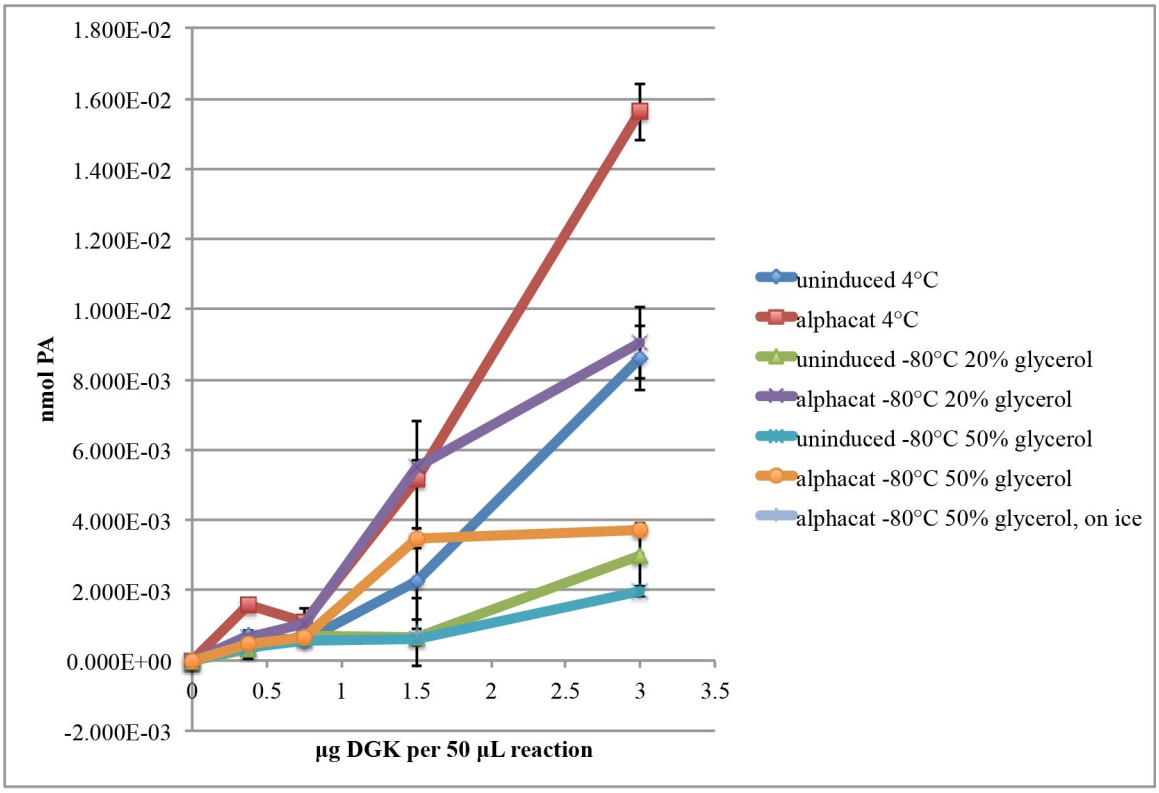

Figure 91. Storage test of alphacat in pT71myc in Rosetta™(DE3) lysates: two weeks. DGK activity assay. The samples used were the same as shown in **Figure 89**, stored for two weeks under the conditions shown. The reaction included 7.5 mM liposomes (53:22:17:8::POPE:POPC:POPS:DOG), 49 mM HEPES, pH 8.0, 4.9 mM $MgCl_2$, 1 mM $CaCl_2$, 1 mM ATP, 70.0 Ci per mmol [γ-^{32}P]-ATP, and, from the lysates, up to 0.9 mM Tris, 5.4 mM NaCl, 180 µM imidazole, 0.009% (v/v) NP-40, 0.018x PIC, and 0.9% (v/v) glycerol, and proceeded for 15 minutes at 30°C. 25.5 minutes elapsed between combining the reaction mix for "alphacat -80°C 50% glycerol on ice" and placing the other tubes in the 30°C water bath. In duplicate: mean ± SD.

Because the switch in substrates caused by the mislabeled lipid limited the conclusions that could be drawn from the alphacat storage conditions experiment, I decided to repeat the experiment. The freshly harvested induced lysate showed higher DGK activity on DOG-containing liposomes than the uninduced lysate did, and this

activity appeared to depend linearly on concentration up through at least 50 ng per µL total protein.

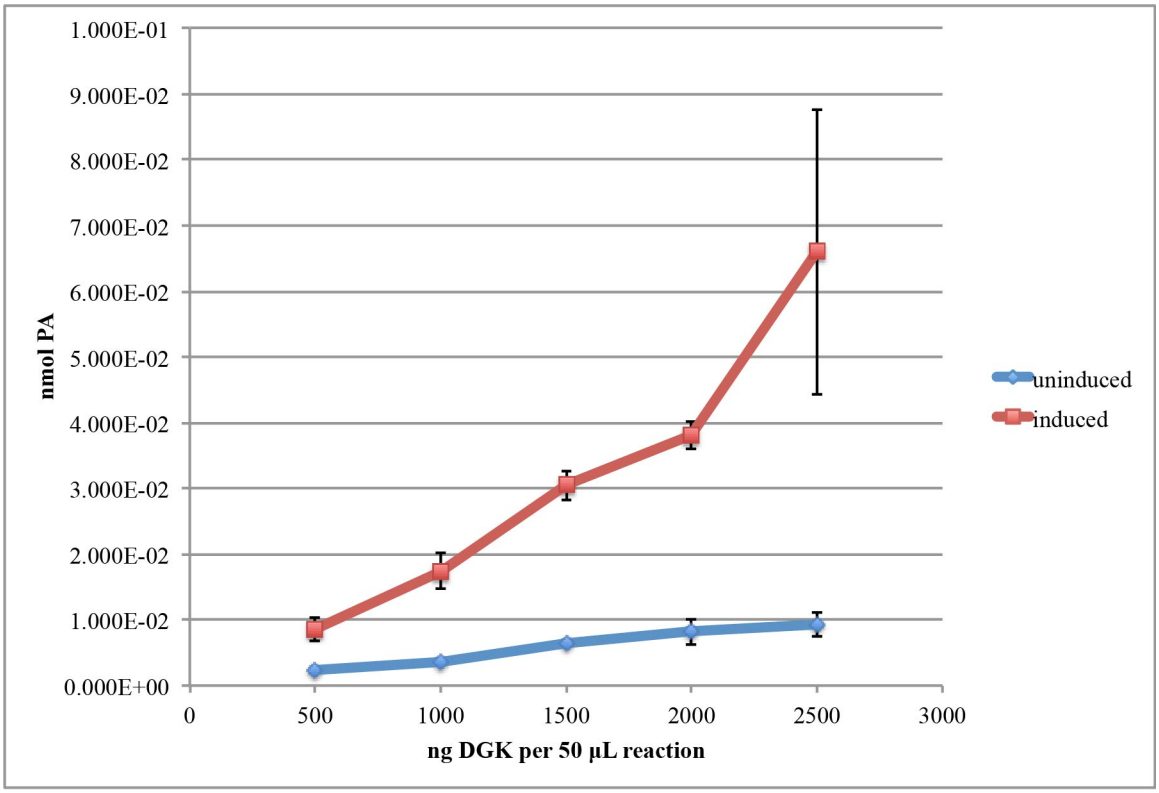

Figure 92. Rosetta™(DE3) lysate overexpressing alphacat in pT71myc shows greater DGK activity toward DOG than uninduced lysate, and this activity depends linearly on the concentration of the enzyme at least up through 50 ng per µL of total protein. I inoculated two 25 mL LB Kan cultures with a freshly growing culture of alphacat in pT71myc in Rosetta™(DE3). When the OD600 was predicted to reach 1.0, I added IPTG to 0.5 mM (or not) and shook the cultures for 20.5 hours at ~15°C, then pelleted the cells by centrifugation and resuspended in 4 mL per gram wet cell pellet lysis buffer (50 mM Tris, pH 8.0, 300 mM NaCl, 10 mM imidazole, 1 mM $CaCl_2$, 5 mM $MgCl_2$, 0.5% NP-40, 1x PIC, 0.5 mM DTT, 1 mg per mL lysozyme) and incubated on ice for ~75 minutes. I vortexed the cells, and they were quite viscous, suggesting that the cells did lyse. I added DNAse I to 10 U per mL and incubated on ice for thirty minutes. I kept the lysates on ice until the DGK assay. The reaction included 7.5 mM liposomes (53:22:17:8::POPE:POPC:POPS:DOG), 49 mM HEPES, pH 8.0, 4.9 mM $MgCl_2$, 1 mM $CaCl_2$, 1 mM ATP, 119 Ci per mmol [γ-^{32}P]-ATP, and, from the lysates, up to 0.5 mM Tris, 3 mM NaCl, 100 µM imidazole, 0.005% (v/v) NP-40, and 0.01x PIC, and proceeded for 15 minutes at 30°C. In duplicate: mean ± SD.

I once again stored aliquots of the lysates either at 4°C, at -80°C in 20% glycerol, or at -80°C in 50% glycerol. After two weeks' storage, the specific activity dropped dramatically, although once again caution must be urged in any quantitative comparison between two different assays (Figure 93). The activity dropped so much that the induced

lysate that had been stored at 4°C for two weeks no longer had any more activity than the uninduced lysate (in contrast to the results shown in Figure 91). The induced lysates stored at -80°C, in either 20% glycerol or 50% glycerol, retained greater activity than their uninduced counterparts, and their activity was comparable to one another (Figure 93). Once concern about this assay is that the activity appeared to no longer depend linearly on the concentration of the protein used: in fact, for nearly all the samples tested, the 30 ng per µL samples (1.5 µg in 50 µL) showed lower activity than the 20 ng per µL samples (1 µg in 50 µL).

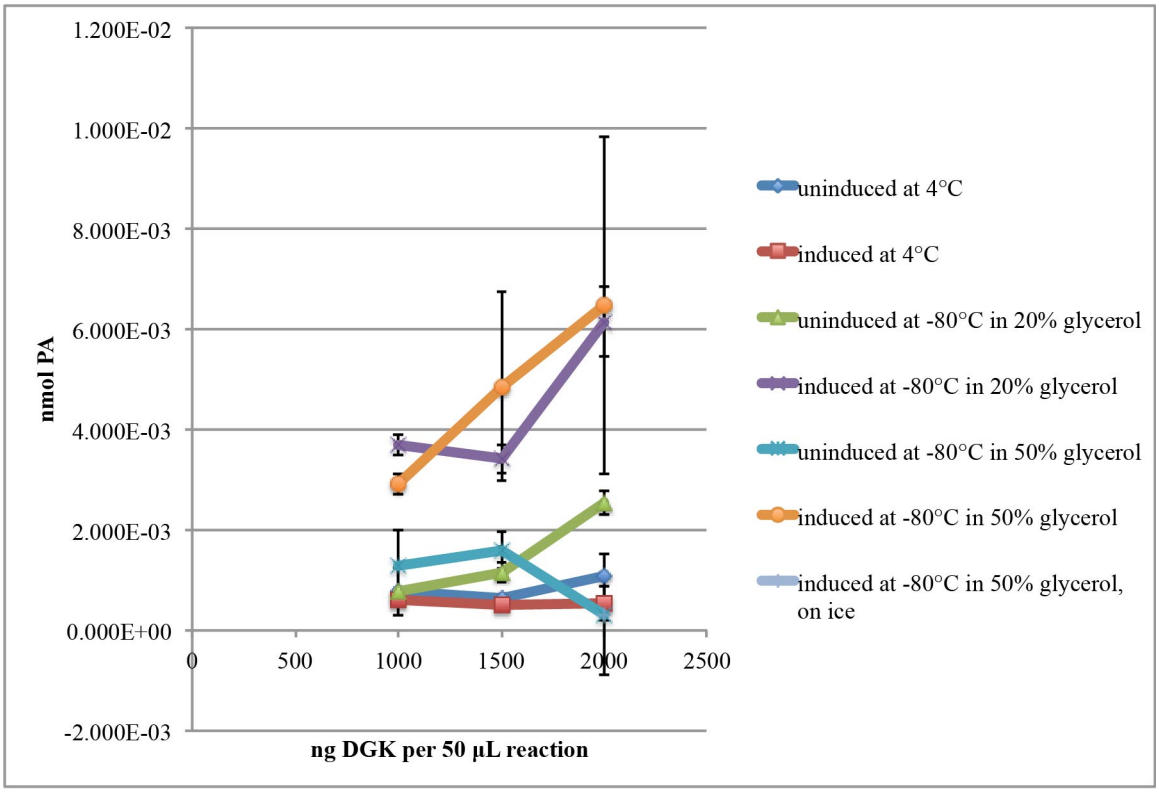

Figure 93. Rosetta™(DE3) lysate overexpressing alphacat in pT71myc lost a considerable amount of DGK activity after two weeks' storage. DGK assay on liposomes of alphacat in pT71myc-overexpressing BL21(DE3) lysates stored for two weeks under the conditions shown. DGK activity assay. The samples used were the same as shown in **Figure 92**, stored for two weeks under the conditions shown. The reaction included 7.5 mM liposomes (53:22:17:8::POPE:POPC:POPS:DOG), 49 mM HEPES, pH 8.0, 4.9 mM $MgCl_2$, 1 mM $CaCl_2$, 1 mM ATP, 60.5 Ci per mmol [γ-^{32}P]-ATP, and, from the lysates, up to 0.5 mM Tris, 3 mM NaCl, 100 µM imidazole, 0.005% (v/v) NP-40, 0.01x PIC and 0.5% (v/v) glycerol, and proceeded for 15 minutes at 30°C. In duplicate: mean ± SD.

After four weeks' storage, the activity of the alphacat lysate that had been stored at 4°C remained no higher than that of the uninduced lysate, and the activity of the lysate that had been stored at -80°C, in either 20% glycerol or 50% glycerol, still retained greater activity than their uninduced counterparts, and their activity remained comparable to one another (Figure 94**A**). The activity, however, was no less than that of the aliquots tested two weeks previously, and, in the case of the lysate stored at -80°C in 20% glycerol, even higher (Figure 94**B**), suggesting that something might have been wrong with the earlier assay.

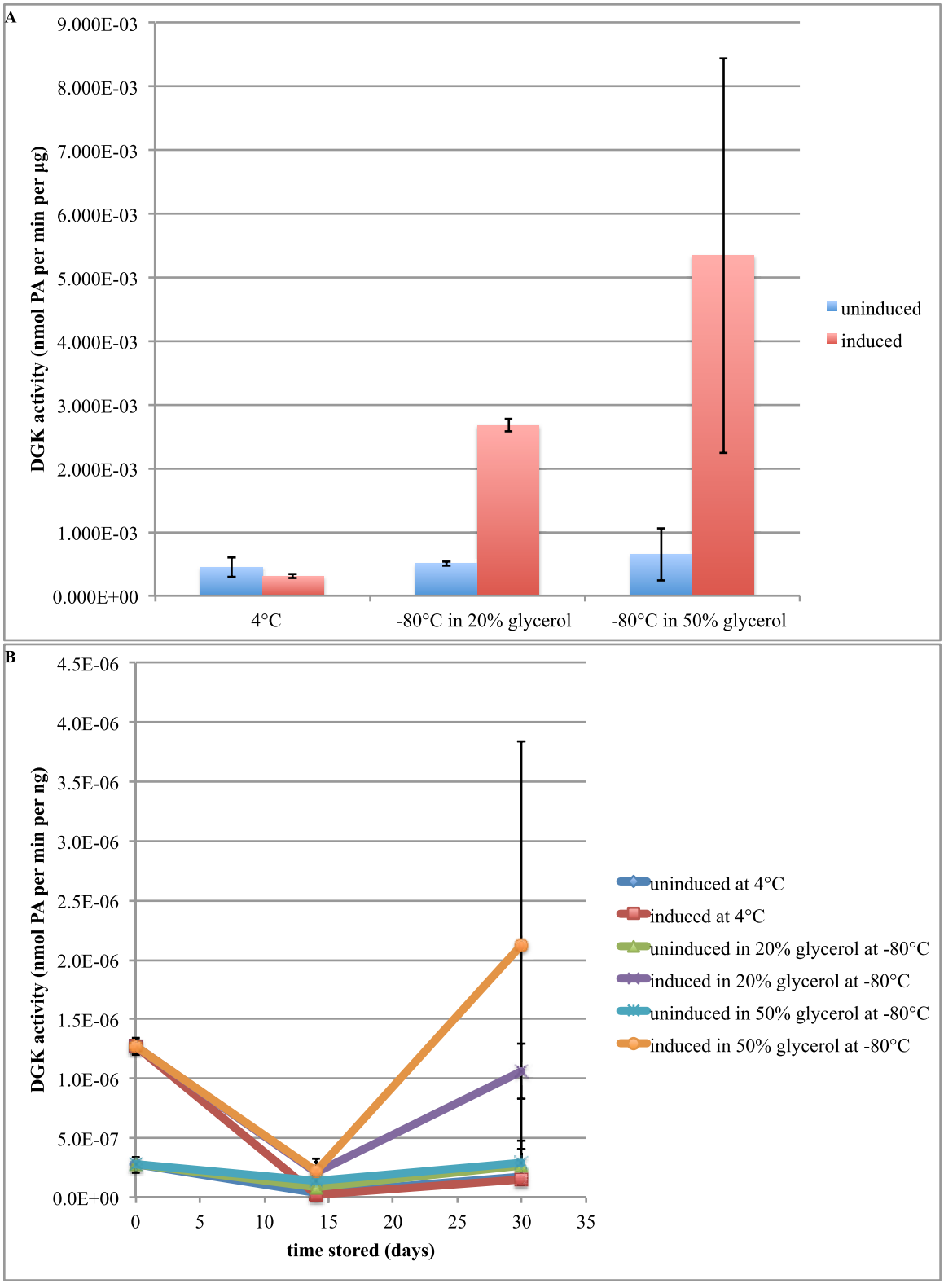
A
9.000E-03
8.000E-03
7.000E-03
6.000E-03
5.000E-03
4.000E-03
3.000E-03
2.000E-03
1.000E-03
0.000E+00
DGK activity (nmol PA per min per µg)
4°C
-80°C in 20% glycerol
-80°C in 50% glycerol
uninduced
induced
B
4.5E-06
4.0E-06
3.5E-06
3.0E-06
2.5E-06
2.0E-06
1.5E-06
1.0E-06
5.0E-07
0.0E+00
DGK activity (nmol PA per min per ng)
0
5
10
15
20
25
30
35
time stored (days)
uninduced at 4°C
induced at 4°C
uninduced in 20% glycerol at -80°C
induced in 20% glycerol at -80°C
uninduced in 50% glycerol at -80°C
induced in 50% glycerol at -80°C

Figure 94. Storage test of alphacat in pT71myc in Rosetta™(DE3) lysates: four weeks. (A) DGK activity assay. The samples used were the same as shown in **Figure 92**, stored for thirty days under the conditions shown. The reaction included 7.5 mM liposomes (53:22:17:8::POPE:POPC:POPS:DOG), 49 mM HEPES, pH 8.0, 4.9 mM $MgCl_2$, 1 mM $CaCl_2$, 1 mM ATP, 114 Ci per mmol [γ-^{32}P]-ATP, and, from the lysates, up to 0.5 mM Tris, 3 mM NaCl, 100 μM imidazole, 0.005% (v/v) NP-40, 0.01x PIC, 0.5% (v/v) glycerol and 2 μg total protein per 50 μL reaction, and proceeded for 15 minutes at 30°C. In duplicate: mean ± SD. **(B)** Specific activity compared to that from previous assays shown in **Figure 92** and **Figure 93**.

After eight weeks' storage, the activity of the alphacat lysate that had been stored at 4°C remained no higher than that of the uninduced lysate, and the activity of the lysate that had been stored at -80°C, in either 20% glycerol or 50% glycerol, still retained greater activity than their uninduced counterparts (Figure 95**A**). This time, however, the lysate that had been stored in 50% glycerol demonstrated greater DGK activity than the lysate that had been stored in 20% glycerol. Indeed, the lysate that had been stored at -80°C in 50% glycerol showed even greater specific activity than when the lysate had been fresh, eight week's previously (Figure 95**B**), supporting the hypothesis that something had been wrong with the assay at two weeks.

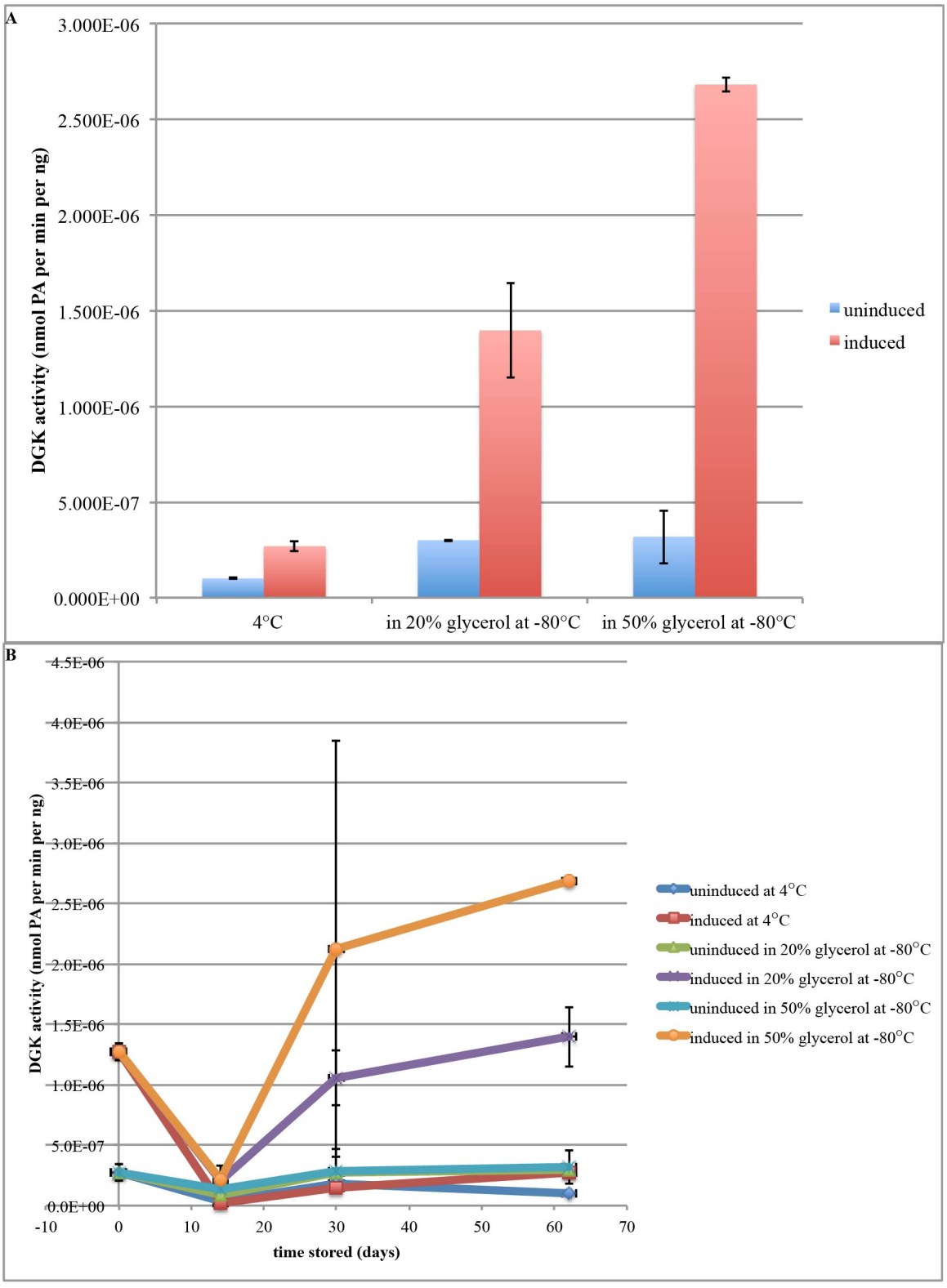

Figure 95. Storage test of alphacat in pT71myc in Rosetta™(DE3) lysates: eight weeks. (A) DGK activity assay. The samples used were the same as shown in **Figure 92**, stored for sixty-two days under the

conditions shown. The reaction included 7.5 mM liposomes (53:22:17:8::POPE:POPC:POPS:DOG), 49 mM HEPES, pH 8.0, 4.9 mM $MgCl_2$, 1 mM $CaCl_2$, 1 mM ATP, 89.2 Ci per mmol [γ-^{32}P]-ATP, and, from the lysates, up to 0.5 mM Tris, 3 mM NaCl, 100 μM imidazole, 0.005% (v/v) NP-40, 0.01x PIC, 0.5% (v/v) glycerol and 2 μg total protein per 50 μL reaction, and proceeded for 15 minutes at 30°C. In duplicate: mean ± SD. **(B)** Specific activity compared to that from previous assays shown in **Figure 92**-**Figure 94**.

It remained unclear how long alphacat lysate could be stored at 4°C before losing its activity. A few hours between lysis and the assay appeared fine in Figure 92, and also in Figure 89, although that used DiC8 and not DOG as a substrate. Induced lysate still retained more activity than uninduced lysate after one week in Figure 90 and after two weeks in Figure 91, although as mentioned before, interpreting these results is complicated by the lysate's activity on ice. Contrariwise, in the second experiment, alphacat stored at 4°C had lost its activity within two weeks (Figure 93) and, even if this experiment is discounted because of apparent problems with this assay (Figure 95**B**), the induced lysate stored at 4°C had clearly lost its activity at four (Figure 94**A**) and eight weeks (Figure 95**A**). Therefore, I tested whether storage of the lysate from a third expression could be stored at 4°C overnight without losing activity. When this lysate was stored overnight at -80°C in 50% glycerol, it maintained higher activity than uninduced lysate, but not when it was stored overnight at 4°C (Figure 96). The first expression (which maintained its activity at 4°C) differed from the second and third expressions (which did not maintain their activity at 4°C) in several ways: the first expression was induced at 18°C, whereas the second and third expressions were induced at lower temperatures; the first expression was lysed in a larger volume of lysis buffer (and therefore was more dilute when it was stored); and the first expression's lysis buffer did not include $MgCl_2$, whereas the second and third expressions were lysed (and stored) in 5 mM $MgCl_2$.

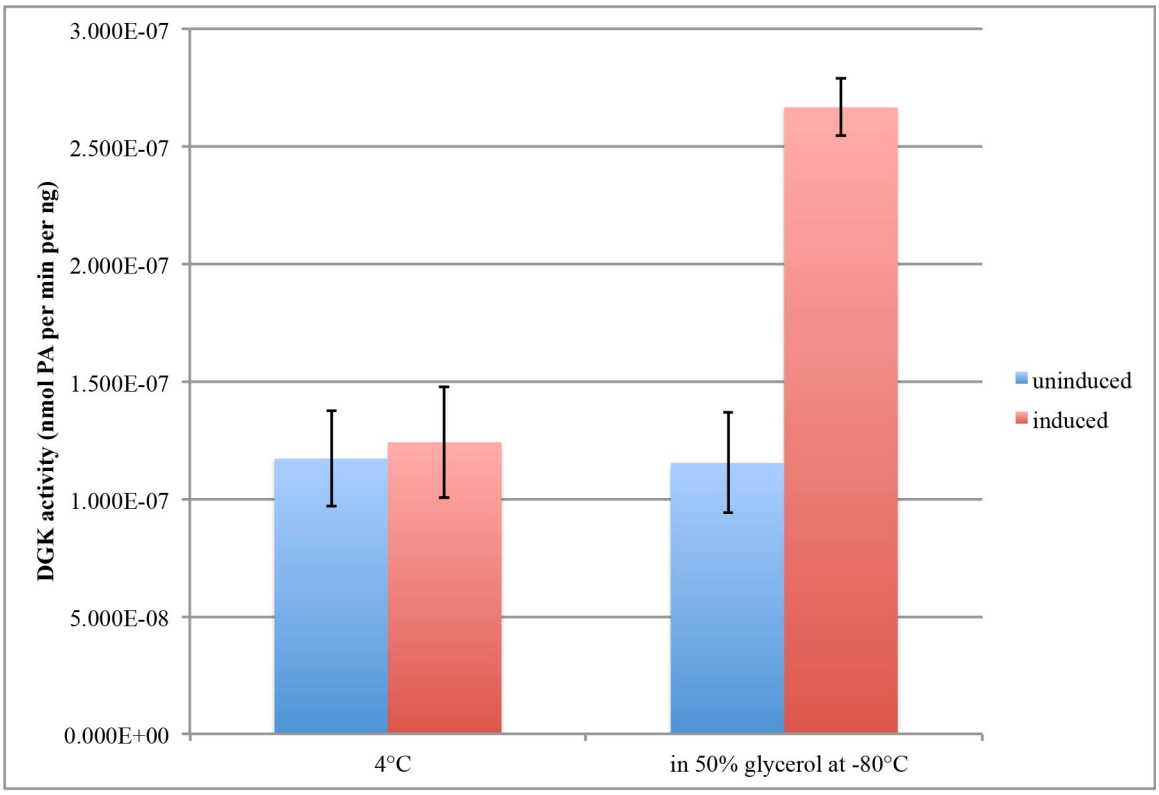

Figure 96. Rosetta™(DE3) lysates overexpressing alphacat in pT71myc lose their activity overnight when stored at 4°C but not when stored at -80°C in 50% glycerol. I inoculated two 25 mL LB Kan cultures with an overnight culture of alphacat in pT71myc in Rosetta™(DE3). When the OD600 was predicted to reach 1.0, I added IPTG to 0.5 mM (or not) and shook the cultures overnight at ~14°C, then pelleted the cells by centrifugation and stored the cell pellets overnight at -80°C. I resuspended in 4 mL per gram wet cell pellet lysis buffer (50 mM Tris, pH 8.0, 300 mM NaCl, 10 mM imidazole, 1 mM $CaCl_2$, 5 mM $MgCl_2$, 0.5% NP-40, 1x PIC, 1 mM DTT, 1 mg per mL lysozyme, 20 U per mL DNAse I) and incubated on ice for ~five hours, and stored the samples for the DGK assay under the conditions shown overnight. The reaction included 7.5 mM liposomes (53:22:17:8::POPE:POPC:POPS:DOG), 49 mM HEPES, pH 8.0, 4.9 mM $MgCl_2$, 1 mM $CaCl_2$, 1 mM ATP, 114 Ci per mmol [γ-^{32}P]-ATP, and, from the lysates, up to 0.1 mM Tris, 0.6 mM NaCl, 20 μM imidazole, 0.001% (v/v) NP-40, 0.002x PIC, and 0.1% glycerol, and proceeded for 15 minutes at 30°C. In duplicate: mean ± SD.

From the alphacat in pT71myc in Rosetta™(DE3) lysate storage experiments, I learned that alphacat lysate maintains its activity when stored at -80°C, in either 20% or 50% glycerol, and that the DGK activity assay sometimes has reproducibility issues that mean that not too much stock can ever be put into a single assay. Whether or not alphacat lysate loses its activity at 4°C may depend on the temperature induction, concentration of storage, and, most intriguingly, the concentration of $MgCl_2$ during

storage. Because these are lysates, and not purified protein, these effects could also depend on components in the lysate besides alphacat: perhaps the bacterial lysate includes another, Mg^{2+}-dependent, enzyme, which is active at 4°C but not when frozen, that processes alphacat in such a way such that it is no longer active.

After expressing *H. sapiens* DGK-theta in High Five™ cells (the expression shown in Figure 73**A**, Figure 74, and Figure 76**B**), I compared the activity of lysates stored either at -80°C or at 4°C for one week. Storage at 4°C for one week decreased the DGK activity as compared to the lysate that had been frozen, but DGK activity remained detectable, and clearly greater than that of the uninfected High Five™ lysate.

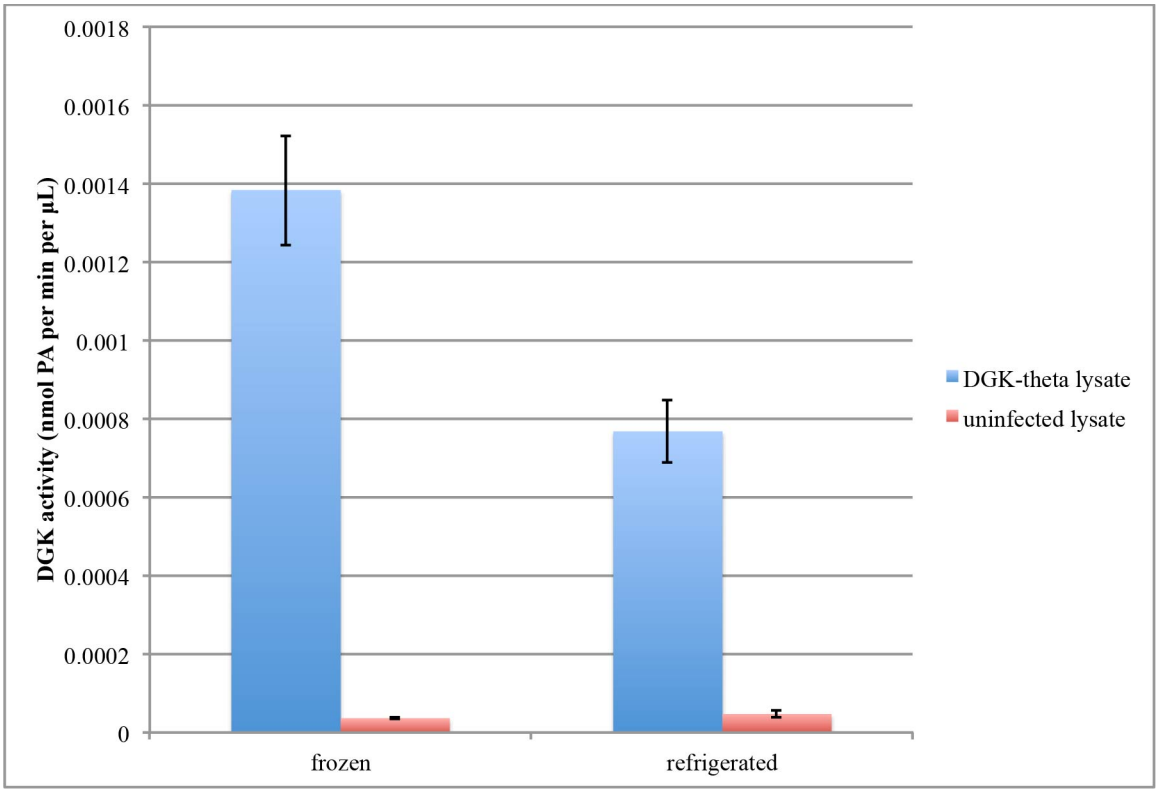

Figure 97. Storage at 4°C, as compared to -80°C, for one week decreases the DGK enzymatic activity of *H. sapiens* DGK-theta-overexpressing High Five™ lysates. DGK activity assay. The samples used were the same as shown in **Figure 73**A, **Figure 74**, and **Figure 76**B, stored for one week either frozen or else at 4°C ("refrigerated"). The reaction included 5 mM liposomes (53:22:17:8::POPE:POPC:POPS:DOG), 48 mM Tris, pH 7.4, 4.8 mM $MgCl_2$, 8.8 mM NaF, 1 mM ATP,

98.3 Ci per mmol [γ-^{32}P]-ATP, and, from the lysates, 0.2 mM Tris, 20 μM EDTA, and 10 μM EDTA, and proceeded for 15 minutes at 37°C. In duplicate: mean ± SD.

As such, I generally stored the enzyme in 50% glycerol at -80°C for activity assays. However, such storage conditions were no guarantee to maintain enzymatic activity. I also observed aliquots of DGK-theta purified from HEK293T cells, having been stored at -80°C in glycerol and maintaining their enzymatic activity for years, that suddenly lost activity, even when those particular aliquots had never been thawed and refrozen, while sister aliquots maintained their activity (Figure 98).

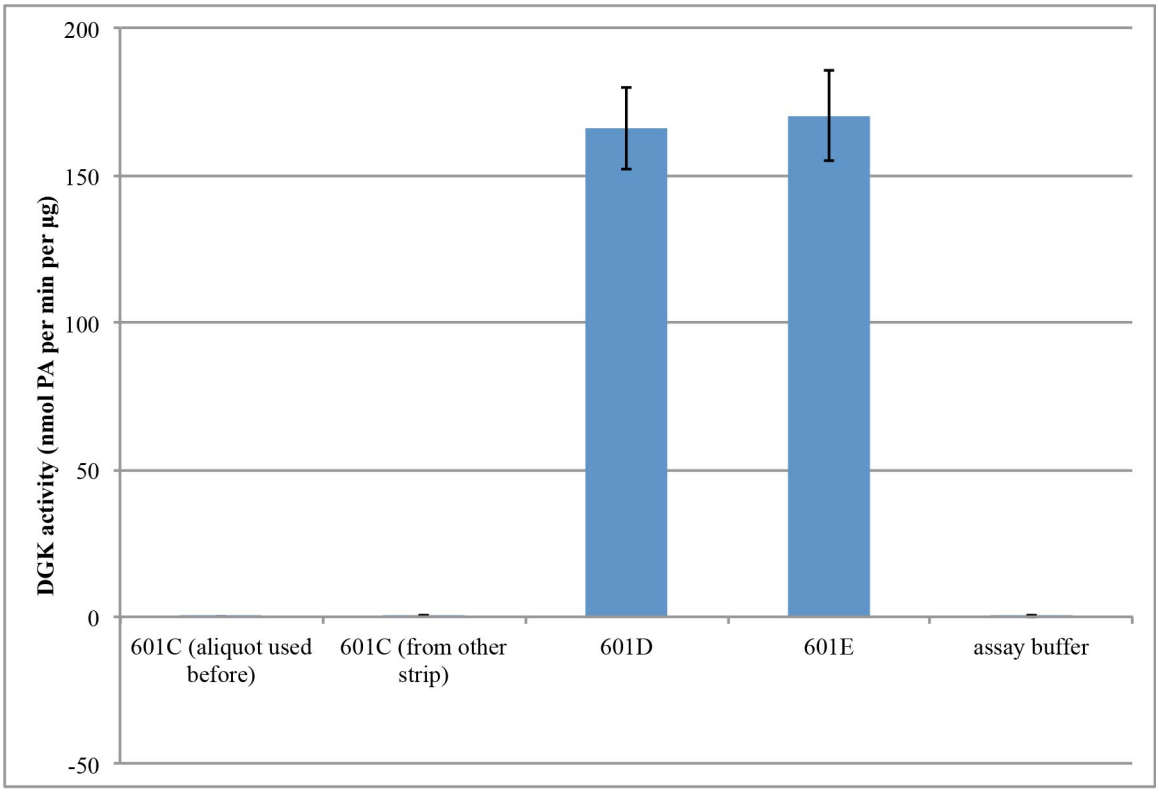

Figure 98. Aliquots of DGK-theta purified from HEK293T cells, stored in 50% glycerol at -80C, can suddenly lose enzymatic activity even while sister aliquots retain theirs. DGK activity assay. The "aliquot used before" had been successfully thawed and refrozen without losing activity. "From other strip" is from the same original sample, aliquoted into separate tubes, and unthawed since originally being frozen. "601D" and "601E" are from other fractions of the purification, frozen at the same time and likewise unthawed. Samples were first preincubated in 0.4% (v/v) NP-40 on ice for ten minutes. The final reaction mixture included 5 mM liposomes (55.3:27.7:9:8::POPE:POPC:POPS:DOG), 50 mM HEPES, pH 7.4, 99 mM NaCl, 1.5 mM $MgCl_2$, 1 mM ATP, 145 Ci per mmol [γ-^{32}P]-ATP, 0.25% (v/v) glycerol, 0.004% (v/v) NP-40, 0.1 μM histone H1, 1 mM DTT, and 6.5 pg per μL purified DGK (as estimated from silver staining and interpolating from the intensity of BSA standards), and proceeded for 15 minutes at 37°C. In duplicate: mean ± SD.

Conclusions

DGK generally maintained its activity in 50% glycerol at -80°C better than it did in 20% glycerol at -80°C, at -20°C, or at 4°C. As such, I generally stored the enzyme in 50% glycerol at -80°C for activity assays. However, such storage conditions were no guarantee to maintain enzymatic activity.

Inactivation of DGK by Incubating While Diluted on Ice or at Room Temperature, and Preincubation and Incubation Conditions That Can Mitigate This Inactivation

Introduction

DGK activity is influenced not only by the conditions of the activity assay, and the conditions of its longterm storage, but also by the conditions to which is has been exposed acutely before the assay.

Results

Incubating purified DGK-theta purified from HEK293T cells on ice for less than two hours before the assay vastly reduced its enzymatic activity (Figure 99**A**). I was surprised by this finding, seeing as the purification of the enzyme takes longer than two hours, but the results were reproducible (Figure 99**B**). I therefore set out to find preincubation conditions that would mitigate this inactivation on ice.

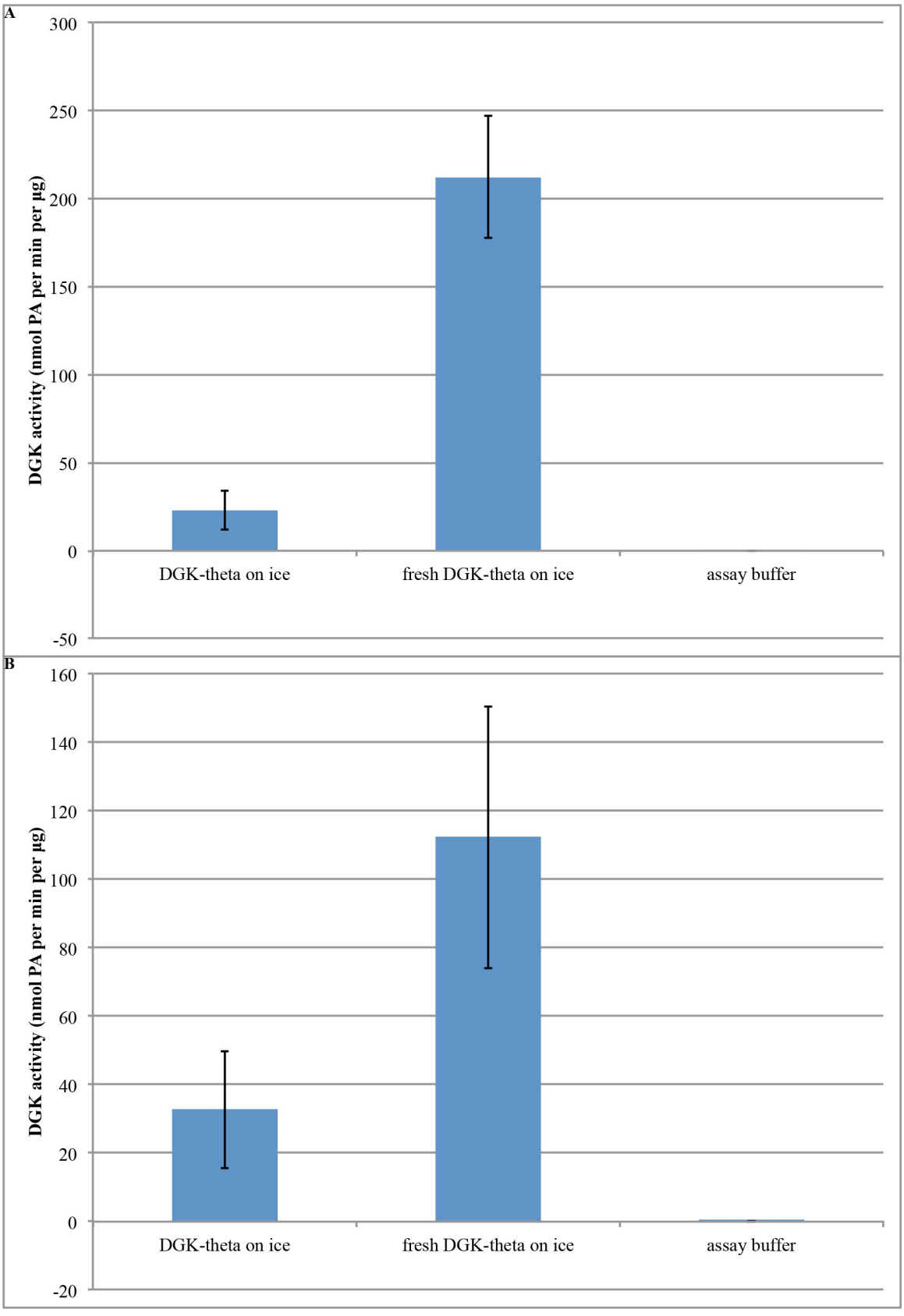
A
300
250
200
150
100
50
0
-50
DGK activity (nmol PA per min per µg)
DGK-theta on ice
fresh DGK-theta on ice
assay buffer
B
160
140
120
100
80
60
40
20
0
-20
DGK activity (nmol PA per min per µg)
DGK-theta on ice
fresh DGK-theta on ice
assay buffer

Figure 99. Incubating purified DGK-theta purified from HEK293T cells on ice for less than two hours before the assay markedly reduces its enzymatic activity. Samples were preincubated for ten minutes in 0.4% NP-40, then incubated on ice in incubation buffer (0.013% NP-40, 50 mM HEPES, 100 mM NaCl, 1 mM DTT, pH 7.4). In triplicate: mean ± SD. **(A)** The samples were incubated in incubation buffer for either 102 ("DGK-theta on ice") or 16 ("fresh DGK-theta on ice") minutes prior to the start of the reaction. The final reaction mixture included 2.75 mM substrate-containing liposomes (50:25:9:16::POPE:POPC:POPS:DOG), 2 mM filler liposomes (60.7:30.3:9::POPE:POPC:POPS), 50 mM HEPES, pH 7.4, 100 mM NaCl, 1.5 mM $MgCl_2$, 1 mM ATP, 131 Ci per mmol [γ-^{32}P]-ATP, 0.04% (v/v) glycerol, 0.0007% (v/v) NP-40, 0.1 μM histone H1, 1 mM DTT, and 1.1 pg per μL purified DGK (as estimated from silver staining and interpolating from the intensity of BSA standards), and proceeded for 16 minutes at 37°C. **(B)** The samples were incubated in incubation buffer for either 78 ("DGK-theta on ice") or 18 ("fresh DGK-theta on ice") minutes prior to the start of the reaction. The final reaction mixture was the same as in (A) except that [γ-^{32}P]-ATP was decreased to 119 Ci per mmol. The reaction proceeded for 15 minutes.

When first thawing aliquots of purified DGK-theta for activity assays, I generally first preincubated in 0.4% (v/v) NP-40 on ice for ten minutes before proceeding. Adjusting the pH of the 0.4% NP-40 preincubation from 8.5 to 7.4 had no effect on the enzymatic activity of DGK-theta purified from HEK293T cells, nor did adding $MgCl_2$ to the preincubation to 15 mM (Figure 100).

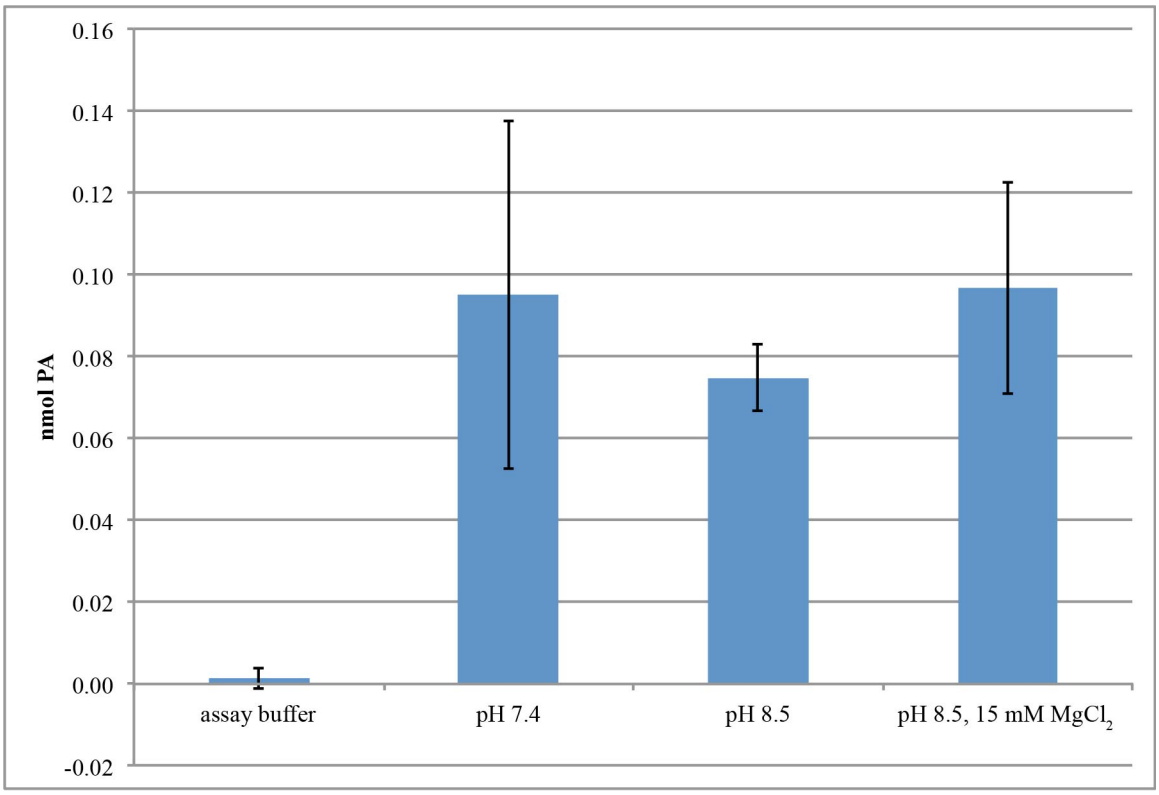

Figure 100. Modifying the pH or the $MgCl_2$ concentration in the 0.4% NP-40 preincubation has no effect on the enzymatic activity of DGK-theta purified from HEK293T cells. DGK activity assay. Samples were first preincubated in 0.4% (v/v) NP-40 on ice under the conditions shown for ten minutes. The final reaction mixture included 5 mM liposomes (55.3:27.7:9:8::POPE:POPC:POPS:DOG), 50 mM HEPES, pH 7.4, 99 mM NaCl, 1.5 mM $MgCl_2$, 1 mM ATP, 145 Ci per mmol [γ-^{32}P]-ATP, 0.004% (v/v) NP-40, 0.1 μM histone H1, and 1 mM DTT, and proceeded for 15 minutes at 37°C. In duplicate: mean ± SD.

When I preincubated purified DGK-theta with DOG-containing liposomes on ice, the DGK activity was higher than purified DGK-theta incubated on ice without liposomes (Figure 101). This observation is consistent with previously reported work showing DGK-theta to be a quasi-scooter[140]: if liposome-binding is partially rate-limiting, then allowing DGK-theta more time to bind the substrate-containing liposomes before assaying the activity would be predicted to increase the apparent activity.

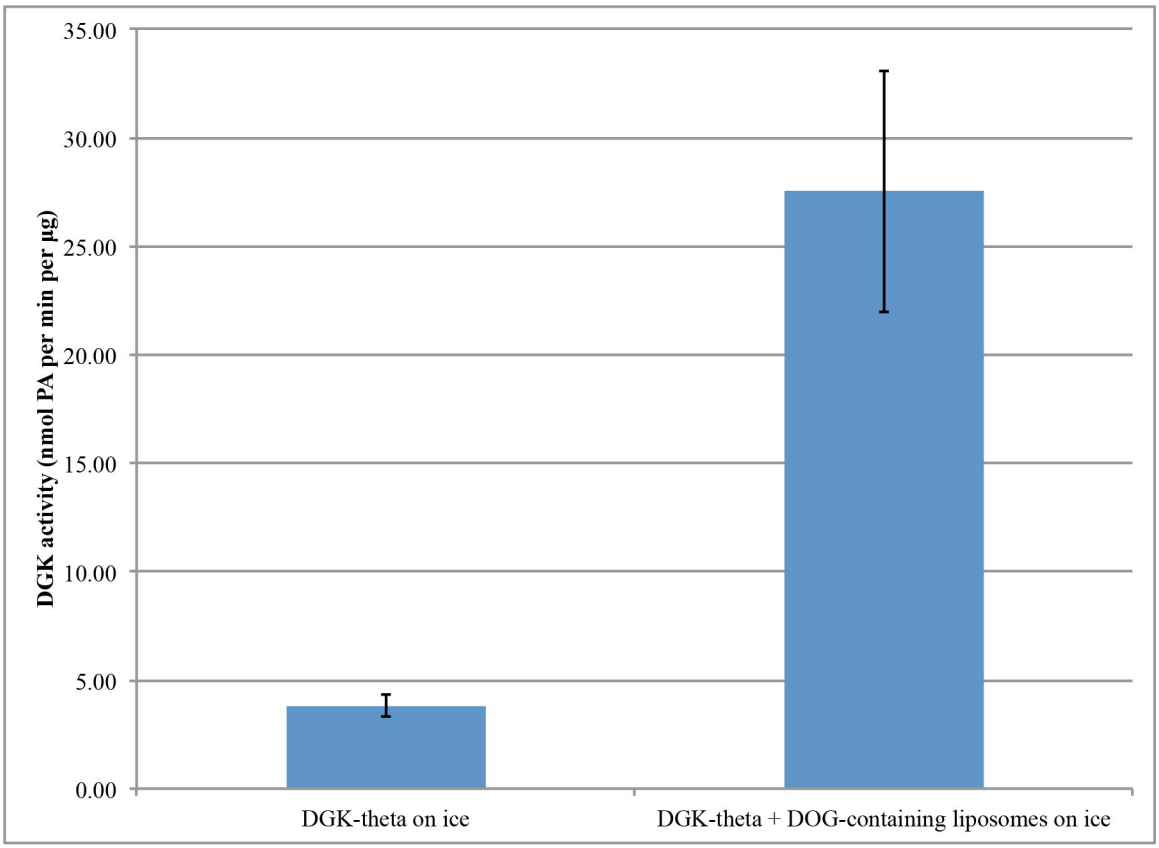

Figure 101. Preincubating with DOG-containing liposomes on ice increases the enzymatic activity of purified DGK-theta. I first preincubated the samples in 0.4% (v/v) NP-40 on ice for ten minutes. I then diluted the samples 1:1 into assay buffer (55.6 mM HEPES, pH 7.4, 111 mM NaCl), with or without 5 mM DOG-containing liposomes (50:25:9:16::POPE:POPC:POPS:DOG), and incubated on ice for two hours. The final reaction mixture included 5 mM liposomes (for "DGK-theta on ice", 55.3:27.7:9:8::POPE:POPC:POPS:DOG; for "DGK-theta + DOG-containing liposomes on ice", 2.5 mM of the original DOG-containing liposomes plus an additional 2.5 mM of 60.7:30.3:9::POPE:POPC:POPS), 36 mM HEPES, pH 7.4, 72 mM NaCl, 1.5 mM $MgCl_2$, 1 mM ATP, 98.3 Ci per mmol [γ-^{32}P]-ATP, 0.2% (v/v) glycerol, 0.1% (v/v) NP-40, 0.1 µM histone H1, 1 mM DTT, and 1.1 pg per µL purified DGK, and proceeded for 15 minutes at 37°C. In triplicate: mean ± SD.

Incubation at room temperature of DGK-theta purified from HEK293T cells vastly reduced its enzymatic activity (Figure 102). I did this particular experiment to see whether the conditions of the O-GlcNAcylation assay inactivated DGK: the lower pH buffer partially did, but the room-temperature incubation inactivated DGK even more so.

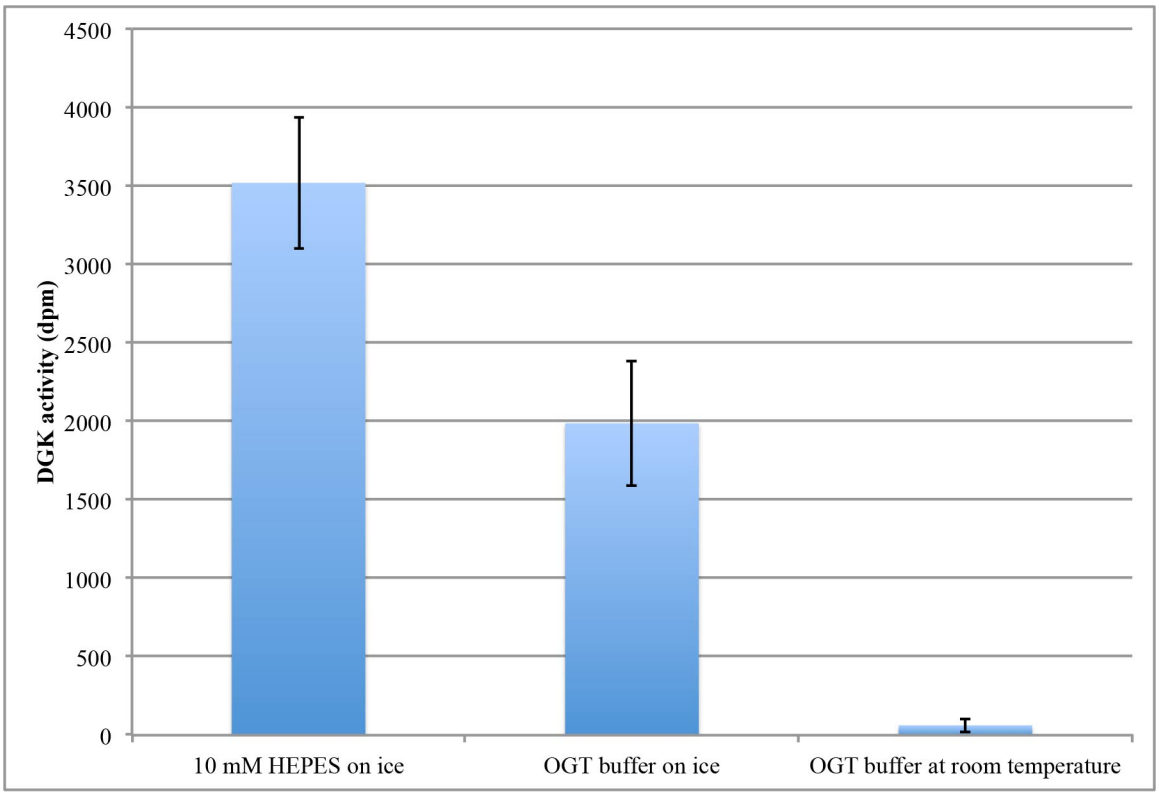

Figure 102. Incubation at room temperature of DGK-theta purified from HEK293T cells vastly reduces its enzymatic activity. DGK activity assay. I incubated purified DGK for 160 minutes in either 10 mM HEPES buffer (10 mM HEPES, pH 7.4, 0.1% (w/v) BSA) or OGT buffer (24 mM sodium cacodylate, pH 6.5, 5.4x PIC, 268 mM GalNAc, 0.67 mM UDP-GlcNAc, 0.006% (w/v) BSA), either at room temperature or on ice. The reaction included 5 mM TX-100 micelles (6 mol% PS, 9 mol% DOG), and 1 mM DTT, and proceeded for 15 minutes at 30°C. In duplicate: mean ± SD.

Irradiation with a 360 nm lamp inactivated DGK time-dependently (Figure 103).

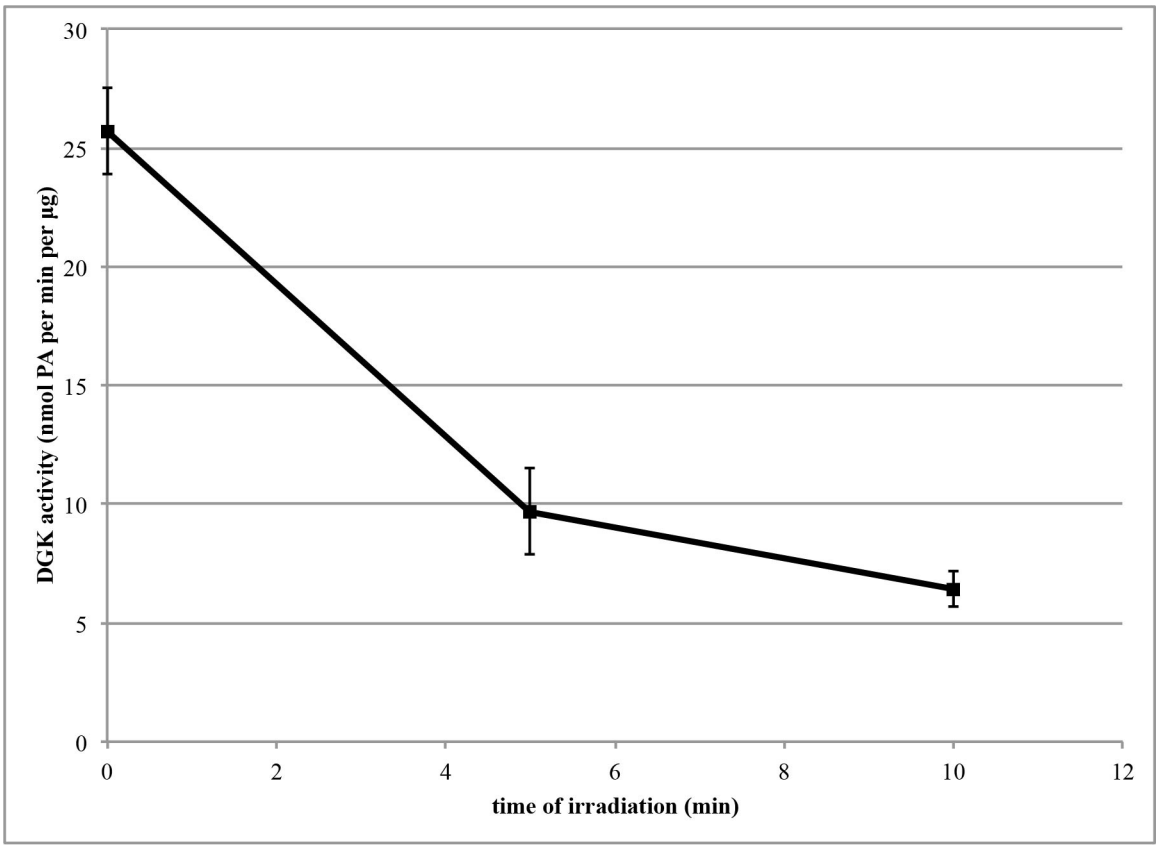

Figure 103. Irradiation with a 360 nm lamp inactivates DGK-theta purified from HEK293T cells time-dependently. DGK activity assay. I first preincubated the samples in 0.4% (v/v) NP-40 on ice for ten minutes. I then diluted the samples into assay buffer (55.6 mM HEPES, pH 7.4, 111 mM NaCl), and then added liposomes (50:25:9:16::POPE:POPC:POPS:DOG). I then irradiated with a 360 nm lamp for the time shown in a water-jacketed quartz cuvette. The final reaction mixture included 2.5 mM substrate-containing liposomes (50:25:9:16::POPE:POPC:POPS:DOG), 2.5 mM filler liposomes (60.7:30.3:9::POPE:POPC:POPS), 50 mM HEPES, pH 7.4, 100 mM NaCl, 1.5 mM $MgCl_2$, 1 mM ATP, 73.5 Ci per mmol [γ-^{32}P]-ATP, 0.05% (v/v) glycerol, 0.0007% (v/v) NP-40, 0.1 µM histone H1, 1 mM DTT, and 1.1 pg per µL purified DGK, and proceeded for 15 minutes at 37°C.

I thought this inactivation might result from the UV lamp's warming up the protein in the quartz cuvette, so I measured the temperature of buffer in the water-jacketed quartz cuvette before and after irradiating it. While the temperature of 100 µL of water in the quartz cuvette with the lamp on was only slightly higher than that protected by cardboard, or with no lamp on at all, it was also only slightly below room temperature (Table 1), and thus I suspected that DGK irradiated at 360 nm was being

subjected to room-temperature inactivation, since I had previously shown that incubation at room temperature inactivates DGK (Figure 102).

Condition	**Temperature (°C)**
100 µL of buffer, in water-jacketed quartz cuvette, irradiated with lamp for 5 minutes	21.1
100 µL of buffer, in water-jacketed quartz cuvette, irradiated with lamp for 5 minutes with cardboard barrier	20.8
100 µL of water in water-jacketed quartz cuvette	20.5
100 uL of water in quartz cuvette (water not flowing in jacket)	22.9
Room temperature	24

Table 1. Temperature as measured by a steel-probed thermometer of buffer in a water-jacketed quartz cuvette under various conditions.

Indeed, incubation at room temperature for 30 minutes inactivated DGK just as much as irradiation at 360 nm did, with or without cardboard between the lamp and the cuvette (Figure 104).

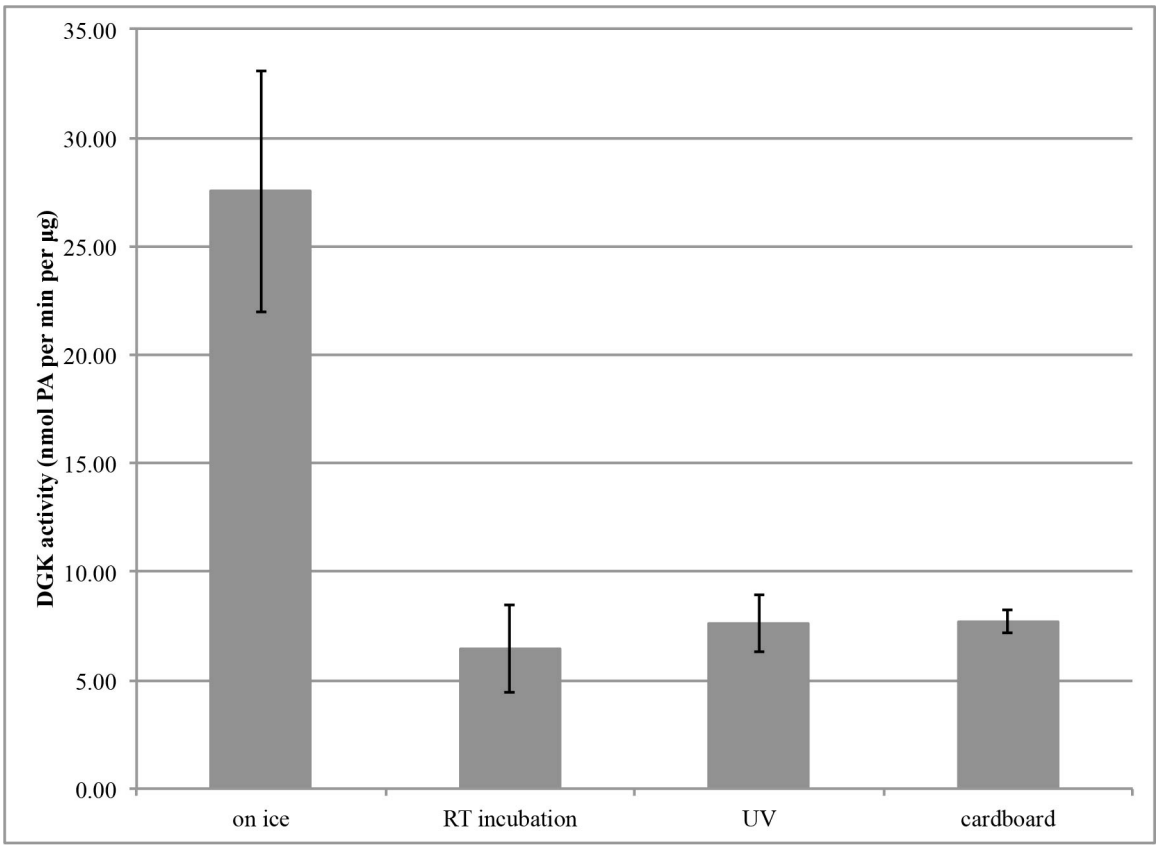

Figure 104. Incubation at room temperature for 30 minutes inactivates DGK-theta purified from HEK293T cells as much as irradiation at 360 nm. DGK activity assay. I first preincubated the samples in 0.4% (v/v) NP-40 on ice for ten minutes. I then diluted the samples 1:1 into assay buffer (55.6 mM HEPES, pH 7.4, 111 mM NaCl) with or 5 mM DOG-containing liposomes (50:25:9:16::POPE:POPC:POPS:DOG), and incubated either on ice (for the "on ice" sample) or at room temperature (RT) for thirty minutes. I then irradiated the "UV" and "cardboard" samples with a 360 nm lamp for four minutes in a water-jacketed quartz cuvette (with a piece of cardboard between the lamp and the cuvette for the "cardboard" sample). The final reaction mixture included 5 mM liposomes (2.5 mM of the original DOG-containing liposomes plus an additional 2.5 mM of 60.7:30.3:9::POPE:POPC:POPS), 36 mM HEPES, pH 7.4, 72 mM NaCl, 1.5 mM $MgCl_2$, 1 mM ATP, 98.3 Ci per mmol [γ-^{32}P]-ATP, 0.2% (v/v) glycerol, 0.1% (v/v) NP-40, 0.1 µM histone H1, 1 mM DTT, and 1.1 pg per µL purified DGK, and proceeded for 15 minutes at 37°C. In triplicate: mean ± SD.

MgATP is one of the substrates of the chemical reaction that DGK catalyzes, and as such may be necessary for DGK to assume a reaction-competent conformation. Histone H1 activates purified DGK-theta[3], and likewise may be necessary for DGK to assume a reaction-competent conformation. These conformational changes might also, in theory, protect DGK from inactivation at room temperature or even on ice. The laboratory has observed conflicting results regarding whether DTT, a reducing agent, has

any effect on DGK activity; DTT could likewise be affecting the conformation of the enzyme, and variable results might reflect variable time spent on ice prior to the assay. I therefore tested whether preincubation with histone H1 and/or MgATP protected DGK from room-temperature inactivation. DTT in the preincubation appeared to have no effect on DGK activity (Figure 105). Incubation at room temperature decreased the activity of DGK. Incubation with histone H1 (without MgATP) on ice decreased DGK activity as much as that which had been incubated at room temperature; it had no additional effect on the DGK that had been incubated at room temperature. Incubation with MgATP, with or without histone H1, precipitously dropped DGK's activity: however, this may have been due the fact that I accidentally added ATP and $MgCl_2$ to 10 mM and 15 mM, respectively, when I had intended to add them to 1 mM and 1.5 mM, and the higher concentration of Mg^{2+}, a divalent cation, may have adversely affected the quality of the liposomes[142].

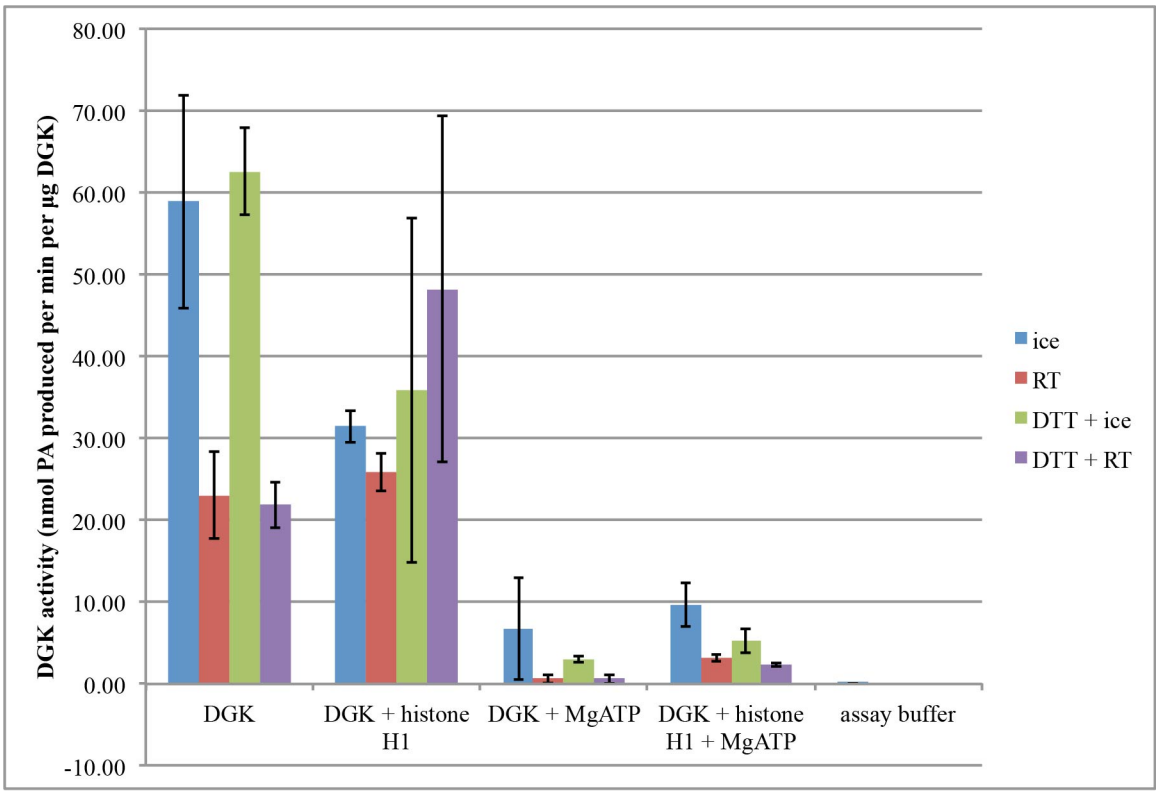

Figure 105. DTT in the preincubation has no effect on the enzymatic activity of DGK-theta purified from HEK293T cells. DGK activity assay. I preincubated purified DGK-theta in 0.4% NP-40 on ice for 27 minutes, either with or without 1 mM DTT. Then I diluted that preincubated DGK into 4 mM liposomes (55.3:27.7:9:8::POPE:POPC:POPS:DOG), with or without 0.625 µM histone H1 and/or 18.75 mM $MgCl_2$ and 12.5 mM ATP, and incubated at 30 minutes either on ice or at room temperature (RT). The final reaction mixture included 5 mM liposomes (55.3:27.7:9:8::POPE:POPC:POPS:DOG), 47 mM HEPES, pH 7.4, 94 mM NaCl, 1.5 (or 15) mM $MgCl_2$, 1 (or 10) mM ATP, 98.3 (or 49.2) Ci per mmol [γ-^{32}P]-ATP, 0.04% (v/v) glycerol, 0.92% (v/v) NP-40, 0.1 µM histone H1, 1 mM DTT, and 1.1 pg per µL purified DGK, and proceeded for 15 minutes at 37°C. In duplicate: mean ± SD.

I retested the effect of histone H1 and/or MgATP preincubation on DGK-theta, this time with the correct MgATP concentration. This time, I preincubated purified DGK with the factors tested in the presence of 0.4% NP-40 on ice for ten minutes. Then I diluted the preincubated DGK into liposomes, and incubated either at room temperature or on ice for 30 minutes. As seen before, a 30-minute incubation at room temperature partially inactivates purified DGK-theta as compared to DGK-theta that had been incubated on ice (Figure 106**A**), even in the presence of liposomes. Preincubation with histone H1 (but not MgATP) increased DGK's activity, even on ice, and room-

temperature incubation no longer inactivated DGK. Preincubation with MgATP (but not histone H1) had no effect on DGK's activity. Preincubation with both histone H1 and MgATP inactivated DGK, either incubated on ice or at room temperature. Preincubation with histone H1 on ice also increased the DGK activity of purified DGK-theta and protected against room temperature inactivation when the activity was assayed using Triton X-100 micelles as a substrate (Figure 106**B**). The implications for possible conformational changes in DGK caused by MgATP, histone H1, and lipid are intriguing (perhaps histone H1 and MgATP pin DGK into a conformation such that the lipid substrate can no longer access the active site?), but the practical implications were that if I first preincubated DGK-theta purified from HEK293T cells on ice for ten minutes in the presence of histone H1, I could protect against later room-temperature inactivation.

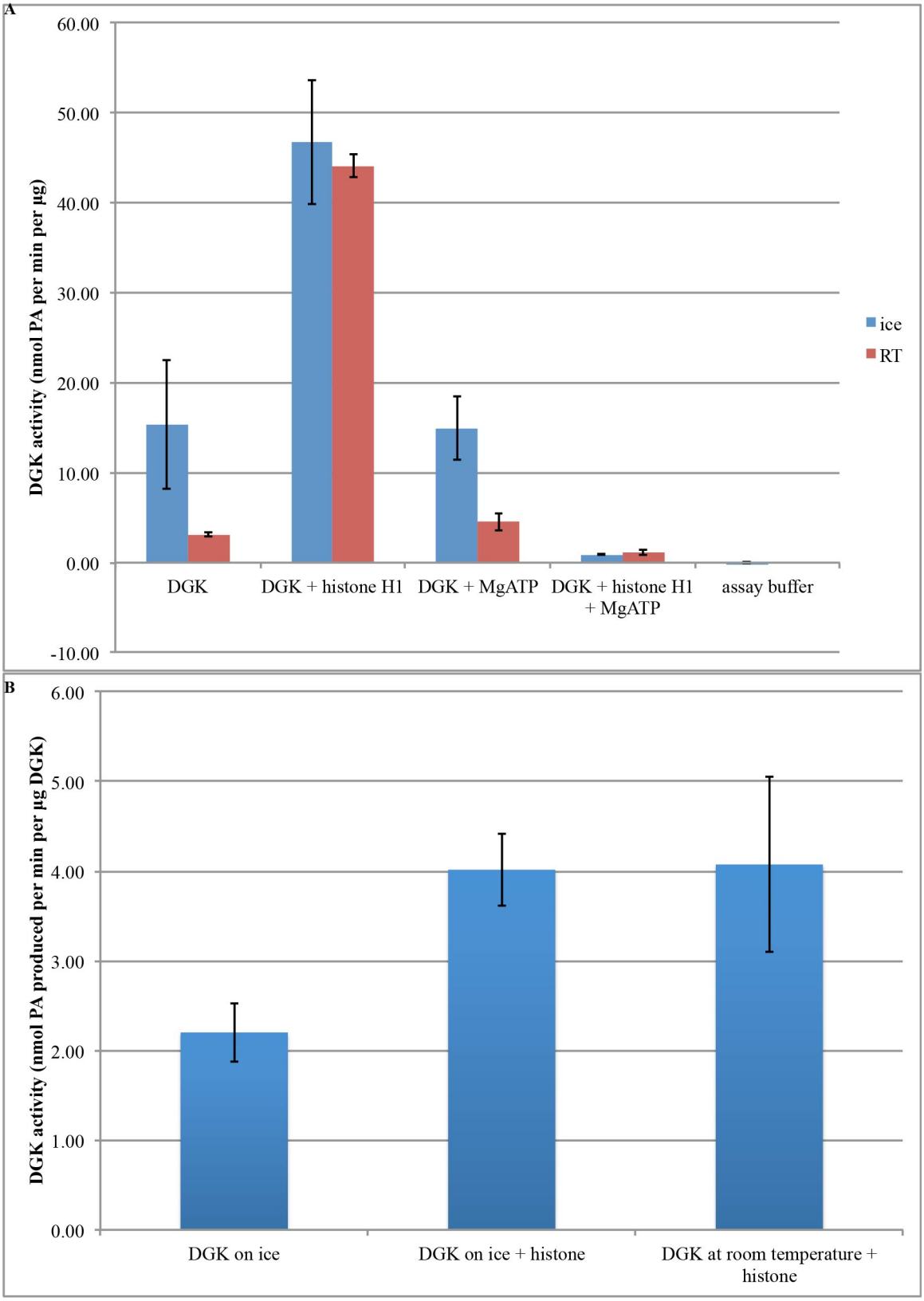
A
60.00
50.00
40.00
30.00
20.00
10.00
0.00
-10.00
DGK activity (nmol PA per min per µg)
ice
RT
DGK
DGK + histone H1
DGK + MgATP
DGK + histone H1 + MgATP
assay buffer
B
6.00
5.00
4.00
3.00
2.00
1.00
0.00
DGK activity (nmol PA produced per min per µg DGK)
DGK on ice
DGK on ice + histone
DGK at room temperature + histone

Figure 106. Preincubation in the presence of histone H1 activates purified DGK-theta and protects against room-temperature inactivation when assayed in both liposomes and detergent micelles. (A) DGK activity assay in liposomes. I preincubated purified DGK-theta on ice in 0.4% NP-40 in the presence or absence of 4 μM histone H1, 30 mM MgCl2, and 20 mM ATP for 10 minutes, then diluted into 5 mM liposomes (55.3:27.7:9:8::POPE:POPC:POPS:DOG) and incubated either on ice or at room temperature for 30 minutes before assaying the activity. The final concentration of histone H1 and MgATP in the assay was the same for all samples. The final reaction mixture included 5 mM liposomes, 50 mM HEPES, pH 7.4, 99 mM NaCl, 1.5 mM $MgCl_2$, 1 mM ATP, 66.7 (or 33.3) Ci per mmol [γ-^{32}P]-ATP, 0.06% (v/v) glycerol, 0.01% (v/v) NP-40, 0.1 μM histone H1, 1 mM DTT, and 1.1 pg per μL purified DGK, and proceeded for 15 minutes at 37°C. In duplicate: mean ± SD. **(B)** DGK activity assay in Triton X-100 micelles. I preincubated purified DGK-theta on ice in 0.4% NP-40 and 1 mM DTT in the presence or absence of 4 μM histone H1 for 10 minutes, then diluted into 2 mM TX-100 micelles (9 mol% POPS) and incubated either on ice or at room temperature for 30 minutes before assaying the activity. The final concentration of histone H1 in the assay was the same for all samples. The final reaction mixture included 2 mM TX-100 micelles (1.5 mM (9 mol% POPS), and 0.5 mM (9 mol% POPS, 32 mol% DOG)), 50 mM HEPES, pH 7.4, 99 mM NaCl, 1.5 mM $MgCl_2$, 1 mM ATP, 60.5 Ci per mmol [γ-^{32}P]-ATP, 0.04% (v/v) glycerol, 0.01% (v/v) NP-40, 0.1 μM histone H1, 1 mM DTT, and 1.1 pg per μL purified DGK, and proceeded for 15 minutes at 37°C.

Indeed, not only did the histone H1 preincubation prevent inactivation by incubating at room temperature, but it also at least partially prevented inactivation caused by irradiating with 360 nm light (Figure 107; compare to Figure 104).

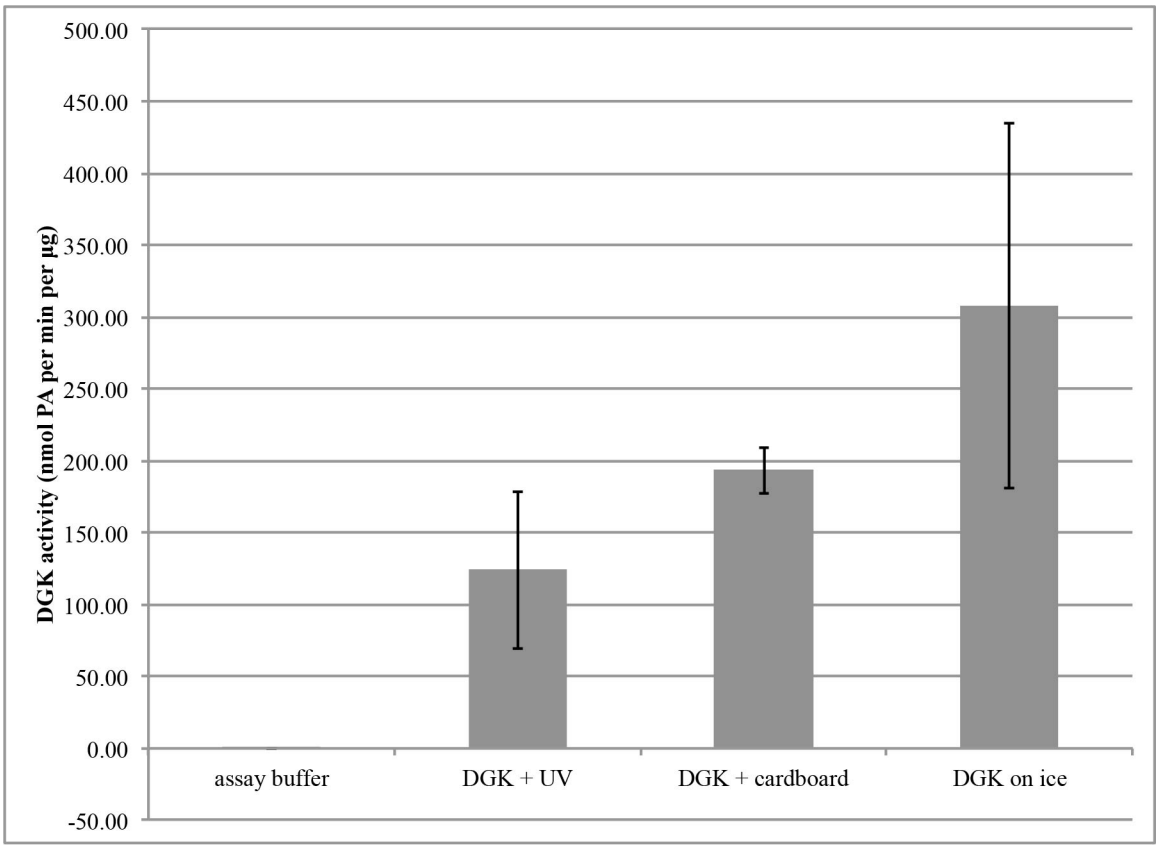

Figure 107. Preincubation in the presence of histone H1 partially prevents inactivation by irradiation with 360 nm light of purified DGK-theta. DGK activity assay. I preincubated purified DGK-theta on ice in preincubation buffer (21 mM HEPES, pH 7.4, 41 mM NaCl, 0.005% (v/v) dodecyl-β-D-maltoside (DDM), 4 µM histone H1, 1 mM DTT) for 10 minutes, then diluted into 1.9 mM liposomes (55.3:27.7:9:8::POPE:POPC:POPS:DOG). I then irradiated the "UV" and "cardboard" samples with a 360 nm lamp for ten minutes in a water-jacketed quartz cuvette. The final reaction mixture included 2 mM liposomes, 50 mM HEPES, pH 7.4, 100 mM NaCl, 1.5 mM $MgCl_2$, 1 mM ATP, 53.1 Ci per mmol [γ-^{32}P]-ATP, 0.04% (v/v) glycerol, 0.0001% (v/v) DDM, 0.1 µM histone H1, 1 mM DTT, and 1.1 pg per µL purified DGK, and proceeded for 15 minutes at 37°C. I calibrated the scintillation counts to a measured amount of [γ-^{32}P]-ATP. In triplicate: mean ± SD.

However, while preincubation with histone H1 on ice protected against room-temperature inactivation in the presence of 1.9 mM liposomes, when the liposome concentration was dropped to 17.5 µM, DGK continued to be inactivated by incubation in the water-jacketed quartz cuvette without irradiation, even when preincubated with histone H1 on ice (Figure 108).

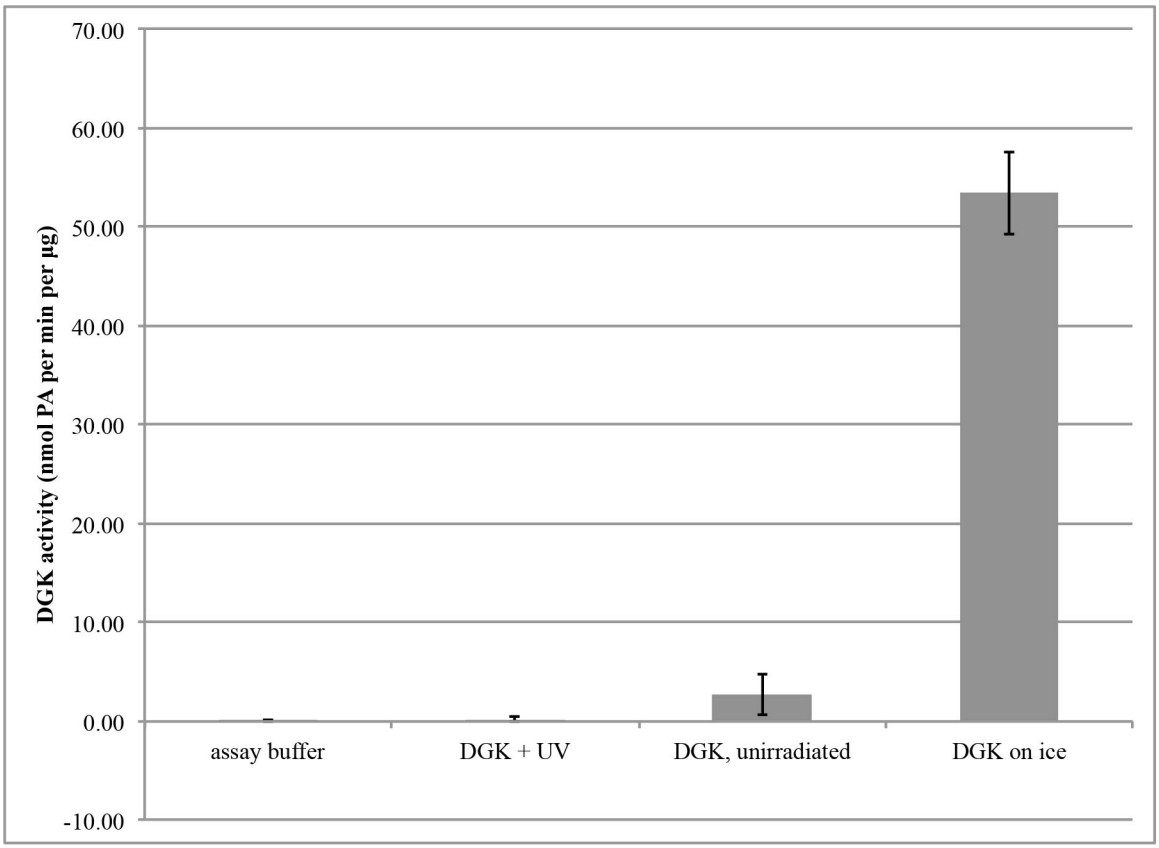

Figure 108. Preincubation with histone H1 is insufficient to protect against room-temperature inactivation of purified DGK-theta in the presence of dilute liposomes. DGK activity assay. I preincubated purified DGK-theta on ice in preincubation buffer (21 mM HEPES, pH 7.4, 41 mM NaCl, 0.005% (v/v) DDM, 4 µM histone H1, 1 mM DTT) for 10 minutes, then diluted into 17.5 µM liposomes (55.3:27.7:9:8::POPE:POPC:POPS:DOG). I then irradiated the "UV" sample with a 360 nm lamp for ten minutes in a water-jacketed quartz cuvette. The "unirradiated" sample was incubated in the cuvette with the lamp turned off. The final reaction mixture included 1 mM liposomes, 50 mM HEPES, pH 7.4, 100 mM NaCl, 1.5 mM $MgCl_2$, 1 mM ATP, 43.8 Ci per mmol [γ-^{32}P]-ATP, 0.04% (v/v) glycerol, 0.0001% (v/v) DDM, 0.1 µM histone H1, 1 mM DTT, and 1.1 pg per µL purified DGK, and proceeded for 15 minutes at 37°C. I calibrated the scintillation counts to a measured amount of [γ-32P]-ATP. In triplicate: mean ± SD.

I then tested whether DGK required an interface in order for preincubation in histone H1 to protect against room-temperature inactivation (Figure 109). Preincubation in the presence of 2 mM liposomes and histone H1 once again prevented room-temperature inactivation. DGK incubated with 17.5 µM liposomes was less active than DGK incubated with 2 mM liposomes, at either temperature. Adding glycerol activated DGK when incubated with 17.5 µM liposomes on ice, but did not protect against room-

temperature inactivation. Incubating in detergent micelles inactivated DGK; they may have disrupted the substrate-containing liposomes in the assay. But the treatment that activated DGK the most, at either temperature, was incubation with ovalbumin, which may have prevented DGK from adhering to the sides of the tube.

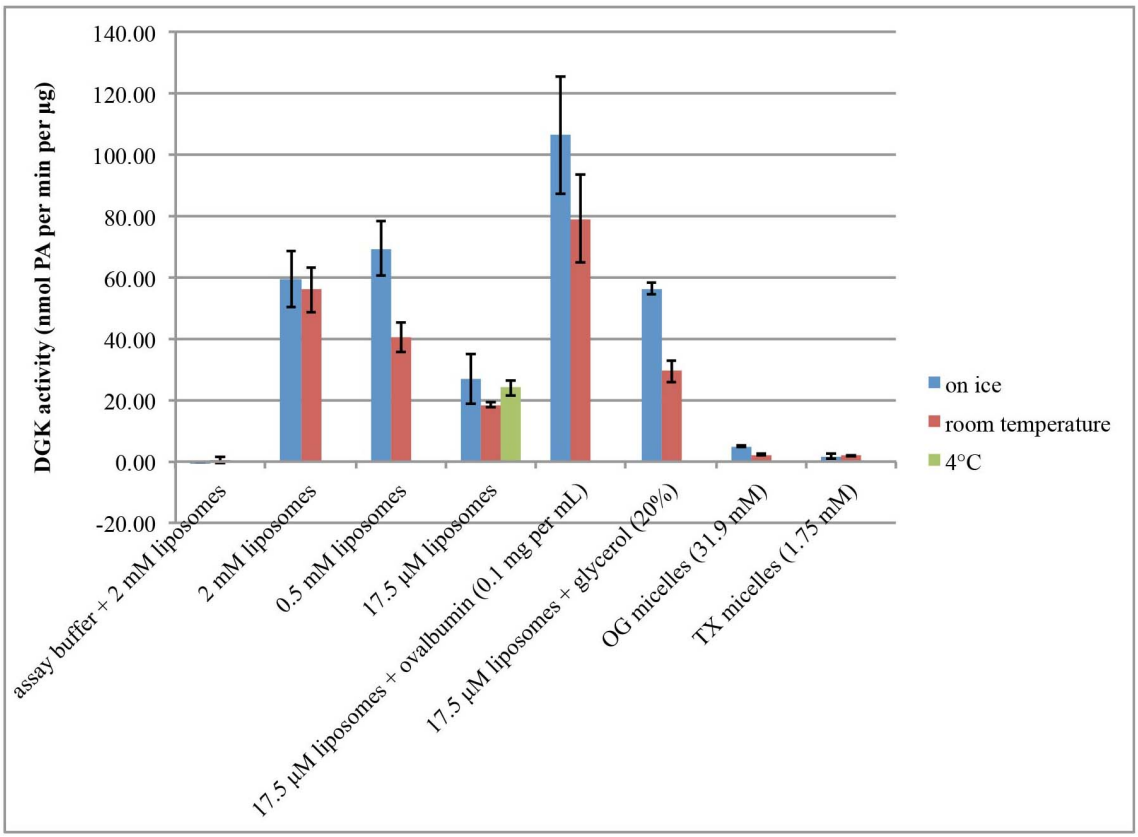

Figure 109. Interface test for room-temperature inactivation of purified DGK-theta. DGK activity assay. Following preincubation with histone H1 on ice, DGK was combined with the components shown and incubated on ice for one hour, prior to being incubated at the temperature indicated for 30 minutes. Detergent micelles included 9 mol% POPS; liposomes were (60.7:30.3:9::POPE:POPC:POPS). The final reaction mixture included 2 mM substrate-containing liposomes (55.3:27.8:9:8:POPE:POPC:POPS:DOG), 1 mM filler liposomes (60.7:30.3:9::POPE:POPC:POPS), 50 mM HEPES, pH 7.4, 100 mM NaCl, 1.5 mM $MgCl_2$, 1 mM ATP, 36.1 Ci per mmol [γ-^{32}P]-ATP, 0.04% (v/v) glycerol, 0.0001% (v/v) DDM, 0.1 µM histone H1, 1 mM DTT, and 1.1 pg per µL purified DGK, and proceeded for 15 minutes at 37°C. I calibrated the scintillation counts to a measured amount of [γ-32P]-ATP. In duplicate: mean ± SD.

I tested that hypothesis by measuring room-temperature inactivation in Eppendorf LoBind tubes, which purport to improve sample recovery as compared to regular Eppendorfs. However, in this experiment, I also included 0.005% (v/v) dodecyl-β-D-

maltoside (DDM) with the DGK at all times, which rescued room-temperature inactivation, beyond which incubation in LoBind tubes or ovalbumin had no additional benefit. As before, the implications for possible conformational changes in DGK caused by detergent are intriguing, but the practical implications were that if I kept DDM at 0.005% at all times, I could protect against room-temperature inactivation of DGK, even in the presence of only dilute liposomes.

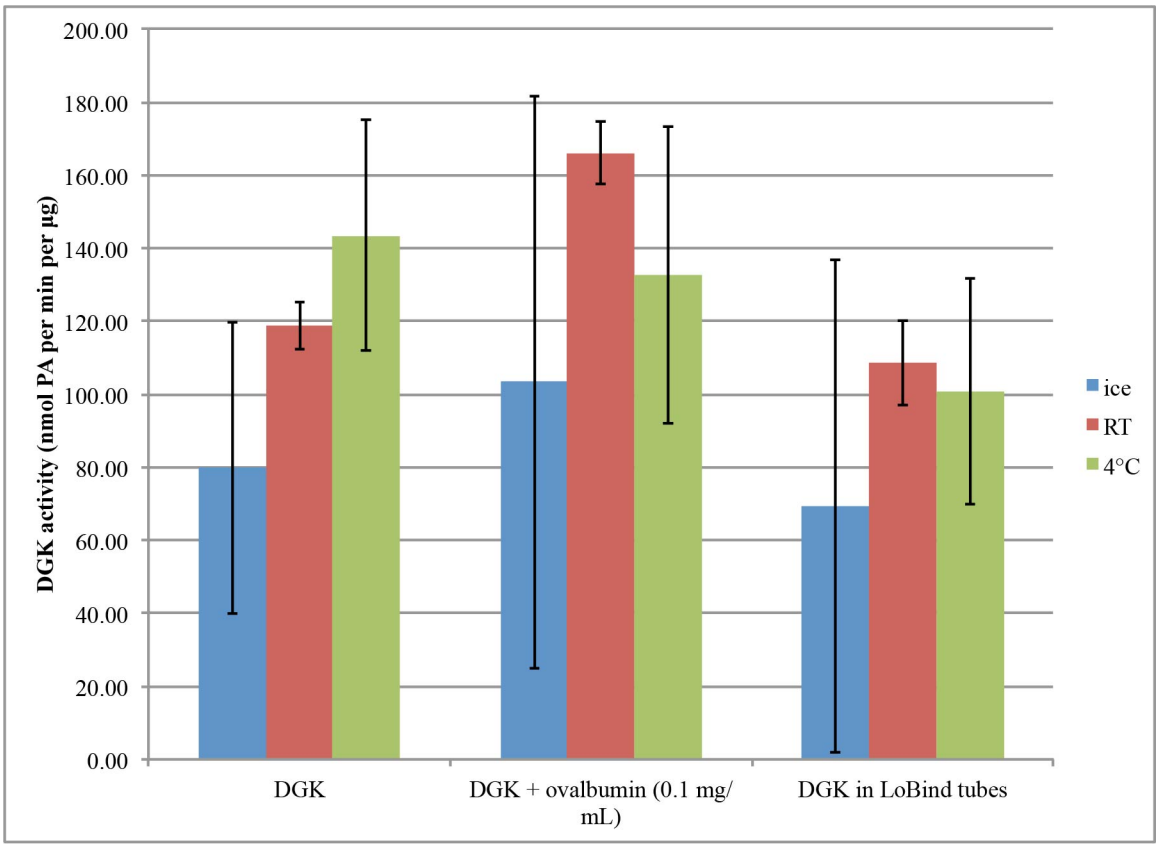

Figure 110. Keeping DDM at 0.005% (v/v) protects against room-temperature inactivation of purified DGK-theta, beyond which incubation in LoBind tubes or ovalbumin had no additional benefit. DGK activity assay. Following preincubation on ice with histone H1, DGK was incubated with each of the following components in the presence of 17.5 µM liposomes (55.3:27.8:9:8:POPE:POPC:POPS:DOG) for one hour on ice, followed by 30 minutes at each of the temperatures shown. DDM was kept at 0.005% at all times. The final reaction mixture included 2 mM liposomes, 50 mM HEPES, pH 7.4, 100 mM NaCl, 1.5 mM $MgCl_2$, 1 mM ATP, 31.2 Ci per mmol [γ-^{32}P]-ATP, 0.04% (v/v) glycerol, 0.005% (v/v) DDM, 0.1 µM histone H1, 1 mM DTT, and 1.1 pg per µL purified DGK, and proceeded for 15 minutes at 37°C. In duplicate: mean ± SD.

However, even when 0.005% DDM was present at all times, DGK still was inactivated when incubated in the water-jacketed quartz cuvette, even without radiation (Figure 111), and even though, as previously mentioned (Table 1), the temperature was even cooler than room temperature.

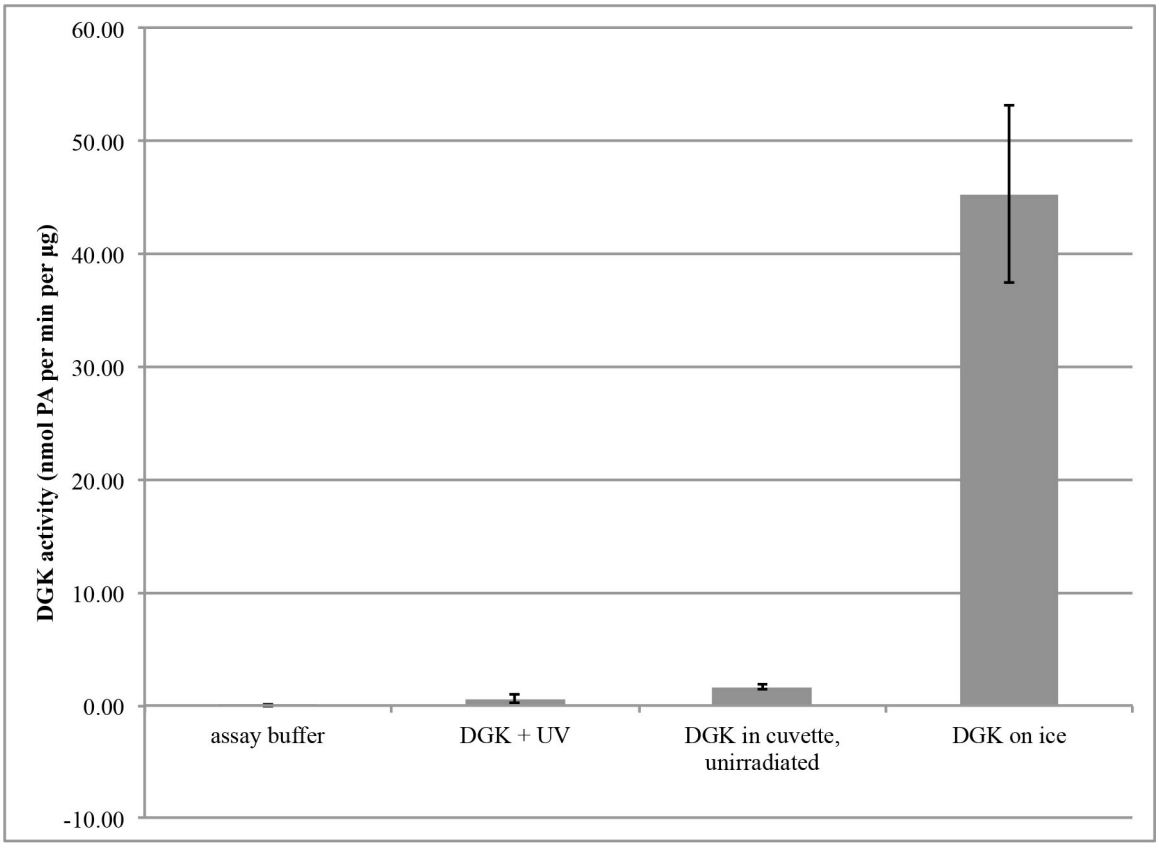

Figure 111. Even with 0.005% (v/v) present at all times, and even with histone H1 preincubation, purified DGK-theta still was inactivated when incubated in the water-jacketed quartz cuvette. DGK activity assay. Following preincubation on ice with histone H1, DGK was incubated with 17.5 µM liposomes (55.3:27.8:9:8:POPE:POPC:POPS:DOG) on ice for 30 minutes, followed by 30 minutes under each of the conditions shown. DDM was kept at 0.005% at all times. The final reaction mixture included 2 mM liposomes, 50 mM HEPES, pH 7.4, 100 mM NaCl, 1.5 mM $MgCl_2$, 1 mM ATP, 49.9 Ci per mmol [γ-^{32}P]-ATP, 0.04% (v/v) glycerol, 0.005% (v/v) DDM, 0.1 µM histone H1, 1 mM DTT, and 1.1 pg per µL purified DGK, and proceeded for 15 minutes at 37°C. In triplicate: mean ± SD.

I wondered whether incubation in the water-jacketed quartz cuvette was uniquely stressful to DGK-theta, more so than the mere rise in temperature. (Caution, however, must always be urged when comparing assays: note for example the difference between

inactivation of DGK incubated with 17.5 μM liposomes in the water-jacketed quartz cuvette in Figure 108 and at room temperature in an Eppendorf in Figure 109.) As such, I compared the activity of DGK-theta in a plastic Eppendorf, either on ice or at room temperature, and in quartz, either in the water-jacketed quartz cuvette with the stir bar, or just a plain quartz cuvette, in case the stirring was what was disturbing DGK. In order to test whether adhesion to the quartz was an issue, I also tested whether adding ovalbumin could improve DGK's tolerance of any of these conditions. I continued to preincubate DGK in 0.1 μM histone H1 on ice for ten minutes before diluting into any liposomes, and I continued to include 0.005% DDM at all times, because I had previously shown those conditions to stabilize DGK (Figure 106 and Figure 110). I found that while preincubation with histone H1 and including 0.005% DDM continued to prevent DGK from room-temperature inactivation in a plastic Eppendorf in the presence of 17.5 μM liposomes, as expected, DGK lost activity when incubated in the quartz cuvette at 4°C, and lost even more activity when incubated in the water-jacketed quartz cuvette with stirring (Figure 112). The inactivation in the quartz cuvette was rescued by including 0.1 mg per mL ovalbumin, suggesting that part of the problem was that DGK was sticking to the quartz. However, the inactivation in the water-jacketed quartz cuvette was only partially rescued by the ovalbumin; that, and the fact that incubation in the water-jacketed quartz cuvette inactivated DGK more than incubation in the plain quartz cuvette did, suggested that in addition to the adhesion problem, there was also a problem with the water-jacketed quartz cuvette, perhaps the shear forces from stirring. Speculating on the nature of the physical basis for the inactivation of DGK by quartz (affinity for electrical charges on the surface of the crystal?) and shear forces (a particularly mechanosensitive

structure?) is tempting, but in practicality, if I wanted to use UV irradiation to study DGK, I needed another vessel for irradiation.

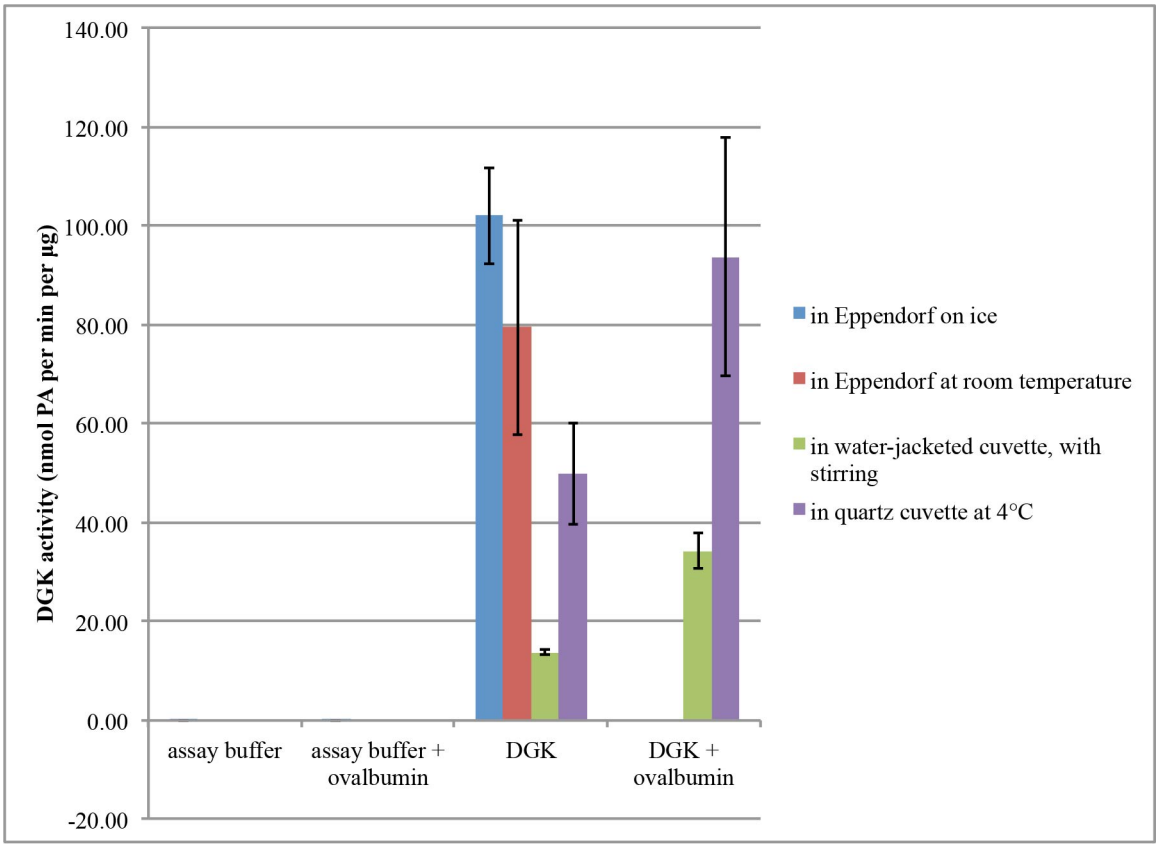

Figure 112. Purified DGK-theta is sensitive to quartz, and is particularly sensitive to the water-jacketed quartz cuvette with stirring. DGK activity assay. DGK + ovalbumin in Eppendorf samples were omitted in the interest of limiting the size of the experiment: compare to **Figure 110**. Following preincubation on ice with histone H1, DGK was incubated with 17.5 µM liposomes (55.3:27.8:9:8:POPE:POPC:POPS:DOG) on ice for 30 minutes, followed by 30 minutes under each of the conditions shown. DDM was kept at 0.005% at all times. The final reaction mixture included 2 mM liposomes, 50 mM HEPES, pH 7.4, 100 mM NaCl, 1.5 mM $MgCl_2$, 1 mM ATP, 39.1 Ci per mmol [γ-^{32}P]-ATP, 0.04% (v/v) glycerol, 0.005% (v/v) DDM, 0.1 µM histone H1, 1 mM DTT, and 1.1 pg per µL purified DGK, and proceeded for 15 minutes at 37°C. In triplicate: mean ± SD.

My next candidate for an irradiation vessel was a 96-well plastic plate. I likewise wanted to test whether UV itself inactivated DGK more than room-temperature incubation itself did, and, anticipating that DGK might stick to the plastic 96-well plate, I decided to also test whether ovalbumin could mitigate any such inactivation. I found that

UV irradiation in the 96-well plate did indeed inactivate DGK, but this inactivation was at least partially rescued by including 0.1 mg per mL ovalbumin (Figure 113).

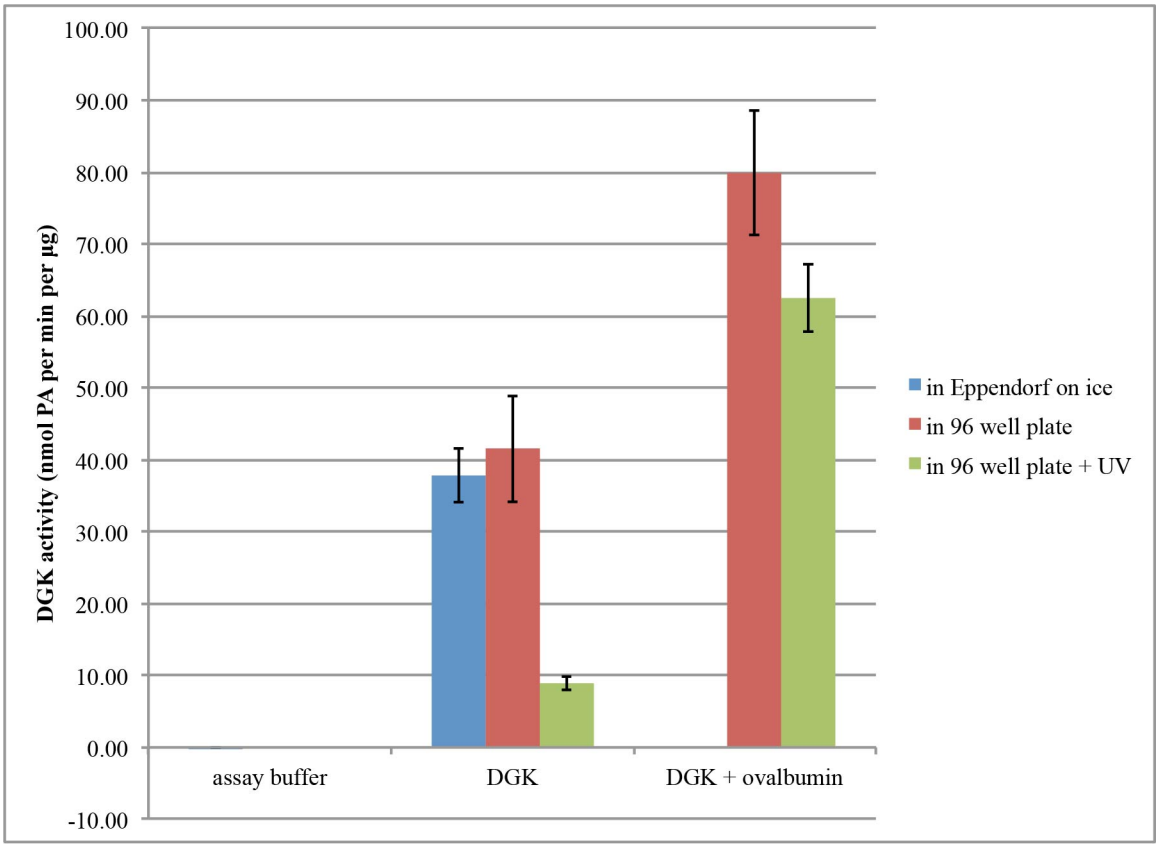

Figure 113. Irradiation with a 360 nm lamp inactivates purified DGK-theta, but incubation in the presence of ovalbumin at least partially prevents this inactivation. DGK activity assay. DGK + ovalbumin in Eppendorf on ice samples were omitted in the interest of limiting the size of the experiment. Following preincubation on ice with histone H1, DGK was incubated with 17.5 µM liposomes (55.3:27.8:9:8:POPE:POPC:POPS:DOG) on ice for 30 minutes, followed by 30 minutes under each of the conditions shown. DDM was kept at 0.005% at all times. The final reaction mixture included 2 mM liposomes, 50 mM HEPES, pH 7.4, 100 mM NaCl, 1.5 mM $MgCl_2$, 1 mM ATP, 35.5 Ci per mmol [γ-^{32}P]-ATP, 0.04% (v/v) glycerol, 0.005% (v/v) DDM, 0.1 µM histone H1, 1 mM DTT, and 1.1 pg per µL purified DGK, and proceeded for 15 minutes at 37°C. In triplicate: mean ± SD.

However, even among experiments done on an ice bucket, in the same cold room, under the same lamp, for the same amount of time, with the same concentration of ovalbumin, the degree of inactivation from irradiation varied among experiments (Figure 114**A-E**). The concentration of DGK in the well, and, consequently, the concentration of glycerol in the well (since the glycerol came from the purified DGK, which had been

stored in glycerol at 80°C), also varied among experiments, but the experiments shown in Figure 114**A**, Figure 114**B**, and Figure 114**C** all used the same concentration of DGK (and therefore glycerol) in the incubation. Because these experiments showed different degrees of inactivation by irradiation, it seems unlikely that the key variable determining susceptibility to inactivation by irradiation is concentration of either DGK or glycerol. The other variables that varied among these experiments were the distance between the lens of the lamp and the 96-well plate (by a few centimeters at most), the angle of the lamp (by several degrees at most), the volume of sample in the well (although I measured the volumes before and after irradiation, and I took the concentration caused by evaporation into account when calculating the specific activity of the enzyme), the time that DGK was thawed before it was irradiated, and the time that elapsed between the DGK was irradiated and the time it was assayed. Any one or combination of these factors might contribute to the degree of inactivation of DGK by irradiating with the 360 nm lamp, protected or not with aluminum foil.

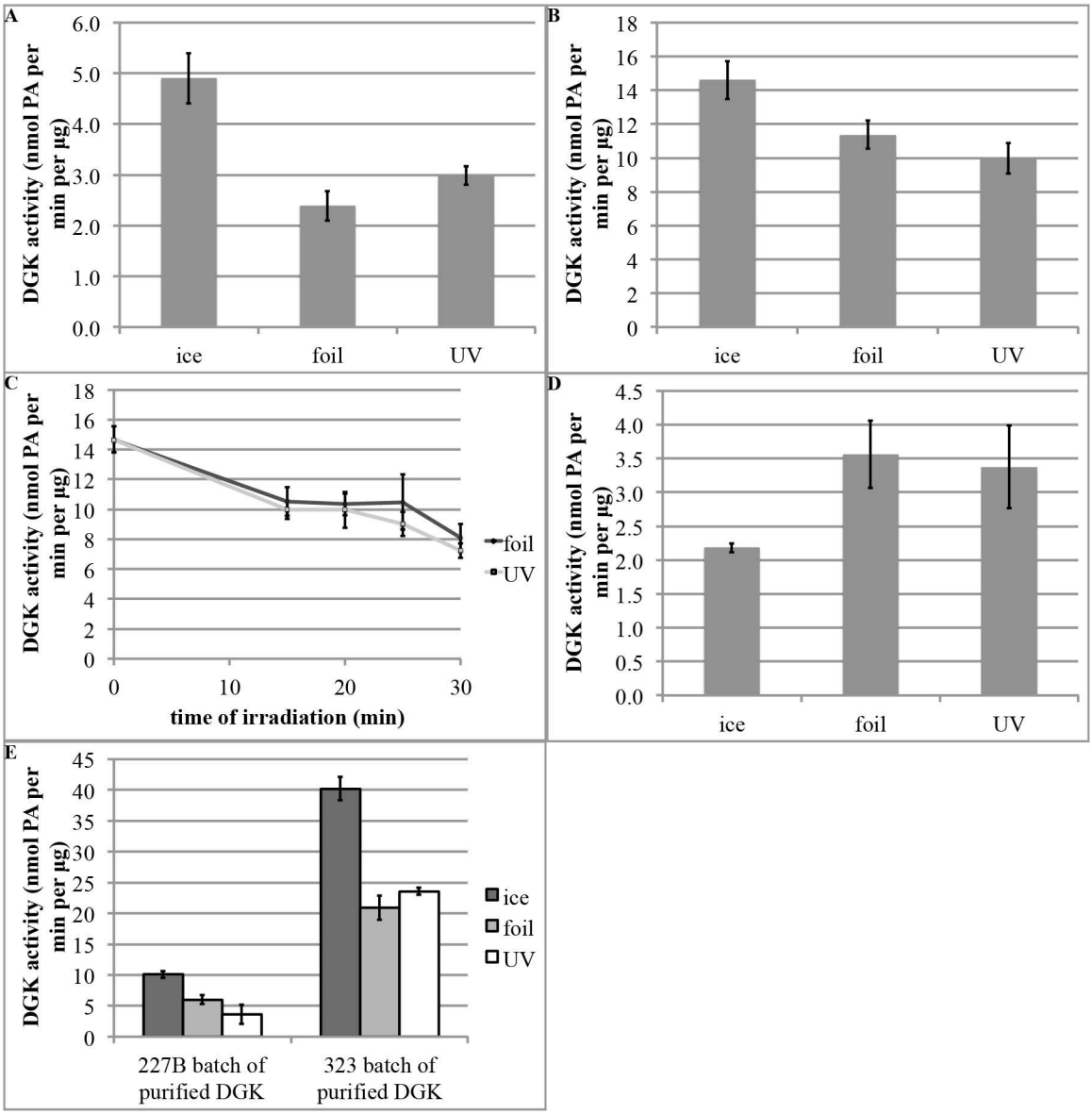

Figure 114. The degree of inactivation under foil during irradiation as compared to incubation on ice varies among experiments. DGK activity assays. **(A)** I incubated purified DGK-theta in preincubation buffer (75 pg per µL DGK-theta, 1.9% (v/v) glycerol, 0.005% (v/v) DDM, 1 mM DTT, 2.5 µM histone H1, 50 mM HEPES, pH 7.4) on ice for ten minutes. I then diluted into irradiation buffer (15 pg per µL DGK-theta, 0.4% (v/v) glycerol, 0.005% (v/v) DDM, 1 mM DTT, 0.5 µM histone H1, 50 mM HEPES, pH 7.4, 100 mM NaCl, 0.1 mg per mL ovalbumin, 1 mM ATP, 1.5 mM $MgCl_2$, 7.5 mM liposomes (53.3:26.7:20::POPE:POPC:POPS)), rocked at room temperature for thirty minutes, then incubated under the conditions shown for another thirty minutes. The final reaction mixture included 5 mM substrate-containing liposomes (56.7:28.3:9:6::POPE:POPC:POPS:DOG), 1.5 mM incubation liposomes, 1.5 mM filler liposomes (49.3:24.7:20:6::POPE:POPC:POPS:compound **3**, 50 mM HEPES, pH 7.4, 100 mM NaCl, 1.5 mM $MgCl_2$, 1 mM ATP, 70.9 Ci per mmol [γ-^{32}P]-ATP, 0.1% (v/v) glycerol, 0.005% (v/v) DDM, 0.1 µM histone H1, 0.02 mg per mL ovalbumin, 1 mM DTT, and 3.0 pg per µL purified DGK, and proceeded for 30 minutes at 37°C. In triplicate: mean ± SD. **(B)** The experiment was the same as that shown in (A) with the exception timepoints were taken at the times shown, I increased [γ-^{32}P]-ATP to 158 Ci per mmol, and the reaction proceeded for 20 minutes at 37°C. In triplicate: mean ± SD. **(C)** The experiment was the

same as that shown in (A) and (B) with the exception that the composition of the filler liposomes was (49.1:24.5:10:6.4::POPE:POPC:POPS:compound **4**, [γ-^{32}P]-ATP was 117 Ci per mmol, and the reaction proceeded for 30 minutes at 37°C. **(D)** I incubated purified DGK-theta in preincubation buffer 2 (996 pg per μL DGK-theta, 16.5% (v/v) glycerol, 0.005% (v/v) DDM, 1 mM DTT, 0.32 μM histone H1, 50 mM HEPES, pH 7.4) on ice for ten minutes. I then diluted into irradiation buffer 2 (307 pg per μL DGK-theta, 5.1% (v/v) glycerol, 0.005% (v/v) DDM, 1 mM DTT, 0.1 μM histone H1, 50 mM HEPES, pH 7.4, 100 mM NaCl, 0.1 mg per mL ovalbumin, 1 mM ATP, 1.5 mM $MgCl_2$, 7.5 mM incubation liposomes), rocked at room temperature for thirty minutes, then incubated under the conditions shown for another thirty minutes. The final reaction mixture included 5 mM substrate-containing liposomes, 43 μM incubation liposomes, 43 μM filler liposomes (compound **4**), 50 mM HEPES, pH 7.4, 100 mM NaCl, 1.5 mM $MgCl_2$, 0.8 mM ATP, 35.7 Ci per mmol [γ-^{32}P]-ATP, 0.04% (v/v) glycerol, 0.005% (v/v) DDM, 0.1 μM histone H1, 0.6 μg per mL ovalbumin, 1 mM DTT, and 1.8 pg per μL purified DGK-theta, and proceeded for 30 minutes at 37°C. In triplicate: mean ± SD. **(E)** 227B and 323 are two different batches of purified DGK-theta. I incubated purified DGK-theta in preincubation buffer (for 227B, 48 pg per μL purified DGK and 1.2% (v/v) glycerol; for 323, 120 pg per μL purified DGK and 2.0% (v/v) glycerol) on ice for ten minutes. I then diluted into irradiation buffer, rocked at room temperature for thirty minutes, then incubated under the conditions shown for another thirty minutes. The final reaction mixture was the same as in (B) except that [γ-^{32}P]-ATP was reduced to 20.9 Ci per mmol. The reaction proceeded for 30 minutes at 37°C. In triplicate: mean ± SD.

One possible explanation for why the time that DGK was thawed before it was irradiated could be an issue is that the DTT might have been breaking down and losing its power as a reducing agent, and that the effect could therefore be perhaps mitigated by using BME as a reducing agent instead. However, when I tested the reducing agent requirement explicitly, while incubating purified DGK-theta with a reducing agent increased its enzymatic activity, the identity of the reducing agent did not seem to matter (Figure 115). It therefore seems unlikely that DTT breakdown could explain the irreproducibility seen in foil inactivation of purified DGK-theta, although out of an abundance of caution, I did replace 1 mM DTT with 3 mM BME in future experiments.

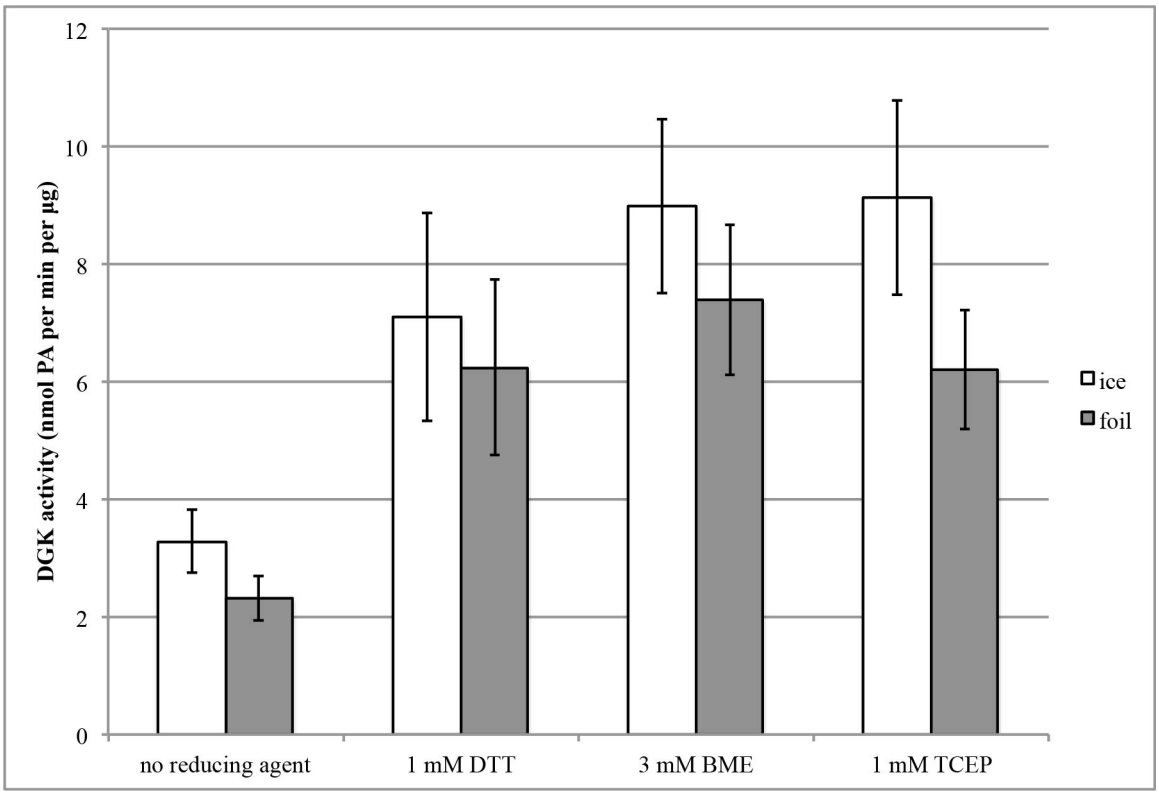

Figure 115. Incubation in the presence of a reducing agent increases purified DGK-theta's enzymatic activity under the conditions tested, but the identity of the reducing agent does not seem to matter. DGK activity assay. I incubated purified DGK-theta in preincubation buffer (67 pg per µL DGK-theta, 1.9% (v/v) glycerol, 0.005% (v/v) DDM, 0.5 µM histone H1, 50 mM HEPES, pH 7.4, and the indicated concentrations of reducing agent) on ice for ten minutes. I then diluted into irradiation buffer (13 pg per µL DGK-theta, 0.4% (v/v) glycerol, 0.005% (v/v) DDM, 0.1 µM histone H1, 50 mM HEPES, pH 7.4, 100 mM NaCl, 0.1 mg per mL ovalbumin, 1 mM ATP, 1.5 mM $MgCl_2$, 7.5 mM liposomes (53.3:26.7:20::POPE:POPC:POPS), and the indicated concentrations of reducing agent), rocked at room temperature for thirty minutes. I then placed the samples either on ice or in a 96-well plate with aluminum foil between the samples and the lamp, and irradiated the samples with a 360 nm lamp for thirty minutes at room temperature. After irradiation, I returned the samples to Eppendorfs, and measured the volume to account for concentration of DGK due to evaporation. The final reaction mixture included 5 mM substrate-containing liposomes (56.7:28.3:9:6::POPE:POPC:POPS:DOG), 1.5 mM incubation liposomes, 50 mM HEPES, pH 7.4, 100 mM NaCl, 1.5 mM $MgCl_2$, 1 mM ATP, 28.4 Ci per mmol [γ-^{32}P]-ATP, 0.08% (v/v) glycerol, 0.005% (v/v) DDM, 0.1 µM histone H1, 0.02 mg per mL ovalbumin, 2.7 pg per µL purified DGK, and the indicated concentrations of reducing agent, and proceeded for 30 minutes at 37°C. In triplicate: mean ± SD.

A relatively recent technological development is the UV light-emitting diode (LED), which produces less heat than the 360 nm lamp I had been using. Indeed, a UV LED flashlight with a peak wavelength of 365 nm did not inactivate purified DGK-theta, even when it was irradiated as long as sixty minutes (Figure 116). Whether the UV LED

flashlight will solve the problem of foil inactivation of purified DGK-theta will therefore depend on whether the UV LED flashlight provides sufficient photon flux to produce probe-, UV-dependent enzymatic inactivation, as the 360 nm UV lamp did.

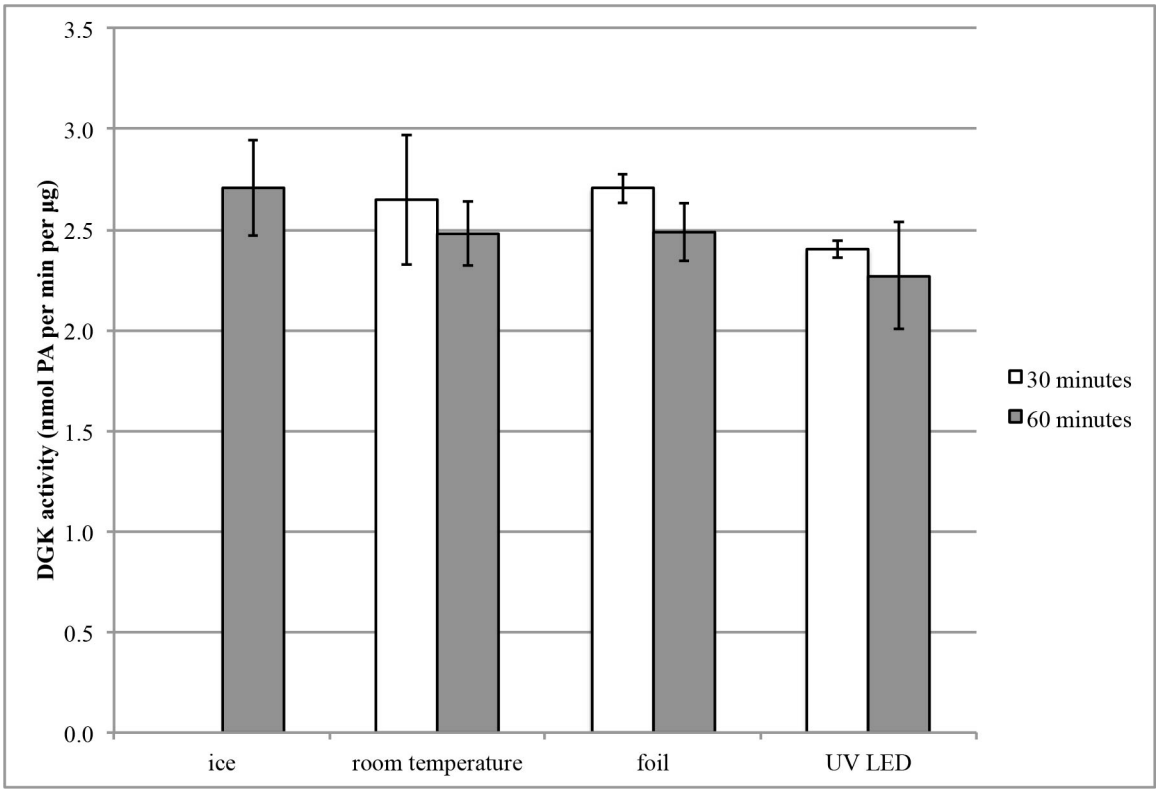

Figure 116. Irradiation with the 365 nm LED for up to sixty minutes does not inactivate purified DGK-theta. DGK activity assay. I incubated purified DGK-theta in preincubation buffer (125 pg per µL DGK-theta, 3.6% (v/v) glycerol, 0.005% (v/v) DDM, 0.5 µM histone H1, 50 mM HEPES, pH 7.4, 3 mM BME) on ice for ten minutes. I then diluted into irradiation buffer (25 pg per µL DGK-theta, 0.7% (v/v) glycerol, 0.005% (v/v) DDM, 0.1 µM histone H1, 50 mM HEPES, pH 7.4, 100 mM NaCl, 0.1 mg per mL ovalbumin, 1 mM ATP, 1.5 mM $MgCl_2$, 7.5 mM liposomes (53.3:26.7:20::POPE:POPC:POPS), and 3 mM BME), rocked at room temperature for thirty minutes. I then placed the samples either on ice or in a 96-well plate, and irradiated the samples with a 365 nm peak wavelength LED flashlight for either thirty minutes (at which point the samples were returned to ice for the remaining thirty minutes) or sixty minutes at room temperature ("foil" samples had aluminum foil between the samples and the flashlight). After irradiation, I returned the samples to Eppendorfs, and measured the volume to account for concentration of DGK due to evaporation. The final reaction mixture included 5 mM substrate-containing liposomes (56.7:28.3:9:6::POPE:POPC:POPS:DOG), 1.5 mM incubation liposomes, 50 mM HEPES, pH 7.4, 100 mM NaCl, 1.5 mM $MgCl_2$, 1 mM ATP, 15.1 Ci per mmol [γ-^{32}P]-ATP, 0.2% (v/v) glycerol, 0.005% (v/v) DDM, 0.1 µM histone H1, 0.02 mg per mL ovalbumin, 5.0 pg per µL purified DGK, and 3 mM BME, and proceeded for 43.5 minutes at ~33°C. In triplicate: mean ± SD.

Conclusions

The maintenance of purified DGK activity is very sensitive to temperature. Incubation at room temperature can greatly decrease the activity of purified DGK, as can incubation on ice. Measures that help protect against this inactivation include keeping detergents such as NP-40 and DDM around at all times, preincubating purified DGK in the presence of histone H1 but not MgATP, and adding ovalbumin to prevent DGK from being lost to adhesion to surfaces. Although raising the temperature may be necessary for an experiment (such as allowing DGK the thermal flexibility that might be required to bind a substrate analog), keeping the temperature as low as possible, by keeping the protein on ice or by using a UV LED instead of a UV lamp, will help preserve the activity of DGK long enough that it can be assayed.

Chapter 5: DGK Activation, Inhibition, and Substrate Specificity

Introduction

In addition to learning about the structure of eukaryotic DGKs, I was also interested in learning about their chemistry. Studying activators and inhibitors of DGKs can give insight into their chemistry as well as their regulation. Studying the substrate specificity requirements can give insight into the structure, topography, and chemical features of the active site. Finding activators of DGKs also has the extremely practical benefit of increasing the observed DGK enzymatic activity: including an activator in an assay can thus make studying the enzymology of DGKs much easier. I was therefore very interested to learn more about activation, inhibition, and substrate specificity of eukaryotic DGKs.

Polybasic Activators and DGKs

Polybasic Activator Introduction

Polybasic proteins such as casein, tau, and histone H1 have been shown to activate *H. sapiens* DGK-theta expressed and purified from HEK293T cells[3]. The question remained whether these proteins likewise activated other eukaryotic DGK isoforms and constructs.

Casein and Alphacat in pT71myc Expressed and Purified from E. coli

Introduction

Polybasic proteins such as casein, tau, and histone HI have been shown to activate *H. sapiens* DGK-theta expressed and purified from HEK293T cells[3]. I therefore tested

whether alphacat in pT71myc expressed in *E. coli* and purified on Ni-NTA (which I showed to elute from the Sephadex® G-100 analytical gel filtration resin in the void in Figure 15) could likewise be activated by casein.

Results

Alphacat clearly had more DGK activity than assay buffer, when assayed either in detergent micelles or in liposomes (Figure 117). However, unlike the reported effect on full-length *H. sapiens* DGK-theta, the addition of casein to the assay buffer decreased the DGK activity of alphacat (Figure 117).

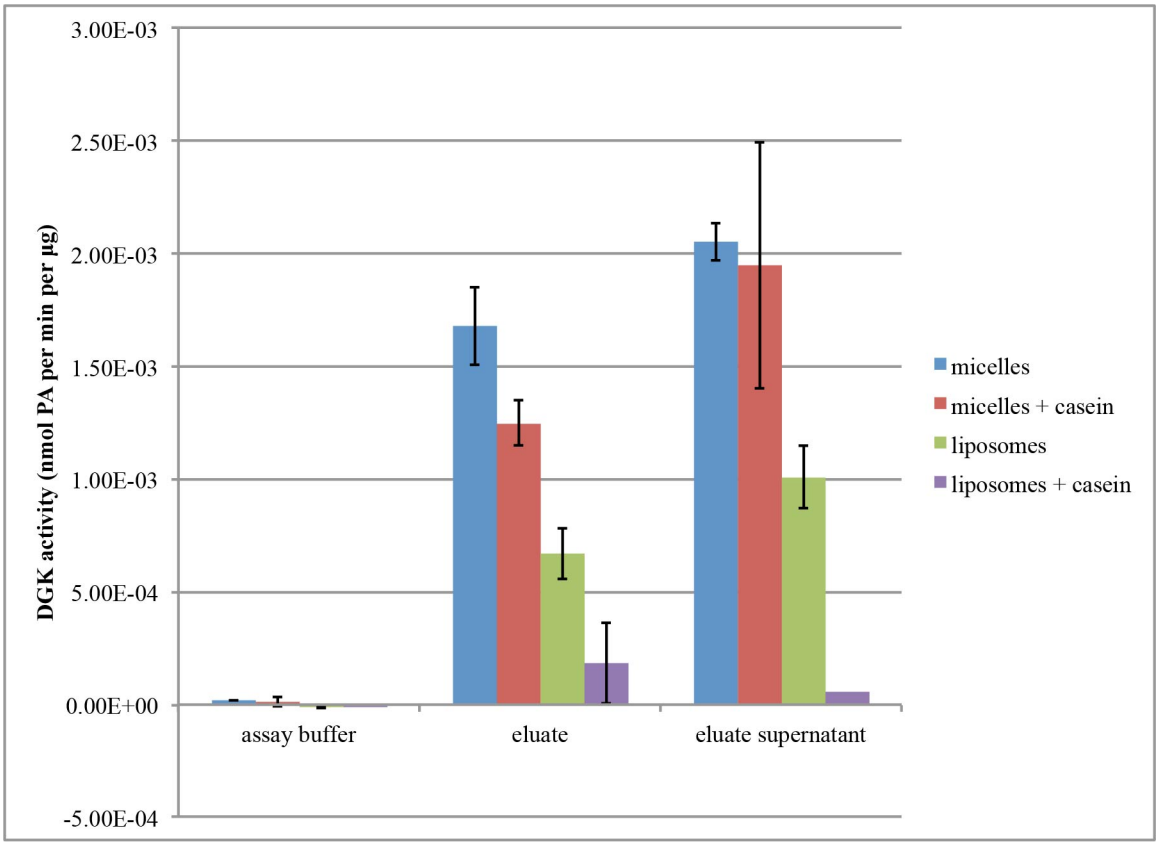

Figure 117. The addition of casein appears to decrease the enzymatic activity of purified alphacat in pT71myc. I stored the samples for four weeks at -80°C in 50% glycerol prior to assaying. The final reaction mixture included either 6.1 mM containing liposomes (53:22:17:8::POPE:POPC:POPS:DOG) or 4.3 mM TX-100 micelles (18.2% POPS, 6 mol% DOG), 44 mM HEPES, pH 8.0, 4.4 mM $MgCl_2$, 0.93 mM

$CaCl_2$, 1 mM ATP, 103 Ci per mmol [γ-^{32}P]-ATP, 2.5 mM Tris, 12.5 mM imidazole, 15 mM NaCl, 5% (v/v) glycerol, 0.1 mg per mL each of α- and β-casein (or not), and either 3.7 ng per μL eluate or 1.8 ng per μL eluate supernatant (as measured by the Bio-Rad Protein Assay), and proceeded for 15 minutes at 30°C. In duplicate: mean ± SD.

Conclusions

Whereas casein activates *H. sapiens* DGK-theta expressed and purified from HEK293T cells[3], it decreases the activity of alphacat in pT71myc expressed in *E. coli* and purified on Ni-NTA. If casein's mechanism of action were on the membrane, making diglyceride a better substrate for DGK, one would predict that casein would exert the same effect on alphacat, but it does not, suggesting that the site of casein's action is on DGK itself. Were it that casein had no effect on alphacat, one might conclude that its binding site on DGK-theta might be outside the catalytic domain. The fact that it decreases alphacat's activity, however, is intriguing. One possible interpretation could be that casein is promoting a conformational change in the catalytic domain that, in the presence of the accessory domains, promotes catalytic turnover, but in their absence, makes turnover more difficult. Another possible explanation is that casein exerts one effect on DGK-theta and another on DGK-alpha. In order to resolve these two possible explanations, the effect of casein on full-length DGK-alpha could be tested.

Polybasic Activators and FLAG-DGKA expressed and purified from D. discoideum

Introduction

Getting at the question of whether polybasic activators affect different eukaryotic isoforms differently, I likewise tested whether casein activated FLAG-DGKA expressed and purified from *D. discoideum.*

Results

The purified FLAG-DGKA was not contaminated with diglyceride, because FLAG-DGKA incubated with micelles without diglyceride showed no detectable DGK activity (Figure 118**A**). The casein was not contaminated with DGK, because casein incubated with substrate-containing micelles likewise showed no detectable DGK activity (Figure 118**A**). When FLAG-DGKA and casein were combined in the presence of substrate-containing micelles, however, together they showed much greater DGK activity than DGKA without casein (Figure 118**A**), suggesting that casein activates FLAG-DGKA, as it does DGK-theta[3]. Activation of purified FLAG-DGKA by casein was reproducible among assays as well as between batches of purified FLAG-DGKA (Figure 66**A** and Figure 118**B**).

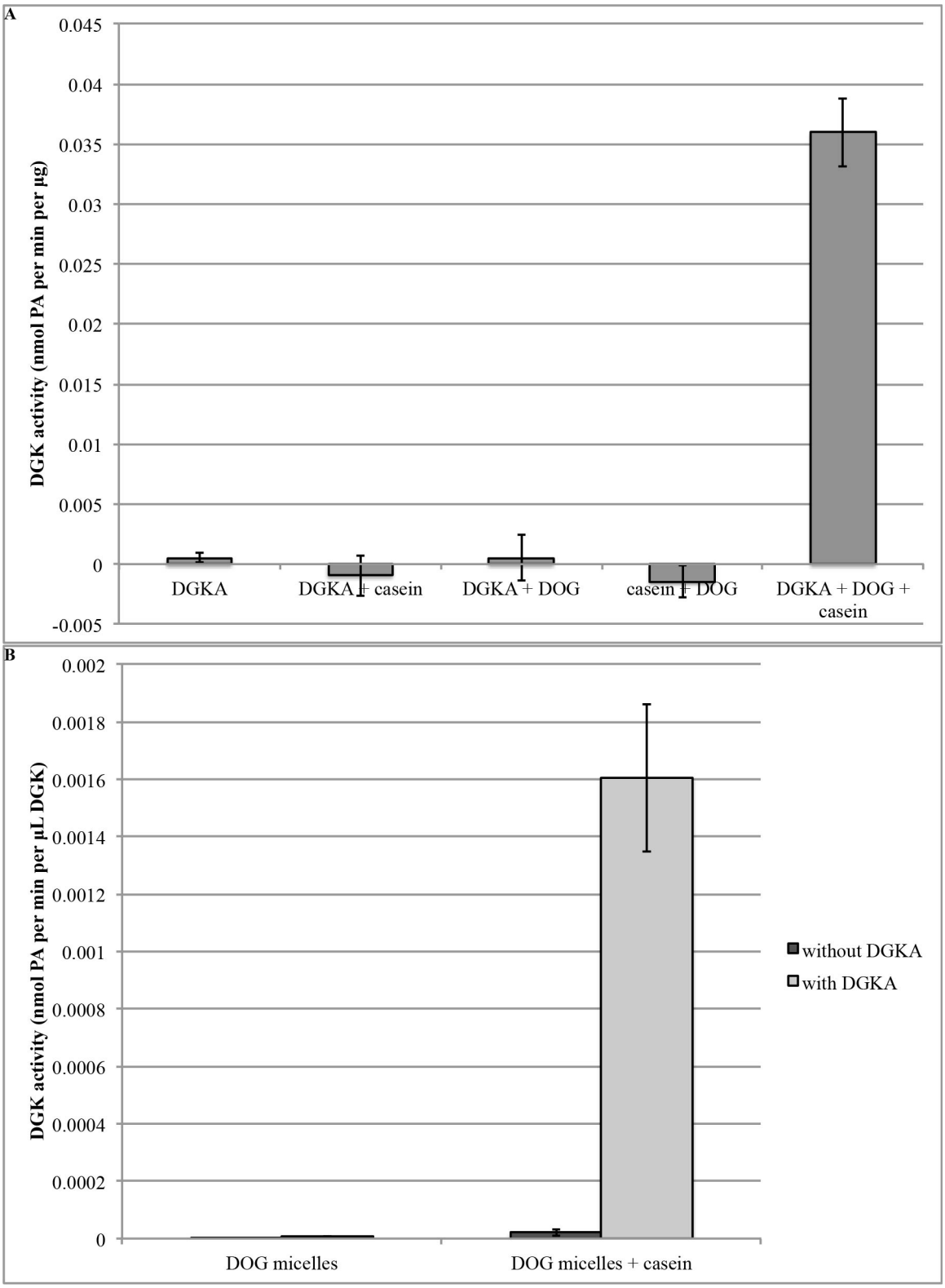

Figure 118. Casein activates purified FLAG-DGKA in detergent micelles. DGK activity assays. **(A)** I stored purified DGKA (shown in **Figure 65**) in 50% glycerol at -80°C for three months prior to assaying.

The reaction included 10 mM TX-100 micelles (9 mol% POPS, with or without 6 mol% DOG), 40 mM Tris, pH 7.0, 4 mM $MgCl_2$, 8 mM NaF, 0.7 ng per µL purified FLAG-DGKA (as estimated from the silver stain in **Figure 65A**), 2 mM TES, 0.2x PIC, 8 µg per µL FLAG peptide, 2% (v/v) glycerol, 1 mM DTT, 1 mM ATP, and 89.1 Ci per mmol [γ-^{32}P]-ATP, and proceeded for 15 minutes at 37°C. I included 3 µL of concentrated stock solutions of casein per 50 µL reaction, where indicated. In duplicate: mean ± SD. **(B)** I stored purified DGKA (shown in **Figure 64**) in 50% glycerol at -80°C for nine days prior to assaying. The reaction included 7 mM TX-100 micelles (9 mol% POPS, 6 mol% DOG), 40 mM Tris, pH 7.0, 4 mM $MgCl_2$, 8 mM NaF, 5 µL purified FLAG-DGKA per 100 µL reaction, 2.5 mM TES, 0.25x PIC, 10 µg per µL FLAG peptide, 2.5% (v/v) glycerol, 1 mM ATP, and 108 Ci per mmol [γ-^{32}P]-ATP, and proceeded for 15 minutes at 30°C. I included 3 µL of concentrated stock solutions of casein per 50 µL reaction, where indicated. In duplicate: mean ± SD.

I also tested the effect of other activators on the activity of FLAG-DGKA in detergent micelles. BL21 has, in its lysate, at least one component that activates DGK-theta, such that when bacterial lysate is added to DGK-theta, its DGK activity is increased. I therefore tested whether the supernatant from BL21 cells likewise activated FLAG-DGKA. I also tested tau, which had been purified from BL21 cells and stored at either -20 or -80°C, as well as BL21 lysate that had been mock-purified, to see whether the effect (if any) could be attributed to tau or to some other bacterial component that co-purified with tau. All of the tested activators increased the DGK activity of FLAG-DGKA, but they also demonstrated greater DGK activity themselves than FLAG-DGKA did (Figure 119). Therefore, while all four activators appeared to activate FLAG-DGKA (as in they demonstrated greater activity than either DGKA or activator alone), it was unclear how to determine quantitatively how much of the DGK activity was resulting from the activated FLAG-DGKA, and how much was resulting from the activator (indeed, FLAG-DGKA could possibly have activated the activators, rather than the other way around).

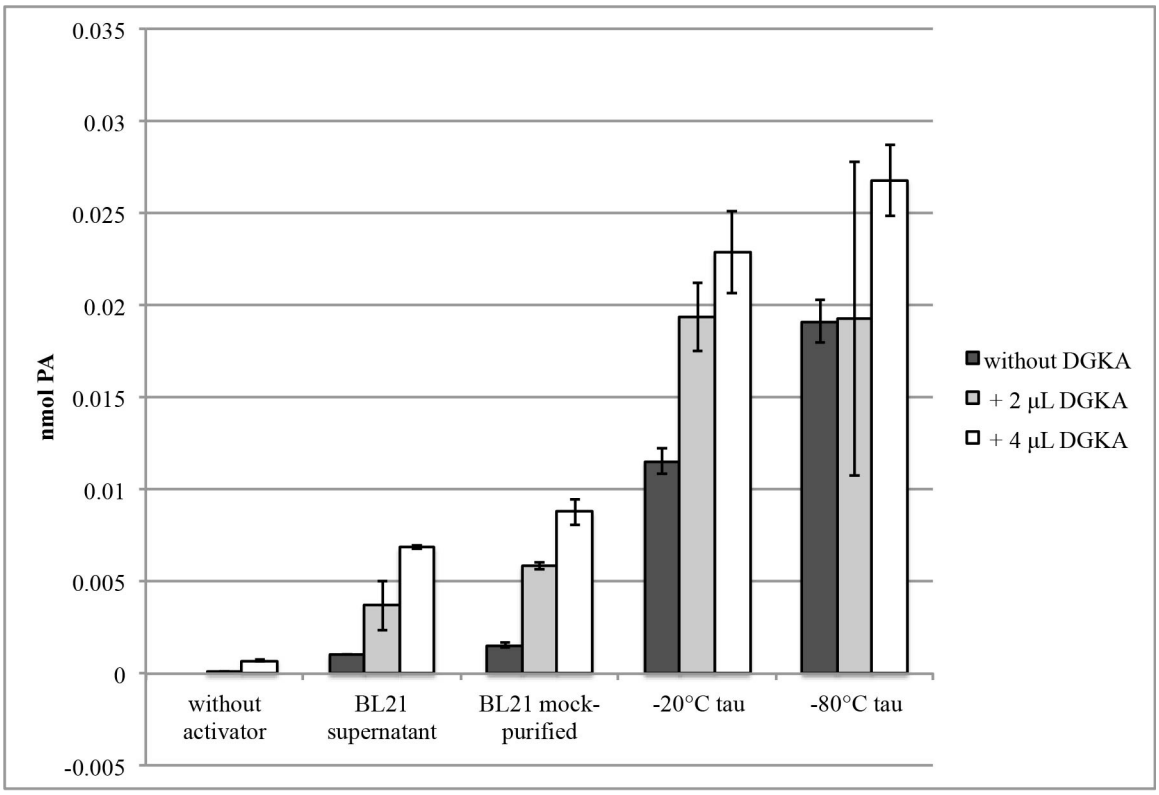

Figure 119. Polybasic activators give high DGK activity in detergent micelles. DGK activity assay. I stored purified DGKA (shown in **Figure 65**) in 50% (v/v) glycerol at -80°C for three months prior to assaying. The reaction included 10 mM TX-100 micelles (9 mol% POPS, 6 mol% DOG), 44 mM Tris, pH 7.4, 4.4 mM $MgCl_2$, 1 mM DTT, 1 mM ATP, 80.1 Ci per mmol [γ-^{32}P]-ATP, and, from the purified DGKA, up to 1.4 ng per µL purified DGKA (as estimated from the silver stain in **Figure 65**A), 4 mM TES, 0.4x PIC, 16 µg per µL FLAG peptide, and 4% (v/v) glycerol, and proceeded for 15 minutes at 37°C. I included 1 µL of concentrated stock solutions of each activator per 50 µL reaction, where indicated. In duplicate: mean ± SD.

Discussion and Conclusions

While all four activators appeared to activate FLAG-DGKA (as in they demonstrated greater activity than either DGKA or activator alone), it was unclear how to determine quantitatively how much of the DGK activity was resulting from the activated FLAG-DGKA, and how much was resulting from the activator (indeed, FLAG-DGKA could possibly have activated the activators, rather than the other way around).

If the DGK activity of the activators was a result of contaminating *E. coli* DGK, I would predict that the DGK activity of the activators would decrease when assayed in liposomes

as compared to detergent micelles, because *E. coli* DGK is an integral membrane protein, and while it could incorporate into detergent micelles and access the substrates therein, it would remain mostly excluded from substrate-containing liposomes. I therefore tested whether these activators activated DGKA in liposomes. Indeed, the activity of each of the activators in the absence of DGKA but in the presence of substrate was lower in liposomes than in micelles, suggesting that previous source of contamination could indeed have been *E. coli* DGK (Figure 66). Casein, as in detergent micelles (Figure 118), activated DGKA in liposomes, as did the other tested activators (Figure 66).

Polybasic Activator Discussion and Conclusions

One reason that these activators may activate *D. discoideum* DGKA (Figure 118 and Figure 66) but not alphacat in pT71myc (Figure 117) could be that DGKA has greater primary sequence homology to DGK-theta than DGK-alpha does[46]. Another possible explanation is that the region of the protein required for activation by casein is found in the N-terminus and not in the catalytic domain included in alphacat. Yet another possible explanation is that post-translational modifications or other processing of DGK provided by a eukaryotic expression host such as HEK293T cells (in the case of DGK-theta[3]) or *D. discoideum* (in the case of DGKA) is required in order for casein to activate the enzyme. The practical implications, however, were that in order to do enzymological studies of purified DGKA, I would need to add an activator to ensure that its DGK activity was detectable.

JG compounds and *D. discoideum* DGKA

Introduction

The laboratory of Professor Glenn Prestwich (Department of Medicinal Chemistry, University of Utah) produced four synthetic diglyceride analogs (named for the person who synthesized them, Dr. Joanna Gajewiak), whose structures are shown in Figure 120.

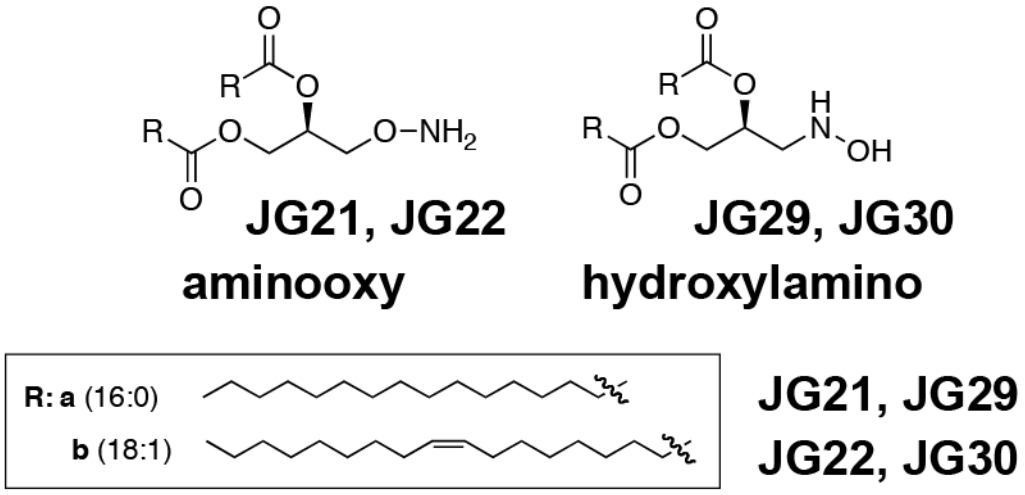

Figure 120. Structures of the JG compounds synthesized by Dr. Joanna Gajewiak of Professor Glenn Prestwich's laboratory (Department of Medicinal Chemistry, University of Utah). The JG compounds are DAG analogs. JG21 and JG22 include an aminooxy group instead of a hydroxyl group, and JG29 and JG30 include a hydroxylamino group. JG21 and 29 include palmitoyl fatty acid chains, and JG22 and JG30 include oleoyl fatty acid chains.

Continuing work started by Ms. Michele Ostroski, I tested whether these DAG analogs activated, inhibited, or could serve as substrates for FLAG-DGKA expressed and purified from *D. discoideum*.

Results

When I included casein, which I had previously shown to activate purified FLAG-DGKA in liposomes (Figure 66), in the reaction, none of the tested JG compounds

appeared to either activate or inhibit DGKA when included in the liposomes at 8 mol%, along with 8 mol% DOG (Figure 121). When DGKA was incubated with liposomes containing 8 mol% JG29 in the absence of DOG, however, I did detect greater DGK activity than DGKA incubated without any liposomes (Figure 121). I therefore concluded that JG29 was able to serve as a substrate for DGKA, albeit at a much lower affinity than DOG. JG30, contrariwise, did not appear to be a substrate for DGKA (Figure 121), even though it has the same head group as JG29, and the two DAG analogs differ only by their fatty acid constituents.

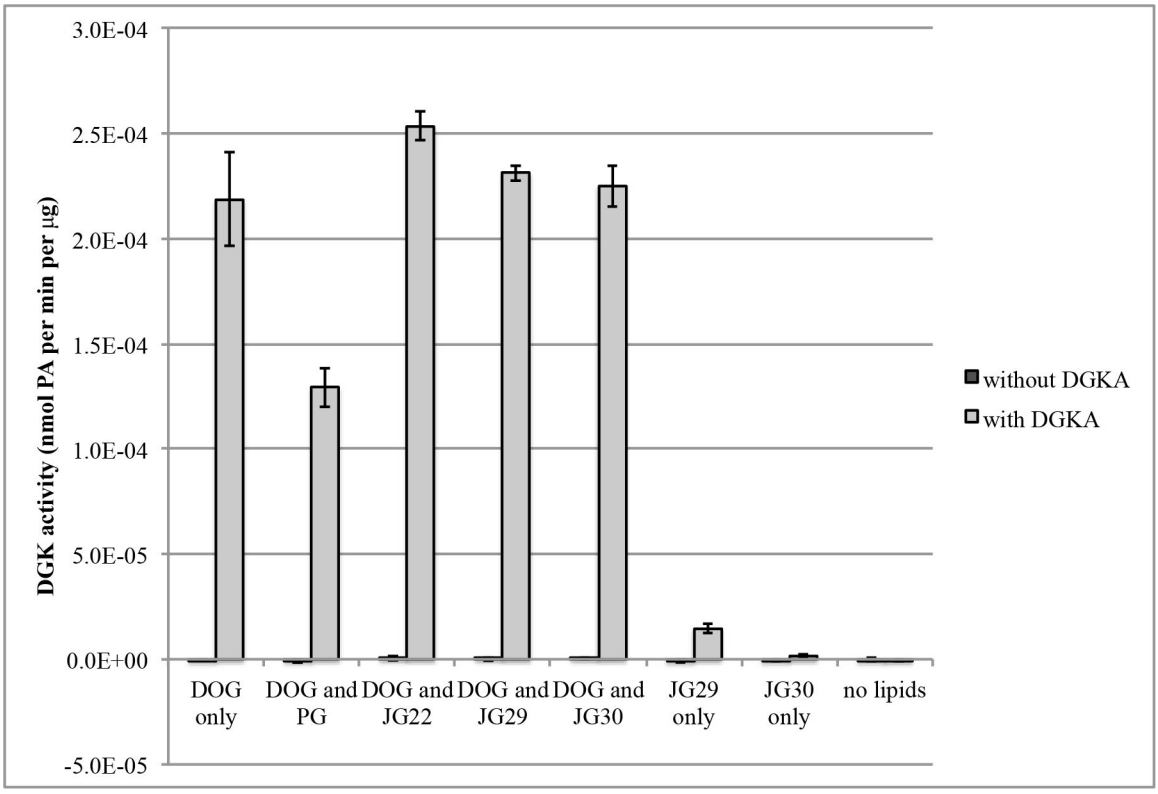

Figure 121. The JG compounds do not appear to affect the activity of purified FLAG-DGKA in the presence of DOG, but JG29 may serve as a substrate. DGK activity assay. I stored purified FLAG-DGKA (shown in **Figure 65**) in 50% (v/v) glycerol at -80°C for three months prior to assaying. The reaction included 5 mM liposomes of the composition shown (for the "DOG only" or "JG only" liposomes, the composition was (40:40:12:8::POPS:POPE:PI:(DOG or JG)), and for the liposomes that contained both DOG and either POPG or one of the JG compounds, the composition was (40:32:12:8:8::POPS:POPE:PI:DOG:(POPG or JG)), 41 mM Tris, pH 7.0, 8.2 mM $MgCl_2$, 8.2 mM NaF, 1 μL of concentrated stock casein per 50 μL reaction, 1 mM DTT, 1 mM ATP, 91.7 Ci per mmol [γ-^{32}P]-ATP, and, from the purified FLAG-DGKA, up to 1.3 ng per μL purified FLAG-DGKA (as estimated from

the silver stain in **Figure 65**A), 3 mM TES, 0.3x PIC, 12 μg per μL FLAG peptide, and 3% (v/v) glycerol, and proceeded for 7.5 minutes at 37°C. In triplicate: mean ± SD.

Discussion and Conclusions

JG29 appeared to be able to serve as a substrate for FLAG-DGKA expressed and purified from *D. discoideum*, whereas JG30 did not, even though it has the same head group as JG29, and the two DAG analogs differ only by their fatty acid constituents. This substrate specificity resulting from different fatty acid chains is consistent with previous reports of DGKA's substrate specificity with regard to the fatty acid chains of different DAGs[47], although palmitoyl and oleoyl side chains of DAG substrates have not been compared explicitly. If JG29 is, indeed, a substrate for DGKA, I would predict it to be a competitive inhibitor of DGKA when DOG is used as a substrate, but, as can be seen in Figure 121, JG29's affinity for DGKA is too low for any such inhibition to be apparent when assayed in liposomes with 8 mol% each JG29 and DOG.

Medium-Chain Diglycerides as Substrates for DGK

Introduction

The substrate specificity of interfacial enzymes such as eukaryotic DGKs includes two components: not only is affinity for the substrate itself important, but so too is the enzyme's ability to bind to the membrane where the substrate resides. If membrane-binding is impaired for some reason, enzymatic activity will be impaired even if the active site is still able to recognize and turn over the lipid substrate.

One way to resolve the question of substrate recognition from that of membrane binding is by using a short-chain substrate analog that is soluble in the aqueous phase without a membrane present. Such soluble substrates can therefore be used to answer the

question of, for example, whether membrane binding causes a conformational change in the enzyme that is required for catalytic turnover (in that case, an enzyme will not be able to use a soluble substrate analog). I wondered whether these eukaryotic DGK constructs could use short-chain diglycerides as substrates.

Results

1,2-dioctanoyl-*sn*-glycerol (DiC8) is a medium-chain diglyceride that has been previously shown to be a substrate for *D. discoideum* DGKA[47]. In that report, 4 mM DiC8 was solubilized by adding OG to 10 mM, below its CMC. When I added 10 mM OG to 4 mM DiC8, however, the mixture remained cloudy. The buffers were similar, but not identical: the buffer reported in Ostroski *et al.* was 50 mM Tris, 10 mM $MgCl_2$, 1 mM DTT, pH 7.4, and the one I used was 55 mM Tris, 5.5 mM $MgCl_2$, pH 7.4. Perhaps the additional $MgCl_2$ and/or the DTT was necessary for solubilizing the DiC8. I did not include DiC8 with 10 mM OG, with or without casein, as a negative control, but the activity of FLAG-DGKA in the presence of 4 mM DiC8 and 10 mM OG is no greater than the DGK activity measured from DOG micelles (without DGKA), with or without casein. As such, I was unable to demonstrate that purified FLAG-DGKA had measurable DGK activity using DiC8 as a substrate (Figure 122), but that could easily have been because of inadequately solubilized lipid substrate.

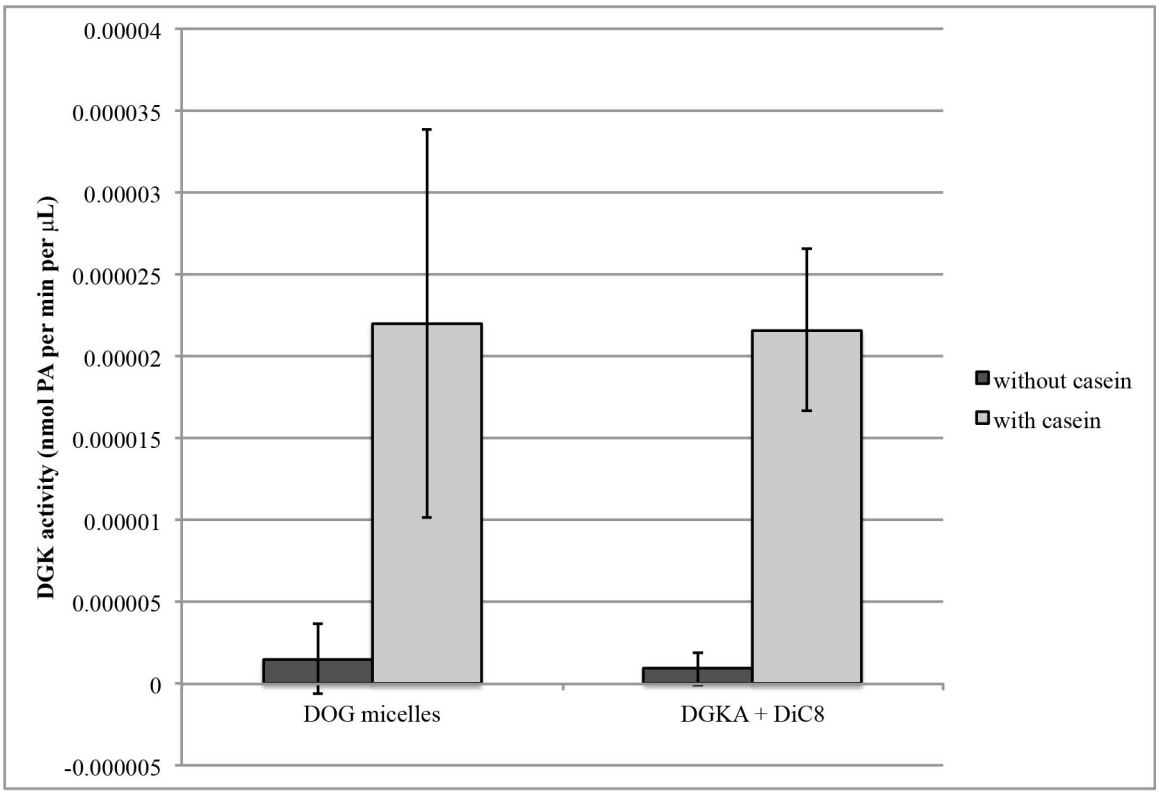

Figure 122. The DGK activity of purified FLAG-DGKA using DiC8 as a substrate is no greater than background activity in DOG micelles. I stored purified FLAG-DGKA (shown in **Figure 64**) in 50% glycerol at -80°C for nine days prior to assaying. The reaction included either 7 mM TX-100 micelles (9 mol% POPS, 6 mol% DOG) or else 4 mM DiC8 plus 10 mM OG, 40 mM Tris, pH 7.0, 4 mM $MgCl_2$, 8 mM NaF, 1 mM ATP, and 108 Ci per mmol [γ-^{32}P]-ATP, and, from the purified FLAG-DGKA, up to 5 μL purified FLAG-DGKA per 100 μL reaction, 2.5 mM TES, 0.25x PIC, 10 μg per μL FLAG peptide, and 2.5% (v/v) glycerol, and proceeded for 15 minutes at 30°C. I included 3 μL of concentrated stock solutions of casein per 50 μL reaction, where indicated. In duplicate: mean ± SD.

I was similarly unable to demonstrate that purified *H. sapiens* DGK-theta had measurable DGK activity on DiC8 (Figure 123). In fact, DGK-theta in the presence of casein in 4 mM DiC8 and 10 mM OG had even less DGK activity than casein in DOG micelles, without DGK-theta. Once again, the lack of activity might be due to insufficiently solubilized lipid substrate.

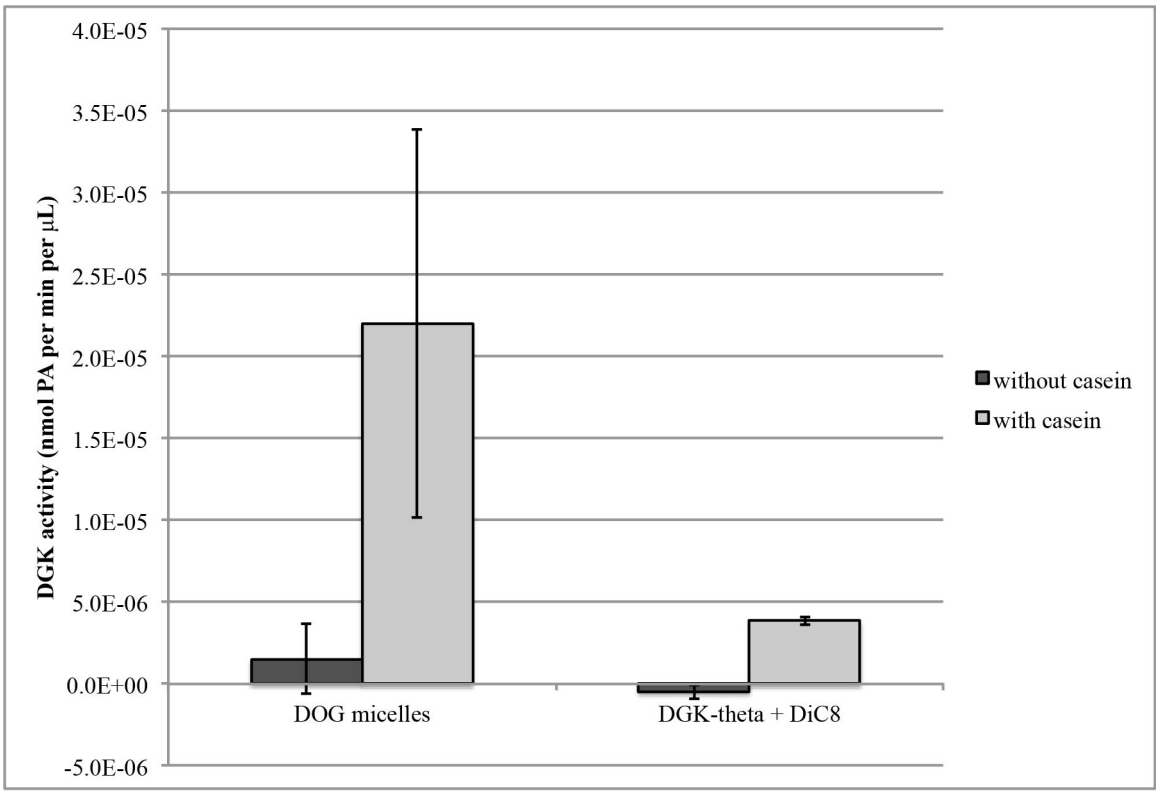

Figure 123. The DGK activity of purified *H. sapiens* DGK-theta using DiC8 as a substrate is no greater than background activity in DOG micelles. The reaction included either 7 mM TX-100 micelles (9 mol% POPS, 6 mol% DOG) or else 4 mM DiC8 plus 10 mM OG, 41 mM Tris, pH 7.0, 4.1 mM $MgCl_2$, 8.3 mM NaF, 1 mM ATP, and 108 Ci per mmol [γ-^{32}P]-ATP, and proceeded for 15 minutes at 30°C. I included 3 µL of concentrated stock solutions of casein per 50 µL reaction, where indicated. In duplicate: mean ± SD.

Because a vial of DiC8 had been labeled as DOG, I also inadvertently tested the DGK activity of alphacat in pT71myc expressed in *E. coli* using DiC8 incorporated into liposomes as a substrate. Induced lysate reproducibly had greater DGK activity than uninduced lysate when using DiC8 as a substrate (Figure 124 and Figure 89). I therefore concluded that alphacat was able to use DiC8 as a substrate. Because the DiC8 was incorporated into liposomes, however, the question of whether alphacat required an interface in order to catalyze the reaction remains unresolved.

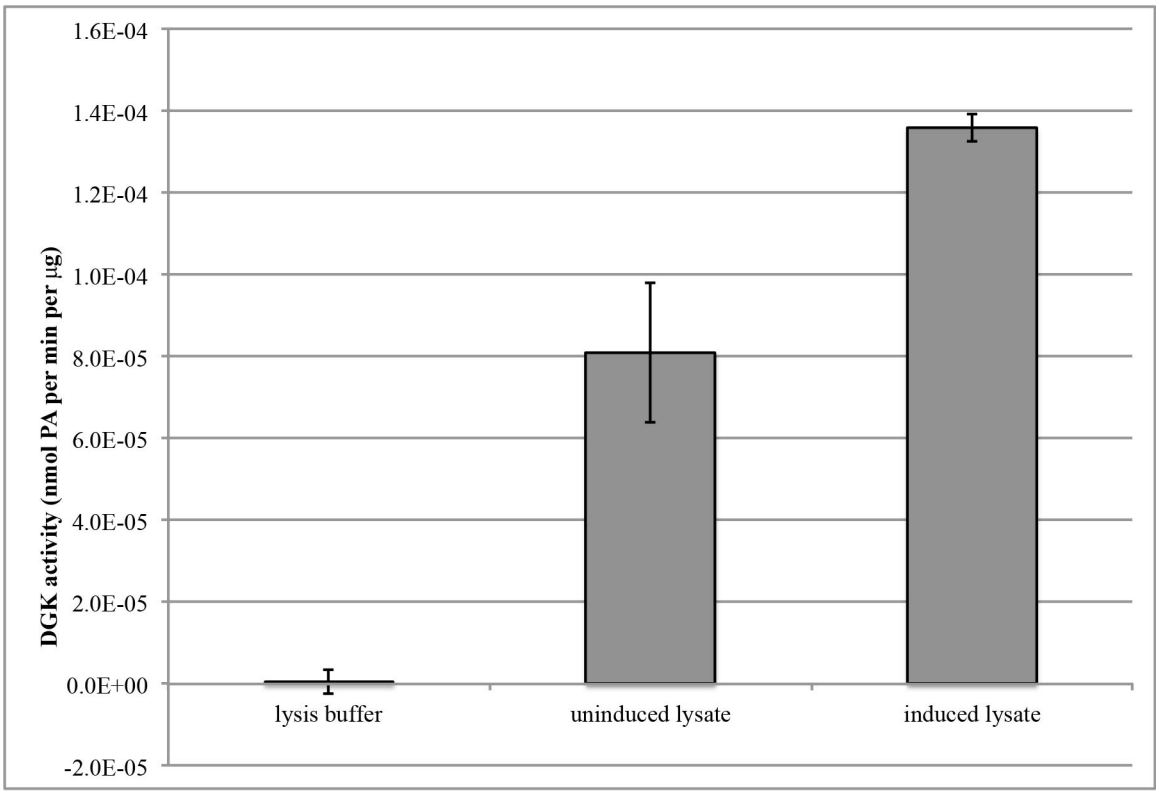

Figure 124. Rosetta™(DE3) lysate overexpressing alphacat in pT71myc is able to use DiC8 incorporated into liposomes as a substrate. DGK activity assay. The samples (**Figure 87**B and F) had been stored in 50% glycerol at -80°C for three weeks prior to assaying their DGK activity. The reaction included 7.5 mM liposomes (53:22:17:8::POPE:POPC:POPS:"DOG"), 49 mM HEPES, pH 8.0, 4.9 mM $MgCl_2$, 1 mM $CaCl_2$, 1 mM ATP, 0.25 mM Tris, 1.5 mM NaCl, 50 µM imidazole, 0.0025% (v/v) NP-40, 0.005x PIC, 0.25% (v/v) glycerol, 0.5 µL protein sample per 50 µL reaction, and 37.3 Ci per mmol [γ-^{32}P]-ATP, and proceeded for 15 minutes at 30°C. In duplicate: mean ± SD.

Conclusions

FLAG-DGKA purified from *D. discoideum* and purified *H. sapiens* DGK-theta were unable to use DiC8 as a substrate, but the lack of activity might have been due to insufficiently solubilized lipid substrate rather than a fundamental inability to use DiC8 as a substrate. *E. coli* lysate overexpressing alphacat in pT71myc was able to use DiC8 as a substrate, but because the DiC8 was incorporated into liposomes, however, the question of whether alphacat required an interface in order to catalyze the reaction remains unresolved.

Buffers and *H. sapiens* DGK-theta expressed and purified from HEK293T cells

Introduction

Studying the effects of different buffer components, such as salts or metal ions, can be of enormous practical value: if I find conditions that optimize DGK's enzymatic activity, I can use less enzyme in the assay, and it will be easier to study its enzymology. Buffer requirements can also lend insight into the chemistry of how DGK catalyzes the reaction. If an increase in salt decreases enzymatic activity, for example, it could be that an internal salt bridge or an ionic interaction between the protein and the substrate is important for catalysis. If metal chelators decrease enzymatic activity, for example, a metal ion might be important for properly positioning the substrate. I therefore studied how different buffer components affected enzymatic activity of purified eukaryotic DGKs.

Results

In order to test the effect of PIP_2 on DGK-theta activity, I needed to find extrusion conditions that could produce PIP_2 liposomes. I did eventually find a buffer that could be used to produce PIP_2 liposomes, but this buffer included 150 mM NaCl. Before testing the effect of PIP_2 on DGK, I therefore first tested the effect of NaCl in the assay buffer. Concentrations of NaCl up to 150 mM did not adversely affect the activity of DGK-theta purified from HEK293T cells, and at 200 mM, appeared to somewhat enhance DGK activity (Figure 125). The molecular basis for this effect could be that the salt ions neutralized charged regions of the enzyme, or destabilized exposed hydrophobic regions which the influenced the fold of the protein, but the practical implications were that I

could assay DGK-theta in the presence of the 150 mM NaCl required to produce PIP_2-containing liposomes.

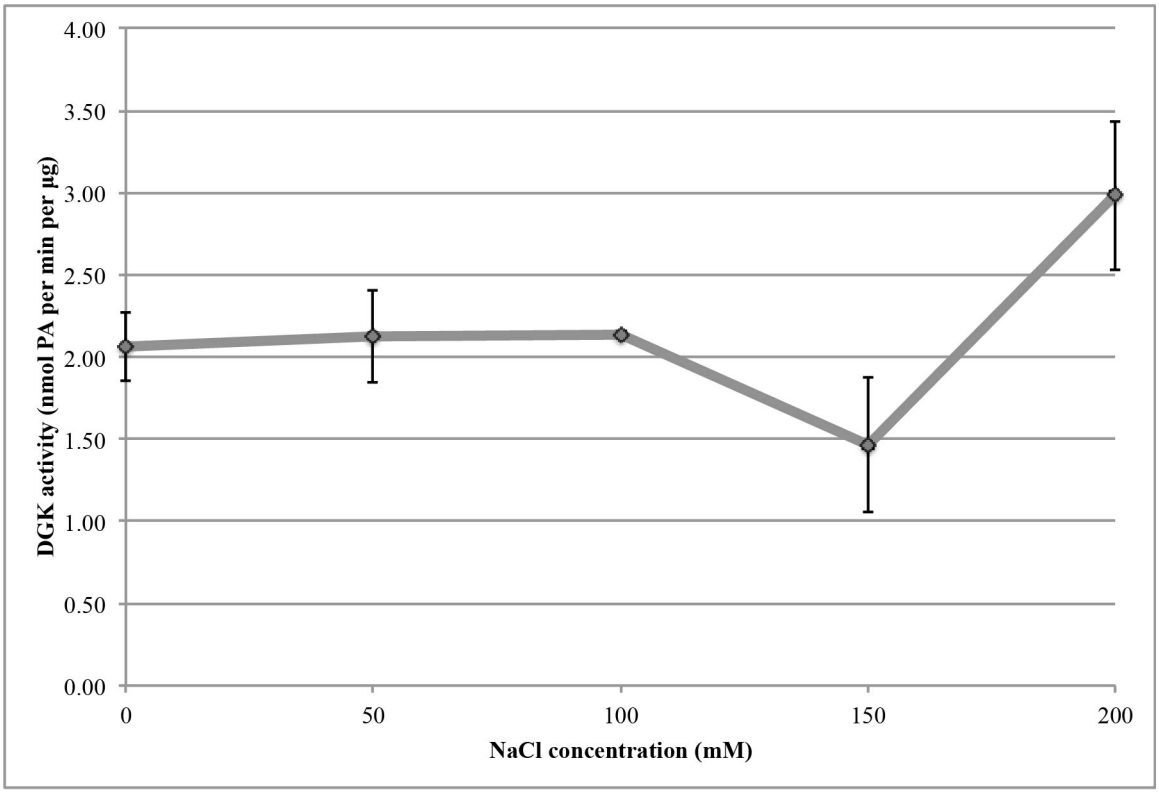

Figure 125. DGK activity of purified *H. sapiens* DGK-theta as a function of NaCl concentration. DGK activity assay. I first incubated purified DGK-theta for four hours on ice in 34% (w/v) sucrose, 1 mg/mL BSA. The reaction included in 7 mM Triton X-100 micelles (9 mol% POPS, 6 mol% DOG), 42 mM Tris, pH 8.2, 4.5 mM $MgCl_2$, 1 mM ATP, 5% (w/v) sucrose, 0.1 mg per mL BSA, 5 ng per µL purified DGK-theta, and 43.1 Ci per mmol [γ-^{32}P]-ATP, and proceeded for 15 minutes. In duplicate: mean ± SD.

The ADP Quest™ kinase assay kit uses propriety buffers, but its protocol warns that at least one of these proprietary reagents is incompatible with HEPES because of its sulfonic acid moiety. I therefore tested the effects of different non-sulfonic-acid-containing buffers whose buffering range include pH 7.5 on the activity of DGK-theta purified from HEK293T cells. Using HEPES at either 50 mM or 5 mM or using triethanolamine or tricine to buffer the assay buffer to pH 7.5, had no effect on DGK activity (Figure 126), as would be expected for reagents whose only role is buffering the

pH of the reaction. Sodium pyrophosphate reduced the DGK activity to undetectable levels (Figure 126), consistent with the pyrophosphate's precipitating out the magnesium so that none was left to coordinate the ATP in the reaction. Imidazole appeared to enhance DGK's activity somewhat (Figure 126). In addition to buffering the pH, imidazole could also be chelating ions such as nickel, zinc, or cobalt: if any of these metals ions inhibit DGK activity, then removing them from the protein by increasing the concentration of imidazole in the buffer would be predicted to increase DGK's activity. The primary sequence of DGK-theta, unlike the other mammalian isoforms, includes four consecutive histidines, which could be a site of chelating such metal ions.

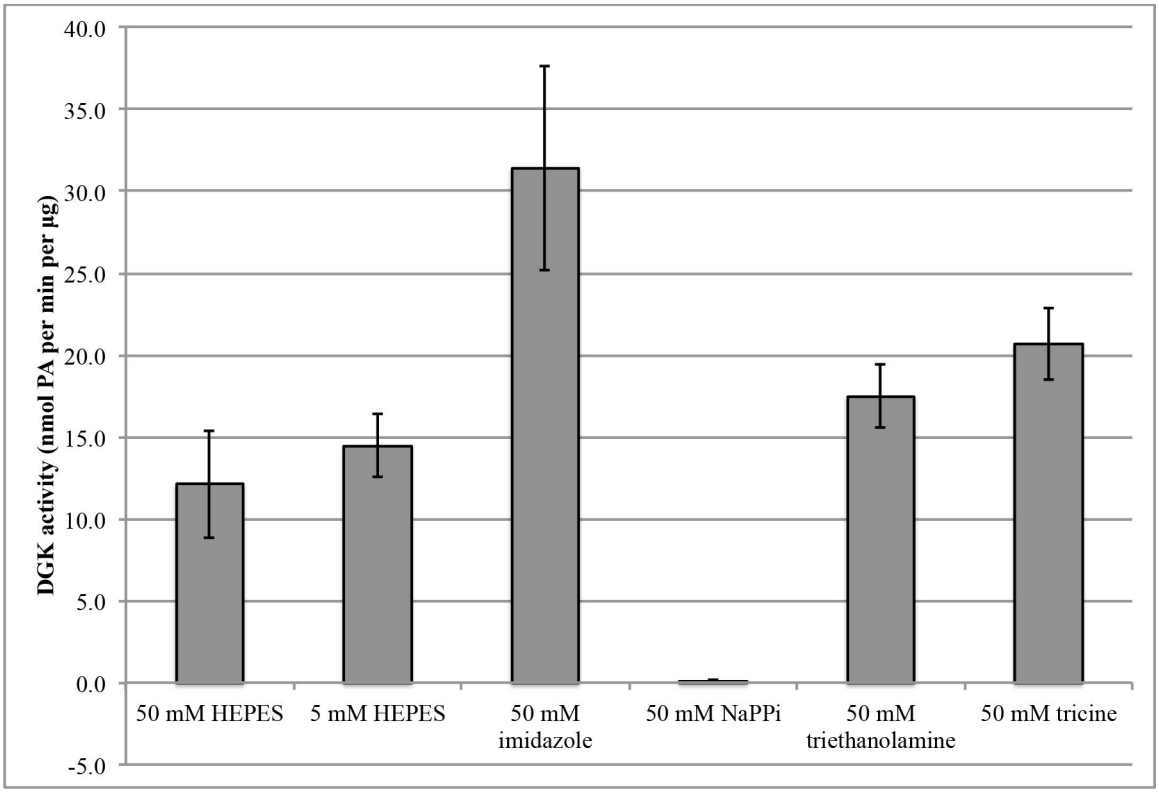

Figure 126. DGK-theta buffer test. DGK activity assay. I incubated purified DGK-theta in preincubation buffer (30 pg per µL DGK-theta, 0.5% (v/v) glycerol, 0.006% (v/v) DDM, 1.1 mM DTT, 0.11 µM histone H1, 1.1 mM liposomes (48:24:20:8::POPE:POPC:POPS:DOG), 111 mM NaCl, 0.11 mg per mL ovalbumin, 55.6 (or 5.6) mM of the buffer in question) on ice for ten minutes. The final reaction mixture included 1 mM liposomes, 100 mM NaCl, 1.5 mM $MgCl_2$, 1 mM ATP, 70.9 Ci per mmol [γ-^{32}P]-ATP, 0.1% (v/v) glycerol, 0.005% (v/v) DDM, 0.1 µM histone H1, 0.02 mg per mL ovalbumin, 1 mM

DTT, and 3.0 pg per μL purified DGK, and proceeded for 30 minutes at 37°C. In triplicate: mean ± SD. $NaPP_i$, sodium pyrophosphate.

Discussion and Conclusions

Concentrations of NaCl up to 150 mM did not adversely affect the activity of DGK-theta purified from HEK293T cells, and at 200 mM, appeared to somewhat enhance DGK activity (Figure 125). The molecular basis for this effect could be that the salt ions neutralized charged regions of the enzyme, or destabilized exposed hydrophobic regions which the influenced the fold of the protein, but the practical implications were that I could assay DGK-theta in the presence of the 150 mM NaCl required to produce PIP_2-containing liposomes. Imidazole appeared to enhance purified DGK-theta's activity somewhat (Figure 126). In addition to buffering the pH, imidazole could also be chelating ions such as nickel, zinc, or cobalt: if any of these metals ions inhibit DGK activity, then removing them from the protein by increasing the concentration of imidazole in the buffer would be predicted to increase DGK's activity. The primary sequence of DGK-theta, unlike the other mammalian isoforms, includes four consecutive histidines, which could be a site of chelating such metal ions.

Hirudin and *H. sapiens* DGK-Theta

Introduction

Hirudin is a thrombin inhibitor found in the salivary glands of the leech *Hirudo medicinalis*[143]. When conducting proteolysis studies on purified *H. sapiens* DGK-theta using thrombin as a protease, I observed that purified Fc-FLAG-DGK-theta bound to Protein A sepharose via an Fc epitope tag that had been digested with thrombin demonstrated higher DGK activity than DGK-theta bound to beads that had been digested

with thrombin in the presence of hirudin (Figure 127). I was surprised because I expected the beads with hirudin to show much higher DGK activity, because the DGK was still bound to the beads, whereas the DGK successfully digested by thrombin (without hirudin to inhibit it) was mostly detached and in the supernatant, not the beads (Figure 127**A**). I therefore wondered whether hirudin inhibits DGK in addition to thrombin (even though the Protein A sepharose beads had been extensively washed and only ~12 nU hirudin per μL would be predicted to remain in the samples assayed).

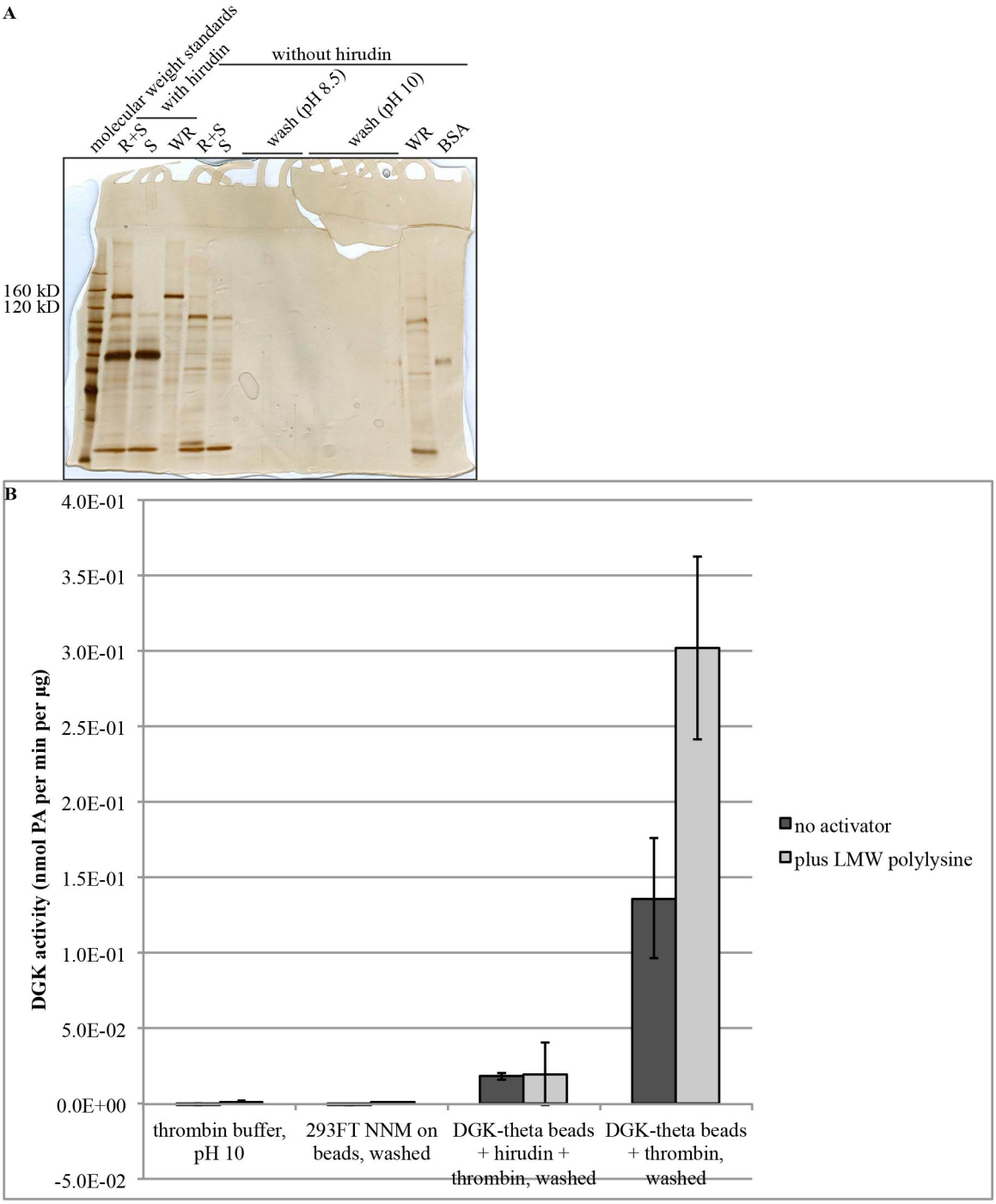

Figure 127. Purified Fc-FLAG-DGK-theta bound to Protein A sepharose via an Fc epitope tag that had been digested with thrombin demonstrates higher DGK activity than DGK-theta bound to beads that had been digested with thrombin in the presence of hirudin. I stored purified Fc-FLAG-DGK-theta bound to Protein A sepharose (shown in **Figure 84E** and **F**) in 50% glycerol at -80°C for four days before thawing and washing with thrombin buffer 1 (10 mM HEPES, 10 mM Tris, 100 mM NaCl, 0.1% (w/v) PEG-8000, pH 8.5). I then incubated 15% (v/v) of the purified Fc-FLAG-DGK-theta bound to Protein A sepharose with 10 mU per µL thrombin (Calbiochem (now EMD Millipore) 605195) in thrombin buffer 1 with or without 15 mU per µL hirudin (Sigma H7380) rotating at 4°C for 22 hours. I washed the

beads with thrombin buffer 1 and thrombin buffer 2 (same as thrombin buffer 2 except pH 10.0 instead of 8.5). **(A)** SDS-PAGE followed by silver staining. R+S, resin plus supernatant; S, supernatant; WR, washed resin. **(B)** DGK activity assay. The samples had been stored in 50% glycerol at -80°C for six weeks prior to assaying. The final reaction included 7.5 mM liposomes (53:22:17:8::POPE:POPC:POPS:DOG), 45 mM HEPES, pH 7.0, 130 mM NaCl, 4.4 mM $MgCl_2$, 1 mM Tris, 0.01% (w/v) PEG-8000, 1 mM ATP, 63.5 Ci per mmol [γ-^{32}P]-ATP, 1 mM DTT, 1.5 ng per µL LMW polylysine, up to 0.7% (v/v) glycerol, and up to 35 pg per µL purified DGK (as estimated from the silver stain in (A)), and proceeded for 15 minutes at 37°C. In duplicate: mean ± SD.

Results

When I tested the effects of increasing concentrations of hirudin on the activity of DGK-theta in liposomes, I was quite surprised to find that only the lowest concentration of hirudin tested inhibited the DGK activity of the non-nuclear membrane fraction of HEK293T cells transiently transfected with DGK-theta (Figure 128**A**). I repeated the experiment with even lower concentrations of hirudin, and confirmed that low, but not too low, concentrations of hirudin inhibit DGK-theta (Figure 128**B**). These concentrations are much lower than the concentrations that are effective for inhibiting thrombin digestion of DGK (Figure 127**A**).

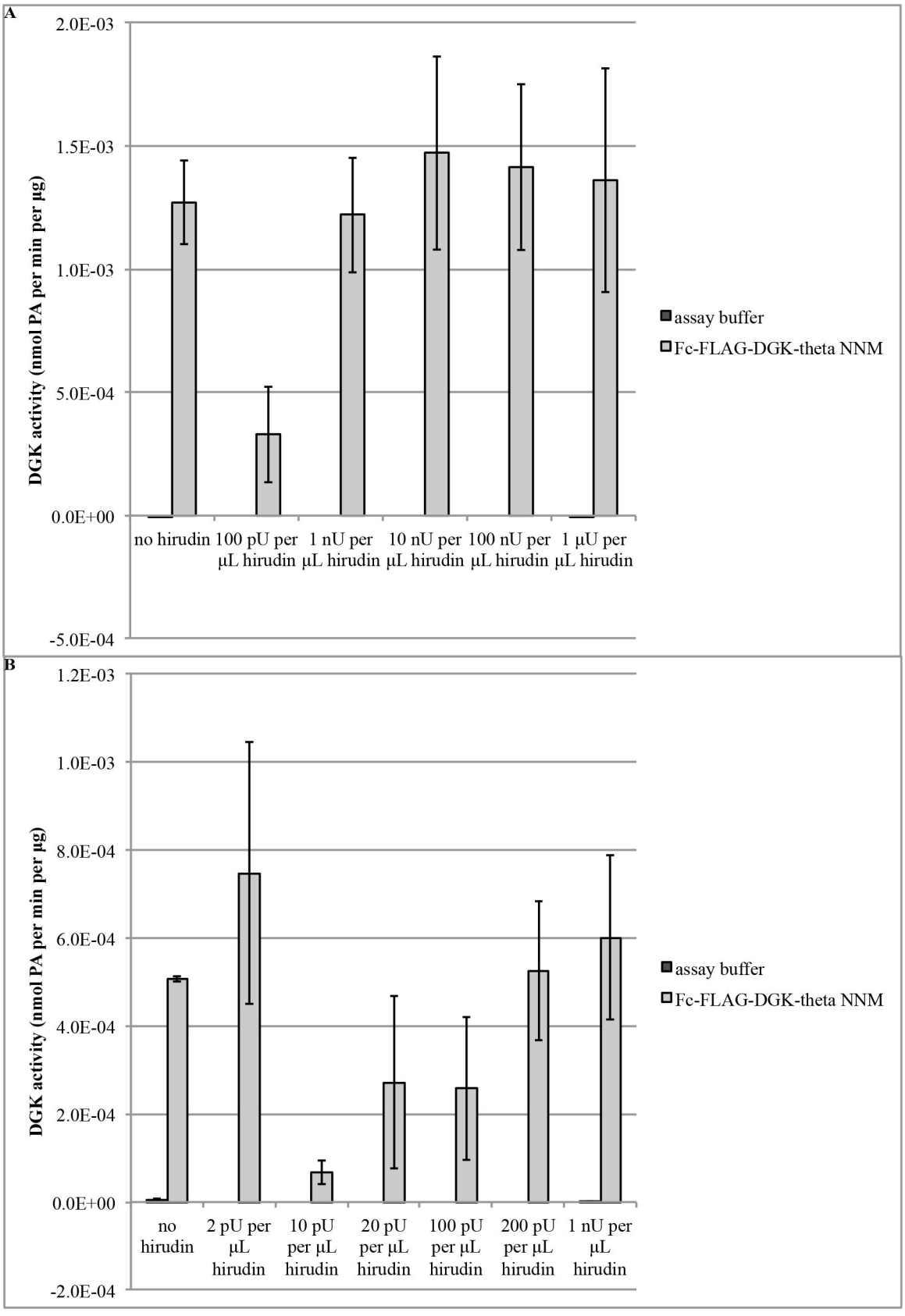
A
2.0E-03
1.5E-03
1.0E-03
5.0E-04
0.0E+00
-5.0E-04
DGK activity (nmol PA per min per µg)
no hirudin
100 pU per µL hirudin
1 nU per µL hirudin
10 nU per µL hirudin
100 nU per µL hirudin
1 µU per µL hirudin
assay buffer
Fc-FLAG-DGK-theta NNM
B
1.2E-03
1.0E-03
8.0E-04
6.0E-04
4.0E-04
2.0E-04
0.0E+00
-2.0E-04
DGK activity (nmol PA per min per µg)
no hirudin
2 pU per µL hirudin
10 pU per µL hirudin
20 pU per µL hirudin
100 pU per µL hirudin
200 pU per µL hirudin
1 nU per µL hirudin
assay buffer
Fc-FLAG-DGK-theta NNM

Figure 128. Low, but not too low, concentrations of hirudin inhibit the DGK activity of NNM from 293FT cells overexpressing Fc-FLAG-DGK-theta. DGK activity assays. **(A)** I stored the NNM of 293FT cells overexpressing Fc-FLAG-DGK-theta (the same expression shown in **Figure 84**E and F) in 50% glycerol at -80°C for seven weeks prior to assaying. The reaction included 7.5 mM liposomes (53:22:17:8::POPE:POPC:POPS:DOG), 49 mM HEPES, pH 7.0, 134 mM NaCl, 4.9 mM $MgCl_2$, 1 mM ATP, 98.3 Ci per mmol [γ-^{32}P]-ATP, 1 mM DTT, and, from the NNM, 6 μM EGTA, 11 μM EDTA, 50 ng per mL quinacrine, 0.01x PIC, 1 mM NAG, 60 μM $NaVO_4$, 120 μM NaF, 0.003% (v/v) NP-40, 0.6% (v/v) glycerol, and 40 ng per μL total protein (as measured by the Bio-Rad Protein Assay), and proceeded for 15 minutes at 37°C. In duplicate: mean ± SD. **(B)** I assayed aliquots of the same NNM samples three days later. The reaction conditions were the same as in (A) with the exception that [γ-^{32}P]-ATP was reduced to 43.1 Ci per mmol. In duplicate: mean ± SD.

Discussion and Conclusions

Low, but not too low, concentrations of hirudin inhibit the DGK activity of NNM from 293FT cells overexpressing Fc-FLAG-DGK-theta. One possible explanation for bell-shaped inhibition (low inhibition at low and high concentrations of inhibitor, and high inhibition at medium concentrations) could be that the hirudin aggregated, such that at high concentrations, the hirudin oligomerized into a form that did not inhibit DGK. The practical implications were that if I wanted to inhibit thrombin digestion of DGK and measure the effects on DGK activity, I would need to find another thrombin inhibitor.

PMSF and *H. sapiens* DGK-Theta

Introduction

Phenylmethylsulfonyl fluoride (PMSF) is another thrombin inhibitor. Before using it in the proteolysis studies, I wanted to first check whether PMSF inhibited DGK, as hirudin did.

Results

I first checked whether PMSF inhibited the DGK activity of lysates of HEK293T cells transiently transfected with Fc-FLAG-DGK-theta. When the concentrations of PMSF tested did not appear to inhibit the NNM of Fc-FLAG-DGK-theta-overexpressing

293FT cells (Figure 129**A**), I then tested whether PMSF, in the same range of concentrations, inhibited purified Fc-FLAG-DGK-theta on Protein A sepharose beads (the sample that would be used in the proteolysis study). The concentrations of PMSF tested did not appear to inhibit purified DGK-theta (Figure 129**B**), although the uncertainty of this experiment is admittedly large.

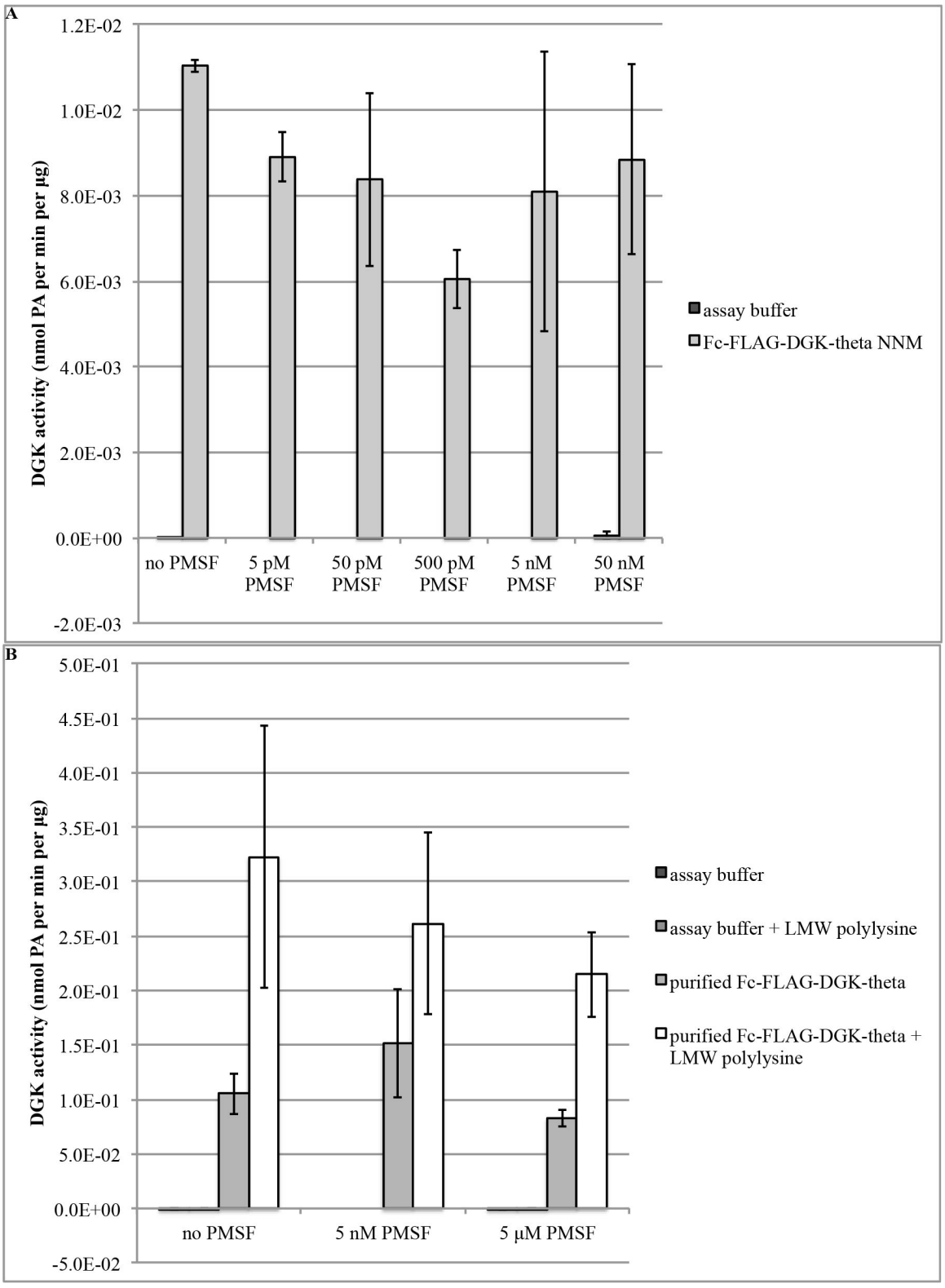

Figure 129. PMSF does not inhibit Fc-FLAG-DGK-theta at the concentrations tested. DGK activity assays. (A) I assayed aliquots of the same NNM samples shown in **Figure 128**B ten days later. The

reaction included 7.5 mM liposomes (53:22:17:8::POPE:POPC:POPS:DOG), 49 mM HEPES, pH 7.0, 135 mM NaCl, 4.9 mM $MgCl_2$, 1 mM ATP, 70.0 Ci per mmol [γ-^{32}P]-ATP, 1 mM DTT, and, from the NNM, 3 μM EGTA, 6 μM EDTA, 25 ng per mL quinacrine, 0.006x PIC, 0.6 mM NAG, 30 μM $NaVO_4$, 60 μM NaF, 0.002% (v/v) NP-40, 0.3% (v/v) glycerol, and 20 ng per μL total protein (as measured by the Bio-Rad Protein Assay), and proceeded for 15 minutes at 37°C. In duplicate: mean ± SD. **(B)** I stored purified Fc-FLAG-DGK-theta bound to Protein A sepharose in 50% glycerol at -80°C for nine weeks since it had been last thawed (**Figure 127**) prior to assaying. The reaction included 7.5 mM liposomes (53:22:17:8::POPE:POPC:POPS:DOG), 47 mM HEPES, pH 7.0, 133 mM NaCl, 4.7 mM $MgCl_2$, 1 mM ATP, 60.5 Ci per mmol [γ-^{32}P]-ATP, 1 mM DTT, 1.5 ng per μL LMW polylysine (or not), and, from the purified Fc-FLAG-DGK-theta, up to 0.5 mM Tris, 0.005% (v/v) glycerol, 0.8% (v/v) glycerol, and 70 pg per μL purified DGK-theta (as estimated from the silver stain in **Figure 127A**), and proceeded for 15 minutes at 37°C. In duplicate: mean ± SD.

Discussion and Conclusions

I had meant to test PMSF concentrations that would remain following digestion of the beads with 1 mM PMSF followed by extensive washing, but I made an arithmetical error, and the concentrations tested here are much larger than would remain. It is unknown whether lower, or higher, concentrations of PMSF would inhibit DGK, but the concentrations tested did not.

Photoaffinity Labels and *H. sapiens* DGK-Theta

Introduction

The laboratory of Professor Michael Best (Department of Chemistry, University of Tennessee) produced photoaffinity labels such that part of the molecule is diglyceride-like, and part of the molecule includes a photoactivatable crosslinker, such as benzophenone. Although these molecules were designed for photoaffinity labeling, because they are diglyceride analogs, I wondered whether they could serve as competitive inhibitors for diglyceride or even as substrates.

Compound 1 and H. sapiens *DGK-Theta*

The structure of compound **1** is shown in Figure 130. It includes two stearic acyl tails as well as the hydroxyl in the 3-position of the glycerol backbone common to 1,2-

diacylglycerol. It also includes benzophenone, a photoactivatable crosslinker, connected at the 1-position of the glycerol backbone via a linker left behind by the click chemistry used in its synthesis[144].

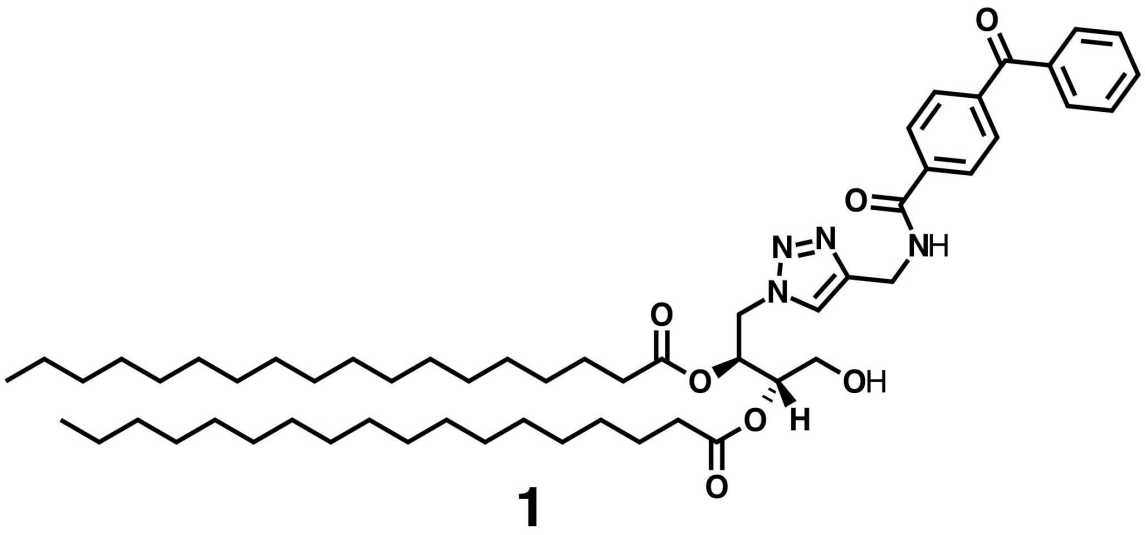

Figure 130. The structure of compound 1.

To confirm that compound **1** was the advertised concentration, and that it remained a single population and had not crosslinked to itself, I ran it on a TLC plate and charred the plate to estimate the intensity of the spots as compared to DOG standards of a known concentration (Figure 131). I estimated it to be perhaps 1/20th the advertised concentration.

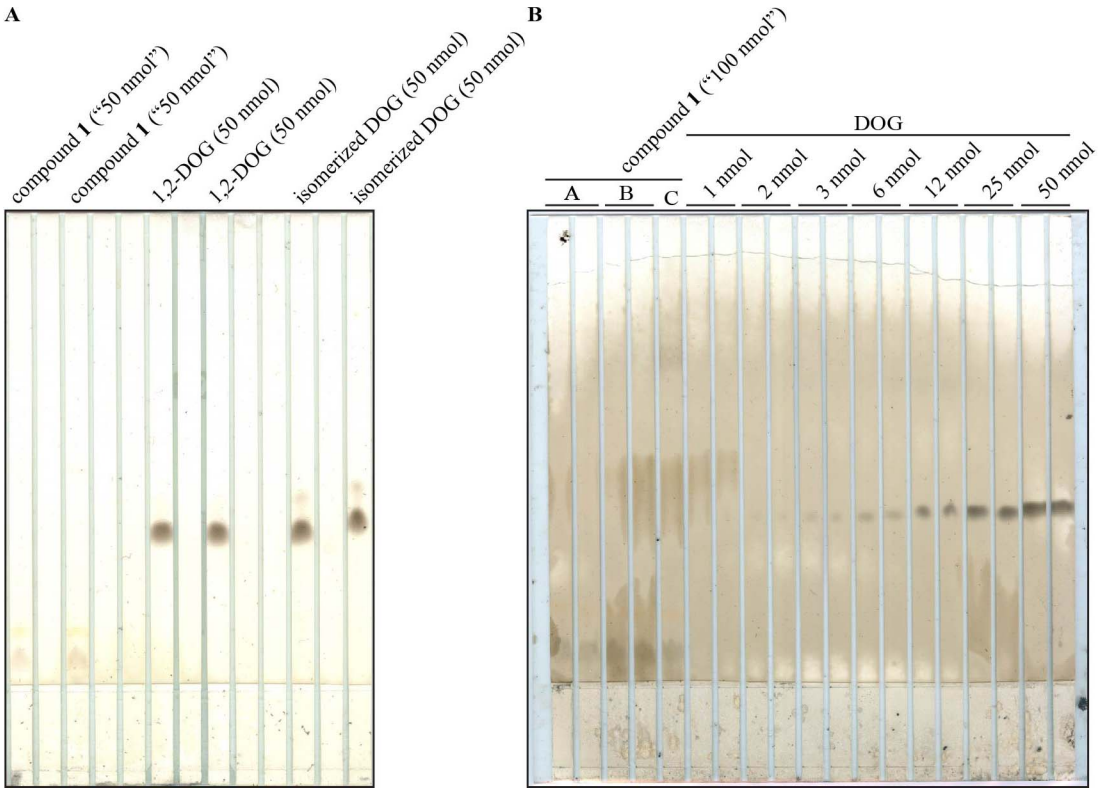

Figure 131. By visualizing the intensity of compound 1 compared to known amounts of DOG on charred TLC plates, I estimated it to be perhaps 1/20th the advertised concentration. (A) After spotting the indicated amounts onto a glass TLC plate, I ran the plate for one hour in fresh tank fluid (85:15:5::toluene:chloroform:methanol), which caused the solvent front to reach the top of the plate. "Isomerized DOG" had been stored in chloroform at room temperature for several months. **(B)** After spotting the indicated amounts onto a glass TLC plate, I ran the plate for thirty minutes in day-old tank fluid and marked the solvent front with pencil before drying. A, B, and C indicate different aliquots of compound 1.

Because compound **1** is a diglyceride analog, I wondered whether it could compete for DOG in a DGK activity assay. In order to work out whether compound **1** was competing for DOG, I first needed to get an idea of what, approximately, DGK-theta's K_m for DOG was. The $K_{m(surface)}$ of purified *H. sapiens* DGK-theta in the presence of polylysine has been reported[3], but only at a single concentration of total liposomes (0.2 mM), and DGK-theta's affinity for DOG has been shown to depend both on the surface and the total concentration of diglyceride[140]. I therefore thought it best to measure myself how DGK-theta's activity depends on the concentration of DOG. I was unable to extrude

liposomes containing 24 mol% DOG. For the liposomes I was able to extrude, at 0.5 mM liposomes, 3 mol% DOG provided much less than half-maximal activity, and I concluded that, at least at 0.5 mM liposomes, DGK-theta's $K_{m(surface)}$ for DOG is greater than 3 mol%, the value reported for 0.2 mM liposomes[3]. One possible source for the discrepancy is the fact that I used 9 mol% POPS, rather than the 8 mol% used for the reported $K_{m(surface)}$; on the other hand, the reported $K_{m(surface)}$ did not depend on whether the liposomes contained 0 or 8 mol% POPS, so POPS-dependence between 8 and 9 mol% seems unlikely. Another possible source of discrepancy is that the liposomes used for the reported $K_{m(surface)}$ used POPC, whereas I used egg PC. (Usually I also used POPC, but several packages of lipid that had been labeled "POPC" were, in fact, PC with other fatty acid chains, which meant that the laboratory ran out of POPC without realizing that I needed to order more.) The primary fatty acid chains in egg PC are palmitoyl and oleoyl, in roughly equal proportions, but other fatty acyls present at detectable levels include linoleoyl, stearoyl, arachidonoyl, palmitoleoyl, docosahexaenoyl, eicosatrienoyl, eicosadienoyl, and myristoyl chains[145]: it is a formal possibility that these other lipid constituents affect DGK's affinity for DOG.

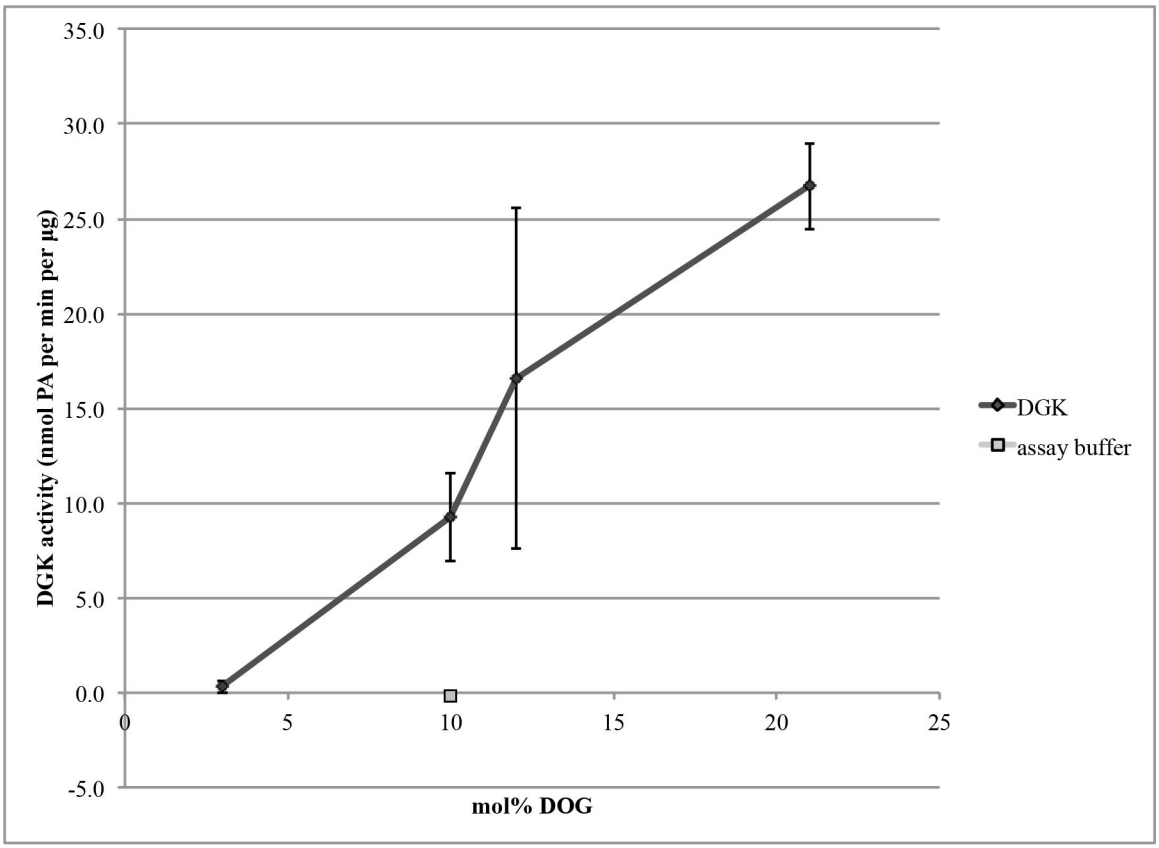

Figure 132. Using 0.2 mM liposomes containing 9 mol% POPS, DGK-theta's $K_{m(surface)}$ for DOG appears to be greater than 3 mol%. DGK activity assay. I first preincubated purified DGK-theta in preincubation buffer (43 pg per µL purified DGK-theta, 1.7% (v/v) glycerol, 0.005% (v/v) DDM, 4 µM histone H1, 1 mM DTT, 31 mM HEPES, pH 7.5, 62 mM NaCl) on ice for ten minutes. The final reaction mixture included 0.5 mM liposomes (2:1::POPE:egg PC; 9 mol% POPS, and the indicated concentrations of DOG), 44 mM HEPES, pH 7.5, 87 mM NaCl, 1 mM DTT, 1.5 mM $MgCl_2$, 1 mM ATP, 26.6 Ci per mmol [γ-^{32}P]-ATP, 0.1 µM histone H1, 0.1 mg per mL ovalbumin, 1.1 pg per µL purified DGK-theta, and 0.04% (v/v) glycerol, and proceeded for 15 minutes at 37°C. In triplicate: mean ± SD.

Of course, another possible explanation was that the liposomes were just bad for some reason, so I confirmed by testing two surface concentrations of DOG at three total concentrations of liposomes. I was also interested in learning what total concentration of liposomes would be required to confidently measure the activity of DGK in 3 mol% DOG liposomes (so that I could more accurately measure any inhibition from compound **1**), so I tested higher total liposome concentrations than in the previous experiment. I confirmed that the activity of purified DGK-theta depends on both the surface and total

concentration of DOG, and that at 2 mM liposomes, 3 mol% DOG gives much less than half-maximal activity, consistent with the $K_{m(surface)}$ of DGK for DOG's being greater than 3 mol% in 2 mM liposomes (Figure 133), as I had observed at 0.5 mM liposomes (Figure 132). This experiment was performed using POPC, not egg PC, so the PC fatty acyl chain constituents did not appear to be the issue, and, because the results repeated, bad liposomes did not appear to be the issue, either. Another possible explanation is that DGK's affinity for DOG does not depend on the total concentration of DOG, but rather on the total concentration of another lipid constituent of the liposomes, such as POPE, POPC, or POPS (although, as mentioned before, the reported $K_{m(surface)}$ did not depend on whether the liposomes contained 0 or 8 mol% POPS[3], and DGK-theta activity has been reported not to depend on PC or PE[140], so that explanation also seems unlikely, particularly when surface dilution kinetic theory predicts that a quasi-scooter would indeed depend on both the surface and the total concentration of lipid substrate). I therefore concluded that, under my experimental conditions, at liposome concentrations of 5 mM or lower, the $K_{m(surface)}$ of purified DGK-theta for DOG is considerably greater than 3 mol%.

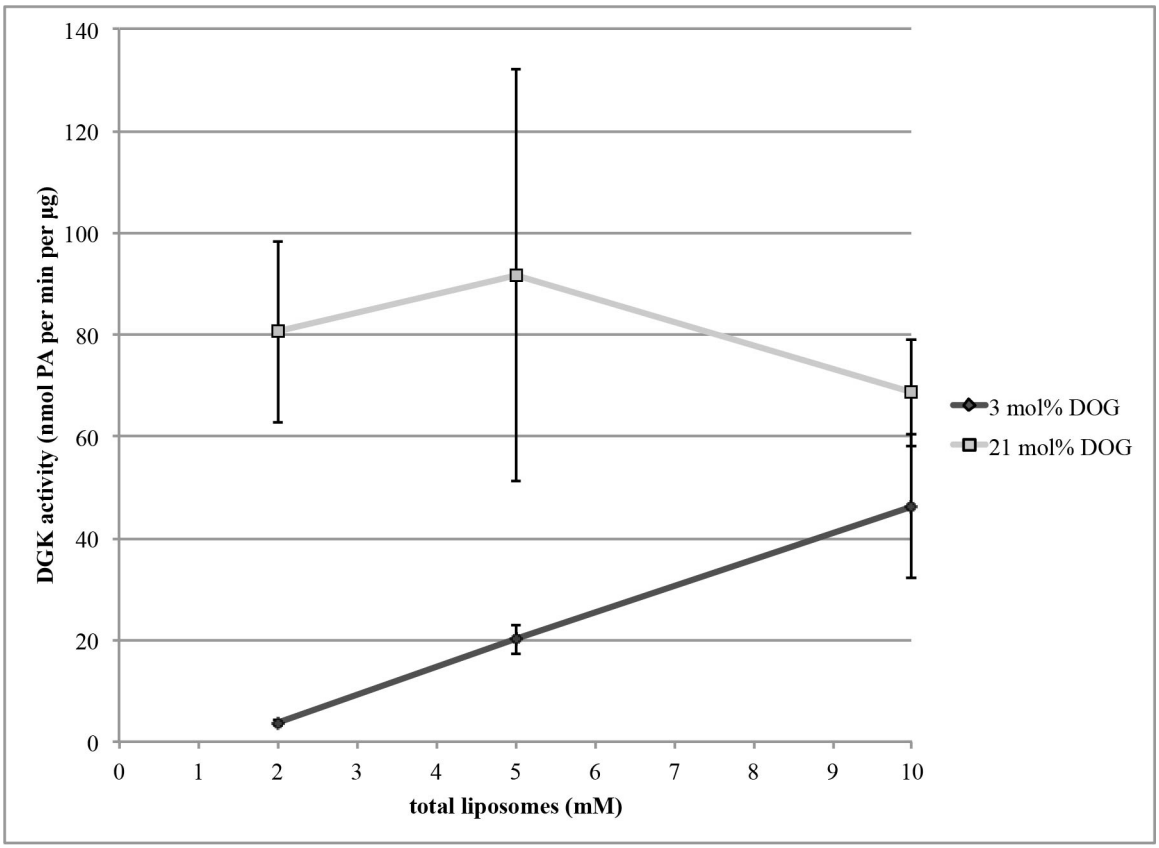

Figure 133. Purified DGK-theta's enzymatic activity depends on both the surface and total concentrations of DOG, and, using liposome concentrations of 5 mM or lower with 9 mol% POPS, its $K_{m(surface)}$ for DOG is greater than 3 mol%. DGK activity assay. I first preincubated purified DGK-theta in preincubation buffer (43 pg per µL purified DGK-theta, 1.7% (v/v) glycerol, 0.005% (v/v) DDM, 4 µM histone H1, 1 mM DTT, 31 mM HEPES, pH 7.5, 62 mM NaCl) on ice for ten minutes. The final reaction mixture included liposomes (2:1::POPE:POPC; 9 mol% POPS, and the indicated concentrations of DOG) at the concentrations shown, 44 mM HEPES, pH 7.5, 87 mM NaCl, 1 mM DTT, 1.5 mM $MgCl_2$, 1 mM ATP, 66.7 Ci per mmol [γ-^{32}P]-ATP, 0.1 µM histone H1, 0.1 mg per mL ovalbumin, 1.1 pg per µL purified DGK-theta, and 0.04% (v/v) glycerol, and proceeded for 15 minutes at 37°C. In triplicate: mean ± SD.

In an effort to boost the DGK activity I could detect, so that I could more reliably measure a decrease in activity that might be caused by compound **1**, I once again tested the dependence of DGK-theta's activity on the surface and total concentration of DOG, this time in the presence of 20 mol% POPS, a lipid that has been reported to activate DGK-theta[140]. In the presence of 20 mol% POPS, the activity of DGK-theta once again depended on both the total and surface concentration of DOG, and, at the liposome concentrations tested, the $K_{m(surface)}$ for DOG was considerably greater than 3 mol%.

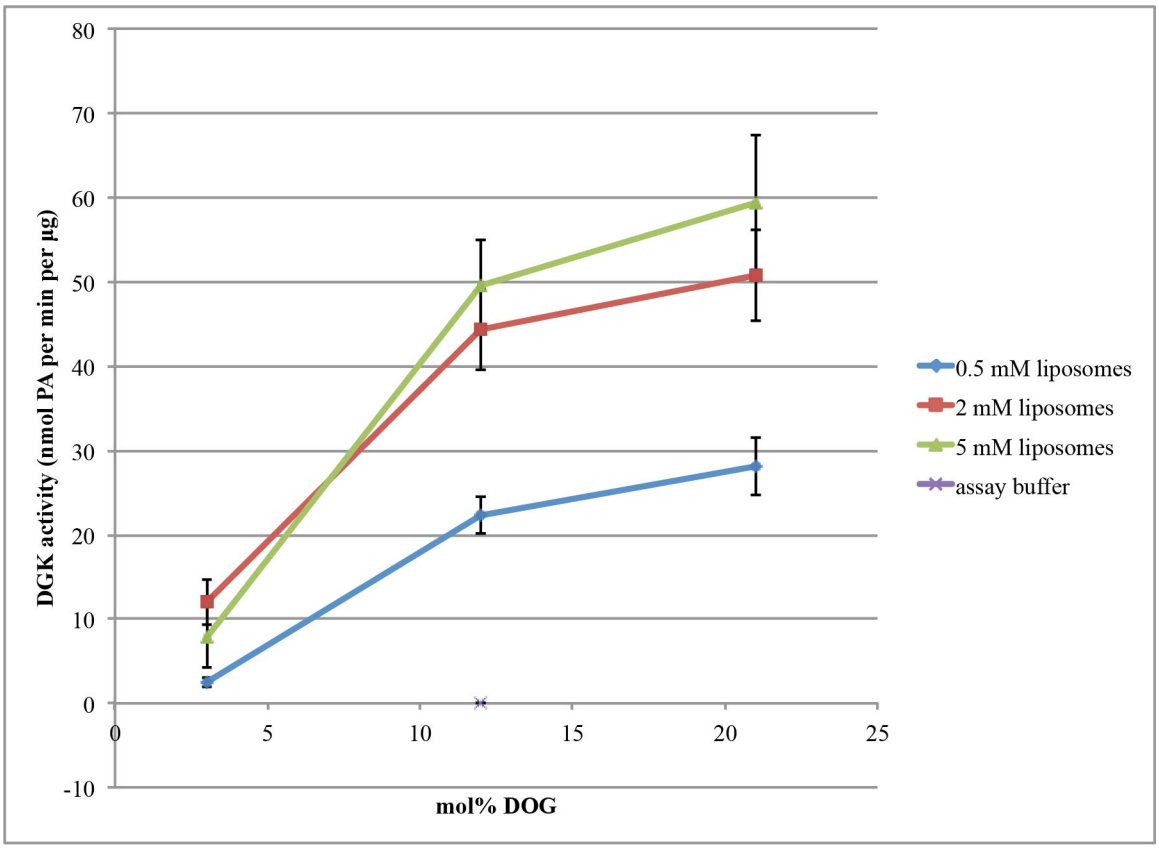

Figure 134. In the presence of 20 mol% POPS, the activity of purified DGK-theta depends on both the total and surface concentration of DOG, and, at the liposome concentrations tested, the $K_{m(surface)}$ for DOG is considerably greater than 3 mol%. DGK activity assay. I first preincubated purified DGK-theta in preincubation buffer (43 pg per µL purified DGK-theta, 1.7% (v/v) glycerol, 0.005% (v/v) DDM, 4 µM histone H1, 1 mM DTT, 31 mM HEPES, pH 7.5, 62 mM NaCl) on ice for ten minutes. The final reaction mixture included liposomes (2:1::POPE:POPC; 20 mol% POPS, and the indicated concentrations of DOG) at the concentrations shown, 44 mM HEPES, pH 7.5, 87 mM NaCl, 1 mM DTT, 1.5 mM $MgCl_2$, 1 mM ATP, 60.5 Ci per mmol [γ-^{32}P]-ATP, 0.1 µM histone H1, 0.1 mg per mL ovalbumin, 1.1 pg per µL purified DGK-theta, and 0.04% (v/v) glycerol, and proceeded for 15 minutes at 37°C. In triplicate: mean ± SD.

If I estimate the $K_{m(surface)}$ of DGK at 0.5 mM liposomes to be 6 mol%, then if an inhibitor is presented at the concentration equal to its K_i, then the maximum (and thus most easily detected) difference in activity between inhibited and uninhibited enzyme would be predicted to be at 8.5 mol% substrate (Figure 135). I therefore tested the effect of three different concentrations of compound **1** in the presence of 8.5 mol% DOG to see whether compound **1** might inhibit DGK-theta. I was quite surprised to observe that compound **1** activated DGK-theta, but not monotonically (Figure 136). One possible

explanation for such an effect could be that compound **1** was interacting with one higher-affinity site that helped the DGK bind the membrane (and encounter DOG) and also with another lower-affinity site that competed for DOG in the active site.

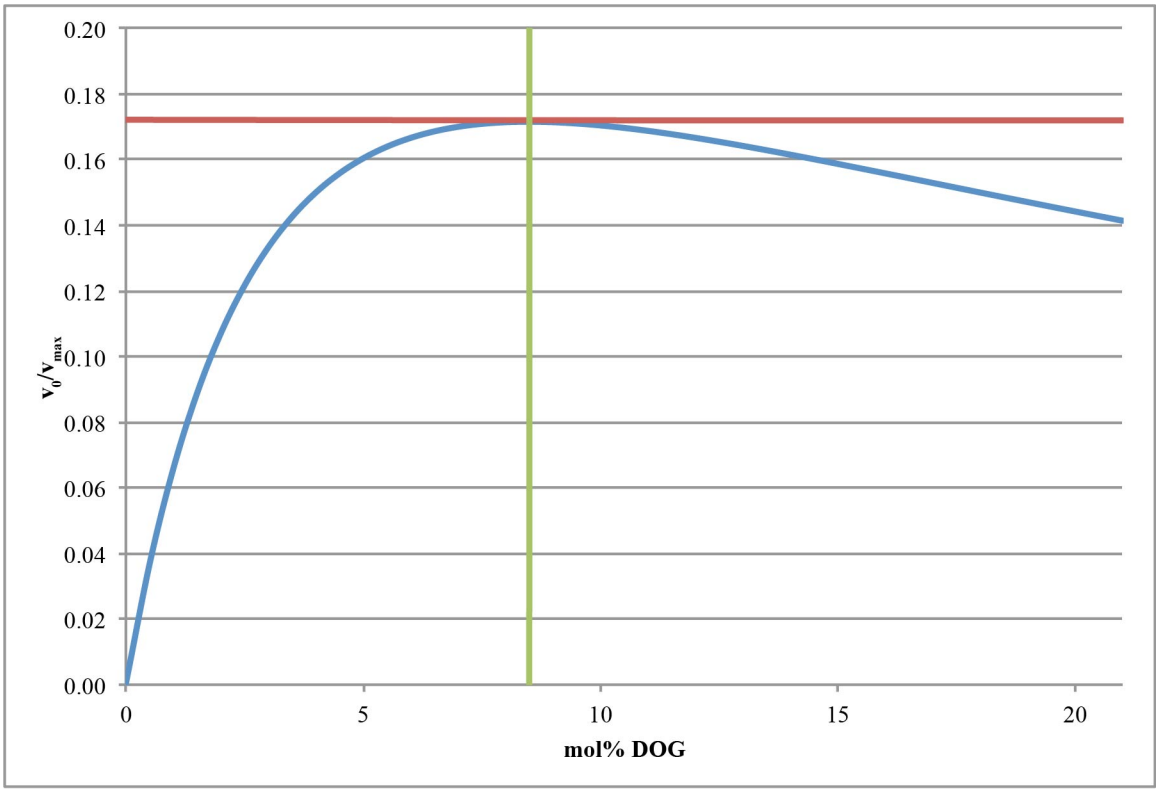

Figure 135. Predicted difference in activity between DGK with and without an inhibitor at the concentration equal to its K_i (blue), plotted as a function of mol% substrate, assuming a $K_{m(surface)}$ of 6 mol%. The red tangent marks where the derivative is equal to zero (i.e., where the local maximum is), and the green orthogonal indicates to which concentration of DOG that maximum corresponds (8.5 mol%).

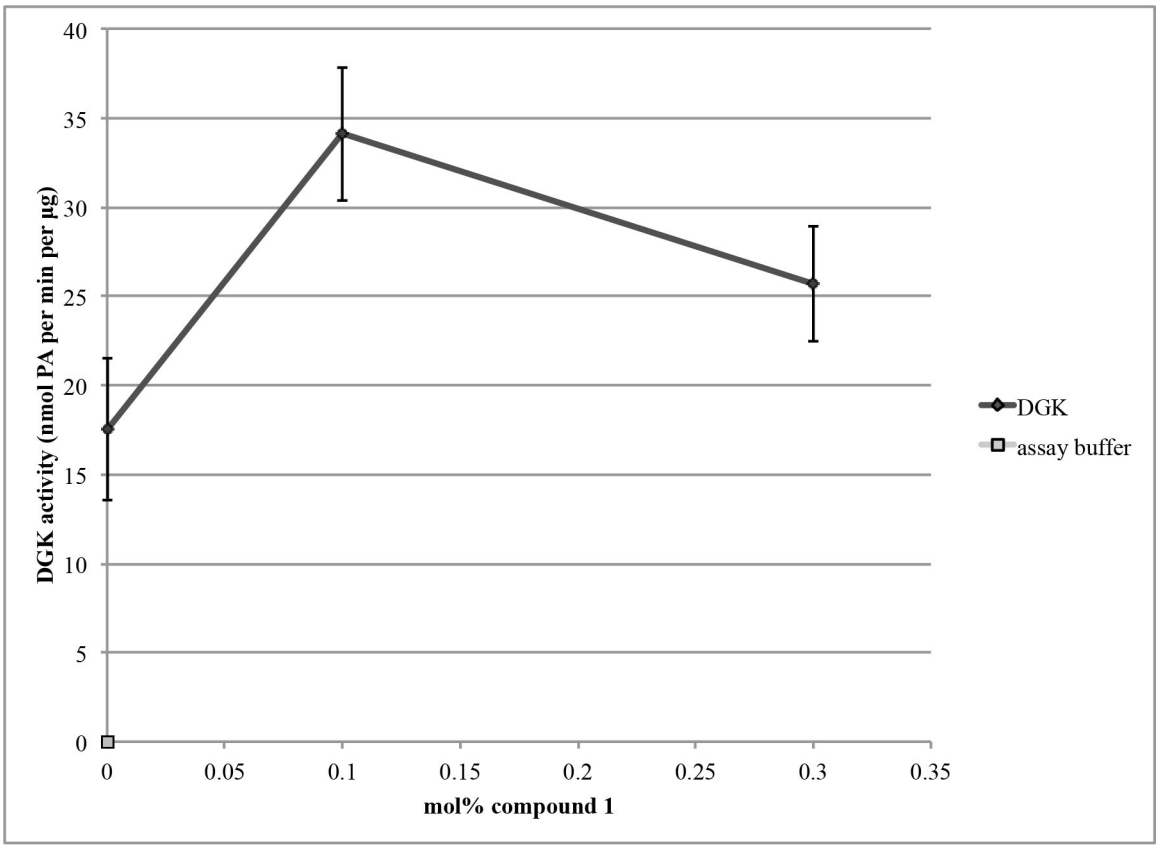

Figure 136. Compound 1 activates purified DGK-theta, but not monotonically. DGK activity assay. I first preincubated purified DGK-theta in preincubation buffer (43 pg per µL purified DGK-theta, 1.7% (v/v) glycerol, 0.005% (v/v) DDM, 0.5 µM histone H1, 1 mM DTT, 45 mM HEPES, pH 7.5, 91 mM NaCl) on ice for ten minutes. The final reaction mixture included 0.5 mM liposomes (2:1::POPE:POPC; 20 mol% POPS, 8.5 mol% DOG, and the indicated concentrations of compound 1), 46 mM HEPES, pH 7.5, 91 mM NaCl, 1 mM DTT, 1.5 mM MgCl2, 1 mM ATP, 60.5 Ci per mmol [γ-32P]-ATP, 0.1 µM histone H1, 0.1 mg per mL ovalbumin, 4.3 pg per µL purified DGK-theta, and 0.2% (v/v) glycerol, and proceeded for 15 minutes at 37°C. In triplicate: mean ± SD.

When I repeated the experiment, the difference in DGK activity between 0 mol% and ~0.4 mol% (the highest concentration I could successfully extrude) compound **1** in the presence of 4 mol% DOG and 20% POPS was not significant (Figure 137). Compound **1** certainly did not appear to inhibit DGK under these conditions. The concentration of compound **1** is admittedly low, especially in the context of 8.5 mol% DOG. It is entirely possible that compound **1** might inhibit DGK at higher

concentrations, but 0.4 mol% was the highest concentration I was able to incorporate into liposomes.

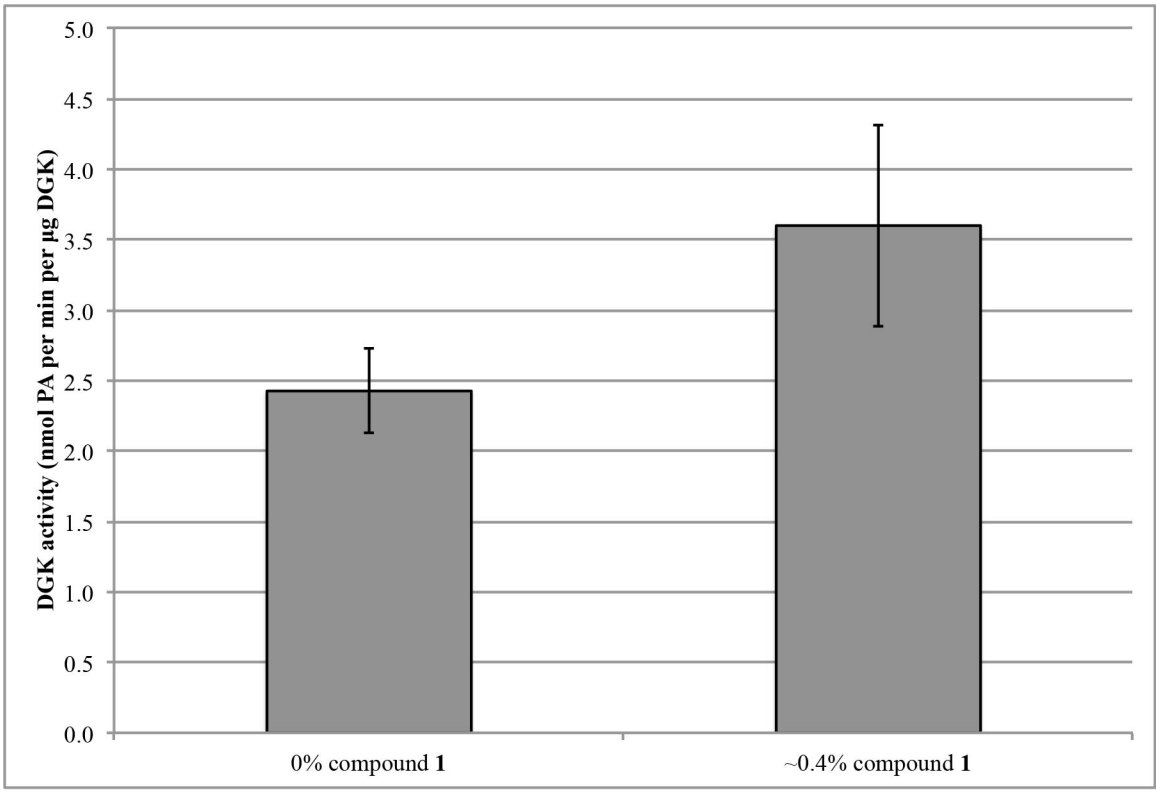

Figure 137. Compound 1 does not inhibit purified DGK-theta under the conditions tested. DGK activity assay. I first preincubated purified DGK-theta in preincubation buffer (43 pg per µL purified DGK-theta, 1.7% (v/v) glycerol, 0.005% (v/v) DDM, 0.1 µM histone H1, 1 mM DTT, 53 mM HEPES, pH 7.5, 105 mM NaCl) on ice for ten minutes. The final reaction mixture included 0.5 mM liposomes (2:1::POPE:POPC; 20 mol% POPS, 8.5 mol% DOG, and the indicated concentrations of compound 1), 46 mM HEPES, pH 7.5, 91 mM NaCl, 1 mM DTT, 1.5 mM MgCl2, 1 mM ATP, 49.9 Ci per mmol [γ-32P]-ATP, 0.1 µM histone H1, 0.1 mg per mL ovalbumin, 17 pg per µL purified DGK-theta, and 0.6% (v/v) glycerol, and proceeded for 15 minutes at 37°C. In triplicate: mean ± SD.

Because compound **1** has a hydroxyl in the 3-position of its carbon backbone, as diacylglycerol does, I also wondered whether DGK-theta could use compound **1** as a substrate. Compound **2** (whose structure is shown in Figure 138) is the product that would be produced by DGK-theta if it were to phosphorylate compound **1** on that hydroxyl. When I subjected compound **2** to TLC in the same solvent system used to separate radiolabeled PA from the other lipids in the DGK assay, compound **2** comigrated

with POPA (and, like compound **1**, was at a much lower concentration than advertised) (Figure 139). Therefore, if indeed DGK were phosphorylating compound **1**, the resulting radiolabeled compound **2** would be predicted to comigrate with radiolabeled PA, and could be contributing to the apparent increase in enzymatic activity seen in Figure 136 and Figure 137.

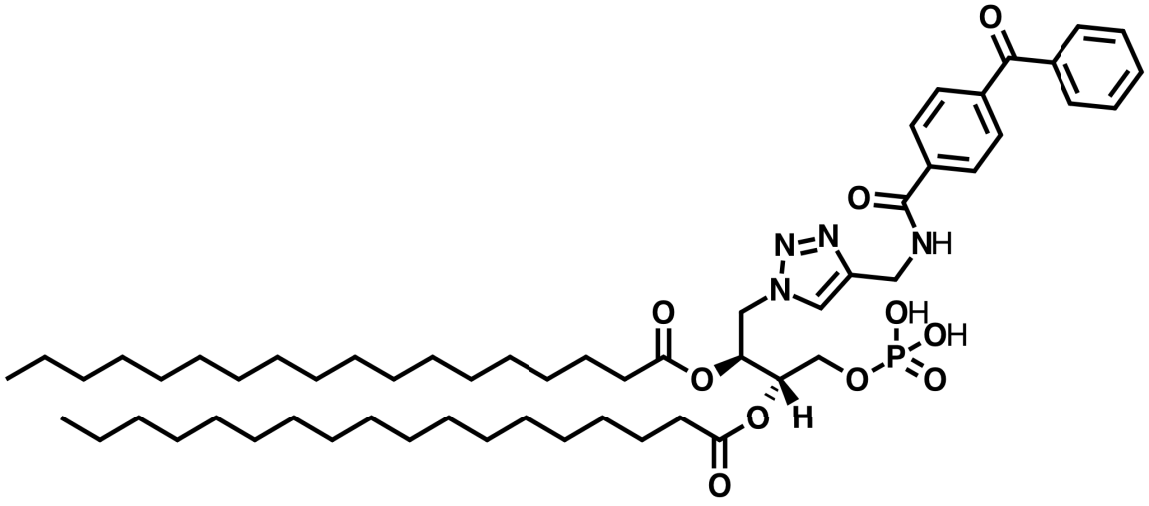

Figure 138. The structure of compound 2.

Figure 139. Compound 2 comigrates with POPA in the PA separation TLC solvent system. After spotting the indicated amounts onto a glass TLC plate, I ran the plate for one hour in fresh tank fluid and marked the solvent front with pencil. I visualized the plate by charring.

I therefore set out to test whether purified DGK-theta could use compound **1** as a substrate by measuring its enzymatic activity on liposomes containing compound **1** but not DOG. I could reproducibly detect greater activity in liposomes that contained ~0.4% compound **1** as compared to liposomes containing none (Figure 140). I therefore concluded that DGK-theta was able to use compound **1** as a substrate.

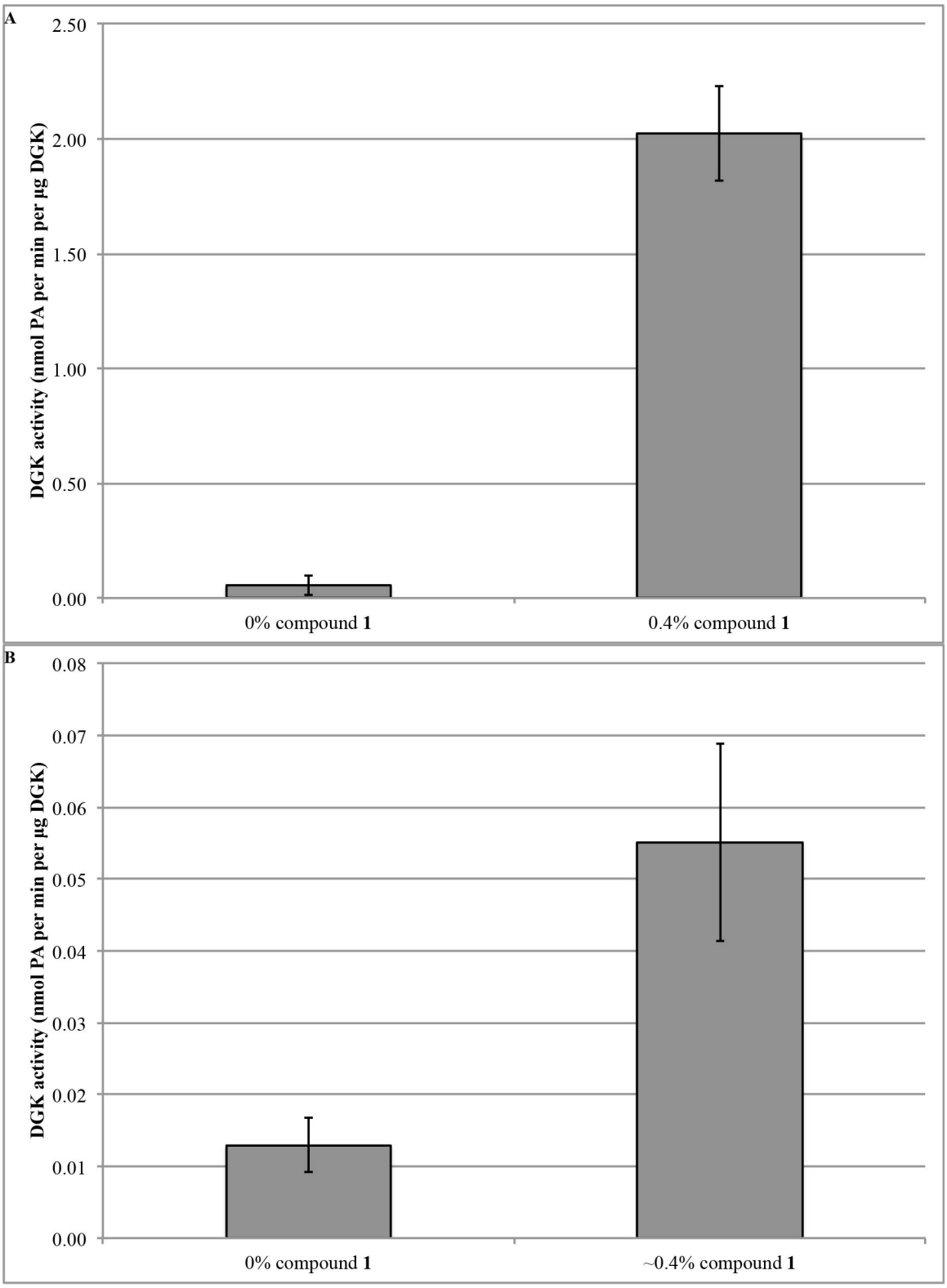

Figure 140. DGK-theta is able to use compound 1 as a substrate. DGK activity assays. **(A)** I first preincubated purified DGK-theta in preincubation buffer 1 (43 pg per µL purified DGK-theta, 1.7% (v/v)

glycerol, 0.005% (v/v) DDM, 1 μM histone H1, 1 mM DTT, 43 mM HEPES, pH 7.5, 85 mM NaCl) on ice for ten minutes. The final reaction mixture included 0.5 mM liposomes (2:1::POPE:POPC; 20 mol% POPS, and the indicated concentrations of compound 1), 46 mM HEPES, pH 7.5, 92 mM NaCl, 1 mM DTT, 1.5 mM MgCl2, 1 mM ATP, 49.9 Ci per mmol [γ-32P]-ATP, 0.1 μM histone H1, 0.1 mg per mL ovalbumin, 2.2 pg per μL purified DGK-theta, and 0.08% (v/v) glycerol, and proceeded for 15 minutes at 37°C. In triplicate: mean ± SD. **(B)** I first preincubated purified DGK-theta in preincubation buffer 2 (43 pg per μL purified DGK-theta, 1.7% (v/v) glycerol, 0.005% (v/v) DDM, 0.1 μM histone H1, 1 mM DTT, 53 mM HEPES, pH 7.5, 105 mM NaCl) on ice for ten minutes. The final reaction mixture included 0.5 mM liposomes (2:1::POPE:POPC; 20 mol% POPS, and the indicated concentrations of compound 1), 46 mM HEPES, pH 7.5, 91 mM NaCl, 1 mM DTT, 1.5 mM MgCl2, 1 mM ATP, 49.9 Ci per mmol [γ-32P]-ATP, 0.1 μM histone H1, 0.1 mg per mL ovalbumin, 17 pg per μL purified DGK-theta, and 0.6% (v/v) glycerol, and proceeded for 15 minutes at 37°C. In triplicate: mean ± SD.

Compound 3 and H. sapiens *DGK-Theta*

Compound **3** is, like compound **1**, a diglyceride-based photoaffinity probe using benzophenone as the photoactivatable crosslinker (Figure 141). Unlike compound **1**, whose fatty acyl chains are stearic (18 carbons), compound **3**'s fatty chains are palmitic (16 carbons). These chains are attached to the glycerol backbone not by an acyl connection, as in compound **1** and diglyceride, but rather by an ether connection, which is predicted to lead to less chain migration.

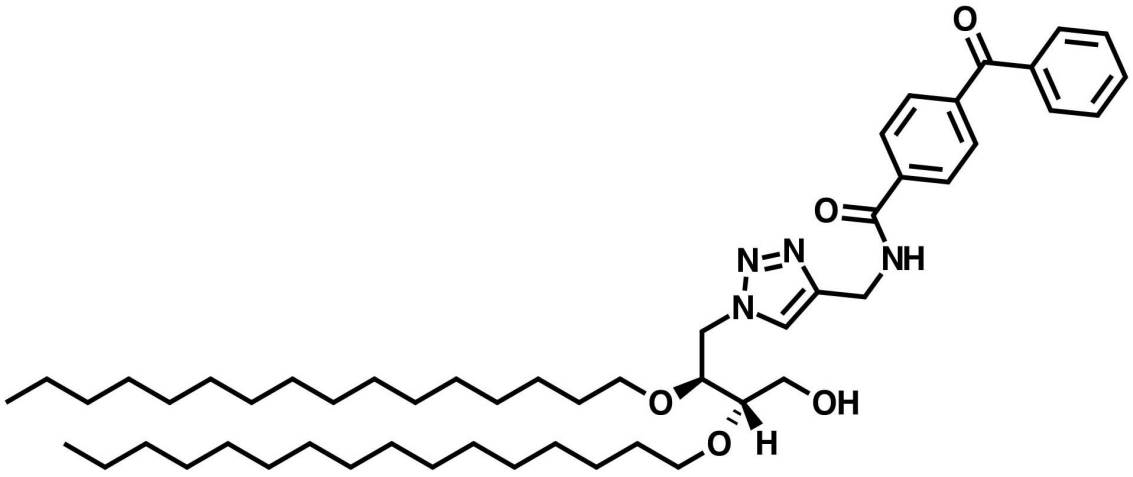

Figure 141. The structure of compound 3.

Especially given my experience with compounds **1** and **2**, I first wanted to measure the concentration of compound **3** before testing whether it was an inhibitor and/or a substrate of DGK. I therefore ran it on a TLC plate and charred the plate to

estimate the intensity of the spots as compared to DOG standards of a known concentration. Unlike compounds **1** and **2**, the intensity of the charred spots corresponding to compound **3** was consistent with the advertised concentration (Figure 142).

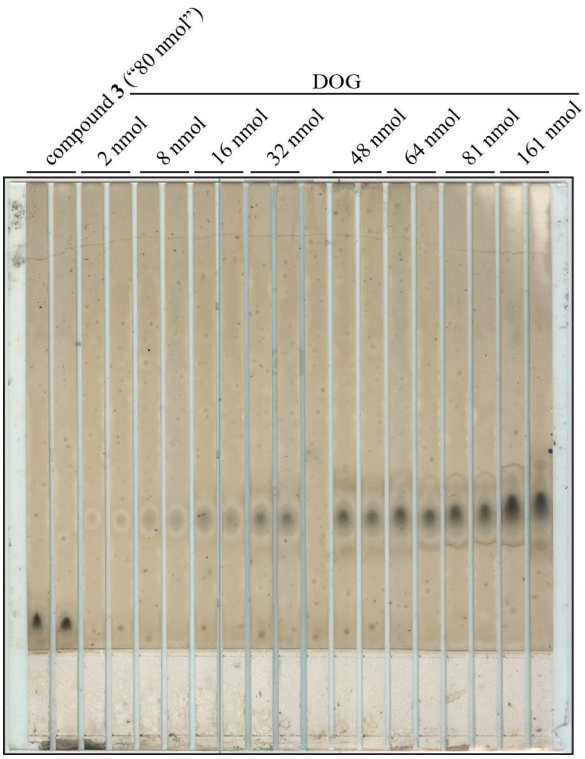

Figure 142. Compound 3's concentration is consistent with the advertised concentration. After spotting the indicated amounts onto a glass TLC plate, I ran the plate for thirty minutes in tank fluid (85:15:5::toluene:chloroform:methanol) that had been made eleven days previously, and marked the solvent front with a pencil before drying. I charred the plate to visualize the spots.

Because compound **3** is a diglyceride analog, I tested whether it could competitively inhibit DGK by measuring the enzymatic activity of purified DGK-theta in the presence of 4 mol% DOG and an increasing concentration of compound **3** (which went into liposomes much more easily than compound **1** did). Instead of inhibiting DGK, compound **3** appeared to enhance DGK-theta's enzymatic activity (Figure 143**A**). As with compound **1** (Figure 136**A**), the activation appeared to not be monotonic.

Activation of purified DGK-theta by compound **3** was reproducible, but not nearly as dramatic when repeated (Figure 143**B**). I therefore concluded that compound **3** activated DGK-theta's enzymatic activity using DOG as a substrate, possibly by helping the enzyme target to the membrane.

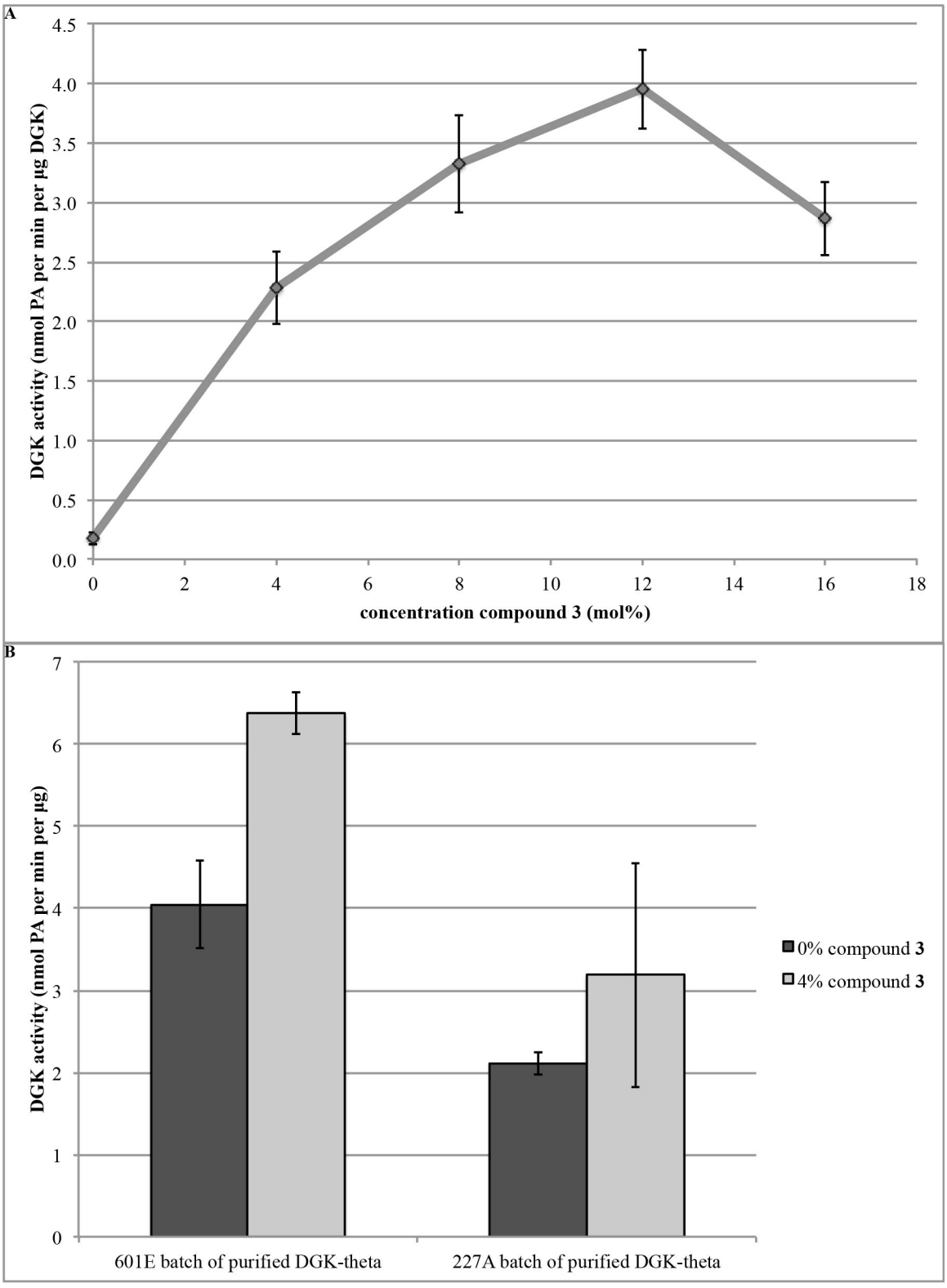

Figure 143. Compound 3 activates purified DGK-theta. DGK activity assays. **(A)** I first preincubated purified DGK-theta in preincubation buffer 1 (37 pg per µL purified DGK-theta, 1.4% (v/v) glycerol,

0.006% (v/v) DDM, 0.1 μM histone H1, 1 mM DTT, 0.1 mg per mL ovalbumin, 52 mM HEPES, pH 7.5, 105 mM NaCl) on ice for ten minutes. The final reaction mixture included 0.5 mM liposomes (2:1::POPE:POPC; 20 mol% POPS, 4 mol% DOG, and the indicated concentrations of compound 3), 51 mM HEPES, pH 7.5, 102 mM NaCl, 1 mM DTT, 0.75 mM MgCl2, 0.5 mM ATP, 85.0 Ci per mmol [γ-32P]-ATP, 0.05 μM histone H1, 0.05 mg per mL ovalbumin, 16 pg per μL purified DGK-theta, and 0.6% (v/v) glycerol, and proceeded for 25 minutes at 37°C. In triplicate: mean ± SD. **(B)** I first preincubated purified DGK-theta ("601E" and "227A" signify two different batches of purified DGK-theta) in preincubation buffer 1 (33 pg per μL purified DGK-theta, up to 1.3% (v/v) glycerol, 0.005% (v/v) DDM, 3 mM MgCl2, 0.2 μM histone H1, 1 mM DTT, 0.1 mg per mL ovalbumin, up to 41 mM HEPES, pH 7.5, up to 83 mM NaCl) on ice for ~thirty minutes. The final reaction mixture included 0.5 mM liposomes (2:1::POPE:POPC; 20 mol% POPS, 4 mol% DOG, and the indicated concentrations of compound 3), 28 mM HEPES, pH 7.5, 98 mM NaCl, 1 mM DTT, 1.5 mM MgCl2, 1 mM ATP, 85.0 Ci per mmol [γ-32P]-ATP, 0.1 μM histone H1, 0.05 mg per mL ovalbumin, 17 pg per μL purified DGK-theta, and 0.6% (v/v) glycerol, and proceeded for 15 minutes at 37°C. In triplicate: mean ± SD.

Compound **3** includes a hydroxyl in the 3-position of the glycerol backbone, as diglyceride does, so I therefore tested whether DGK-theta could use compound **3** as a substrate. (The migration pattern of the phosphorylated product of compound **3** in the PA separation TLC solvent system is unknown, so I do not know whether such radiolabeled spots might be contributing to the activity detected in Figure 143.) Early experiments measuring the enzymatic activity of DGK-theta on liposomes containing compound **3** without DOG were either inconclusive (Figure 144**B**, **C**) or demonstrated that DGK-theta's K_m for compound **3** must be very high (Figure 144**A**), but when I increased the liposome concentration to 7.5 mM, the DGK-theta concentration to 60 pg per μL, and the time of the assay to sixty minutes, I could confidently measure DGK-theta's activity on liposomes containing compound **3** to be greater than its activity on liposomes without compound **3** (Figure 145). I therefore concluded that compound **3** is a substrate for DGK-theta, albeit one with very low affinity.

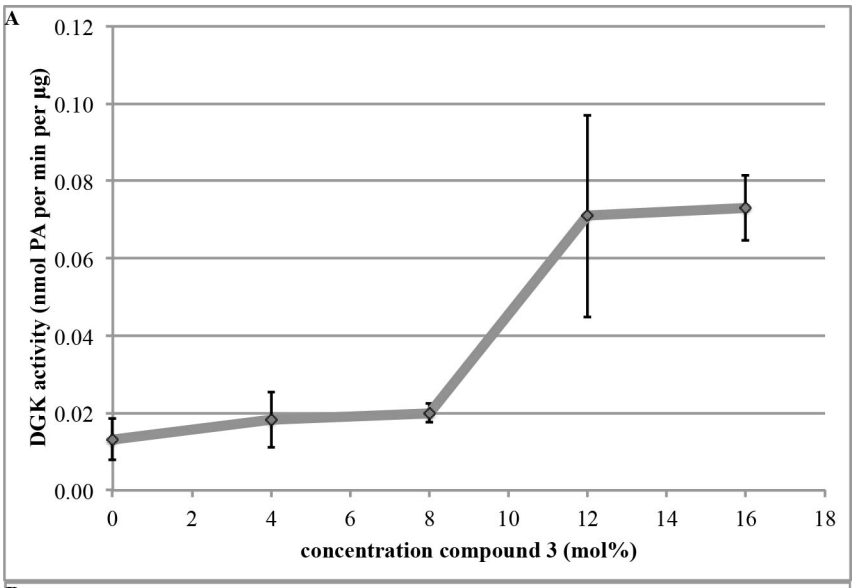
A
DGK activity (nmol PA per min per µg)
0.12
0.10
0.08
0.06
0.04
0.02
0.00
0
2
4
6
8
10
12
14
16
18
concentration compound 3 (mol%)

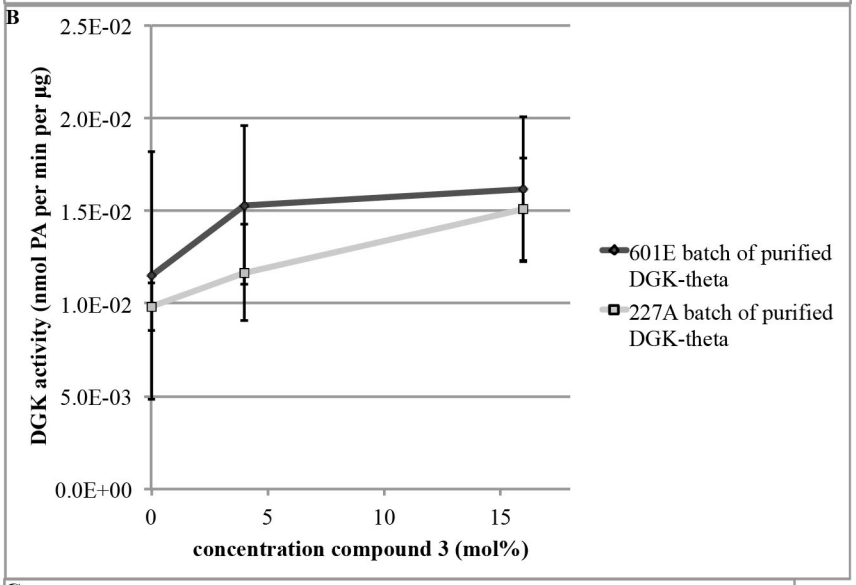
B
DGK activity (nmol PA per min per µg)
2.5E-02
2.0E-02
1.5E-02
1.0E-02
5.0E-03
0.0E+00
0
5
10
15
concentration compound 3 (mol%)
601E batch of purified DGK-theta
227A batch of purified DGK-theta

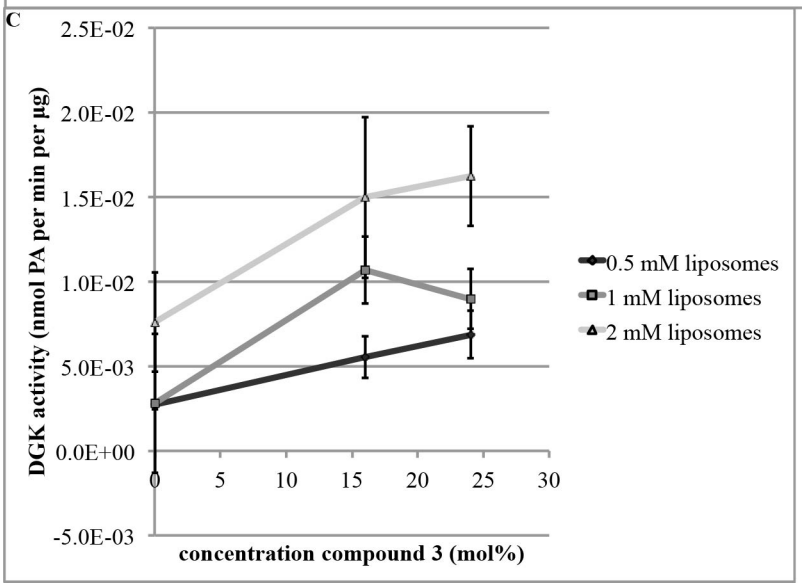
C
DGK activity (nmol PA per min per µg)
2.5E-02
2.0E-02
1.5E-02
1.0E-02
5.0E-03
0.0E+00
-5.0E-03
0
5
10
15
20
25
30
concentration compound 3 (mol%)
0.5 mM liposomes
1 mM liposomes
2 mM liposomes

Figure 144. Early experiments measuring the enzymatic activity of DGK-theta on liposomes containing compound 3 without DOG were inconclusive. DGK activity assays. **(A)** I first preincubated purified DGK-theta in preincubation buffer 1 (37 pg per µL purified DGK-theta, 1.4% (v/v) glycerol, 0.006% (v/v) DDM, 0.1 µM histone H1, 1 mM DTT, 0.1 mg per mL ovalbumin, 52 mM HEPES, pH 7.5, 105 mM NaCl) on ice for ten minutes. The final reaction mixture included 0.5 mM liposomes (2:1::POPE:POPC; 20 mol% POPS, and the indicated concentrations of compound 3), 51 mM HEPES, pH 7.5, 102 mM NaCl, 1 mM DTT, 0.75 mM MgCl2, 0.5 mM ATP, 85.0 Ci per mmol [γ-32P]-ATP, 0.05 µM histone H1, 0.05 mg per mL ovalbumin, 16 pg per µL purified DGK-theta, and 0.6% (v/v) glycerol, and proceeded for 25 minutes at 37°C. In triplicate: mean ± SD. **(B)** I first preincubated purified DGK-theta ("601E" and "227A" signify two different batches of purified DGK-theta) in preincubation buffer 2 (33 pg per µL purified DGK-theta, up to 1.3% (v/v) glycerol, 0.005% (v/v) DDM, 3 mM MgCl2, 0.2 µM histone H1, 1 mM DTT, 0.1 mg per mL ovalbumin, up to 41 mM HEPES, pH 7.5, up to 83 mM NaCl) on ice for ~thirty minutes. The final reaction mixture included 0.5 mM liposomes (2:1::POPE:POPC; 20 mol% POPS, and the indicated concentrations of compound 3) at the concentrations shown, 48 mM HEPES, pH 7.5, 95 mM NaCl, 1 mM DTT, 1.5 mM MgCl2, 1 mM ATP, 73.5 Ci per mmol [γ-32P]-ATP, 0.1 µM histone H1, 0.05 mg per mL ovalbumin, 17 pg per µL purified DGK-theta, and 0.6% (v/v) glycerol, and proceeded for 15 minutes at 37°C. In triplicate: mean ± SD. **(C)** I first preincubated purified DGK-theta in preincubation buffer 3 (80 pg per µL purified DGK-theta, 2% (v/v) glycerol, 0.005% (v/v) DDM, 3 mM MgCl2, 0.2 µM histone H1, 1 mM DTT, 0.1 mg per mL ovalbumin, 40 mM HEPES, pH 7.5, 80 mM NaCl) on ice for half an hour. The final reaction mixture included liposomes (2:1::POPE:POPC; 20 mol% POPS, and the indicated concentrations of compound 3) at the concentrations shown, 28 mM HEPES, pH 7.5, 98 mM NaCl, 1 mM DTT, 1.5 mM MgCl2, 1 mM ATP, 85.0 Ci per mmol [γ-32P]-ATP, 0.1 µM histone H1, 0.05 mg per mL ovalbumin, 40 pg per µL purified DGK-theta, and 1% (v/v) glycerol, and proceeded for thirty minutes at 37°C. In triplicate: mean ± SD.

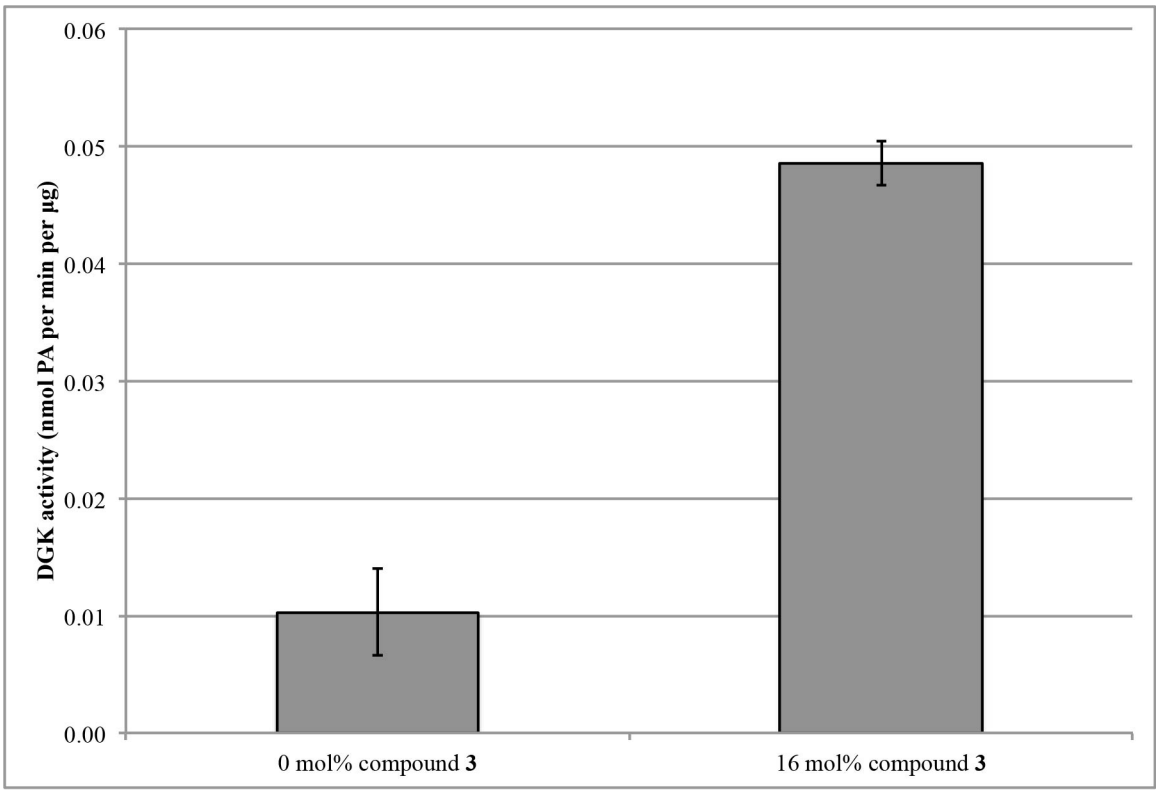

Figure 145. DGK-theta can use compound 3 as a substrate. DGK activity assay. I first preincubated purified DGK-theta in preincubation buffer 1 (150 pg per µL purified DGK-theta, 6% (v/v) glycerol, 0.006% (v/v) DDM, 0.3 µM histone H1, 1 mM DTT, 0.1 mg per mL ovalbumin, 63 mM HEPES, pH 7.5,

126 mM NaCl) on ice for half an hour. The final reaction mixture included (2:1::POPE:POPC; 20 mol% POPS, and the indicated concentrations of compound 3), 50 mM HEPES, pH 7.5, 100 mM NaCl, 1 mM DTT, 1.5 mM $MgCl_2$, 1 mM ATP, 98.3 Ci per mmol [γ-^{32}P]-ATP, 0.1 μM histone H1, 0.05 mg per mL ovalbumin, 60 pg per μL purified DGK-theta, and 2% (v/v) glycerol, and proceeded for one hour at 37°C. In triplicate: mean ± SD.

Compound 4 and H. sapiens *DGK-Theta*

Compound **4** is, like compounds **1** and **3**, a diglyceride-based photoaffinity probe using benzophenone as the photoactivatable crosslinker (Figure 146). Like compound **3**, its fatty chains are palmitic and attached to the glycerol backbone via an ether connection. Unlike compounds **1**, **2**, and **3**, it was not synthesized using click chemistry, and as a result, it has a shorter linker between its benzophenone moiety and its DAG-like moiety.

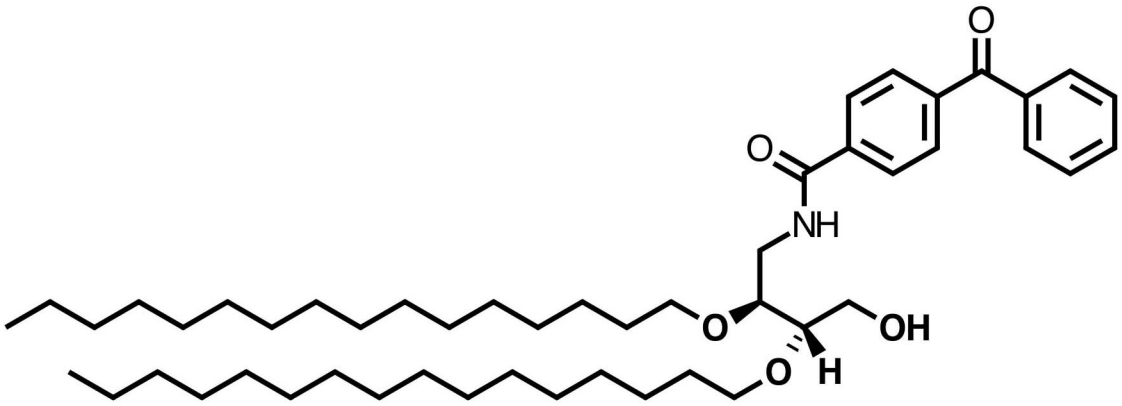

Figure 146. The structure of compound 4.

Especially given my experience with compounds **1** and **2**, I first wanted to measure the concentration of compound **4** before testing whether it was an inhibitor and/or a substrate of DGK. I therefore ran it on a TLC plate and charred the plate to estimate the intensity of the spots as compared to DOG standards of a known concentration. Unlike compounds **1** and **2**, but like compound **3**, the intensity of the

charred spots corresponding to compound **4** was consistent with the advertised concentration (Figure 147).

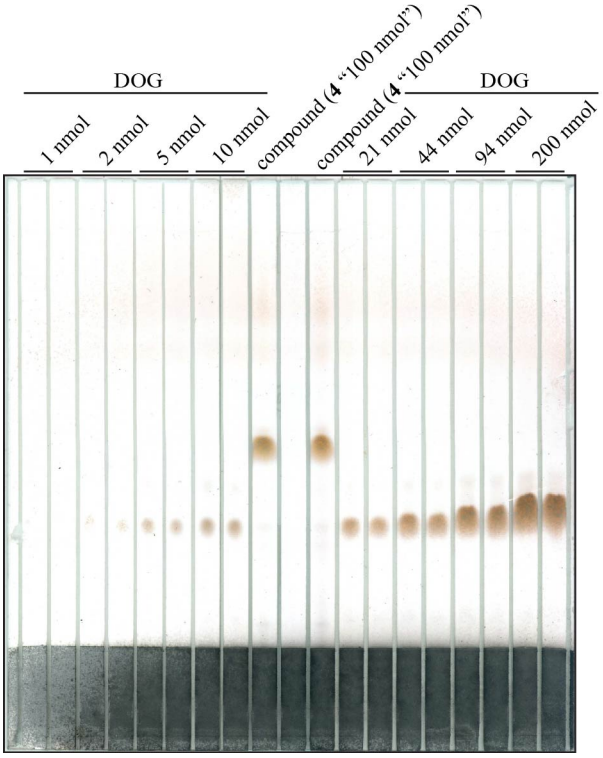

Figure 147. Compound 4's concentration is consistent with the advertised concentration. After spotting the indicated amounts onto a glass TLC plate, I ran the plate for thirty minutes in fresh tank fluid (85:15:5::toluene:chloroform:methanol). I charred the plate to visualize the spots.

Because compound **4** is a diglyceride analog, I tested whether it could competitively inhibit DGK by measuring the enzymatic activity of purified DGK-theta in the presence of 5 mol% DOG and an increasing concentration of compound **4** (which went into liposomes much more easily than compound **1** did, but not so easily as compound **3**). Compound **4** did not appear to inhibit DGK-theta (Figure 148), and, unlike compounds **1** (Figure 136 and Figure 137) and **3** (Figure 143), it did not appear to activate DGK-theta, either (Figure 148).

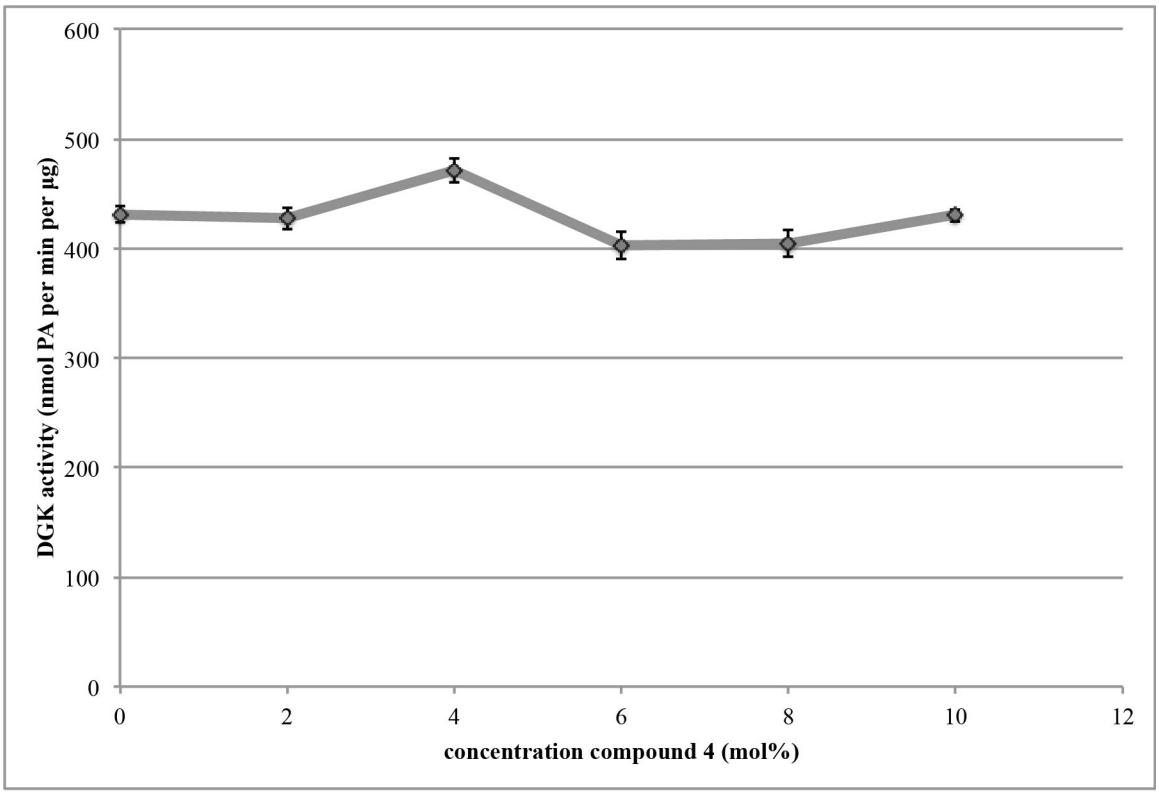

Figure 148. Compound 4 appears to neither activate nor inhibit purified DGK-theta under the conditions tested. DGK activity assay. I first preincubated purified DGK-theta in preincubation buffer (1.1 pg per µL purified DGK-theta, 0.02% (v/v) glycerol, 0.005% (v/v) DDM, 0.5 µM histone H1, 1 mM DTT, 50 mM HEPES, pH 7.5, 100 mM NaCl) on ice for half an hour. The final reaction mixture included 7.5 mM liposomes (2:1::POPE:POPC; 20 mol% POPS, 5 mol% DOG, and the indicated concentrations of compound 4), 50 mM HEPES, pH 7.5, 100 mM NaCl, 1 mM DTT, 1.5 mM MgCl2, 1 mM ATP, 37.3 Ci per mmol [γ-32P]-ATP, 0.1 µM histone H1, 0.1 mg per mL ovalbumin, 0.22 pg per µL purified DGK-theta, and 0.006% (v/v) glycerol, and proceeded for thirty minutes at 37°C. In triplicate: mean ± SD.

Compound **4** includes a hydroxyl in the 3-position of the glycerol backbone, as diglyceride does, so I therefore tested whether DGK-theta could use compound **4** as a substrate. (The migration pattern of the phosphorylated product of compound **4** is unknown, so I do not know whether such radiolabeled spots might be contributing to the activity detected in Figure 148: it is a formal possibility that compound **4** is, in fact, inhibiting DGK-theta to exactly the same extent that it is a substrate, so that the loss and gain in radiolabeled spots perfectly balance one another, but that explanation seems extremely unlikely.) I measured the enzymatic activity of purified DGK-theta to be

greater on liposomes containing 10 mol% compound **4** than on liposomes containing 0% compound **4** (Figure 149). I therefore concluded that DGK-theta is able to use compound **4** as a substrate.

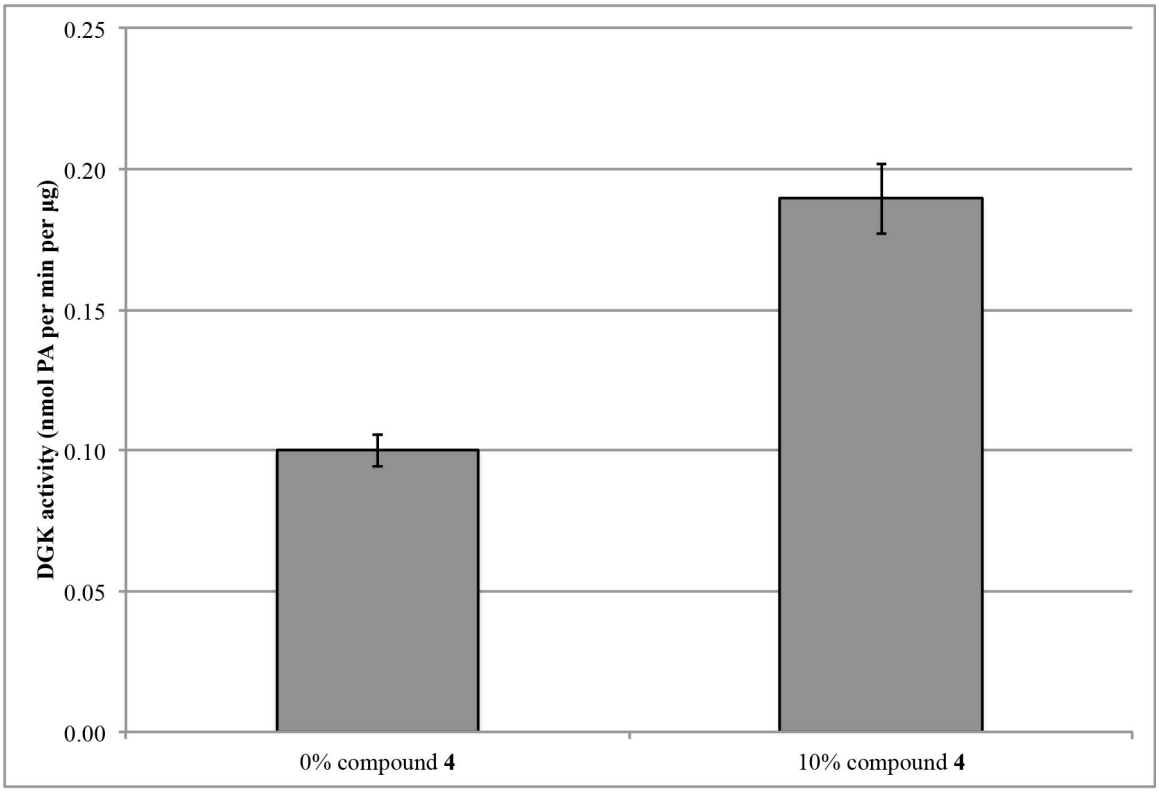

Figure 149. Purified DGK-theta is able to use compound 4 as a substrate. DGK activity assay. I first preincubated purified DGK-theta in preincubation buffer (300 pg per µL purified DGK-theta, 8% (v/v) glycerol, 0.005% (v/v) DDM, 0.5 µM histone H1, 1 mM DTT, 50 mM HEPES, pH 7.5, 100 mM NaCl) on ice for fifteen minutes. The final reaction mixture included 7.5 mM liposomes (2:1::POPE:POPC; 20 mol% POPS, and the indicated concentrations of compound 4), 50 mM HEPES, pH 7.5, 100 mM NaCl, 1 mM DTT, 1.5 mM MgCl2, 1 mM ATP, 85.0 Ci per mmol [γ-32P]-ATP, 0.1 µM histone H1, 0.1 mg per mL ovalbumin, 60 pg per µL purified DGK-theta, and 1.5% (v/v) glycerol, and proceeded for one hour at 37°C. In triplicate: mean ± SD.

Conclusions

Under my experimental conditions, at liposome concentrations of 5 mM or lower, the $K_{m(surface)}$ of purified DGK-theta for DOG is considerably greater than 3 mol%.

Compounds **1** and **3** activate purified DGK-theta, but not monotonically, possibly by helping the enzyme target to the membrane, and can also be used as a substrate by the

enzyme. Compound **4**, contrariwise, does not appear to activate DGK-theta under the conditions tested, but DGK-theta is also able to use it as a substrate.

Chapter 6: Bimolecular Fluorescence Complementation (BiFC) to Probe DGK-Theta's Protein-Protein interactions

Introduction

Bimolecular fluorescence complementation (BiFC) is a method for observing protein-protein interactions[146]. The basic idea is that half of a fluorescent protein is fused to protein A, and the other half of the fluorescent protein is fused to protein B; if and when proteins A and B interact, the two halves of the fluorescent protein come together and fluoresce. One advantage to this method is that no exogenous staining molecules are required to visualize the interaction. Another advantage is that the method provides very high signal to noise, because in the absence of the interaction between proteins A and B, the two halves of the fluorescent molecule remain separate and do not fluoresce. The fact that unassociated proteins produce no signal is also a limitation to the method: with no signal from unassociated proteins, the kinetics of real-time association cannot be measured. Another challenge is that the method requires overexpression of recombinant proteins, and, as always is a risk with overexpressed proteins, the observed effects might be more an artifact of overexpression than a result of the endogenous molecules' interactions.

Methods

"YN" signifies residues 1-154 (or the N-terminus) of enhanced yellow fluorescent protein (eYFP), a mutant of green fluorescent protein (GFP), which is a protein from the Northwest Pacific jellyfish *Aequoria victoria*, that has been engineered to have red-

shifted excitation and emission wavelengths[147] as well as a single excitation peak[148]. "YC" signifies residues 155-238 (or the C-terminus) of eYFP.

I transformed the FLAG/YN-Smad3 and FLAG/YC-Smad4 constructs each into the One Shot® TOP 10 (Life Technologies™) strain of *E. coli*, selecting for transformants using the antibiotic carbenicillin, and made glycerol stocks of the transformed bacteria.

In order to use the YN-Smad3 and YC-Smad4 constructs for cloning DGK BiFC constructs, I needed to know the sequence of those constructs. I therefore designed sequencing primers to be at least eighteen nucleotides long, ending with GC rich content, and homologous to regions approximately 100 nucleotides from the sequence of interest. For YN-Smad3, the forward sequencing primer I designed was GGGCGACACCCTGGTGAACCGC and the reverse sequencing primer I designed was CGGGCAGGAGGAGAAATGGTGCG, and for YC-Smad4, the forward sequencing primer I designed was CCGCCGCCGGGATCACTCTCGGC and the reverse sequencing primer I designed was GCATTGTGCATAGTTTGATGTGCC. The sequences produced by the reverse primers were more robust than the sequences produced by the forward primers, and I was able to successfully sequence the YN-Smad3 and YC-Smad4 constructs.

In order to generate the DGK-theta BiFC constructs, I decided to use PCR to amplify either YN (from YN-Smad3) or YC (from YC-Smad4) with the appropriate restriction digestion sites for ligating into the DGK-theta in pCDNA3.1 (+) plasmid. For inserting the YFP fragments upstream of DGK-theta (to produce a fusion protein with the YFP fragment attached to the N-terminus of DGK-theta), I used a HindIII site upstream

and an EcoRI site downstream of the YFP fragments (Figure 150). For inserting the YFP fragments downstream of DGK-theta (to produce a fusion protein with the YFP fragment attached to the C-terminus of DGK-theta), I used an XbaI site upstream and a XhoI site downstream of the YFP fragments (Figure 151).

The forward primer I designed for PCRing the YN fragment, for fusion either upstream or downstream of DGK-theta, was gctaCTCGAG***AC***atggactacaaagac (Figure 150**A**). This primer begins with a four-nucleotide overhang, for improving the efficiency of digestion at the following XhoI restriction site (for fusing the YN fragment to the C-terminus of DGK-theta). The XhoI site is followed by two nucleotides, which ensure that the YN fragment is translated in the same reading frame as DGK-theta (for the construct in which YN is attached C-terminally to DGK-theta). The primer ends with fifteen nucleotides homologous to the beginning of the FLAG tag in the FLAG/YN-Smad3 template.

The reverse primer I designed for PCRing the YN fragment, likewise for adding either upstream or downstream of DGK-theta, was CGATtctagaCgaattcGGCCATGATA (Figure 150**B**). This primer also begins with a four-nucleotide overhang, for improving the efficiency of digestion at the following XbaI restriction site (for fusing the YN fragment to the C-terminus of DGK-theta). The XbaI site is followed by a single nucleotide, which ensures that DGK-theta is translated in the same reading frame as YN (for the construct in which YN is attached N-terminally to DGK-theta). The single nucleotide is followed by an EcoRI restriction site (for fusing the YN fragment to the N-terminus of DGK-theta). The primer ends with ten nucleotides homologous to the reverse complement of the end of YN in the FLAG/YN-Smad3 template.

The produced PCR fragment of YN, therefore, is predicted to begin with a four nucleotide overhang, followed by an XhoI restriction site, followed by a two nucleotide spacer, followed by FLAG-YN as it encoded in the FLAG/YN-Smad3 template, followed by an EcoRI site immediately C-terminal to YN, followed by a single nucleotide spacer, followed by an XbaI restriction site, followed by a four nucleotide overhang (Figure 150**B**). When digested by EcoRI and HindIII (whose restriction site is already present in the FLAG/YN-Smad3 template, between the FLAG tag and YN) and ligated into DGK-theta in pCDNA3.1 (+) plasmid that has been likewise digested, the predicted protein product begins with YN, followed by a glutamate and a phenylalanine, followed by DGK-theta, which from the pCDNA3.1(+) also includes a five-amino-acid tail whose sequence is AAARV: this is the YN-DGK-theta construct (Figure 150**C**). Alternatively, EcoRI- and HindIII-digested PCR product can be ligated into pCDNA3.1(+) empty vector, in order to produce free YN, which can be used as a negative control for spontaneous interaction between YN and YC. When the PCR product is digested by XhoI and XbaI and ligated into DGK-theta in pCDNA3.1 (+) plasmid that has been likewise digested, the predicted protein product begins with DGK-theta, followed by a five-amino-acid linker whose sequence is AAARD, followed by the FLAG tag, followed by a single leucine, followed by YN, followed by three amino acids whose sequence is EFV: this is the DGK-theta-YN construct (Figure 150**C**). Free YN can also be produced by digesting the PCR product with XhoI and XbaI and then ligating into pCDNA3.1 (+) empty vector.

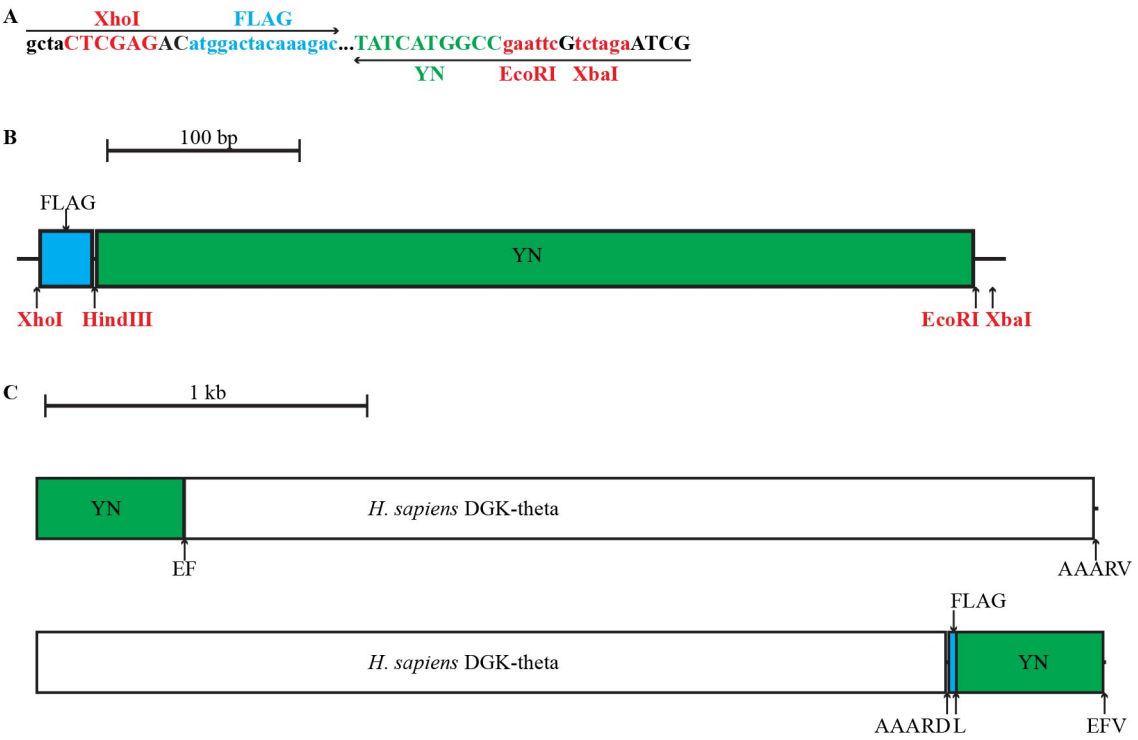

Figure 150. Cloning strategy for generating YN DGK BiFC constructs. (A) Primers designed for PCR of YN, using FLAG/YN-Smad3 as a template. **(B)** Predicted PCR product. **(C)** YN-DGK-theta construct (top) and DGK-theta-YN construct (bottom).

The forward primer I designed for PCRing the YC fragment to fuse to the N-terminus of DGK-theta was GCTAaagcttATGgacaagcagaagaag (Figure 151**A**). This primer begins with a four-nucleotide overhang, for improving the efficiency of digestion at the following HindIII restriction site. The HindIII site is followed by a start codon. The primer ends with fifteen nucleotides homologous to beginning of YC in the FLAG/YC-Smad4 template.

The reverse primer I designed for PCRing the YC fragment to fuse to either the N- or C-terminus of DGK-theta was CGATtctagaCgaattcCTTGTACAGC (Figure 151**A**). This primer begins with a four-nucleotide overhang, for improving the efficiency of digestion at the following XbaI restriction site. The XbaI site is followed by a single nucleotide, for ensuring that the stop codon in the XbaI site is in the same translational

reading frame as the fusion protein, such that fusion protein will end with four amino acids after the end of YC. The single nucleotide spacer is followed by an EcoRI site. The primer ends with ten nucleotides homologous to the reverse complement of the end of YC in the FLAG/YC-Smad4 template.

The produced PCR fragment using these two primers, therefore, is predicted to begin with a four-nucleotide overhang, followed by a HindIII site, followed by a start codon, followed by YC, as it is encoded in the FLAG/YC-Smad4 template, followed by an EcoRI site immediately C-terminal to YC, followed by a single-nucleotide spacer, followed by an XbaI site, followed by a four-nucleotide overhang (Figure 151**B**). When digested by EcoRI and HindIII and ligated into DGK-theta in pCDNA3.1 (+) plasmid that has been likewise digested, the predicted protein product begins with YC, followed by a glutamate and a phenylalanine, followed by DGK-theta, which from the pCDNA3.1(+) also includes a five-amino-acid tail whose sequence is AAARV: this is the YC-DGK-theta construct (Figure 151**C**).

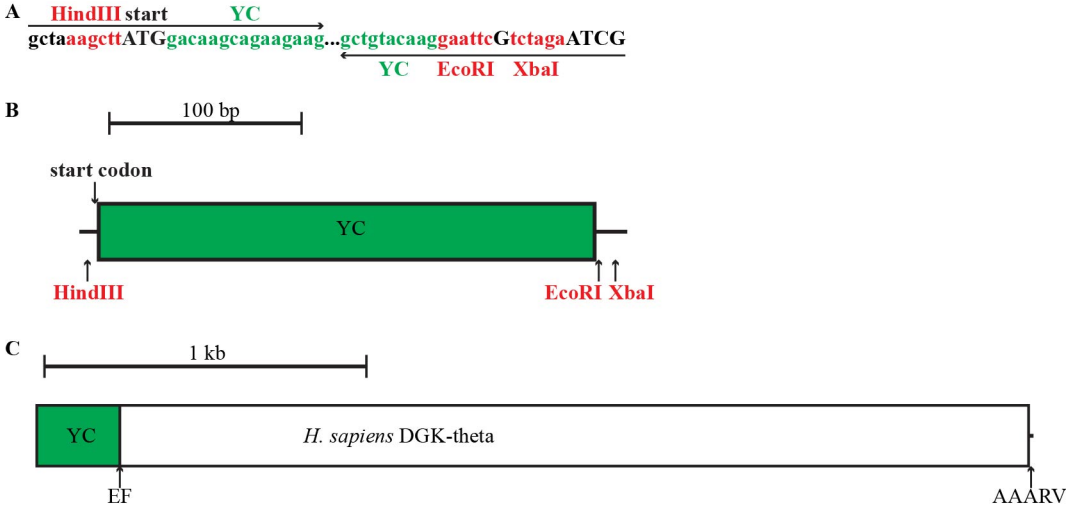

Figure 151. Cloning strategy for generating the YC-DGK-theta BiFC construct. (A) Primers designed for PCR of YC, using FLAG/YC-Smad4 as a template. **(B)** Predicted PCR product. **(C)** YC-DGK-theta construct.

The forward primer I designed for PCRing the YC fragment to fuse to the C-terminus of DGK-theta was gctaCTCGAG***ag***ATGgacaagcagaag (Figure 152**A**). This primer begins with a four-nucleotide overhang, for improving the efficiency of digestion at the following XhoI restriction site. The XhoI site is followed by two nucleotides, which ensure that YC is translated in the same reading frame as DGK-theta. The two nucleotides are followed by a start codon. The primer ends with twelve nucleotides homologous to the beginning of YC in the FLAG/YC-Smad4 template.

The produced PCR product using this primer and the reverse primer shown in Figure 151**A**, therefore, is predicted to begin with a four-nucleotide overhang, followed by an XhoI site, followed by a two-nucleotide spacer, followed by a start codon, followed by YC, as it is encoded in the FLAG/YC-Smad4 template, followed by an EcoRI site immediately C-terminal to YC, followed by a spacer nucleotide (to make sure that the downstream stop codon is in frame), followed by an XbaI site, followed by a four-nucleotide overhang (Figure 152**B**). When digested by XhoI and XbaI and ligated into DGK-theta in pCDNA3.1 (+) plasmid that has been likewise digested, the predicted protein product begins with DGK-theta, followed by a five-amino-acid linker whose sequence is AAARE, followed by YC, and ending with three amino acids whose sequence is EFV: this is the DGK-theta-YC construct (Figure 152**C**).

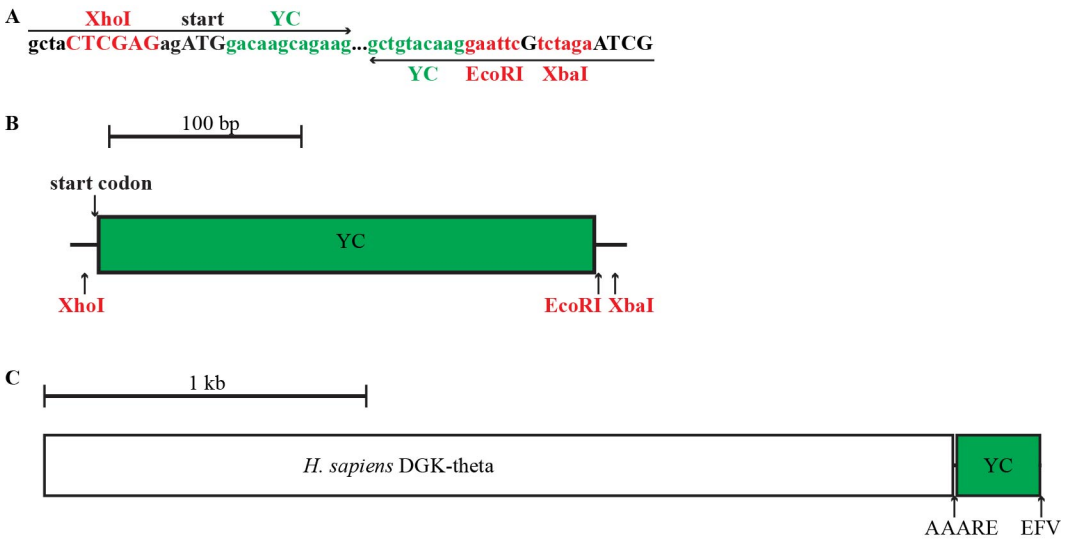

Figure 152. Cloning strategy for generating the DGK-theta-YC BiFC construct. (A) Primers designed for PCR of YC, using FLAG/YC-Smad4 as a template. **(B)** Predicted PCR product. **(C)** DGK-theta-YC construct.

After my first attempt at PCR, the YN primers produced robust PCR products of approximately the correct size, but the YC primers did not. Adjusting the annealing temperature of the PCR reaction did not help. Adding DMSO to the PCR reaction did not help. Reducing the template concentration, reducing the initial annealing temperature, and increasing the time of the annealing steps produced PCR products of approximately the correct size faintly detectable by ethidium bromide staining following agarose electrophoresis for the XhoI YC PCR product, but not for the HindIII YC product. Using previous PCR attempts as the template for more rounds of PCR eventually produced enough of a PCR product for HindIII YC that was approximately the correct size and faintly detectable by ethidium bromide staining following agarose electrophoresis, but the YC PCR products were never as robustly amplified as the YN PCR products. PCR purification of the PCR products using either the QIAGEN or Invitrogen™ (now Life Technologies™) kits appeared to work equally well.

Because of the poor yields from the attempts to PCR the YC fragment, I designed new primers. The fact that increasing the primer:template ratio, decreasing the annealing temperature, and increasing the annealing time improved the amplification of the PCR product suggested that the problem with the first set of primers was that their affinity for the template was too low. For the next set of primers, therefore, I increased the length of the primer that was homologous to the template, in order to increase its affinity. In order to make room for the increased homologous region, each primer included only one restriction site. I therefore designed the new set of primers such that one set of PCR primers would produce the YC fragment with the HindIII and EcoRI sites required for fusing the YC fragment upstream of DGK-theta, and a second set of PCR primers would produce the YC fragment with the XhoI and XbaI sites required for fusing the YC fragment downstream of DGK-theta.

The forward primer I designed for this second attempt to PCR the YC fragment to fuse to the N-terminus of DGK-theta was cgacaagcttatgGACAAGCAGAAGAAGAACGG (Figure 153**A**). Similarly to the previous primer, it begins with a four-nucleotide overhang, including a GC anchor, for improving the efficiency of digestion at the following HindIII restriction site. Following the HindIII site is a start codon. The primer ends with twenty nucleotides (as opposed to only fifteen in the previous primer) homologous to the beginning of YC. I hoped that the longer homologous region would improve PCR efficiency. This primer is calculated to have a T_m of 66°C, a homologous T_m of 55°C, and a GC content of 48%.

The reverse primer I designed for this second attempt to PCR the YC fragment to fuse to the N-terminus of DGK-theta was

gcatGAATTCCTTGTACAGCTCGTCCATGCC (Figure 153**A**). Similarly to the previous primer, it begins with a four-nucleotide overhang, including a GC anchor, for improving the efficiency of digestion at the following EcoRI restriction site. The primer ends with twenty-one nucleotides (as opposed to only ten in the previous primer) homologous to the end of YC. I hoped that the longer homologous region (allowed by removing the XbaI site) would improve PCR efficiency. This primer is calculated to have a T_m of 66°C, a homologous T_m of 61°C, and a GC content of 52%.

The PCR product predicted to be produced by these two primers is very similar to that produced by the first round of primers (Figure 153**B**; compare to Figure 151**B**), and, because the PCR product would be inserted into DGK-theta in pCDNA3.1 (+) via HindIII and EcoRI sites, the final YC-DGK-theta construct would be the same (Figure 153**C**; compare to Figure 151**C**).

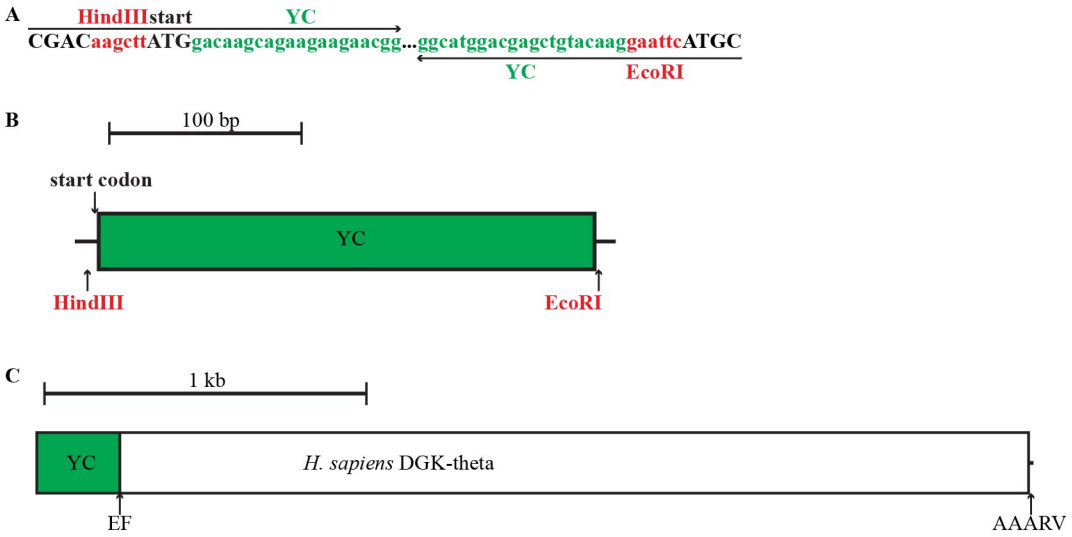

Figure 153. Cloning strategy for generating the YC-DGK-theta BiFC construct, attempt 2. (A) Primers designed for PCR of YC, using FLAG/YC-Smad4 as a template. **(B)** Predicted PCR product. **(C)** YC-DGK-theta construct.

The forward primer I designed for this second attempt to PCR the YC fragment to fuse to the C-terminus of DGK-theta was

gctaCTCGAGAGGACAAGCAGAAGAAGAACGG (Figure 154**A**). Similarly to the previous primer, it begins with a four-nucleotide overhang, including a GC anchor, for improving the efficiency of digestion at the following XhoI restriction site. As before, the XhoI site is followed by two nucleotides, which ensure that YC is translated in the same reading frame as DGK-theta. Unlike the previous primer, this time I omitted the start codon. The primer ends with twenty nucleotides homologous to the beginning of YC (as opposed to only twelve nucleotides in the first primer). I hoped that the longer homologous region would improve PCR efficiency. This primer is calculated to have a T_m of 66°C, a homologous T_m of 58°C, and a GC content of 53%.

The reverse primer I designed for this second attempt to PCR the YC fragment to fuse to the C-terminus of DGK-theta was CGATtctagaCCTTGTACAGCTCGTCCATGCC (Figure 154**A**). Similarly to the previous primer, it begins with a four-nucleotide overhang, including a GC anchor, for improving the efficiency of digestion at the following XbaI restriction site. As before, the XbaI site is followed by a single nucleotide to ensure that the stop codon in the XbaI site is translated in the same reading frame as the fusion protein. I omitted the EcoRI site, and the primer ends with twenty-one nucleotides homologous to the end of YC (as opposed to only ten in the first primer). I hoped that the longer homologous region (allowed by removing the EcoRI site) would improve PCR efficiency. This primer is calculated to have a T_m of 66°C, a homologous T_m of 59°C, and a GC content of 53%.

The PCR product predicted to be produced by these primers, unlike the PCR product predicted to be produced in the first cloning attempt, is missing the start codon

and the EcoRI site (Figure 154**B**). As such, the tail of the fusion protein, after the end of the YC coding sequence, is reduced to only a single valise (Figure 154**C**).

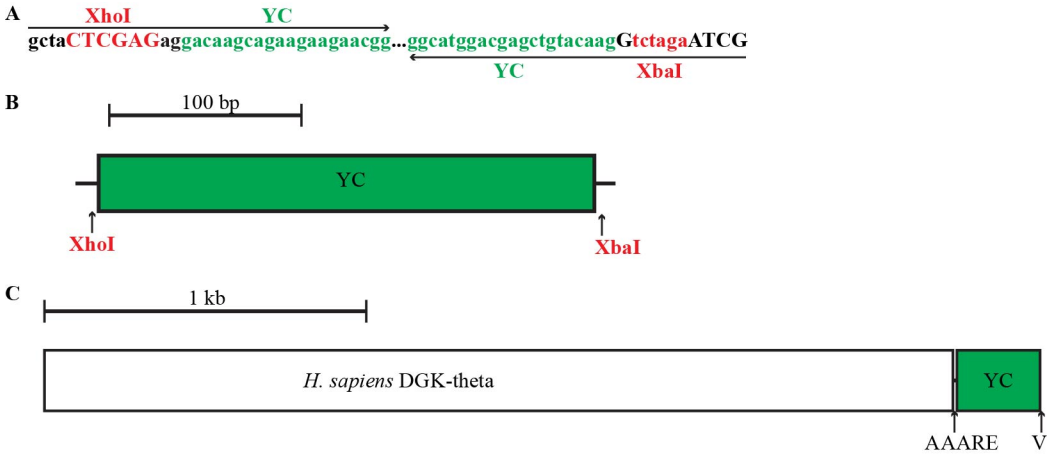

Figure 154. Cloning strategy for generating the DGK-theta-YC BiFC construct, attempt 2. (A) Primers designed for PCR of YC, using FLAG/YC-Smad4 as a template. **(B)** Predicted PCR product. **(C)** DGK-theta-YC construct.

With the new PCR primers, the YC PCR products were more robust than with the previous primers, but still not as robust as the YN PCR products.

I isolated the DNA from glycerol stocks of One Shot® TOP 10 (Life Technologies™) strain of *E. coli* that had been labeled as transformed with pCDNA3.1 (+) empty vector and from DGK-theta in pCDNA3.1(+). When I digested the isolated DNA with either HindIII and EcoRI or with XhoI and XbaI, I discovered that the glycerol stock that had been labeled as pcDNA3.1 (+) empty vector was, in fact, DGK-theta in pCDNA3.1 (+). The glycerol stock that had been labeled DGK-theta in pCDNA3.1 (+) was, in fact, DGK-theta in pCDNA3.1 (+), but that was different from the sequence that I had been told was DGK-theta in pCDNA3.1 (+). The original sequence (and the one from the glycerol stock) included two EcoRI sites, one on either side of DGK-theta; the sequence that I had been working with, which had also been labeled DGK-theta in

pCDNA3.1(+), was the original sequence that had been digested with NotI and religated to remove the extra EcoRI sites.

As a control for ligation, I always also included a reaction without insert, to assess the number of background colonies from incompletely digested plasmids that had religated without incorporating the insert. Ligations that using XhoI and XbaI sites gave high background. XhoI's enzymatic activity has been reported to be impaired by CpG dinucleotide methylation[149], and thus more restriction enzyme may be required for supercoiled plasmid than for linear DNA. In order to assess whether XhoI was the culprit, I redigested the previously digested plasmid either with XhoI or XbaI. The plasmid that was redigested with XbaI, when ligated and transformed into *E. coli*, still gave a large number of background colonies, suggesting that incomplete digestion by XbaI was not the problem. The plasmid that was redigested with XhoI, contrariwise, when ligated and transformed into *E. coli* gave many more colonies than the originally digested plasmid, suggesting that at least part of the source of the high background was due to incomplete digestion at the XhoI site. Subsequent digestion, first by XbaI to linearize the plasmid followed by XhoI, likewise gave low background, and I therefore used sequential rather than simultaneous digestion for the XhoI / XbaI sites.

My early attempts at ligating the digested PCR products into the digested plasmids were unsuccessful, probably because I had too much insert in the ligation reactions. I thought that large amounts of insert would favor ligation, but apparently too much insert reduced ligation efficiency. I therefore picked colonies even when the number of colonies was no higher than on the background plates, in the hopes that any

colonies were successful transformants, and that the low number of colonies reflected repression from too much insert, and not from high background.

In order to assess whether the transformants had successfully incorporated the insert, I performed diagnostic PCR using cultures that had been inoculated from single colonies from the transformed plate. Because the YN forward primer relies on the FLAG tag, which would be removed after HindIII digestion, for constructs that were cloned via HindIII I used T7 as a forward primer instead for the diagnostic PCR. The T7 primer is considerably shorter than the other primers, and failure to PCR may partially be a result of poor compatibility in T_m within the primer pair. For clones that appeared promising by diagnostic PCR, I isolated the DNA and sent it for sequencing, using either the T7 primer for N-terminal fusions or for the fragments ligated into the vector alone, or a primer I designed for sequencing the C-terminal fusions based on homology to the C-terminal region of DGK-theta, ggccctaaggtgcacatgc. I then discovered that the sequence I had been working with to design the constructs ("DGK-theta in pCDNA3.1(+)") had yet another discrepancy from the actual physical sequence. The actual sequence had one more nucleotide between the end of the DGK-theta coding region and the XhoI site, meaning that the C-terminal fusion constructs I had designed were out of frame when cloned into the real sequence.

In an attempt to solve the frame-shift problem, I digested the DGK-YC (via XhoI and XbaI) construct with NotI, to leave an appropriately sized sticky end such that when the sticky end was removed by mung bean nuclease, the resulting blunt ends, when ligated together, would be in the appropriate frame. For 4 μg of construct that had been digested with NotI and gel-purified, however, a 15-minute digestion at 30°C with 10 U of

mung bean nuclease completely chewed up the construct (Figure 155). Another possible explanation for the appearance of the construct in Figure 155 is that recovery from gel-purification following NotI digestion was much worse than the recovery from gel-purification of DGK-theta in pCDNA3.1 (+) following HindIII and EcoRI digestion.

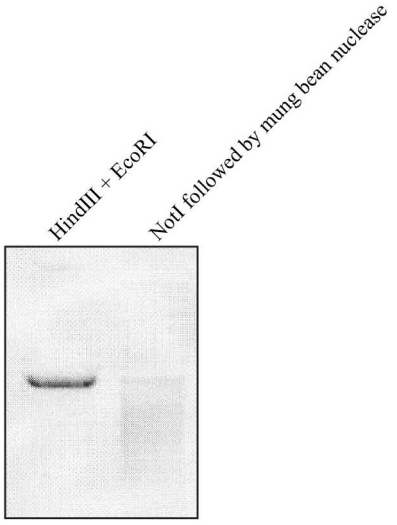

Figure 155. Very little pCDNA3.1 (+) is left after digestion with NotI and mung bean nuclease under the conditions shown. Electrophoresis of a 1% (w/v) agarose gel visualized by ethidium bromide staining. Left, DGK-theta in pCDNA3.1 (+) that had been digested with HindIII and EcoRI and gel-purified. Right, DGK-YC (via XhoI and XbaI) in pCDNA3.1 (+) that had been digested with NotI, gel-purified, digested with mung bean nuclease, and PCR-purified.

In order to solve the frame-shift problem, then, I designed yet a third set of primers that would produce C-terminally fused constructs that would be in the appropriate frame.

The forward primer I designed for fusing YN to the C-terminus of DGK-theta, in the appropriate frame, was gctaCTCGAGCatggactacaaagacg (Figure 156**A**). As with the other primers, it begins with a four-nucleotide overhang, including a GC anchor, for improving the efficiency of digestion at the following XhoI restriction site. The XhoI site, unlike in previous primers, is immediately followed by one, not two nucleotides, so that YN will be translated in the same reading frame as DGK-theta. The primer ends

with sixteen nucleotides homologous to the beginning sequence of the FLAG tag, including the start codon. This primer is calculated to have a T_m of 62°C and a homologous T_m of 45°C. The predicted PCR product (Figure 156**B**) is very similar to that produced by the first set of YN primers (Figure 150**B**), but because of the frame shift, the linker sequence between the end of the DGK-theta coding sequence and the beginning of the FLAG tag was now GGRSS (Figure 156**C**; compare to Figure 150**C**).

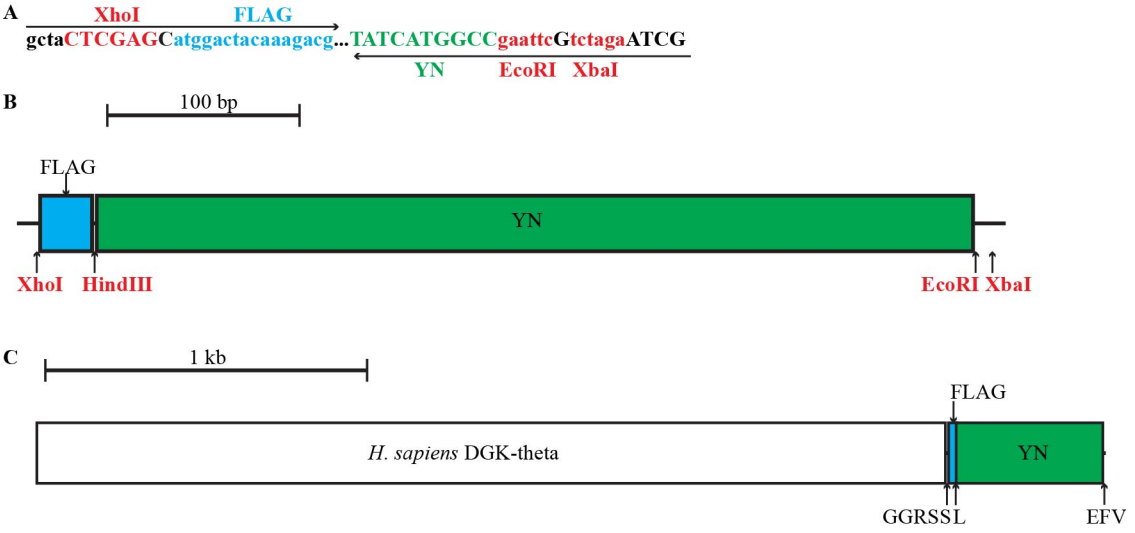

Figure 156. Cloning strategy for generating DGK-theta-YN, attempt 2. (A) Primers designed for PCR of YN, using FLAG/YN-Smad3 as a template. **(B)** Predicted PCR product. **(C)** DGK-theta-YN construct.

The forward primer I designed for fusing YC to the C-terminus of DGK-theta, in the appropriate frame, was gctaCTCGAGGGACAAGCAGAAGAAGAACG. This primer is very similar to the second forward primer I designed for fusing YC to the C-terminus of DGK-theta, but instead of a two-nucleotide spacer between the XhoI site and the beginning of the YC sequence, it has a one-nucleotide spacer, so that YC will be translated in the same reading frame as DGK-theta. The primer ends with nineteen nucleotides homologous to the beginning sequence of YC, ending with another GC anchor. This primer is calculated to have a T_m of 65°C and a homologous T_m of 52°C.

As with the redesign of the YN primers, the predicted PCR product (Figure 157**B**) is very similar to that produced by the second set of YC primers (Figure 154**B**), but because of the frame shift, the linker sequence between the end of the DGK-theta coding sequence and the beginning of the YC coding sequence was now GGRSR (Figure 157**C**; compare to Figure 154**C**).

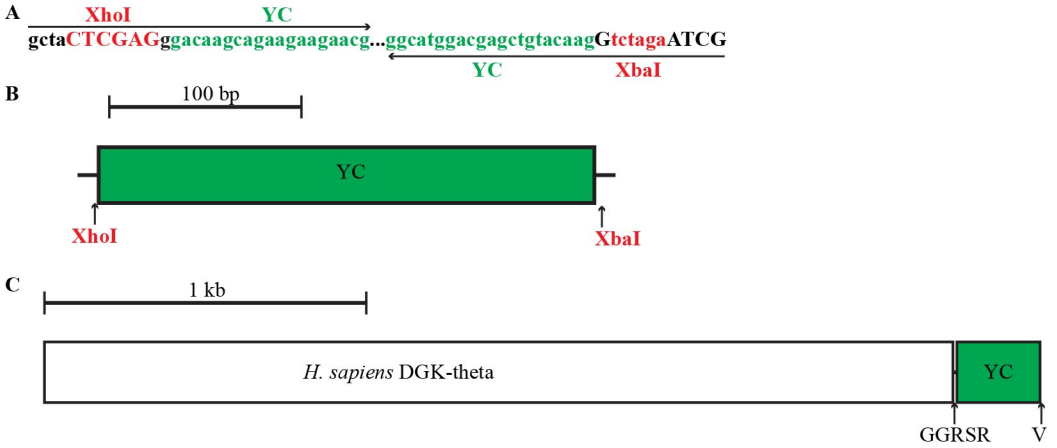

Figure 157. Cloning strategy for generating the DGK-theta-YC BiFC construct, attempt 3. (A) Primers designed for PCR of YC, using FLAG/YC-Smad4 as a template. **(B)** Predicted PCR product. **(C)** DGK-theta-YC construct.

I also designed primers for diagnostic PCR to determine whether the clones successfully incorporated the insert. I designed the forward primer GGTGAGCAAGGGCGAGGAGC to detect the presence of YN, and the forward primer GCAGAAGAAGAACGGCATCAAGG to detect the presence of YC. These primers were designed to complement the 5' region of the sequence, and successful PCR would be predicted only if the YFP fragments were incorporated. The reverse primers that were used to generate the constructs could be used with these forward primers for diagnostic PCR.

PCR using this third set of primers finally gave PCR products that were robustly detected by ethidium bromide staining and agarose electrophoresis (Figure 158). The

intensity of the recovered bands also depended strongly on which tube of template was used. The new success, therefore, may have either been due to superior primer design, or else due to some problem with the tubes of template used previously (such as incorrect concentration measurement, etc.).

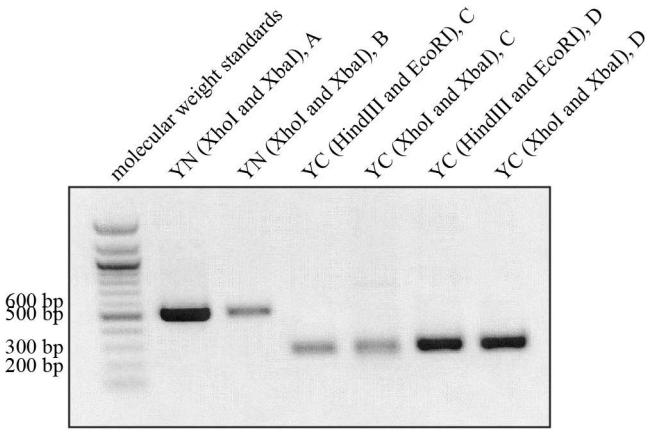

Figure 158. The newest sets of primers robustly produce PCR products, although the yield also depends on the tube of template used. Agarose electrophoresis visualized by ethidium bromide staining of PCR products of YFP fragments using the third set of primers. "HindIII and EcoRI" signify the primers used to amplify the BiFC constructs for fusion to the N-terminus of DGK-theta, and "XhoI and XbaI" signify the primers used to amplify the constructs for fusion to the C-terminus of DGK-theta. A, B, C, and D signify different tubes of template. The migration patterns of the PCR products are consistent with their predicted sizes (523 bp for YN using the "XhoI and XbaI" primers, 294 bp for YC using the "HindIII and EcoRI" primers, and 277 bp for YC using the "XhoI and XbaI" primers).

I PCR-purified these PCR products and then digested either with HindIII or EcoRI, or with XbaI and XhoI (because the PCR products are linear, subsequent digestion was not necessary). I PCR-purified the digests, and assessed the DNA concentration by agarose electrophoresis visualized by ethidium bromide staining. I ligated these digested PCR products at a 3:1 molar ratio with DGK-theta in pCDNA3.1 (+) that had likewise been digested with either HindIII and EcoRI, or by XbaI followed by XhoI, and PCR-purified. I transformed the ligations into *E. coli*, and the number of colonies on the transformed plates greatly exceeded the number of colonies on the control plates (digested plasmid without insert). I inoculated cultures with single colonies from

these plates, and performed diagnostic PCR on the cultures using the forward primers I had designed for diagnostic PCR, and the reverse primers used for the original PCR to build the insert. I assessed the diagnostic PCR by running the diagnostic PCR products on an agarose gel (Figure 159). I isolated the DNA from clones that had produced robust bands of the correct size, and submitted for sequencing. I made glycerol stocks of good clones confirmed by DNA sequencing.

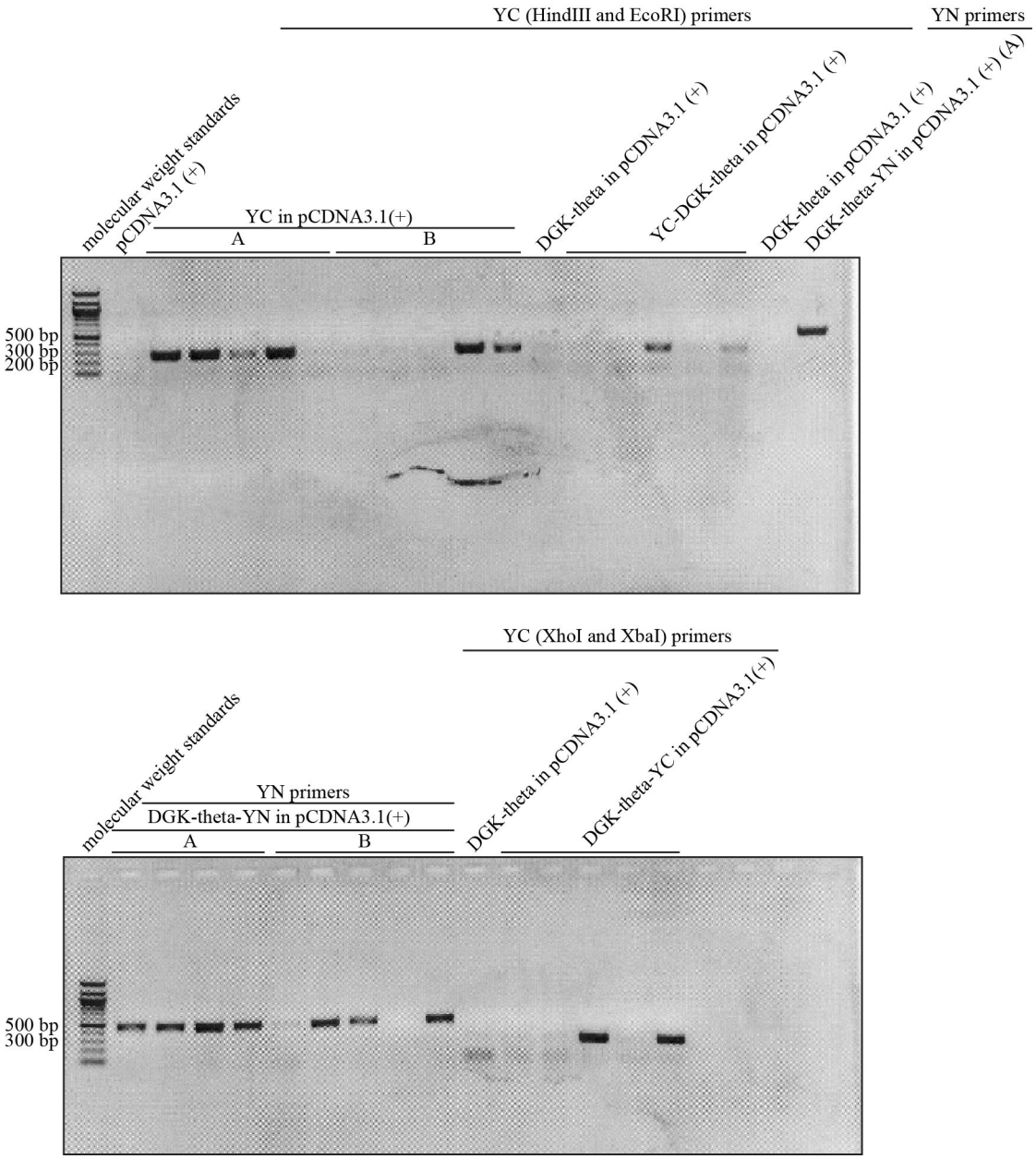

Figure 159. Diagnostic PCR of some BiFC clones. Agarose electrophoresis visualized by ethidium bromide staining. A, B, C, and D correspond to the PCR products shown in **Figure 158**.

I was therefore able to successfully generate clones of YN, YC, YN-DGK-theta, YC-DGK-theta, DGK-theta-YN, and DGK-theta-YC, all in pCDNA3.1 (+).

BiFC and *H. sapiens* DGK-theta dimerization in HEK293T cells

Introduction

As previously mentioned, oligomerization of LCB5 family proteins is not unprecedented: purified *Salmonella typhimurium* YegS recombinantly expressed in *E. coli* elutes as a dimer from a Superdex G200 resin[92], *E. coli* YegS[93] and *Staphylococcus aureus* DgkB[94] recombinantly expressed in *E. coli* each crystallize as dimers, and *H. sapiens* DGK-epsilon recombinantly expressed in COS-7 cells has been reported to dimerize based on its migration in PFO-PAGE[43]. We therefore wondered whether *H. sapiens* DGK-theta was likewise dimerizing. More traditional methods that would be used to measure dimerization of a protein, such as size exclusion chromatography or analytical ultracentrifugation require large amounts of purified protein. (The migration pattern of an unpurified protein in size exclusion chromatography or PFO-PAGE could be followed by a sensitive assay such as Western blotting, but if the protein is unpurified, it is impossible to show conclusively that the protein is dimerizing and not merely interacting with another, similarly-sized protein.) If DGK-theta dimerizes, it would be predicted that, if the fusion proteins are in the proper orientation, DGK-theta would produce a BiFC signal. Advantages of this approach include the fact that it does not require large amounts of purified protein, and that it would reflect the dimerization state *in vivo*.

Results

For positive controls, I used the FLAG/YN-Smad3 and FLAG/YC-Smad4 constructs[2]. Smad3 and Smad4 are proteins that form a heteromeric complex in response

to TGF-β stimulation[150], and BiFC has been used to monitor their interaction[151]. "YN" signifies residues 1-154 (or the N-terminus) of enhanced yellow fluorescent protein (eYFP), a mutant of green fluorescent protein (GFP), which is a protein from the Northwest Pacific jellyfish *Aequoria victoria*, that has been engineered to have red-shifted excitation and emission wavelengths[147] as well as a single excitation peak[148]. "YC" signifies residues 155-238 (or the C-terminus) of eYFP. When I transfected HEK293T cells with FLAG/YN-Smad3 or FLAG/YN-Smad4 alone, I did not observe any fluorescence, but when I transfected the two constructs together, I observed robust fluorescence (Table 2), consistent with successful BiFC. I therefore concluded that the YN-Smad3 and YN-Smad4 constructs were suitable positive controls for the DGK-theta dimerization BiFC experiment.

Transfection	**Observed signal**
None	No
Mock	No
GFP	Yes
YN-Smad3 alone	No
YC-Smad4 alone	No
Both YN-Smad3 and YC-Smad4	Yes

Table 2. The FLAG/YN-Smad3 and FLAG/YN-Smad4 constructs produce a BiFC signal when cotransfected, but not when transfected separately. I transfected the DNA (2 μg per well of a 6-well dish) into HEK293T cells using HiFect® Reagent (Lonza) and Opti-MEM® Reduced Serum Medium (Life Technologies™) for 3.5 hours, and observed the cells on a fluorescent microscope three days later using a GFP filter, through which the eYFP signal bled. GFP served as a positive control; the untransfected and mock-transfected cells served as negative controls for autofluorescence.

For negative controls, I cloned the YN or YC fragments alone into pCDNA3.1(+).

When I transfected HEK293T cells with these constructs, the cells gave no detectable signal when excited at 514 nm (Figure 160**E**), suggesting that the YN and YC fragments do not have high enough affinity for one another to drive BiFC of their fused proteins. When cells transfected with the FLAG/YN-Smad3 and FLAG/YN-Smad4 positive controls and excited with the same laser intensity, they gave a robust YFP signal (Figure 160**C** and **D**), which I interpreted as successful BiFC. I therefore concluded that the YN and YC constructs were a suitable control for the DGK-theta dimerization BiFC experiment.

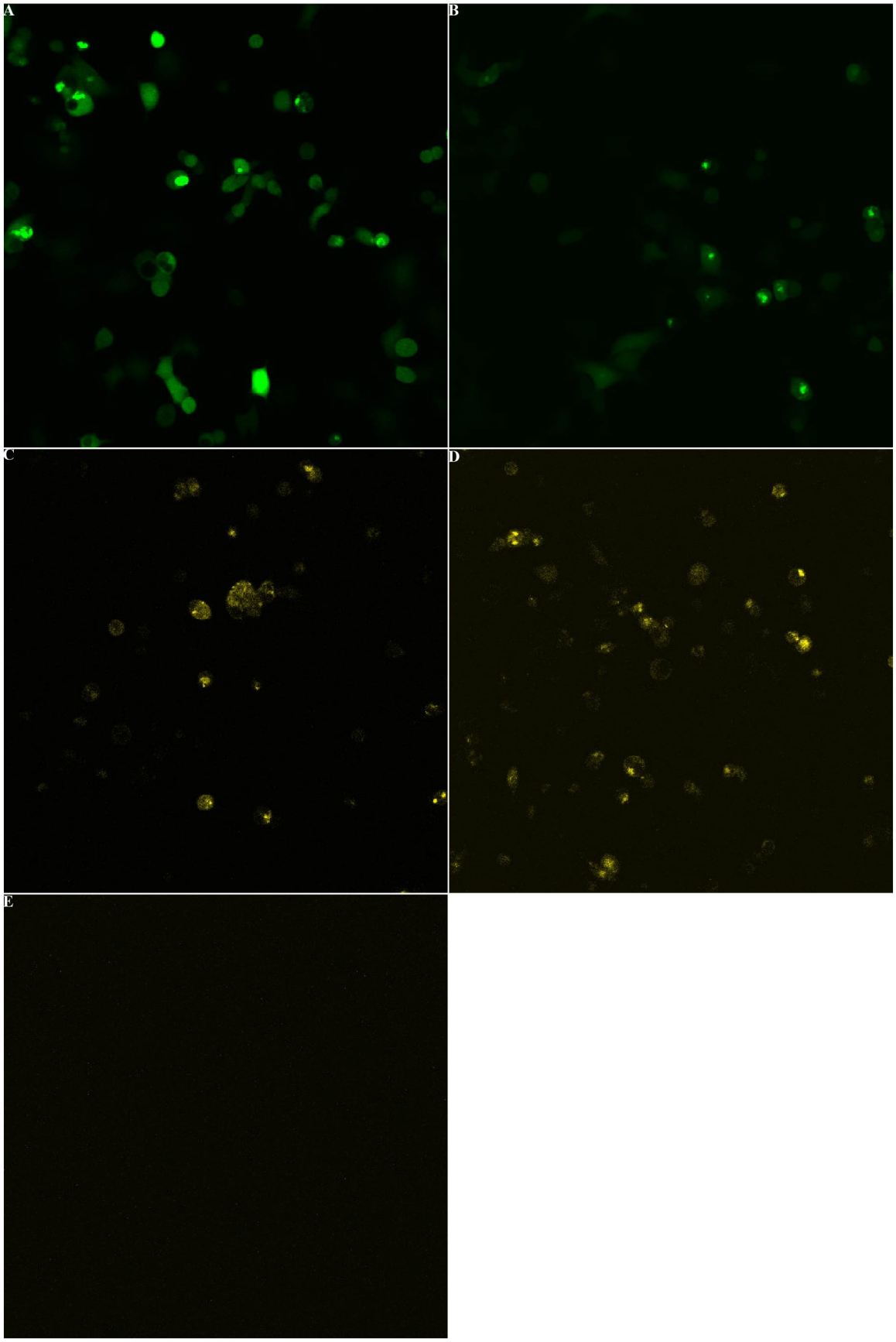
A
B
C
D
E

Figure 160. YN and YC (the negative controls) do not produce a BiFC signal, even though the positive controls in the same transfection do. I transfected the DNA (2 μg per 35-mm coverslip-bottomed dish) into HEK293T cells using HiFect® Reagent and Opti-MEM® Reduced Serum Medium for three and a quarter hours, and observed the cells two days later on a Zeiss laser scanning microscope (LSM) 510 Inverted META. **(A)** and **(B)**: two representative panels from cells transfected with GFP-C2 as a positive control for transfection. The excitation wavelength was 488 nm, and the signal was observed through a 505-530nm filter. **(C)** and **(D)**: two representative panels from cells transfected with FLAG/YN-Smad3 and FLAG/YN-Smad4. The excitation wavelength was 514 nm, and the signal was observed through a 530-600nm filter. **(E)** Cells transfected with YN and YC. The excitation wavelength was 514 nm, and the signal was observed through a 530-600nm filter.

I cloned the YN and the YC fragments to either the N-terminus or the C-terminus of DGK-theta to produce four constructs: YN-DGK-theta, YC-DGK-theta, DGK-theta-YN, and DGK-theta-YC, in case the orientation of the YFP fragment limited the efficiency of BiFC. In order to confirm the expression of these constructs, I immunoblotted lysates from HEK293T cells that had been transiently transfected with them. HEK293T cells expressed a GFP-antibody-immunoreactive band between 27 and 35 kD, which could be faintly detected in the untransfected cells (Figure 161**A**). The anti-GFP antibody only faintly detected two bands between 15 and 27 kD in lysates expressing YN and YC. The higher of these bands ran a bit faster than would be predicted for YN's predicted molecular weight of 19.3 kD. The lower of these bands ran quite a bit slower than would be predicted for YC's predicted molecular weight of 11.9 kD.

The anti-GFP antibody recognized a smear of proteins in the lysate coexpressing YN-Smad3 and YC-Smad4 (Figure 161**B**), whose molecular weights are predicted to be 71.5 kD and 59.2 kD respectively, and, therefore, would have been predicted to run off the gel.

The anti-DGK and anti-GFP antibodies both recognize the same two bands in lysates coexpressing DGK-theta-YN and DGK-theta-YC (Figure 161**B**). These two

bands, however, migrating just faster and just slower than the 130 kD molecular weight marker, electrophoresed a little more slowly than the predicted protein products would: the predicted molecular weight of DGK-theta-YN is 120.1 kD, and the predicted weight of DGK-theta-YC is 110.7 kD. The anti-DGK-theta antibody recognized three bands in the lysates coexpressing YN-DGK-theta and YC-DGK-theta, the upper two of which were also recognized by the anti-GFP antibody (Figure 161**B**) and were presumably the two YFP-fragment-fused constructs. The molecular weight of YN-DGK-theta is predicted to be 119.5 kD, and the molecular weight of YC-DGK-theta is predicted to be 113.1 kD. The lowest band, which was recognized by the anti-DGK but not the anti-GFP antibody, was presumably DGK-theta where translation began at the start codon at DGK-theta, whose resulting molecular weight is predicted to be 101.7 kD (from the alternative start site in YN-DGK-theta) or 101.9 kD (from the alternative start site in YC-DGK-theta). All three of these bands electrophoresed more slowly than would be predicted from their sequence. The discrepancies between the predicted and the observed migration patterns may reflect post-translational processing.

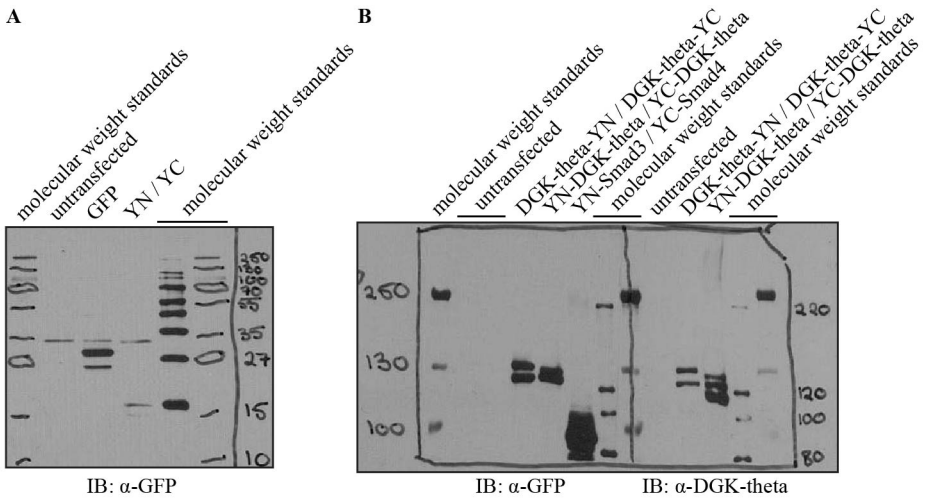

Figure 161. The BiFC constructs successfully express. I transfected the DNA (2 µg per well of a 6-well plate) into HEK293T cells using HiFect® Reagent and Opti-MEM® Reduced Serum Medium for four and a quarter hours. Two days late I washed the cells with FB, then added lysis buffer (FB, 0.1% (v/v) Triton X-100, 1x PIC) and incubated on ice. I resuspended the cells in the lysis buffer, and loaded 10 µg total protein (as measured by the Bio-Rad Protein Assay) per lane. Immunoblot following SDS-PAGE. (A) 15% acrylamide; immunoblot against GFP (abcam® ab6556 (1:5000 (v/v))). (B) 6% acrylamide. Left, immunoblot against GFP (abcam® ab6556 (1:5000(v/v))). Right, immunoblot against DGK-theta C-term (1:500 (v/v)).

Because the BiFC constructs were detected by the appropriate antibodies and were not detected in the untransfected cells, and because the constructs were of approximately the correct molecular weight, I concluded that they were successfully expressing. The presence of untagged DGK might dilute the BiFC signal in cells expressing YN-DGK-theta or YC-DGK-theta. Also, the relative amounts of each construct in each coexpression cannot be estimated from the immunoblot, because the intensity of the band might reflect the affinity of the antibody for the epitope (which might be enhanced by its three-dimensional context) rather than its abundance.

When I co-transfected the DGK-theta-YN and DGK-theta-YC constructs (the two constructs that appear not to produce any untagged DGK that might dilute the signal) into HEK293T cells, the DGK BiFC constructs gave no detectable signal, at either of the two ratios of transfection tested (Figure 162**D** and **E**). Not surprisingly, the positive control

of FLAG/YN-Smad3 cotransfected with FLAG/YN-Smad4 gave a weaker signal when excited at 488 nm (Figure 162**C**) than it did at 514 nm (Figure 160**C** and **D**), but the signal was still discernible. I confirmed the expression of DGK BiFC constructs by immunoblotting (Figure 162).

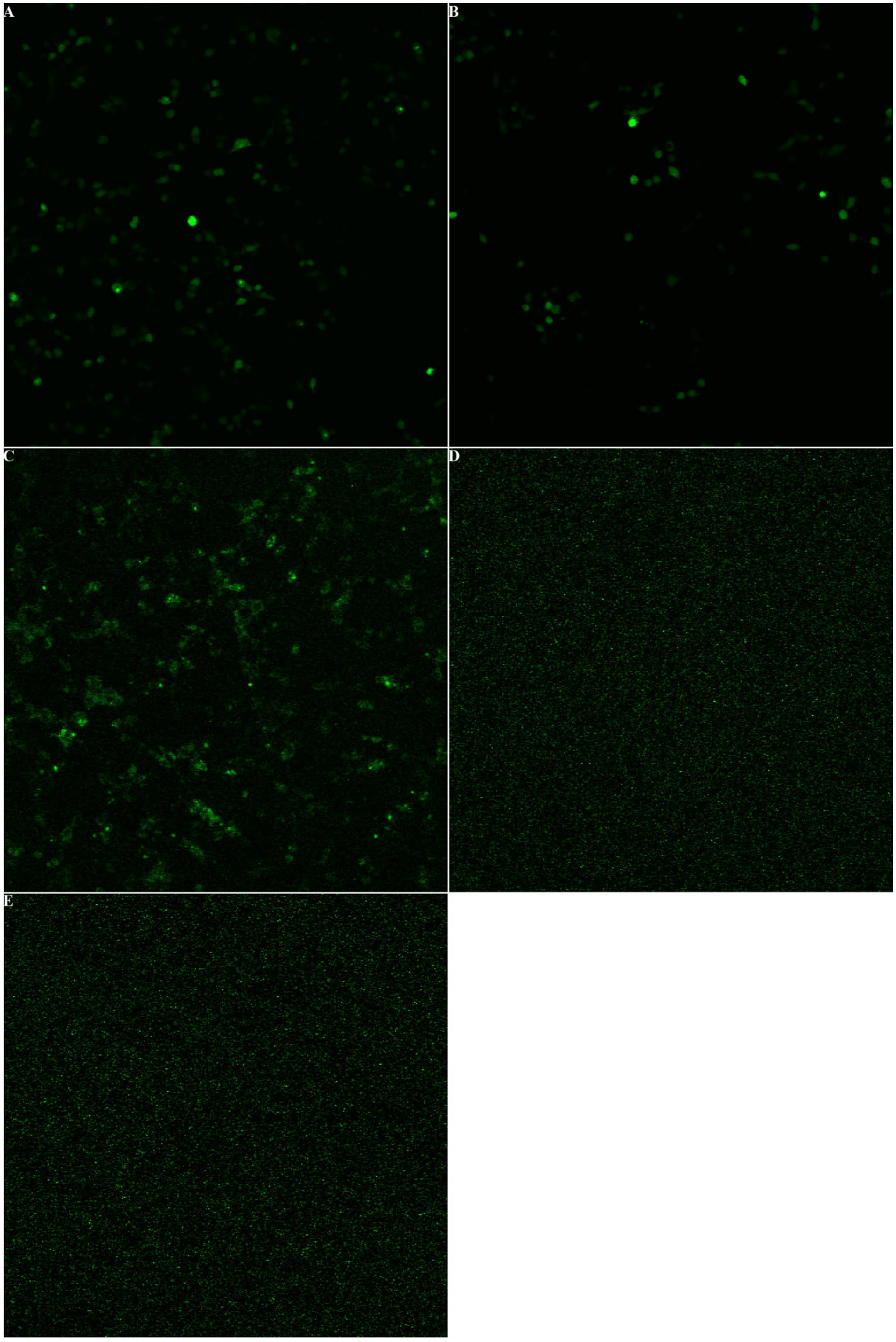
A
B
C
D
E

Figure 162. DGK-theta-YN / DGK-theta-YC do not produce a BiFC signal. I transfected the DNA (2 µg for each construct or 4 µg per well in a six-well plate) into HEK293T cells using HiFect® Reagent and Opti-MEM® Reduced Serum Medium for 3.5 hours, and observed the cells two days later on a Zeiss laser scanning microscope (LSM) 510 Inverted META. The excitation wavelength was 488 nm, and the signal was observed through a 505nm+ filter. **(A)** and **(B)**: two representative panels from cells transfected with GFP-C2 as a positive control for transfection. **(C)** Cells transfected with FLAG/YN-Smad3 and FLAG/YN-Smad4. (**D)** Cells transfected with DGK-YN-theta and DGK-YC-theta in a 1:1 ratio. **(E)** Cells transfected with DGK-YN-theta and DGK-YC-theta in a 0.9:1.1 ratio.

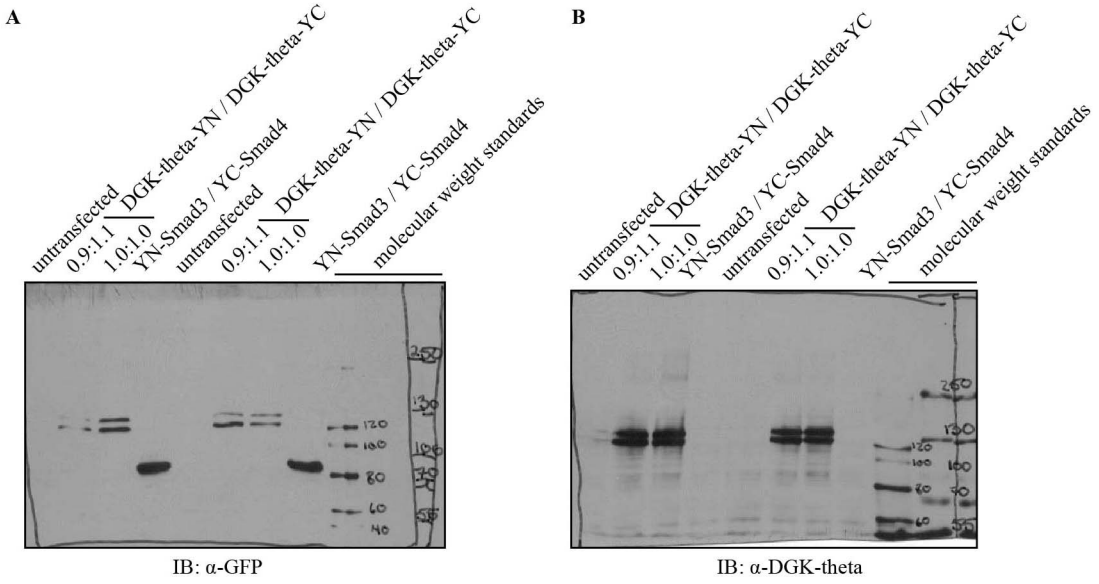

Figure 163. DGK-theta-YN / DGK-theta-YC express. After imaging the cells shown in **Figure 162**, I removed the medium, added lysis buffer (FB, 0.1% (v/v) Triton X-100, 1x PIC), and incubated on ice. I resuspended the cells in the lysis buffer, and loaded 15 µg total protein (as measured by the Bio-Rad Protein Assay) per lane. SDS-PAGE of a 6% acrylamide gel, followed by immunoblotting against (A) GFP (abcam® ab6556 (1:5000 (v/v))), and (B) DGK-theta Cterm (1:500 (v/v)).

The DGK BiFC signal could very well depend on the orientation of the YFP fragments relative to the DGK interface: that was the very reason that I made four DGK BiFC constructs and not just two. I therefore transfected HEK293T cells with each of the remaining three possible combinations: YN-DGK-theta and YC-DGK-theta, YN-DGK-theta and DGK-YC-theta, and DGK-YN-theta and YC-DGK-theta. Although positive controls for transfection (Figure 164**A**) and BiFC (Figure 164**B**) gave a clearly detectable signal, I could not detect any BiFC signal for any of the DGK-BiFC combinations,

cotransfected at multiple ratios (Figure 164**C-I**). Immunoblotting against DGK-theta and GFP confirmed the expression of all the constructs.

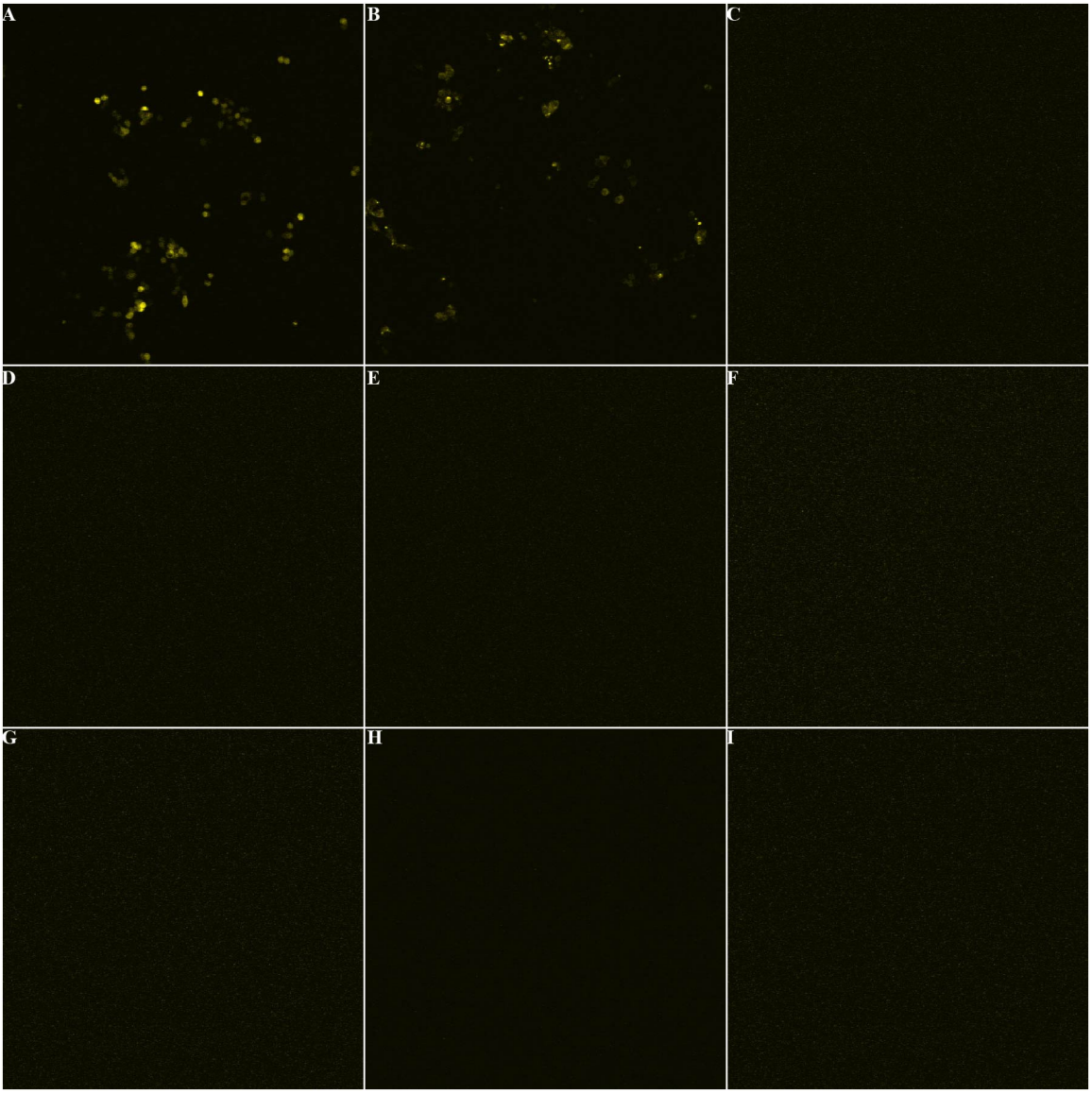

Figure 164. None of the tested DGK BiFC construct combinations produce a BiFC signal. I transfected the DNA (2 µg for each construct or 4 µg per well in a six-well plate) into HEK293T cells using HiFect® Reagent and Opti-MEM® Reduced Serum Medium for 3.5 hours, and observed the cells two days later on a Zeiss laser scanning microscope (LSM) 510 Inverted META. The excitation wavelength was 514 nm, and the signal was observed through a 530-600nm filter. Representative panels are shown. **(A)** Cells transfected with GFP-C2 as a positive control for transfection. **(B)** Cells transfected with FLAG/YN-Smad3 and FLAG/YN-Smad4 in a 1:1 ratio as a positive control for BiFC. **(C)** Cells transfected with YN-DGK and YC in a 1:1 ratio as a negative control. **(D)** Cells transfected with YN and YC-DGK in a 1:1 ratio as a negative control. **(E)** Cells transfected with YN-DGK and YC-DGK in a 1:1 ratio. **(F)** Cells transfected with YN-DGK and DGK-YC in a 1:1 ratio. **(G)** Cells transfected with YN-DGK and DGK-YC

in a 1.25:0.75 ratio. **(H)** Cells transfected with DGK-YN and YC-DGK in a 1:1 ratio. **(I)** Cells transfected with DGK-YN and YC-DGK in a 1:25:0.75 ratio.

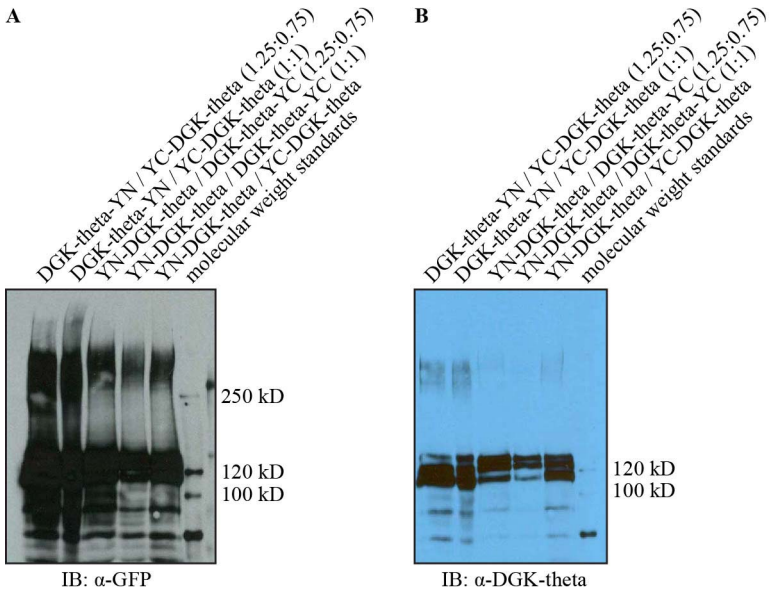

Figure 165. The DGK BiFC constructs expressed. After imaging the cells shown in **Figure 164**, I removed the medium and resuspended the cells in lysis buffer (FB, 0.1% (v/v) TX-100, 1x PIC). I loaded 14 µL per lane. SDS-PAGE of a 15% acrylamide gel followed by immunoblotting against (A) GFP (abcam® ab6556 (1:5000 (v/v))) and (B) DGK-theta Cterm (1:350 (v/v)).

Discussion and Conclusions

The negative controls (YN and YC) do not produce a BiFC signal, even though the positive controls (YN-Smad3 and YC-Smad4) in the same transfection do. The DGK BiFC constructs express, but none of the tested DGK BiFC construct combinations produce a BiFC signal.

One possible explanation for the lack of BiFC signal for any of the cotransfections tested is that DGK-theta, unlike the other LCB5 family proteins mentioned, might not dimerize. On the other hand, even if DGK-theta was dimerizing, the DGK BiFC signal could very well be weaker than that of the positive control, because its affinity for itself could be lower than the affinity between Smad3 and Smad4. Even for an equal affinity, we would expect half the BiFC signal (because, if the DGK-theta

dimerized randomly, one-quarter would be DGK-theta-YN/DGK-theta-YN pairs, and give no signal, and one-quarter would be DGK-theta-YC/DGK-theta-YC pairs, and give no signal, leaving only half of the dimerized DGK in DGK-theta-YN/DGK-theta-YC pairs). For BiFC constructs in which the DGK was fused to the C-terminus of the YFP fragments and included its own start codon, the signal would be even further diluted by competition from untagged DGK-theta. Yet another possible explanation is that the DGK-theta dimerization interface might not be compatible with any of the four combinations tested, such that DGK-theta did dimerize but gave no BiFC signal using these constructs. Thus, while I failed to find any evidence using the BiFC approach that DGK-theta dimerizes, I cannot conclude that DGK-theta does not dimerize, only that any oligomeric interaction between DGK-theta and itself is undetectable using these particular constructs.

BiFC and the interaction between tau and *H. sapiens* DGK-theta in mammalian cells

Introduction

Purified *H. sapiens* DGK-theta's enzymatic activity is activated *in vitro* by polybasic proteins including tau[3]. If DGK-theta and tau directly interact physically, they would be expected to produce a BiFC signal when attached to the appropriate YFP fragments. Using the DGK-theta BiFC constructs described in the previous subchapter, we therefore decided to use a BiFC approach to see whether we could see a BiFC signal produced by a DGK-theta/tau interaction. Phorbol esters such as phorbol 12-myristate 13-acetate (PMA) have been shown to increase DGK activity and enhance the association

of DGKs with other proteins[38], so we were also curious whether any BiFC-reflected association between DGK-theta and tau depended on PMA. Because PMA also activates protein kinase C (PKC), I also tested whether any such PMA-induced effect depended on pretreatment with PKC inhibitors.

Results

I looked at the YFP signal of two of the DGK BiFC constructs discussed previously (DGK-theta-YN and DGK-theta-YC) when coexpressed with two tau BiFC constructs, YN-tau40 and YC-tau40. Of the combinations tested, however, only the positive control for BiFC (FLAG/YN-Smad3 cotransfected with FLAG/YC-Smad4, described in the previous subchapter) gave a BiFC signal.

Whenever I checked the expression of YN-tau40 by immunoblot (among four different expressions, in both HEK293T and COS7 cells), I never saw any anti-GFP antibody-immunoreactive band of the appropriate size in any of the transfected lysates, even though the anti-GFP antibody was able to recognize YN fused to either end of DGK-theta (Figure 161**B**, Figure 163**A**, and Figure 165**A**) and therefore would be predicted to recognize YN on tau40 as well. What I did observe was a band that was immunoreactive to the anti-GFP antibody, but not the anti-tau antibody, that migrated slightly faster than GFP (whose molecular weight is 27 kD) (Figure 166).

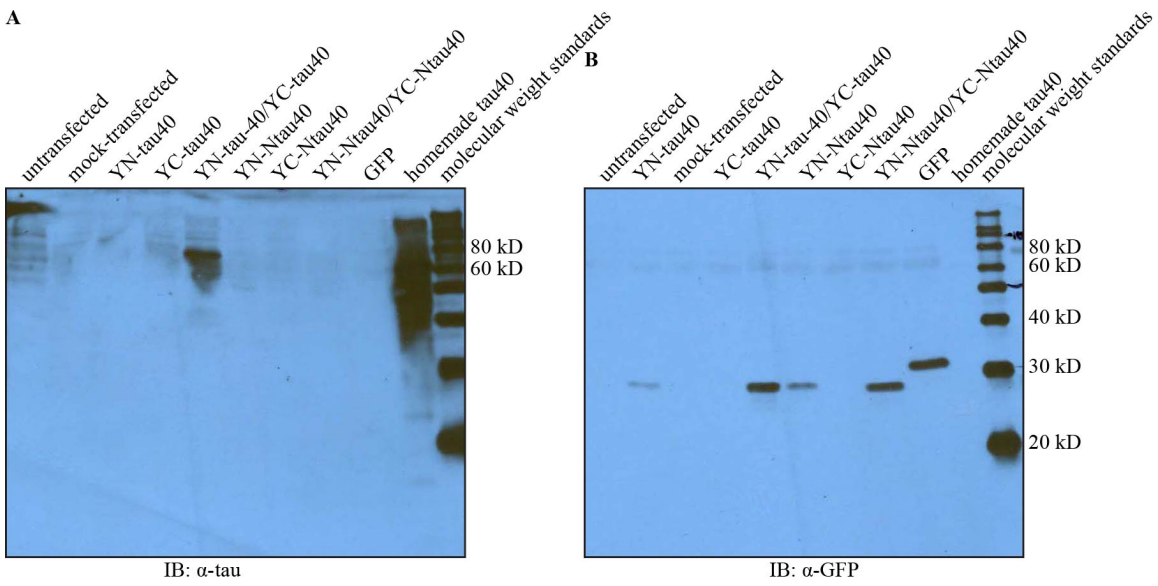

Figure 166. The anti-GFP antibody does not recognize a band of the appropriate size in YN-tau40-transfected lysates, but does recognize a band migrating slightly faster than GFP (27 kD). I transfected the DNA (0.5 µg for each construct or 1 µg per well in a twelve-well plate) into COS-7 cells using HiFect® Reagent and Opti-MEM® Reduced Serum Medium for four hours, and observed the cells on a fluorescent microscope two days later. Seeing no BiFC signal, I removed the medium by aspiration, and added lysis buffer (FB, 1x PIC, 0.5% (v/v) NP-40) to the cells on ice and scraped. I loaded 12 µL lysate per lane. SDS-PAGE of a 10% acrylamide gel followed by immunoblotting against (A) tau (1:30,000 (v/v)), and (B) GFP (abcam® ab6556 (1:1000 (v/v))).

Much later, when I was finally able to access the original sequencing data for the YN-tau40 constructs, I found a single nucleotide insertion in the fourth amino acid of the tau40 sequence, such that only the first three amino acids of tau40 are expressed, followed by a string of thirty-six amino acids (resulting from the frame shift and thus not from tau40), followed by a prematurely introduced stop codon, producing a protein with a predicted size of 25 kD that includes all of the YN but almost none of the tau40, consistent with the anti-GFP-immunoreactive band I saw in Figure 166. The "YN-tau40" construct, therefore, was not helpful for addressing whether DGK and tau can produce a BiFC signal, seeing as it did not encode tau. Unfortunately, in two out of three experiments attempting to reproduce reported observations of a PMA-induced BiFC signal, I focused on the constructs reported to produce that result, YN-tau40 and DGK-

theta-YC, and tried to optimize expression with varying ratios of transfected DNA. As a result did not test the other combination, YC-tau40 and DGK-theta-YN in those experiments.

I observed that when HEK293T cells were treated with PMA, they released the plate and rounded up (Figure 167), which resulted in an increase in autofluorescence. This increase in autofluorescence could explain the PMA-dependent increase in "BiFC" signal that was reportedly observed in the "YN-tau40" and DGK-theta-YC cotransfected cells.

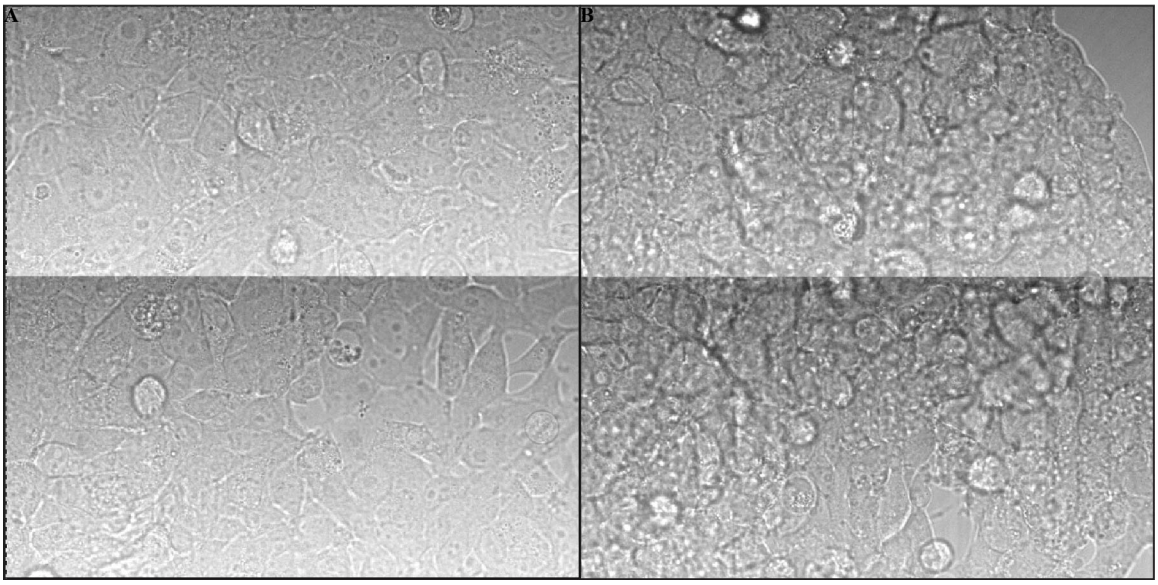

Figure 167. Treating HEK293T cells with 500 nM PMA causes them to release the plate and round up. HEK293T cells that I had transfected with 1 μg each of YN and DGK-theta-YC in a 35 mm coverslip-bottomed dish for three hours and observed two days later on an Olympus I fluorescence microscope on brightfield. **(A)** Brightfield before PMA treatment. **(B)** Brightfield five minutes after adding PMA to 500 nM, refocused due to the z-drift caused by the cells' motion.

The first experiment I tried with the tau and DGK BiFC constructs did include YC-tau40 coexpressed with YN-DGK-theta. Before I could conclude anything about the lack of BiFC signal from the coexpression, I first needed to confirm that the constructs expressed, which I tested by immunoblotting the lysates of the cells. I never did access

the sequence of the YC-tau40 construct, but I estimated from the size of YC and the published sequence of tau40 that the fusion construct must be at least 91 kD. I first immunoblotted against GFP, which I had previously shown to recognize both the YN and YC fragments when fused to target proteins (Figure 161**B**, Figure 163**A**, and Figure 165**A**). In the lysates cotransfected with YN and with YC-tau40, I observed a faint immunoreactive band greater than 70 kD not visible in the mock-transfected lysate (Figure 168**A**), consistent with YC-tau40 expression. However, this band was the same size as the immunoreactive band in the adjacent lane, and thus may have resulted from lane contamination, which can result from the interface between the stacking and separating phases of the gels' drying out during casting. In order to confirm the expression of YC-tau40, I therefore ran a fresh gel and immunoblotted against tau-5. The anti-tau-5 antibody recognized three new bands in the lysates transfected with YC-tau40 not seen in the mock-transfected lysate, but all of these bands migrated faster than the 70 kD molecular weight marker (Figure 168**B**). These bands are consistent with some sort of recombinant expression of tau or part of tau, but because these bands do not coincide with the anti-GFP-immunoreactive band, and because they are too small to be the YC-fused protein, I therefore concluded that the "YC-tau40" construct was not properly expressing as a fusion protein of YC and tau40. Whether this failure to express is due to some complication from this particular expression (such as proteolytic processing by the HEK293FT cells) or due to some problem with the construct (such as a frameshift, as seen in the YN-tau40 construct, or a second start codon at the beginning of the tau40 sequence) is unclear because I was unable to access the sequence of the YC-tau40 construct.

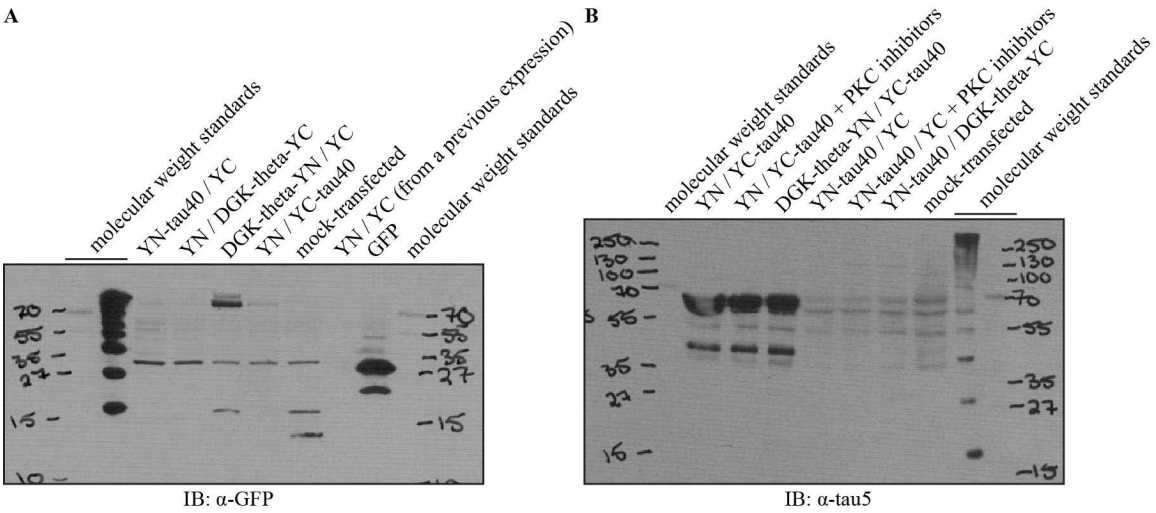

Figure 168. The YC-tau40 construct did not properly express in HEK293FT cells as a fusion protein of YC and tau40. I transiently transfected HEK293FT cells with 0.75 µg of each DNA construct (for a total of 1.5 µg DNA per 35 mm glass-bottomed plate) for three hours, and observed the cells on an Olympus I fluorescence microscope two days later. Seeing no BiFC signal, I removed the medium by aspiration, and resuspended the cells in lysis buffer (FB, 10 mM NaCl, 1x PIC, 0.1% (v/v) Triton X-100). I loaded 20 µg total protein (as measured by the Bio-Rad Protein Assay) per lane. (A) SDS-PAGE of a 15% acrylamide gel followed by immunoblotting against GFP (abcam® ab6556 (1:500 (v/v))). (B) SDS-PAGE of an 8% acrylamide gel followed by immunoblotting against tau5 (1:5000 (v/v)).

Discussion and Conclusions

Because neither the YN-tau40 construct nor the YC-tau40 construct expressed, I did not observe any BiFC signal between the tau and DGK BiFC constructs. Previous reports of a PMA-dependent BiFC signal could be explained by the reaction of control cells to PMA, and did not depend on the presence of the BiFC constructs. It remains to be seen whether a direct DGK-tau interaction could be observed by a BiFC approach, but any such approach would require cloning new tau BiFC constructs, and confirming their proper translational frame by DNA sequencing.

Chapter 7: Proteolysis to Probe Structure

Introduction

We were curious as to whether the N-terminal accessory domains of mammalian DGK auto0inhibited the C-terminal catalytic domain, and whether activation by polybasic proteins and/or lipids operated via any such N-terminal auto-inhibition. An obvious approach to answer this question would be to express the C-terminal catalytic domain by itself and compare its activity and activation to that of full-length DGK, but I experienced solubility challenges for recombinantly expressed truncations of DGK. I therefore wondered whether we could approach this problem by allowing the protein to fold (in the setting of a mammalian cell, for mammalian DGK) first, and then truncating it via proteolysis after the protein has folded.

Results

I used the Peptide Cutter tool[152] on the ExPASy (which originally stood for "Expert Protein Analysis System"), the Swiss Institute of Bioinformatics (SIB)'s bioinformatics resource portal[153], to determine which commonly available proteases would digest mammalian DGK isoforms into tractable fragments. For the sequences I examined, the most promising protease was thrombin, which was predicted to cut *H. sapiens* DGK-theta in two places, at position 127 (between the first and second C1 domains), and at position 394, just before the RA domain (Figure 169). Digestion of untagged DGK-theta would therefore be predicted to produce three fragments: a 13 kD N-terminal fragment including the first C1 domain, a 28 kD middle fragment including the second two C1 domains, and a 60 kD C-terminal fragment including the RA and

LCB5 domains. Incomplete digestion would also produce a 41 kD N-terminal fragment including all three C1 domains, and an 88 kD C-terminal fragment including the second two C1 domains, the RA domain, and the LCB5 domain. The predicted size of these fragments would be modified by the addition of any epitope tags to the N- or C-terminus of the DGK-theta construct used.

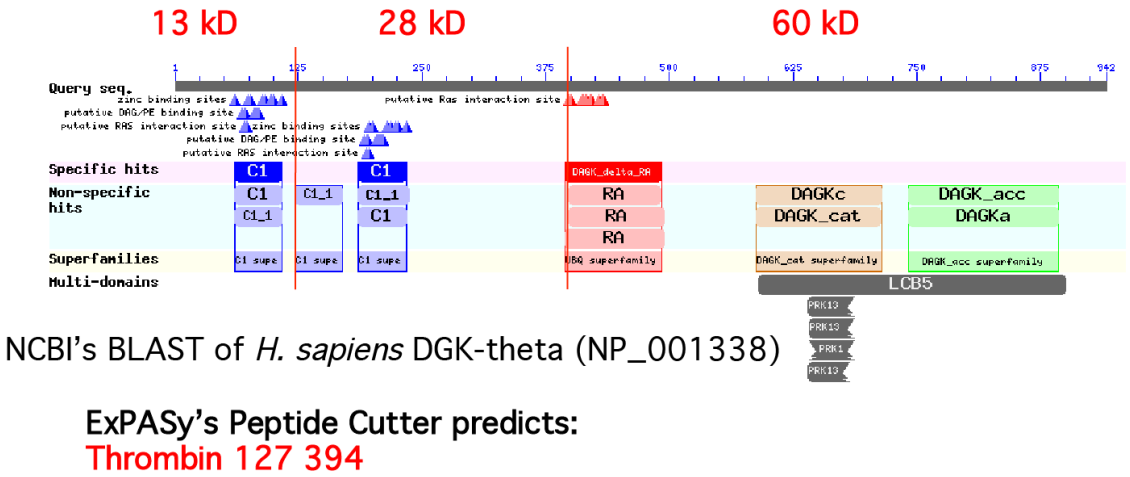

Figure 169. Schematic of predicted thrombin digestion sites on *H. sapiens* DGK-theta. I performed a BLAST search of the sequence of *H. sapiens* DGK-theta (NP_001338), which automatically annotated the sequence according to the Conserved Domain Database with three C1 domains, an RA domain, and an LCB5 domain. Red vertical lines indicate the location of the predicted thrombin sites relative to the annotated domains in the sequence.

In order to test whether the thrombin in the freezer was still active, I tested its activity on a synthetic chromogenic substrate, N-(p-Tosyl)-Gly-Pro-Arg p-nitroanilide acetate salt[154], by measuring the absorbance at 385 nm of the substrate as a function of time in the presence of six different concentrations of thrombin. For the three most concentrated samples of thrombin, the reaction had already gone to completion on ice in the time it took to mix the reaction and measure the absorbance of it, and all of the tested concentrations went to completion within four hours at 4°C (Figure 170). I therefore concluded that the thrombin in the freezer was still active.

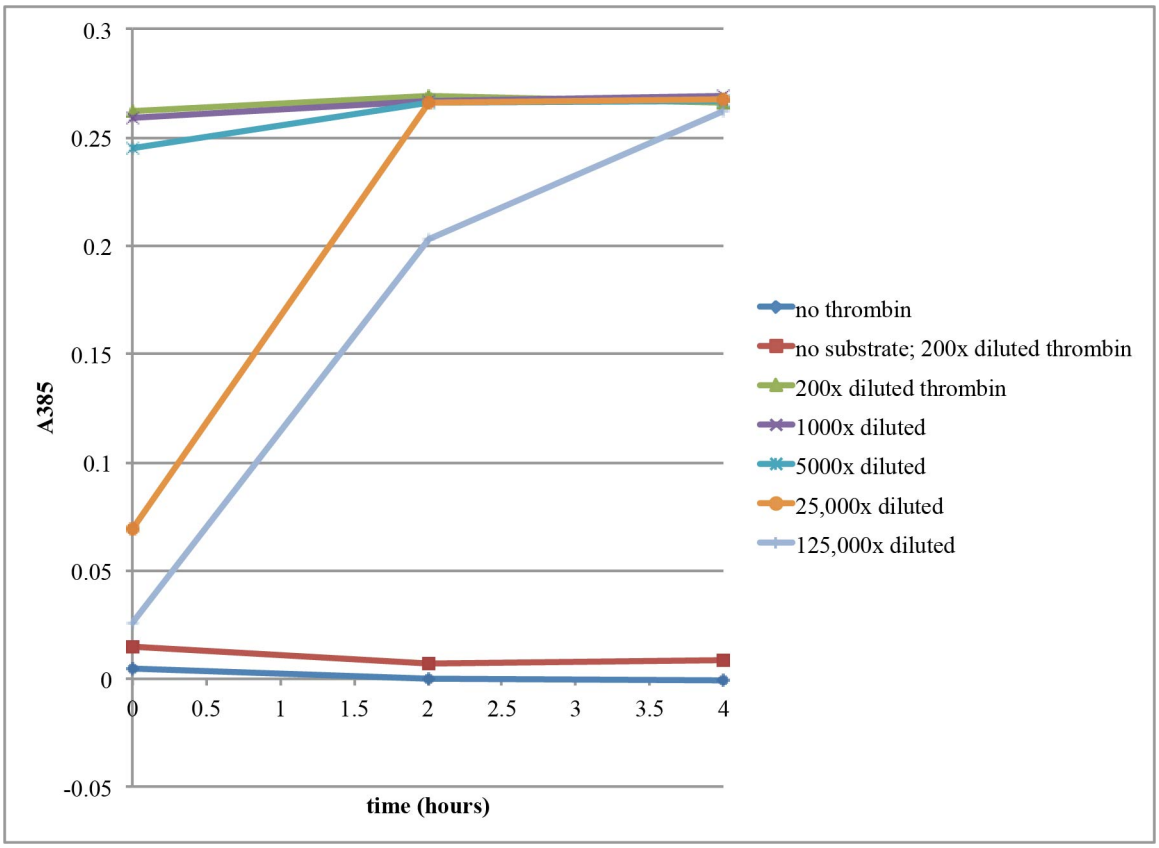

Figure 170. The thrombin in the freezer was still active on a chromogenic substrate under the conditions tested. Absorbance at 385 nm as a function of time of chromogenic substrate (16.4 μM) in the presence of six different concentrations of thrombin, in 10 mM HEPES, 10 mM Tris, pH 7.8, 100 mM NaCl, 0.1% (w/v) PEG-8000.

I next tested conditions for digesting purified *H. sapiens* DGK-theta with the thrombin. The construct of DGK-theta I first used included a 25 kD C-terminal tag, such that the predicted sizes of the fragments would be 13 kD and 113 kD after a single cut at the first site, 41 kD and 85 kD after a single cut at the second site, and 28 kD after cuts at both sites (Figure 171). I incubated two different samples of purified DGK-theta with four different concentrations of thrombin, collected timepoints, and assessed the degree of digestion by silver staining following SDS-PAGE. The predominant band that migrated between the 120 and 160 kD molecular weight markers (Figure 172) was consistent in size to be full-length DGK-theta, whose molecular weight including the 25

kD C-terminal tag was predicted to be 126 kD. Incubation with thrombin that had been diluted 312,500-fold had no obvious effect on DGK-theta's migration pattern, even after 16 hours at 4°C (Figure 172**A**). Contrariwise, when I diluted the thrombin only 500-fold, the intensity of the heaviest band noticeably decreased as a function of time, and new bands that migrated between the 100 and 120 kD molecular weight markers emerged (Figure 172**B**), consistent with the predicted size of 113 kD after a single cut at the first site. The accompanying 13 kD band that would be produced by cutting at this site would have run off this 8% acrylamide gel. Cutting at the second size would be predicted to produce a band at 41 kD, but no new bands appeared during the timecourse that run between the 40 and 50 kD molecular weight markers. New bands running between the 30 and 40 kD molecular weight markers, between the 50 kD and 60 kD markers, and between the 100 kD molecular weight marker and the previously described 113 kD band do appear (Figure 172**B**); whether these fragments result from post-translational modification of predicted fragments, contaminating proteases in the thrombin sample, or cryptic thrombin sites in the epitope tag is unclear. These fragments are not visible in the samples incubated without thrombin, suggesting that they are not resulting from nonspecific degradation or from contaminated proteases from the purified DGK-theta. When I tested digestion of another batch of purified DGK-theta, once again, only in the highest concentration of thrombin tested did the predicted band migrating between 100 and 120 kD appear, as did the mystery band just above the 30 kD molecular weight marker (Figure 172**C**). I concluded that while the concentrations of thrombin tested in Figure 170 were perfectly adequate for digesting 16.4 μM chromogenic substrate, higher

concentrations would be required to generate the LCB5-including protein fragment of DGK-theta purified from HEK293T cells.

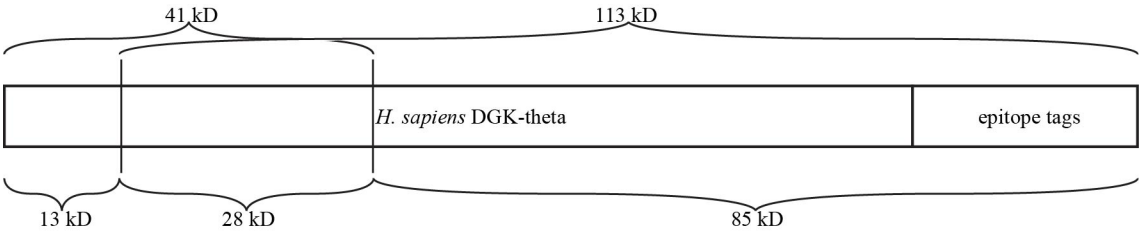

Figure 171. Schematic of predicted thrombin digestion sites on *H. sapiens* DGK-theta when 25 kD of C-terminal epitope tags are included. Vertical lines indicate the locations of the predicted thrombin sites.

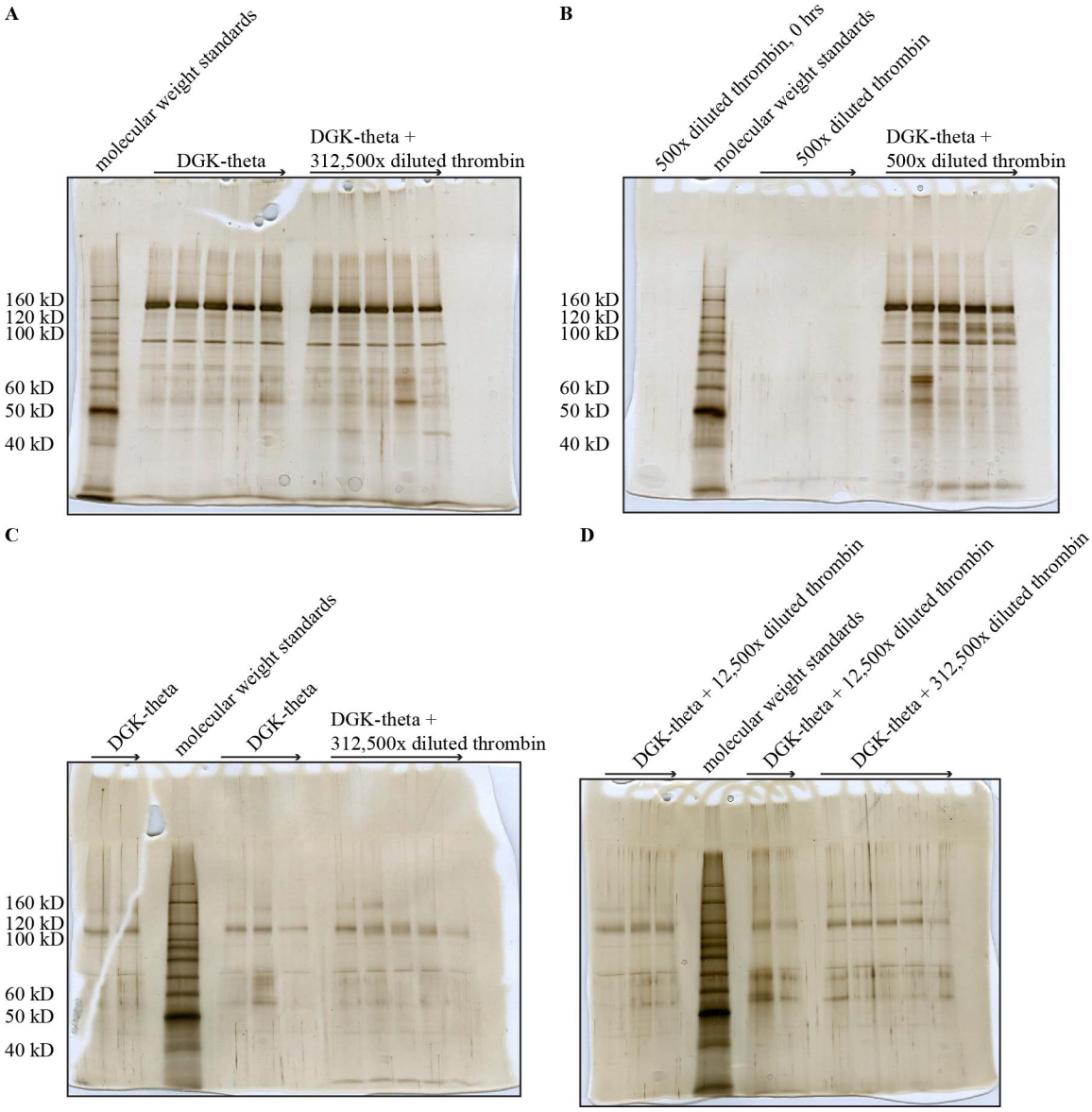

Figure 172. Higher concentrations of thrombin are required to generate the LCB5-including protein fragment of DGK-theta purified from HEK293T cells than to digest the chromogenic substrate. I incubated DGK-theta, which had been purified from cytosol on Protein A beads and washed with thrombin buffer (10 mM HEPES, 10 mM Tris, pH 7.8, 100 mM NaCl, 0.1% (w/v) PEG-8000), with different concentrations of thrombin in thrombin buffer at 4°C and took timepoints at 0, 2, 4, 8, and 16 hours. I quenched the reaction of each timepoint by adding SDS-gel-loading buffer to 1x. SDS-PAGE of 8% acrylamide gels followed by silver staining. Arrows indicate the passage of time. **(A)** Left, no thrombin. Right, 312500x diluted thrombin. **(B)** 500x diluted thrombin. Left, no DGK-theta. Right, DGK-theta cytosol purified on Protein A beads. **(C)** 414A batch of purified DGK-theta. Left, no thrombin. Right, 500x diluted thrombin. **(D)** 414A batch of purified DGK-theta. Left, 12,500x diluted thrombin. Right, 312,500x diluted thrombin.

I therefore incubated purified DGK-theta in the presence of undiluted thrombin at either 4°C, 16°C, or 37°C, collected timepoints, and once again assessed the degree of

digestion by silver staining following SDS-PAGE. There was no detectable difference between the timepoints taken from the incubations at 37°C and 16°C (i.e., the reaction appeared to be complete by thirty minutes' incubation at 37°C, and two hours' incubation at 16°C, the earliest timepoints taken for each), but the reaction did appear to progress more slowly at 4°C than at 16°C or 37°C (Figure 173). In the samples with thrombin, no detectable full-length DGK-theta remained after two hours. In the samples incubated at 4°C, a band between 100 and 120 kD (consistent with the 113 fragment that would be produced by a single cut) appeared at 2 hours, but disappeared overnight, consistent with cutting first at the first site, and then cutting a second time. New bands also appeared between 30 and 40 kD and between 70 and 80 kD in all the completely digested samples, but the intensity of these bands did not appear to sum to equal the intensity of the original full-length DGK-theta. It was unclear where the rest of the DGK-theta was going: as above, DGK-theta incubated in the absence of thrombin experienced no degradation, so it was unlikely to be resulting from nonspecific degradation or a contaminating protease in the DGK-theta.

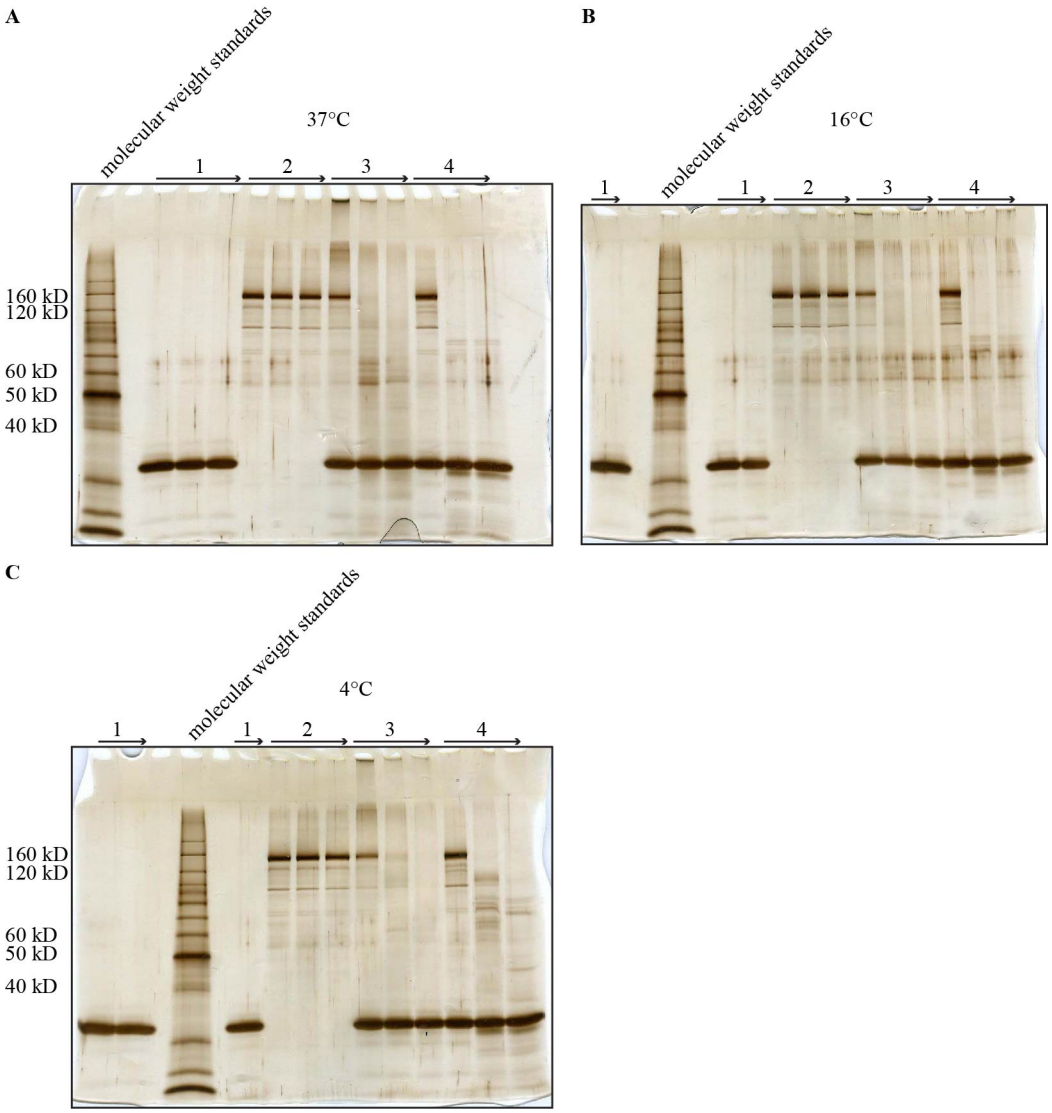

Figure 173. Higher concentrations of thrombin digest purified DGK-theta, but do not produce the expected pattern of bands. I stored the purified DGK-theta shown in **Figure 172**A and B for six days in 50% glycerol at -80°C prior to thawing and washing with thrombin buffer (10 mM HEPES, 10 mM Tris, pH 7.8, 100 mM NaCl, 0.1% (w/v) PEG-8000). Some of the purified DGK-theta I heat-inactivated at 100°C for twenty minutes. I incubated the DGK-theta with 3 µL thrombin per 30 µL reaction (10x diluted) (or not) in thrombin buffer at the indicated temperature. I took timepoints from the 37°C reaction at 0 minutes, 30 minutes, and two hours, and I took timepoints from the 16°C and 4°C reactions at 0 hours, two hours, and overnight. I quenched the reaction of each timepoint by adding SDS-gel-loading buffer to 1x. SDS-PAGE of 10% acrylamide gels followed by silver staining. 1, thrombin (no DGK); 2, DGK (no thrombin); 3, heat-denatured DGK plus thrombin; 4, DGK plus thrombin. Arrows indicate the passage of time. **(A)** 37°C incubations. **(B)** 16°C incubations. **(C)** 4°C incubations.

In order to find an optimal thrombin concentration for producing the C-terminal fragment of DGK-theta, I incubated DGK-theta with lower concentrations of thrombin

(though not so low as in the experiment shown in Figure 172) at 4°C, collected timepoints, and once again assessed the degree of digestion by silver staining following SDS-PAGE. As before, new bands appeared between 120 and 160 kD, between 100 and 120 kD, between 60 and 70 kD, between 30 and 40 kD, and between 25 and 30 kD, some of which are consistent with the predicted fragments of 13 kD, 28 kD, 41 kD, 113 kD, and 126 kD. As before, the sum of the intensities of these bands did not appear to equal the intensity of the original DGK-theta. None of these bands were visible in the Protein A sepharose and thrombin samples, suggesting that they are came from the DGK-theta purification.

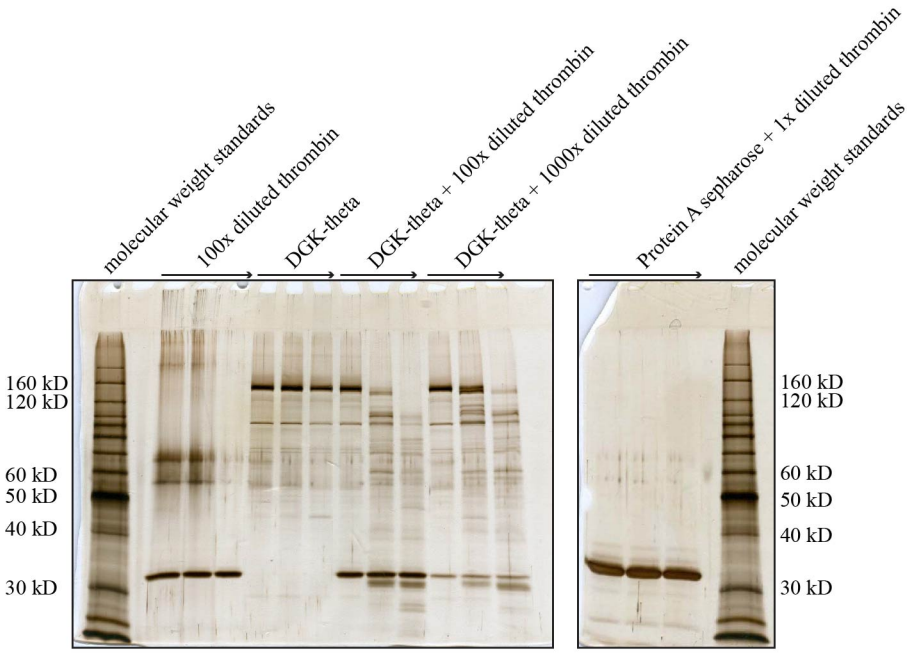

Figure 174. Incubation of purified DGK-theta with moderate amounts of thrombin produces new bands detectable by silver staining, some of which are consistent with the predicted size, but do not appear to total the intensity of the original band. I stored the purified DGK-theta shown in **Figure 173** for four days in 50% glycerol at -80°C prior to thawing and washing with thrombin buffer (10 mM HEPES, 10 mM Tris, pH 7.8, 100 mM NaCl, 0.1% (w/v) PEG-8000). I incubated the DGK-theta with different concentrations of thrombin in thrombin buffer at 4°C, and took timepoints at 0, 2, and 20 hours. I quenched the reaction of each timepoint by adding SDS-gel-loading buffer to 1x. SDS-PAGE of 10% acrylamide gels followed by silver staining. Arrows indicate the passage of time.

Because of uncertainty resolving which of the produced bands was actually the C-terminal band I was looking for, I decided to immunoblot against the Fc tag on the C-terminus to follow thrombin digestion of DGK-theta. However, when I immunoblotted against Fc, I was unable to detect any of the DGK-theta. On the other hand, the secondary antibody wasn't able to recognize the Magic Mark™ XP Western Protein Standard (Life Technologies™) molecular weight standards, either, so the lack of recognition was probably an antibody problem rather than a construct problem. Contrariwise, the anti-DGK-theta antibody was readily able to detect the DGK-theta (Figure 175). Protein A sepharose and thrombin produced no anti-DGK-theta-antibody immunoreactive bands (Figure 175**A**). As I had observed with the silver stains, when DGK-theta was incubated over time in the absence of thrombin, full-length DGK-theta persisted (Figure 175**B**), suggesting that the digested bands were not produced by nonspecific degradation or by proteases copurifying with DGK-theta. Contrariwise, when DGK-theta was incubated with thrombin, the immunoreactive band corresponding with full-length DGK-theta disappeared as a function of time and was undetectable after 22 hours, and lower immunoreactive bands appeared as time progressed (Figure 175**C**). The first band to appear, visible at 2.5 hours and even faintly at the 0 hour timepoint (and therefore produced in the time taken to mix the reaction), migrated between the 80 and 100 kD molecular weight markers, and was consistent with the 85 kD fragment that would be predicted to be formed by thrombin's cutting at the second thrombin site. The corresponding peptide, at 41 kD, would be predicted to have run off the gel, and, furthermore, was unlikely to be able to be detected by the monoclonal antibody directed against the C-terminus of DGK-theta. After 5.5 hours, two more immunoreactive bands

appeared: one that migrated between 100 and 120 kD and thus was consistent with the 113 kD fragment produced by thrombin's cutting at the first site, and one that migrated between 60 and 80 kD, whose identity was unclear. By 22 hours, two more immunoreactive bands appeared: one that ran just above the mystery band, also between 60 and 80 kD, whose identity was equally mysterious, and one that ran between the dye front and the 60 kD molecular weight marker. Only three possible immunoreactive bands were expected (126 kD for full-length, 113 kD for the C-terminus left from cutting at the first site, and 88 kD for the C-terminus left from cutting at the second site), yet I observed five different bands. As with the silver stain, the intensity of these bands did not appear to sum to the intensity of the original, full-length band (although using the immunoblot signal as a measure of protein abundance assumes that antibody has equal affinity for all the proteolyzed fragments, which it very well might not have). Consistent with the Fc tag's being on the C-terminus of the construct, the immunoreactive bands remained largely in the pellet fraction, consistent with still being bound to the Protein A sepharose resin.

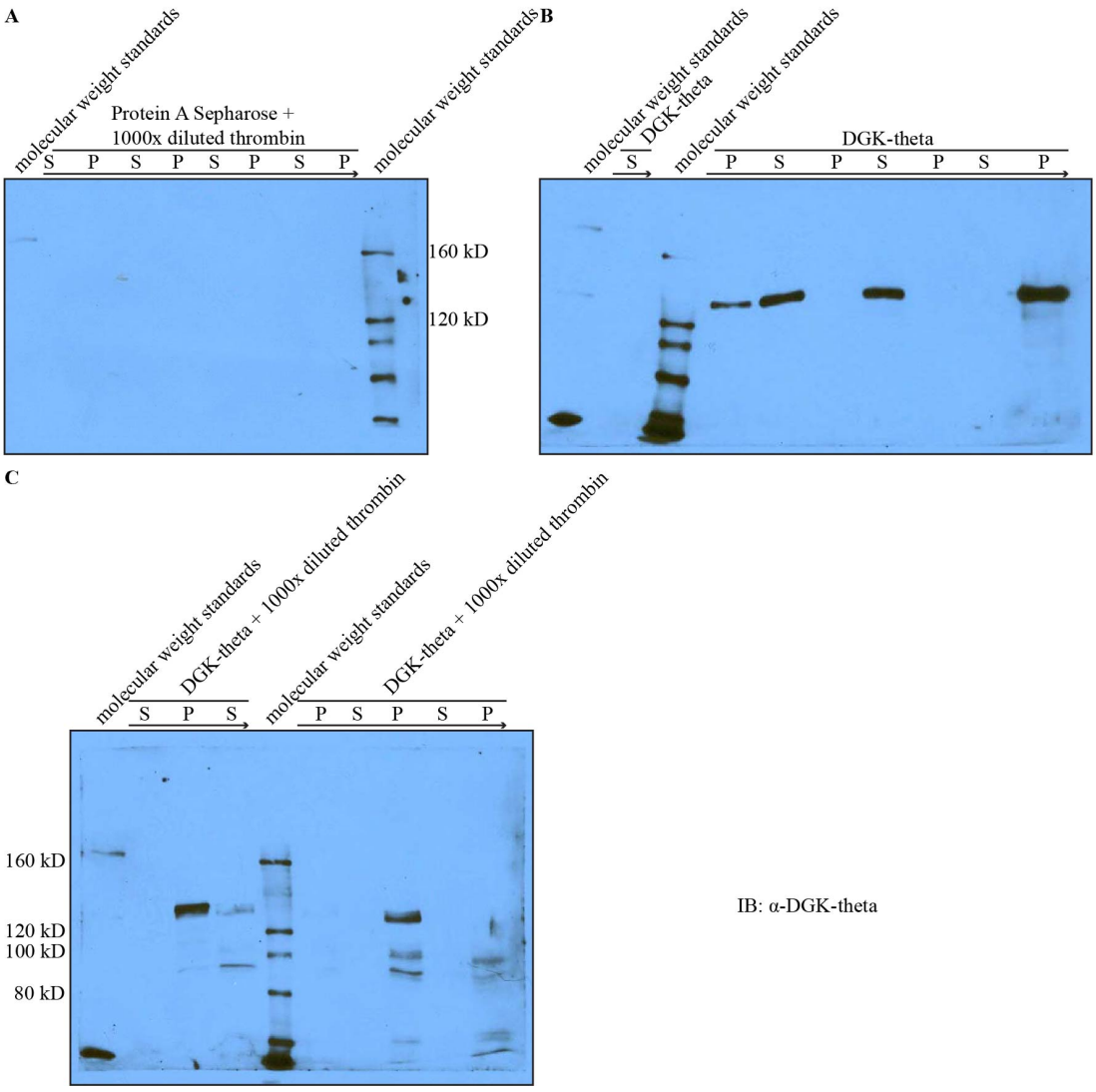

Figure 175. Incubation of purified DGK-theta with thrombin produces new bands detectable by immunoblotting against DGK-theta, some of which are consistent with the predicted size. I stored the purified DGK-theta shown in **Figure 174** for four days in 50% glycerol at -80°C prior to thawing and washing with thrombin buffer (10 mM HEPES, 10 mM Tris, pH 7.8, 100 mM NaCl, 0.1% (w/v) PEG-8000). I incubated the DGK-theta with or without 1000x diluted thrombin in thrombin buffer at 4°C, and took timepoints at 0, 2.5, 5.5, and 22 hours. For each timepoint, I microfuged the sample to separate the supernatant from the pellet. I quenched the reaction of each timepoint by adding SDS-gel-loading buffer to 1x. SDS-PAGE of 6% acrylamide gels followed by immunoblotting against DGK-theta (1:350 (v/v)). Arrows indicate the passage of time. S, supernatant; P, pellet. **(A)** Protein A sepharose with thrombin. **(B)** DGK-theta without thrombin. **(C)** DGK-theta with thrombin.

Concerned that the old thrombin from the freezer might be contaminated with other proteases, which would explain the presence of unexpected bands and also why the intensity of those bands was less than expected, I bought some new, supposedly highly

purified thrombin (Calbiochem (now EMD Millipore) 605195). I compared the digestion of purified DGK-theta with the old thrombin vs. the new thrombin. The new thrombin digested almost all of the full-length DGK-theta such that no full-length band was detectable after one hour, but in this experiment the old thrombin likewise completely digested DGK-theta within one hour (Figure 176), although the conditions were supposedly the same as in Figure 175. Also unlike previous experiments, in this experiment the intensity of the signal of DGK-theta incubated in the absence of thrombin also decreased over time (Figure 176). At the time, I interpreted these results as problems of inherent irreproducibility of this approach, but in hindsight, primary antibody reuse may be a problem. At the time I was in the habit of reusing dilutions of primary antibody, to be frugal. However, such reuse can lead to irreproducibility among blots: antibodies that have been diluted longer may have weaker affinity for their epitopes because of degradation or denaturation, and dilutions that have been used more than once may have lower concentrations of antibody because antibody molecules may have been left adhered to previous blots. The differences between Figure 175 and Figure 176B, therefore, may reflect more about antibody irreproducibility than thrombin digestion irreproducibility. But, as was seen in previous experiments, the intensity of the faster-running fragments was once again considerably lower than that of the full-length enzyme, making it very difficult to monitor the size and number of newly appearing bands.

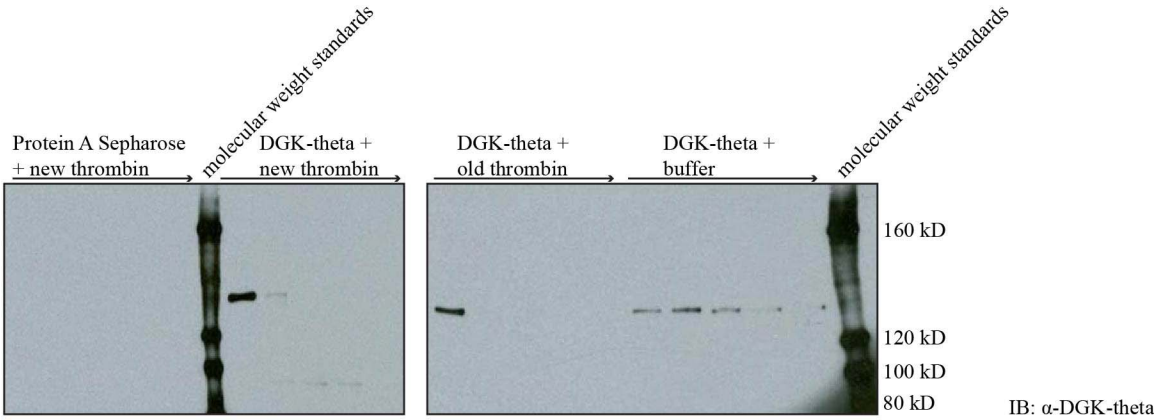

Figure 176. Irreproducibility in immunoblotting detection among thrombin digestions might have resulted from primary antibody reuse. I stored the purified DGK-theta shown in **Figure 175** for eleven days in 50% glycerol at -80°C prior to thawing and washing with thrombin buffer (10 mM HEPES, 10 mM Tris, pH 7.8, 100 mM NaCl, 0.1% (w/v) PEG-8000). I incubated the DGK-theta with either 1000x diluted old thrombin or else 1 mU per µL new (Calbiochem) thrombin in thrombin buffer at 4°C, and took timepoints at 0, 1, 2, 4, and 18 hours. I quenched the reaction of each timepoint by adding SDS-gel-loading buffer to 1x. SDS-PAGE of 6% acrylamide gels followed by immunoblotting against DGK-theta (1:350 (v/v)). Arrows indicate the passage of time.

At this point, I ran out of purified DGK-theta and needed to purify more. Once I had expressed and purified Fc-FLAG-DGK-theta from 293FT cells (Figure 84**A**-**B**), I tested the digestion of this new construct by thrombin. With 28 kD of N-terminal epitope tags, the predicted size of the fragments produced by thrombin digestion of this construct are 41 kD and 88 kD after a single cut at the first thrombin site, 69 kD and 60 kD after a single cut at the second thrombin site, and 28 kD after cutting at both sites (Figure 177). The conditions that had robustly digested the previous batch of purified DGK-theta did not digest this batch of purified DGK-theta any more than heat-denatured thrombin did (Figure 178**A**). Silver staining confirmed that two hours at 4°C with 1 mU per µL of the Calbiochem thrombin was insufficient to digest this new batch of purified DGK-theta (Figure 178**B**). I therefore needed to work out afresh thrombin digestion conditions for this new batch of purified DGK-theta.

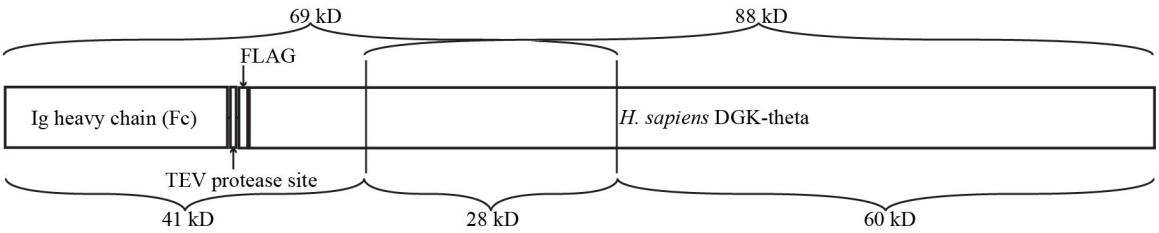

Figure 177. Schematic of predicted thrombin digestion sites on the Fc-FLAG-DGK-theta construct. Vertical lines indicate the locations of the predicted thrombin sites.

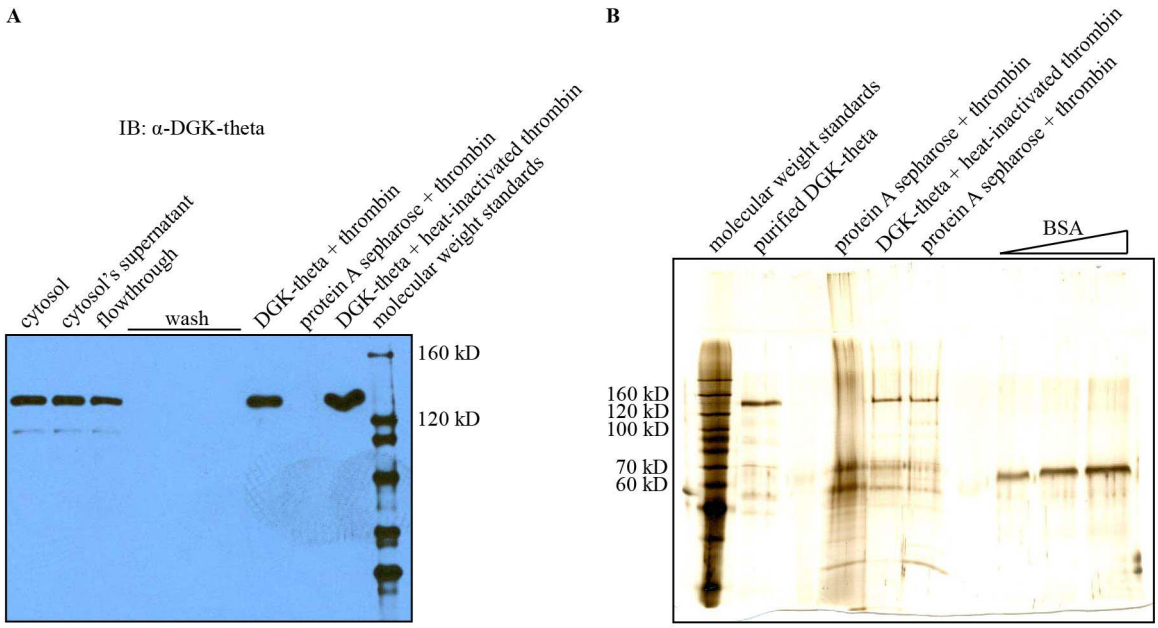

Figure 178. Purified Fc-FLAG-DGK-theta requires different thrombin digestion conditions than the C-terminally tagged DGK-theta construct. I stored the purified DGK-theta shown in **Figure 84**A-B for two days in 50% (v/v) glycerol at -80°C prior to thawing and washing with thrombin buffer (10 mM HEPES, 10 mM Tris, 100 mM NaCl, 0.1% (w/v) PEG-8000, pH 7.5). I incubated the DGK-theta or protein A sepharose with 1 mU per µL thrombin (Calbiochem) in thrombin buffer at 4°C for two hours. I quenched the reaction by adding SDS-gel-loading buffer to 1x. **(A)** SDS-PAGE followed by immunoblotting against DGK-theta (1:350 (v/v)). **(B)** SDS-PAGE of an 8% acrylamide gel followed by silver staining.

When I increased the thrombin concentration tenfold, the band migrating between the 120 and 160 kD molecular weight markers corresponding to full-length DGK-theta decreased in intensity as a function of time in the samples incubated with thrombin, but not heat-inactivated thrombin, such that by 22 hours the band had completely disappeared (Figure 179). The intensity of the thrombin band was greatly decreased for the heat-

inactivated thrombin samples (Figure 179**A**), so perhaps thrombin's failure to digest DGK-theta resulted less from heat-inactivation as it did from thrombin's being left behind in the PCR tube following the heat inactivation. As the full-length DGK-theta disappeared, a new band migrating between the 100 and 120 kD molecular weight markers appeared, which is puzzling, because none of the products of Fc-FLAG-theta following thrombin digestion were predicted to be that size. New bands also appeared that migrated between the 90 and 100 kD molecular weight markers (which, if it were running slightly more slowly than predicted due to post-translational modifications, could be the 88 kD C-terminal fragment after a single cut at the first thrombin site) and between the 50 and 60 kD molecular weight markers (which could be the 60 kD C-terminal fragment after a cut at the second thrombin site). When I blotted against the C-terminus of DGK-theta, the band migrating between the 120 and 220 kD molecular weight markers, consistent with full-length Fc-FLAG-DGK-theta, likewise faded intensity over time in the samples incubated with thrombin but not heat-inactivated thrombin (Figure 179**B**). Bands migrating between the 80 and 100 kD molecular weight markers and between the 60 and 80 kD molecular weight markers, consistent with the C-terminal 88 kD fragment that would be left after a single cut at the first thrombin site and with the C-terminal 60 kD fragment that would be left after a cut at the second thrombin site, appeared over time, although no immunoreactive bands were detectable after 22 hours. These results are consistent with digestion of Fc-FLAG-DGK-theta at the two predicted thrombin sites. However, the intensity of the two product bands were much, much less than the intensity of the full-length protein, possibly as a result of digestion by another protease contaminant of thrombin, or possibly as a result of impaired antibody

recognition (since the candidate product bands were still visible in the silver stain after 22 hours, although it is not clear why the bands would be recognized after 4 hours but not 22 hours: perhaps antibody recognition depended on some key post-translational modification that was lost after proteolytic truncation).

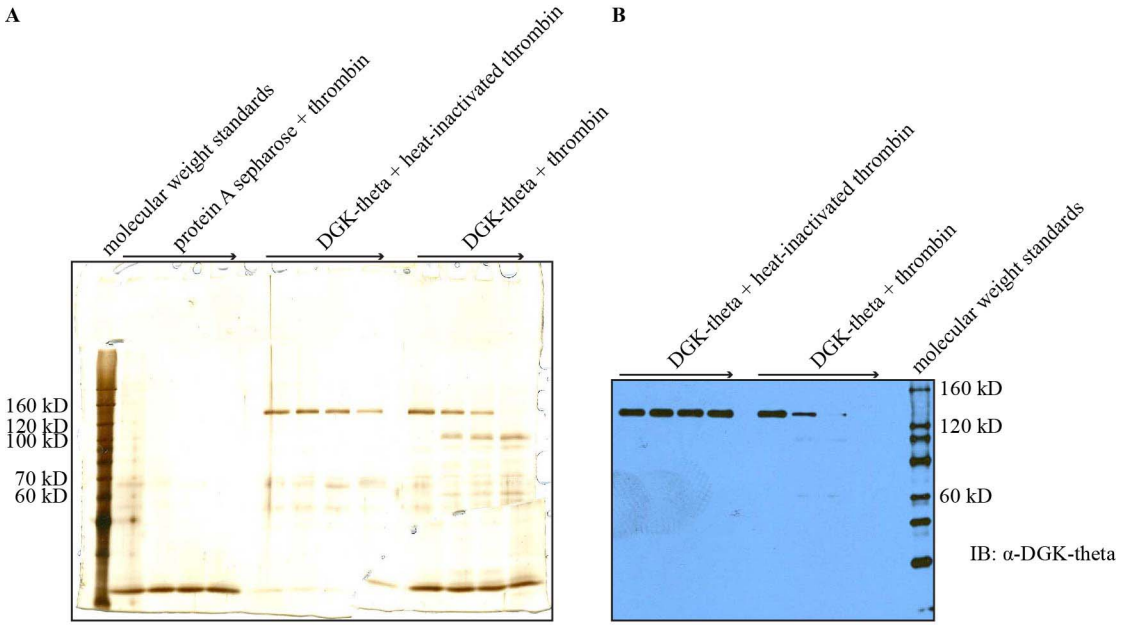

Figure 179. Increased concentrations of thrombin are able to digest Fc-FLAG-DGK-theta purified from 293FT cytosol. I stored the purified DGK-theta shown in **Figure 178** for six days in 50% (v/v) glycerol at -80°C prior to thawing and washing with thrombin buffer (10 mM HEPES, 10 mM Tris, 100 mM NaCl, 0.1% (w/v) PEG-8000, pH 7.5). I incubated the DGK-theta or protein A sepharose with 10 mU per µL thrombin (Calbiochem) in thrombin buffer at 4°C for 0, 2, 4, and 22 hours. I heat-inactivated thrombin by incubating it at 100°C for twenty minutes. I quenched the reaction of each timepoint by adding SDS-gel-loading buffer to 1x. SDS-PAGE followed by **(A)** silver staining, and **(B)** immunoblotting against DGK-theta (1:350 (v/v)).

I repeated the thrombin digestion with Fc-FLAG-DGK-theta I had purified from HEK293FT non-nuclear membranes, and collected aliquots from which to assay the DGK activity, to determine whether removal of the N-terminus of Fc-FLAG-DGK-theta freed it from autoinhibition. As with the Fc-FLAG-DGK-theta purified from cytosol, Fc-FLAG-DGK-theta purified from non-nuclear membranes produced an anti-DGK-theta-C-terminal-antibody-immunoreactive band that migrated between 120 and 160 kD whose

intensity decreased as a function of time when incubated with thrombin to a greater extent than when incubated with heat-inactivated thrombin (Figure 180). As before, incubation with thrombin produced smaller, immunoreactive bands, and as before, the intensity of these bands also faded with time. When I measured the enzymatic activity of the samples, the supernatant from the Fc-FLAG-DGK-theta that had been digested with thrombin gave higher activity on liposomes than the supernatant from the Fc-FLAG-DGK-theta that had been incubated with the heat-inactivated thrombin (Figure 181**A**), consistent with digestion's releasing DGK from the Fc tag and therefore releasing it from the Protein A sepharose into the supernatant. Activity of purified DGK-theta still attached to beads was noisy, consistent with a high variability of how many beads were included in the reaction volume. The activation power of LMW polylysine was modest. I tried to estimate specific activity by estimating the concentration of DGK-theta that was in the supernatant by SDS-PAGE followed by silver staining. Although the thrombin was clearly visible (as would be expected for the supernatant), the DGK-theta was too dilute to visualize by silver staining (Figure 181**B**).

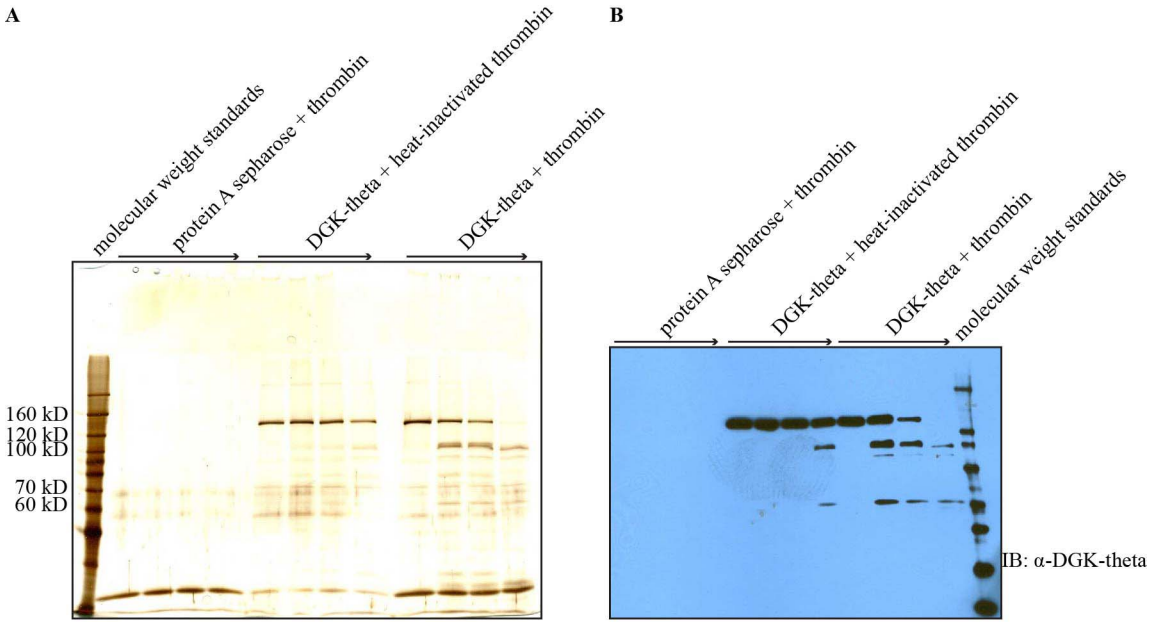

Figure 180. Thrombin is also able to digest Fc-FLAG-DGK-theta purified from 293FT non-nuclear membranes. I stored Fc-FLAG-DGK-theta purified from HEK293FT non-nuclear membranes on protein A sepharose (**Figure 84**C-D) for four weeks in 50% (v/v) glycerol at -80°C prior to thawing and washing with thrombin buffer (10 mM HEPES, 10 mM Tris, 100 mM NaCl, 0.1% (w/v) PEG-8000, pH 7.5). I incubated the DGK-theta or protein A sepharose with 10 mU per µL thrombin (Calbiochem) in thrombin buffer at 4°C for 0, 2, 4, and 21 hours. I heat-inactivated thrombin by incubating it at 100°C for twenty minutes. I quenched the reaction of each timepoint by adding SDS-gel-loading buffer to 1x or by adding glycerol to 50% and freezing at -80°C. SDS-PAGE of 8% acrylamide gels followed by **(A)** silver staining and **(B)** immunoblotting against DGK-theta (1:350 (v/v)).

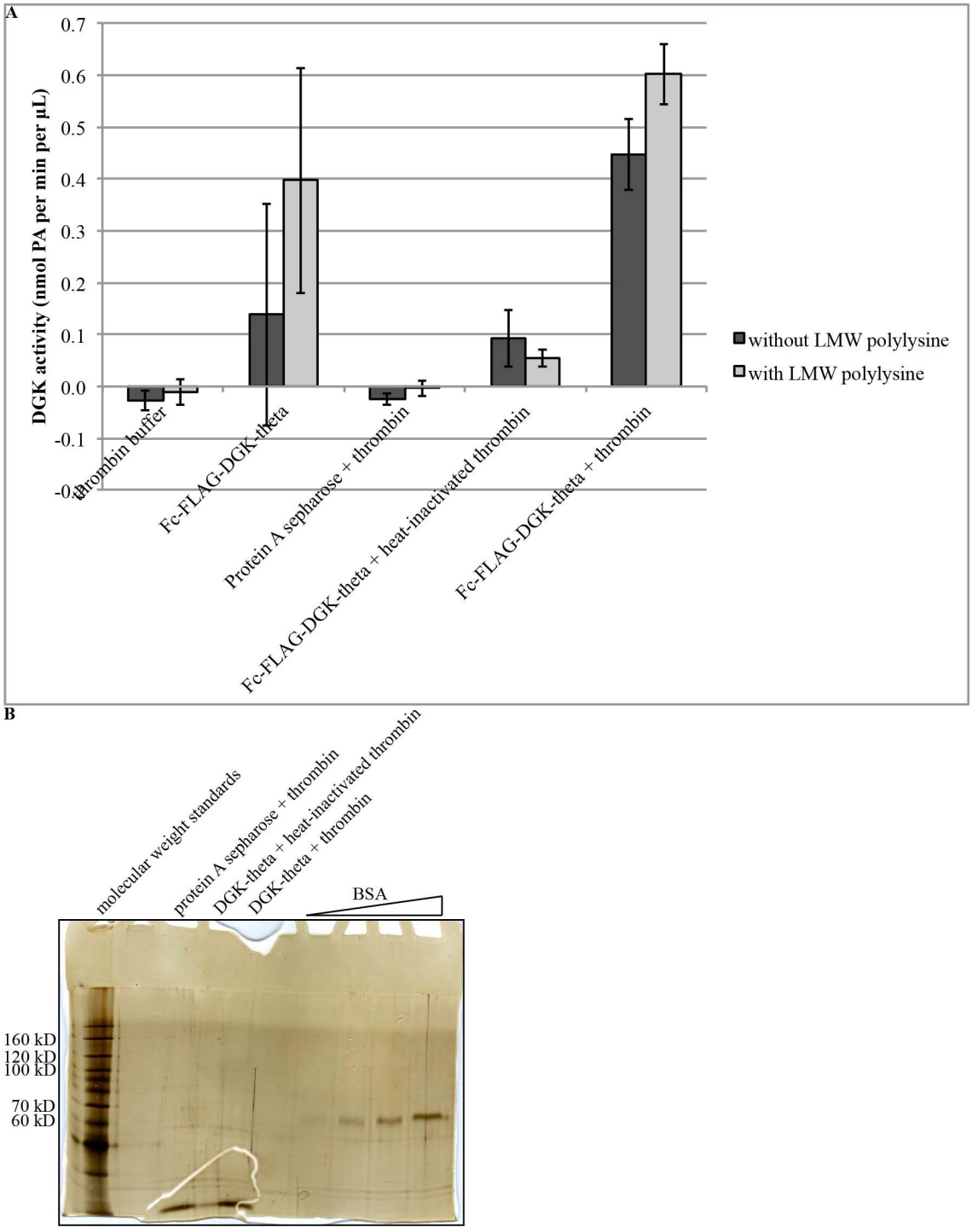

Figure 181. The supernatant from the Fc-FLAG-DGK-theta that has been digested with thrombin gives higher activity on liposomes than the supernatant from the Fc-FLAG-DGK-theta that has been incubated with the heat-inactivated thrombin, although the concentration of DGK-theta in the supernatant, and therefore the specific activity, is difficult to measure. (A) DGK activity assay. I stored the samples shown in **Figure 180**A-B for twelve days in 50% (v/v) glycerol at -80°C prior to assaying. I assayed the resin for Fc-FLAG-DGK-theta (as a positive control), and the supernatants of the

thrombin-digested samples. The reaction included 7.5 mM liposomes (53:22:17:8::POPE:POPC:POPS:DOG), 45 mM HEPES, pH 7.0, 130 mM NaCl, 1 mM Tris, 0.01% (w/v) PEG-8000, 1 mM DTT, 4.4 mM $MgCl_2$, 1 mM ATP, 89.2 Ci per mmol [γ-^{32}P]-ATP, 1.5 ng per μL LMW polylysine, 1.1% (v/v) glycerol, and 1.1 μL purified DGK-theta per 50 μL reaction, and proceeded for 15 minutes at 37°C. In duplicate: mean ± SD. **(B)** SDS-PAGE of an 8% acrylamide gel followed by silver staining of the supernatants removed from the Protein A sepharose beads following thrombin digestion for 21 hours.

I therefore scaled up the thrombin digestion, now that I had worked out the digestion conditions (overnight at 4°C with 10 mU thrombin per μL), with the hopes of being able to confidently measure the amount of DGK-theta in the supernatant, so that I could confidently measure the specific activity. Although I could clearly detect thrombin in the supernatant, as expected, and although digested Fc-FLAG-DGK-theta was clearly detectable in the resin plus supernatant, none of the digested DGK-theta was visible in the supernatant (Figure 182**A**), but rather was still on the resin (Figure 182**B**). However, thrombin was also detected on the resin, leaving the question of whether the DGK-theta was only lightly adhered and could be washed off, or whether the two halves of the protein were interacting with one another, or whether the protein was aggregating. I therefore washed the beads three times with thrombin buffer (10 mM HEPES, 10 mM Tris, 100 mM NaCl, 0.1% PEG-8000), followed by four times with thrombin buffer with NaCl increased to 524 mM. One ~70 kD band and one ~60 kD band came off in the washes (Figure 182**C**): these may correspond to the 69 kD N-terminal fragment that would be predicted to be produced by a single cut at the second thrombin site, and the 60 kD C-terminal fragment that would be predicted to be produced by a cut at the second thrombin site. However, the 69 kD fragment would be predicted to be still attached to the protein A Sepharose beads, which means that we must also consider that any signal in a "supernatant" might also result from a bead that had been accidentally aspirated while

removing the supernatant. Two predominant bands remained on the beads: one migrating between 100 and 120 kD, and one between 30 and 40 kD.

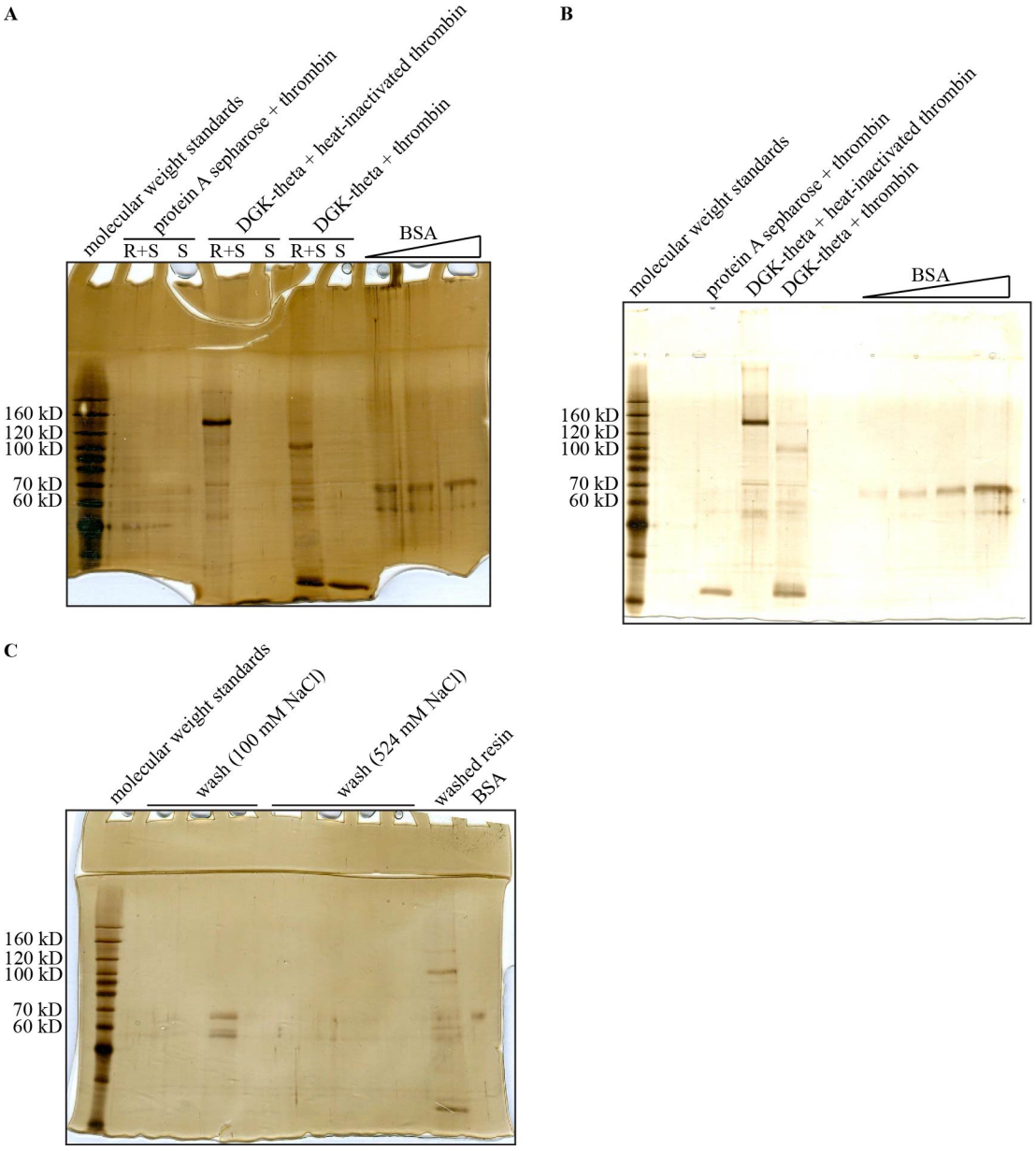

Figure 182. Digested Fc-FLAG-DGK-theta remains on the protein A sepharose after thrombin digestion, even after washing with salt. I stored the Fc-FLAG-DGK-theta purified from HEK293FT non-nuclear membranes on protein A sepharose (shown in **Figure 180**) for fifteen days in 50% (v/v) glycerol at -80°C prior to thawing and washing with thrombin buffer (10 mM HEPES, 10 mM Tris, 100 mM NaCl, 0.1% (w/v) PEG-8000, pH 7.5). I incubated the DGK-theta or protein A sepharose with 10 mU per µL thrombin (Calbiochem) in thrombin buffer at 4°C for 21 hours. I heat-inactivated thrombin by incubating it at 100°C for twenty minutes. After removing a resin + supernatant aliquot, I microfuged to separate the resin from the supernatant. SDS-PAGE of 8% acrylamide gels followed by silver staining. R+S, resin + supernatant; S, supernatant. **(A)** The dye front had not run off the gel when it was stained, but was cut off

during development. **(B)** I stored the beads shown in (A) for four days in 50% (v/v) glycerol at -80°C prior to resuspending them in an equivalent volume of thrombin buffer used for the samples in (A) for loading onto the gel. **(C)** I stored the beads shown in (A) overnight in 50% (v/v) glycerol at -80°C prior to washing in thrombin buffer and wash buffer (same as thrombin buffer but with NaCl increased to 524 mM).

Because even thrombin that had been heat-inactivated by incubating at 100°C for twenty minutes still digested Fc-FLAG-DGK-theta to some extent after 21 hours' at 4°C (Figure 180**B**), I was interested in finding another negative control for thrombin digestion. As previously mentioned, hirudin is a thrombin inhibitor found in the salivary glands of the leech *Hirudo medicinalis*[143]. Hirudin indeed inhibited thrombin digestion of Fc-FLAG-DGK-theta purified from HEK293FT cytosol (Figure 183), but as before, the salt wash did not remove either of the predominant products from the protein A sepharose (Figure 183**A** and **B**). In another thrombin digestion, this time of Fc-FLAG-DGK-theta purified from HEK293T non-nuclear membranes, a high pH wash did not remove these products from the resin, either (Figure 183**C** and **D**). Because hirudin inhibits DGK-theta's enzymatic activity (Figure 128), DGK-theta incubated with hirudin-inhibited thrombin was not an appropriate negative control for determining whether removal of the N-terminus relieves autoinhibition of DGK-theta. I therefore needed yet another inhibitor as a negative control.

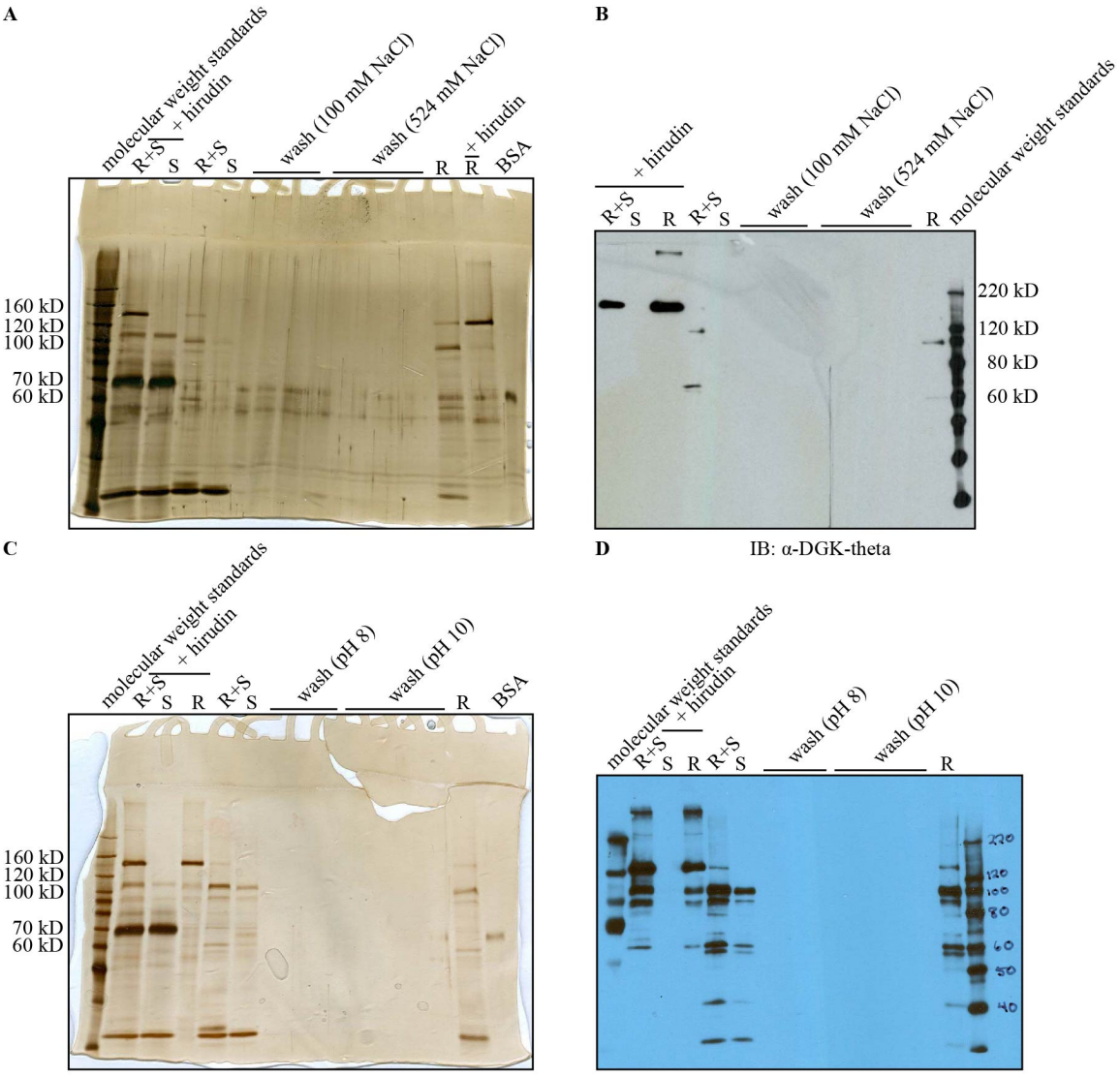

Figure 183. Washing with salt or high pH does not remove thrombin-digested Fc-FLAG-DGK-theta, purified from either HEK293FT cytosol or non-nuclear membranes, from protein A sepharose. I stored the Fc-FLAG-DGK-theta purified from HEK293FT cytosol on protein A sepharose (shown in **Figure 179**) for four weeks in 50% (v/v) glycerol at -80°C prior to thawing and washing with thrombin buffer 1 (10 mM HEPES, 10 mM Tris, 100 mM NaCl, 0.1% (w/v) PEG-8000, pH 7.5). I incubated the DGK-theta with 10 mU per µL thrombin (Calbiochem) and 15 mU per µL hirudin (Sigma-Aldrich® H7380) (or not) in thrombin buffer at 4°C for 18 hours. After removing a resin + supernatant aliquot, I microfuged to separate the resin from the supernatant. I washed the resin with thrombin buffer 1 and with wash buffer 1 (same as thrombin buffer 1 but with NaCl increased to 524 mM). R+S, resin + supernatant; S, supernatant; R, washed resin. SDS-PAGE of 8% acrylamide gels followed by **(A)** silver staining, and **(B)** immunoblotting against DGK-theta (1:350 (v/v)). I stored the Fc-FLAG-DGK-theta purified from HEK293FT non-nuclear membranes on protein A sepharose (shown in **Figure 182**) for eighteen days in 50% (v/v) glycerol at -80°C prior to thawing and washing with thrombin buffer 2 (10 mM HEPES, 10 mM Tris, 100 mM NaCl, 0.1% (w/v) PEG-8000, pH 8.5). I incubated the DGK-theta with 10 mU per µL thrombin (Calbiochem) and 15 mU per µL hirudin (Sigma-Aldrich® H7380) (or not) in thrombin buffer at 4°C for 21 hours. After removing a resin + supernatant aliquot, I microfuged to separate the resin from the supernatant. I washed the resin with thrombin buffer 2 and with wash buffer 2 (same as thrombin buffer 2

but pH adjusted to 10). **(C)** SDS-PAGE followed by silver staining. This figure is reproduced from **Figure 127**A for ease of comparison. **(D)** SDS-PAGE followed by immunoblotting against DGK-theta. (1:350 (v/v)).

As mentioned previously, PMSF is another thrombin inhibitor, but before using it in the proteolysis studies, I wanted to first check whether PMSF inhibited DGK, as hirudin did. After confirming that 1 mM PMSF did not inhibit DGK-theta (Figure 129), I once again digested DGK-theta with thrombin, this time with 1 mM PMSF as a negative control. To assess inhibition by PMSF, I also incubated DGK-theta without thrombin. To assess whether any of the background bands resulted from HEK293FT non-nuclear membrane proteins copurified with DGK-theta, I also digested mock-purified HEK293FT non-nuclear membranes (untransfected cells that were subjected to the same purification protocol as the cells transiently transfected with Fc-FLAG-DGK-theta were). 1 mM PMSF was insufficient to prevent thrombin (10 mU per μL) digestion of purified Fc-FLAG-DGK-theta overnight at 4°C (Figure 184). As before, washing with a high-pH buffer did not remove the digested fragments of DGK-theta from the Protein-A sepharose resin (Figure 184). When I measured the enzymatic activity of the digested DGK-theta, it showed considerably more DGK activity than the undigested DGK-theta (Figure 185**A**). The activity of the resin and supernatant together appeared greater than the sum of the activity of the resin and of the supernatant separately, suggesting that the two halves of the protein (or other components of the supernatant and the pellet fractions) might have cross-activated. Alternatively, the activity might have resulted from a component that had been washed away when the resin was washed. In order to distinguish between the two scenarios, I combined the supernatant and the resin together and assayed their activity. The activity of the combined supernatant and washed resin actually may have

been slightly lower than the sum of the activities of the supernatant and washed resin (Figure 185**C**), and is substantially lower than the activity of the resin plus supernatant, before they were separated and the resin washed (Figure 185). The activity of the beads plus supernatant was noisy, as observed previously (Figure 180), consistent with stochasticity of whether a bead happened to be included in the sample taken for the reaction or not; on the other hand, such an effect would also have been predicted for the washed resin, and was not observed (Figure 185). Because the activity of the combined supernatant and washed resin was less than that of the original resin plus supernatant, I therefore concluded that the components on the resin and the components in the supernatant did not cross-activate. It is possible that the active component in the resin plus supernatant fraction was a weakly bound factor, and thus not in the supernatant, that then washed away during either the thrombin buffer washes or the high pH washes. However, in that case it would have to be a very potently active component, seeing as no predominant bands appear in any of the washes (Figure 184). Another, more plausible, explanation is that the resin retained the active component (consistent with the bands seen in Figure 184), but that the resin lost its activity during the course of the washing. One possible cause for a loss in activity could be the extra ~four hours spent at 4°C during the course of washing (after all, I have shown the activity of purified DGK-theta to be sensitive to incubation on ice (Figure 99), and Figure 185 does not include a fresh-from-the-freezer control, so the resin may have also lost some activity during the overnight thrombin digestion). Alternatively, a fragment lost to the supernatant or in the washing might help stabilize the protein, and its loss might make the remaining DGK-theta less

stable. Yet another possible explanation is that the washing at pH 10 damaged or otherwise inactivated the Fc-FLAG-DGK-theta on the resin.

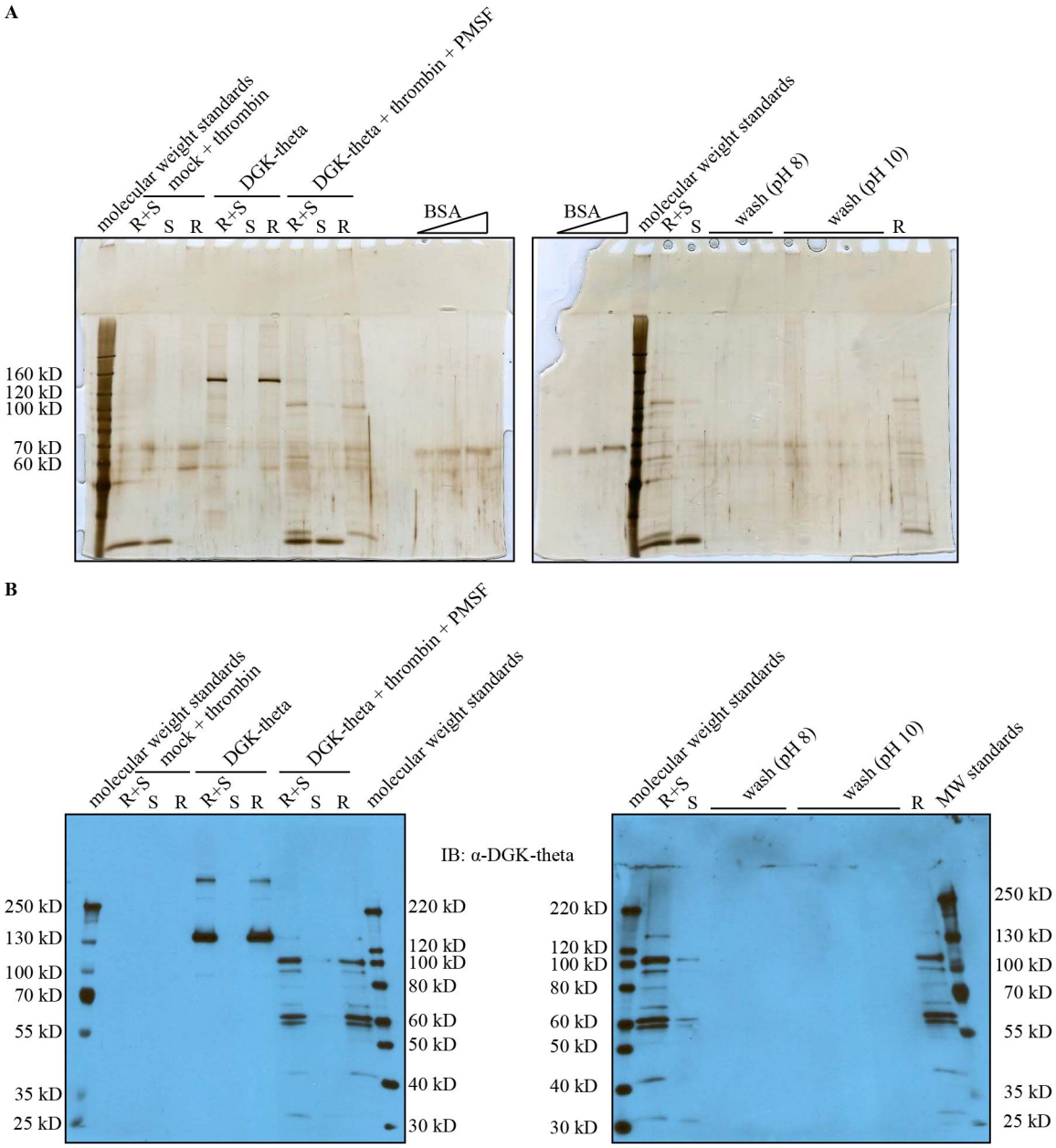

Figure 184. 1 mM PMSF is insufficient to prevent 10 mU per µL thrombin from digesting purified Fc-FLAG-DGK-theta overnight at 4°C. I stored the Fc-FLAG-DGK-theta purified from HEK293FT non-nuclear membranes on protein A sepharose (shown in **Figure 183**C-D) for two months in 50% (v/v) glycerol at -80°C prior to thawing and washing with thrombin buffer (10 mM HEPES, 10 mM Tris, 100 mM NaCl, 0.1% (w/v) PEG-8000, pH 85). I incubated either purified Fc-FLAG-DGK-theta or else mock-purified HEK293FT non-nuclear membranes with 10 mU per µL thrombin (Calbiochem) and 1 mM PMSF in thrombin buffer at 4°C for 21 hours. After removing a resin + supernatant aliquot, I microfuged to separate the resin from the supernatant. I washed the resin with thrombin buffer and with wash buffer 1

(same as thrombin buffer but with pH increased to 10). R+S, resin + supernatant; S, supernatant; R, washed resin; "mock", mock-purified HEK293FT non-nuclear membranes. SDS-PAGE of 8% acrylamide gels followed by **(A)** silver staining, and **(B)** immunoblotting against DGK-theta (1:350 (v/v)).

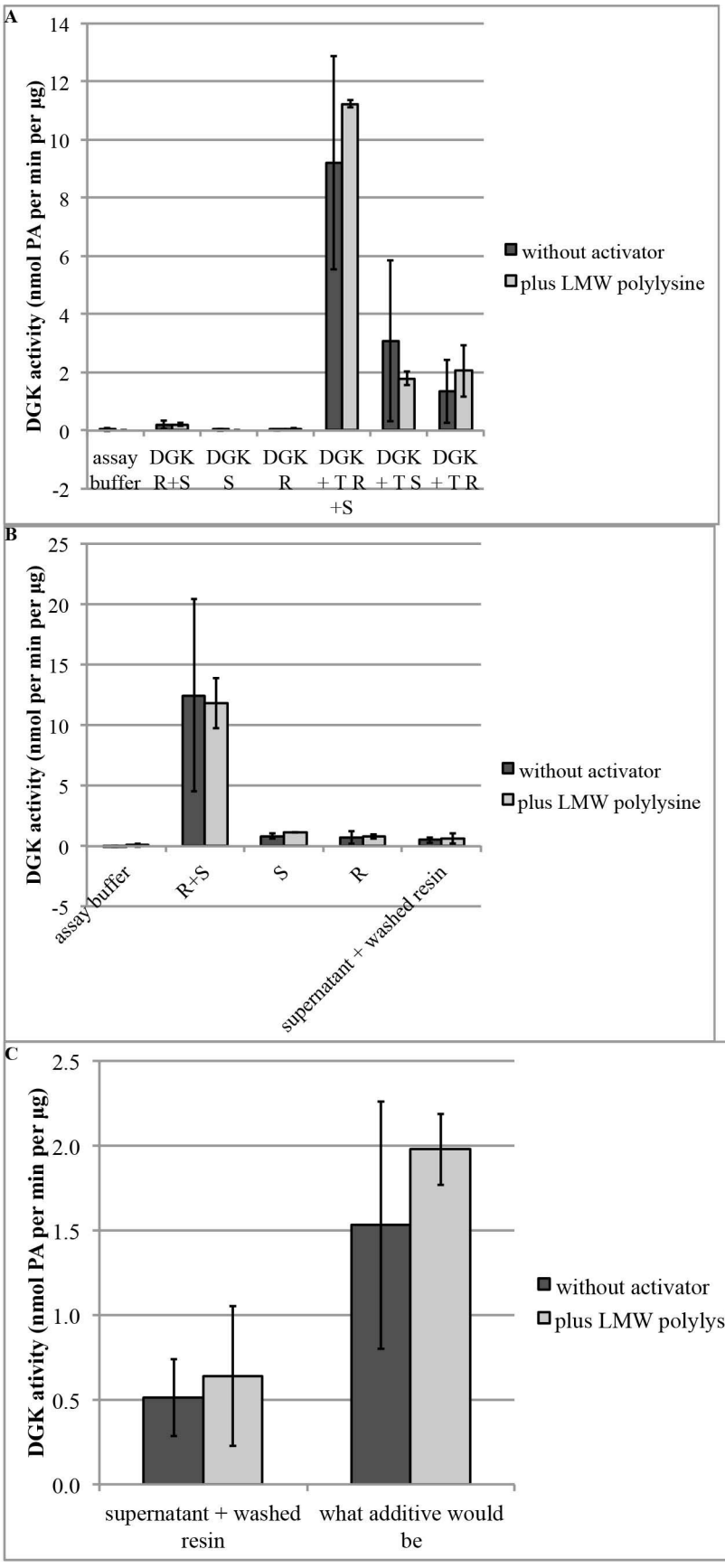
A
DGK activity (nmol PA per min per µg)
14
12
10
8
6
4
2
0
-2
assay buffer
DGK R+S
DGK S
DGK R
DGK +T R +S
DGK +T S
DGK +T R
without activator
plus LMW polylysine
B
DGK activity (nmol per min per µg)
25
20
15
10
5
0
-5
assay buffer
R+S
S
R
supernatant + washed resin
without activator
plus LMW polylysine
C
DGK ativity (nmol PA per min per µg)
2.5
2.0
1.5
1.0
0.5
0.0
supernatant + washed resin
what additive would be
without activator
plus LMW polylysine

Figure 185. Thrombin-digested DGK-theta shows considerably greater DGK enzymatic activity than undigested DGK-theta DGK activity assays, but the two digested components do not cross-activate when recombined. R+S, resin + supernatant; S, supernatant; R, washed resin; T, thrombin. **(A)** I stored the samples shown in **Figure 184** for three days in 50% (v/v) glycerol at -80°C prior to assaying. The reaction included 7.5 mM liposomes (53:22:17:8::POPE:POPC:POPS:DOG), 48 mM HEPES, pH 7.0, 134 mM NaCl, 1 mM DTT, 4.4 mM $MgCl_2$, 1 mM ATP, 103 Ci per mmol [γ-^{32}P]-ATP, 1.5 ng per µL LMW polylysine, and from the purified DGK-theta, up to 0.3 mM Tris, 0.003% (w/v) PEG-8000, 1.4% (v/v) glycerol, and 14 pg per µL purified DGK-theta (concentration estimated by silver staining), and proceeded for 15 minutes at 37°C. In triplicate: mean ± SD. **(B)** I stored the samples shown in **Figure 184** for one week in 50% (v/v) glycerol at -80°C prior to assaying. The reaction included 7.5 mM liposomes (53:22:17:8::POPE:POPC:POPS:DOG), 49 mM HEPES, pH 7.0, 134 mM NaCl, 1 mM DTT, 4.4 mM $MgCl_2$, 1 mM ATP, 89.2 Ci per mmol [γ-^{32}P]-ATP, 1.5 ng per µL LMW polylysine, and from the purified DGK-theta, up to 0.1 mM Tris, 0.001% (w/v) PEG-8000, 0.7% (v/v) glycerol, and 2.4 pg per µL purified DGK-theta (concentration estimated by silver staining), and proceeded for 15 minutes at 37°C. In triplicate: mean ± SD. **(C)** The same data as in (B), redisplayed to show what the additive activity would be.

Discussion and Conclusions

In conclusion, while I was able to use thrombin to digest DGK-theta after folding, none of the washing conditions I tested (including high salt and high pH) were able to remove the digested C-terminal fragments from the protein A sepharose beads to which the N-terminal fragments were still bound via their Fc tag. Digestion with thrombin appeared to activate DGK-theta, but whether the activation was due to relief from auto-inhibition or some other effect from the thrombin could not be resolved because the different fragments of DGK-theta could not be separated. Other systems that have been reported to pursue a similar strategy of allowing a protein to fold before proteolytically digesting it used denaturation by guanidine chloride to separate the different fragments of the protein[155,156]. Future directions with using this strategy to express truncations of mammalian DGK might therefore wish to consider using denaturation to separate the pieces, but conditions for unfolding and refolding DGK-theta while recovering enzymatic activity would have to be worked out before being able to answer the question of whether such truncation relieves auto-inhibition.

Chapter 8: Photoaffinity labeling

Introduction

Photoaffinity labeling approaches have been successfully used to map the binding sites of ligands on receptors and the active sites of enzymes. I therefore decided to try a photoaffinity labeling approach in an attempt to identify the lipid substrate binding sites on mammalian DGK.

Sucrose-loaded vesicle (SLV) pulldown

Introduction

One method to measure covalent crosslinking of photoaffinity labels to DGK is by sucrose-loaded vesicle (SLV) pulldown. When large unilamellar vesicles (LUVs) are made in the presence of high concentrations of sucrose, then diluted into a buffer without sucrose, the buffer inside the vesicles is denser than the buffer outside the vesicles, and the SLVs will sink to the bottom of a tube when centrifuged[157] (Figure 186). SLVs have therefore been used to measure the binding of proteins to membranes. If a lipid incorporated into SLVs covalently attached to a protein, as would be predicted if the probes were photoaffinity labeling DGK, then I would predict to see a probe- and UV-dependent increase in SLV pulldown of DGK.

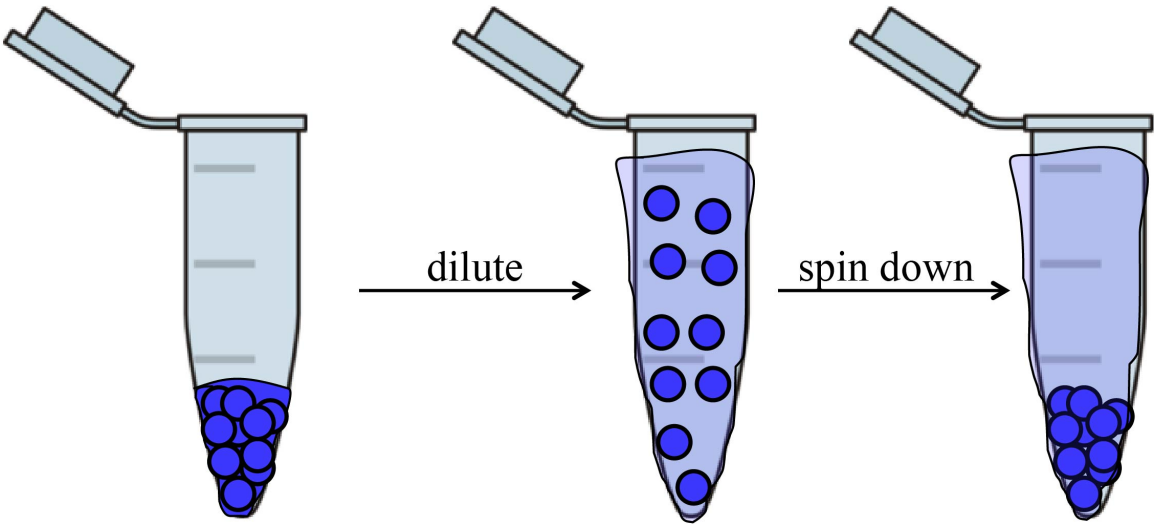

Figure 186. Schematic for making SLVs. LUVs are first made in a buffer with a high concentration of sucrose, represented by the blue color. When the vesicles are diluted into buffer without sucrose, the interior of the SLVs (still blue) has a higher concentration of sucrose than the buffer outside the SLVs (a more translucent blue). As such, the SLVs are denser than the surrounding buffer, and will pellet when centrifuged.

Methods

I made sucrose-loaded vesicles (SLVs) in the same way as I made liposomes (see "Radiometric Endpoint DGK Assay" sub-subchapter of the "Diacylglycerol Kinase (DGK) Activity Assays" subchapter of the "General Methods" chapter), except that I included 170 mM sucrose in the buffer used to hydrate and extrude the lipids. I generally also included 1,2-dioleoyl-*sn*-glycero-3-phosphoethanolamine-*N*-(7-nitro-2-1,3-benzoxadiazol-4-yl) (NBD-PE), a fluorescent lipid, to 1 μg per μL. In order to measure the recovery of the lipids, I loaded samples into a 96-well plate and used a plate reader to excite at 485 nm and measure the emission at 528 nm, scaling to an empty well for sensitivity. I stored SLVs at 4°C.

Measuring how much DGK-theta is pulled down by SLVs without covalent crosslinking

In order to be able to confidently measure an increase in pulldown (such as a probe- and UV-dependent increase in SLV pulldown of DGK that photoaffinity labeling would be predicted to produce), I would need to first find conditions under which not all of the DGK was pulled down by SLVs without photoaffinity labeling, so that I would be able to detect a probe- and UV-dependent increase in pulldown. I therefore incubated purified DGK-theta in duplicate with 1 mM SLVs (2:1::POPE:POPC) including varying concentrations of 1-palmitoyl-2-oleoyl-*sn*-glycero-3-phosphate (POPA), removed an aliquot ("vesicles"), then centrifuged to separate into supernatant and pellet. I measured the enzymatic activity of these samples as one method to detect how much DGK partitioned into the different fractions. Reproducibility among samples was an issue: one replicate of DGK-theta incubated with SLVs containing 20% PA, for example, gave considerably greater activity than the other replicate, even though both were made from the same master mix and thus should have had the same total amount of DGK-theta in them (Figure 188). Another issue with using DGK activity as a proxy for DGK concentration is that the enzyme's specific activity could very well depend on its chemical environment: I have previously shown DGK to be activated in the presence of liposomes (Figure 101), so the samples from the vesicles or pellets might have higher specific activity than the samples from supernatant and actually reflect a lower concentration of enzyme. Alternatively, the samples from the supernatant might have higher specific activity if more of the activating histone H1 (which had been included in

the preincubation to prevent room-temperature inactivation (Figure 106**A**)) partitioned to the supernatant.

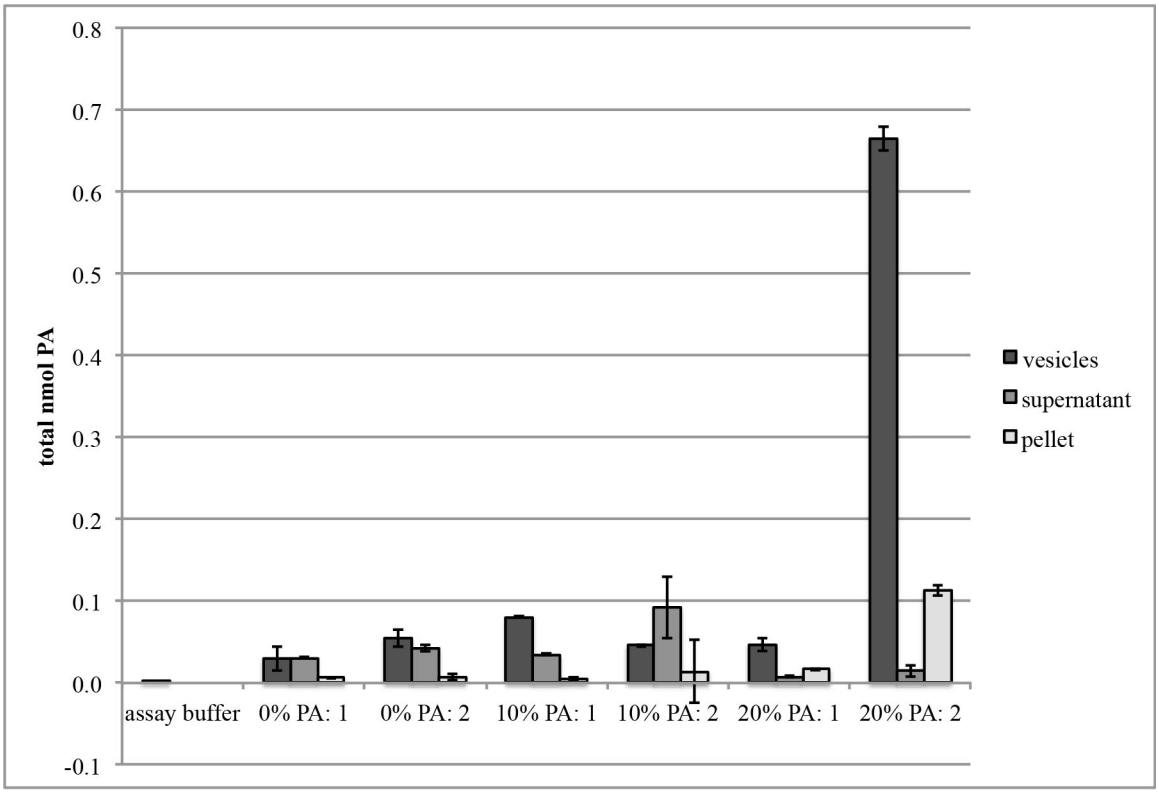

Figure 187. Using enzymatic activity to determine the partitioning of purified DGK-theta on SLVs does not give reproducible results between replicates. DGK activity assay. I first preincubated purified DGK-theta in preincubation buffer (1.1 ng per µL purified DGK-theta, 41% (v/v) glycerol, 0.2% (v/v) NP-40, 1.4 µM histone H1, 1 mM DTT) on ice for ten minutes. I then diluted into SLV buffer (1 mM SLVs (2:1::POPE:POPC, and the indicated concentrations of POPA), 50 mM HEPES, pH 7.5, 100 mM NaCl, 1 mM ATP, 1.5 mM MgCl2, 81 pg per µL purified DGK-theta, 3% (v/v) glycerol, 0.015% (v/v) NP-40, 0.1 µM histone H1, 0.1 mM DTT), and incubated at room temperature for thirty minutes. I separated into two replicates, and then the supernatant from the pellet by centrifuging at 136,000 x g for 75 minutes at 25°C, and resuspended the pellet in DGK assay buffer. The final reaction mixture included 2 mM liposomes (55.3:27.7:9:8::POPE:POPC:POPS:DOG), 50 mM HEPES, pH 7.5, 100 mM NaCl, 1 mM DTT, 1.6 mM MgCl2, 1 mM ATP, 99.8 Ci per mmol [γ-32P]-ATP, 0.09 µM histone H1, and from the SLVs, up to 33 µM SLVs, 0.0005% (v/v) NP-40, and 0.1% (v/v) glycerol, and proceeded for 15 minutes at 37°C. In duplicate: mean ± SD. Because the goal of this assay was to determine the partitioning of DGK (and hence it is unknown how much DGK is in each fraction), the DGK activity is represented as total nmol PA rather than specific activity. Vesicles: samples removed before centrifugation. "1" and "2" signify replicates in pulldown.

I therefore also immunoblotted against DGK-theta in these samples, and quantified the signal by interpolating into DGK-theta standards loaded onto the same gel (Figure 188**A**). The proportion of DGK-theta in the pellet did appear to rise as a function

of POPA (Figure 188**C**), but this effect resulted not from an increase in signal from the pellet, but a decrease in signal from the vesicles (Figure 188**B**). The discrepancy in activity between the two replicates of the 20% PA samples (Figure 187) was not accompanied by any such discrepancy in the amount of DGK recognized by the antibody (Figure 188), reaffirming that measuring DGK activity is probably not a good way to measure how much DGK-theta is present in an aliquot. On the other hand, antibody recognition might also depend on the chemical environment: for example, the presence of histone H1 might influence recognition between DGK-theta and the antibody. I therefore blotted against histone H1 to determine how histone H1 was distributed among the samples. However, I was unable to detect histone H1 on these blots (Figure 189), even though I was using conditions that had been reported to reliably detect as little as 10 ng of histone H1 on other blots. One possible explanation is that some reaction component (the SLVs, for example, or perhaps the NP-40) hindered antibody recognition of histone H1. Although quantitatively measuring how much DGK-theta was in the supernatant and the pellet was clearly going to be a challenge, I was able to conclude that not all of the DGK-theta pelleted with the SLVs under the conditions tested, and I should be able to detect an increase due to photoaffinity labeling.

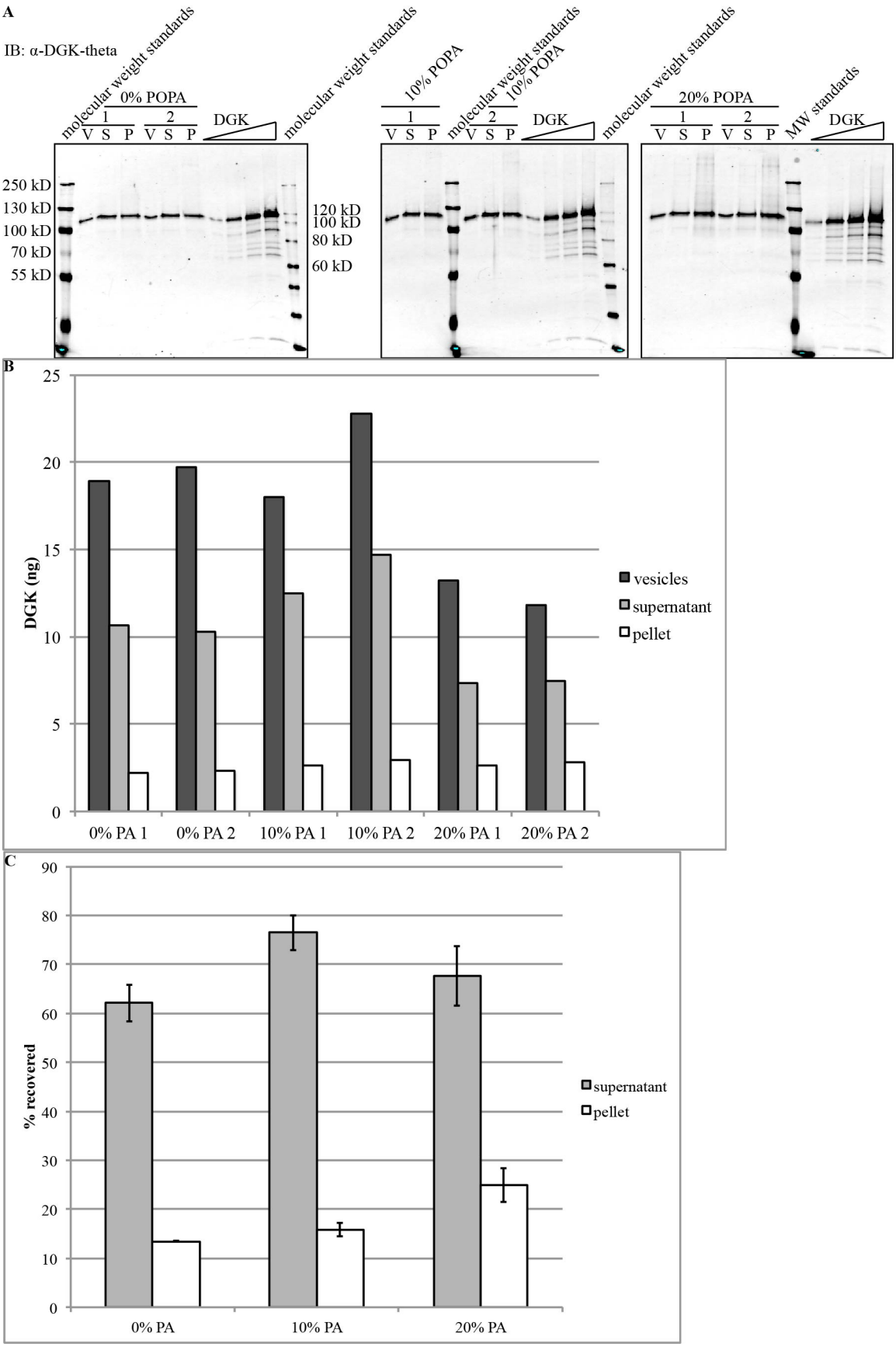
A
IB: α-DGK-theta
molecular weight standards
0% POPA
1
2
V S P V S P
DGK
molecular weight standards
10% POPA
molecular weight standards
10% POPA
molecular weight standards
20% POPA
MW standards
250 kD
130 kD
100 kD
70 kD
55 kD
120 kD
100 kD
80 kD
60 kD
B
DGK (ng)
25
20
15
10
5
0
vesicles
supernatant
pellet
0% PA 1
0% PA 2
10% PA 1
10% PA 2
20% PA 1
20% PA 2
C
% recovered
90
80
70
60
50
40
30
20
10
0
supernatant
pellet
0% PA
10% PA
20% PA

Figure 188. Not all of the DGK-theta pelleted with the SLVs under the conditions tested. The same samples as shown in **Figure 187**. **(A)** SDS-PAGE of 8% acrylamide gels followed by immunoblotting against DGK-theta (1:350 (v/v)). V, vesicles; S, supernatant; P, pellet. "1" and "2" signify replicates in pulldown. I also loaded various concentrations of purified DGK-theta onto each gel as a standard. **(B)** Quantification of the signal from (A), calculated by comparing to the signal from the DGK-theta standard loaded onto each blot. **(C)** The same data as in (B), but redisplayed as a percent of the signal from vesicles (after accounting for mass lost to the aliquot removed), and averaged over the two replicates. Mean ± SD.

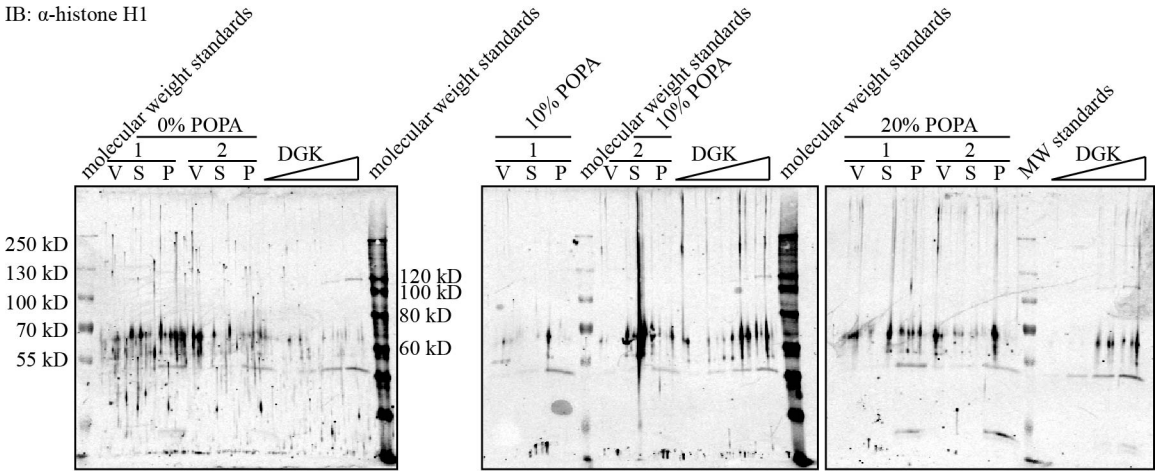

Figure 189. The anti-histone H1 antibody was unable to measurably detect histone H1 by immunoblot under the conditions tested. The same membranes shown in **Figure 188**A, immunoblotted against histone H1 (1:500 (v/v)). The anti-DGK-theta antibody was a mouse antibody, while the anti-histone H1 antibody was a rabbit antibody, therefore the signals were observed on different channels on the Odyssey® Infrared Imaging System, and the anti-DGK-theta signal is not contributing to these immunoblots.

I wanted to be sure that the DGK-theta would be able to encounter any photoaffinity label in the SLV, but, as I mentioned above, also wanted the amount of DGK pulled down by the control SLVs to be low enough that I would be able to detect a photoaffinity-labeling-induced increase. One way of accomplishing both would be to first incubate the DGK-theta with liposomes of a composition such that the DGK-theta would bind the membrane, then change the chemical environment such that any DGK-theta not covalently attached would release the membrane. I therefore tested how much DGK-theta was pulled down in the context of 20 mol% POPA and increasing concentrations of salt, with the idea that I could incubate the DGK-theta first with

liposomes containing 20 mol% POPA and low salt, and then increase the concentration of salt to remove the non-covalently attached DGK. When I immunoblotted the fractions against DGK-theta, increasing concentrations of salt appeared to increase the amount of immunoreactive DGK in the pellet, but did not decrease the amount of immunoreactive DGK in the supernatant (Figure 190). Once again, reproducibility between replicates was poor: not only did the two 500 mM NaCl replicates vary greatly in the amount of DGK-theta detected in the SLVs before centrifugation (Figure 190), but the 100 mM NaCl replicates also differed from the 100 mM 20% POPA samples in the previous experiment (compare Figure 188 and Figure 190).

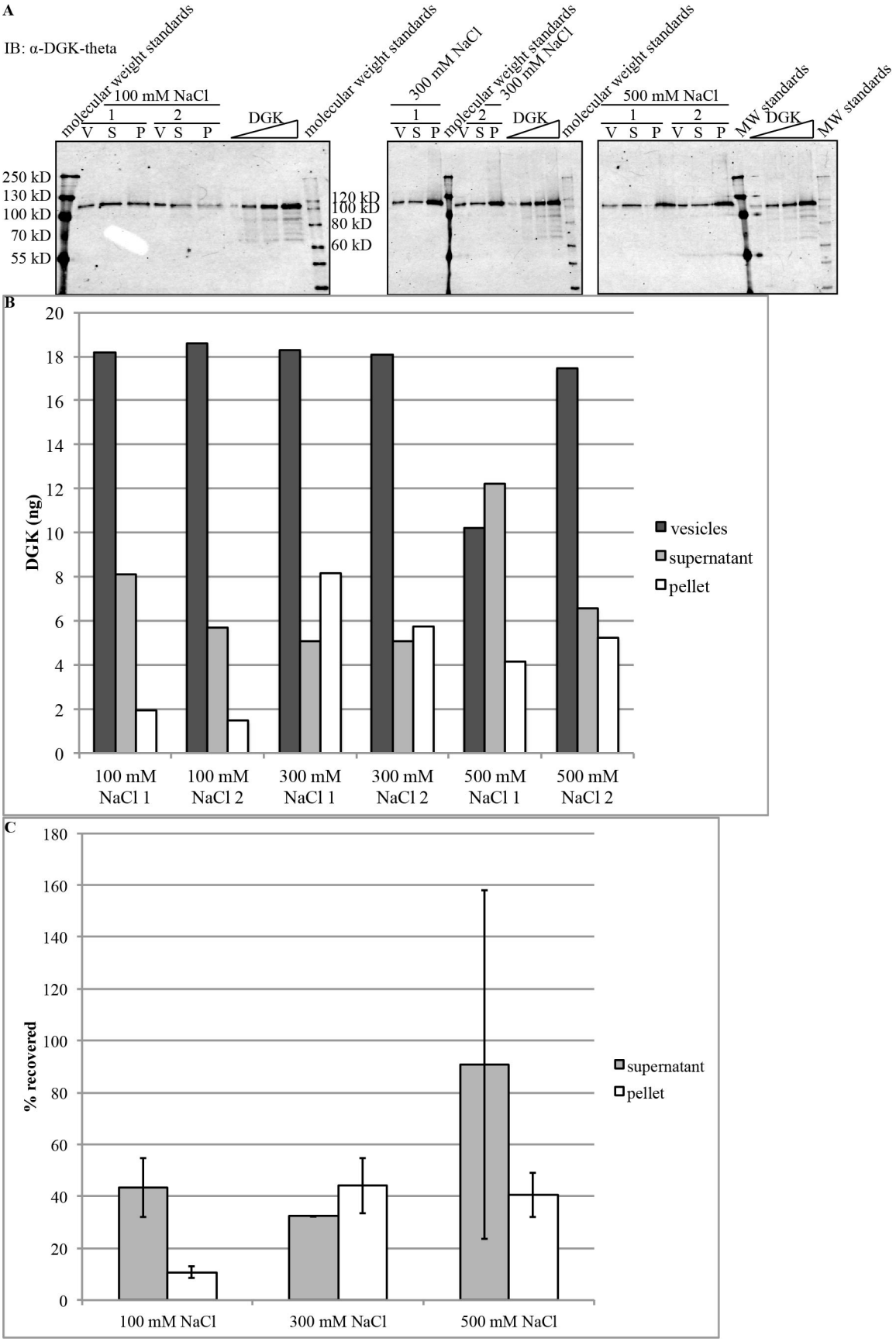
A
IB: α-DGK-theta
molecular weight standards
100 mM NaCl
1
2
V S P V S P
DGK
molecular weight standards
300 mM NaCl
1
2
V S P V S P
DGK
molecular weight standards
300 mM NaCl
500 mM NaCl
1
2
V S P V S P
MW standards
DGK
MW standards
250 kD
130 kD
100 kD
70 kD
55 kD
120 kD
100 kD
80 kD
60 kD
B
DGK (ng)
20
18
16
14
12
10
8
6
4
2
0
100 mM NaCl 1
100 mM NaCl 2
300 mM NaCl 1
300 mM NaCl 2
500 mM NaCl 1
500 mM NaCl 2
vesicles
supernatant
pellet
C
% recovered
180
160
140
120
100
80
60
40
20
0
100 mM NaCl
300 mM NaCl
500 mM NaCl
supernatant
pellet

Figure 190. Increasing concentrations of salt appeared to increase the amount of immunoreactive DGK in the pellet following SLV pulldown, but did not decrease the amount of immunoreactive DGK in the supernatant. I stored the 20% POPA SLVs (used in **Figure 187**-**Figure 189**) for eighteen days at 4°C prior to use. I first preincubated purified DGK-theta in preincubation buffer (1.1 ng per μL purified DGK-theta, 41% (v/v) glycerol, 0.2% (v/v) NP-40, 1.4 μM histone H1, 1 mM DTT) on ice for ten minutes. I then diluted into SLV buffer (1 mM SLVs (53.3:26.7:20::POPE:POPC:POPA), 50 mM HEPES, pH 7.5, the indicated concentrations of NaCl, 1 mM ATP, 1.5 mM MgCl2, 81 pg per μL purified DGK-theta, 3% (v/v) glycerol, 0.015% (v/v) NP-40, 0.1 μM histone H1, 0.1 mM DTT), and incubated at room temperature for thirty minutes. I separated into two replicates, and then the supernatant from the pellet by centrifuging at 136,000 x g for 75 minutes at 25°C, and resuspended the pellet in DGK assay buffer. **(A)** SDS-PAGE of 10% acrylamide gels, followed by immunoblotting against DGK-theta (1:350 (v/v)). V, vesicles; S, supernatant; P, pellet. "1" and "2" signify replicates in pulldown. I also loaded various concentrations of purified DGK-theta onto each gel as a standard. **(B)** Quantification of the signal from (A), calculated by comparing to the signal from the DGK-theta standard loaded onto each blot. **(C)** The same data as in (B), but redisplayed as a percent of the signal from vesicles (after accounting for mass lost to the aliquot removed), and averaged over the two replicates. Mean ± SD.

The amount of DGK in the pellet in the higher salt treatment increased, but the specific activity decreased (Figure 191), which could be consistent with histone H1's remaining in the supernatant, but could also be consistent with differences in efficiency of anti-DGK-theta antibody recognition (which could depend on the presence of lipid, for example, and thus might vary between the supernatant and pellet samples). I once again immunoblotted against histone H1 to resolve how it fractionated among the SLVs, and once again I was unable to detect histone H1 signal quantitatively (Figure 192). I was therefore faced with the problem that my method of quantifying DGK-theta (recognition by the anti-DGK-theta antibody) might depend on the presence of histone H1, which I was unable to measure.

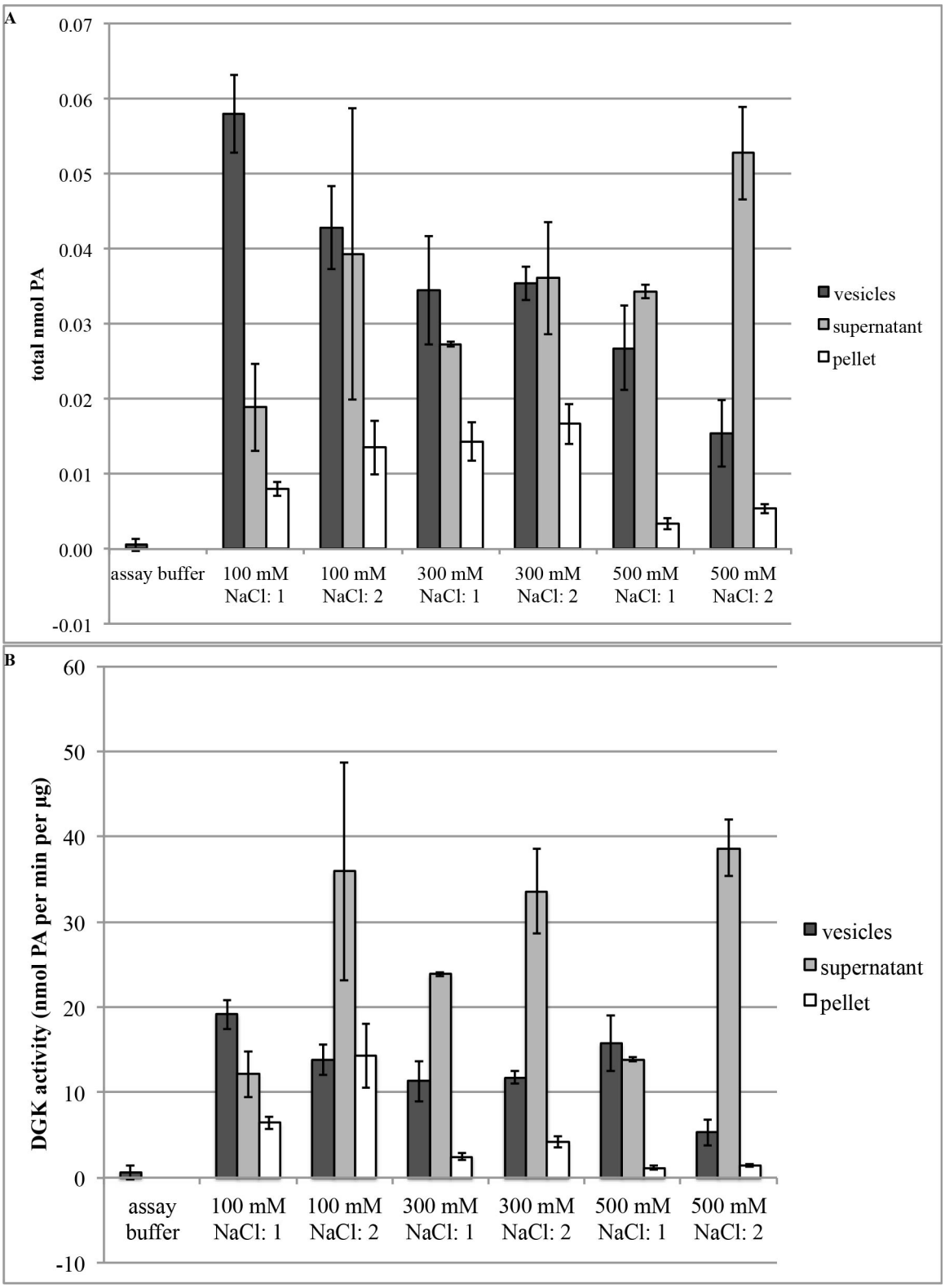

Figure 191. Both the total and specific activity varies between replicates. DGK activity assay of the samples shown in **Figure 190**, immediately after separating into supernatant and pellet. The final reaction mixture included 2 mM liposomes (55.3:27.7:9:8::POPE:POPC:POPS:DOG), 50 mM HEPES, pH 7.5, 100

mM NaCl, 1 mM DTT, 1.6 mM MgCl2, 1 mM ATP, 43.2 Ci per mmol [γ-32P]-ATP, 0.1 μM histone H1, and from the SLVs, up to 100 μM SLVs, 0.0015% (v/v) NP-40, and 0.3% (v/v) glycerol, and proceeded for 15 minutes at 37°C. In duplicate: mean ± SD. Vesicles: samples removed before centrifugation. "1" and "2" signify replicates in pulldown. **(A)** Total nmol PA. **(B)** Specific activity (using the concentration of DGK-theta in each fraction calculated from the immunoblots shown in **Figure 190**).

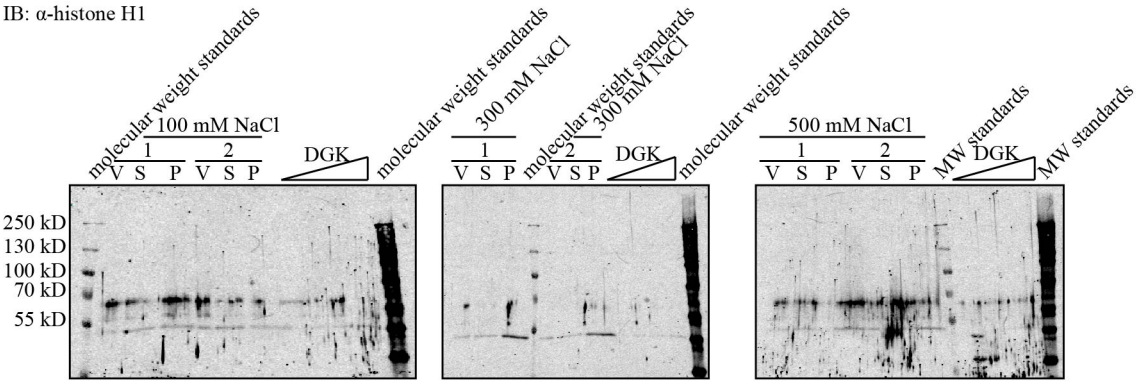

Figure 192. The anti-histone H1 antibody once again was unable to measurably detect histone H1 by immunoblot under the conditions tested. The same membranes as shown in **Figure 190**, immunoblotted against histone H1 (1:500 (v/v)). The anti-DGK-theta antibody was a mouse antibody, while the anti-histone H1 antibody was a rabbit antibody, therefore the signals were observed on different channels on the Odyssey® Infrared Imaging System, and the anti-DGK-theta signal is not contributing to these immunoblots.

I therefore decided to try to detect DGK-theta's presence by immunoblotting against an epitope tag, in this case, the histidine tag, whose affinity for its antibody would not be predicted to depend on the presence of histone H1. After stripping the membranes, however, the antibody detection by either of two mouse anti-histidine antibodies detected not much stronger a signal than anti-mouse secondary antibody alone (Figure 193**A-C**), making quantification difficult. When I blotted against histidine using a rabbit antibody (Figure 193**D**), a new band appeared coincident with the anti-DGK-theta immunoreactive band (Figure 193**A-C**) not seen in the anti-histone H1 blot (Figure 192), consistent with recognition of the fusion protein. Once again, however, the signal remained to weak to be useful for quantitatively measuring protein recovery.

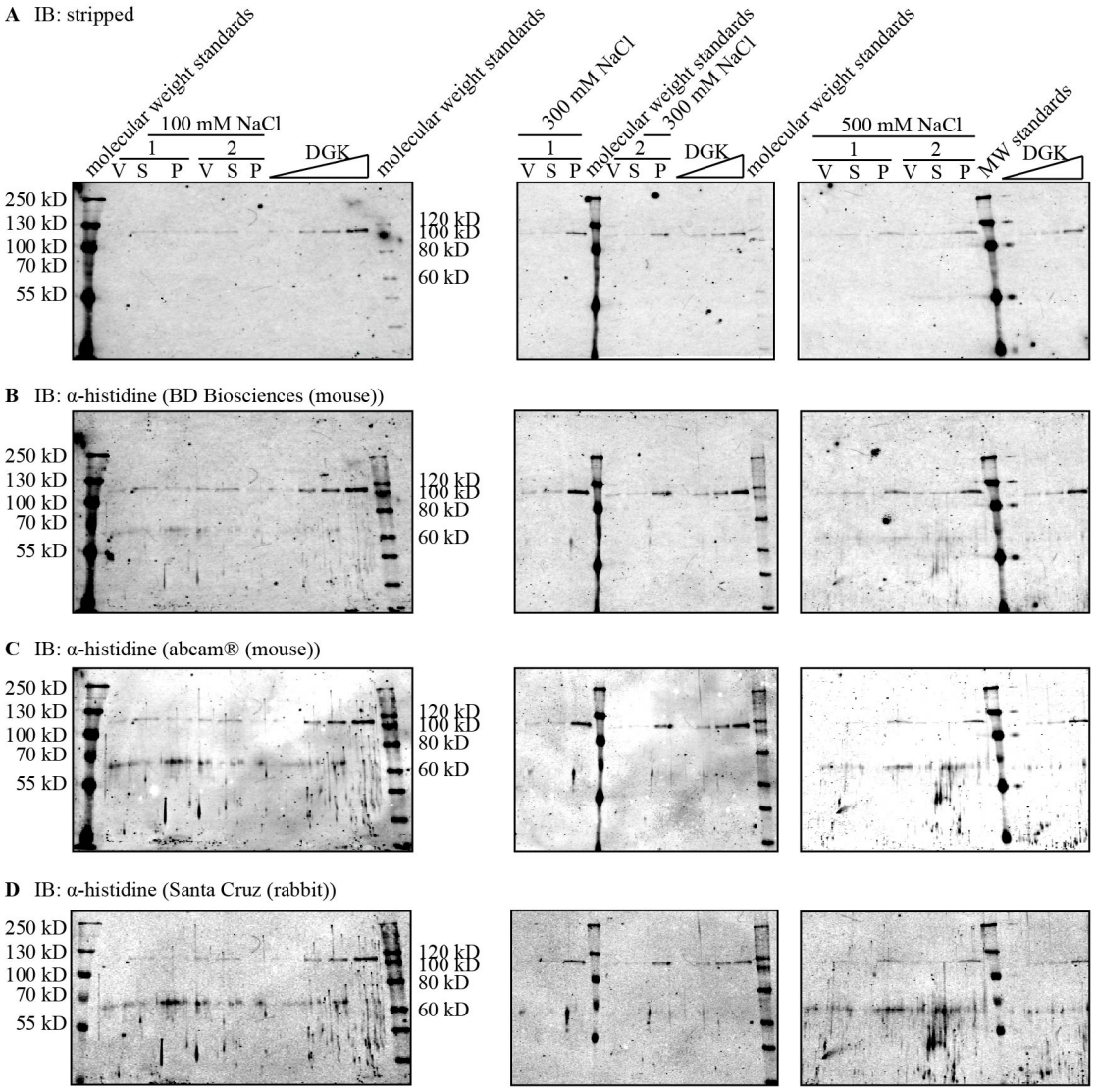

Figure 193. The signal from immunoblotting against histidine was too weak to quantitatively measure DGK-theta recovery following SLV pulldown in the presence of salt. (A) The same membranes as shown in **Figure 192**, stripped with NewBlot™ Nitro Stripping Buffer and redeveloped with IRDye® 680LT goat anti-mouse IgG. The anti-DGK-theta antibody used in **Figure 190** was also a mouse antibody, so the lingering signal probably is from anti-DGK-theta that remained after stripping. **(B)** The same membranes immunoblotted against histidine (BD Biosciences 631212 (1:5000 (v/v)), also a mouse antibody). **(C)** The same membranes immunoblotted against His6 (abcam® ab6196 (1:2500 (v/v)), also a mouse antibody). **(D)** The same membranes immunoblotted against histidine (Santa Cruz Biotechnology, Inc. sc-803 (1:2000 (v/v)), a rabbit antibody).

Positive control: eGFP-C1b

Because I was having issues quantitatively measuring the amount of DGK-theta pulled down by SLVs and reproducing previous results, it was suggested to me to first

make sure that the probes successfully photoaffinity labeled a positive control before expending too much effort optimizing the DGK-theta conditions. I therefore transiently transfected HEK293T cells with DNA that had been labeled "PKC delta C1b 2x in pEGFP-C2", which supposedly encoded two copies of the C1b domain from *H. sapiens* PKC-δ fused in tandem to the C-terminus of eGFP, but DNA sequencing confirmed that only one copy of the C1b domain was encoded (Figure 194). The transfected cells fluoresced green two days after transfection, consistent with expression of the eGFP. I lysed the cells, fractionated into nuclei, cytosol, and non-nuclear membranes, then assessed the partitioning of the fusion protein using SDS-PAGE followed by Coomassie staining and immunoblotting against GFP. No new bands in the transfected samples not seen in the mock-transfected samples were visible by Coomassie staining (Figure 195**A**), but a predominant band that migrated between the 35 and 40 kD molecular weight markers was robustly recognized by the anti-GFP antibody in the transfected but not mock-transfected samples (Figure 195**B**), consistent with the expression of a fusion protein with the predicted molecular weight of 38.5 kD. Of the fractions tested, the cytosol appeared to have the most eGFP-C1b expression (Figure 195**C**).

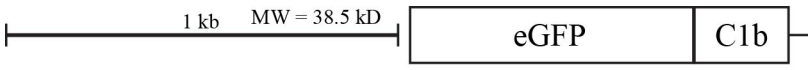

Figure 194. Schematic of the eGFP-C1b construct. I submitted the purified DNA to GENEWIZ® for sequencing using their EGFP-C sequencing primer (CATGGTCCTGCTGGAGTTCGTG), and was thereby able to sequence the construct from the end of the eGFP coding region through to the stop codon. The upstream coding region of eGFP is inferred. As such, the predicted molecular weight is 38.5 kD.

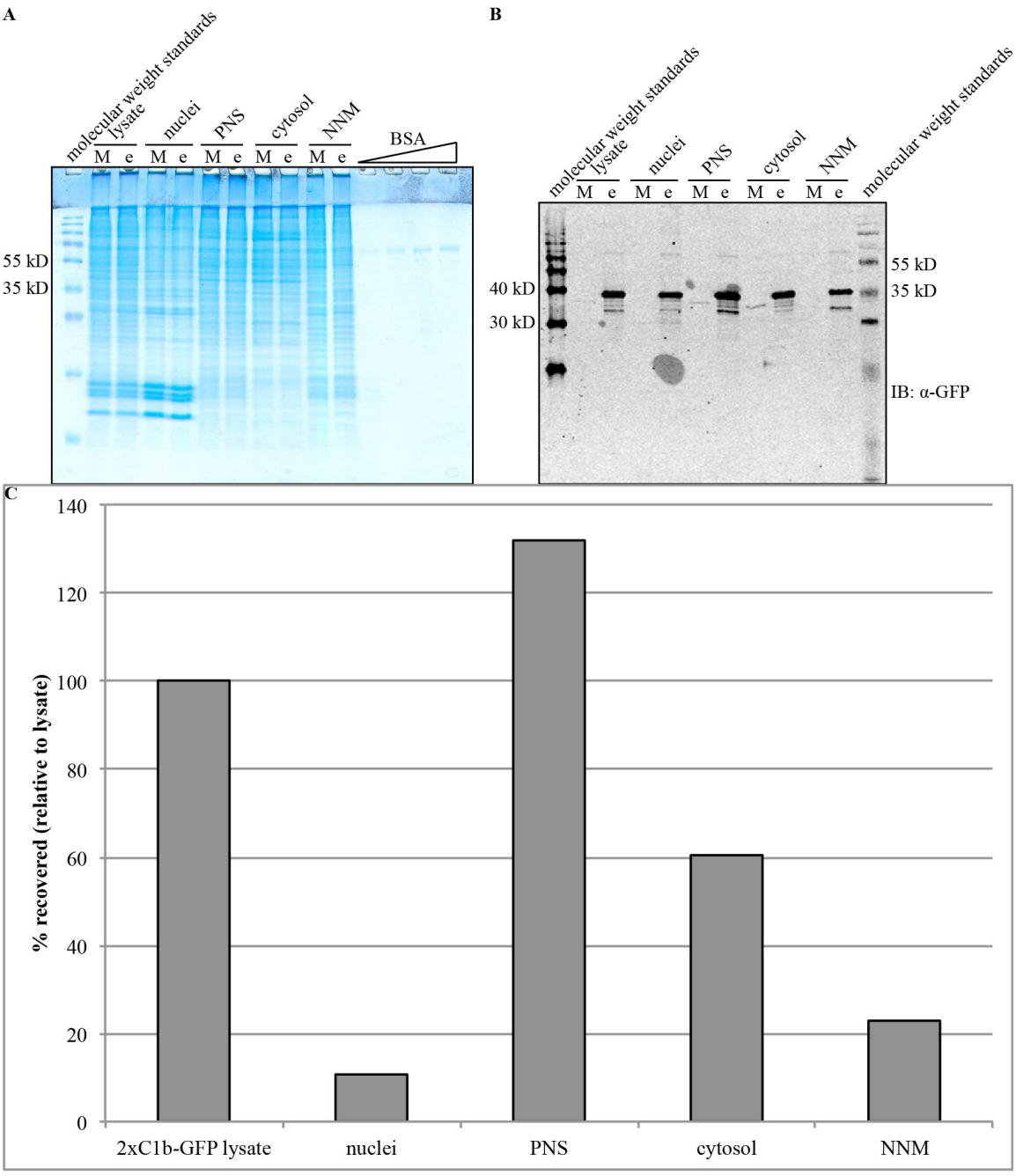

Figure 195. eGFP-C1b-transfected HEK293T cells express a band that migrates between the 35 and 40 kD molecular weight markers during SDS-PAGE that is recognized by an anti-GFP antibody and fractionates mostly to the cytosol. I transfected two 15 cm plates each of HEK293T cells with either eGFP-C1b or without DNA (mock-transfected) for two days. I rinsed each plate twice with cold PBS, added cold lysis buffer (20 mM HEPES, pH 7.4, 0.5 mM EGTA, 1 mM EDTA, 4 µg per mL quinacrine, 1x PIC, 5 mM NaVO4, 10 mM NaF, 5 mM DTT, 0.25% (v/v) NP-40), and incubated on ice for five minutes before scraping and homogenizing twelve times with a glass cell homogenizer. I stored the lysate at -80°C for four days prior to thawing by shaking the tubes gently in water. The lysates appeared not completely lysed, so I homogenized twelve more times. I separated the nuclei from the post-nuclear supernatant (PNS) by centrifugation. I fractionated the resulting supernatant by centrifuging at 110,000 x g for 65 minutes at

4°C: the resulting supernatant was the cytosol, and the resulting pellet was the non-nuclear membranes (NNM). **(A)** SDS-PAGE of a 15% acrylamide gel followed by Coomassie staining. I loaded 10 μg protein (as measured by the Bio-Rad Protein Assay) per lane. M; mock-transfected; e, eGFP-C1b. **(B)** SDS-PAGE of a 15% acrylamide gel followed by immunoblotting against GFP (abcam® ab6556 (1:3000 (v/v))). I loaded 1 μg protein (as measured by the Bio-Rad Protein Assay) per lane. **(C)** Quantification of the immunoblot signal from (B), normalized to the signal from the lysate.

I first precleared the eGFP-C1b-expressing cytosol with SLVs to remove nonspecifically-associating protein from the sample, and then pulled down with SLVs again to confirm that not all of the eGFP-C1b had been removed in the first step, and that a low enough proportion of the eGFP-C1b came down with the pellet so that I would be able to detect any probe- and UV-dependent increase in pulldown. I could easily detect the remaining eGFP-C1b after preclearing (Figure 196**A**-**B**), so I concluded that preclearing did not remove all the eGFP-C1b. As before, the reproducibility of partitioning among replicates was poor (Figure 196), so I would only be able to detect with confidence at least a twofold increase in pulldown. In the experiment, I might be able to increase the precision by doing more blots of each replicate, to reduce the uncertainty due to transfer.

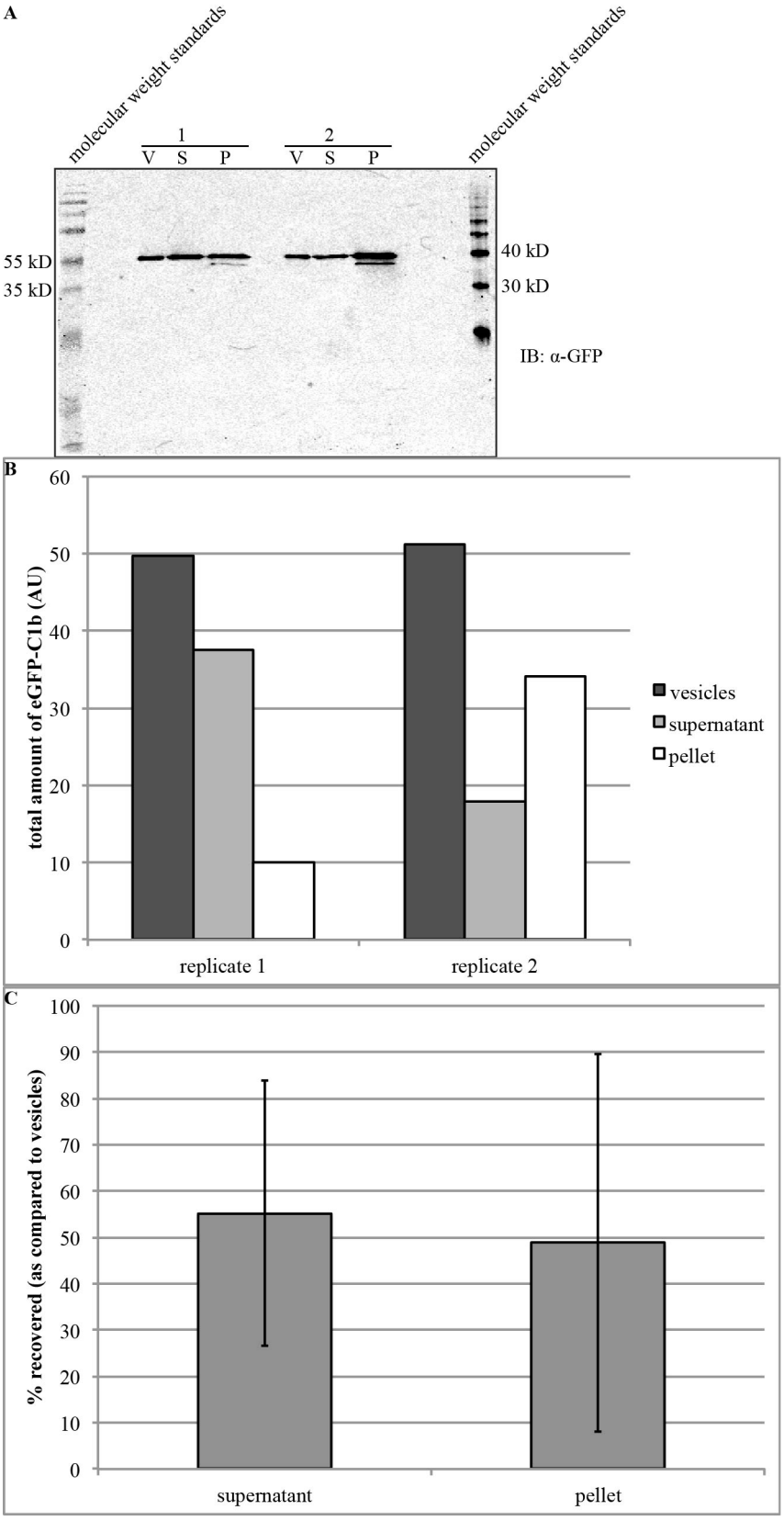
A
molecular weight standards
1
V S P
2
V S P
molecular weight standards
55 kD
35 kD
40 kD
30 kD
IB: α-GFP
B
total amount of eGFP-C1b (AU)
60
50
40
30
20
10
0
vesicles
supernatant
pellet
replicate 1
replicate 2
C
% recovered (as compared to vesicles)
100
90
80
70
60
50
40
30
20
10
0
supernatant
pellet

Figure 196. eGFP-C1b is easily detectable by immunoblot after preclearing with SLVs, but reproducibility between SLV pulldown replicates is poor. I stored the eGFP-C1b cytosol (shown in **Figure 195**) at -80°C for five days before thawing and preclearing by incubating with preclearing buffer (1 mM freshly made SLVs (53.3:26.7:20::POPE:POPC:POPS), 51 mM HEPES, pH 7.5, 101 mM NaCl, 0.1 μM histone H1, 1 mM ATP, 1.5 mM MgCl2, and from the eGFP-C1b cytosol, 100 ng per μL protein (as measured by the Bio-Rad Protein Assay), 34 μM EGTA, 68 μM EDTA, 0.3 μg per μL quinacrine, 0.07x PIC, 0.3 mM NaVO4, 0.7 mM NaF, 0.02% (v/v) NP-40), rocking at room temperature for thirty minutes. I pelleted the SLVs by centrifuging at 136,000 x g for 75 minutes at 25°C: the resulting supernatant was the precleared cytosol. I then pulled down the precleared cytosol in duplicate by incubating with SLV buffer (1 mM SLVs, 52 mM HEPES, pH 7.5, 103 mM NaCl, 0.08 μM histone H1, 0.8 mM ATP, 1.3 mM MgCl2, and from the precleared cytosol, up to 84 ng per μL protein (assuming 100% recovery after preclearing), 29 μM EGTA, 57 μM EDTA, 0.2 μg per μL quinacrine, 0.06x PIC, 0.3 mM NaVO4, 0.6 mM NaF, 0.01% (v/v) NP-40), rocking at room temperature for thirty minutes. I pelleted the SLVs by centrifuging at 136,000 x g for 75 minutes at 25°C. **(A)** SDS-PAGE of a 15% acrylamide gel, followed by immunoblotting against GFP (abcam® ab6556 (1:3000 (v/v))). V, vesicles; S, supernatant; P, pellet. "1" and "2" indicate two replicates. **(B)** Quantification of the signal in (A), adjusted for the volumes of the samples to calculate the total amount of protein in each fraction. Because there is no eGFP-C1b standard on this membrane, the units are arbitrary and assume equal efficiency of antibody recognition in each sample. **(C)** The same data shown in (B), redisplayed as a percent of the vesicle from signals and averaged over the two replicates. Mean ± SD.

I observed an additional, faster-migrating band in the pellet of the eGFP-C1b SLV pulldown (Figure 196**A**), so, concerned about antibody specificity in the context of the SLVs (since no nonspecific bands from the mock-transfected cells were recognized in the immunoblot testing the expression of the recombinant protein (Figure 195**B**)), I immunoblotted against both SLV pulldowns of the mock-transfected HEK293T cytosol as well as of SLV pulldowns without cytosol. A GFP-immunoreactive band was indeed apparent in the mock-transfected pulldown and, to a lesser extent, the buffer pulldown (Figure 197), but this band was distinct in size from the eGFP-C1b band and did not contribute to the quantification of eGFP-C1b.

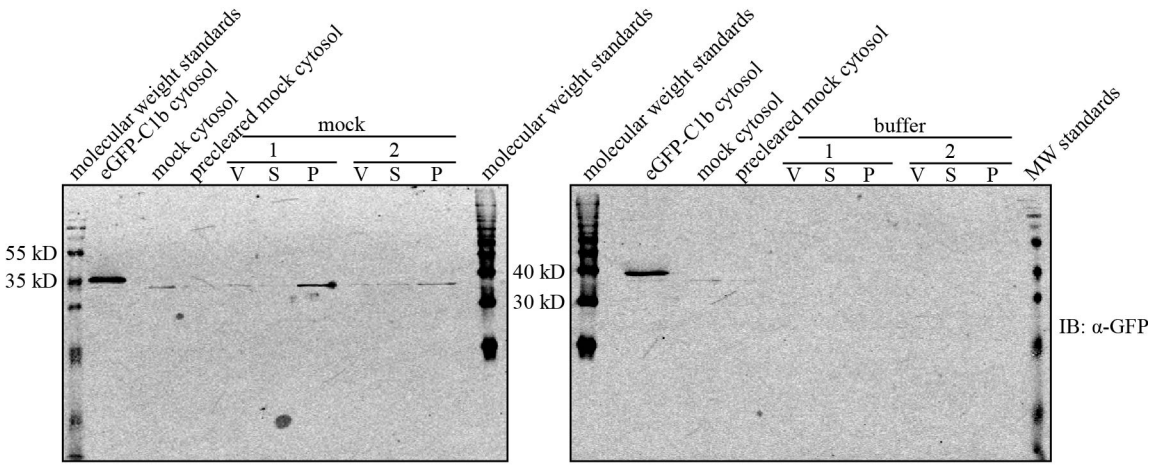

Figure 197. SLV pulldowns of mock-transfected HEK293T cytosol and of buffer produce an immunoreactive band, but it is distinct in size from eGFP-C1b and does not contribute to its quantification. I precleared the mock-transfected 293FT cytosol (shown in **Figure 195**) by incubating with preclearing buffer (1 mM SLVs (53.3:26.7:20::POPE:POPC:POPS), 51 mM HEPES, pH 7.5, 101 mM NaCl, 0.1 μM histone H1, 1 mM ATP, 1.5 mM MgCl2, and from the eGFP-C1b cytosol, 100 ng per μL protein (as measured by the Bio-Rad Protein Assay), 34 μM EGTA, 68 μM EDTA, 0.3 μg per μL quinacrine, 0.07x PIC, 0.3 mM NaVO4, 0.7 mM NaF, 0.02% (v/v) NP-40), rocking at room temperature for thirty minutes. I pelleted the SLVs by centrifuging at 136,000 x g for 75 minutes at 25°C: the resulting supernatant was the precleared cytosol. I then pulled down either precleared mock-transfected HEK293T cytosol or else just buffer in duplicate by incubating with SLV buffer (1 mM SLVs, 52 mM HEPES, pH 7.5, 103 mM NaCl, 0.08 μM histone H1, 0.8 mM ATP, 1.3 mM MgCl2, and from the precleared cytosol, up to 84 ng per μL protein (assuming 100% recovery after preclearing), 29 μM EGTA, 57 μM EDTA, 0.2 μg per μL quinacrine, 0.06x PIC, 0.3 mM NaVO4, 0.6 mM NaF, 0.01% (v/v) NP-40), rocking at room temperature for thirty minutes. I pelleted the SLVs by centrifuging at 136,000 x g for 75 minutes at 25°C. SDS-PAGE of 15% acrylamide gels, followed by immunoblotting against GFP (abcam® ab6556 (1:3000 (v/v))). V, vesicles; S, supernatant; P, pellet. "1" and "2" indicate two replicates.

When I tested whether irradiation in the presence of compound **1** (whose structure is shown in Figure 130) increased the SLV pulldown of precleared eGFP-C1b-overexpressing cytosol in a probe- and UV- dependent way, I first found that much more of the eGFP-C1b fractionated into the supernatant (Figure 198 and Figure 199) than in the previous experiment (Figure 196), even though SLVs of identical concentration and composition were used in an identical buffer, underscoring the difficulties in reproducibility in SLV recovery. The percentage of eGFP-C1b that fractionated into the pellet did not increase in a probe- and UV-dependent way, under the conditions tested.

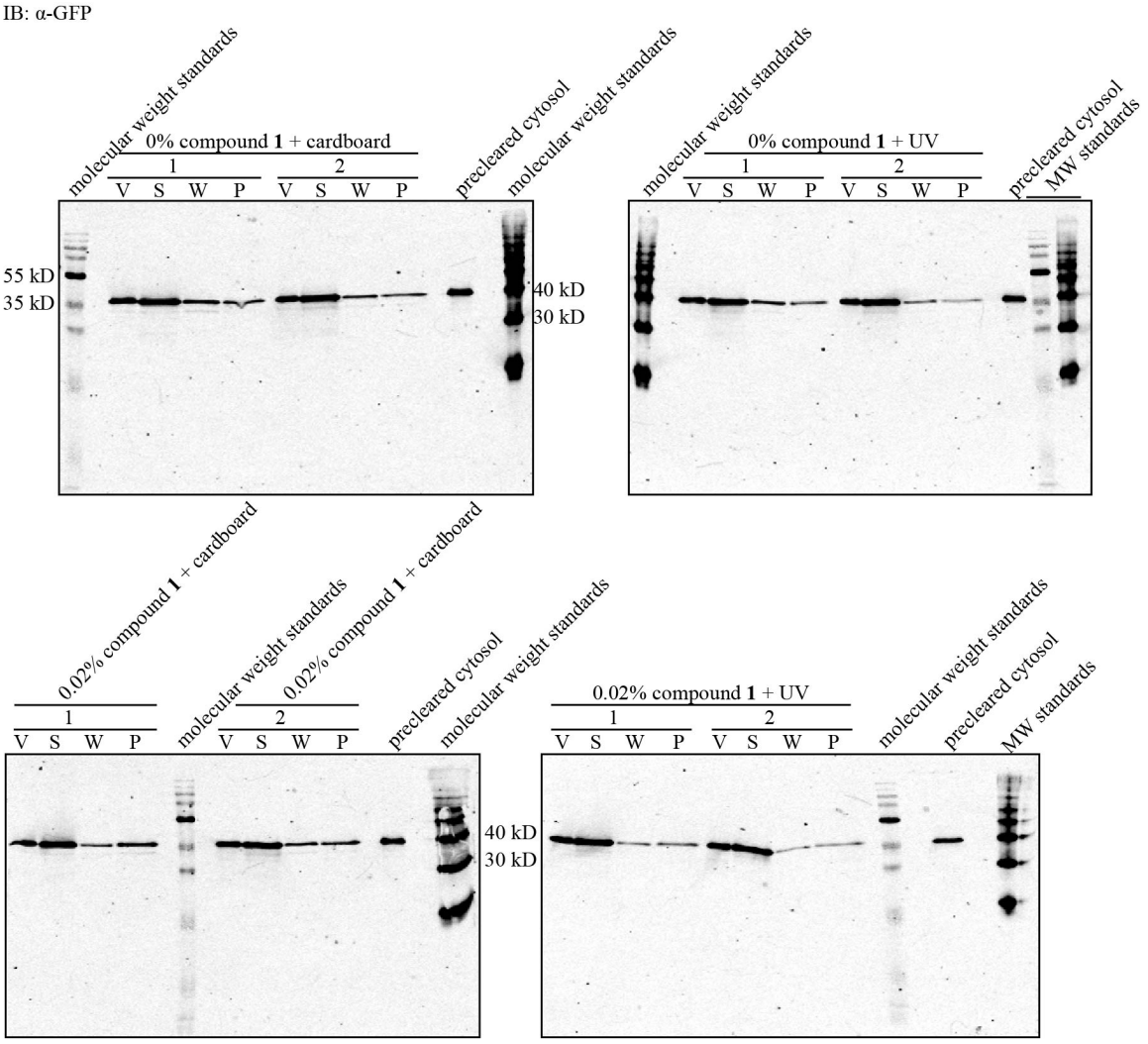

Figure 198. Reproducibility of how eGFP-C1b fractionates in SLV pulldown is low among experiments, and the percentage of eGFP-C1b that fractionated into the pellet did not increase in a probe- and UV-dependent way, under the conditions tested. I precleared the eGFP-C1b cytosol (shown in **Figure 195**) by incubating with preclearing buffer (1 mM freshly made SLVs (52.2:26.3:20::POPE:POPC:POPS), 51 mM HEPES, pH 7.5, 101 mM NaCl, 0.1 μM histone H1, 1 mM ATP, 1.5 mM MgCl2, and from the eGFP-C1b cytosol, 100 ng per μL protein (as measured by the Bio-Rad Protein Assay), 34 μM EGTA, 68 μM EDTA, 0.3 μg per μL quinacrine, 0.07x PIC, 0.3 mM NaVO4, 0.7 mM NaF, 0.02% (v/v) NP-40), rocking at room temperature for thirty minutes. I pelleted the SLVs by centrifuging at 136,000 x g for 75 minutes at 25°C: the resulting supernatant was the precleared cytosol. I then pulled down the precleared cytosol by incubating with SLV buffer (1 mM SLVs (2:1::POPE:POPC, 20 mol% POPS, plus the indicated concentration of compound 1), 52 mM HEPES, pH 7.5, 103 mM NaCl, 0.08 μM histone H1, 0.8 mM ATP, 1.3 mM MgCl2, and from the precleared cytosol, up to 84 ng per μL protein (assuming 100% recovery after preclearing), 29 μM EGTA, 57 μM EDTA, 0.2 μg per μL quinacrine, 0.06x PIC, 0.3 mM NaVO4, 0.6 mM NaF, 0.01% (v/v) NP-40), rocking at room temperature, protected from light, for thirty minutes. I then irradiated the samples with a 360 nm lamp for six minutes in a water-jacketed quartz cuvette with stirring, with or without cardboard between the lamp and cuvette. I pelleted the SLVs in duplicate by centrifuging at 136,000 x g for 75 minutes at 25°C. I resuspended the

pellets in assay buffer, and pelleted the SLVs a second time, storing the resulting supernatant as “wash”. SDS-PAGE of 15% acrylamide gels, followed by immunoblotting against GFP (abcam® ab6556 (1:3000 (v/v))). V, vesicles; S, supernatant; W, wash; P, pellet. “1” and “2” indicate two replicates.

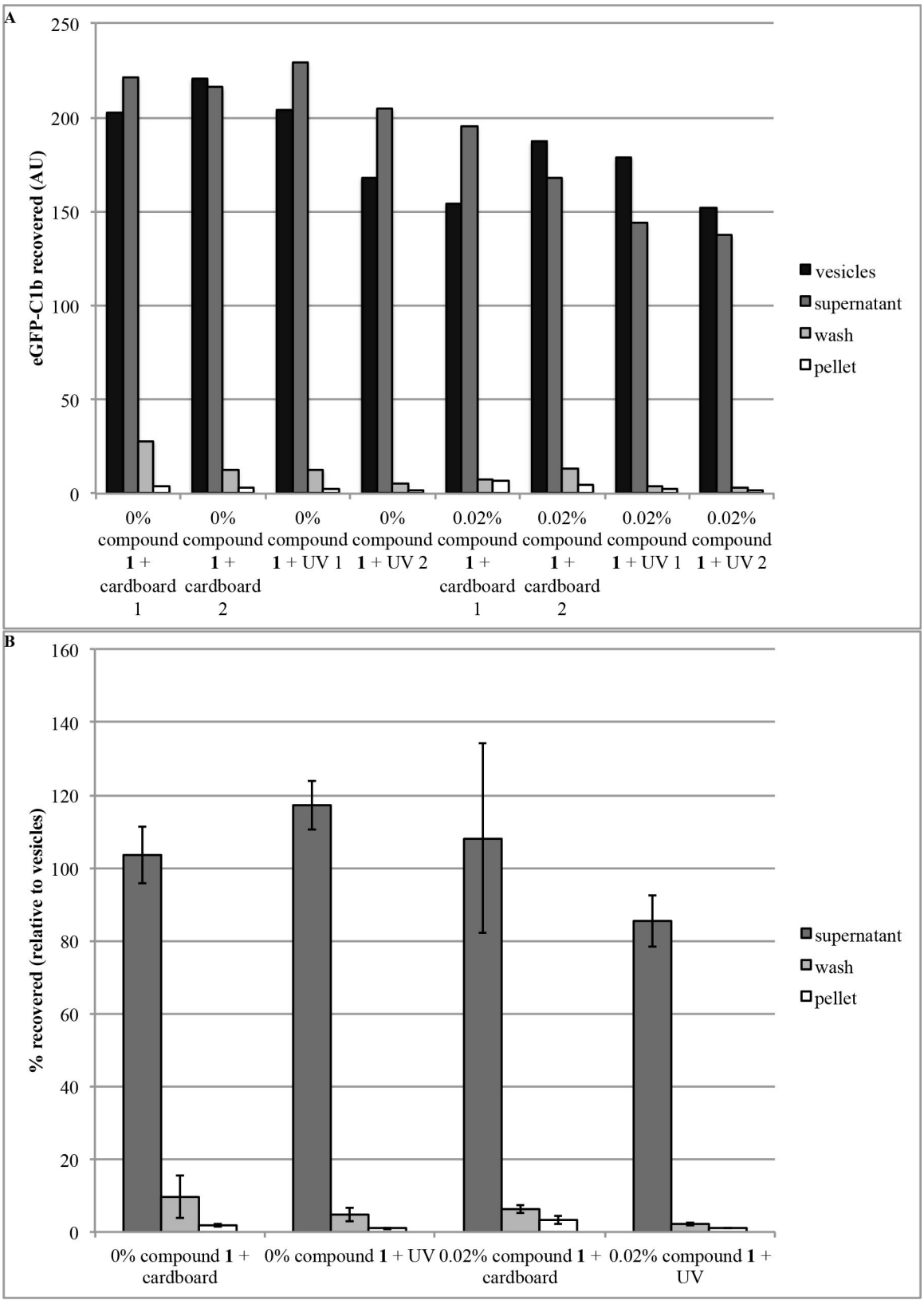
A
250
200
150
100
50
0
eGFP-C1b recovered (AU)
vesicles
supernatant
wash
pellet
0% compound 1 + cardboard 1
0% compound 1 + cardboard 2
0% compound 1 + UV 1
0% compound 1 + UV 2
0.02% compound 1 + cardboard 1
0.02% compound 1 + cardboard 2
0.02% compound 1 + UV 1
0.02% compound 1 + UV 2
B
160
140
120
100
80
60
40
20
0
% recovered (relative to vesicles)
supernatant
wash
pellet
0% compound 1 + cardboard
0% compound 1 + UV
0.02% compound 1 + cardboard
0.02% compound 1 + UV

Figure 199. Reproducibility of how eGFP-C1b fractionates in SLV pulldown is low among experiments, and the percentage of eGFP-C1b that fractionated into the pellet did not increase in a probe- and UV-dependent way, under the conditions tested. (A) Quantification of the signal in **Figure 198**, adjusted for the volumes of the samples to calculate the total amount of protein in each fraction. Because there is no eGFP-C1b standard on this membrane, the units are arbitrary and assume equal efficiency of antibody recognition in each sample. **(B)** The same data shown in (A), redisplayed as a percent of the vesicle from signals and averaged over each set of two replicates. Mean ± SD.

A number of factors could possibly explain why irradiating in the presence of the probe would not increase the amount of eGFP-C1b recovered in the pellet: perhaps the experiment did not include enough protein or enough probe, perhaps the probe had gone bad (it is, after all, a photoreactive molecule), perhaps the time of irradiation wasn't long enough, perhaps other components in the buffer were absorbing some of the 360 nm light, etc. In order to have a positive control for the positive control, therefore, I next tested whether DAG could increase SLV pulldown of eGFP-C1b. I chose four concentrations of DAG to test: 0 mol%; the concentration used in the previous experiment (0.53 mol% (this was before I realized the concentration of compound **1** was less than advertised (Figure 131))); the supposed K_d[158] of PKCδ's C1b domain for DAG (7800 nM = 0.78 mol% of 1 mM liposomes); and a value considerably higher than the reported K_d (2.5 mol%). The proportion of eGFP-C1b copelleting with the SLVs did appear to increase DAG-dependently (Figure 200 and Figure 201), as predicted, but the amount of eGFP-C1b pulled down remained far less than half. One possible explanation for why the DAG pulled down as little eGFP-C1b as it did is that eGFP-C1b, while overexpressed, is presumably not the only DAG-binding protein in the HEK293T cytosol, and these other proteins could compete with eGFP-C1b. A purified protein might therefore be a better choice as a positive control for photoaffinity labeling of DGK.

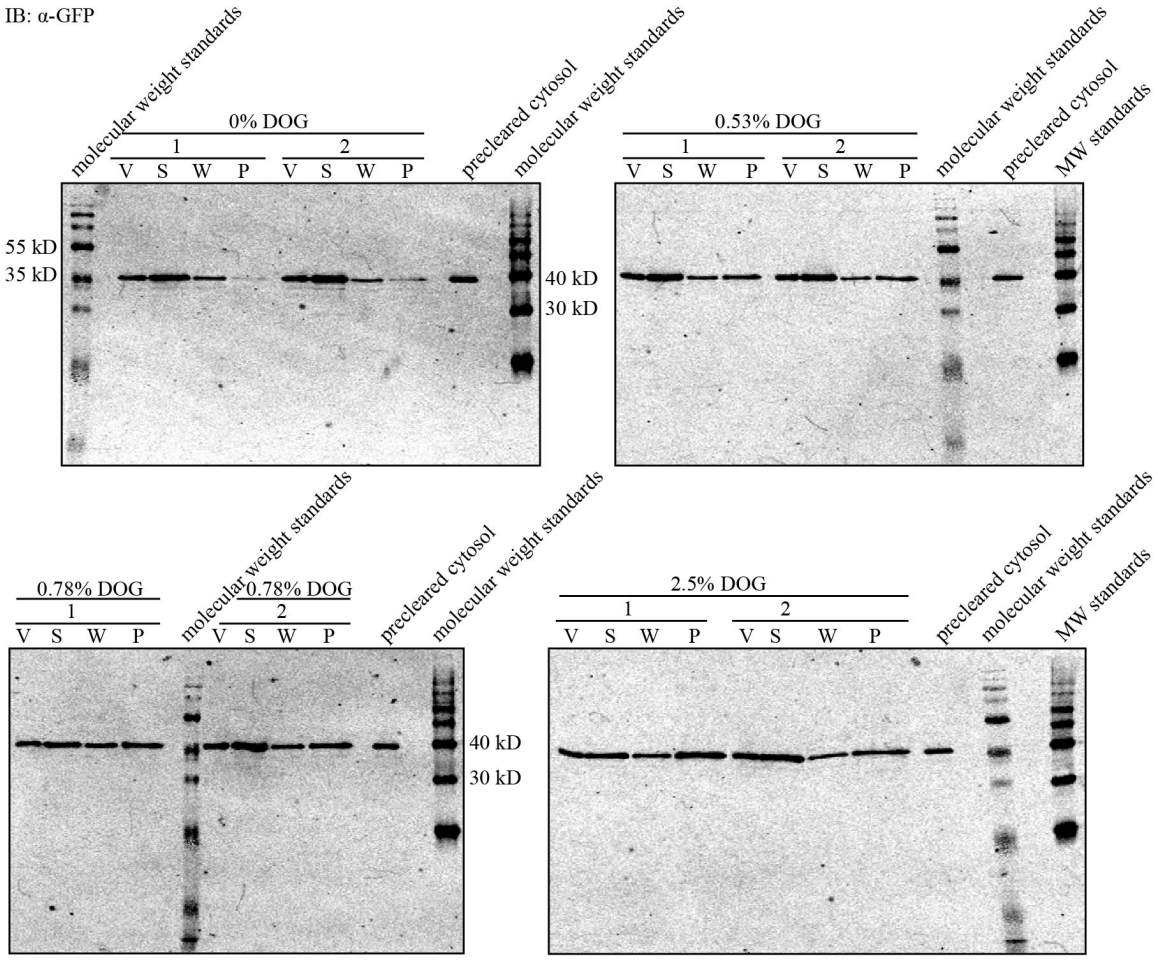

Figure 200. The proportion of eGFP-C1b copelleting with the SLVs did appear to increase DAG-dependently, but the amount of eGFP-C1b pulled down remained far less than half. I precleared the eGFP-C1b cytosol (shown in **Figure 195**) by incubating with preclearing buffer (1 mM freshly made SLVs (52.2:26.3:20::POPE:POPC:POPS), 51 mM HEPES, pH 7.5, 101 mM NaCl, 0.1 μM histone H1, 1 mM ATP, 1.5 mM MgCl2, and from the eGFP-C1b cytosol, 100 ng per μL protein (as measured by the Bio-Rad Protein Assay), 34 μM EGTA, 68 μM EDTA, 0.3 μg per μL quinacrine, 0.07x PIC, 0.3 mM NaVO4, 0.7 mM NaF, 0.02% (v/v) NP-40), rocking at room temperature for thirty minutes. I pelleted the SLVs by centrifuging at 136,000 x g for 75 minutes at 25°C: the resulting supernatant was the precleared cytosol. I then pulled down the precleared cytosol by incubating with SLV buffer (0.67 mM SLVs (2:1::POPE:POPC, 20 mol% POPS, plus the indicated concentration of DOG) (0.78% DOG SLVs were 1 mM to match the reported Kd[158]), 52 mM HEPES, pH 7.5, 103 mM NaCl, 0.08 μM histone H1, 0.8 mM ATP, 1.3 mM MgCl2, and from the precleared cytosol, up to 84 ng per μL protein (assuming 100% recovery after preclearing), 29 μM EGTA, 57 μM EDTA, 0.2 μg per μL quinacrine, 0.06x PIC, 0.3 mM NaVO4, 0.6 mM NaF, 0.01% (v/v) NP-40), rocking at room temperature for thirty minutes. I pelleted the SLVs in duplicate by centrifuging at 136,000 x g for 75 minutes at 25°C. I resuspended the pellets in assay buffer, and pelleted the SLVs a second time, storing the resulting supernatant as "wash". SDS-PAGE of 15% acrylamide gels, followed by immunoblotting against GFP (abcam® ab6556 (1:3000 (v/v))). V, vesicles; S, supernatant; W, wash; P, pellet. "1" and "2" indicate two replicates.

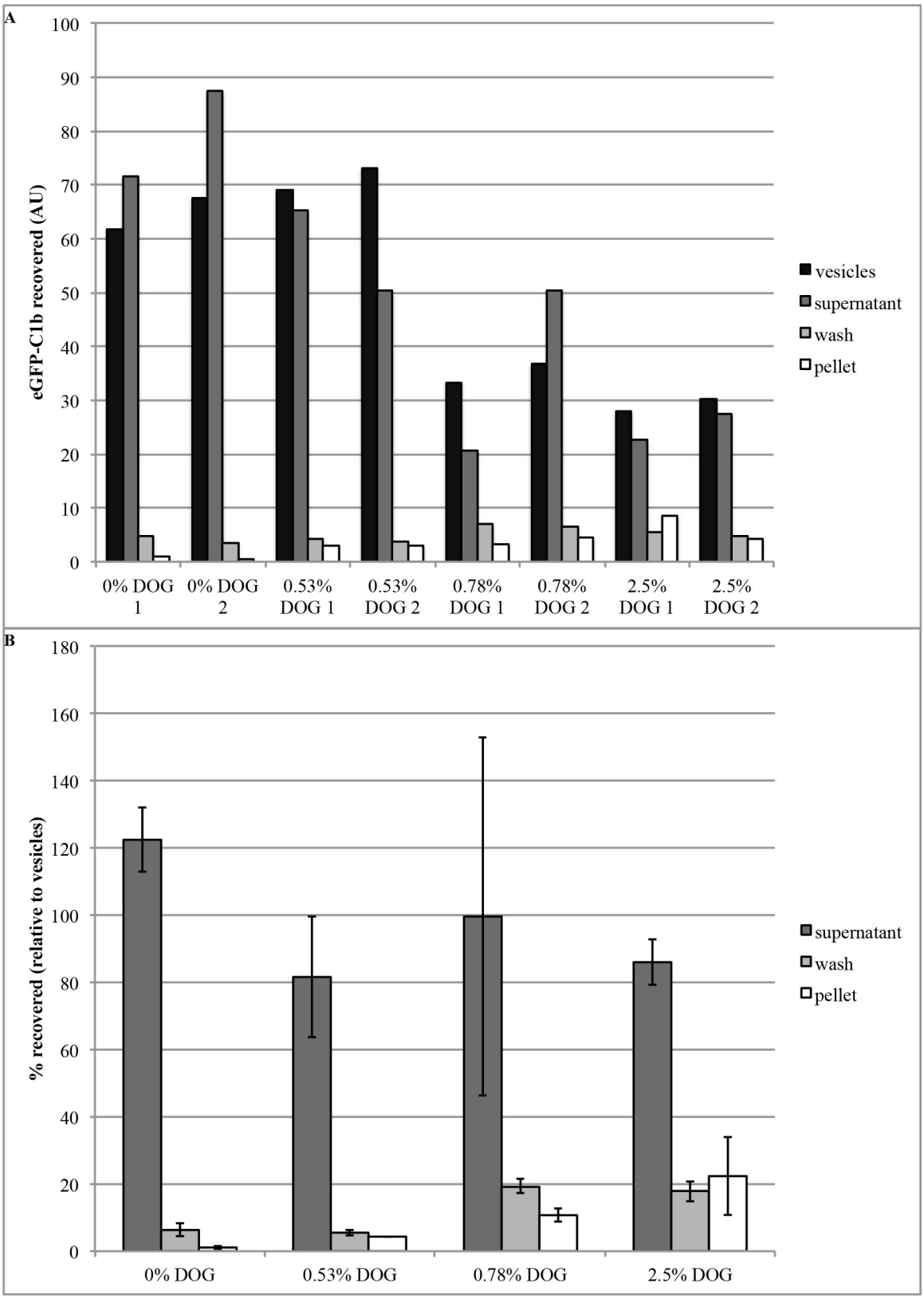
A
eGFP-C1b recovered (AU)
100
90
80
70
60
50
40
30
20
10
0
0% DOG 1
0% DOG 2
0.53% DOG 1
0.53% DOG 2
0.78% DOG 1
0.78% DOG 2
2.5% DOG 1
2.5% DOG 2
vesicles
supernatant
wash
pellet
B
% recovered (relative to vesicles)
180
160
140
120
100
80
60
40
20
0
0% DOG
0.53% DOG
0.78% DOG
2.5% DOG
supernatant
wash
pellet

Figure 201. The proportion of eGFP-C1b copelleting with the SLVs did appear to increase DAG-dependently, but the amount of eGFP-C1b pulled down remained far less than half. (A) Quantification of the signal in **Figure 200**, adjusted for the volumes of the samples to calculate the total amount of protein in each fraction. Because there is no eGFP-C1b standard on this membrane, the units are arbitrary and assume equal efficiency of antibody recognition in each sample. **(B)** The same data shown in (A), redisplayed as a percent of the vesicle from signals and averaged over each set of two replicates. Mean ± SD.

Positive Control: GST-hPKCδ

I was able to show that eGFP-C1b copelleted with SLVs DAG-dependently, but ultimately we wanted a positive control known to bind compound **1**, not necessarily DAG. The paper describing the synthesis of compound **1** also reported that compound **1** had an affinity to purified PKCδ comparable to that of DAG[144]. I therefore ordered commercial *H. sapiens* PKCδ, with a GST tag fused to the N-terminus (Enzo Life Sciences® SE-346, MW predicted to be 104 kD). Because I planned to measure SLV fractionation via immunoblotting, I first tested which antibodies recognized the recombinant, purified GST-hPKCδ. Neither a mouse-anti-PKCα nor an anti-GST primary antibody detected GST-hPKCδ at any of the concentrations tested (Figure 202**A**). An anti-GST antibody directly coupled to horseradish peroxidase (HRP) was able to recognize the GST-hPKCδ (Figure 202**B**), but the blot was too messy to be able to show that this antibody could detect it quantitatively (Figure 202**C**). I therefore ordered a new anti-GST antibody. This antibody easily detected GST-hPKCδ (Figure 203**A** and **B**), and its signal showed a good linear dependence on the concentrations tested at 1:10,000 (Figure 203**C**), 1:5000, and 1:1000 (v/v) dilutions (Figure 203**D**). The signal was considerably stronger at 1:5000 than at 1:10,000 (although caution must be exercised any time different LiCor scans are compared); contrariwise, the signal at 1:1000 was not much stronger than at 1:5000. I therefore opted to use the 1:5000 dilution of the Novus® anti-GST antibody in order to detect SLV pulldown of GST-hPKCδ.

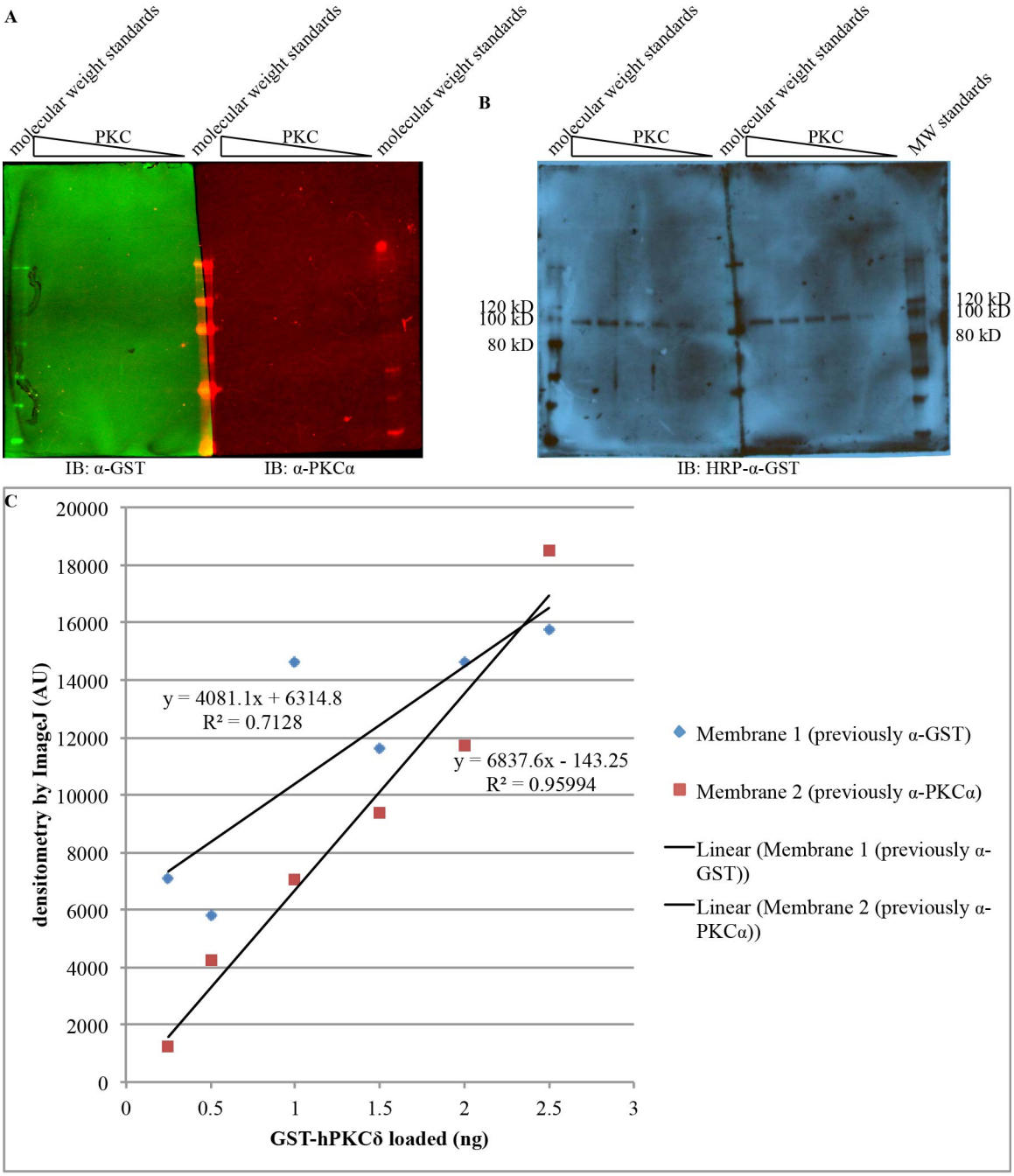

Figure 202. Neither a mouse-anti-PKCα nor an anti-GST primary antibody detected GST-hPKCδ at any of the concentrations tested, and the signal to noise ratio for an anti-GST antibody directly coupled to horseradish peroxidase was insufficient for quantitative immunoblotting. SDS-PAGE of 8% acrylamide gels followed by immunoblotting against **(A)** (left) GST (1:50,000 (v/v)) and (right) PKCα (Upstate® (now EMD Millipore) 05-154). **(B)** The same membranes as in (A), immunoblotted against GST with an antibody conjugated to horseradish peroxidase (HRP). **(C)** Quantification of the signal in (B) using densitometry as measured by ImageJ[68] (v1.46r).

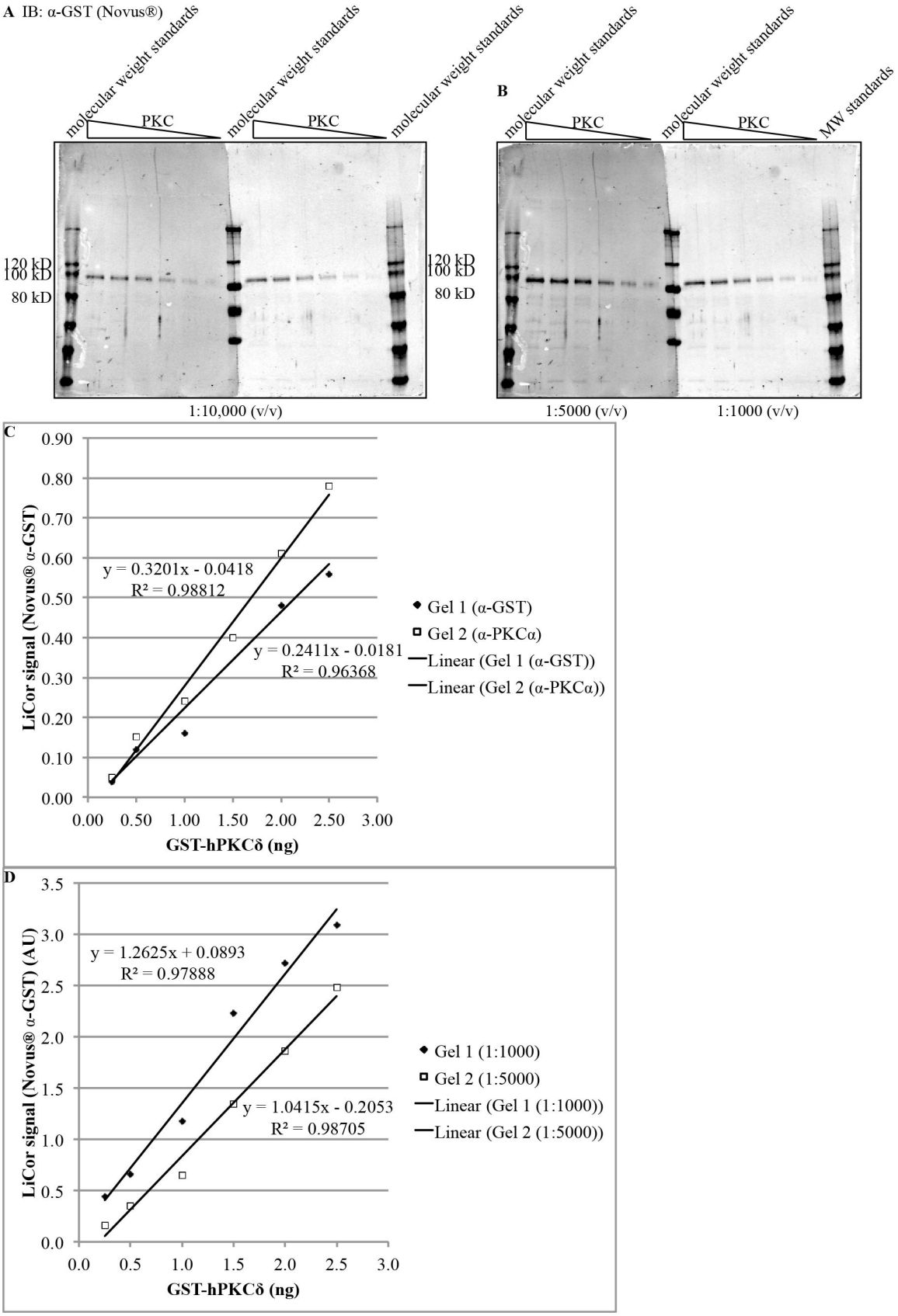
A IB: α-GST (Novus®)
molecular weight standards
PKC
molecular weight standards
PKC
molecular weight standards
120 kD
100 kD
80 kD
1:10,000 (v/v)
B
molecular weight standards
PKC
molecular weight standards
PKC
MW standards
120 kD
100 kD
80 kD
1:5000 (v/v)
1:1000 (v/v)
C
LiCor signal (Novus® α-GST)
GST-hPKCδ (ng)
y = 0.3201x - 0.0418
R² = 0.98812
y = 0.2411x - 0.0181
R² = 0.96368
Gel 1 (α-GST)
Gel 2 (α-PKCα)
Linear (Gel 1 (α-GST))
Linear (Gel 2 (α-PKCα))
D
LiCor signal (Novus® α-GST) (AU)
GST-hPKCδ (ng)
y = 1.2625x + 0.0893
R² = 0.97888
y = 1.0415x - 0.2053
R² = 0.98705
Gel 1 (1:1000)
Gel 2 (1:5000)
Linear (Gel 1 (1:1000))
Linear (Gel 2 (1:5000))

Figure 203. 1:5000 (v/v) is the best dilution for using the Novus® anti-GST antibody to detect GST-hPKCδ. (A) The membranes shown in **Figure 202**, stripped (with NewBlot™ Nitro Stripping Buffer) and reprobed against GST (Novus® (1:10,000 (v/v))). **(B)** The same membranes reprobed against GST (Novus®): left, 1:1000 (v/v); right, 1:5000 (v/v). **(C)** Quantification of the signal in (A), subtracting out the signal of the stripped blot. **(D)** Quantification of the signal in (B), subtracting out the signal of the stripped blot.

When I tried to confirm DAG-dependent SLV pulldown of purified GST-hPKCδ, however, I was unable to detect any of the SLV samples (Figure 204**A**), and the signal from the GST-hPKCδ standard was considerably weaker than in the antibody dilution tests (Figure 204**B**).

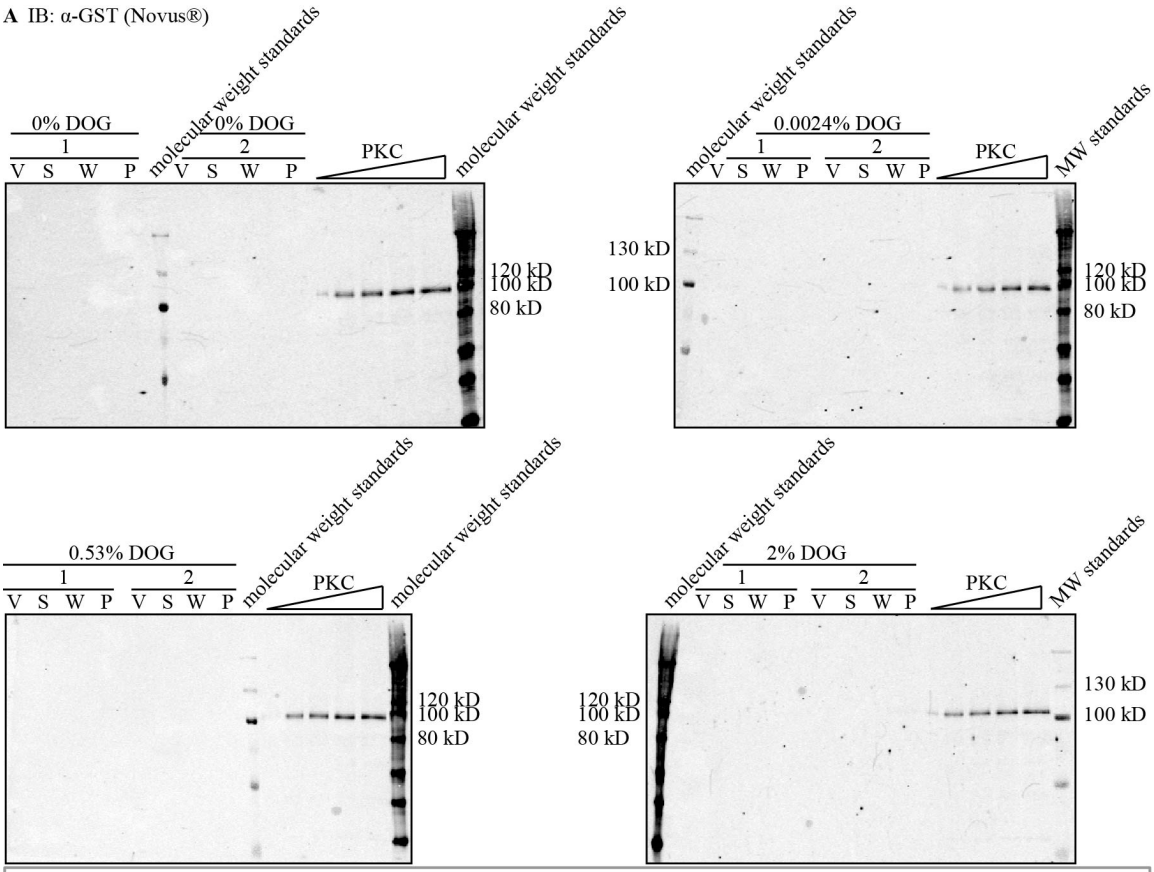
A IB: α-GST (Novus®)
0% DOG
1
2
V S W P V S W P
molecular weight standards
PKC
molecular weight standards
120 kD
100 kD
80 kD
0.0024% DOG
MW standards
130 kD
100 kD
0.53% DOG
2% DOG

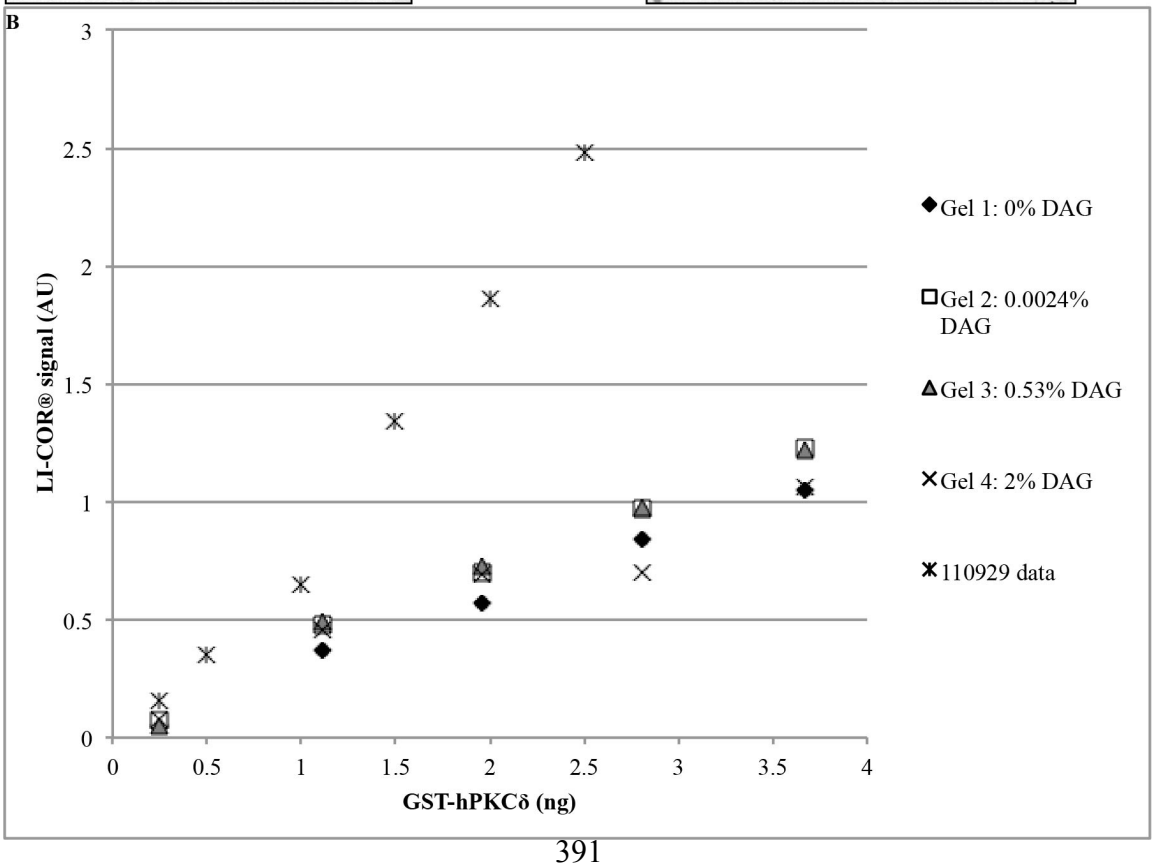
B
LI-COR® signal (AU)
GST-hPKCδ (ng)
0
0.5
1
1.5
2
2.5
3
3.5
4
Gel 1: 0% DAG
Gel 2: 0.0024% DAG
Gel 3: 0.53% DAG
Gel 4: 2% DAG
110929 data

Figure 204. The anti-GST immunoblot signal was considerably weaker than in the previous experiment. I pulled down purified GST-hPKCδ by incubating in duplicate with SLV buffer (0.25 mM SLVs (20 mol% POPS, the indicated concentration of DOG, and the rest filled with POPC), 55 mM HEPES, pH 7.5, 110 mM NaCl, 0.1 mM $CaCl_2$, 86 pg per μL GST-hPKCδ), rocking at room temperature for thirty minutes. I supplemented PC/PE SLVs to 1 mM to assist in pelleting the SLVs (GST-hPKCδ is not predicted to bind these SLVs, so their presence should not affect the pulldown). I pelleted the SLVs by centrifuging at 136,000 x *g* for ninety minutes at 25°C. I resuspended the pellets in assay buffer, and pelleted the SLVs a second time, storing the resulting supernatant as "wash". **(A)** SDS-PAGE of 8% acrylamide gels, followed by immunoblotting against GST (Novus® (1:5000 (v/v))). V, vesicles; S, supernatant; W, wash; P, pellet. "1" and "2" indicate two replicates. **(B)** Quantification of the signal of the GST-hPKCδ standards in (A), redisplaying the data shown in **Figure 203**D for comparison (as "110929 data").

I thought perhaps the lipid from the SLVs was interfering with antibody recognition of GST-hPKCδ, so I incubated GST-hPKCδ with SLVs and took timepoints to see whether antibody recognition depended on the presence of lipid. Antibody recognition of GST-hPKCδ clearly deteriorated as a function of time incubated at room temperature, but this was not a problem with the lipid interfering with antibody detection, because the signal from GST-hPKCδ incubated in buffer was even weaker and also deteriorated as a function of time (Figure 205).

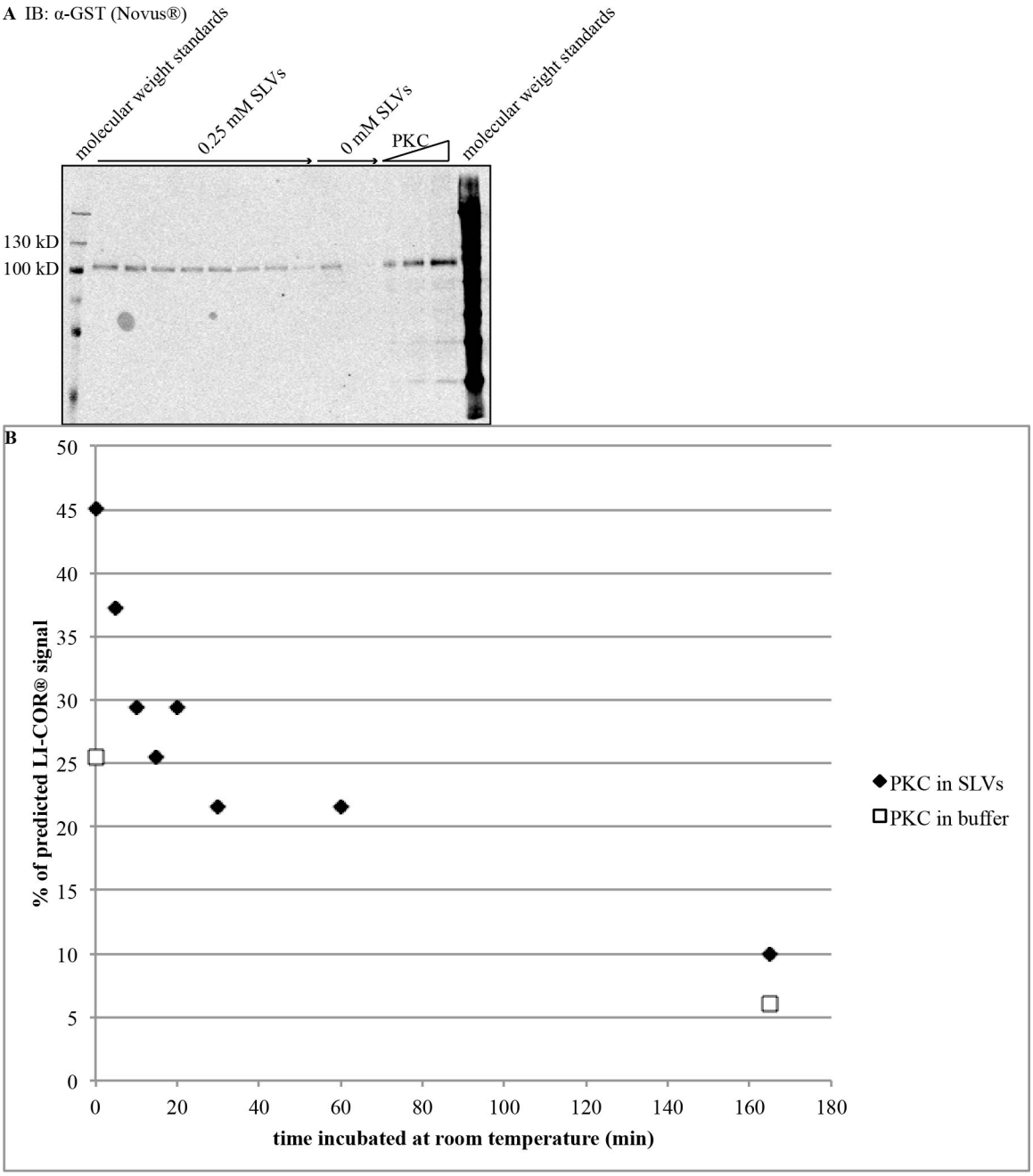

Figure 205. Antibody recognition of GST-hPKCδ by the anti-GST antibody decreases as a function of time. I incubated purified GST-hPKCδ in SLV buffer (0 or 0.25 mM SLVs (80:20:0.0024:POPC:POPS:DOG), 55 mM HEPES, pH 7.5, 110 mM NaCl, 500 pg per μL GST-hPKCδ), collecting timepoints at 0, 5, 10, 15, 20, 30, 60, and 165 minutes. I quenched each timepoint by adding SDS-PAGE gel-loading buffer to 1x and freezing at -20°C. **(A)** SDS-PAGE of an 8% acrylamide gel followed by immunoblotting against GST (Novus® (1:5000 (v/v))). Arrows indicate the passage of time. **(B)** Quantification of the signal in (A), using the GST-hPKCδ standards to calculate what the predicted LI-COR® signal would be.

I therefore wondered whether the decline in antibody recognition was a result of GST-hPKCδ's adhering to the sides of the tube. This hypothesis would explain why the signal decreased as a function of time, why GST-hPKCδ incubated with SLVs would give a stronger signal (because the SLVs would compete for tube-binding), and why the signal given by the GST-hPKCδ standard when it was freshly made (before it had time to adhere to the tube) was considerably stronger than on any of the blots since then. BSA, a protein traditionally used to prevent purified proteins from adhering to tubes, binds lipids and thus is not a good choice for including with a protein whose properties might be lipid-dependent, such as DGK. I therefore tested whether adding 0.1 μg per μL ovalbumin protected against this time-dependent loss of antibody recognition. In order to distinguish between changes in antibody recognition and changes in the amount of protein available, I also subjected the samples to silver staining. The silver-stained gel tore at the region where the GST-hPKCδ was predicted to migrate (Figure 206**A**), making interpretation exceedingly difficult. A bubble also unfortunately coincided with some of the GST-hPKCδ bands during the transfer of the immunoblot, but even so, incubating with ovalbumin clearly improved antibody recognition (Figure 206**B** and **C**). I therefore concluded that the difficulties in antibody recognition of GST-hPKCδ were due to protein adhesion, that protein adhesion could be mitigated by including ovalbumin in the reaction mix, and therefore included ovalbumin as a precaution in future experiments with GST-hPKCδ.

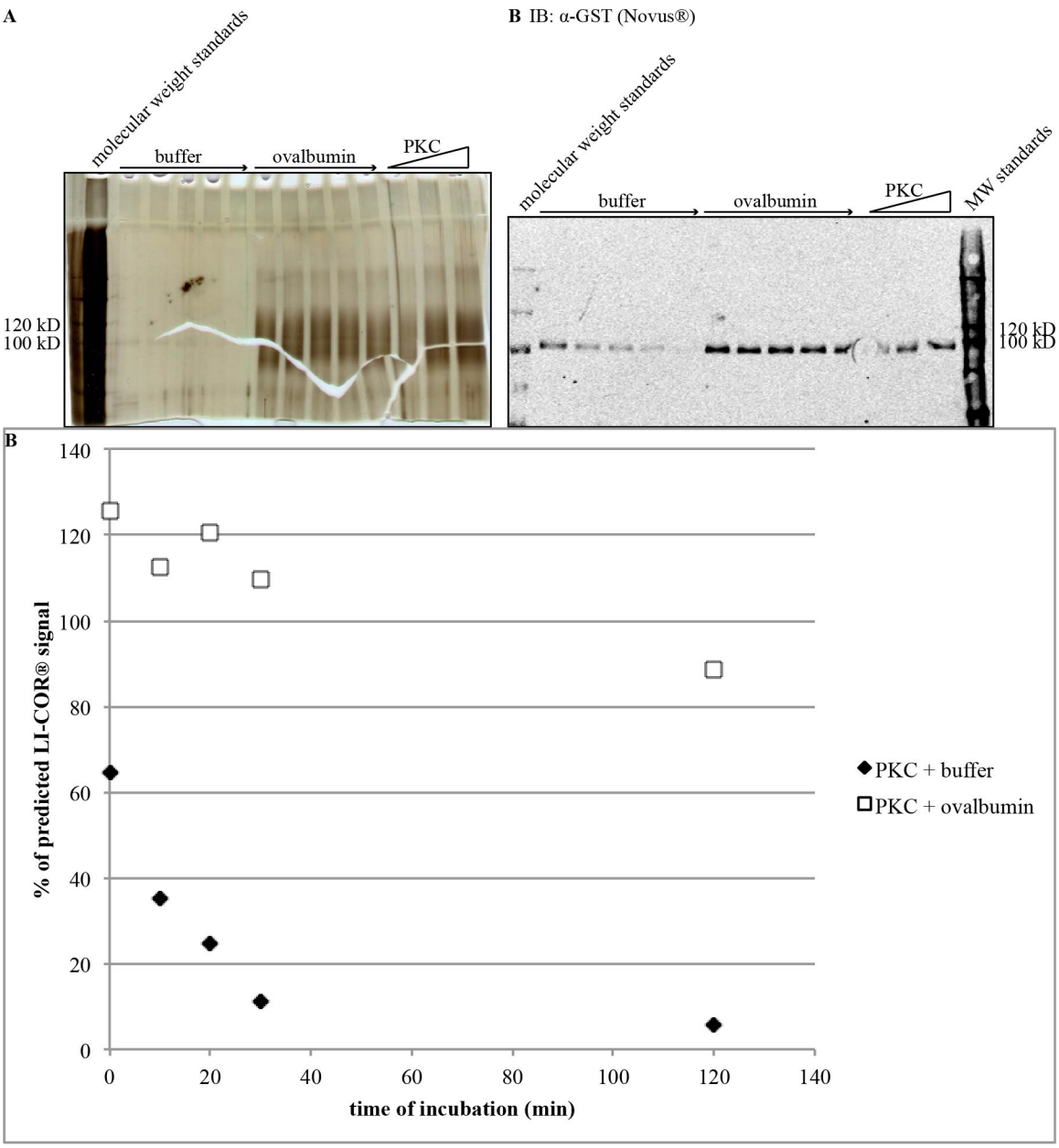

Figure 206. Including 0.1 mg per mL ovalbumin improves recognition of GST-hPKCδ by the anti-GST antibody. I incubated purified GST-hPKCδ in incubation buffer (54 mM HEPES, pH 7.5, 109 mM NaCl, 1 ng per µL GST-hPKCδ, with or without 0.1 mg per mL ovalbumin), collecting timepoints at 0, 10, 20, 30, and 120 minutes. I quenched each timepoint by adding SDS-PAGE gel-loading buffer to 1x and freezing at -20°C. SDS-PAGE of 8% acrylamide gels followed by **(A)** silver staining and **(B)** immunoblotting against GST (Novus® (1:5000 (v/v))). Arrows indicate the passage of time. **(C)** Quantification of the signal in (B), using the GST-hPKCδ standards to calculate what the predicted LI-COR® signal would be. The recovery of more than 100% the predicted signal might be due to uncertainty from the GST-hPKCδ standard because of the bubble.

I therefore once again tried to confirm DAG-dependent SLV pulldown of GST-hPKCδ, this time in the presence of ovalbumin in order to prevent GST-hPKCδ from adhering to the side of the tube and ensure better antibody detection. Ultimately I was interested not in how much protein was in the supernatant and the pellet, but rather how much of the protein is bound to the lipid. In order to calculate how much protein was bound to the lipid, I also needed to measure how the lipid partitioned between the supernatant and the pellet as well as how much of the protein sediments in the pellet in the absence of lipid, according to Equation 5[159]. I could measure how the lipid partitioned because when making the SLVs I included a fluorescent lipid, NBD-PE. When I measured lipid partitioning, however, more than half of the lipid ended up in the supernatant, not the pellet (Figure 207). The fact that the proportion of protein that pelleted in the absence of lipid (1 – β) was greater than the proportion of SLVs that pelleted (α) (Figure 208 and Figure 208) meant that it was impossible to calculate from the partitioning of the protein between supernatant and pellet how much of the protein was bound to lipid.

$$A_v = \frac{\beta * A_b + (\beta - 1)A_t}{\alpha + \beta - 1}$$

Equation 5. The fraction of protein associated with vesicles (A_v) can be calculated from the amount of protein in the top fraction (A_t), the amount of protein in the bottom fraction (A_b), the fraction of sedimented vesicles (α), and the fraction of the protein in the supernatant in the absence of vesicles (β).

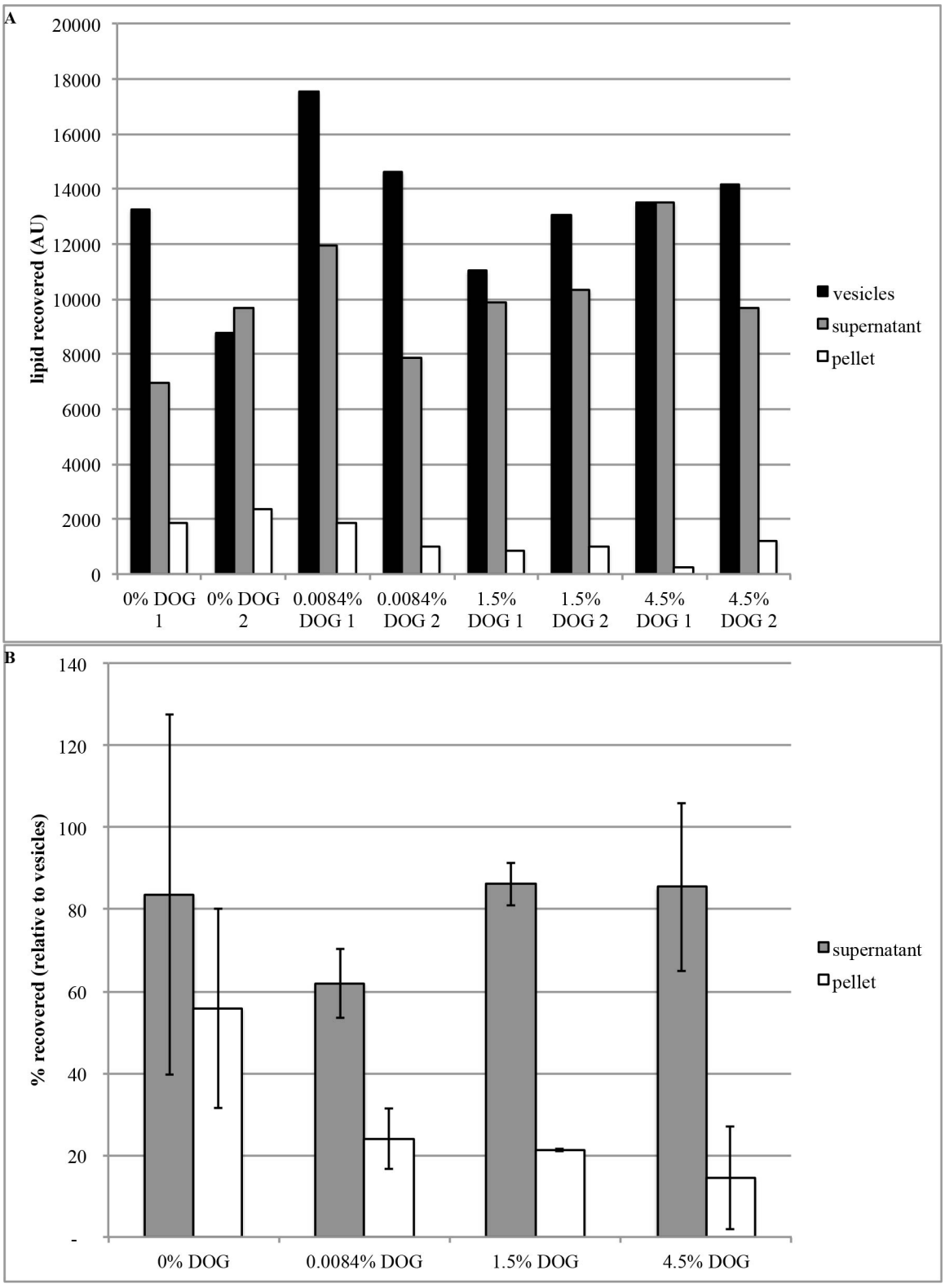

Figure 207. More than half the lipid is in the supernatant following SLV pulldown. I pulled down purified GST-hPKCδ by incubating in duplicate with SLV buffer (0.25 mM SLVs (20 mol% POPS, the

indicated concentration of DOG, and the rest filled with POPC), 55 mM HEPES, pH 7.5, 109 mM NaCl, 500 pg per μL GST-hPKCδ, 0.1 mg per mL ovalbumin), rocking at room temperature for thirty minutes. I removed aliquots as "vesicles", and stored protected from light while I pelleted the SLVs by centrifuging at 136,000 x *g* for ninety minutes at 25°C. **(A)** Recovery of the lipids as measured by the emission at 528 nm in response to excitation at 485 nm. "1" and "2" indicate two replicates. **(B)** The same data shown in (A), redisplayed as a percent of the vesicle from signals and averaged over each set of two replicates. Mean ± SD.

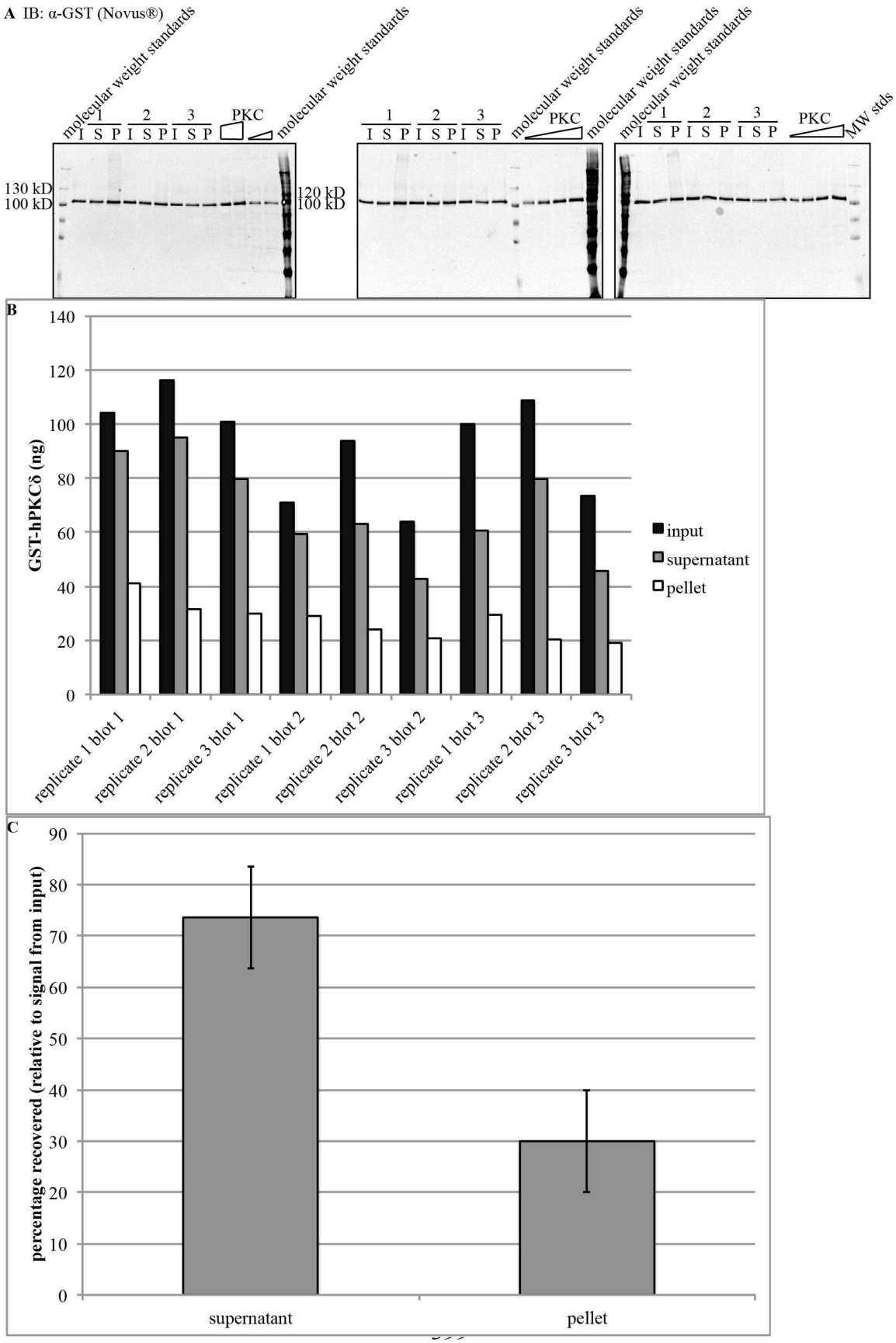
A IB: α-GST (Novus®)
molecular weight standards
1
2
3
I S P I S P I S P
PKC
molecular weight standards
130 kD
100 kD
120 kD
100 kD
MW stds
B
GST-hPKCδ (ng)
140
120
100
80
60
40
20
0
input
supernatant
pellet
replicate 1 blot 1
replicate 2 blot 1
replicate 3 blot 1
replicate 1 blot 2
replicate 2 blot 2
replicate 3 blot 2
replicate 1 blot 3
replicate 2 blot 3
replicate 3 blot 3
C
percentage recovered (relative to signal from input)
90
80
70
60
50
40
30
20
10
0
supernatant
pellet

Figure 208. More GST-hPKCδ sediments in the absence of SLVs than SLVs sediment. I measured the sedimentation of GST-hPKCδ in the absence of SLVs (α in **Equation 5**) by incubating purified GST-hPKCδ in duplicate with sedimentation buffer (55 mM HEPES, pH 7.5, 109 mM NaCl, 500 pg per μL GST-hPKCδ, 0.1 mg per mL ovalbumin), rocking at room temperature for thirty minutes. I removed aliquots as "input", then sedimented the protein by centrifuging at 136,000 x *g* for ninety minutes at 25°C. **(A)** SDS-PAGE of 8% acrylamide gels followed by immunoblotting against GST (Novus® (1:1000 (v/v))). "1", "2", and "3" indicate three replicates, blotted three times to account for uncertainty due to the transfer. MW stds, molecular weight standards. **(B)** Quantification of the signal in (A). I first measured the LI-COR® signal from GST-hPKCδ with ovalbumin standards of known concentration, and calculated a linear fit to the signal as a function of concentration (Microsoft® Excel®). R^2 values for these linear fits were greater than 0.91. I then used the linear fit to calculate how much GST-hPKCδ was present in each loaded sample based on its LI-COR® signal. I then used the volume loaded to calculate the concentration, and used the total volume of the sample to calculate the total amount of GST-hPKCδ. **(C)** The same data as in (B), but redisplayed as a proportion of input, and averaged over the three transfers of each of the three replicates. Mean ± SD.

A closer inspection of the reference that showed that PKCδ had equal affinities for all the functionalized DAG analogues[144] revealed that the way the authors did the experiment was by varying the total concentration of lipid without changing the lipid composition. Because all the liposomes tested included 20% POPS, it could very well be that they were measuring PKCδ's affinity for POPS, and not for the DAG analogues. Because I therefore did not, in fact, have evidence that PKCδ had an affinity for these particular probes, I had no reason to continue to pursue GST-hPKCδ as a positive control for probe- and UV-dependent SLV pulldown of DGK-theta.

Positive control: His_6-hPKCε

Still looking for a positive control to show probe- and UV-dependent SLV pulldown, I searched the literature for other proteins that had demonstrated a DAG-dependent (and not just, as with the PKCδ reference, total-lipid dependent) increase in SLV pulldown, and found that PKCε was such a protein[160].

I therefore ordered commercial purified human PKCε with a hexahistidine fused to the N-terminus (ProSpec PKA-322) and, as I did previously with GST-hPKCδ, worked out conditions for recognizing the purified protein by immunoblot. I found that if I

loaded enough His_6-hPKCε, including 0.005% DDM improved antibody recognition (Figure 209). Unlike GST-hPKCδ, adding ovalbumin to His_6-hPKCε did not so much improve antibody recognition as change the shape of the curve: it appeared to enhance antibody recognition at lower concentrations of His_6-hPKCε, but impede recognition at higher concentrations.

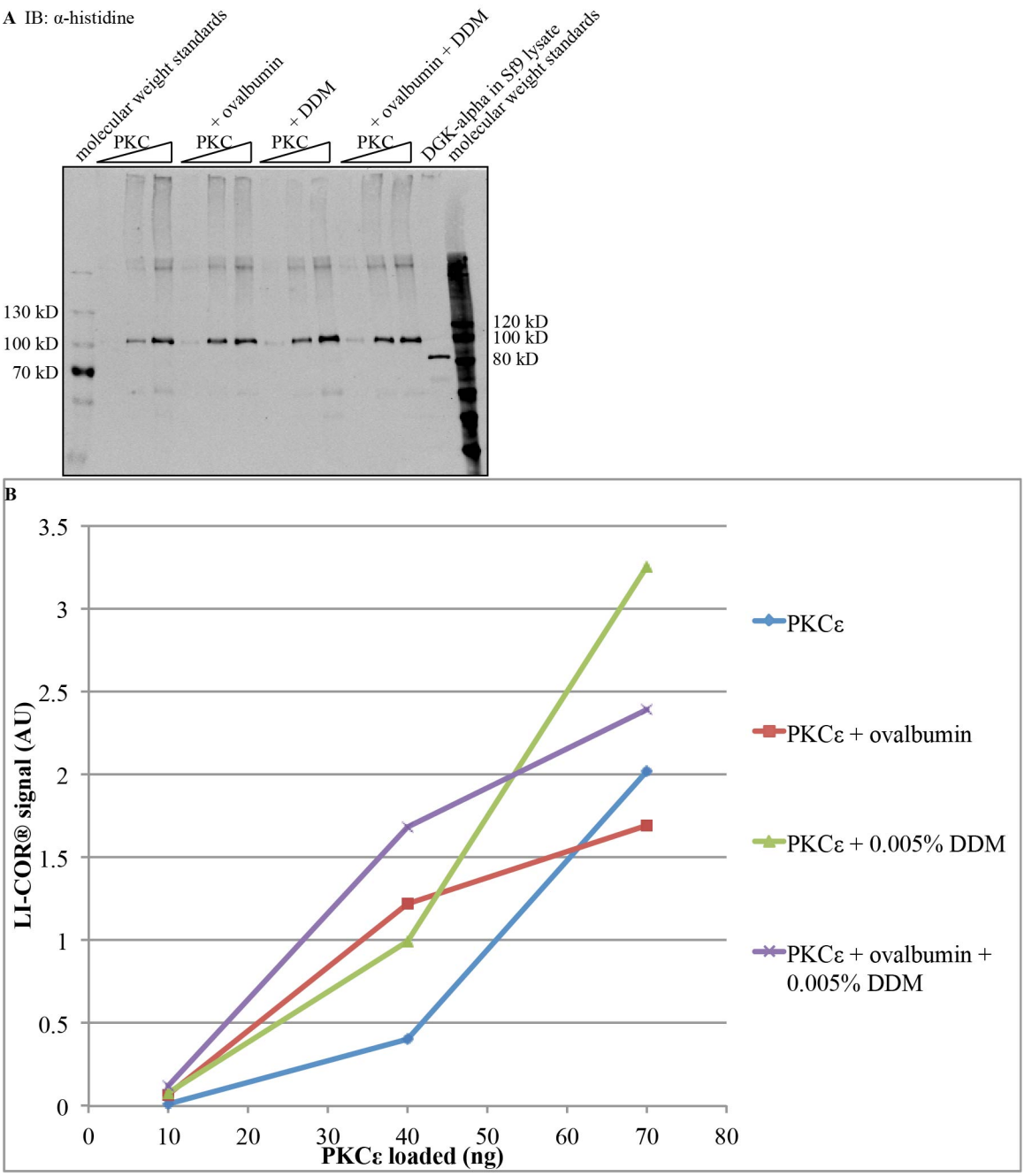

Figure 209. Including 0.005% DDM improves antibody recognition of His_6-hPKCε by the anti-histidine antibody. (A) SDS-PAGE of 8% acrylamide gels followed by immunoblotting against histidine (Santa Cruz Biotechnology, Inc. sc-803 (1:100 (v/v))). Where indicated, ovalbumin was included at 0.1 mg per mL, and DDM was included at 0.005% (v/v). As a positive control for histidine recognition, I also included the lysate of Sf9 cells that had been infected with baculovirus encoding His_6-tagged *R. norvegicus* DGK-alpha. **(B)** Quantification of the signal in (A). The displayed R^2 values were calculated in Microsoft® Excel®.

Once I was confident that I had found conditions under which I could detect His_6-hPKCε fractionation, I tested whether I could confirm DAG-dependent SLV pulldown of His_6-hPKCε. As a positive control for the positive control, I also tested whether PMA increased SLV pulldown of His_6-hPKCε. However, as I had observed with the SLV pulldowns of GST-hPKCδ, lipid recovery in the pellet after SLV pulldown was exceedingly poor (Figure 210). When I tried to measure how much of the His_6-PKCε sedimented in the absence of SLVs, I found that, as I had previously experienced, reproducibility between the two replicates was also exceedingly poor (Figure 211). I was therefore unable to calculate any meaningful numbers for the proportion of His_6-hPKCε bound to lipid from the proportion of His_6-hPKCε that fractionated into either the supernatant or the pellet.

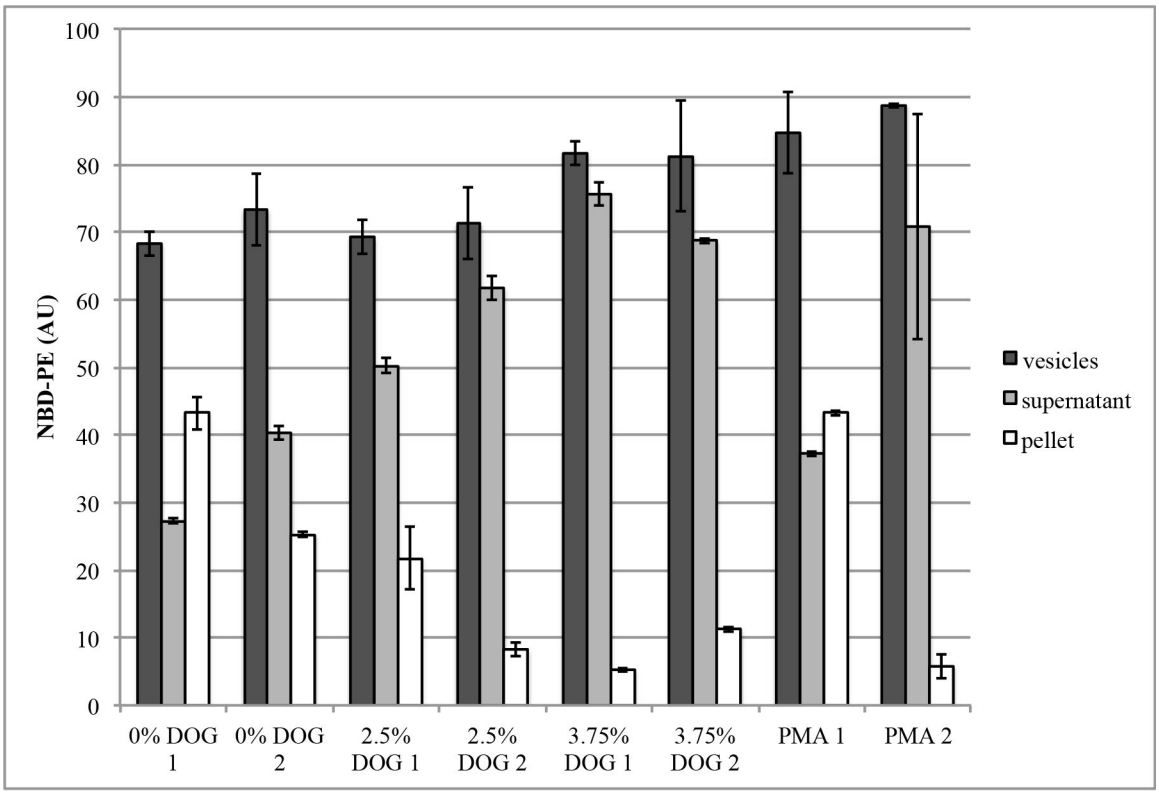

Figure 210. Lipid recovery in the pellet following SLV pulldown was exceedingly poor. I pulled down purified His_6-hPKCε by incubating in duplicate with SLV buffer (0.1 mM SLVs (20 mol% POPS, the indicated concentration of DOG, and the rest filled with POPC; "PMA" lipids included both 1.25% DOG and 200 nM PMA, as well as 0.2% (v/v) DMSO), 20 mM Tris, pH 7.5, 100 mM NaCl, 0.2 mM EGTA, 0.005% (v/v) DDM, 1.3 ng per µL (15 nM) His_6-hPKCε, 1.3% (v/v) glycerol, 0.1 mg per mL ovalbumin), rocking at room temperature for fifteen minutes. I removed aliquots as "vesicles", and stored protected from light while I pelleted the SLVs by centrifuging at 136,000 x *g* for thirty minutes at 25°C. I measured the recovery of the lipids by measuring the emission at 528 nm in response to excitation at 485 nm. "1" and "2" indicate two replicates. Measured in triplicate, mean ± SD.

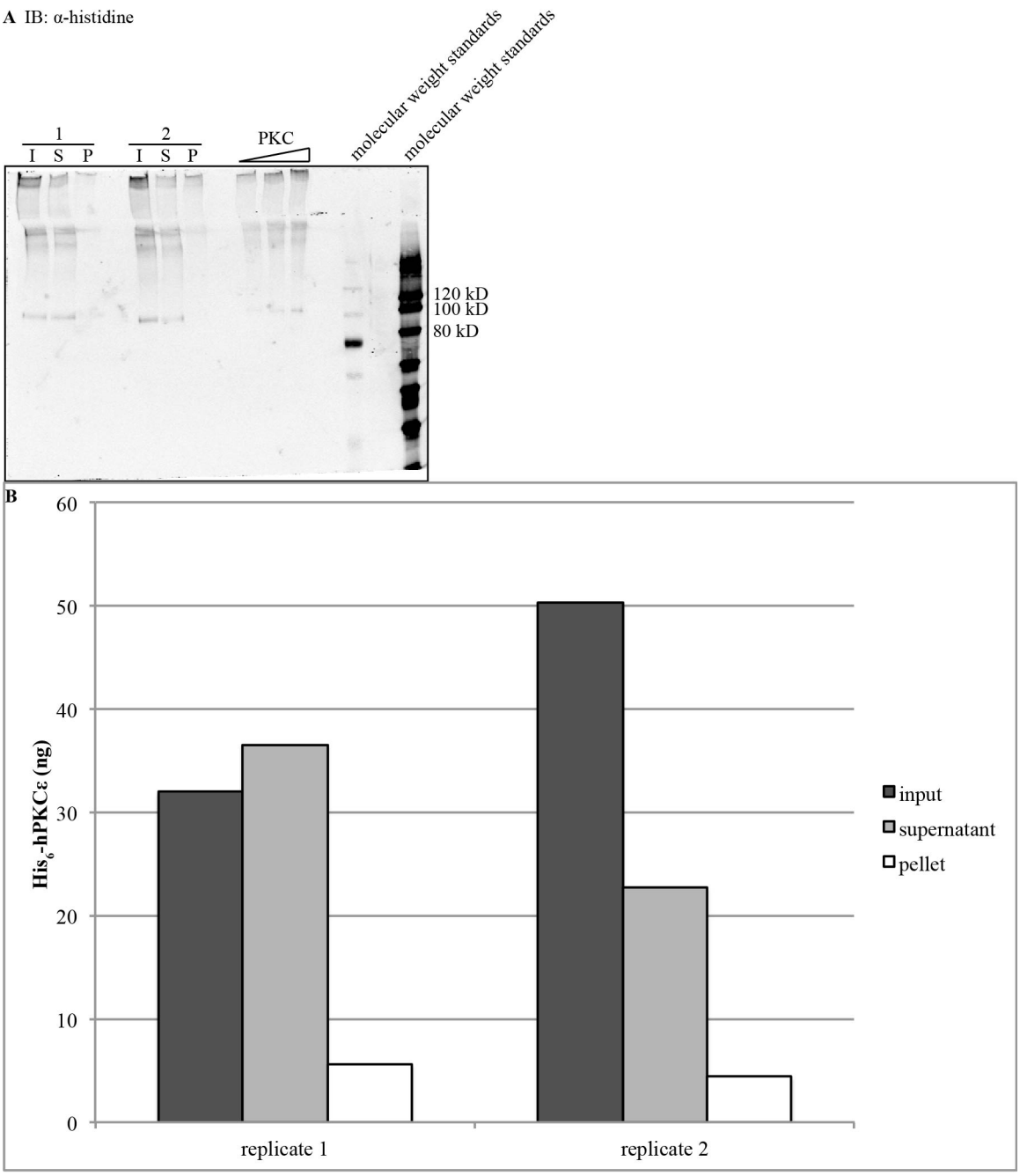

Figure 211. Reproducibility between replicates in sedimentation of His_6-hPKCε in the absence of SLVs was poor. I measured the sedimentation of His_6-hPKCε in the absence of SLVs (α in **Equation 5**) by incubating purified His_6-hPKCε in duplicate with sedimentation buffer (20 mM Tris, pH 7.5, 100 mM NaCl, 0.2 mM EGTA, 0.005% (v/v) DDM, 1.3 ng per μL (15 nM) His_6-hPKCε, 1.3% (v/v) glycerol, 0.1 mg per mL ovalbumin), rocking at room temperature for fifteen minutes. I removed aliquots as "input", then sedimented the protein by centrifuging at 136,000 x *g* for thirty minutes at 25°C. **(A)** SDS-PAGE of an 8% acrylamide gel followed by immunoblotting against histidine (Santa Cruz Biotechnology, Inc. sc-803 (1:200 (v/v))). "1" and "2" indicate two replicates. **(B)** Quantification of the signal in (A). I first measured the LI-COR® signal from His_6-hPKCε standards of known concentration, and calculated a linear fit to the signal as a function of concentration (Microsoft® Excel®). The R^2 value for this linear fit was

greater than 0.99. I then used the linear fit to calculate how much His_6-hPKCε was present in each loaded sample based on its LI-COR® signal. I then used the volume loaded to calculate the concentration, and used the total volume of the sample to calculate the total amount of His_6-hPKCε.

I was curious as to why lipid recovery during the course of producing the SLVs (Figure 212) was considerably better than during the pulldown with His_6-hPKCε (Figure 210). The concentration of liposomes was slightly lower during the pulldown with protein (0.1 mM during pulldown as opposed to 0.16 mM during SLV preparation), and the buffer was different. The most suspicious of the buffer components seemed to me to be the DDM. I therefore tested DDM individually, as well as the entire buffer system, on SLV recovery. I found that the most important factor in lipid recovery was not the concentration or the buffer composition, but the order in which I removed it from the centrifuge (Figure 213): the greatest recoveries were from the replicates removed first, and the lowest recoveries were from the replicates removed last. It seems unlikely this result is purely a function of time, since the tubes had been sitting in the centrifuge for thirty minutes while centrifuging, and a few minutes after the centrifuge stopped, whereas the time to remove them from the centrifuge could not have taken more than a minute. It seems more likely a function of angle: I did not rotate the centrifuge as I removed the tube, and some tubes were undoubtedly jostled more than others depending on the angle at which I removed them from their different positions in the stationary rotor.

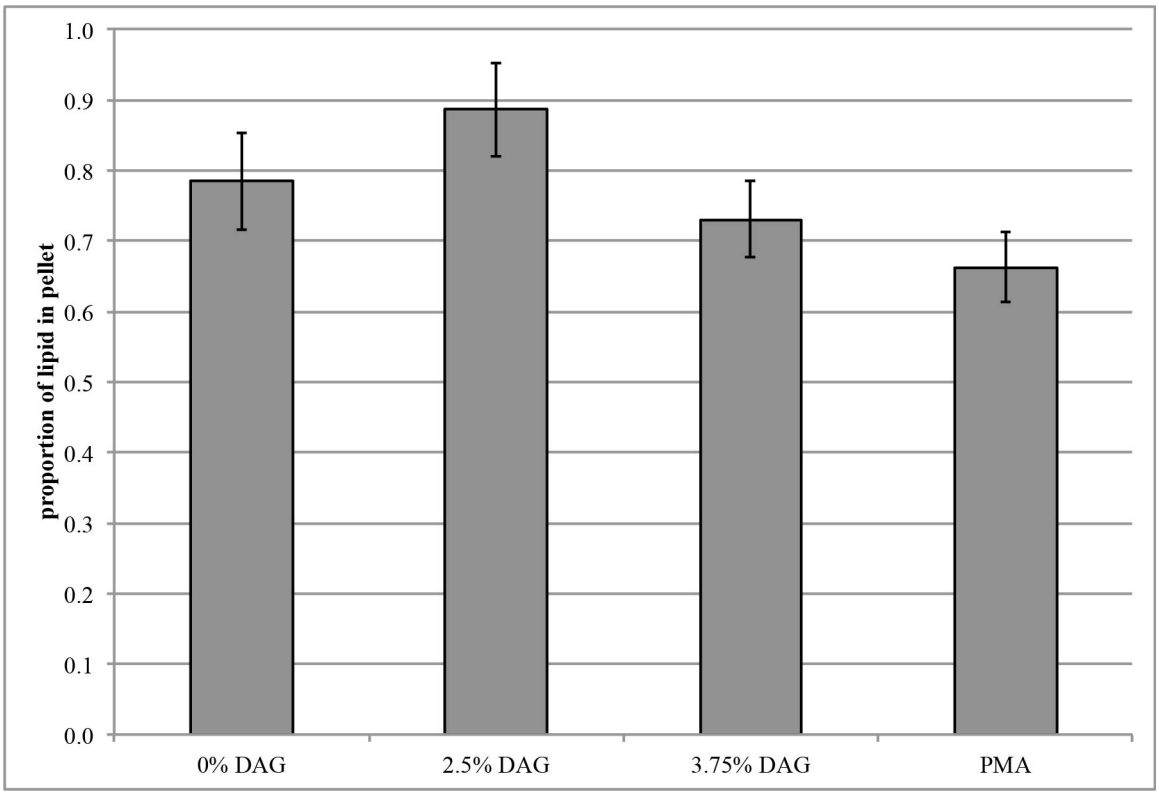

Figure 212. Recovery of SLVs during SLV preparation was considerably better than during pulldown. Recovery of the SLVs (used in **Figure 210**) during their preparation, as measured by the emission at 528 nm in response to excitation at 485 nm. Measured in triplicate, mean ± SD.

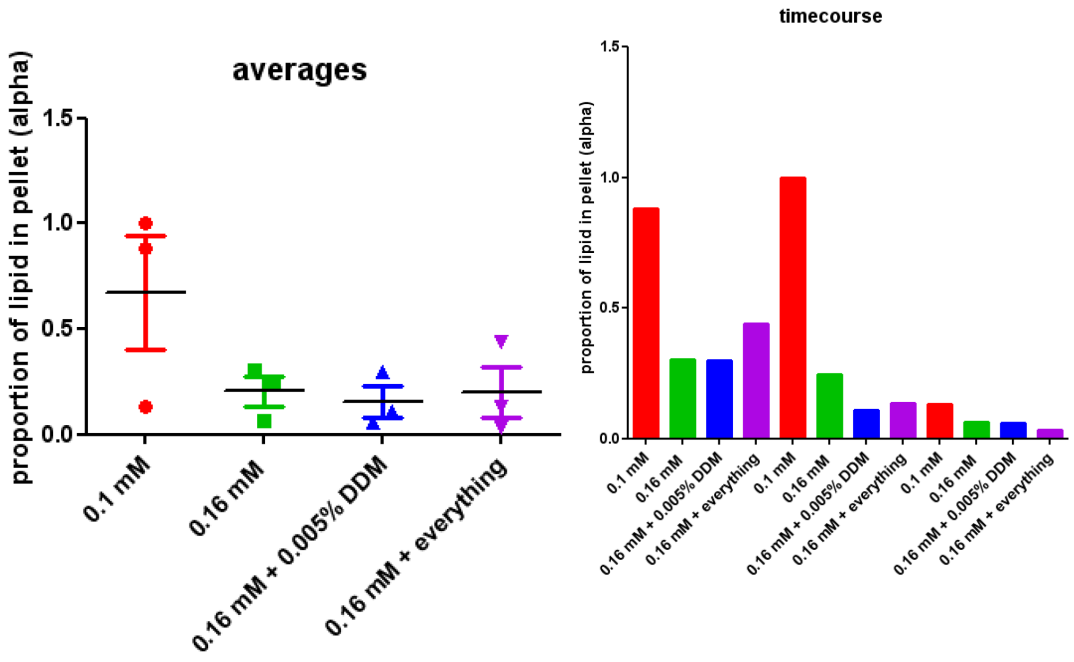

Figure 213. Lipid recovery following SLV pulldown depends strongly on the order in which the tubes are removed from the rotor. I incubated SLVs under different conditions, in triplicate, to test which variables were important in SLV recovery. "0.16 mM" signifies the reproduction of the original SLV recovery (0.16 mM SLVs (77.5:20:2.5::POPC:POPS:DOG), 20 mM Tris, pH 7.5, 80 mM NaCl, 40 mM sucrose). "0.1 mM" dropped the SLV concentration to 0.1 mM. "0.16 mM + 0.005% DDM" added DDM to 0.005% (v/v). "0.16 mM + everything" also included 1.3% (v/v) glycerol, 0.1 mg per mL ovalbumin, 100 mM NaCl, 0.2 mM EGTA, and 0.005% (v/v) DDM. I incubated for 15 minutes, rocking at room temperature. I pelleted the lipids by centrifuging at 136,000 x *g* for thirty minutes at 25°C. I measured the recovery of the lipids by measuring the emission at 528 nm in response to excitation at 485 nm. Left, results organized by condition. The markers indicate the three data points, the black horizontal line indicates the mean, and the colored spread indicates the SD. Right, results organized by the order in which I removed them from the rotor, from left to right.

Conclusions

As mentioned previously, when the lipid fractionates into the pellet in a lower proportion than the protein that fractionates into the pellet in the absence of lipid, it is impossible to use the protein SLV pulldown data in order to measure how much protein is bound to lipid (Equation 5)[159]. I showed that the proportion of lipid that fractionates into the pellet is extremely sensitive to even minor changes in sample preparation, as simple as the order in which the tubes are removed from the centrifuge, and as such I was

unable to reproducibly fractionate the lipid in the pulldowns into the pellet to a greater degree than the protein in the absence of lipid. As such, I decided that SLV pulldown was not a robust method for measuring protein-lipid interactions. I would therefore need to find another way to measure photoaffinity labeling of DGK.

Triton X-114 partitioning

Introduction

The cloud point of Triton X-114 (TX-114) is around room temperature[161], which means that at cold temperatures (on ice, for example), it forms a single, micellar phase, but at warm temperatures (at 37°C, for example), it forms two distinct phases: a bottom, detergent-rich phase and a top, detergent-poor phase[69]. TX-114 partitioning is therefore a method that has been used to enrich for membrane-anchored proteins[162]: the presence of the membrane anchor causes the protein to preferentially partition into the detergent-rich phase and out of the detergent-poor phase. Because the photoaffinity label is a lipid, one might predict that DGK covalently attached to the photoaffinity label to more preferentially partition into the detergent-rich phase as compared to DGK that had not been photoaffinity labeled.

Results

As with the SLV pulldown, for the TX-114 partitioning I decided to start with looking at how purified DGK-theta partitioned into TX-114 before crosslinking, to be sure that I would be able to detect a probe- and UV-dependent increase. Following a previously published protocol[163] I decided to use 1% (v/v) TX-114 to phase-partition purified DGK-theta, but, in the reaction conditions tested, 1% (v/v) TX-114 was

insufficient to form two phases at 37°C. I added TX-114 to 15% (v/v), which was enough to produce two distinct phases, but in that case the bottom phase was much larger than the top phase. Diluting the mixture to 12% (v/v) TX-114 was sufficient to produce two phases approximately equal in size. I collected samples both before the phase separation as well as from each of the two separated phases.

Because TX-114 has been reported to interfere with SDS-PAGE[162], I first ethanol-precipitated the samples to remove the TX-114 from the protein. We had recently switched brands of Eppendorfs, and the brand of tube I used was not quite clear, making it difficult to visually assess the success of ethanol precipitation; however, the presence of ovalbumin and histone H1 as carrier proteins should have increased the efficiency of protein precipitation (as in Figure 13); on the other hand, the carrier proteins may have partitioned differently from DGK-theta (i.e., if all of the ovalbumin and histone H1 partitioned into the detergent-poor phase, they would be unable to assist in the precipitation of DGK-theta that was in the detergent-rich phase). When I immunoblotted the samples against DGK-theta, reproducibility among replicates was poor (Figure 214**A-B**). Part of the irreproducibility may have resulted from protein loss during the ethanol precipitation: the "before" samples (removed before partitioning) gave a much weaker signal than would be expected given the theoretical amount in the sample (Figure 214**C**), which is consistent with protein loss during ethanol precipitation. A loss of protein in the "before" samples was, however, surprising, given the large concentration of ovalbumin and histone H1 in the samples, which should have assisted in precipitation. Other possible explanations for the poor recovery of DGK-theta in the "before" samples could be that residual TX-114 remaining after the ethanol precipitation, however low in

concentration, interfered with antibody recognition, or that the presence of TX-114 interfered with efficiency of protein precipitation.

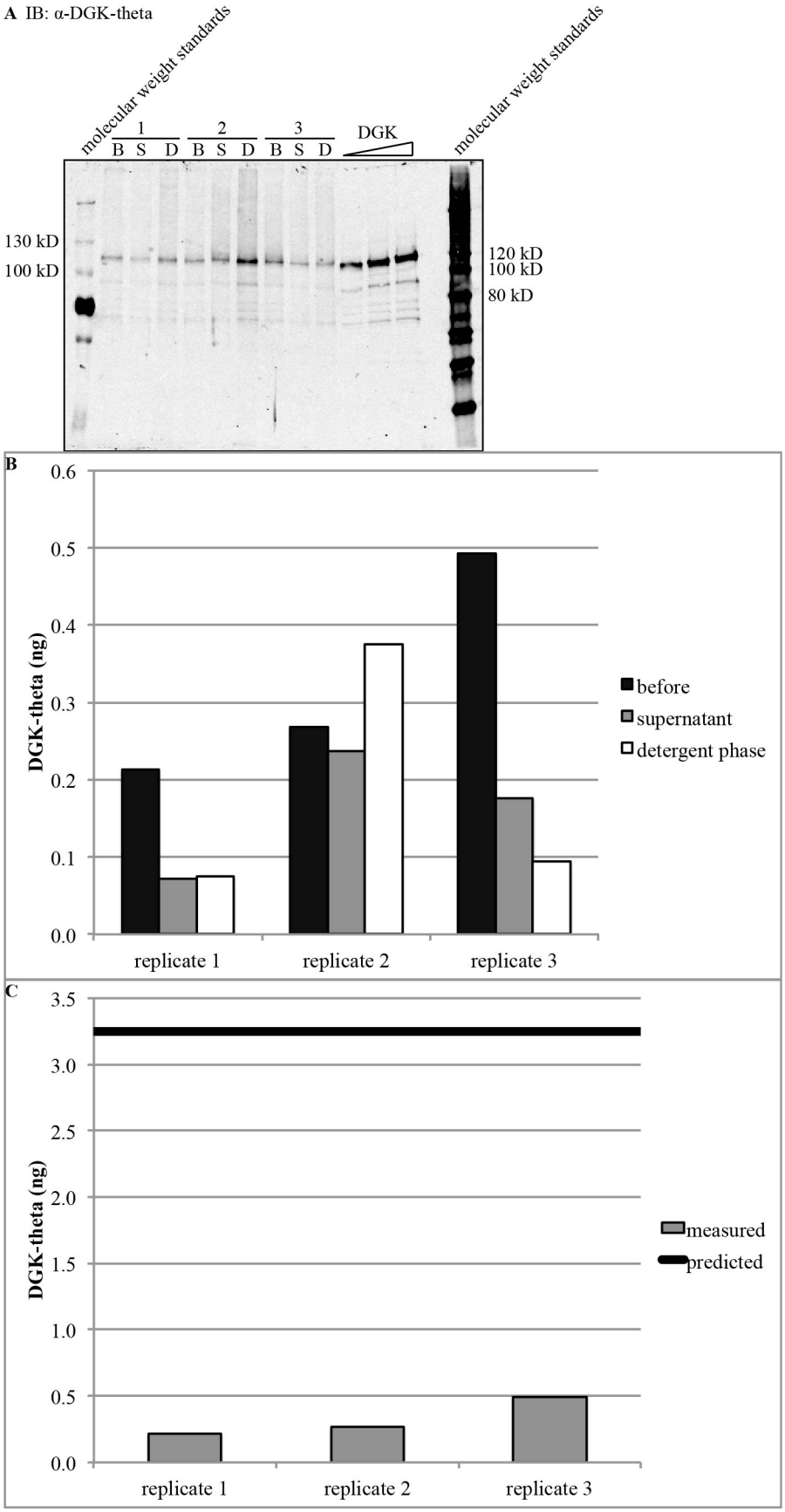
A IB: α-DGK-theta
molecular weight standards
1
2
3
DGK
B S D B S D B S D
molecular weight standards
130 kD
100 kD
120 kD
100 kD
80 kD
B
DGK-theta (ng)
0.6
0.5
0.4
0.3
0.2
0.1
0.0
replicate 1
replicate 2
replicate 3
before
supernatant
detergent phase
C
DGK-theta (ng)
3.5
3.0
2.5
2.0
1.5
1.0
0.5
0.0
replicate 1
replicate 2
replicate 3
measured
predicted

Figure 214. TX-114 partitioning of purified DGK-theta varies among replicates, and recovery following ethanol precipitation is poor. I first preincubated purified DGK-theta in preincubation buffer (50 mM HEPES, pH 7.5, 0.005% (v/v) DDM, 0.22 μM histone H1, 1 mM DTT, 79 pg per μL purified DGK-theta, 1.6% (v/v) glycerol) on ice for ten minutes. I then diluted into incubation buffer (50 mM HEPES, pH 7.5, 100 mM NaCl, 0.005% (v/v) DDM, 1 mM ATP, 1.5 mM $MgCl_2$, 1 mM DTT, 7.5 mM liposomes (53.3:26.7:20::POPE:POPC:POPS), 1 μM histone H1, 0.1 mg per mL ovalbumin, 0.7% (v/v) glycerol, 36 pg per μL DGK-theta), and incubated for thirty minutes, rocking at room temperature. I added TX-114 to 1% (v/v) (which decreased the other buffer components to 46 mM HEPES, pH 7.5, 92 mM NaCl, 0.005% (v/v) DDM, 0.9 mM ATP, 1.4 mM $MgCl_2$, 0.9 mM DTT, 6.9 mM liposomes, 0.09 μM histone H1, 0.09 mg per mL ovalbumin, 0.7% glycerol, and 33 pg per μL DGK-theta), separated into three replicates, vortexed, and incubated on ice for 10 minutes, followed by 37°C for five minutes. When no separate phases were apparent, I incubated at 50°C for twenty minutes. When still no separate phases were apparent, I added TX-114 to 15% (v/v) (which decreased the other buffer components to 39 mM HEPES, pH 7.5, 79 mM NaCl, 0.004% (v/v) DDM, 0.8 mM ATP, 1.2 mM $MgCl_2$, 0.8 mM DTT, 5.9 mM liposomes, 0.08 μM histone H1, 0.08 mg per mL ovalbumin, 0.6% glycerol, and 29 pg per μL DGK-theta) and incubated at 50°C for five minutes before microfuging to form two distinct phases. In order to make the bottom and top phases more equal in size, I added buffer to dilute the TX-114 to 12% (which adjusted the other buffer components to 42 mM HEPES, pH 7.5, 83 mM NaCl, 0.003% (v/v) DDM, 0.6 mM ATP, 0.9 mM $MgCl_2$, 0.6 mM DTT, 4.7 mM liposomes, 0.06 μM histone H1, 0.06 mg per mL ovalbumin, 0.5% glycerol, and 22 pg per μL DGK-theta), incubated on ice for five minutes, mixed, and incubated on ice for another five minutes. I removed aliquots as "before", then incubated at 50°C for five minutes before microfuging to form two phases of approximately equal size. I separated the phases before ethanol-precipitating the protein and resuspending in SDS-PAGE gel-loading buffer. **(A)** SDS-PAGE of an 8% acrylamide gel followed by immunoblotting against DGK-theta (1:350 (v/v)). B, before; S, supernatant; D, detergent phase. "1", "2", and "3" signify three different replicates. **(B)** Quantification of the signal in (A). I first measured the LI-COR® signal from DGK-theta standards of known concentration, and calculated a linear fit to the signal as a function of concentration (Microsoft® Excel®). The R^2 value for this linear fit was greater than 0.98. I then used the linear fit to calculate how much DGK-theta was present in each loaded sample based on its LI-COR® signal. I then used the volume loaded to calculate the concentration, and used the total volume of the sample to calculate the total amount of DGK-theta. **(C)** The same data of the "before" fractions shown in (B), compared to the amount of DGK-theta theoretically loaded.

I had only collected enough "before" sample for the one immunoblot, but I still had aliquots of samples taken from the separated phases left over. I therefore subjected those samples to SDS-PAGE followed by Coomassie staining in order to confirm that appropriate amounts of ovalbumin were recovered in the top phases (consistent with its partitioning to the detergent-poor phase in sufficiently high concentration to be efficiently recovered from ethanol-precipitation). On the same gel, I also compared ovalbumin standards that either had or had not been ethanol-precipitated, to estimate how much of the protein was lost during precipitation. Comparison of the precipitated and non-precipitated standards shows that a small but definitely detectable amount of ovalbumin was lost at the concentrations tested, although, if anything, less protein was lost at lower

concentrations than at higher concentrations (Figure 215**A**-**B**), suggesting that sufficient carrier protein was present at these concentrations to prevent much protein loss. Quantifying the amount of ovalbumin recovered in the pellet was complicated by the fact that the signal for all of the pellets was weaker than the lowest concentration of standard loaded, requiring extrapolation rather than interpolation, and as a consequence gave negative numbers for calculating the amount of ovalbumin in the detergent phase (Figure 215**C**), which was clearly incorrect. However, the recovery of ovalbumin in the top, detergent-poor phase was robust: in fact, I calculated more ovalbumin to be in the top phase than was theoretically loaded into the entire sample, which was also clearly incorrect.

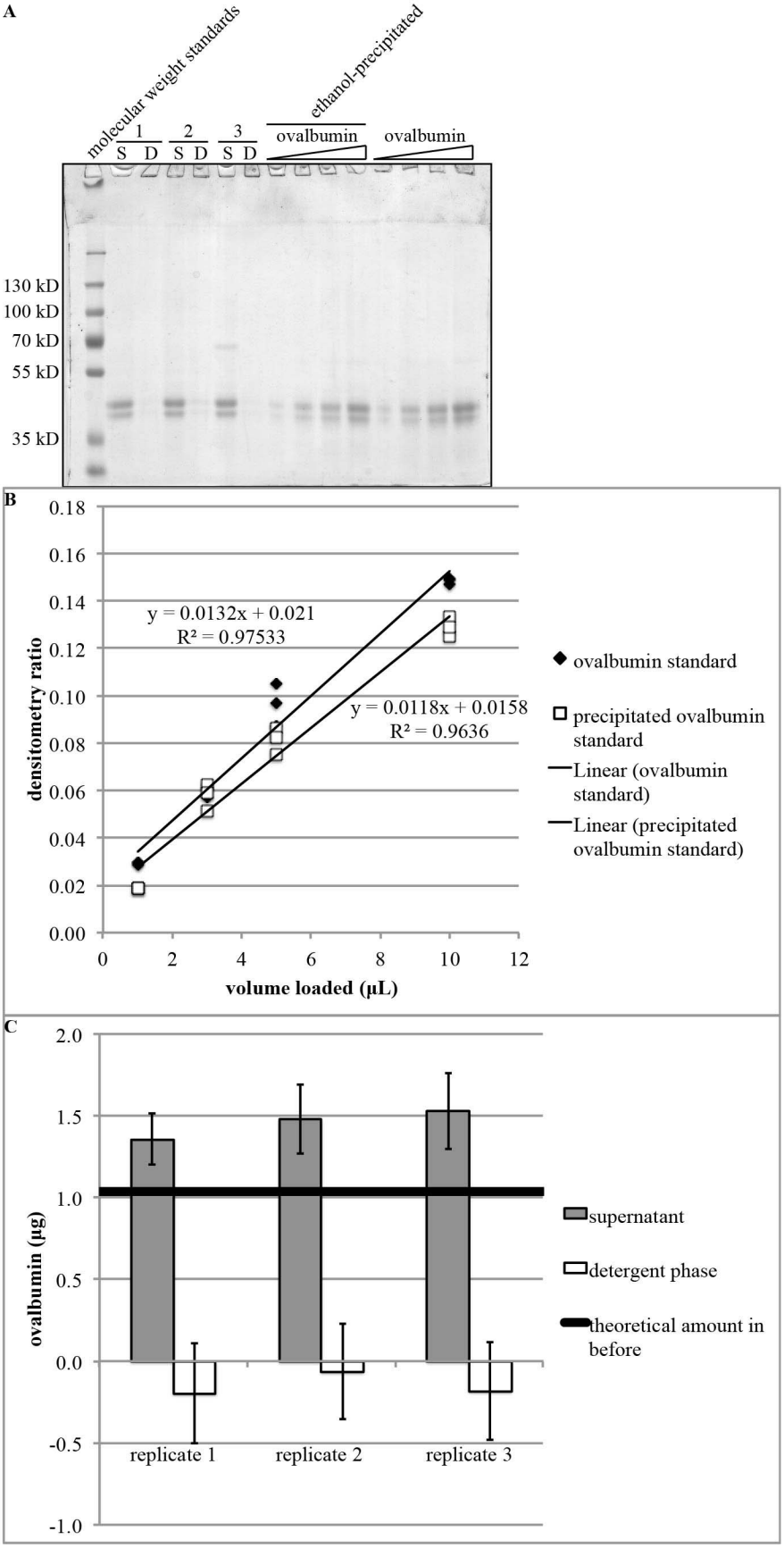
A
molecular weight standards
1
2
3
S D S D S D
ethanol-precipitated
ovalbumin
ovalbumin
130 kD
100 kD
70 kD
55 kD
35 kD
B
0.18
0.16
0.14
0.12
0.10
0.08
0.06
0.04
0.02
0.00
densitometry ratio
y = 0.0132x + 0.021
R² = 0.97533
y = 0.0118x + 0.0158
R² = 0.9636
0
2
4
6
8
10
12
volume loaded (µL)
ovalbumin standard
precipitated ovalbumin standard
Linear (ovalbumin standard)
Linear (precipitated ovalbumin standard)
C
2.0
1.5
1.0
0.5
0.0
-0.5
-1.0
ovalbumin (µg)
replicate 1
replicate 2
replicate 3
supernatant
detergent phase
theoretical amount in before

Figure 215. While a small amount of ovalbumin is lost to ethanol-precipitation, most remains in the supernatant following TX-114 partitioning. The same samples immunoblotted in **Figure 214A**, as well as ovalbumin standards that either had or had not been ethanol-precipitated. **(A)** SDS-PAGE of an 8% acrylamide gel followed by Coomassie staining. **(B)** Quantification of the signal in (A). I scanned the gel, sandwiched in a clear binder sheet, as a 1200 dots per inch (dpi) .tiff file. I measured the densitometry of the files by ImageJ[68] (v1.46r) without calibration, three times from the file. I normalized the relative densitometry of each lane to the total densitometry of all the lanes on that replicate. **(C)** The same data as in (B), redisplayed as a proportion of the theoretical amount loaded, and averaged over the three densitometry measurements. Mean ± SD.

Conclusions

Although quantitatively measuring ovalbumin's partitioning was problematic, I was able to conclude that most if not all of the ovalbumin was partitioning into the top phase, as predicted, and thus sufficient amounts of ovalbumin should have been present to serve as a carrier protein to mitigate ethanol-precipitation losses of DGK-theta in the top, detergent-poor phase. As such, the poor recovery of DGK-theta in the top phase, or at least the poor reproducibility of recovery of DGK-theta in the top phase (Figure 214), suggested that it would be difficult to detect a probe- and UV-dependent decrease of such recovery. I therefore concluded that TX-114 partitioning would not be a very promising approach to detect photoaffinity labeling of DGK-theta.

Probe- and UV-dependent enzymatic inactivation

Introduction

If the photoaffinity labels covalently attached to the active site of DGK, I would expect to see probe- and UV-dependent enzymatic inactivation, because the covalently attached lipid would occlude the active site.

Results

After working out conditions under which I could irradiate DGK-theta with 360 nm light without inactivating it, I found that when I irradiated DGK-theta in the presence

of liposomes containing compound **1**, I was unable to detect probe- and UV-dependent inactivation (Figure 216). Under these same reaction conditions (liposome composition and concentration, buffer composition, etc.), DGK-theta could use compound **1** as a substrate (Figure 140), which suggested that compound **1** was able to access the active site including, presumably, the lipid substrate binding site, but was unable to covalently attach to DGK-theta in that orientation.

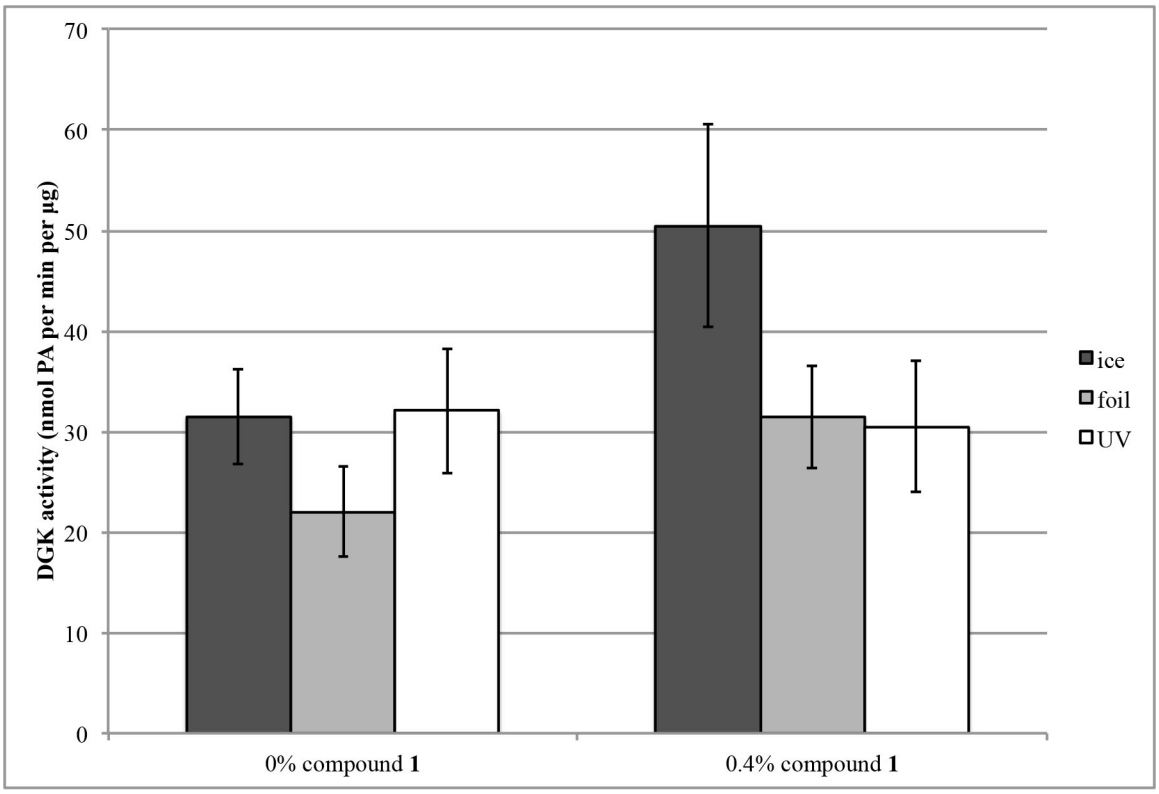

Figure 216. Compound 1 does not inactivate purified DGK-theta in a probe- and UV-dependent way. DGK activity assay. I first preincubated purified DGK-theta in preincubation buffer (43 mM HEPES, pH 7.5, 0.005% (v/v) DDM, 2 µM histone H1, 1 mM DTT, 43 pg per µL purified DGK-theta, 1.7% (v/v) glycerol) on ice for ten minutes. I then diluted into incubation buffer (0.5 mM liposomes (2:1::POPE:POPC, 20 mol% POPS, plus the indicated concentration of compound **1**), 48 mM HEPES, pH 7.5, 95 mM NaCl, 0.005% (v/v) DDM, 0.2 µM histone H1, 1 mM DTT, 0.1 mg per mL ovalbumin, 1 mM ATP, 1.5 mM $MgCl_2$, 4.3 pg per µL purified DGK-theta, 0.2% (v/v) glycerol) and incubated on ice for thirty minutes. The "ice" samples remained on ice. I placed the other samples in a 96-well plate, and placed aluminum foil over the "foil" samples. I irradiated the samples with a 360 nm lamp at room temperature in a chemical fume hood for 30 minutes. I returned the samples to Eppendorfs, and measured the volume to account for concentration of DGK due to evaporation. The final DGK activity assay reaction included 2 mM substrate-containing liposomes (47.7:23.8:20:8.5::POPE:POPC:POPS:DOG), 0.25 mM crosslinking liposomes, 0.25 mM filler liposomes (such that the final liposome composition in the reactions

were all the same), 51 mM HEPES, pH 7.5, 101 mM NaCl, 1 mM DTT, 0.005% (v/v) DDM, 1.5 mM $MgCl_2$, 1 mM ATP, 30.3 Ci per mmol [γ-^{32}P]-ATP, 0.1 μM histone H1, 0.05 mg per mL ovalbumin, 2.1 pg per μL purified DGK-theta, and 0.08% (v/v) glycerol, and proceeded for 15 minutes at 37°C. In triplicate: mean ± SD.

I was similarly unable to observe probe- and UV-dependent inactivation of DGK-theta when irradiated in the presence of compound **3** (Figure 217), likewise under the same reaction conditions that I had previously used to show that DGK-theta was able to use compound **3** as a substrate (Figure 144). I also considered the possibility that compound **3** might be covalently attaching to the DGK-theta at a site distinct from the lipid substrate binding site, such as the C1 domain, and tested whether crosslinking to liposomes anchored the protein to the liposomes (if the protein were anchored, I would predict to see higher activity in anchoring liposomes that included DAG than anchoring liposomes that did not include DAG), but I did not see any such difference (Figure 217). Like compound **1**, compound **3** is apparently able to access the active site of DGK-theta, because DGK-theta is able to use it as a substrate, but does not lead to the probe- and UV-dependent enzymatic inactivation that would be predicted to result from photoaffinity labeling.

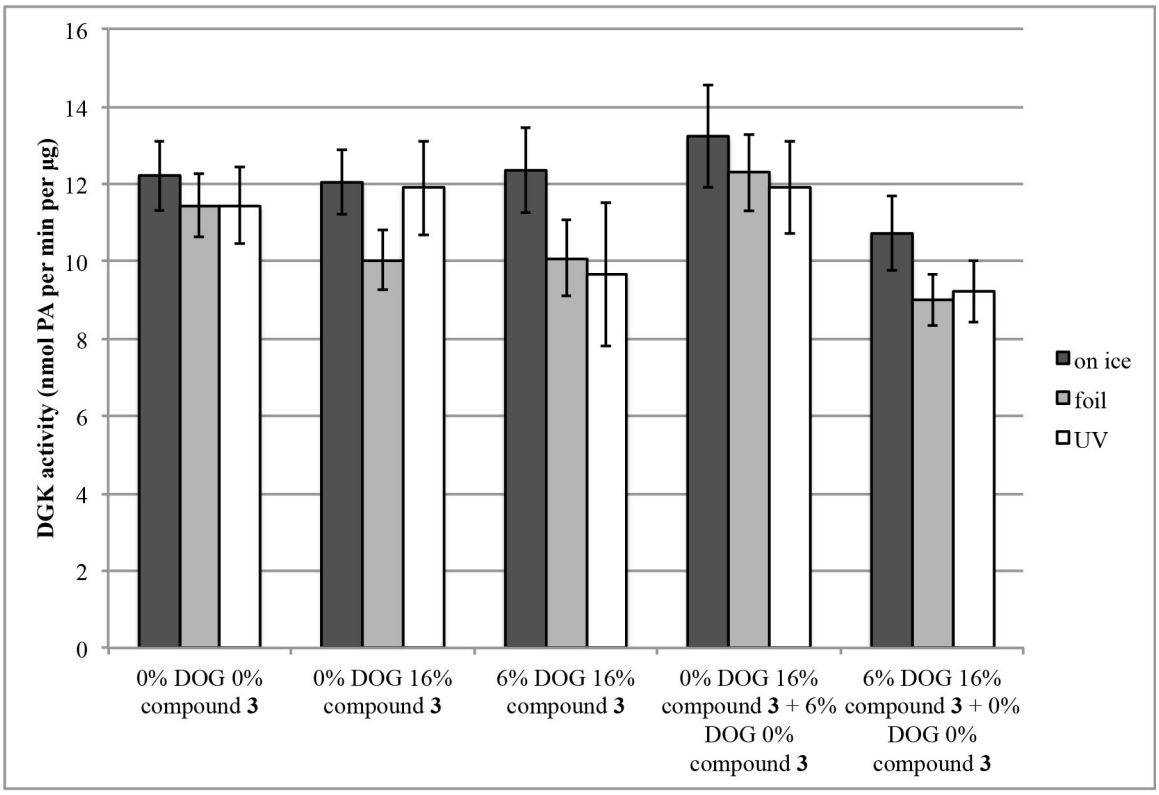

Figure 217. Compound 3 does not inactivate purified DGK-theta in a probe- and UV-dependent way, nor does it appear to anchor it to the crosslinking liposomes. DGK activity assay. I first preincubated purified DGK-theta in preincubation buffer (50 mM HEPES, pH 7.5, 0.005% (v/v) DDM, 0.4 µM histone H1, 1 mM DTT, 80 pg per µL purified DGK-theta, 1.6% (v/v) glycerol) on ice for ten minutes. I then diluted into incubation buffer (0.5 mM liposomes (2:1::POPE:POPC, 20 mol% POPS, plus the indicated concentration of compound **3** and DOG) (for the samples with two sets of liposomes, the concentration of each set of liposomes was 0.5 mM for a total liposome concentration of 1 mM), 50 mM HEPES, pH 7.5, 100 mM NaCl, 0.005% (v/v) DDM, 0.2 µM histone H1, 1 mM DTT, 0.1 mg per mL ovalbumin, 1 mM ATP, 1.5 mM $MgCl_2$, 40 pg per µL purified DGK-theta, 0.8% (v/v) glycerol) and incubated for thirty minutes, rocking at room temperature. The "on ice" samples remained on ice. I placed the other samples in a 96-well plate, and placed aluminum foil over the "foil" samples. I irradiated the samples with a 360 nm lamp at room temperature in a chemical fume hood for 30 minutes. I returned the samples to Eppendorfs, and measured the volume to account for concentration of DGK due to evaporation. The final DGK activity assay reaction included 2 mM substrate-containing liposomes (48:24:20:8::POPE:POPC:POPS:DOG), 0.25 mM crosslinking liposomes, 0.25 mM filler liposomes (such that the final liposome composition in the reactions were all the same), 50 mM HEPES, pH 7.5, 100 mM NaCl, 1 mM DTT, 0.005% (v/v) DDM, 1.5 mM $MgCl_2$, 1 mM ATP, 42.5 Ci per mmol [γ-^{32}P]-ATP, 0.1 µM histone H1, 0.05 mg per mL ovalbumin, 20 pg per µL purified DGK-theta, and 0.4% (v/v) glycerol, and proceeded for 15 minutes at 37°C. In triplicate: mean ± SD.

The distance of the linker between the photoreactive moiety and the affinity-conferring moiety has been reported to influence the efficiency of photoaffinity labeling[164]: if the linker is too long, the molecule might bind to its target in the appropriate site, but the photoreactive part of the molecule might be too far away from

the protein to covalently attach to it. Because compounds **1** and **3** appeared to be accessing the active site (otherwise, they couldn't be substrates), but did not appear to be photoaffinity labeling DGK-theta (since they weren't producing probe- and UV-dependent inactivation under those conditions), the Best group designed and sent us compound **4** (Figure 146), with a shorter linker between the DAG-like moiety and the benzophenone. With compound **4**, I did indeed observe probe- and UV-dependent enzymatic inactivation of purified DGK-theta (Figure 218**A**), as would be predicted by covalent attachment to the active site. This probe- and UV-dependent inactivation was reproducible, although the magnitude of the effect varied among experiments (Figure 218**B**).

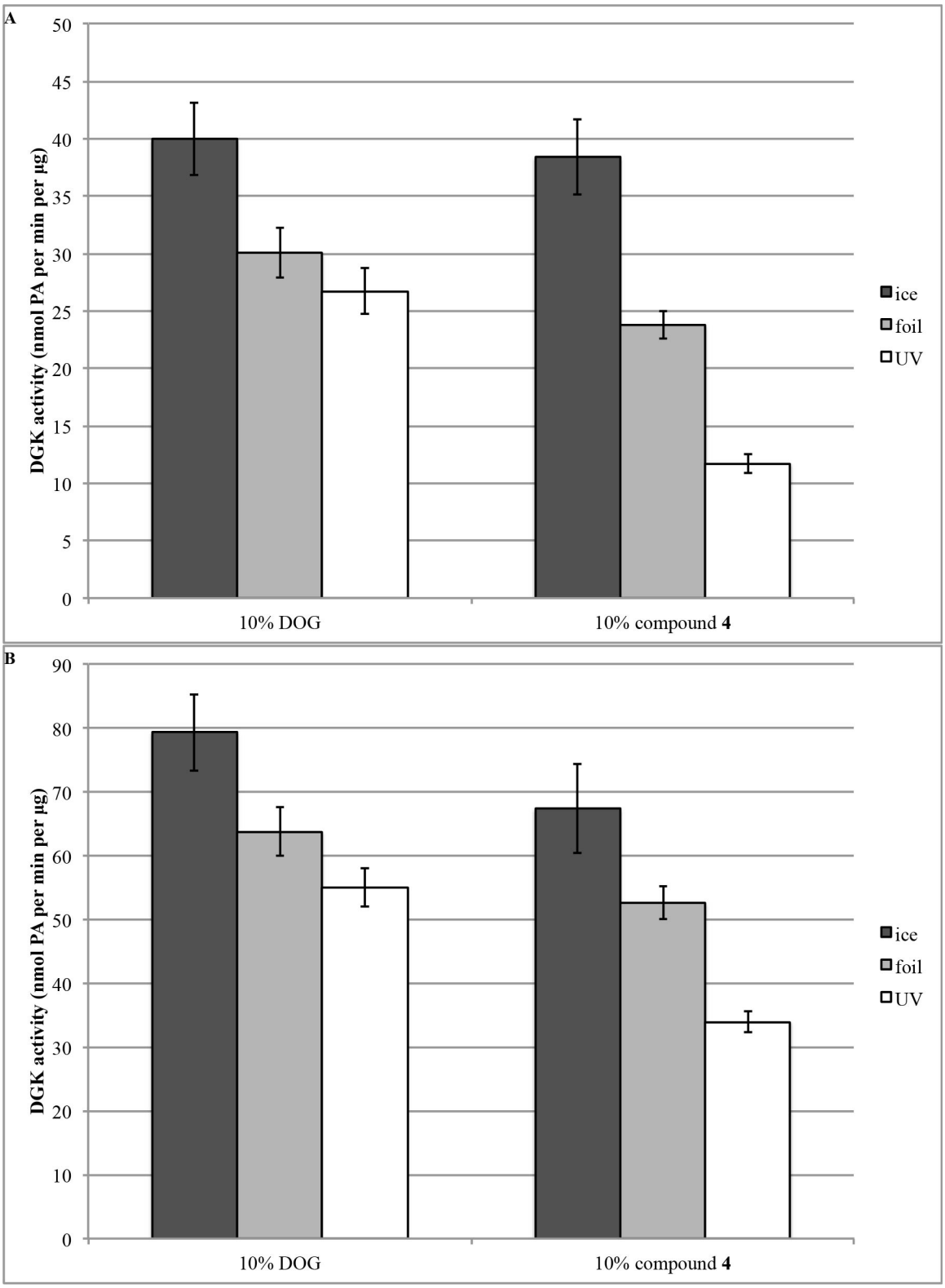

Figure 218. Compound 4 reproducibly enzymatically inactivates purified DGK-theta in a probe- and UV-dependent way. DGK activity assays. **(A)** I first preincubated purified DGK-theta in preincubation

buffer 1 (50 mM HEPES, pH 7.5, 0.005% (v/v) DDM, 1.25 μM histone H1, 1 mM DTT, 37 pg per μL purified DGK-theta, 1.0% (v/v) glycerol) on ice for ten minutes. I then diluted into incubation buffer (7.5 mM liposomes (46.7:23.3:20:10::POPE:POPC:POPS:DOG or compound **4**), 50 mM HEPES, pH 7.5, 100 mM NaCl, 0.005% (v/v) DDM, 0.5 μM histone H1, 1 mM DTT, 0.1 mg per mL ovalbumin, 1 mM ATP, 1.5 mM $MgCl_2$, 15 pg per μL purified DGK-theta, 0.4% (v/v) glycerol) and incubated for thirty minutes, rocking at room temperature. The "on ice" samples remained on ice. I placed the other samples in a 96-well plate, and placed aluminum foil over the "foil" samples. I irradiated the samples with a 360 nm lamp on an ice bucket in a chemical fume hood for thirty minutes. I returned the samples to Eppendorfs, and measured the volume to account for concentration of DGK due to evaporation. The final DGK activity assay reaction included 7.5 mM substrate-containing liposomes (46.7:23.3:20:10::POPE:POPC:POPS:DOG), 1.5 mM crosslinking liposomes, 1.5 mM filler liposomes (such that the final liposome composition in the reactions were all the same), 50 mM HEPES, pH 7.5, 100 mM NaCl, 1 mM DTT, 0.005% (v/v) DDM, 1.5 mM $MgCl_2$, 1 mM ATP, 30.7 Ci per mmol [γ-^{32}P]-ATP, 0.1 μM histone H1, 0.02 mg per mL ovalbumin, 3.0 pg per μL purified DGK-theta, and 0.08% (v/v) glycerol, and proceeded for thirty minutes at 37°C. In triplicate: mean ± SD. **(B)** The experiment was the same as in (A) with the exception that preincubation buffer 2 (50 mM HEPES, pH 7.5, 0.005% (v/v) DDM, 1.67 μM histone H1, 1 mM DTT, 50 pg per μL purified DGK-theta, 1.3% (v/v) glycerol) was used instead of preincubation buffer 1, and in the DGK assay reaction, [γ-^{32}P]-ATP was 89.2 Ci per mmol. In triplicate: mean ± SD.

For the largest experiments, I noticed that instead of a UV-dependent inactivation of DGK-theta, as I had observed in the smaller experiments (Figure 218), compound **4** appeared to inactivate DGK-theta even without irradiation (Figure 219). I therefore wondered whether ambient light was causing compound **4** to crosslink to DGK while the tubes were sitting during the course of preparing the experiment, because this preparation time took longer for larger experiments than for smaller ones. Benzophenones are reported to be more stable in ambient light than other photoreactive molecules such as diazirines, aryl azides, or diazo esters[165], but they are still photoreactive molecules. Although I had thought glass was opaque to ultraviolet (which is why one cannot get sunburned indoors, even when sitting in a sunbeam), most glass actually transmits the longer UV-A (320 nm – 400 nm) radiation[166], which includes the 360 nm wavelength used to activate benzophenones.

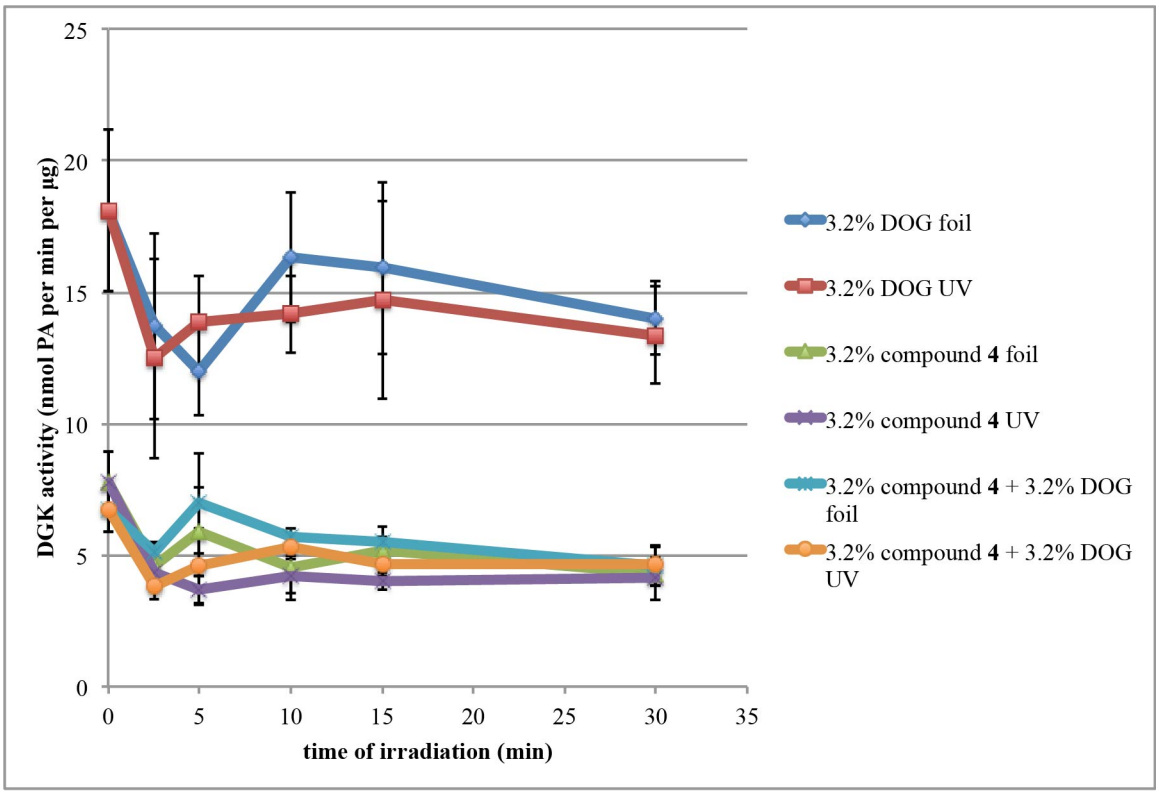

Figure 219. In large experiments, compound 4 inactivates purified DGK-theta even without UV irradiation. DGK activity assay. I first preincubated purified DGK-theta in preincubation buffer (50 mM HEPES, pH 7.5, 0.005% (v/v) DDM, 2.5 µM histone H1, 1 mM DTT, 75 pg per µL purified DGK-theta, 1.9% (v/v) glycerol) on ice for ten minutes. I then diluted into incubation buffer (7.5 mM liposomes (2:1::POPE:POPC, 20 mol% POPS, and the indicated concentrations of DOG and compound **4**), 50 mM HEPES, pH 7.5, 100 mM NaCl, 0.005% (v/v) DDM, 0.5 µM histone H1, 1 mM DTT, 0.1 mg per mL ovalbumin, 1 mM ATP, 1.5 mM $MgCl_2$, 15 pg per µL purified DGK-theta, 0.4% (v/v) glycerol) and incubated for thirty minutes, rocking at room temperature, protected from light. The "on ice" samples remained on ice. I placed the other samples in a 96-well plate, and placed aluminum foil over the "foil" samples. I irradiated the samples with a 360 nm lamp on an ice bucket in a chemical fume hood, removing timepoints to ice at the indicated times. I returned the samples to Eppendorfs, and measured the volume to account for concentration of DGK due to evaporation. The final DGK activity assay reaction included 5 mM substrate-containing liposomes (56.7:28.3:9:6::POPE:POPC:POPS:DOG), 1.5 mM crosslinking liposomes, 1.5 mM filler liposomes (such that the final liposome composition in the reactions were all the same), 50 mM HEPES, pH 7.5, 100 mM NaCl, 1 mM DTT, 0.005% (v/v) DDM, 1.5 mM $MgCl_2$, 1 mM ATP, 63.5 Ci per mmol [γ-^{32}P]-ATP, 0.1 µM histone H1, 0.02 mg per mL ovalbumin, 3.0 pg per µL purified DGK-theta, and 0.08% (v/v) glycerol, and proceeded for thirty minutes at 37°C. In triplicate: mean ± SD.

I therefore decided to test whether ambient light through the window glass of the laboratory was causing compound **4** to crosslink to DGK by comparing the enzymatic activity of DGK that had been incubated either with or without compound **4**, and then either protected from sunlight by aluminum foil or exposed to ambient light through the

windows. Indeed, I observed probe- and ambient light-dependent inactivation of DGK-theta (Figure 220), at least partially explaining the different degrees of inactivation seen in different assays (Figure 218). The lack of UV-dependent inactivation seen in Figure 219, therefore, might be explained if all the DGK-theta incubated in the presence of compound **4** had already been crosslinked due to the ambient light before exposure to the 360 nm lamp. I was therefore careful in all future experiments to protect the probes from sunlight at all times. Most fluorescent light bulbs do not include 360 nm light in their spectra[167], so I continued working under fluorescent light, such that I would be able to see what I was pipetting.

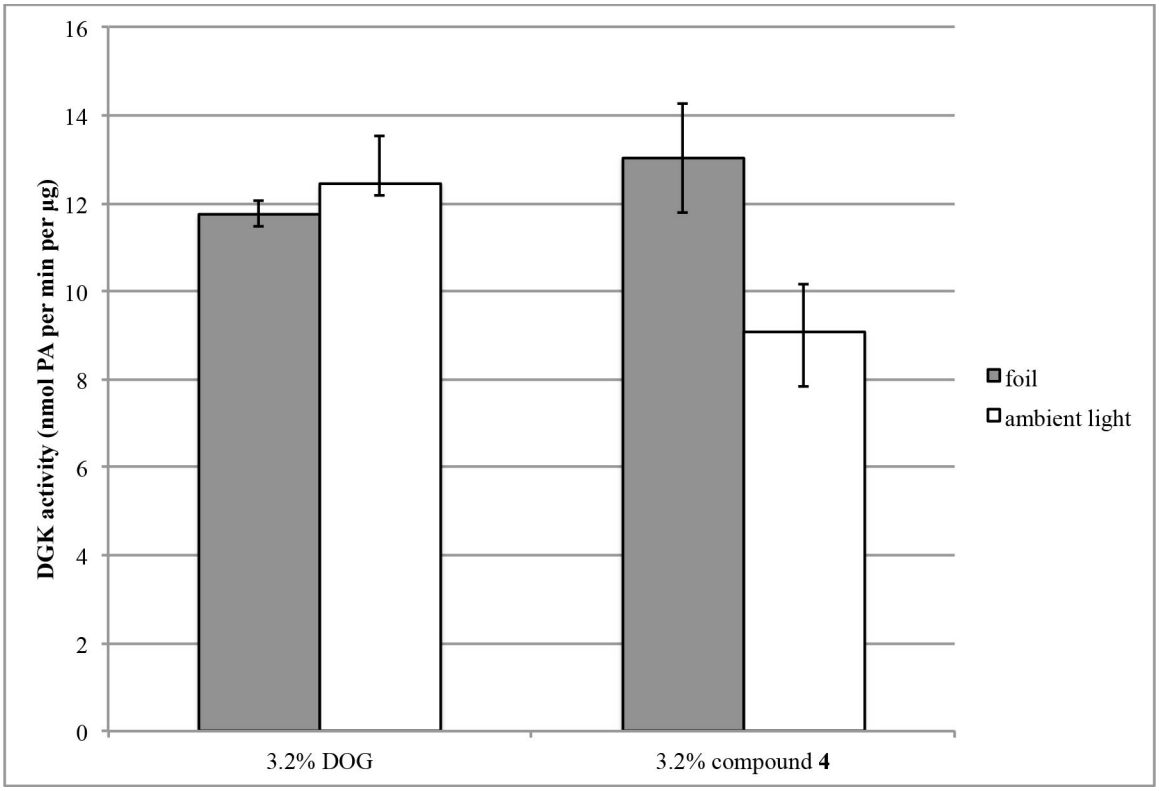

Figure 220. Compound 4 inactivates DGK-theta in an ambient light-dependent way. DGK activity assay. The lipids and the "foil" samples were kept either under foil at all times or else with the lights off and the shades closed. I first preincubated purified DGK-theta in preincubation buffer (50 mM HEPES, pH 7.5, 0.005% (v/v) DDM, 2.5 µM histone H1, 1 mM DTT, 75 pg per µL purified DGK-theta, 1.9% (v/v) glycerol) on ice for ten minutes. I then diluted into incubation buffer (7.5 mM liposomes (51.2:25.6:20:3.2::POPE:POPC:POPS:DOG or compound **4**), 50 mM HEPES, pH 7.5, 100 mM NaCl,

0.005% (v/v) DDM, 0.5 μM histone H1, 1 mM DTT, 0.1 mg per mL ovalbumin, 1 mM ATP, 1.5 mM $MgCl_2$, 15 pg per μL purified DGK-theta, 0.4% (v/v) glycerol) and incubated for thirty minutes, rocking at room temperature, either under foil or with the lights on and the shades open. I then placed the samples on ice for thirty minutes, either under foil or with the lights on and the shades open. The final DGK activity assay reaction included 5 mM substrate-containing liposomes (56.7:28.3:9:6::POPE:POPC:POPS:DOG), 1.5 mM crosslinking liposomes, 1.5 mM filler liposomes (such that the final liposome composition in the reactions were all the same), 50 mM HEPES, pH 7.5, 100 mM NaCl, 1 mM DTT, 0.005% (v/v) DDM, 1.5 mM $MgCl_2$, 1 mM ATP, 74.9 Ci per mmol [γ-^{32}P]-ATP, 0.1 μM histone H1, 0.02 mg per mL ovalbumin, 3.0 pg per μL purified DGK-theta, and 0.08% (v/v) glycerol, and proceeded for thirty minutes at 37°C. In triplicate: mean ± SD.

In order to show that the probe was binding to a DAG-specific site, I wanted to show that DAG would be able to compete for probe- and UV-dependent inactivation of DGK-theta. In a normal photoaffinity labeling experiment, one would just flood the experiment with a vast excess of substrate to show conclusive competition. For soluble substrates, such an option is viable, but since lipids need to be incorporated into a two-dimensional interface, setting up such a competition experiment is more challenging. I was able to show probe- and UV-dependent inactivation of DGK-theta at the relatively high concentration of probe of 3.2 mol%. The theoretical upper bound of DOG, therefore, would be in 3.2 mol% probe, 96.8 mol% DOG liposomes, or at most a 30.3-fold excess of DOG. However, the amount of DOG I can incorporate into liposomes is also limited. As previously mentioned, the highest concentration of DOG I have been able to successfully incorporate into liposomes is 21 mol%, or only a 6.6-fold excess of DOG. I therefore tested whether I could detect a delay in the timecourse of crosslinking by compound **4** to DGK-theta in the presence of competing DOG. I made a mistake during the assay in which I forgot to replace the foil for the foil samples between 5 and 10 minutes. I should also note that I was pipetting in the dark for this particular experiment, and thus may not have pulled up quite the entire volume while pipetting because it was difficult to see, and as such the specific activity of any given sample is

possibly underestimated. I did not see any probe- and UV-dependent inactivation of DGK-theta during the first five minutes of the experiment (Figure 221**A**), so I concluded that the foil controls were safe to be used as such, even for timepoints past five minutes. I continued to observe probe- and UV-dependent inactivation of DGK-theta, and this effect appeared to emerge clearly only after fifteen minutes of irradiation (using a lamp that had not been previously warmed up) (Figure 221**B**). Including an equimolar amount of DOG during the irradiation did not appear to delay the timecourse of inactivation (Figure 221**B**).

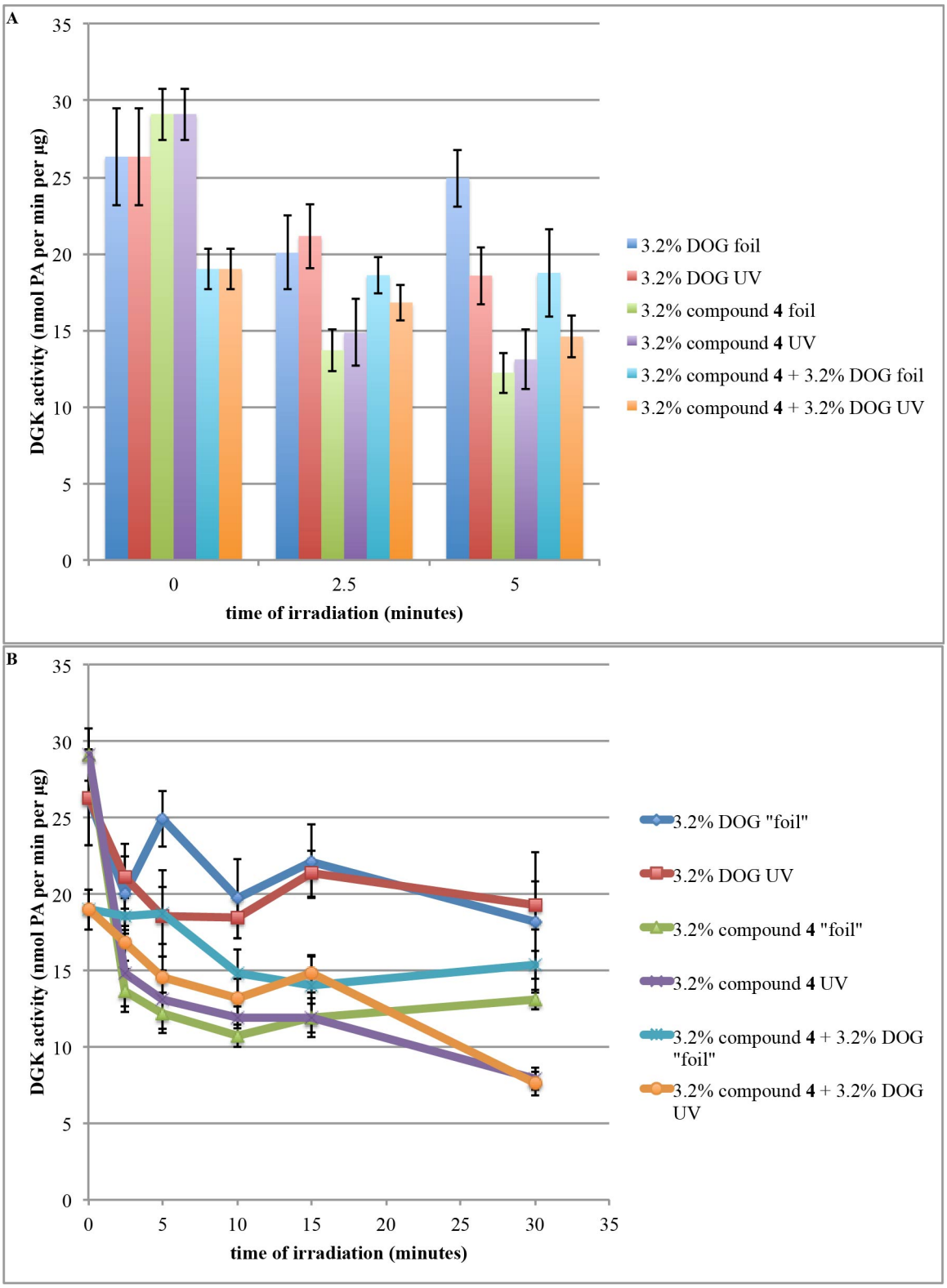

Figure 221. Compound 4 does not inactivate DGK-theta until after at least fifteen minutes of irradiation (using a lamp that had not been previously warmed up), and including an equimolar

amount of DOG did not delay the timecourse of inactivation, under the conditions tested. DGK activity assay. I first preincubated purified DGK-theta in preincubation buffer (50 mM HEPES, pH 7.5, 0.005% (v/v) DDM, 2.5 μM histone H1, 1 mM DTT, 75 pg per μL purified DGK-theta, 1.9% (v/v) glycerol) on ice for ten minutes. I then diluted into incubation buffer (7.5 mM liposomes (2:1::POPE:POPC, 20 mol% POPS, and the indicated concentrations of DOG and compound **4**), 50 mM HEPES, pH 7.5, 100 mM NaCl, 0.005% (v/v) DDM, 0.5 μM histone H1, 1 mM DTT, 0.1 mg per mL ovalbumin, 1 mM ATP, 1.5 mM $MgCl_2$, 15 pg per μL purified DGK-theta, 0.4% (v/v) glycerol) and incubated for thirty minutes, rocking at room temperature, protected from light. The "on ice" samples remained on ice. I placed the other samples in a 96-well plate, and placed aluminum foil over the "foil" samples. I irradiated the samples with a 360 nm lamp on an ice bucket in a chemical fume hood, removing timepoints to ice at the indicated times. I forgot to replace the foil for the foil samples between 5 and 10 minutes. After irradiation, I returned the samples to Eppendorfs, and measured the volume to account for concentration of DGK due to evaporation. The final DGK activity assay reaction included 5 mM substrate-containing liposomes (56.7:28.3:9:6::POPE:POPC:POPS:DOG), 1.5 mM crosslinking liposomes, 1.5 mM filler liposomes (such that the final liposome composition in the reactions were all the same), 50 mM HEPES, pH 7.5, 100 mM NaCl, 1 mM DTT, 0.005% (v/v) DDM, 1.5 mM $MgCl_2$, 1 mM ATP, 50.8 Ci per mmol [γ-^{32}P]-ATP, 0.1 μM histone H1, 0.02 mg per mL ovalbumin, 3.0 pg per μL purified DGK-theta, and 0.08% (v/v) glycerol, and proceeded for thirty minutes at 37°C. In triplicate: mean ± SD.

By this point, I had used up all of the first batch of compound **4** (due at least in part to a large batch of liposomes lost to a bad lot of DOG), and the Best group sent us a second batch. I resuspended the dried down lipid into chloroform, and noticed at that time there was quite a lot of what appeared to be dust in the vial. When I subjected this batch to TLC and charred it, I noticed that, as compared to the first batch (Figure 147), the main spot migrated closer to the DOG than the previous batch did (Figure 222). That difference, however, could probably be explained in very small changes in experimental conditions. For example, this plate was run in December, whereas the previous plate was run in August, which meant the humidity of the room was probably lower. The amount of water that a TLC plate absorbs can affect how molecules interact with it; one way to control for that is to first run the plates in hexane and/or heat them, but I did not do that for these plates. Another point of concern is that, as compared to the first batch, this second batch produced, in addition to the spot running just before the DOG, a smear running near the top of the plate approximately equal in intensity. This other smear might indicate contaminants from the dust or from other byproducts from the synthesis of

the probe; on the other hand, because, as mentioned, the humidity of the plate can affect TLC migration patterns on it, these other components may have been present in the first batch, as well, but comigrated with the main spot under those particular chromatography conditions. I concluded that this batch of compound **4** included two major populations, such that the total intensity of the presumed compound **4** spot was consistent with perhaps about half the concentration of what it was supposed to be.

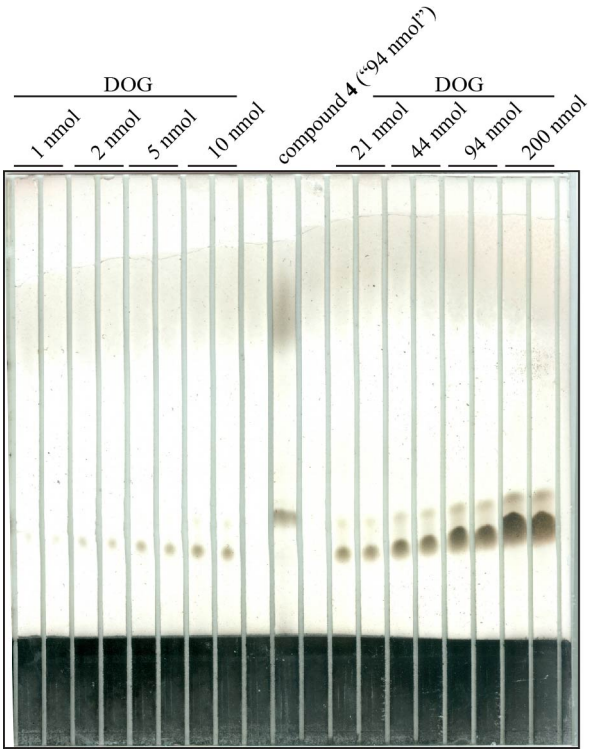

Figure 222. The second batch of compound 4's concentration is consistent with ~half the advertised concentration. After spotting the indicated amounts onto a glass TLC plate, I ran the plate for thirty minutes in fresh tank fluid (85:15:5::toluene:chloroform:methanol). I charred the plate to visualize the spots.

This second batch of compound **4** likewise produced probe- and UV-dependent enzymatic inactivation of DGK (Figure 223).

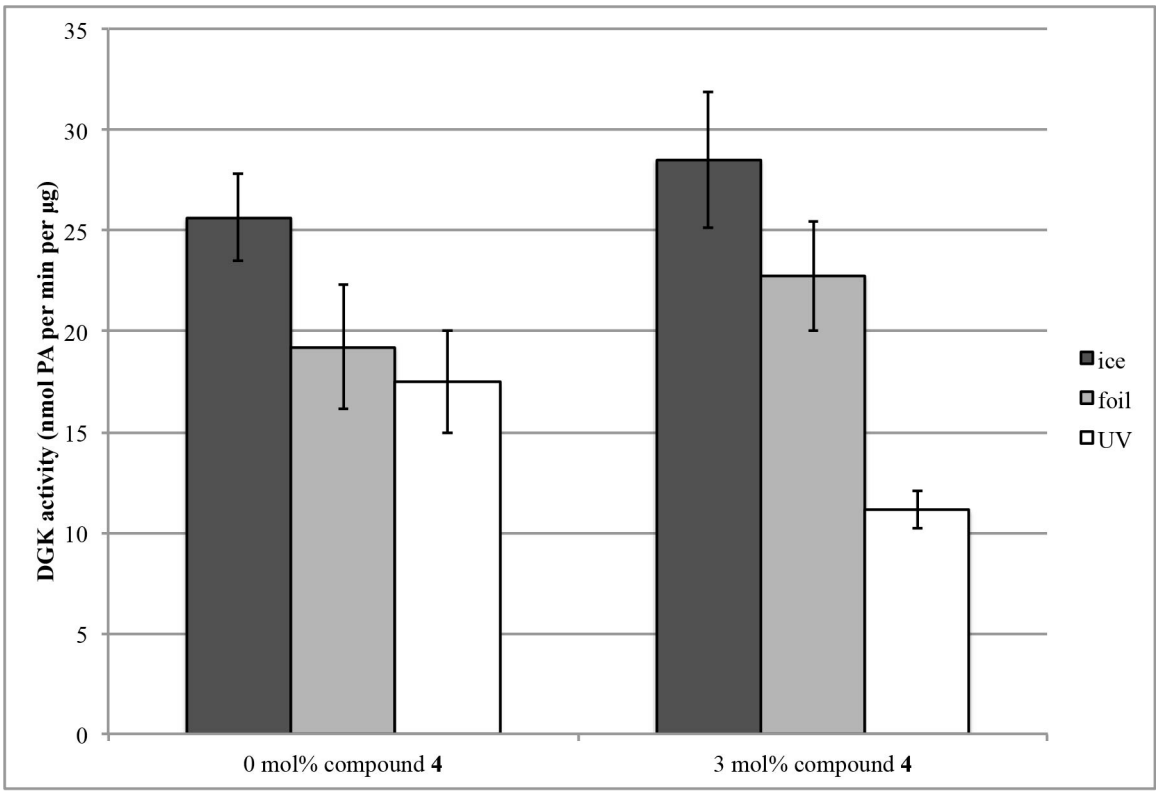

Figure 223. The second batch of compound 4 inactivates purified DGK-theta in a probe- and UV-dependent way. I first preincubated purified DGK-theta in preincubation buffer (50 mM HEPES, pH 7.5, 0.005% (v/v) DDM, 2.5 µM histone H1, 1 mM DTT, 75 pg per µL purified DGK-theta, 1.9% (v/v) glycerol) on ice for ten minutes. I then diluted into incubation buffer (7.5 mM liposomes (2:1::POPE:POPC, 20 mol% POPS, and the indicated concentration of compound **4**), 50 mM HEPES, pH 7.5, 100 mM NaCl, 0.005% (v/v) DDM, 0.5 µM histone H1, 1 mM DTT, 0.1 mg per mL ovalbumin, 1 mM ATP, 1.5 mM $MgCl_2$, 15 pg per µL purified DGK-theta, 0.4% (v/v) glycerol) and incubated for half and hour, rocking at room temperature, protected from light. The "on ice" samples remained on ice. I placed the other samples in a 96-well plate, and placed aluminum foil over the "foil" samples. I irradiated the samples with a 360 nm lamp on an ice bucket in a chemical fume hood for thirty minutes. After irradiation, I returned the samples to Eppendorfs, and measured the volume to account for concentration of DGK due to evaporation. The final DGK activity assay reaction included 5 mM substrate-containing liposomes (56.7:28.3:9:6::POPE:POPC:POPS:DOG), 1.5 mM crosslinking liposomes, 1.5 mM filler liposomes (such that the final liposome composition in the reactions were all the same), 50 mM HEPES, pH 7.5, 100 mM NaCl, 1 mM DTT, 0.005% (v/v) DDM, 1.5 mM $MgCl_2$, 1 mM ATP, 98.3 Ci per mmol [γ-^{32}P]-ATP, 0.1 µM histone H1, 0.02 mg per mL ovalbumin, 3.0 pg per µL purified DGK-theta, and 0.08% (v/v) glycerol, and proceeded for thirty minutes at 37°C. In triplicate: mean ± SD.

I therefore repeated the DOG competition timecourse with this new batch of compound **4**, doubling the concentration of DOG, and taking later timepoints, in the hopes of seeing evidence of delayed crosslinking in the samples with competing DOG. To simplify this experiment, I irradiated at a high concentration and then diluted for the

assay. Although these timepoint dilutions included 7.5 mM liposomes to provide an interface for the DGK, 0.005% DDM, and 0.1 μM histone H1, the resulting activity assay was too noisy to be conclusive (Figure 224), possibly because of the small volumes taken for the dilutions (which might lead to high variation).

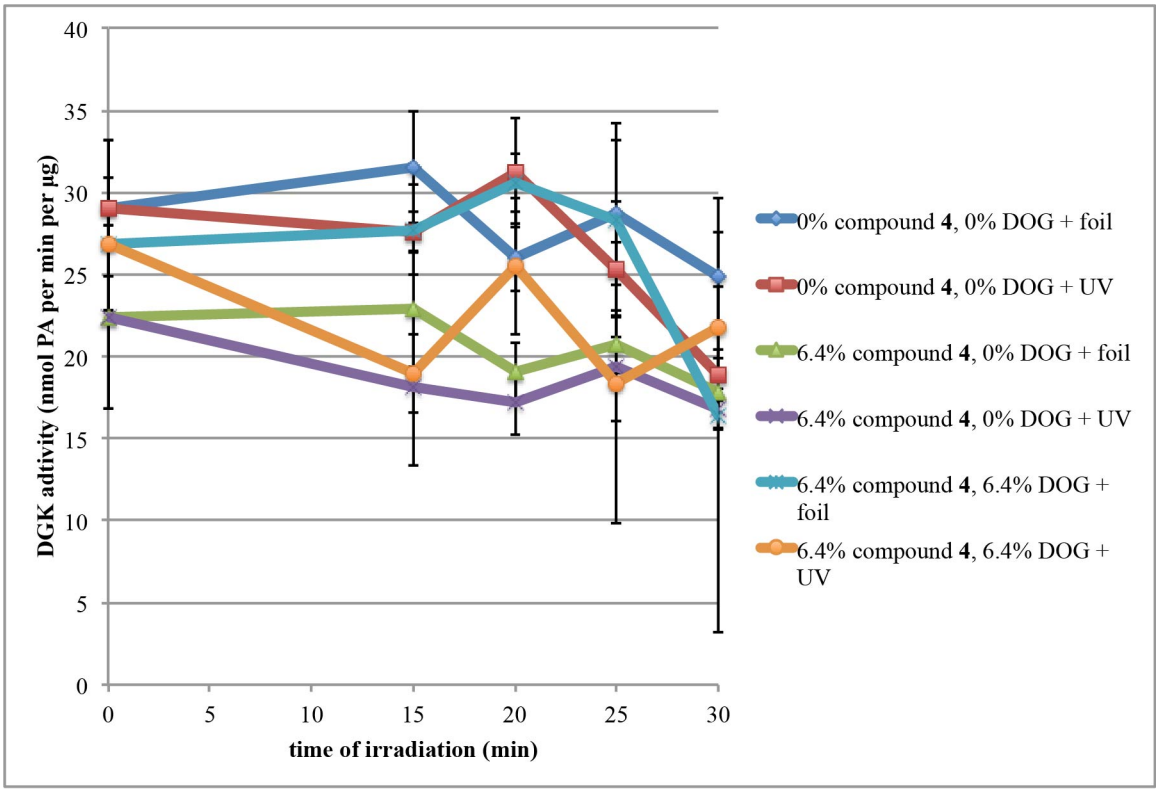

Figure 224. Small pipetting volumes result in large uncertainty. DGK activity assay. I first preincubated purified DGK-theta in preincubation buffer (50 mM HEPES, pH 7.5, 0.008% (v/v) DDM, 0.4 μM histone H1, 1 mM DTT, 1.3 ng per μL purified DGK-theta, 23% (v/v) glycerol) on ice for ten minutes. I then diluted into incubation buffer (6.2 mM liposomes (2:1::POPE:POPC, 20 mol% POPS, and the indicated concentrations of DOG and compound **4**), 55 mM HEPES, pH 7.5, 100 mM NaCl, 0.005% (v/v) DDM, 0.1 μM histone H1, 1 mM DTT, 0.1 mg per mL ovalbumin, 1 mM ATP, 1.5 mM $MgCl_2$, 313 pg per μL purified DGK-theta, 5.6% (v/v) glycerol) and incubated for thirty minutes, rocking at room temperature. I then placed the samples in a 96-well plate, and placed aluminum foil over the "foil" samples. I irradiated the samples with a 360 nm lamp on an ice bucket in a chemical fume hood, removing timepoints to ice at the indicated times. After irradiation, I returned the samples to Eppendorfs, and measured the volume to account for concentration of DGK due to evaporation. I then diluted into dilution buffer (0.4 mM crosslinking liposomes, 7.5 mM dilution liposomes (53.3:26.7:20::POPE:POPC:POPS), 50 mM HEPES, pH 7.5, 85 mM NaCl, 0.005% (v/v) DDM, 0.1 μM histone H1, 1 mM DTT, 7 μg per mL ovalbumin, 71 μM ATP, 107 μM $MgCl_2$, 22 pg per μL DGK-theta, 0.4% (v/v) glycerol), and stored on ice protected from light until the DGK assay was ready. The final DGK activity assay reaction included 5 mM substrate-containing liposomes (56.7:28.3:9:6::POPE:POPC:POPS:DOG), 18 μM crosslinking liposomes, 50 mM HEPES, pH 7.5, 100 mM NaCl, 1 mM DTT, 0.005% (v/v) DDM, 1.5 mM $MgCl_2$, 1 mM ATP, 78.4 Ci per mmol [γ-

^{32}P]-ATP, 0.1 μM histone H1, 0.3 μg per mL ovalbumin, 0.89 pg per μL purified DGK-theta, and 0.02% (v/v) glycerol, and proceeded for thirty minutes at 37°C. In triplicate: mean ± SD.

I therefore repeated the experiment, using larger volumes (for greater certainty), and increasing the concentration of DOG to 19.2%. This time, possibly because of the larger volumes, I once again observed probe- and UV-dependent inactivation of DGK (Figure 225**A**). This inactivation was also time-dependent, as would be expected for photocrosslinking to the active site. In fact, this inactivation fit well to a linear fit, as would be predicted; on the other hand, inactivation of the samples protected by foil also fit well to a linear fit as a function of time (Figure 225**B**). I was surprised to see that the presence of DOG in the irradiating liposomes did not impair this probe- and UV-dependent inactivation, as I had predicted for competing at the same site, but actually seemed to enhance the inactivation. One possible explanation for that could be if the DOG helped the DGK bind the membrane (for example, by interacting with another DOG-binding site besides the active site): if more DGK were targeted to the membrane, I would predict that more would encounter the probe, and more would be inactivated.

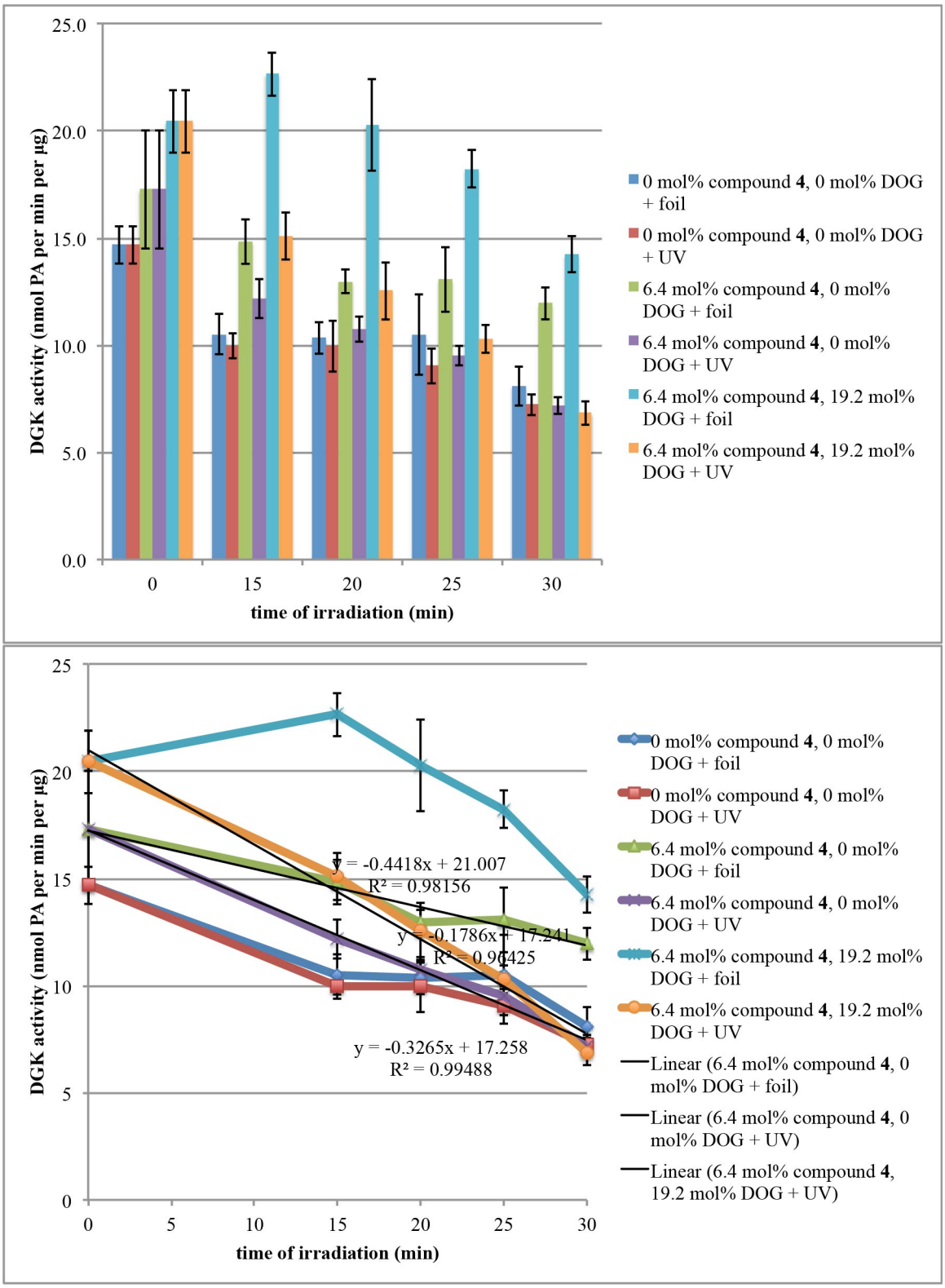

Figure 225. Compound 4 inactivates purified DGK-theta in a probe-, UV-, and time-dependent way, but including DOG does not reduce crosslinking. DGK activity assay. I first preincubated purified

DGK-theta in preincubation buffer (50 mM HEPES, pH 7.5, 0.005% (v/v) DDM, 2.5 μM histone H1, 1 mM DTT, 75 pg per μL purified DGK-theta, 1.9% (v/v) glycerol) on ice for ten minutes. I then diluted into incubation buffer (7.5 mM liposomes (2:1::POPE:POPC, 20 mol% POPS, and the indicated concentrations of DOG and compound **4**), 50 mM HEPES, pH 7.5, 100 mM NaCl, 0.005% (v/v) DDM, 0.5 μM histone H1, 1 mM DTT, 0.1 mg per mL ovalbumin, 1 mM ATP, 1.5 mM $MgCl_2$, 15 pg per μL purified DGK-theta, 0.4% (v/v) glycerol) and incubated for thirty minutes, rocking at room temperature, protected from light. I then placed the samples in a 96-well plate, and placed aluminum foil over the "foil" samples. I irradiated the samples with a 360 nm lamp on an ice bucket in a chemical fume hood, removing timepoints to ice at the indicated times. After irradiation, I returned the samples to Eppendorfs, and measured the volume to account for concentration of DGK due to evaporation. The final DGK activity assay reaction included 5 mM substrate-containing liposomes (56.7:28.3:9:6::POPE:POPC:POPS:DOG), 1.5 mM crosslinking liposomes, 1.5 mM filler liposomes (such that the final liposome composition in the reactions were all the same), 50 mM HEPES, pH 7.5, 100 mM NaCl, 1 mM DTT, 0.005% (v/v) DDM, 1.5 mM $MgCl_2$, 1 mM ATP, 119 Ci per mmol [γ-^{32}P]-ATP, 0.1 μM histone H1, 0.02 mg per mL ovalbumin, 3.0 pg per μL purified DGK-theta, and 0.08% (v/v) glycerol, and proceeded for thirty minutes at 37°C. In triplicate: mean ± SD.

The Best group also sent another compound, compound **5** (structure shown in Figure 226). Like compound **4**, the fatty chains are attached by ether, not acyl, linkages in order to reduce chain migration, and like compound **4**, compound **5** includes a shorter linker between the DAG-like moiety and photoreactive moiety. However, unlike compounds **1**-**4**, compound **5** used diazirine as the photoreactive component instead of benzophenone. As compared to benzophenones, diazirines have the disadvantages that they are less stable in ambient light and that they react preferentially with O-H bonds (as in water) over C-H bonds, but diazirines also have the considerable advantage that they are much smaller than benzophenones, and would therefore be predicted to interact with targets in orientations that might be sterically prohibited with benzophenones. Compound **5** arrived as a lipid film, and was yellowish in color and, like the second batch of compound **4**, there was what appeared to be dust in the vial.

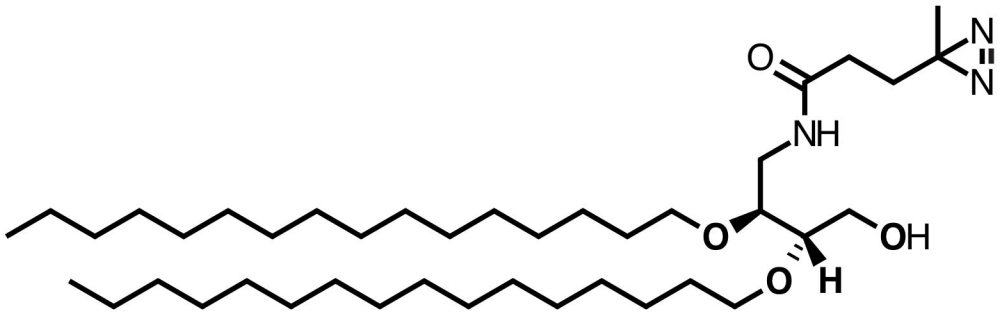

Figure 226. Schematic showing the structure of compound 5.

As with the other photoaffinity probes, I first wanted to confirm the concentration of compound **5**, and confirm that it migrated as a single spot and not a smear, and therefore subjected it to TLC. Because the solvent had been made six days previously, the DOG standards' migration patterned differed from other TLC plates shown, but under these conditions, compound **5** migrated as two major populations, with a high-migrating smear as the second batch of compound **4** did, with a total intensity that appeared consistent with the advertised concentration (Figure 227).

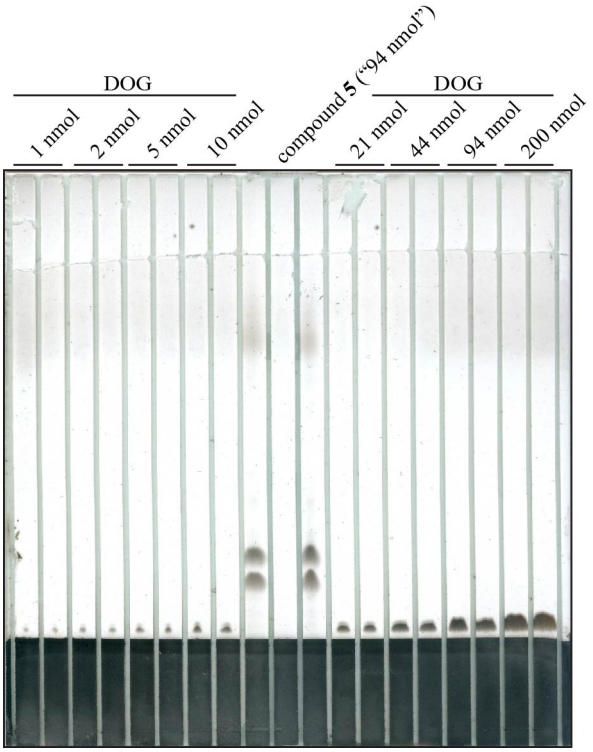

Figure 227. Compound 5's concentration is consistent with the advertised concentration. After spotting the indicated amounts onto a glass TLC plate, I ran the plate for thirty minutes in tank fluid (85:15:5::toluene:chloroform:methanol) that had been made six days previously. I charred the plate to visualize the spots.

When I irradiated purified DGK-theta in the presence of liposomes containing compound **5**, under the same conditions that produced probe- and UV-dependent inactivation with compound **4**, I was unable to observe any probe- and UV-dependent inactivation (Figure 228).

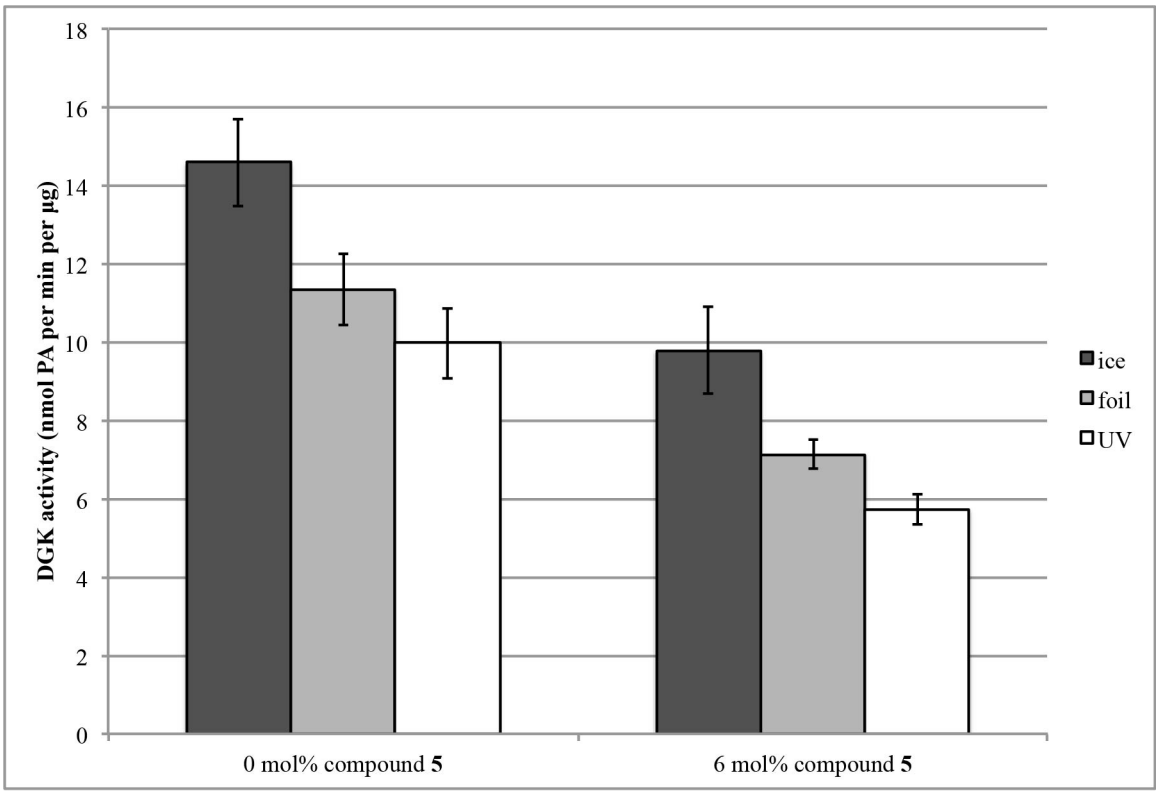

Figure 228. Compound 5 does not inactivate DGK in a probe- and UV-dependent way, under the conditions tested. DGK activity assay. I first preincubated purified DGK-theta in preincubation buffer (50 mM HEPES, pH 7.5, 0.005% (v/v) DDM, 2.5 µM histone H1, 1 mM DTT, 75 pg per µL purified DGK-theta, 1.9% (v/v) glycerol) on ice for ten minutes. I then diluted into incubation buffer (7.5 mM liposomes (2:1::POPE:POPC, 20 mol% POPS, and the indicated concentration of compound **5**), 50 mM HEPES, pH 7.5, 100 mM NaCl, 0.005% (v/v) DDM, 0.5 µM histone H1, 1 mM DTT, 0.1 mg per mL ovalbumin, 1 mM ATP, 1.5 mM $MgCl_2$, 15 pg per µL purified DGK-theta, 0.4% (v/v) glycerol) and incubated for thirty minutes, rocking at room temperature, protected from light. I then placed the samples in a 96-well plate, and placed aluminum foil over the "foil" samples. I irradiated the samples with a 360 nm lamp for thirty minutes on an ice bucket at 4°C. After irradiation, I returned the samples to Eppendorfs, and measured the volume to account for concentration of DGK due to evaporation. The final DGK activity assay reaction included 5 mM substrate-containing liposomes (56.7:28.3:9:6::POPE:POPC:POPS:DOG), 1.5 mM crosslinking liposomes, 1.5 mM filler liposomes (such that the final liposome composition in the reactions were all the same), 50 mM HEPES, pH 7.5, 100 mM NaCl, 1 mM DTT, 0.005% (v/v) DDM, 1.5 mM $MgCl_2$, 1 mM ATP, 158 Ci per mmol [γ-^{32}P]-ATP, 0.1 µM histone H1, 0.02 mg per mL ovalbumin, 3.0 pg per µL purified DGK-theta, and 0.08% (v/v) glycerol, and proceeded for twenty minutes at 37°C. In triplicate: mean ± SD. The *p* value between the 6 mol% compound **5** foil vs. UV samples was calculated to be 0.134 by one-way analysis of variance (Holm-Sidak method, SigmaPlot 12).

Mass spectrometry

If any of the probes successfully photoaffinity labeled DGK, I would predict that the molecular weight of the protein would increase by the mass of the probe. Such a shift is theoretically possible to observe by SDS-PAGE. Because I was able to observe probe-,

UV-, and time-dependent inactivation of DGK-theta in the presence of compound **4**, I decided to pursue that probe for crosslinking studies. After irradiating DGK in the presence of liposomes containing compound **4**, I subjected the samples to SDS-PAGE. The band corresponding to DGK-theta was just barely visible by SimplyBlue™ (Life Technologies™) staining (Figure 229**A**), but clearly visible by silver staining (Figure 229**B**). I was unable to detect any probe- and UV-dependent gel shift; on the other hand, the resolution of this gel may have been insufficient to detect a 778 Da shift on a ~120 kD protein. I ran this gel for the purpose of visualizing the complexity of the sample for the mass spectrometry studies; perhaps if I had run the gel longer, I could have achieved better resolution.

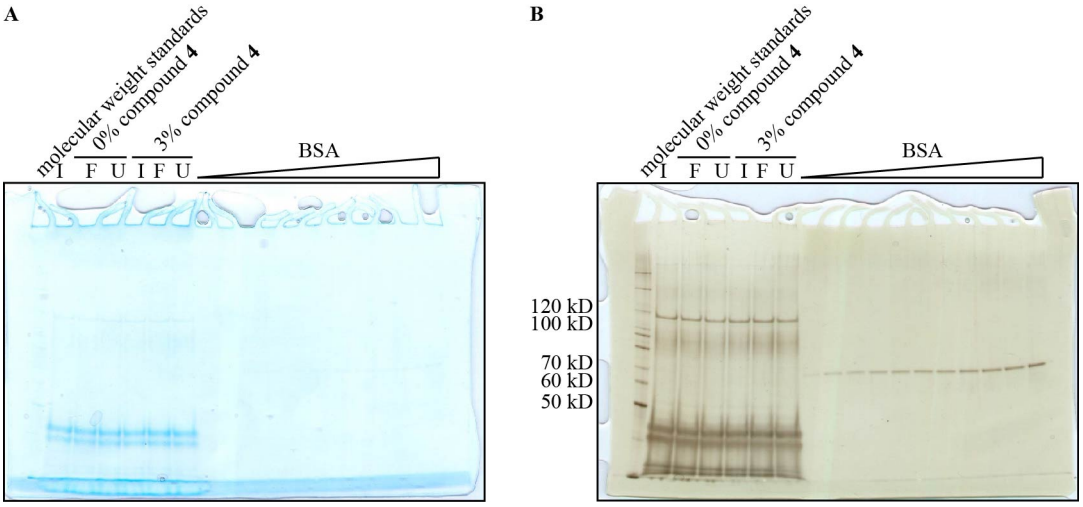

Figure 229. No gel shift following crosslinking of purified DGK-theta to compound 4 was detectable by SDS-PAGE of a Criterion™ XT (Bio-Rad) 3-8% Tris-Acetate gel, under the conditions tested. I first preincubated purified DGK-theta in preincubation buffer (52 mM HEPES, pH 7.5, 0.02% (v/v) DDM, 0.4 μM histone H1, 4 mM DTT, 1.3 ng per μL purified DGK-theta, 36% (v/v) glycerol) on ice for ten minutes. I then diluted into incubation buffer (7.5 mM liposomes (2:1::POPE:POPC, 20 mol% POPS, and the indicated concentration of compound **4**), 50 mM HEPES, pH 7.5, 100 mM NaCl, 0.005% (v/v) DDM, 0.1 μM histone H1, 1 mM DTT, 0.1 mg per mL ovalbumin, 1 mM ATP, 1.5 mM $MgCl_2$, 306 pg per μL purified DGK-theta, 8.8% (v/v) glycerol) and incubated for thirty minutes, rocking at room temperature, protected from light. I then placed the samples in a 96-well plate, and placed aluminum foil over the "foil" samples. I irradiated the samples with a 360 nm lamp for thirty minutes on an ice bucket at 4°C. SDS-PAGE of a Criterion™ XT (Bio-Rad) 3-8% Tris-Acetate gel, followed by **(A)** SimplyBlue™ staining, then rinsed and **(B)** silver stained. I, ice; F, foil; U, UV.

I excised the bands from lanes 4 and 7 (the samples irradiated with UV), destained, washed with methanol, and submitted for LC/MS/MS. Amino acid coverage of the control sample was low (27%), and even lower for the crosslinked sample (22%) (Figure 230). One reason for the lower amino acid coverage could be that if compound **4** had covalently attached to the protein, the resulting peptides would have a greater hydrophobicity, which can make the labeled peptides difficult to extract from the gel matrix[168]. Certain adjacent tryptic peptides were disproportionately absent from the crosslinked sample as compared to the control sample. For example, ARPGPGPGPGPER was found six times in the control peptide, APGPAAAPGHSFR was found eleven times, and IPCTSVAPSLVRVPVAHCFGPR was found three times. Of these peptides, ARPGPGPGPGPER and IPCTSVAPSLVRVPVAHCFGPR were found in the crosslinked sample, but APGPAAAPGHSFR was not, even though it was the most abundant in the control sample. If peptides were covalently modified with compound **4**, I would predict them to be disproportionately absent from the crosslinked sample, either because the mass of the crosslinked peptide had been shifted and thus no longer appeared as the unmodified mass, or else because the crosslinked peptide remained in the gel matrix. I found two such disproportionately absent peptides in these samples, and, even more encouragingly, both coincided with regions of the protein predicted by primary sequence homology to include DAG-binding sites. While the presence of such disproportionately absent peptides was encouraging, any such subtractive analysis must be used cautiously.

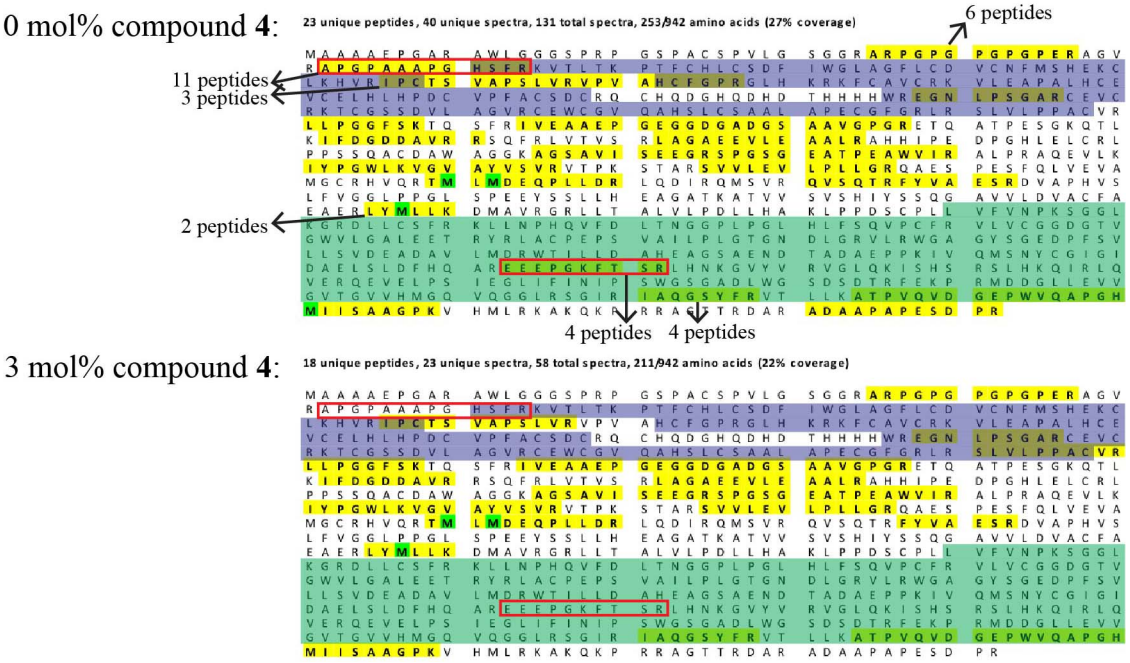

Figure 230. Amino acid coverage of in-gel trypsin-digested DGK crosslinked with compound 4 is low, but certain peptides are disproportionately absent in the crosslinked as compared to control sample. I excised the bands from lanes 4 and 7 (the samples irradiated with UV) as well as a control region of the gel shown in **Figure 229**, destained, washed with methanol, and submitted for LC/MS/MS. The samples were digested in-gel with trypsin. Peptides were removed from the gel and fractionated by reverse-phase HPLC (Magic C18AQ), and eluting peptides were sprayed directly into an LTQ Orbitrap Velos. Peptide sequences were identified from isotopically resolved masses in MS and MS/MS spectra using Mascot[169] and Proteome Discoverer[170]. Amino acid coverage of DGK subjected to LC/MS/MS following irradiation in the presence of liposomes of the composition shown. Detected peptides are highlighted in yellow. Peptides disproportionately absent in the sample with compound 4 are marked in red. The three C1 domains and the catalytic domain of DGK, which are predicted to contain DAG-binding sites, are shaded in blue and green, respectively. Oxidized sites are marked in bright green.

I therefore repeated the crosslinking experiment, to see whether the same peptides would be disproportionately absent. This time, the samples were digested in-solution, so that crosslinked peptides would not be left behind in any polyacrylamide gel matrix. This time, I also assayed the DGK activity of the samples. I once again observed probe-dependent inactivation of DGK activity (Figure 231**A**). Amino acid coverage of the in-solution digested samples was indeed improved as compared to the in-gel samples, including the control samples (Figure 231**B**), suggesting that the improvement may have been due to factors other than increased hydrophobicity conferred by the attachment of

compound **4**'s anchoring the protein in the gel matrix. The APGPAAAPGHSFR and EEEPGKFTSR peptides were once again absent in the crosslinked sample, consistent with covalent attachment on this peptide and consequent mass shift of the peptide, but coverage in those regions of the protein was just generally poor, so that peptides could not be said to be disproportionately absent. A new peptide, IAQGSYFR, also in the catalytic domain, was disproportionately absent in the crosslinked as compared to the control samples. However, when the set of masses was searched for masses consistent with 778 Da's being added to any of the peptides, no such mass shifts were found.

A

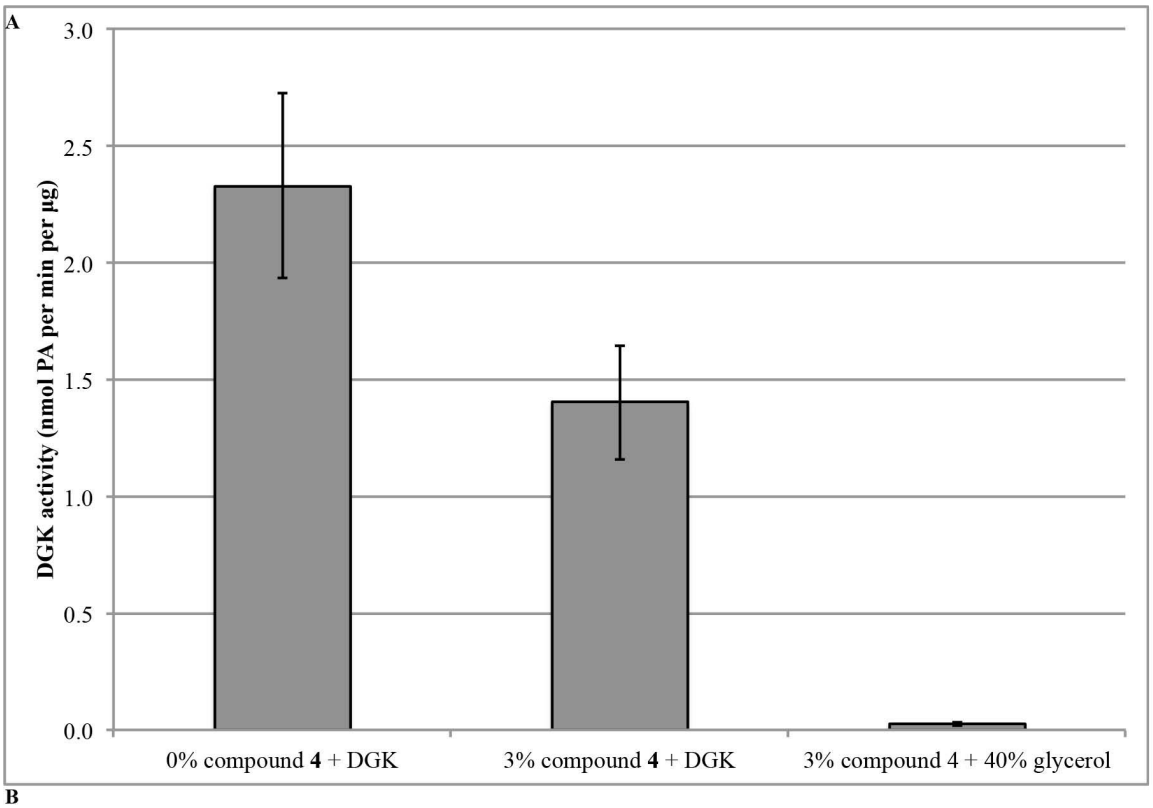

B

0 mol% compound **4**:

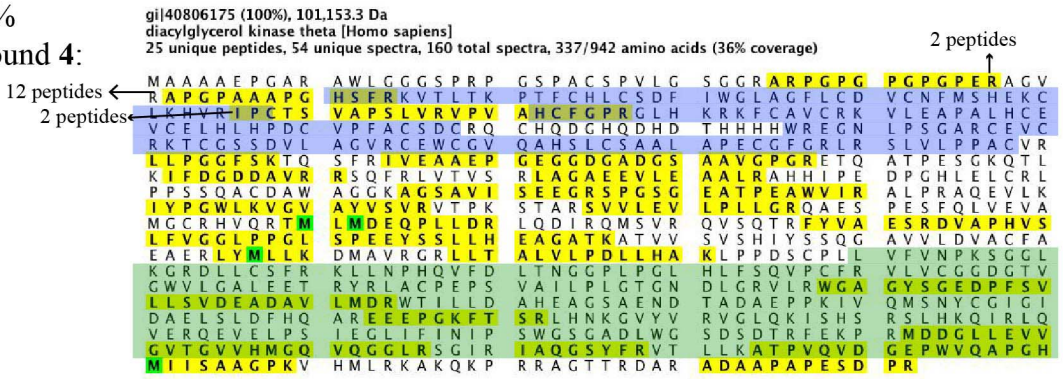

6.4 mol% compound **4**:

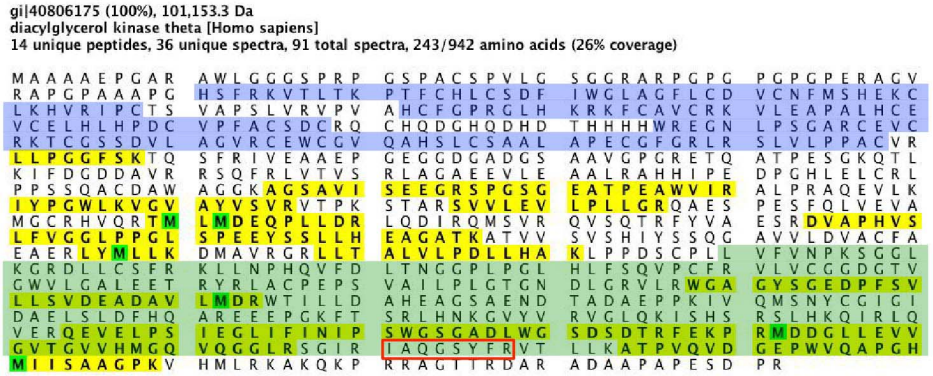

Figure 231. Amino acid coverage of in-solution trypsin-digested DGK crosslinked with compound 4 is somewhat improved, and certain peptides are once again disproportionately absent in the crosslinked as compared to control sample. **(A)** DGK activity assay. I first preincubated purified DGK-theta in preincubation buffer (50 mM HEPES, pH 7.5, 0.005% (v/v) DDM, 0.4 μM histone H1, 1 mM DTT, 875 pg per μL purified DGK-theta, 25% (v/v) glycerol) on ice for ten minutes. I then diluted into incubation buffer (7.5 mM liposomes (2:1::POPE:POPC, 20 mol% POPS, and the indicated concentration of compound **4**), 50 mM HEPES, pH 7.5, 100 mM NaCl, 0.005% (v/v) DDM, 0.1 μM histone H1, 1 mM DTT, 0.1 mg per mL ovalbumin, 1 mM ATP, 1.5 mM $MgCl_2$, 204 pg per μL purified DGK-theta, 5.9% (v/v) glycerol) and incubated for thirty minutes, rocking at room temperature, protected from light. I then placed the samples in a 96-well plate, and irradiated the samples with a 360 nm lamp for thirty minutes on an ice bucket at 4°C. After irradiation, I returned the samples to Eppendorfs, and measured the volume to account for concentration of DGK due to evaporation. I then diluted into dilution buffer (50 mM HEPES, pH 7.5, 0.5 μM histone H1, 0.005% (v/v) DDM, 1 mM DTT, 1 mM dilution liposomes (53.3:26.7:20::POPE:POPC:POPS:DOG), 0.003 mg per mL ovalbumin, 29 μM ATP, 43 μM $MgCl_2$, 11 mM NaCl, 5.8 pg per μL purified DGK-theta, 0.17% (v/v) glycerol). The final DGK activity assay reaction included 5 mM substrate-containing liposomes (56.7:28.3:9:6::POPE:POPC:POPS:DOG), 43 μM crosslinking liposomes, 43 μM filler liposomes (such that the final liposome composition in the reactions were all the same), 50 mM HEPES, pH 7.5, 98 mM NaCl, 1 mM DTT, 0.005% (v/v) DDM, 1.5 mM $MgCl_2$, 1 mM ATP, 24.0 Ci per mmol [γ-^{32}P]-ATP, 0.1 μM histone H1, 0.02 mg per mL ovalbumin, 3.0 pg per μL purified DGK-theta, and 0.08% (v/v) glycerol, and proceeded for twenty minutes at 37°C. In triplicate: mean ± SD. I calculated a p value comparing 0% compound 4 + DGK to 6.4% compound 4 + DGK to be < 0.021 by one-way analysis of variance (Holm-Sidak method, SigmaPlot 12). **(B)** Amino acid coverage of DGK subjected to LC/MS/MS following irradiation in the presence of liposomes of the composition shown. Aliquots of samples were removed prior to dilution into dilution buffer, digested in-solution with trypsin, and fractionated by reverse-phase HPLC (Magic C18AQ), and eluting peptides were sprayed directly into an LTQ Orbitrap Velos. Peptide sequences were identified from isotopically resolved masses in MS and MS/MS spectra using Mascot[169] and Proteome Discoverer[170]. Detected peptides are highlighted in yellow. Peptides disproportionately absent in the sample with compound 4 are marked in red. The three C1 domains and the catalytic domain of DGK, which are predicted to contain DAG-binding sites, are shaded in blue and green, respectively. Oxidized sites are marked in bright green. The same peptide disproportionately absent following in-gel trypsin digestion (**Figure 230**) was also absent, but because amino acid coverage was generally poor in this region of the protein, it could not be said to be disproportionately absent.

I therefore wondered whether the probe was fragmenting during the course of the LC/MS/MS, such that any labeled peptides would be shifted not by the full 778 Da, but by the mass of a fragment of the probe. Before doing mass spectrometry on compound **4**, I first tested its solubility in several solvents commonly used in mass spectrometry of lipids[171–175] to see which ones were appropriate for testing the fragmentation pattern of compound **4**. I therefore either spotted compound **4** directly from the vial, or else resuspended it in each of the solvents to be tested, then spotted onto a TLC plate and visualized how much had made it on to the plate by charring. I found that compound **4** appeared quite soluble in chloroform and in 1:2::chloroform:methanol, pretty soluble in

20:40:3:chloroform:methanol:1 M aqueous ammonium acetate, somewhat soluble in acetonitrile, only slightly soluble in 70:30::acetonitrile:water, and not at all soluble in 75:25::methanol:acetonitrile (Figure 232). Caution must be used when using acetonitrile as a solvent, because it dissolves the adhesive between the polytetrafluoroethylene lining and the cap of the vials we use for lipids. Compound **4** is also somewhat soluble in methanol (Figure 232). I concluded that chloroform should be an adequate solvent for resuspending compound **4** for loading into the mass spectrometer. While compound **4** was not completely soluble in methanol, some of it definitely partitioned into the methanol, so as long as the amount of probe loaded was well above the detection limit of the instrument, methanol should likewise be a suitable solvent for resuspending compound **4** for loading into the mass spectrometer.

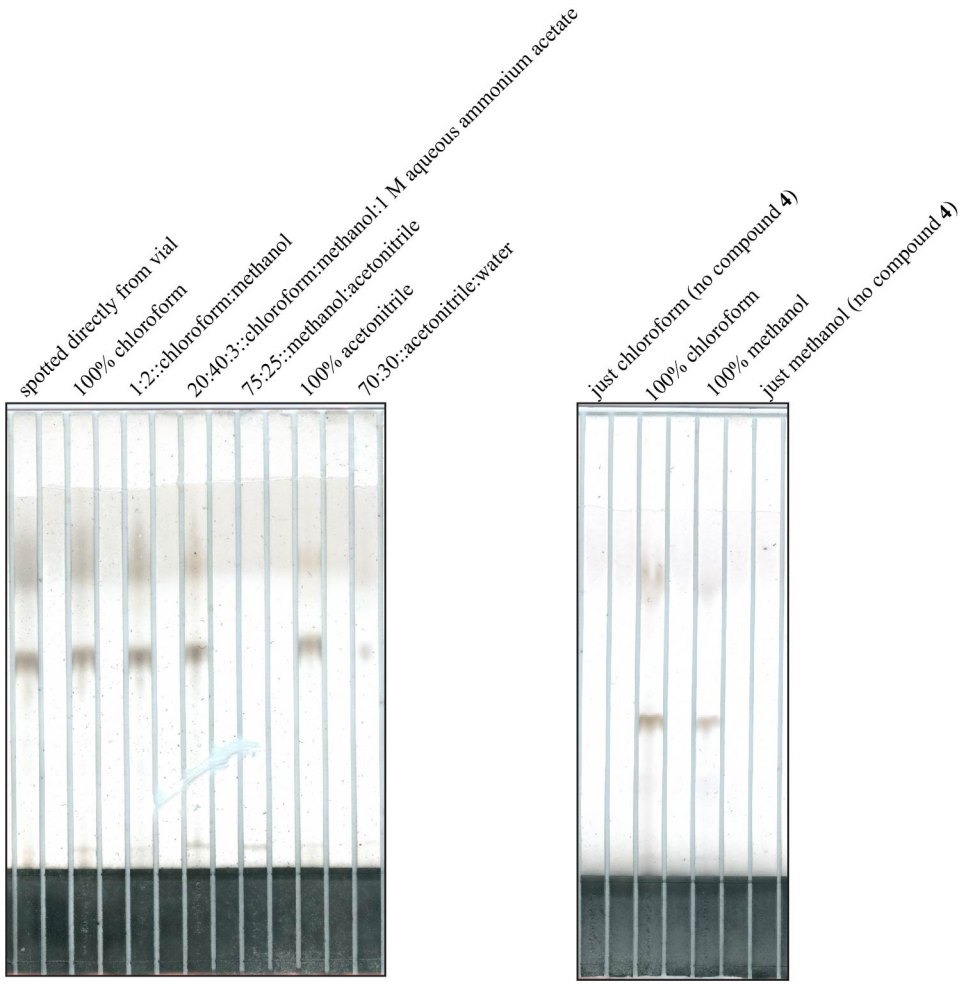

Figure 232. The solubility of compound 4 among solvents varies. TLC of compound 4 resuspended in different solvents, run in freshly made 85:15:5::toluene:chloroform:methanol, dried, sprayed with 40% sulfuric acid, and charred.

When compound **4** was resuspended in 53 mM ammonium formate in methanol and scanned in positive ion mode on a AB Sciex 4000 Q Trap spectrum, it gave a predominant peak at 987.2 Da (Figure 233). The predicted peak at 778 Da was very small, no greater than noise, even though at a concentration of 100 μg per mL the molecule should be clearly detectable. The lack of detection was probably not a problem with the instrument: the spectra we observed 23 May 2013 (Figure 233**A**) are well reproduced by the spectra we observed 30 May 2013 (Figure 233**B**), and the Haughey lab

had used the instrument several times in the intervening week with no reported problems with their other samples.

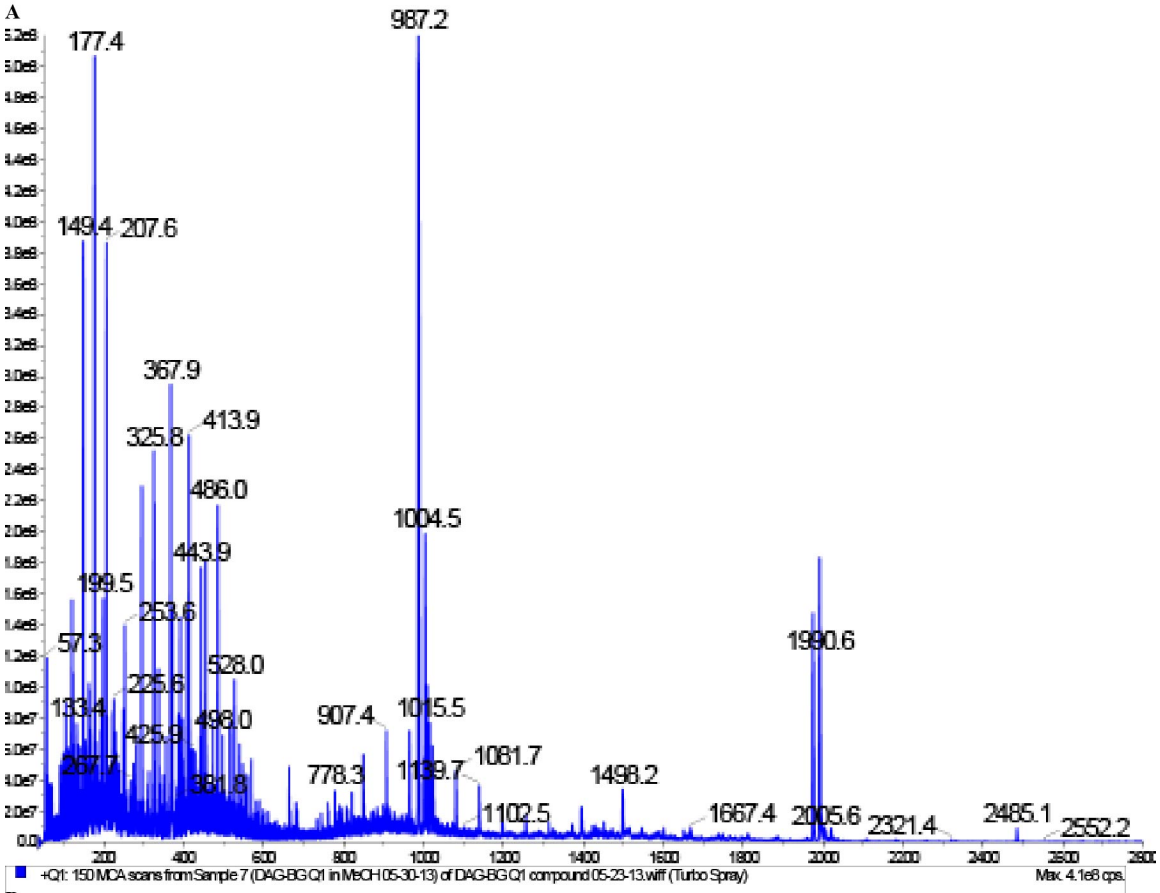
A
177.4
987.2
149.4
207.6
367.9
413.9
325.8
486.0
1004.5
443.9
199.5
253.6
57.3
528.0
1990.6
225.6
183.4
907.4
1015.5
498.0
425.9
1081.7
267.7
778.3
1139.7
1498.2
381.8
1102.5
1667.4
2005.6
2321.4
2485.1
2552.2
+Q1: 150 MCA scans from Sample 7 (DAG-BG Q1 in MeCH 05-30-13) of DAG-BG Q1 compound 05-23-13.wiff (Turbo Spray)
Max. 4.1e8 cps.

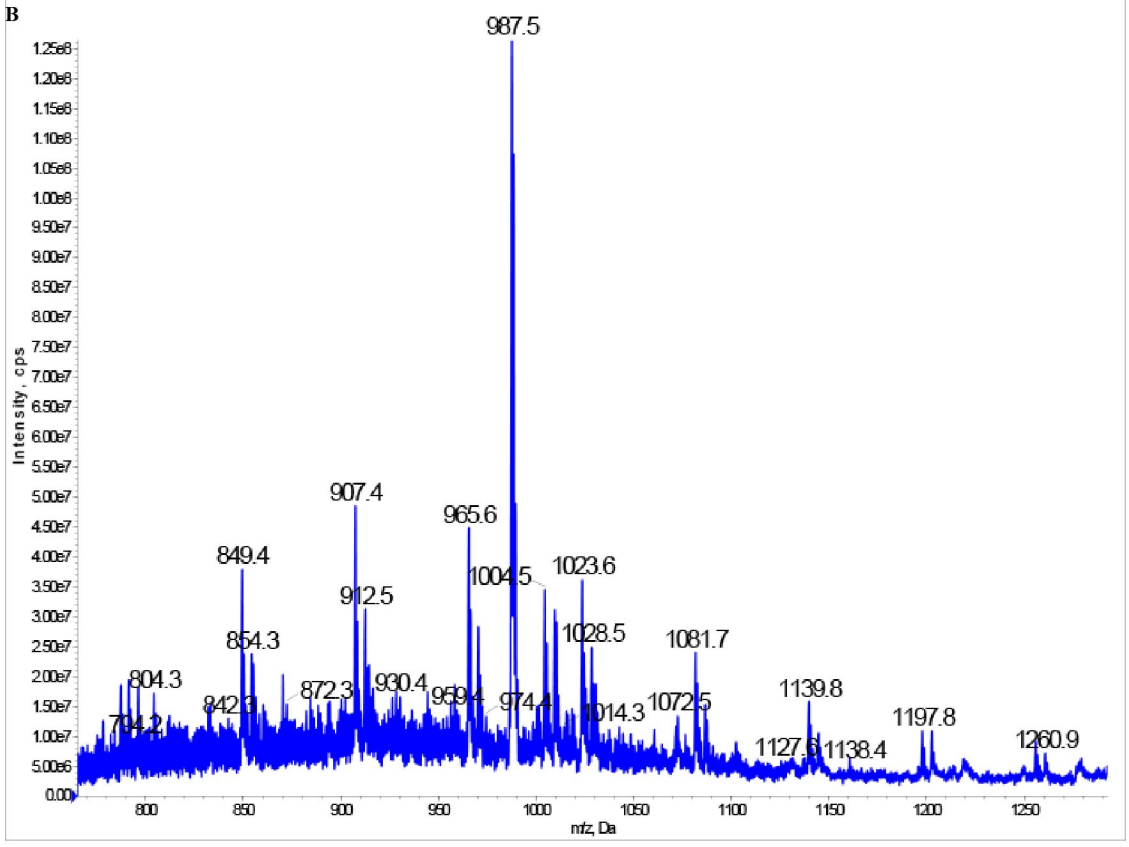
B
987.5
907.4
965.6
849.4
1004.5
1023.6
912.5
1028.5
1081.7
854.3
804.3
872.3
930.4
959.4
974.4
1014.3
1072.5
1139.8
842.3
794.2
1127.6
1138.4
1197.8
1260.9
Intensity, cps
m/z, Da

Figure 233. When the second batch of compound 4 is subjected to LC/MS/MS, it produces a peak at 987 Da, not at the predicted molecular weight of 778 Da. AB Sciex 4000 Q Trap spectrum of the probe (100 µg per mL) in 53 mM ammonium formate in methanol in positive ion mode. **(A)** Spectrum measured 23 May 2013. **(B)** Spectrum measured 30 May 2013.

Although compound **4** was mostly soluble in methanol (Figure 232), such that, even if not all of the probe partitioned into the methanol, surely enough should have at 100 µg per mL to be detectable, I wondered whether changing the solvent to chloroform would increase the amount of the 778 Da peak detected. When we scanned the probe in 53 mM ammonium formate in chloroform, however, we observed the same predominant peak at 987.5 Da (Figure 234). I therefore concluded that the lack of detection of a 778 Da peak was probably not a problem with the molecule's solubility in methanol.

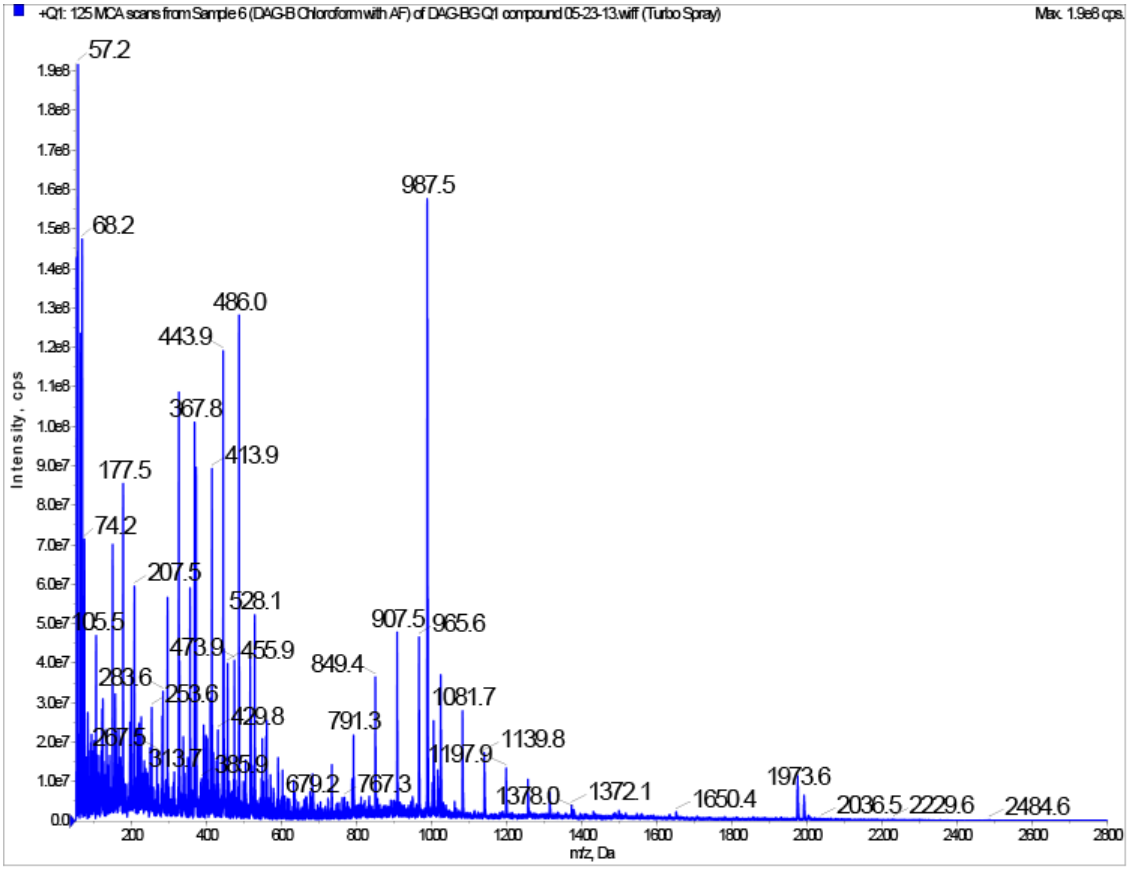

Figure 234. Using 53 mM ammonium formate in chloroform as a solvent does not increase the proportion of the 778 Da peak during LC/MS/MS of compound 4. AB Sciex 4000 Q Trap spectrum of the probe (100 µg per mL) in 53 mM ammonium formate in chloroform (1% methanol), in positive ion mode.

The spectrum of just 53 mM ammonium formate in methanol (Figure 235**A**) also showed the 987 peak, although not as high an amplitude as in the probe scans. This peak was not seen in a scan of methanol alone (Figure 235**B**), so can probably be attributed to the 53 mM ammonium formate (and is probably contributing to the 987.5 peak seen in Figure 233 and Figure 234). An alternative explanation is that the 53 ammonium formate in methanol sample was confused with the compound **4** dissolved in 53 ammonium formate in methanol sample.

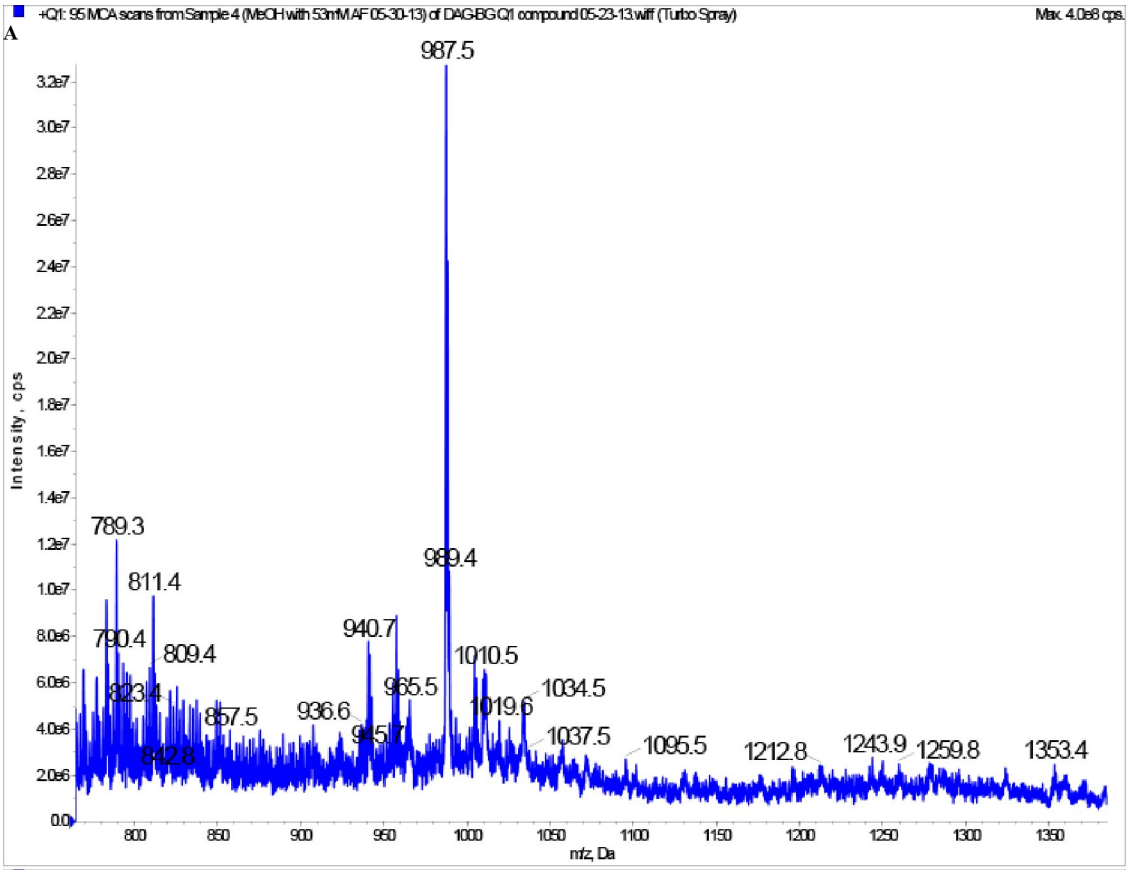
A
+Q1: 95 MCA scans from Sample 4 (MeOH with 53mM AF 05-30-13) of DAG-BG Q1 compound 05-23-13.wiff (Turbo Spray)
Max. 4.0e8 cps.
Intensity, cps
m/z, Da
987.5
789.3
989.4
811.4
940.7
790.4
809.4
1010.5
965.5
1034.5
823.4
857.5
936.6
1019.6
945.7
1037.5
842.8
1095.5
1212.8
1243.9
1259.8
1353.4

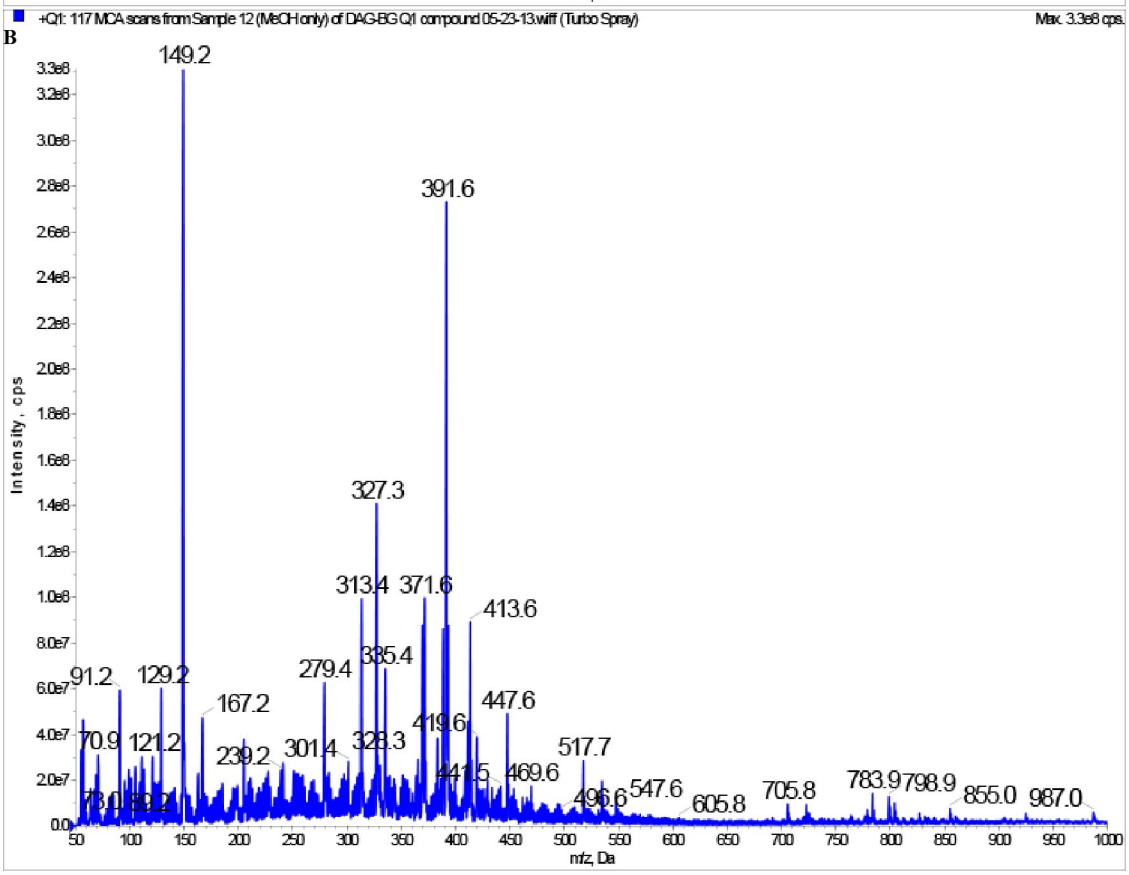
B
+Q1: 117 MCA scans from Sample 12 (MeOH only) of DAG-BG Q1 compound 05-23-13.wiff (Turbo Spray)
Max. 3.3e8 cps.
Intensity, cps
m/z, Da
149.2
391.6
327.3
313.4
371.6
413.6
385.4
279.4
91.2
129.2
167.2
447.6
419.6
70.9
121.2
328.3
301.4
239.2
517.7
441.5
469.6
496.6
547.6
605.8
705.8
783.9
798.9
855.0
987.0

Figure 235. The 987.5 Da peak also appears in LC/MS/MS scans of 53 mM ammonium formate in methanol, but not of methanol alone. AB Sciex 4000 Q Trap spectrum in positive ion mode of **(A)** 53 mM ammonium formate in methanol and **(B)** methanol.

Although some of the 987.5 Da peak was probably coming from the ammonium formate (unless the samples were mixed up), the fact that the amplitude is higher in the scans with probe (Figure 233 and Figure 234) suggested that at least some of the amplitude of the peak came from compound **4** (or contaminants from the vial containing compound **4**). 987.4 Da is the molecular weight that would be predicted for compound **4** were another benzophenone attached via a ketone linkage (as in Figure 236**A**). I am not familiar with the synthesis used to produce compound **4**, so I am not sure how plausible this structure is as a synthetic byproduct, but it seemed promising, because such a contaminant could conceivably explain why, even if there were no compound **4** present, I reproducibly observed probe- and UV-dependent inactivation of DGK, seeing as this structure still has the DAG-like part of the molecule to target it to the enzyme, and a photoactivatable crosslinker (in fact, three). When we fragmented the 987.5 Da peak, the fragmentation spectrum (Figure 236**B**) showed a product at 745.7 Da. A product ion size of 745.7 Da was very promising because not one but two plausible fragments of the structure proposed in Figure 236**A** would be predicted to have a molecular weight of 746.0 Da (Figure 236**C**). These product ions are plausible because cleavage at branch points, such as in Figure 236**C**, produces more stable carbocations, due to hyperconjugation and inductive effects, and more stable cations will be more prevalent in product ion spectra. On the other hand, when the (albeit smaller in amplitude) 987 peak from the solvent alone was likewise fragmented, it also produced a 745.7 Da fragment. (We forgot to save that scan, so I cannot include it as a figure.) Unless the ammonium

formate bottle were somehow contaminated by the probe, or unless the samples were mixed up, it seems exceedingly unlikely that it would have a molecule of the same molecular weight and same fragmentation pattern in it.

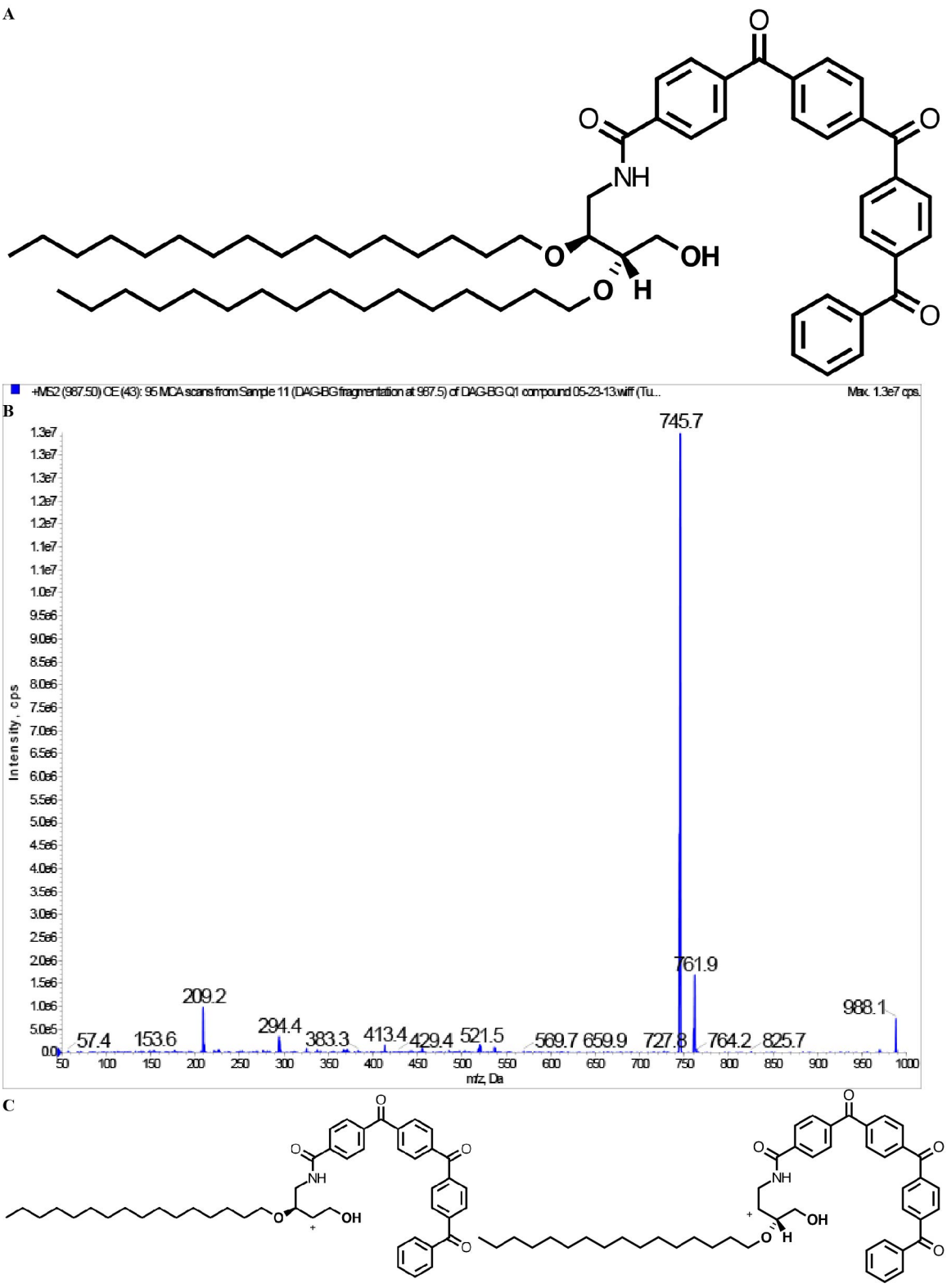

Figure 236. The 987 Da peak's size and fragmentation pattern is consistent with compound 4 with an additional benzophenone added via a ketone linkage. (A) Structure of compound **4** with an additional

benzophenone added via a ketone linkage. Its predicted molecular weight is 987.4 Da. (The additional keto-benzophenone could be added at any location of the molecule and the total predicted molecular weight would remain 987.4 Da.) **(B)** Fragmentation spectrum of the 987.5 peak from the AB Sciex 4000 Q Trap spectrum of the probe (100 μg per mL) in 53 mM ammonium formate in methanol in positive ion mode (shown in **Figure 233**B). **(C)** Structure of proposed fragments from the 987 peak, if they derived from the structure shown in (A).

To be thorough, we also checked the spectrum of the probe in negative ion mode, but there were no additional peaks seen in the probe spectrum (Figure 237**A**) that were not seen in the solvent spectrum (Figure 237**B**).

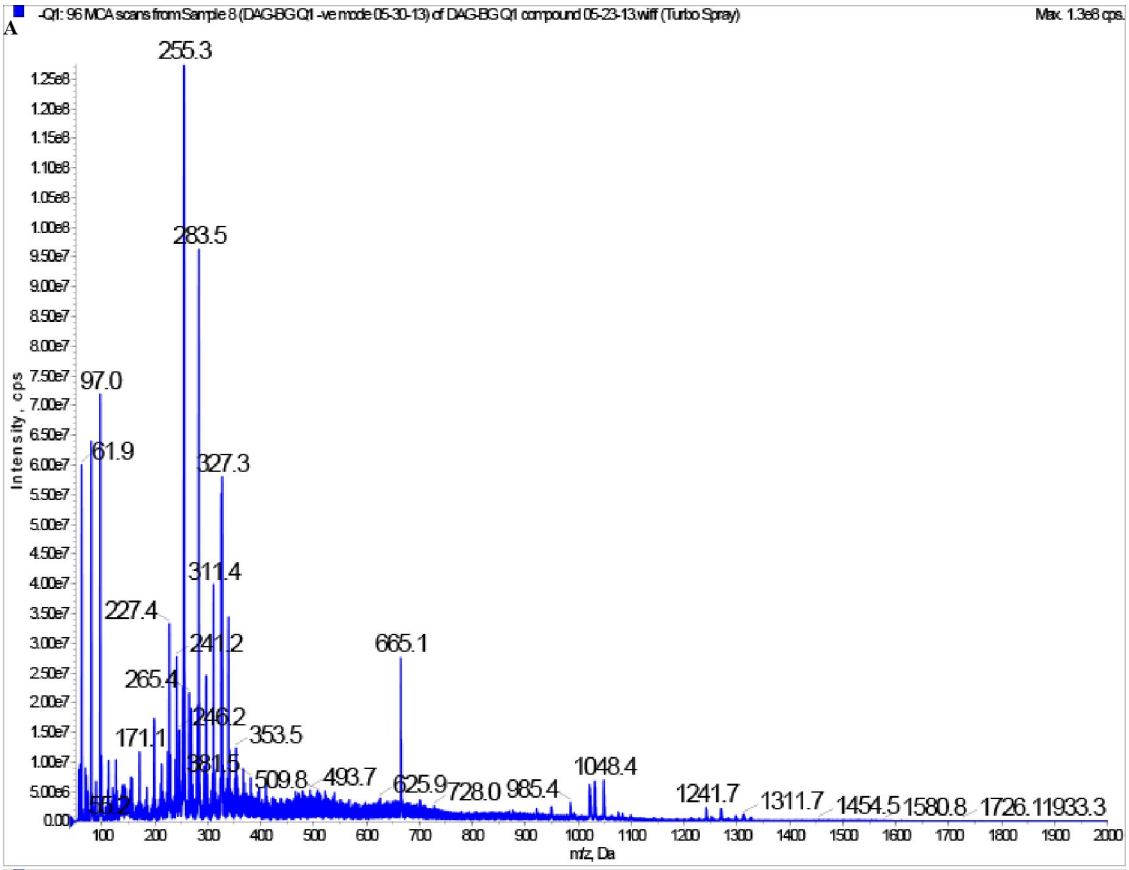
A
-Q1: 96 MCA scans from Sample 8 (DAG-BG Q1 -ve mode 05-30-13) of DAG-BG Q1 compound 05-23-13.wiff (Turbo Spray)
Max. 1.3e8 cps.
Intensity, cps
m/z, Da
255.3
283.5
97.0
61.9
327.3
311.4
227.4
241.2
665.1
265.4
246.2
353.5
171.1
381.5
509.8
493.7
625.9
728.0
985.4
1048.4
1241.7
1311.7
1454.5
1580.8
1726.1
1933.3

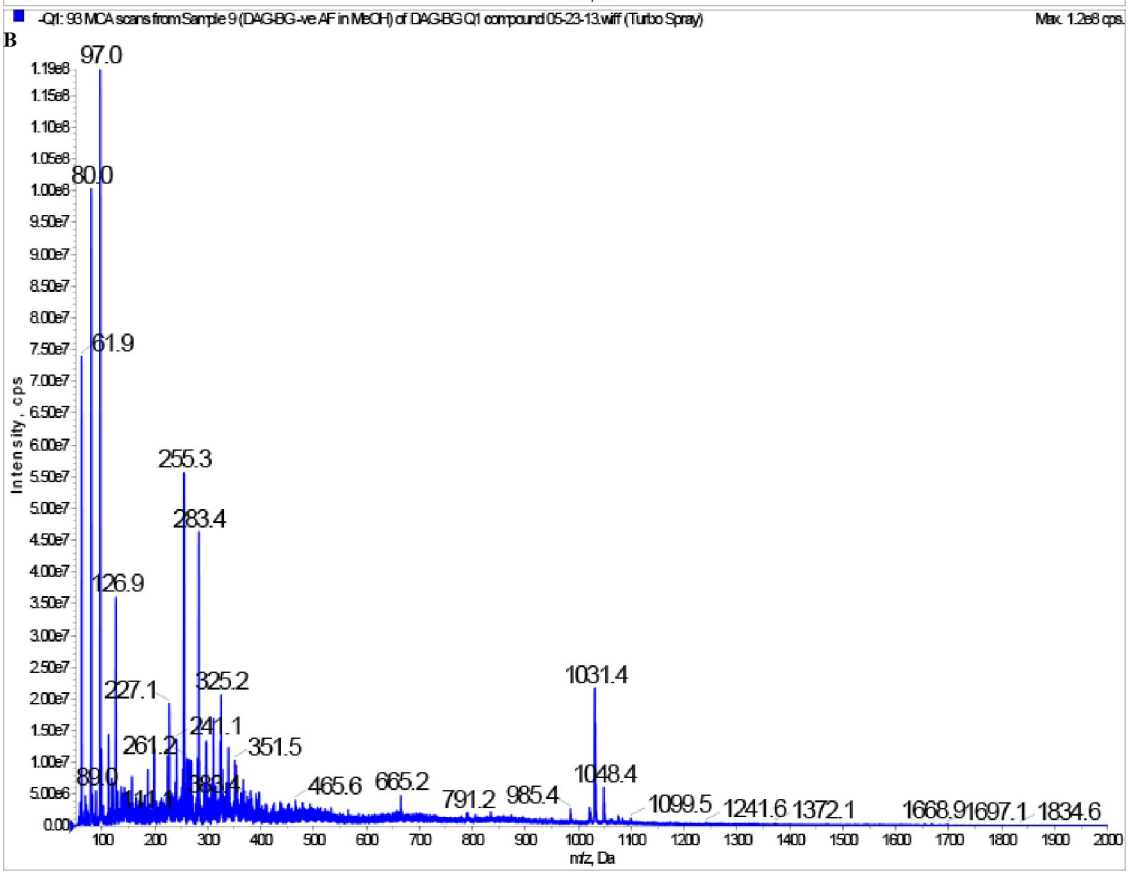
B
-Q1: 93 MCA scans from Sample 9 (DAG-BG -ve AF in MeOH) of DAG-BG Q1 compound 05-23-13.wiff (Turbo Spray)
Max. 1.2e8 cps.
Intensity, cps
m/z, Da
97.0
80.0
61.9
255.3
283.4
126.9
325.2
1031.4
227.1
241.1
261.2
351.5
1048.4
89.0
111.1
381.4
465.6
665.2
791.2
985.4
1099.5
1241.6
1372.1
1668.9
1697.1
1834.6

Figure 237. The scan of compound 4 in negative ion mode shows no additional peaks over solvent alone. (A) AB Sciex 4000 Q Trap spectrum of the probe (100 µg per mL) in 53 mM ammonium formate in methanol in negative ion mode. **(B)** AB Sciex 4000 Q Trap spectrum of 53 mM ammonium formate in methanol in negative ion mode.

I was therefore left with two possible conclusions. The first hypothesis was that the Best group had sent us not compound **4** but rather the molecule shown in Figure 236**A**, which would explain the predominant peak of 987.5 Da (Figure 233 and Figure 234) whose product ion is 745.7 Da (Figure 236). Challenges to this hypothesis include the fact that the Best group reported MALDI spectra of the probe they sent us to be consistent with the predicted molecular weight, the predicted molecular weight plus a proton, and the predicted molecular weight plus a sodium ion, as well as the fact that the methanol plus ammonium formate also gave a predominant peak of 987.5 Da (Figure 235**A**) whose product ion is 745.7 Da. In order to reconcile this hypothesis, then, not only would the Best lab had to have mixed up the samples when they did the MALDI, but we would also have to have mixed up the samples when we did the LC/MS/MS of the methanol plus ammonium formate solvent only scan. Furthermore, because I am not familiar with the synthesis of compound **4**, the alternate structure may or may not be a plausible alternative product.

The second hypothesis was that the probe sent to us started off as compound **4**, but, in the time between when the Best group synthesized it and the time we subjected it to LC/MS/MS, something happened to it, consistent with its being a photoreactive molecule, which would explain the Best group's MALDI spectra. Challenges to this hypothesis include the fact that we did not detect any LC/MS/MS peaks of 1556, as would be expected if two molecules of compound **4** crosslinked to one another, and that I did not see any smearing on the TLC plate (Figure 232), as might be predicted if the

compound had linked to itself many times, or indeed any major differences between how the molecule migrated on TLC shortly after it arrived (Figure 222) as compared to how it migrated at the time we were unable to detect a 778 Da peak by LC/MS/MS (Figure 232), as might be predicted for chemical modification. On the other hand, as we had previously observed, small changes in humidity may affect how molecules migrate on TLC, making the different TLC plates difficult to compare.

I therefore wrote to the Best group asking them to send us fresh compound **4**, in case something had happened to the second batch. They very kindly sent us a third batch, once again confirming the molecular weight by MS (Figure 238). This batch arrived wrapped in aluminum foil, but also included what appeared to be dust, hair, and broken glass in the vial. I once again confirmed the concentration and migration pattern by TLC. As before, compound **4** migrated as a single spot whose total intensity was consistent with that of the predicted molecular weight (Figure 239), consistent with the batch not being a smear of probe crosslinked to itself. Unlike the previous batches (Figure 147 and Figure 222), however, which migrated faster than the DOG standards, this batch of compound **4** migrated more slowly than the DOG standards (Figure 239), even though the same solvent systems, lot number of DOG, and brand of TLC plate were used. This discrepancy in TLC migration might be evidence that this batch of compound **4** is, in fact, a different molecule from the previous batches, consistent with the first hypothesis aired in the penultimate paragraph; on the other hand, it might merely reflect inconsistencies in humidity and how much water the plate had absorbed.

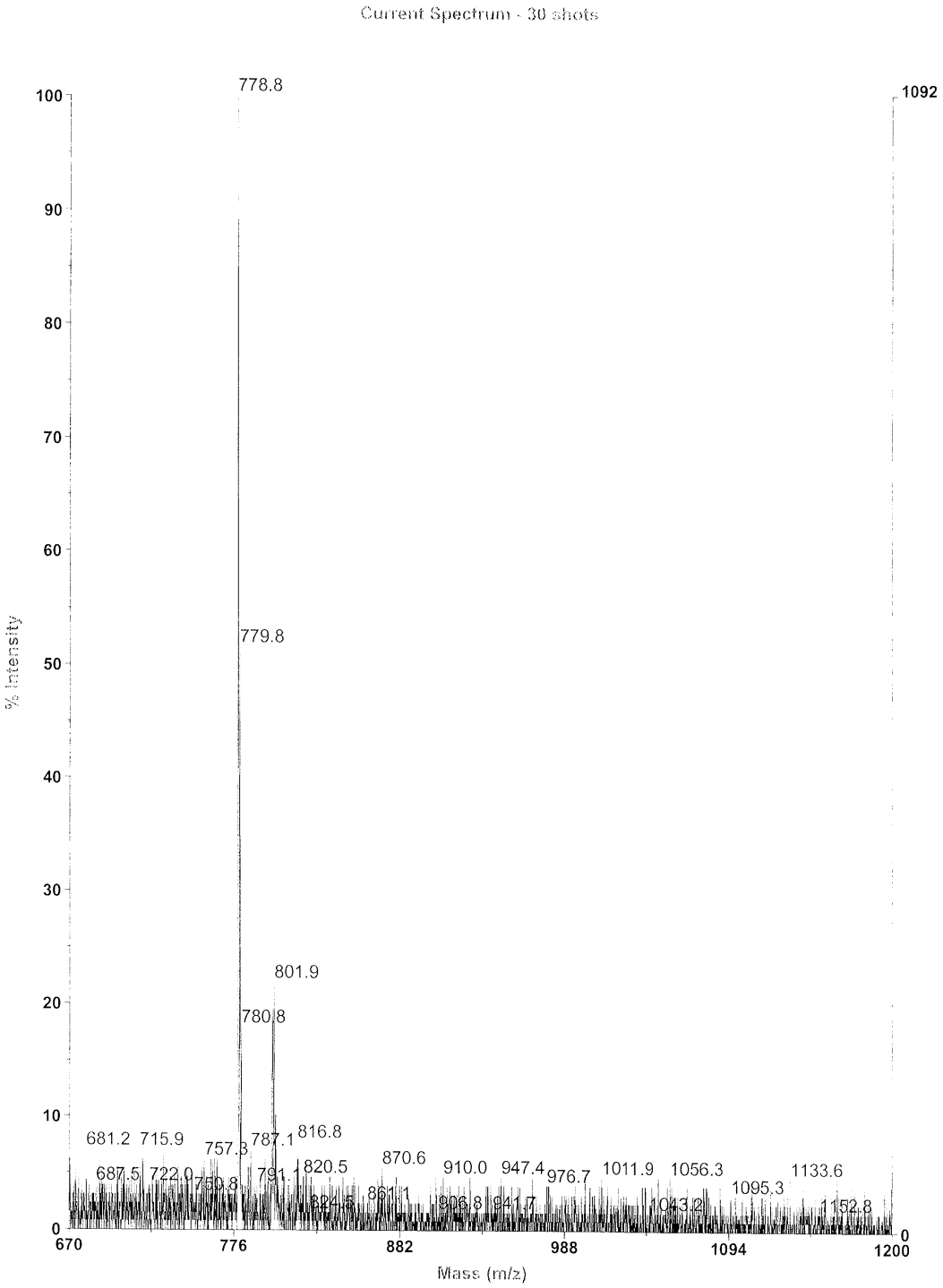

Figure 238. The mass spectrum of the third batch of compound 4, as measured by the Best lab, is consistent with its predicted molecular weight. MS spectra performed by Best group on the third batch of compound **4**.

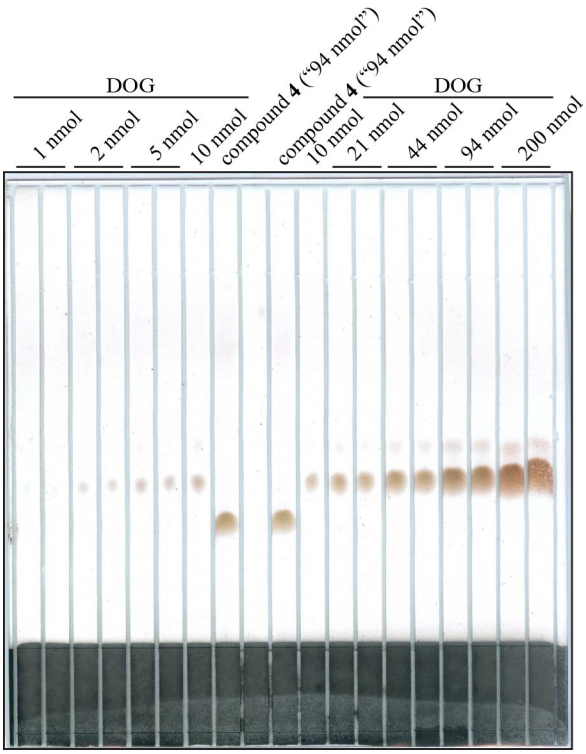

Figure 239. The third batch of compound 4 migrates differently on TLC than the previous two batches, but its concentration is consistent with what was advertised. TLC of the third batch of compound 4 as compared to DOG standards, run in an 85:15:5::toluene:chloroform:methanol solvent system, dried, sprayed with 40% (v/v) sulfuric acid, and charred.

In order to confirm the molecular weight of the new batch of compound **4**, I submitted it to LC/MS/MS, as I had with the previous batch. This time, a peak of 779.0 Da, consistent with the predicted molecular weight of 778 Da, was easily detectable in positive ion mode, and the corresponding peak of 777 Da was easily detectable in negative ion mode (Figure 240). The 779.0 Da peak gave a product ion of 536.7 Da (Figure 241**A**), consistent with the predicted molecular weight of 536.7 Da of not one but two plausible fragment structures (Figure 241**B**). In fact, these are the very fragments that correspond to the fragments proposed for the second batch of compound **4** shown in Figure 236**C**, possibly providing more evidence that, if these kinds of molecules are likely to fragment at the ether linkage, the second batch of compound **4** really was the

molecule shown in Figure 236**A**. From the LC/MS/MS spectra of the third batch of compound **4**, though, I concluded that this batch, was, indeed, predominantly compound **4**, and that under at least these LC/MS/MS conditions, it fragmented to produce a 536.7 Da piece. This piece retains the benzophenone moiety, so a peptide that had been modified by compound **4** might, after LC/MS/MS, be modified by a mass addition of 536.7 Da, not 778 Da. I therefore asked for the data we had already collected, from the mass spectrometry experiment shown in Figure 231**B**, to be searched for peptides with a shifted mass of 536.7 Da, in case the second batch really was compound **4** and just had something happen to it between that experiment and the LC/MS/MS shown in Figure 233 - Figure 237. No such mass shifts were found. In case the second batch of compound **4** was really the structure shown in Figure 236**A**, I also asked for the data to be searched for a peptides with a shifted mass of either 985.7 Da, the size of the structure with the additional keto-benzophenone, and 744.4 Da, the size of the product ion. No such mass shifts were found.

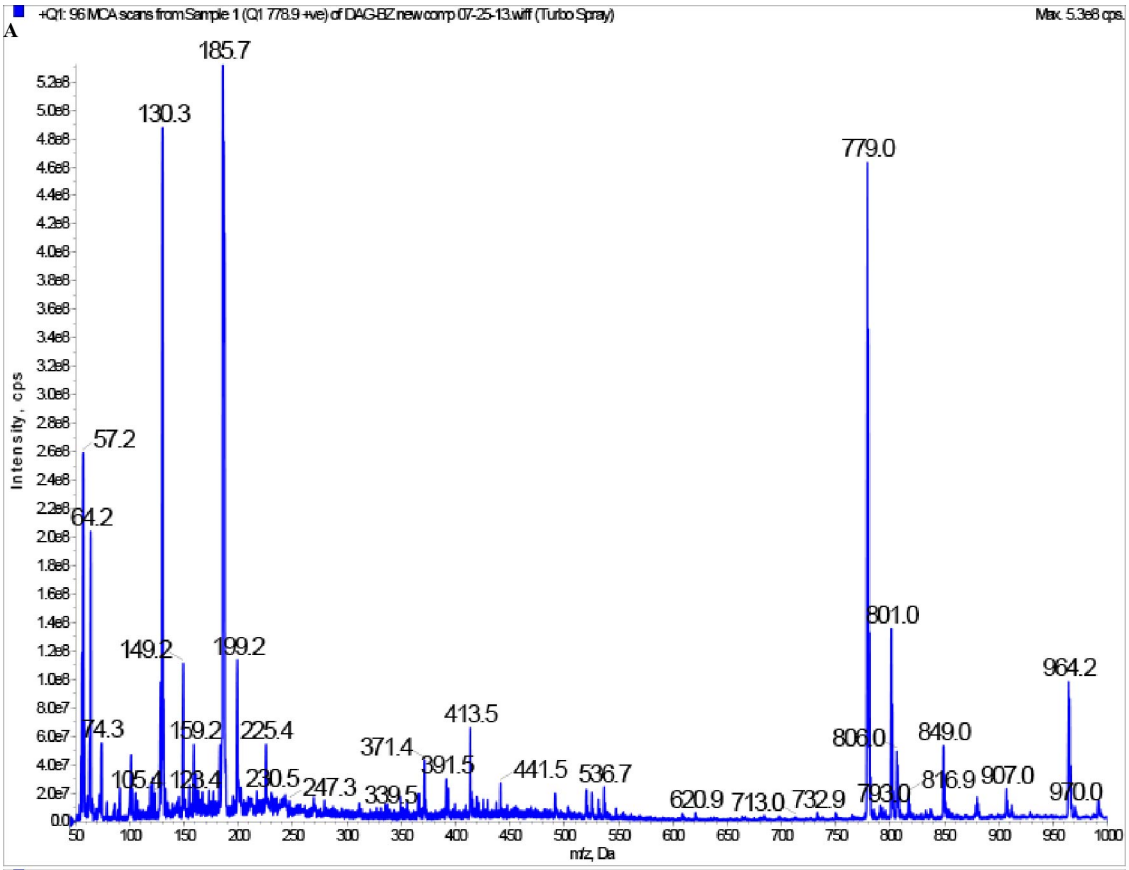
A
+Q1: 96 MCA scans from Sample 1 (Q1 778.9 +ve) of DAG-BZ new comp 07-25-13.wiff (Turbo Spray)
Max. 5.3e8 cps.
Intensity, cps
m/z, Da
185.7
130.3
779.0
57.2
64.2
801.0
149.2
199.2
964.2
413.5
74.3
159.2
225.4
371.4
806.0
849.0
891.5
441.5
536.7
105.4
128.4
230.5
247.3
339.5
620.9
713.0
732.9
793.0
816.9
907.0
970.0

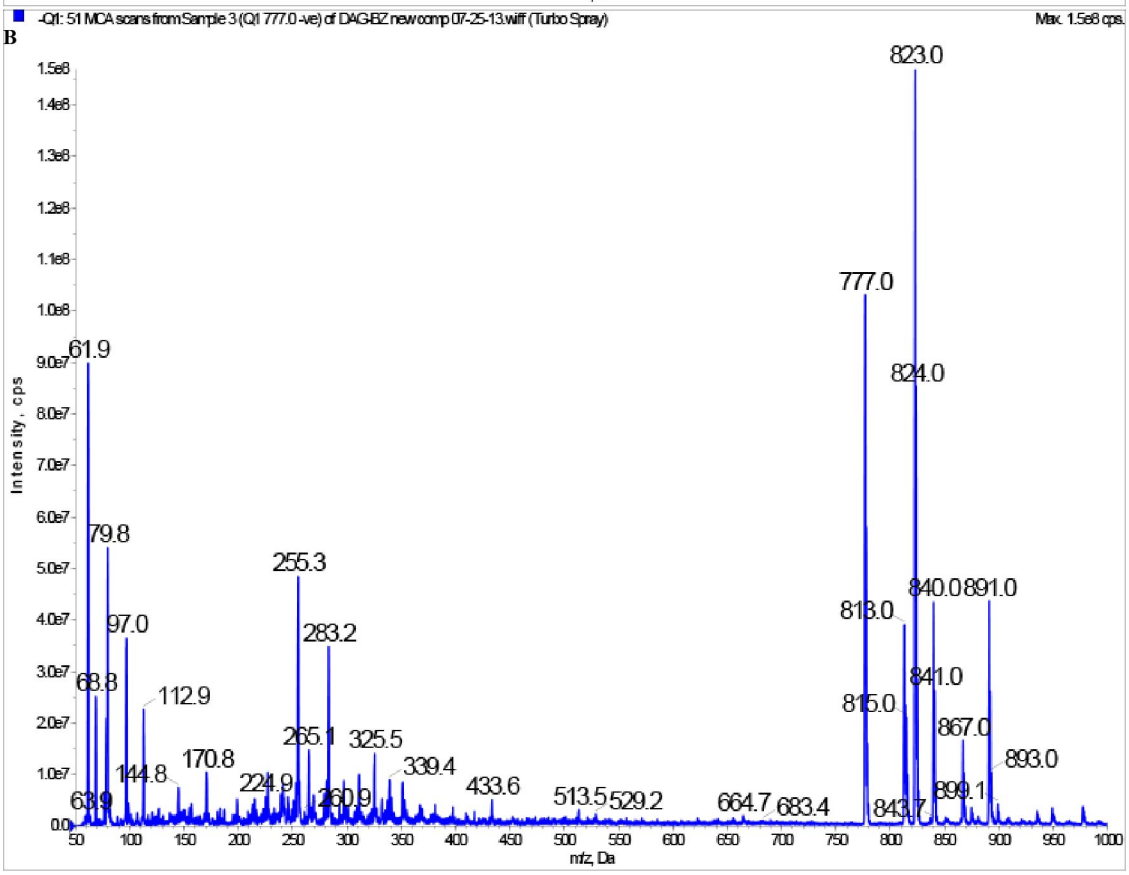
B
-Q1: 51 MCA scans from Sample 3 (Q1 777.0 -ve) of DAG-BZ new comp 07-25-13.wiff (Turbo Spray)
Max. 1.5e8 cps.
Intensity, cps
m/z, Da
823.0
777.0
61.9
824.0
79.8
255.3
840.0
891.0
813.0
97.0
283.2
841.0
68.8
112.9
815.0
867.0
265.1
325.5
893.0
170.8
339.4
144.8
224.9
433.6
899.1
63.9
260.9
513.5
529.2
664.7
683.4
843.7

Figure 240. The third batch of compound 4 produces peaks in positive and negative ion mode in LC/MS/MS consistent with its predicted molecular weight. AB Sciex 4000 Q Trap spectrum of the third batch compound 4 (66.7 µg per mL) in 2:l::methanol:chloroform in **(A)** positive ion mode, and **(B)** negative ion mode.

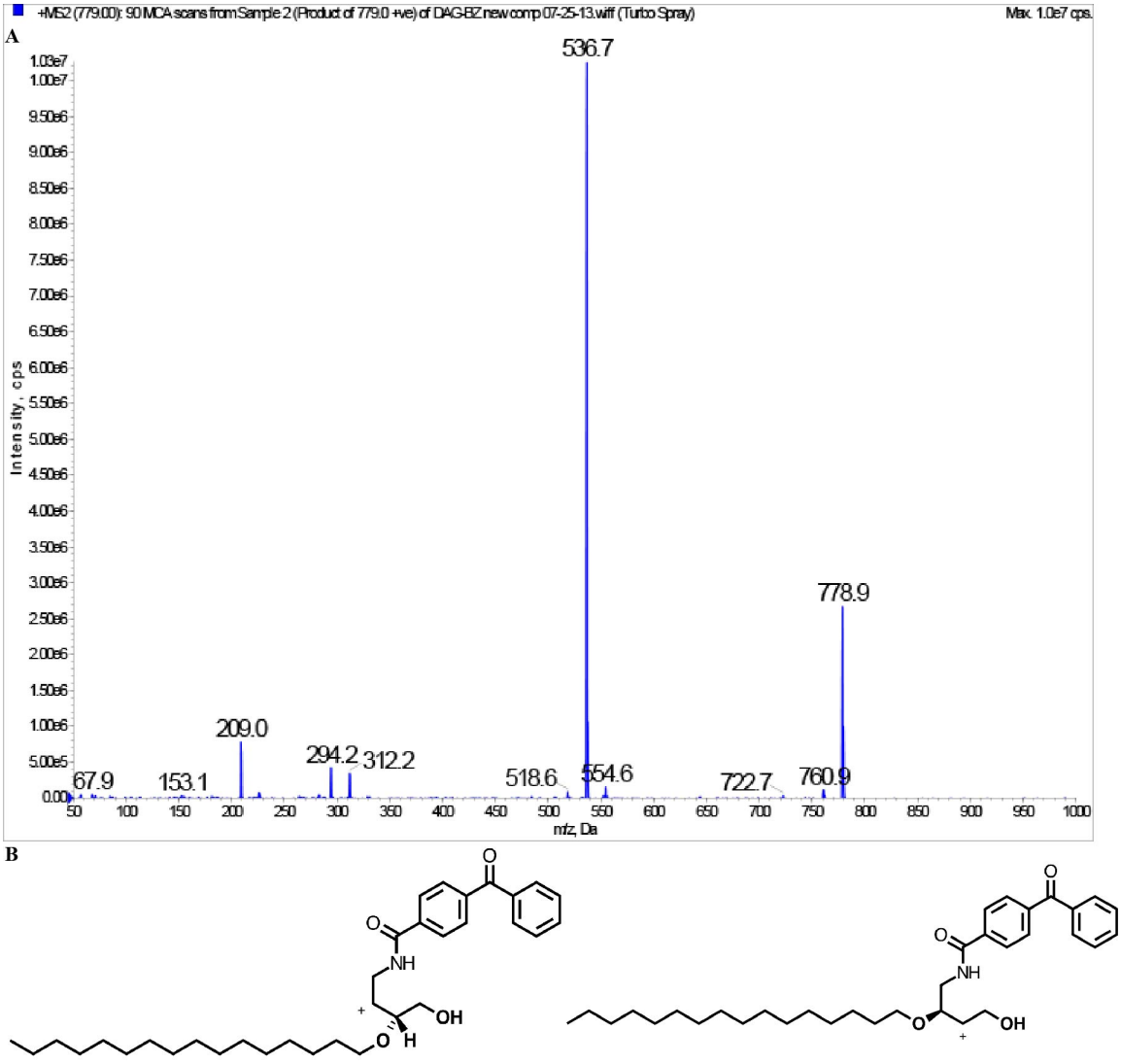

Figure 241. The product ion of the 779 Da LC/MS/MS peak of the third batch of compound 4 is consistent with two plausible fragment structures. (A) The product ion from the 779 Da peak shown in **Figure 240**A. **(B)** Proposed fragment structures for the product ion shown in (A).

There are a number of possible explanations for why we did not observe the mass shifts in question. One could be, of course, that compound **4** is not, in fact, covalently attaching to DGK-theta, even though the probe-, UV-, and time-dependent inactivation of DGK-theta, as well as the disproportionate absence of certain peptides in the crosslinked

vs. control samples, are all consistent with such covalent attachment. Another could be that compound **4** is attaching to part of the protein from which peptides were not detected by LC/MS/MS: the amino acid coverage is, after all quite low. Another explanation could be that the covalent attachment of compound **4** (or a fragment thereof) causes the covalently modified peptides to be too hydrophobic to elute from the Magic C18AQ column, and thus the peptides never made it into the mass spectrometer. Yet another explanation could be that the modified peptides were filtered out of the collected data because their isotopic distribution was insufficiently peptide-like.

I thought that perhaps the process of incorporating compound **4** into liposomes might chemically modify it (by oxidation, etc.) (which would mean the mass shift we would expect to see after photoaffinity labeling might be different than the mass shift produced by LC/MS/MS of compound **4** dissolved into 2:l::methanol:chloroform), but I also thought that the standard composition of liposomes used in the activity assay (2:1::POPE:POPC) would complicate the MS spectrum beyond interpretation. I therefore tried to make 100% compound **4** liposomes from the third batch for LC/MS/MS analysis: however, the lipid film of compound **4** never uniformly resuspended into the liposome resuspension buffer (50 mM HEPES, 100 mM NaCl, pH 7.5, 1 mM DTT), even after continuously bath sonicating for more than two hours. I was therefore unable to make 100% compound **4** liposomes, so was unable to perform LC/MS/MS on compound **4** in the chemical environment more relevant to the protein crosslinking experiments.

When I tested whether this third batch of compound **4** still produced probe- and UV-dependent inactivation of DGK, however, I did not observe the probe- and UV-dependent inactivation of DGK-theta I had observed with the previous two batches

(Figure 242). I had made the sample volume in this experiment large enough that I could remove aliquots to look for a potential gel-shift, by both immunoblotting and silver staining, and to repeat the mass spectrometry, looking for peptide shifts of the appropriate size. As such, I had irradiated at a high concentration and then diluted for the assay, as in the experiment shown in Figure 224. However, I used larger volumes for the dilution, which may explain while the uncertainty is lower here than in Figure 224. Figure 224 was too noisy to be conclusive; contrariwise, the uncertainty in Figure 242 is low enough that I can say with confidence that this batch of compound **4** did *not* inactivate DGK-theta in a probe- and UV-dependent way. In this experiment, compound **4** appeared to activate DGK-theta, as compounds **1** (Figure 136) and **3** did (Figure 143), but as I had not observed with the previous batches of compound **4** (Figure 148, Figure 218-Figure 221, Figure 223; some of those might be complicated by the fact that ambient light may have been inactivating DGK-theta and balancing any activation by compound **4**, but in Figure 220 on I took precautions to protect the liposomes from sunlight). Thinking perhaps that the pipets had lost their calibration, and the different samples had different volumes of diluted irradiated enzyme, I checked the calibration of my pipets. I found that while the calibration of the P2 pipet was off, it was only off by about 10% (Table 3), which would not be enough to account either for why compound **4** failed to inactivate DGK-theta in a UV-dependent way (previous batches inactivated DGK-theta approximately 50%), or why compound **4** now appeared to activate DGK-theta by approximately 100%.

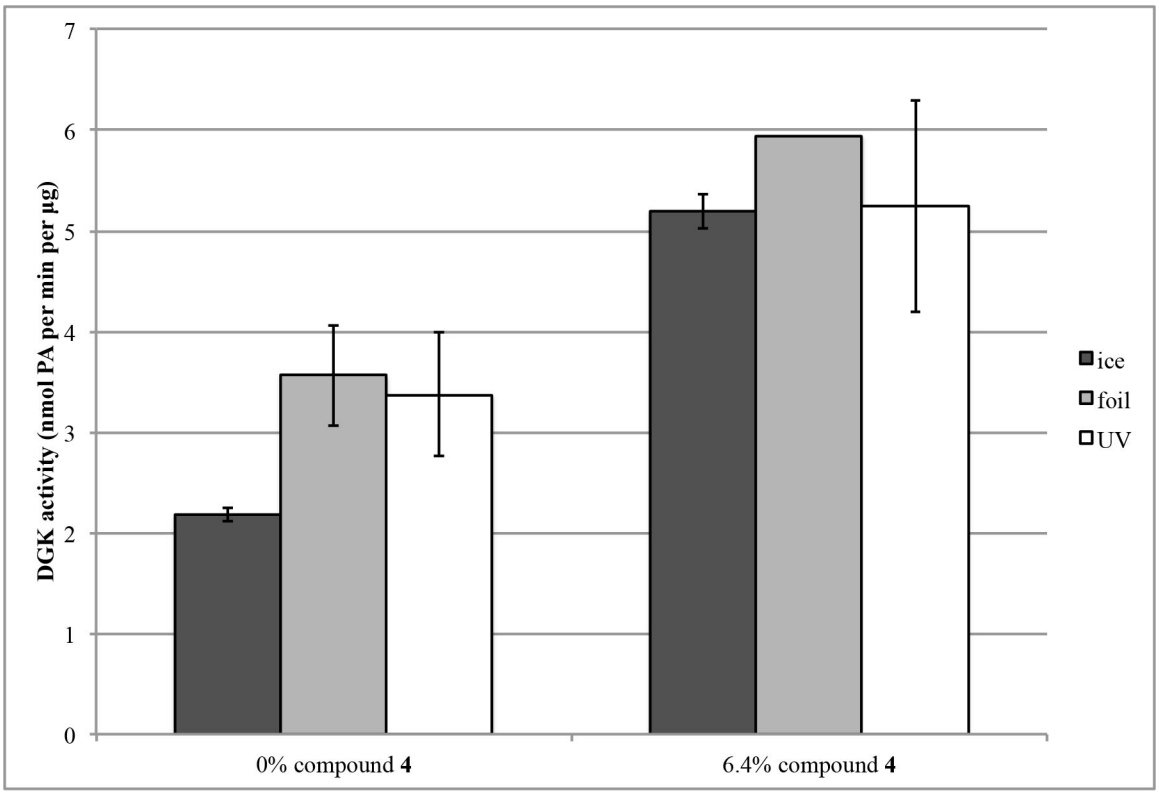

Figure 242. The third batch of compound 4 does not show probe- and UV-dependent inactivation of purified DGK-theta under the conditions tested. DGK activity assay. I first preincubated purified DGK-theta in preincubation buffer (50 mM HEPES, pH 7.5, 0.005% (v/v) DDM, 0.3 µM histone H1, 1 mM DTT, 996 pg per µL purified DGK-theta, 17% (v/v) glycerol) on ice for ten minutes. I then diluted into incubation buffer (7.5 mM liposomes (2:1::POPE:POPC, 20 mol% POPS, and the indicated concentration of compound **4**), 50 mM HEPES, pH 7.5, 100 mM NaCl, 0.005% (v/v) DDM, 0.1 µM histone H1, 1 mM DTT, 0.1 mg per mL ovalbumin, 1 mM ATP, 1.5 mM $MgCl_2$, 307 pg per µL purified DGK-theta, 5.1% (v/v) glycerol) and incubated for thirty minutes, rocking at room temperature, protected from light. I then placed the samples either on ice or in a 96-well plate, and irradiated the samples with a 360 nm lamp for thirty minutes on an ice bucket at 4°C ("foil" samples had aluminum foil between the samples and the lamp). After irradiation, I returned the samples to Eppendorfs, and measured the volume to account for concentration of DGK due to evaporation. I then diluted into dilution buffer (50 mM HEPES, pH 7.5, 0.5 µM histone H1, 0.005% (v/v) DDM, 1 mM DTT, 1 mM dilution liposomes (53.3:26.7:20::POPE:POPC:POPS:DOG), 0.003 mg per mL ovalbumin, 29 µM ATP, 43 µM $MgCl_2$, 11 mM NaCl, 8.8 pg per µL purified DGK-theta, 0.15% (v/v) glycerol). The final DGK activity assay reaction included 5 mM substrate-containing liposomes (56.7:28.3:9:6::POPE:POPC:POPS:DOG), 43 µM crosslinking liposomes, 43 µM filler liposomes (such that the final liposome composition in the reactions were all the same), 50 mM HEPES, pH 7.5, 98 mM NaCl, 1 mM DTT, 0.005% (v/v) DDM, 1.5 mM $MgCl_2$, 0.8 mM ATP, 35.7 Ci per mmol [γ-^{32}P]-ATP, 0.1 µM histone H1, 0.0006 mg per mL ovalbumin, 1.8 pg per µL purified DGK-theta, and 0.03% (v/v) glycerol, and proceeded for thirty minutes at 37°C. In triplicate, except for the 6.4% compound 4 plus foil sample, where I accidentally scrapped the silica of the TLC plate from two of the lanes into the same vial, and which I have therefore omitted, and am showing the remaining singlicate. Mean ± SD.

Pipet	Volume measured (µL)	Mass (g)	Discrepancy (%)
P1000	1000	1.0125	1.25
P200	200.0	0.1989	-0.55
P100	100.0	0.1008	0.8
P20	20.00	0.0199	-0.5
P2	2.000	0.0022	10

Table 3. Errors in pipet calibration are not large enough to explain why the third batch of compound 4 did not inactivate purified DGK-theta in a probe- and UV-dependent way. Pipet calibration. I measured the indicated volume of ddH2O onto a weighboat and measured its mass using an analytical balance.

I therefore repeated the crosslinking experiment to see whether the results were anomalous. As mentioned, the experiment shown in Figure 242 required more concentrated protein, so I had used a new batch of purified DGK-theta. I therefore compared the two batches of DGK-theta, and the second and third batch of compound **4**. I also used larger volumes to reduce any variance from pipetting. I found that while the new batch of enzyme had a greater specific activity than the old batch, neither one showed UV- and probe-dependent inactivation, even for the second batch of compound **4** (Figure 243). Nor did I observe activation, as I did in the previous experiment (Figure 242). However, both also showed inactivation in the foil control (Figure 243), suggesting the possibility that either or both batches of probe might be inactivating the enzyme in a UV-dependent way that is masked by the inactivation caused by incubating the enzyme under the UV lamp, with or without foil. As previously mentioned, variables that might be contributing to this inactivation under foil include the distance between the lens of the lamp and the 96-well plate (by a few centimeters at most), the angle of the lamp (by several degrees at most), the volume of sample in the well (although I measured the

volumes before and after irradiation, and I took the concentration caused by evaporation into account when calculating the specific activity of the enzyme), the time that DGK was thawed before it was irradiated, and the time that elapsed between the DGK was irradiated and the time it was assayed. As previously mentioned, future directions include testing the reducing agent requirement explicitly, as well as acquiring a UV LED, and testing whether using that as a photon source reduces inactivation of DGK.

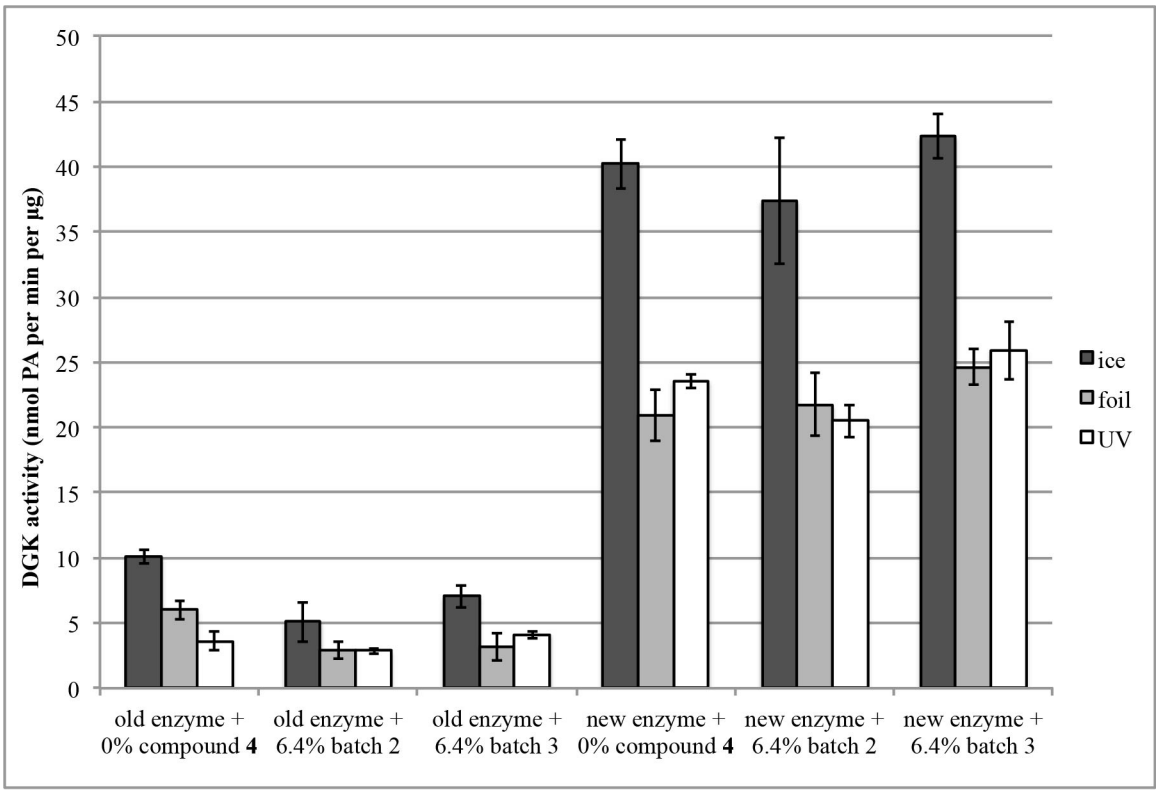

Figure 243. Batch 3 of compound 4 does not inactivate either batch of purified DGK-theta in a UV- and probe-dependent way, but neither does batch 2 anymore. DGK activity assay. 227B and 323 are two different batches of purified DGK-theta. I incubated purified DGK-theta in preincubation buffer (for 227B, 48 pg per µL purified DGK and 1.2% (v/v) glycerol; for 323, 120 pg per µL purified DGK and 2.0% (v/v) glycerol) on ice for ten minutes. I then diluted into irradiation buffer (0.4% (v/v) glycerol, 0.005% (v/v) DDM, 1 mM DTT, 0.5 µM histone H1, 50 mM HEPES, pH 7.4, 100 mM NaCl, 0.1 mg per mL ovalbumin, 1 mM ATP, 1.5 mM $MgCl_2$, 7.5 mM liposomes (2:1::POPE:POPC, 20 mol% POPS, and the indicated concentration of the indicated batch of compound **4**)), and incubated for thirty minutes, rocking at room temperature, protected from light. I then placed the samples either on ice or in a 96-well plate, and irradiated the samples with a 360 nm lamp for thirty minutes on an ice bucket at 4°C ("foil" samples had aluminum foil between the samples and the lamp). After irradiation, I returned the samples to Eppendorfs, and measured the volume to account for concentration of DGK due to evaporation. The final DGK assay reaction mixture included 5 mM substrate-containing liposomes (56.7:28.3:9:6::POPE:POPC:POPS:DOG),

1.5 mM incubation liposomes, 1.5 mM filler liposomes (such that the final liposome composition in the reactions were all the same), 50 mM HEPES, pH 7.4, 100 mM NaCl, 1.5 mM $MgCl_2$, 1 mM ATP, 20.9 Ci per mmol [γ-^{32}P]-ATP, 0.1% (v/v) glycerol, 0.005% (v/v) DDM, 0.1 μM histone H1, 0.02 mg per mL ovalbumin, 1 mM DTT, and 3.0 pg per μL purified DGK, and proceeded for 30 minutes at 37°C. In triplicate: mean ± SD.

The 365 nm peak wavelength UV LED flashlight did not inactivate purified DGK-theta even after sixty minutes of irradiation (Figure 116), but neither did it provide probe- and UV-dependent inactivation of purified DGK-theta using the third batch of compound **4**. One possible explanation for why Figure 244 does not reproduce the results of Figure 218, Figure 220, Figure 221**B**, Figure 223, Figure 225, and Figure 231**A** could be that the UV LED flashlight does not produce sufficient photon flux. Another explanation is that batch 2 and batch 3 are in fact different molecules (an interpretation supported by Figure 147, Figure 222, Figure 233, Figure 236, and Figure 239-Figure 241), and the molecule whose structure is shown in Figure 236**A** is able to probe-, UV-, and time-dependently inactivate DGK, while compound **4** is not. In order to distinguish between these two explanations, the next logical experiment would be to test whether the UV LED flashlight could reproduce probe- and UV-dependent inactivation of purified DGK-theta using the second batch of compound **4**.

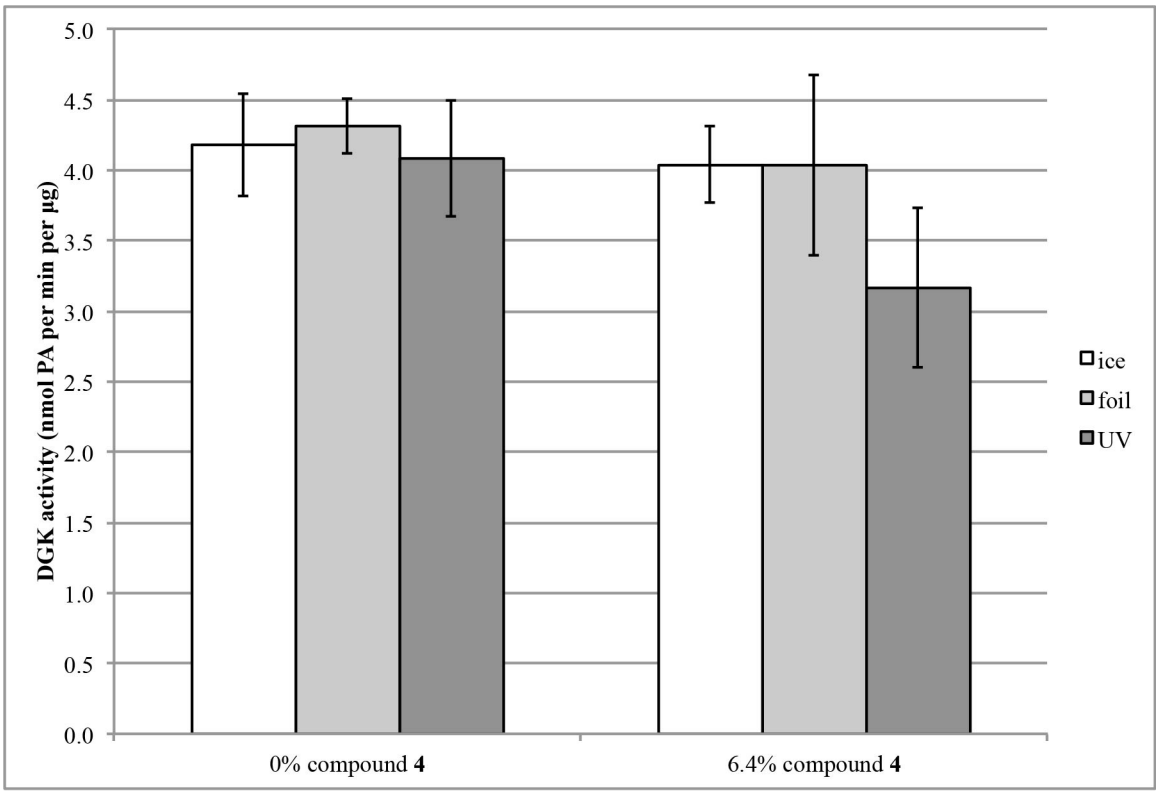

Figure 244. Batch 3 of compound 4 does not cause probe-, UV LED-dependent inactivation of purified DGK-theta. DGK activity assay. I incubated purified DGK-theta in preincubation buffer (50 mM HEPES, pH 7.5, 0.005% (v/v) DDM, 0.5 µM histone H1, 3 mM BME, 176 pg per µL purified DGK, 5.1% (v/v) glycerol) on ice for ten minutes. I then diluted into irradiation buffer (35 pg per µL DGK, 1.0% (v/v) glycerol, 0.005% (v/v) DDM, 3 mM BME, 0.1 µM histone H1, 50 mM HEPES, pH 7.4, 100 mM NaCl, 0.1 mg per mL ovalbumin, 1 mM ATP, 1.5 mM $MgCl_2$, 7.5 mM liposomes (2:1::POPE:POPC, 20 mol% POPS, and the indicated concentration of the third batch of compound **4**)), and incubated for thirty minutes, rocking at room temperature, protected from light. I then placed the samples either on ice or in a 96-well plate, and irradiated the samples with a 365 nm peak wavelength LED flashlight for sixty minutes at room temperature ("foil" samples had aluminum foil between the samples and the flashlight). After irradiation, I returned the samples to Eppendorfs, and measured the volume to account for concentration of DGK due to evaporation. The final DGK assay reaction mixture included 5 mM substrate-containing liposomes (56.7:28.3:9:6::POPE:POPC:POPS:DOG), 1.5 mM incubation liposomes, 1.5 mM filler liposomes (such that the final liposome composition in the reactions were all the same), 50 mM HEPES, pH 7.4, 100 mM NaCl, 1.5 mM $MgCl_2$, 1 mM ATP, 10.8 Ci per mmol [γ-^{32}P]-ATP, 0.2% (v/v) glycerol, 0.005% (v/v) DDM, 0.1 µM histone H1, 0.02 mg per mL ovalbumin, 3 mM BME, and 7.0 pg per µL purified DGK, and proceeded for 30 minutes at 37°C. In triplicate: mean ± SD.

If the UV LED flashlight merely has insufficient photon flux, another strategy to solve the foil inactivation problem (using a homemade circuit to allow a higher amplitude of illumination from the LED, perhaps) will have to be worked out. In that case, if the third batch of compound **4** does produce probe- and UV-dependent inactivation of DGK-

theta, as the previous batches did, future directions include repeating LC/MS/MS of this crosslinked protein and searching for mass shifts of the covered peptides. If no such shifted peptides are found, future directions include finding conditions to improve amino acid coverage of crosslinked DGK-theta, such as by digesting with more proteases in addition to trypsin, optimizing the elution of covalently modified peptides from the Magic C18AQ column, and searching all of the data and not filtering for peptide-like isotopic distributions (seeing as a peptide covalently modified with compound **4** or a fragment thereof might no longer be peptide-like). If still no such peptides are found, the intriguing possibility remains that perhaps the structure shown in Figure 236**A** may photoaffinity label DGK-theta while compound **4** may not. In that case, the compound shown in Figure 236**A** could be synthesized and tested for photoaffinity labeling DGK-theta explicitly.

Photoaffinity Labeling Conclusions

SLV pulldown and TX-114 partitioning are not promising methods for assessing photoaffinity labeling of DGK, due in part to purified DGK's propensity to aggregate. Compounds **1** and **3** did not provide probe- and UV-dependent inactivation of purified DGK, even under the same conditions under which they were able to act as substrates, suggesting that they were getting into the active site, but that the benzophenone moiety might not have been properly oriented to crosslink to the enzyme. The first two batches of compound **4**, with a shorter linker between the DAG-like moiety and the benzophenone, were able to give probe-, UV-, and time-dependent inactivation of purified DGK-theta, as would be expected if they were photoaffinity labeling the enzyme. Enzyme crosslinked with the second batch of compound **4**, when subjected to

LC/MS/MS, exhibited disproportionately absent peptides in the crosslinked vs. the control sample, as would be expected if the probe were photoaffinity labeling the enzyme. No peptides shifted by the predicted molecular weight were found. When the second batch of compound **4** was subjected to LC/MS/MS to determine its fragmentation pattern, the size and fragmentation pattern were inconsistent with the predicted structure. The third batch of compound **4** did give the predicted size and fragmentation pattern, but migrated differently on TLC than the first two batches did, suggesting that it was perhaps a different molecule. I was unable to find probe-, UV-dependent enzymatic inactivation using the third batch of compound **4**, but at this point I was experiencing difficulties with the UV lamp and was likewise unable to reproduce probe-, UV-dependent enzymatic inactivation using the second batch of compound **4**. Future directions include testing whether, under conditions that reproduce probe-, UV-dependent enzymatic inactivation using batch 2 of compound **4**, batch 3 likewise reproduces probe-, UV-dependent enzymatic inactivation, and, for either batch, using LC/MS/MS to identify the crosslinked residue(s) on DGK-theta in order to gain insight into which residues are near diglyceride binding sites on its surface.

Chapter 9: Conclusions

Constructs of the catalytic domain of *S. scrofa* DGK-alpha could be expressed in *Escherichia coli* and extracted, refolded, and purified from inclusion bodies, but when subjected to analytical gel filtration chromatography, these constructs eluted in the void volume in what appeared to be microscopic aggregates unsuitable for x-ray crystallography. Adding glutathione S-transferase, thioredoxin, or maltose binding protein as N-terminal fusion tags did not improve the constructs' solubility. Coexpressing with bacterial chaperones increased the yield in the supernatant after high-speed centrifugation, but the protein still eluted in the void upon analytical gel filtration chromatography. DGK constructs expressed in insect cells were likewise insoluble and unsuitable for x-ray crystallography. Even DGK constructs expressed in mammalian cells likewise eluted in the void upon analytical gel filtration chromatography, suggesting that they were aggregating and unsuitable for x-ray crystallography. This tendency of overexpressed recombinant eukaryotic DGK to aggregate may be providing insight into its structure as an interfacial enzyme.

Loss of enzymatic activity of purified DGK could be mitigated by including 50% (v/v) glycerol and storing at -80°C, and by including detergent, lipid, and protein activators following thawing.

Certain polybasic proteins and substrate analogs increase the *in vitro* enzymatic activity of purified DGK, whereas hirudin decreases its activity under certain conditions. DGK is able to use certain diglyceride analogs as substrates.

Bimolecular fluorescence complementation was unable to show whether DGK-theta dimerized or interacted with tau when overexpressed in mammalian cells.

Thrombin was able to digest DGK-theta after folding, but none of the washing conditions tested were able to separate the digested fragments, so while digestion with thrombin appeared to activate DGK-theta, whether the activation was due to relief from auto-inhibition or some other effect from the thrombin could not be resolved.

SLV pulldown and TX-114 partitioning are not promising methods for assessing photoaffinity labeling of DGK, due in part to purified DGK's previously mentioned propensity to aggregate. Photoaffinity labels were able to enzymatically inactivate purified DGK-theta in a probe-, ultraviolet-, and time-dependent way, but only when the linker between the substrate analog moiety and the photoactivatable moiety was sufficiently short. Mass spectrometry studies were unable to detect peptides shifted by the predicted molecular weight of the photoaffinity labels or their fragments. This work should guide future studies of the structure of eukaryotic DGKs, interfacial enzymes, and protein-lipid interactions.

References

1. Petro, E. J. & Raben, D. M. Bacterial expression strategies for several Sus scrofa diacylglycerol kinase alpha constructs: solubility challenges. *Sci. Rep.* **3** Article number: 1609, doi:10.1038/srep01609**,** (2013).
2. Guo, Y., Rebecchi, M. & Scarlata, S. Phospholipase Cbeta2 binds to and inhibits phospholipase Cdelta1. *J. Biol. Chem.* **280,** 1438–1447 (2005).
3. Tu-Sekine, B. & Raben, D. M. Dual regulation of diacylglycerol kinase (DGK)-θ: polybasic proteins promote activation by phospholipids and increase substrate affinity. *J. Biol. Chem.* **287,** 41619–41627 (2012).
4. Takeishi, Y., Goto, K. & Kubota, I. Role of diacylglycerol kinase in cellular regulatory processes: a new regulator for cardiomyocyte hypertrophy. *Pharmacol. Ther.* **115,** 352–359 (2007).
5. Ali, H. *et al.* Selective translocation of diacylglycerol kinase zeta in hippocampal neurons under transient forebrain ischemia. *Neurosci. Lett.* **372,** 190–195 (2004).
6. Kanoh, H. & Ohno, K. Partial purification and properties of diacylglycerol kinase from rat liver cytosol. *Arch. Biochem. Biophys.* **209,** 266–275 (1981).
7. Besterman, J. M., Pollenz, R. S., Booker, E. L., Jr & Cuatrecasas, P. Diacylglycerol-induced translocation of diacylglycerol kinase: use of affinity-purified enzyme in a reconstitution system. *Proc. Natl. Acad. Sci. U. S. A.* **83,** 9378–9382 (1986).
8. Stathopoulos, V. M. *et al.* Identification of two cytosolic diacylglycerol kinase isoforms in rat brain, and in NIH-3T3 and ras-transformed fibroblasts. *Biochem. J.* **272,** 569–575 (1990).

9. Chen, Q., Klemm, N. & Jeng, I. Characterization of two cytosolic diacylglycerol kinase forms. *J. Neurochem.* **60,** 1212–1219 (1993).

10. Shim, Y. H., Lin, C. H. & Strickland, K. P. The purification and properties of monoacylglycerol kinase from bovine brain. *Biochem. Cell Biol. Biochim. Biol. Cell.* **67,** 233–241 (1989).

11. Ogawara, H. *et al.* Inhibitors of diacylglycerol kinase from Drechslera sacchari. *J. Antibiot. (Tokyo)* **47,** 499–501 (1994).

12. Yada, Y., Ozeki, T., Kanoh, H. & Nozawa, Y. Purification and characterization of cytosolic diacylglycerol kinases of human platelets. *J. Biol. Chem.* **265,** 19237–19243 (1990).

13. Hodgkin, M., Gardner, S. & Wakelam, M. The identification of several stearoyl-arachidonyl selective diacylglycerol kinases in the particulate fraction of porcine testes. *Biochem. Soc. Trans.* **21,** 490S (1993).

14. Redman, C., Lefevre, J. & MacDonald, M. L. Inhibition of diacylglycerol kinase by the antitumor agent calphostin C. Evidence for similarity between the active site of diacylglycerol kinase and the regulatory site of protein kinase C. *Biochem. Pharmacol.* **50,** 235–241 (1995).

15. Jiang, Y., Sakane, F., Kanoh, H. & Walsh, J. P. Selectivity of the diacylglycerol kinase inhibitor 3-{2-(4-[bis-(4-fluorophenyl)methylene]-1-piperidinyl)ethyl}-2,3-dihydro -2-thioxo-4(1H)quinazolinone (R59949) among diacylglycerol kinase subtypes. *Biochem. Pharmacol.* **59,** 763–772 (2000).

16. Jiang, Y., Qian, W. J., Hawes, J. W. & Walsh, J. P. A domain with homology to neuronal calcium sensors is required for calcium-dependent activation of diacylglycerol kinase alpha. *J. Biol. Chem.* **275,** 34092–34099 (2000).

17. Lemaitre, R. N., King, W. C., MacDonald, M. L. & Glomset, J. A. Distribution of distinct arachidonoyl-specific and non-specific isoenzymes of diacylglycerol kinase in baboon (Papio cynocephalus) tissues. *Biochem. J.* **266,** 291–299 (1990).

18. Walsh, J. P., Suen, R., Lemaitre, R. N. & Glomset, J. A. Arachidonoyl-diacylglycerol kinase from bovine testis. Purification and properties. *J. Biol. Chem.* **269,** 21155–21164 (1994).

19. Walsh, J. P., Suen, R. & Glomset, J. A. Arachidonoyl-diacylglycerol kinase. Specific in vitro inhibition by polyphosphoinositides suggests a mechanism for regulation of phosphatidylinositol biosynthesis. *J. Biol. Chem.* **270,** 28647–28653 (1995).

20. Thomas, W. E. & Glomset, J. A. Multiple Factors Influence the Binding of a Soluble, Ca2+-Independent, Diacylglycerol Kinase to Unilamellar Phosphoglyceride Vesicles. *Biochemistry* **38,** 3310–3319 (1999).

21. Thomas, W. E. & Glomset, J. A. Affinity purification and catalytic properties of a soluble, Ca2+-independent, diacylglycerol kinase. *Biochemistry* **38,** 3320–3326 (1999).

22. Inoue, H., Yoshioka, T. & Hotta, Y. Partial purification and characterization of membrane-associated diacylglycerol kinase of Drosophila heads. *Biochim. Biophys. Acta* **1122,** 219–224 (1992).

23. Wissing, J. B. & Wagner, K. G. Diacylglycerol kinase from suspension cultured plant cells : characterization and subcellular localization. *Plant Physiol.* **98,** 1148–1153 (1992).

24. Kanoh, H., Kondoh, H. & Ono, T. Diacylglycerol kinase from pig brain. Purification and phospholipid dependencies. *J. Biol. Chem.* **258,** 1767–1774 (1983).

25. Kanoh, H. & Ono, T. Utilization of diacylglycerol in phospholipid bilayers by pig brain diacylglycerol kinase and Rhizopus arrhizus lipase. *J. Biol. Chem.* **259,** 11197–11202 (1984).

26. Bishop, H. H. & Strickland, K. P. Comparisons of monoacylglycerols and diacylglycerols of varying fatty acid composition as substrates for the acylglycerol kinase(s) of rat brain. *Lipids* **15,** 285–291 (1980).

27. Kanoh, H., Yamada, K., Sakane, F. & Imaizumi, T. Phosphorylation of diacylglycerol kinase in vitro by protein kinase C. *Biochem. J.* **258,** 455–462 (1989).

28. Sakane, F., Yamada, K. & Kanoh, H. Different effects of sphingosine, R59022 and anionic amphiphiles on two diacylglycerol kinase isozymes purified from porcine thymus cytosol. *FEBS Lett.* **255,** 409–413 (1989).

29. Sakane, F., Yamada, K., Imai, S. & Kanoh, H. Porcine 80-kDa diacylglycerol kinase is a calcium-binding and calcium/phospholipid-dependent enzyme and undergoes calcium-dependent translocation. *J. Biol. Chem.* **266,** 7096–100 (1991).

30. Lin, C. H., Bishop, H. & Strickland, K. P. Properties of diacylglycerol kinase purified from bovine brain. *Lipids* **21,** 206–211 (1986).

31. Kato, M. & Takenawa, T. Purification and characterization of membrane-bound and cytosolic forms of diacylglycerol kinase from rat brain. *J. Biol. Chem.* **265,** 794–800 (1990).

32. Kahn, D. W. & Besterman, J. M. Cytosolic rat brain synapsin I is a diacylglycerol kinase. *Proc. Natl. Acad. Sci. U. S. A.* **88,** 6137–6141 (1991).

33. Younes, A. *et al.* Ceramide is a competitive inhibitor of diacylglycerol kinase in vitro and in intact human leukemia (HL-60) cells. *J. Biol. Chem.* **267,** 842–847 (1992).

34. Schaap, D. *et al.* Purification, cDNA-cloning and expression of human diacylglycerol kinase. *FEBS Lett.* **275,** 151–158 (1990).

35. Haq, E., Sharma, S. & Khuller, G. K. Purification of diacylglycerol kinase from Microsporum gypseum and its phosphorylation by the catalytic subunit of protein kinase A. *Arch. Biochem. Biophys.* **392,** 219–225 (2001).

36. Sakane, F., Yamada, K., Kanoh, H., Yokoyama, C. & Tanabe, T. Porcine diacylglycerol kinase sequence has zinc finger and E-F hand motifs. *Nature* **344,** 345–348 (1990).

37. Katagiri, T., Mizoguchi, T. & Shinozaki, K. Molecular cloning of a cDNA encoding diacylglycerol kinase (DGK) in Arabidopsis thaliana. *Plant Mol. Biol.* **30,** 647–653 (1996).

38. Topham, M. K. & Prescott, S. M. Diacylglycerol Kinase ζ Regulates Ras Activation by a Novel Mechanism. *J. Cell Biol.* **152,** 1135–1144 (2001).

39. Takahashi, M., Yamamoto, T., Sakai, H. & Sakane, F. Calcium negatively regulates an intramolecular interaction between the N-terminal recoverin homology

and EF-hand motif domains and the C-terminal C1 and catalytic domains of diacylglycerol kinase α. *Biochem. Biophys. Res. Commun.* **423,** 571–576 (2012).

40. Sanjuán, M. A., Jones, D. R., Izquierdo, M. & Mérida, I. Role of diacylglycerol kinase alpha in the attenuation of receptor signaling. *J. Cell Biol.* **153,** 207–220 (2001).

41. Imai, S., Kai, M., Yasuda, S., Kanoh, H. & Sakane, F. Identification and characterization of a novel human type II diacylglycerol kinase, DGK kappa. *J. Biol. Chem.* **280,** 39870–39881 (2005).

42. Lung, M. *et al.* Diacylglycerol kinase epsilon is selective for both acyl chains of phosphatidic acid or diacylglycerol. *J. Biol. Chem.* **284,** 31062–31073 (2009).

43. Dicu, A. O., Topham, M. K., Ottaway, L. & Epand, R. M. Role of the hydrophobic segment of diacylglycerol kinase epsilon. *Biochemistry* **46,** 6109–6117 (2007).

44. Luo, B., Prescott, S. M. & Topham, M. K. Association of diacylglycerol kinase zeta with protein kinase C alpha: spatial regulation of diacylglycerol signaling. *J. Cell Biol.* **160,** 929–937 (2003).

45. Sakane, F., Kai, M., Wada, I., Imai, S. & Kanoh, H. The C-terminal part of diacylglycerol kinase alpha lacking zinc fingers serves as a catalytic domain. *Biochem. J.* **318 (Pt 2),** 583–590 (1996).

46. De la Roche, M. A. *et al.* Dictyostelium discoideum has a single diacylglycerol kinase gene with similarity to mammalian θ isoforms. *Biochem. J.* **368,** 809 (2002).

47. Ostroski, M., Tu-Sekine, B. & Raben, D. M. Analysis of a Novel Diacylglycerol Kinase from Dictyostelium discoideum: DGKA. *Biochemistry* **44,** 10199–10207 (2005).

48. Ahmed, S. *et al.* The cysteine-rich domain of human proteins, neuronal chimaerin, protein kinase C and diacylglycerol kinase binds zinc. Evidence for the involvement of a zinc-dependent structure in phorbol ester binding. *Biochem. J.* **280,** 233–241 (1991).

49. Sakane, F., Imai, S., Yamada, K. & Kanoh, H. The regulatory role of EF-hand motifs of pig 80K diacylglycerol kinase as assessed using truncation and deletion mutants. *Biochem. Biophys. Res. Commun.* **181,** 1015–1021 (1991).

50. Liu, Z., Chang, G. Q. & Leibowitz, S. F. Diacylglycerol kinase zeta in hypothalamus interacts with long form leptin receptor. Relation to dietary fat and body weight regulation. *J. Biol. Chem.* **276,** 5900–5907 (2001).

51. Gómez-Merino, F. C. *et al.* AtDGK2, a novel diacylglycerol kinase from Arabidopsis thaliana, phosphorylates 1-stearoyl-2-arachidonoyl-sn-glycerol and 1,2-dioleoyl-sn-glycerol and exhibits cold-inducible gene expression. *J. Biol. Chem.* **279,** 8230–8241 (2004).

52. Gómez-Merino, F. C. *et al.* Arabidopsis AtDGK7, the smallest member of plant diacylglycerol kinases (DGKs), displays unique biochemical features and saturates at low substrate concentration: the DGK inhibitor R59022 differentially affects AtDGK2 and AtDGK7 activity in vitro and alters plant growth and development. *J. Biol. Chem.* **280,** 34888–34899 (2005).

53. Prodeus, A., Berno, B., Topham, M. K. & Epand, R. M. The basis of the substrate specificity of the epsilon isoform of human diacylglycerol kinase is not a consequence of competing hydrolysis of ATP. *Chem. Phys. Lipids* **166C,** 26–30 (2012).

54. Yamada, K., Sakane, F., Matsushima, N. & Kanoh, H. EF-hand motifs of alpha, beta and gamma isoforms of diacylglycerol kinase bind calcium with different affinities and conformational changes. *Biochem. J.* **321 (Pt 1),** 59–64 (1997).

55. Liu, G. *et al.* NMR Structure of the Diacylglycerol kinase alpha, NESGC target HR532. *Northeast Struct. Genomics Consort.* <http://www.rcsb.org/pdb/explore/explore.do?structureId=1TUZ> (2005).

56. Miyamoto, K. *et al.* Solution Structure of The C1 Domain of The Human Diacylglycerol Kinase Delta. <http://www.rcsb.org/pdb/explore/explore.do?structureId=1R79> (2004).

57. Harada, B. T. *et al.* Regulation of enzyme localization by polymerization: polymer formation by the SAM domain of diacylglycerol kinase delta1. *Struct. Lond. Engl. 1993* **16,** 380–387 (2008).

58. Bradford, M. M. A rapid and sensitive method for the quantitation of microgram quantities of protein utilizing the principle of protein-dye binding. *Anal. Biochem.* **72,** 248–254 (1976).

59. Reynolds, J. A. & Tanford, C. Binding of Dodecyl Sulfate to Proteins at High Binding Ratios. Possible Implications for the State of Proteins in Biological Membranes. *Proc. Natl. Acad. Sci.* **66,** 1002–1007 (1970).

60. Shapiro, A. L., Viñuela, E. & Maizel, J. V., Jr. Molecular weight estimation of polypeptide chains by electrophoresis in SDS-polyacrylamide gels. *Biochem. Biophys. Res. Commun.* **28,** 815–820 (1967).

61. Meyer, T. S. & Lamberts, B. L. Use of coomassie brilliant blue R250 for the electrophoresis of microgram quantities of parotid saliva proteins on acrylamide-gel strips. *Biochim. Biophys. Acta BBA - Gen. Subj.* **107,** 144–145 (1965).

62. Kerényi, L. & Gallyas, F. A highly sensitive method for demonstrating proteins in electrophoretic, immunoelectrophoretic and immunodiffusion preparations. *Clin. Chim. Acta* **38,** 465–467 (1972).

63. Blackshear, P. J. Systems for polyacrylamide gel electrophoresis. *Methods Enzymol.* **104,** 237–255 (1984).

64. Hames, B. D. *Gel Electrophoresis of Proteins: a Practical Approach*. (Oxford University Press, 1998).

65. Merril, C. R. DEVELOPMENT AND MECHANISMS OF SILVER STAINS FOR ELECTROPHORESIS. *Acta Histochem. Cytochem.* **19,** 655–667 (1986).

66. Rabilloud, T. Mechanisms of protein silver staining in polyacrylamide gels: a 10-year synthesis. *Electrophoresis* **11,** 785–794 (1990).

67. SAMBROOK, F., & MANIATIS. *Molecular Cloning: A Laboratory Manual SECOND EDITION*. (Cold Spring Harbor Laboratory, 1989).

68. Schneider, C. A., Rasband, W. S. & Eliceiri, K. W. NIH Image to ImageJ: 25 years of image analysis. *Nat. Methods* **9,** 671–675 (2012).

69. Neugebauer, J. M. Detergents: an overview. *Methods Enzymol.* **182,** 239–253 (1990).

70. Loewenthal, H. J. E. & Zass, E. *A Guide for the Perplexed Organic Experimentalist*. (Wiley, 1990).

71. Avanti Polar Lipids - TLC Solvent Systems - Lipid Migration. <http://avantilipids.com/index.php?option=com_content&id=1690&Itemid=409> (2013).

72. Bishop, W. R., Ganong, B. R. & Bell, R. M. Attenuation of sn-1,2-diacylglycerol second messengers by diacylglycerol kinase. Inhibition by diacylglycerol analogs in vitro and in human platelets. *J. Biol. Chem.* **261,** 6993–7000 (1986).

73. Lundberg, G. A. & Sommarin, M. Diacylglycerol kinase in plasma membranes from wheat. *Biochim. Biophys. Acta* **1123,** 177–183 (1992).

74. Charter, N. W., Kauffman, L., Singh, R. & Eglen, R. M. A generic, homogenous method for measuring kinase and inhibitor activity via adenosine 5'-diphosphate accumulation. *J. Biomol. Screen.* **11,** 390–399 (2006).

75. Cook, P. F. & Cleland, W. W. *Enzyme Kinetics and Mechanism*. (Garland Science, 2007).

76. Durfee, T. *et al.* The complete genome sequence of Escherichia coli DH10B: insights into the biology of a laboratory workhorse. *J. Bacteriol.* **190,** 2597–2606 (2008).

77. Hanahan, D., Jessee, J. & Bloom, F. R. Plasmid transformation of Escherichia coli and other bacteria. *Methods Enzymol.* **204,** 63–113 (1991).

78. Tu, A.-H. T. Transformation of Escherichia coli Made Competent by Calcium Chloride Protocol. *ASM MicrobeLibrary* <http://www.microbelibrary.org/component/resource/laboratory-test/3152-transformation-of-escherichia-coli-made-competent-by-calcium-chloride-protocol> (2008).

79. Knudsen, E. T., Rolinson, G. N. & Sutherland, R. Carbenicillin: a new semisynthetic penicillin active against Pseudomonas pyocyanea. *Br. Med. J.* **3,** 75–78 (1967).

80. Fuller, B. J. Cryoprotectants: the essential antifreezes to protect life in the frozen state. *Cryo Letters* **25,** 375–388 (2004).

81. LOVELOCK, J. E. The protective action of neutral solutes against haemolysis by freezing and thawing. *Biochem. J.* **56,** 265–270 (1954).

82. Strains and Vectors - Strains - Bacterial Strains - EMBL. *Eur. Mol. Biol. Lab.* <http://www.embl.de/pepcore/pepcore_services/strains_vectors/strains/bacterial_strains/> (2013).

83. Rosetta™(DE3) Competent Cells - EMD4Biosciences | EMD Millipore USA. <http://www.emdmillipore.com/life-science-research/rosettade3-competent-cells/EMD_BIO-70954/p_pUWb.s1Ow04AAAEjRhl9.zLX?WFSimpleSearch_NameOrID=rosetta&BackButtonText=search+results> (2013).

84. THE LAC REPRESSOR. <http://biology.kenyon.edu/BMB/Chime/Mat/MASTER.HTM> (1999).

85. Nash, J. A., Ballard, T. N. S., Weaver, T. E. & Akinbi, H. T. The Peptidoglycan-Degrading Property of Lysozyme Is Not Required for Bactericidal Activity In Vivo. *J. Immunol.* **177,** 519–526 (2006).

86. Kashyap, D. R. *et al.* Peptidoglycan recognition proteins kill bacteria by activating protein-sensing two-component systems. *Nat. Med.* **17,** 676–683 (2011).

87. LATHE, G. H. & RUTHVEN, C. R. The separation of substances and estimation of their relative molecular sizes by the use of columns of starch in water. *Biochem. J.* **62,** 665–674 (1956).

88. Whitaker, J. R. Determination of Molecular Weights of Proteins by Gel Filtration of Sephadex. *Anal. Chem.* **35,** 1950–1953 (1963).

89. Scopes, R. K. *Protein Purification: Principles and Practice*. (Springer, 1994).

90. Marchler-Bauer, A. *et al.* CDD: conserved domains and protein three-dimensional structure. *Nucleic Acids Res.* **41,** D348–352 (2013).

91. Palmer, I. and Wingfield, P. T. Preparation and Extraction of Insoluble (Inclusion-Body) Proteins from Escherichia coli. *Current Protocols in Protein Science*. 38:6.3.1–6.3.18 (2004). doi: 10.1002/0471140864.ps0603s38

92. Nichols, C. E. *et al.* Characterization of Salmonella typhimurium YegS, a putative lipid kinase homologous to eukaryotic sphingosine and diacylglycerol kinases. *Proteins Struct. Funct. Bioinforma.* **68,** 13–25 (2007).

93. Bakali H., M. A., Nordlund, P. & Hallberg, B. M. Expression, purification, crystallization and preliminary diffraction studies of the mammalian DAG kinase homologue YegS from Escherichia coli. *Acta Crystallograph. Sect. F Struct. Biol. Cryst. Commun.* **62,** 295–297 (2006).

94. Miller, D. J., Jerga, A., Rock, C. O. & White, S. W. Analysis of the Staphylococcus aureus DgkB Structure Reveals a Common Catalytic Mechanism for the Soluble Diacylglycerol Kinases. *Structure* **16,** 1036–1046 (2008).

95. Ramjeesingh, M., Huan, L. J., Garami, E. & Bear, C. E. Novel method for evaluation of the oligomeric structure of membrane proteins. *Biochem. J.* **342 (Pt 1),** 119–123 (1999).

96. Renzi, F. *et al.* Large-scale purification and crystallization of the endoribonuclease XendoU: troubleshooting with His-tagged proteins. *Acta Crystallograph. Sect. F Struct. Biol. Cryst. Commun.* **62,** 298–301 (2006).

97. Krebs, M. R. H., Devlin, G. L. & Donald, A. M. Protein particulates: another generic form of protein aggregation? *Biophys. J.* **92,** 1336–1342 (2007).

98. BioUltra Biological Buffers. *Sigma-Aldrich* <http://www.sigmaaldrich.com/life-science/metabolomics/bioultra-reagents/biological-buffers.html> (2013).

99. Han, J. C. & Han, G. Y. A procedure for quantitative determination of tris(2-carboxyethyl)phosphine, an odorless reducing agent more stable and effective than dithiothreitol. *Anal. Biochem.* **220,** 5–10 (1994).

100. Guo, W., Sun, Y. W., Luo, G. S. & Wang, Y. J. Interaction of PEG with ionic surfactant SDS to form template for mesoporous material. *Colloids Surf. Physicochem. Eng. Asp.* **252,** 71–77 (2005).

101. Thomas, J. G., Ayling, A. & Baneyx, F. Molecular chaperones, folding catalysts, and the recovery of active recombinant proteins from E. coli. To fold or to refold. *Appl. Biochem. Biotechnol.* **66,** 197–238 (1997).

102. De Marco, A. Protocol for preparing proteins with improved solubility by co-expressing with molecular chaperones in Escherichia coli. *Nat. Protoc.* **2,** 2632–2639 (2007).

103. Haacke, A., Fendrich, G., Ramage, P. & Geiser, M. Chaperone over-expression in Escherichia coli: apparent increased yields of soluble recombinant protein kinases are due mainly to soluble aggregates. *Protein Expr. Purif.* **64,** 185–193 (2009).

104. National Center for Biotechnology Information. <http://www.ncbi.nlm.nih.gov/> (2013).

105. Altschul, S. F. *et al.* Gapped BLAST and PSI-BLAST: a new generation of protein database search programs. *Nucleic Acids Res.* **25,** 3389–3402 (1997).

106. Kipnis, Y., Papo, N., Haran, G. & Horovitz, A. Concerted ATP-induced allosteric transitions in GroEL facilitate release of protein substrate domains in an all-or-none manner. *Proc. Natl. Acad. Sci.* **104,** 3119–3124 (2007).

107. Bartlett, J. M. S. & Stirling, D. A short history of the polymerase chain reaction. *Methods in Molecular Biology*™ **226,** 3–6 (2003). doi: 10.1385/1-59259-384-4:3

108. SalI | New England Biolabs. <https://www.neb.com/products/r0138-sali> (2013).

109. Cleavage Close to the End of DNA Fragments | New England Biolabs. <https://www.neb.com/tools-and-resources/usage-guidelines/cleavage-close-to-the-end-of-dna-fragments> (2013).

110. NotI | New England Biolabs. <https://www.neb.com/products/r0189-noti> (2013).

111. Schoenmakers, T. J., Visser, G. J., Flik, G. & Theuvenet, A. P. CHELATOR: an improved method for computing metal ion concentrations in physiological solutions. *BioTechniques* **12,** 870–874, 876–879 (1992).

112. Dyson, M. R., Shadbolt, S. P., Vincent, K. J., Perera, R. L. & McCafferty, J. Production of soluble mammalian proteins in Escherichia coli: identification of protein features that correlate with successful expression. *BMC Biotechnol.* **4,** 32 (2004).

113. Douette, P. *et al.* Escherichia coli fusion carrier proteins act as solubilizing agents for recombinant uncoupling protein 1 through interactions with GroEL. *Biochem. Biophys. Res. Commun.* **333,** 686–693 (2005).

114. Esposito, D. & Chatterjee, D. K. Enhancement of soluble protein expression through the use of fusion tags. *Curr. Opin. Biotechnol.* **17,** 353–358 (2006).

115. Santner, A. A. *et al.* Sweeping Away Protein Aggregation with Entropic Bristles: Intrinsically Disordered Protein Fusions Enhance Soluble Expression. *Biochemistry* **51,** 7250–7262 (2012).

116. Smith, D. B. Generating fusions to glutathione S-transferase for protein studies. *Methods Enzymol.* **326,** 254–270 (2000).

117. Smith, D. B. & Johnson, K. S. Single-step purification of polypeptides expressed in Escherichia coli as fusions with glutathione S-transferase. *Gene* **67,** 31–40 (1988).

118. LaVallie, E. R. *et al.* A thioredoxin gene fusion expression system that circumvents inclusion body formation in the E. coli cytoplasm. *Biotechnol. Nat. Publ. Co.* **11,** 187–193 (1993).

119. Richarme, G. & Caldas, T. D. Chaperone properties of the bacterial periplasmic substrate-binding proteins. *J. Biol. Chem.* **272,** 15607–15612 (1997).

120. Sachdev, D. & Chirgwin, J. M. Fusions to maltose-binding protein: control of folding and solubility in protein purification. *Methods Enzymol.* **326,** 312–321 (2000).

121. De Marco, A., Deuerling, E., Mogk, A., Tomoyasu, T. & Bukau, B. Chaperone-based procedure to increase yields of soluble recombinant proteins produced in E. coli. *BMC Biotechnol.* **7,** 32–32 (2007).

122. Kane, J. F. Effects of rare codon clusters on high-level expression of heterologous proteins in Escherichia coli. *Curr. Opin. Biotechnol.* **6,** 494–500 (1995).

123. Carstens, C.-P. Use of tRNA-Supplemented Host Strains for Expression of Heterologous Genes in *E. coli*. *Methods in Molecular Biology* **205,** 225–234 (2002). doi: 10.1385/1-59259-301-1:225

124. Palmer, E. & Freeman, T. Investigation Into the use of C- and N-terminal GFP Fusion Proteins for Subcellular Localization Studies Using Reverse Transfection Microarrays. *Comp. Funct. Genomics* **5,** 342–353 (2004).

125. Gan, X. & Gould, S. J. Identification of an inhibitory budding signal that blocks the release of HIV particles and exosome/microvesicle proteins. *Mol. Biol. Cell* **22,** 817–830 (2011).

126. Magnan, C. N., Randall, A. & Baldi, P. SOLpro: accurate sequence-based prediction of protein solubility. *Bioinforma. Oxf. Engl.* **25,** 2200–2207 (2009).

127. Smialowski, P. *et al.* Protein solubility: sequence based prediction and experimental verification. *Bioinforma. Oxf. Engl.* **23,** 2536–2542 (2007).

128. Sakikawa, C., Taguchi, H., Makino, Y. & Yoshida, M. On the Maximum Size of Proteins to Stay and Fold in the Cavity of GroEL underneath GroES. *J. Biol. Chem.* **274,** 21251–21256 (1999).

129. Houry, W. A., Frishman, D., Eckerskorn, C., Lottspeich, F. & Hartl, F. U. Identification of in vivo substrates of the chaperonin GroEL. *Nature* **402,** 147–154 (1999).

130. Liberek, K., Marszalek, J., Ang, D., Georgopoulos, C. & Zylicz, M. Escherichia coli DnaJ and GrpE heat shock proteins jointly stimulate ATPase activity of DnaK. *Proc. Natl. Acad. Sci. U. S. A.* **88,** 2874–2878 (1991).

131. Martínez-Alonso, M., García-Fruitós, E., Ferrer-Miralles, N., Rinas, U. & Villaverde, A. Side effects of chaperone gene co-expression in recombinant protein production. *Microb. Cell Factories* **9,** 64 (2010).

132. Wiech, H., Buchner, J., Zimmermann, R. & Jakob, U. Hsp90 chaperones protein folding in vitro. *Nature* **358,** 169–170 (1992).

133. Narberhaus, F. Alpha-crystallin-type heat shock proteins: socializing minichaperones in the context of a multichaperone network. *Microbiol. Mol. Biol. Rev. MMBR* **66,** 64–93 (2002).

134. Close, T. J. Dehydrins: A commonalty in the response of plants to dehydration and low temperature. *Physiol. Plant.* **100,** 291–296 (1997).

135. Buchberger, A., Schröder, H., Hesterkamp, T., Schönfeld, H.-J. & Bukau, B. Substrate Shuttling Between the DnaK and GroEL Systems Indicates a Chaperone Network Promoting Protein Folding. *J. Mol. Biol.* **261,** 328–333 (1996).

136. Long, F., Cho, W. & Ishii, Y. Expression and purification of 15N- and 13C-isotope labeled 40-residue human Alzheimer's β-amyloid peptide for NMR-based structural analysis. *Protein Expr. Purif.* **79,** 16–24 (2011).

137. Park, D.-W. *et al.* Improved recovery of active GST-fusion proteins from insoluble aggregates: solubilization and purification conditions using PKM2 and HtrA2 as model proteins. *BMB Rep.* **44,** 279–284 (2011).

138. Black, M. M., Stockum, C., Dickson, J. M., Putterill, J. & Arcus, V. L. Expression, purification and characterisation of GIGANTEA: A circadian clock-controlled regulator of photoperiodic flowering in plants. *Protein Expr. Purif.* **76,** 197–204 (2011).

139. Ullrich, A. *et al.* Rat Insulin Genes: Construction of Plasmids Containing the Coding Sequences. *Science* **196,** 1313–1319 (1977).

140. Tu-Sekine, B., Ostroski, M. & Raben, D. M. Modulation of diacylglycerol kinase theta activity by alpha-thrombin and phospholipids. *Biochemistry* **46,** 924–932 (2007).

141. Tu-Sekine, B., Goldschmidt, H., Petro, E. & Raben, D. M. Diacylglycerol kinase θ: regulation and stability. *Adv. Biol. Regul.* **53,** 118–126 (2013).

142. McLaughlin, S., Mulrine, N., Gresalfi, T., Vaio, G. & McLaughlin, A. Adsorption of divalent cations to bilayer membranes containing phosphatidylserine. *J. Gen. Physiol.* **77,** 445–473 (1981).

143. Markwardt, F. Hirudin as an inhibitor of thrombin. *Methods Enzymol.* **19,** 924–932 (1970).

144. Smith, M. D. *et al.* Synthesis and Convenient Functionalization of Azide-Labeled Diacylglycerol Analogues for Modular Access to Biologically Active Lipid Probes. *Bioconjug. Chem.* **19,** 1855–1863 (2008).

145. Avanti Polar Lipids - Egg PC 99%. <http://avantilipids.com/index.php?option=com_content&view=article&id=260&Itemid=212&catnumber=840051> (2013).

146. Kerppola, T. K. Visualization of molecular interactions by fluorescence complementation. *Nat. Rev. Mol. Cell Biol.* **7,** 449–456 (2006).

147. Ormö, M. *et al.* Crystal structure of the Aequorea victoria green fluorescent protein. *Science* **273,** 1392–1395 (1996).

148. Lybarger, L. *et al.* Dual-color flow cytometric detection of fluorescent proteins using single-laser (488-nm) excitation. *Cytometry* **31,** 147–152 (1998).

149. XhoI | New England Biolabs. <https://www.neb.com/products/r0146-xhoi> (2013).

150. Moustakas, A., Souchelnytskyi, S. & Heldin, C. H. Smad regulation in TGF-beta signal transduction. *J. Cell Sci.* **114,** 4359–4369 (2001).

151. Remy, I., Montmarquette, A. & Michnick, S. W. PKB/Akt modulates TGF-β signalling through a direct interaction with Smad3. *Nat. Cell Biol.* **6,** 358–365 (2004).

152. Gasteiger, E. *et al.* Protein Identification and Analysis Tools on the ExPASy Server. *The Proteomics Protocols Handbook* 571–607 (Humana Press, 2005).

153. Artimo, P. *et al.* ExPASy: SIB bioinformatics resource portal. *Nucleic Acids Res.* **40,** W597–W603 (2012).

154. Lottenberg, R., Christensen, U., Jackson, C. M. & Coleman, P. L. Assay of coagulation proteases using peptide chromogenic and fluorogenic substrates. *Methods Enzymol.* **80 Pt C,** 341–361 (1981).

155. Henry Arnaud, C. Cut-And-Paste GFP. *Chem. Eng. News* **87,** 13 (2009).

156. Kent, K. P., Oltrogge, L. M. & Boxer, S. G. Synthetic Control of Green Fluorescent Protein. *J. Am. Chem. Soc.* **131,** 15988–15989 (2009).

157. Rebecchi, M., Peterson, A. & McLaughlin, S. Phosphoinositide-specific phospholipase C-delta 1 binds with high affinity to phospholipid vesicles containing phosphatidylinositol 4,5-bisphosphate. *Biochemistry* **31,** 12742–12747 (1992).

158. Stahelin, R. V. *et al.* Mechanism of Diacylglycerol-induced Membrane Targeting and Activation of Protein Kinase Cδ. *J. Biol. Chem.* **279,** 29501–29512 (2004).

159. Mosior, M. & Newton, A. C. Mechanism of Interaction of Protein Kinase C with Phorbol Esters. *J. Biol. Chem.* **270,** 25526–25533 (1995).

160. Medkova, M. & Cho, W. Differential membrane-binding and activation mechanisms of protein kinase C-alpha and -epsilon. *Biochemistry* **37,** 4892–4900 (1998).

161. Brusca, J. S. & Radolf, J. D. Isolation of integral membrane proteins by phase partitioning with Triton X-114. *Methods Enzymol.* **228,** 182–193 (1994).

162. Bordier, C. Phase separation of integral membrane proteins in Triton X-114 solution. *J. Biol. Chem.* **256,** 1604–1607 (1981).

163. Lee, A. *et al.* Rat liver membrane glycoproteome: enrichment by phase partitioning and glycoprotein capture. *J. Proteome Res.* **8,** 770–781 (2009).

164. Rowland, M. M. *et al.* Phosphatidylinositol 3,4,5-trisphosphate activity probes for the labeling and proteomic characterization of protein binding partners. *Biochemistry* **50,** 11143–11161 (2011).

165. Dormán, G. & Prestwich, G. D. Benzophenone Photophores in Biochemistry. *Biochemistry* **33,** 5661–5673 (1994).

166. Deitzer, G. F. Does glass block UV light? <http://www.bio.net/bionet/mm/plant-ed/1999-March/004186.html> (1999).

167. Producing Light. <http://www1.union.edu/newmanj/Physics100/Light%20Production/producing_light.htm> (2013).

168. Dimova, K. *et al.* Structural insights into the calmodulin-Munc13 interaction obtained by cross-linking and mass spectrometry. *Biochemistry* **48,** 5908–5921 (2009).

169. Mascot search engine | Protein identification software for mass spec data. <http://www.matrixscience.com/> (2013).

170. Thermo Omics Portal. <http://portal.thermo-brims.com/> (2013).

171. Fong, B., Ma, L. & Norris, C. Analysis of phospholipids in infant formulas using high performance liquid chromatography-tandem mass spectrometry. *J. Agric. Food Chem.* **61,** 858–865 (2013).

172. Norris, C., Fong, B., MacGibbon, A. & McJarrow, P. Analysis of phospholipids in rat brain using liquid chromatography-mass spectrometry. *Lipids* **44,** 1047–1054 (2009).

173. Liebisch, G. *et al.* High throughput quantification of cholesterol and cholesteryl ester by electrospray ionization tandem mass spectrometry (ESI-MS/MS). *Biochim. Biophys. Acta BBA - Mol. Cell Biol. Lipids* **1761,** 121–128 (2006).

174. Saville, J. T., Zhao, Z., Willcox, M. D. P., Blanksby, S. J. & Mitchell, T. W. Detection and Quantification of Tear Phospholipids and Cholesterol in Contact Lens Deposits: The Effect of Contact Lens Material and Lens Care Solution. *Invest. Ophthalmol. Vis. Sci.* **51,** 2843–2851 (2010).

175. Ismaiel, O. A., Jenkins, R. G. & Thomas Karnes, H. Investigation of endogenous blood lipids components that contribute to matrix effects in dried blood spot samples by liquid chromatography-tandem mass spectrometry. *Drug Test. Anal.* **5,** 710–715 (2013).

CURRICULUM VITAE

Elizabeth Jane Petro

123 West Barre Street #402
Baltimore, MD 21201
ejpetro@gmail.com
(480)335-9617

Born April 26, 1985 in Milwaukee, WI

Education

- B.S. *with General Honors* in Biological Chemistry *with Honors*, minor in Classical Studies, The University of Chicago, Chicago, IL (2002-2006)
- Ph.D. in Biological Chemistry, Biological Chemistry Graduate Program, The Johns Hopkins University School of Medicine, Baltimore, MD (2006-2013)

Research Experience

- Undergraduate Research Assistant, Department of Biochemistry and Molecular Biology, The University of Chicago, Chicago, IL (February 2004-June 2006)
    - Research Advisor: Anthony A. Kossiakoff, Ph.D.
- Graduate Research Assistant, Department of Biological Chemistry, The Johns Hopkins University School of Medicine, Baltimore, MD (August 2006-November 2006)
    - Research Advisor: Pierre A. Coulombe, Ph.D.
    - Rotation Project Title: "Interferon-gamma and catagen induction in C57Bl/6 N12 K17 -/- mouse backskin"
- Graduate Research Assistant, Department of Biological Chemistry, The Johns Hopkins University School of Medicine, Baltimore, MD (December 2006-December 2013)
    - Research Advisor: Daniel M. Raben, Ph.D.
    - Thesis Title: "Seeking the lipid substrate binding site: structural studies of eukaryotic diacylglycerol kinases"

Teaching Experience

- Organic Chemistry Tutor, Department of Chemistry, The University of Chicago, Chicago, IL (October 2004-December 2004)
- Metabolism Teaching Assistant, Department of Biological Chemistry, The Johns Hopkins University School of Medicine, Baltimore, MD (October 2007; October 2008)
- Biochemical and Biophysical Principles Tutor, Department of Biological Chemistry, The Johns Hopkins University School of Medicine, Baltimore, MD (October 2008)
- Oral Exam Tutor, Department of Biological Chemistry, The Johns Hopkins University School of Medicine, Baltimore, MD (May 2011-August 2011)

- Metabolism Conference Leader, Department of Biological Chemistry, The Johns Hopkins University School of Medicine, Baltimore, MD (November 2009; November 2010; November 2012)

Professional Affiliations

- American Chemical Society (2006-present)
- American Association for the Advancement of Science (2006-present)
- Sigma Xi (2006-present)
- Phi Beta Kappa (2006-present)
- The Biophysical Society (2007)
- Association for Women in Science (2011-present)
- The American Society for Biochemistry and Molecular Biology (2013-present)
- Society for Experimental Biology and Medicine (2013-present)

Honors and Awards

- University Scholar Award, The University of Chicago, Chicago, IL (2002-2006)
- National Merit Finalist Scholarship, The University of Chicago, Chicago, IL (2002-2006)
- Dean's List, The University of Chicago, Chicago, IL (2003-2006)
- Sigma Xi, Associate Member, The University of Chicago, Chicago, IL (2006)
- Phi Beta Kappa, The University of Chicago, Chicago, IL (2006)
- B.S. in the College with General Honors, The University of Chicago, Chicago, IL (2006)
- B.S. in Biological Chemistry with Honors, The University of Chicago, Chicago, IL (2006)
- Honorable Mention, National Science Foundation Graduate Research Fellowship, National Science Foundation (2008)
    - Proposed Research Essay Title: "How lipids and post-translational modifications affect the membrane-binding and the enzymatic activity of diacylglycerol kinase A"
- American Heart Association Predoctoral Fellowship, American Heart Association, Mid-Atlantic Affiliate (2008-2010)
    - Project Title: "Structure, function, and enzymology of human diacylglycerol kinase zeta"
- WCC / Eli Lilly Travel Award, American Chemical Society Women Chemists Committee and Eli Lilly and Company (2013)
    - Abstract Title: "Photoaffinity labeling the lipid binding site of mammalian diacylglycerol kinase"

Presentations

- **E. Petro**, J. Horn, and A. Kossiakoff. "Stability studies of a phage-optimized human growth hormone variant." 16th Annual Argonne Symposium for Undergraduates in Science, Engineering, and Mathematics, Argonne, IL (November 2005)

- Biological Chemistry Honors Thesis Presentation, Department of Chemistry, The University of Chicago, Chicago, IL (April 2006)
- "Activation and inhibition of a *Dictyostelium discoideum* diacylglycerol kinase." Thursday Evening Research Discussion Series, Department of Biological Chemistry, The Johns Hopkins University School of Medicine, Baltimore, MD (February 2008)
- "Structural studies of mammalian diacylglycerol kinases." Biological Chemistry Student Seminar, Department of Biological Chemistry, The Johns Hopkins University School of Medicine, Baltimore, MD (June 2011)
- "Photoaffinity labeling of diacylglycerol kinase (DGK): seeking the lipid substrate binding site." Biological Chemistry Student Seminar, Department of Biological Chemistry, The Johns Hopkins University School of Medicine, Baltimore, MD (June 2012)
- "Photoaffinity labeling of diacylglycerol kinase (DGK): seeking the lipid substrate binding site." Thursday Evening Research Discussion Series, Department of Biological Chemistry, The Johns Hopkins University School of Medicine, Baltimore, MD (June 2012)
- "Seeking the lipid substrate binding site: photoaffinity labeling of diacylglycerol kinase (DGK)." Biological Chemistry Student Seminar, Department of Biological Chemistry, The Johns Hopkins University School of Medicine, Baltimore, MD (June 2013)
- "Taking a photoaffinity labeling approach to find the lipid binding site on an interfacial enzyme, mammalian diacylglycerol kinase (DGK)." Chemistry at Florham Seminar Series, Fairleigh Dickinson University, Hackensack, NJ (October 2013)
- "Seeking the lipid substrate binding site: structural studies of eukaryotic diacylglycerol kinases." Biological Chemistry Thesis Seminar, Department of Biological Chemistry, The Johns Hopkins University School of Medicine, Baltimore, MD (**expected** 2013)

Posters

- "Photoaffinity labeling of diacylglycerol kinase (DGK): seeking the lipid substrate binding site." Third Annual Biological Chemistry Welcome Party & Lab Olympics Poster Session, Department of Biological Chemistry, The Johns Hopkins University School of Medicine, Baltimore, MD (August 2012)
- **E. Petro**, B. Tu-Sekine, M. Rowland, S. Eni Eni, M. Best, L. DeVine, R. Cole, and D. Raben. "Photoaffinity labeling the lipid binding site of mammalian diacylglycerol kinase." The American Society for Biochemistry and Molecular Biology Annual Meeting, Boston, MA (April 2013)
- **E. Petro**, B. Tu-Sekine, M. Rowland, S. Eni Eni, M. Best, L. DeVine, R. Cole, and D. Raben. "Photoaffinity labeling the lipid binding site of mammalian diacylglycerol kinase." Sigma Xi Mid-Atlantic Regional Meeting, Fairfax, VA (April 2013)
- Third Annual Flemmys Bad Data Social, Graduate Peer Mentoring Program, The Johns Hopkins University School of Medicine, Baltimore, MD (May 2013)

- **E. Petro**, B. Tu-Sekine, M. Rowland, S. Eni Eni, M. Best, L. DeVine, R. Cole, and D. Raben. "Photoaffinity labeling the lipid binding site of mammalian diacylglycerol kinase." Graduate Student Association Annual Poster Session, The Johns Hopkins University School of Medicine, Baltimore, MD (May 2013)
- **E. Petro**, B. Tu-Sekine, M. Rowland, S. Eni Eni, M. Best, L. DeVine, R. Cole, and D. Raben. "Photoaffinity labeling the lipid binding site of mammalian diacylglycerol kinase." The 246th American Chemical Society National Meeting & Exposition, Indianapolis, IN (September 2013)

Peer-Reviewed Publications

- J. Horn, B. Kraybill, **E. Petro**, S. Coales, J. Morrow, Y. Hamuro, and A. Kossiakoff. "The Role of Protein Dynamics in Increasing Binding Affinity for an Engineered Protein-Protein Interaction Established by H/D Exchange Mass Spectrometry." *Biochemistry* 45: 8488-8498 (2006)
- B. Tu-Sekine, H. Goldschmidt, **E. Petro**, and D. Raben. "Diacylglycerol kinase θ: Regulation and Stability." *Advances in Biological Regulation* 53:118-126 (2013)
- **E. Petro** and D. Raben. "Bacterial expression strategies for several *Sus scrofa* diacylglycerol kinase alpha constructs: solubility challenges." *Scientific Reports* 3:1609 (2013)